Geological characterization of sand-prone subaqueous delta systems: a case study of the Upper Jurassic Sognefjord Formation (Troll Field, Northern North Sea, offshore Norway) and global examples

Stefano Patruno

Imperial College London

Department of Earth Science and Engineering

Submitted in accordance with the requirements of the University of London for the degree of Doctor of Philosophy and the Diploma of Imperial College

April 2013

I, Stefano Patruno, hereby declare that the work presented in this thesis is my own, and that all else is appropriately referenced.

ABSTRACT

Core sedimentology, stratigraphic architecture and 3D seismic geomorphology are integrated in order to: (a) demonstrate the criteria for recognition of coarse-grained subaqueous deltas in the stratigraphic record; (b) compare them with modern examples; (c) develop a new method to extract progradation rates from ancient shallow-marine clinoforms; and (d) refine the depositional model of the Upper Jurassic Sognefjord Formation, which forms the main reservoir in the super-giant Troll Field (Norwegian North Sea).

The Sognefjord Formation is a 10-200 m thick clastic wedge, deposited in ca. 6 Myr, by a fully marine deltaic system that was sourced from the Norwegian mainland. A series of 10-60 m thick, westerly-dipping subaqueous clinoform sets are developed within this unit and can be mapped for several tens of kilometres along strike. Within each clinoform set, clinothems are formed by regressively stacked sandstone-rich bedsets, devoid of subaerial facies and separated by thin mudstone intervals. Near-horizontal trajectories are observed in each clinoform set, and the sets are stacked vertically. In the eastern half of the field, individual clinoforms are relatively gently dipping (1-6°) and bound thin (10-30 m) clinothems dominated by fine-grained, hummocky cross-stratified sandstones. Towards the west, clinoforms gradually become steeper (5-14°) and bound thicker (15-60 m) clinothems that comprise medium-grained sandstones in their upper parts. Topsets are usually well developed.

Quantification of clinoform age and progradation rates is constrained by regionally correlatable bioevents, and relies on exponential age-depth interpolations. The facies break that mirrors the foreset-to-bottomset transition, which represents storm wave base, is subsequently dated, and progradation rates are measured along transects tied to well correlations and seismic interpretations. The results indicate falls in progradation rate (from 500 to 30 km/Myr) and net sediment flux (from 90 to 10 km^2/Myr), and a simultaneous rise in vertical sedimentation rate (from 15 to 70 m/Myr) towards the basin; these variations are attributed to the progradation of the subaqueous delta into progressively deeper waters associated with along-shore currents that provide net sediment transport out of the study area, as well as sculpting the linear, elongated clinoforms.

Coarse-grained subaqueous deltas provide a new interpretative template that may be applicable to other ancient clinoform-bearing shallow-marine sandstones with reservoir potential, whilst calculation of progradation rates provides a tool to improve reservoir characterisation and near-field exploration by enhancing prediction of reservoir distribution and character.

ACKNOWLEDGEMENTS

My supervisors, Chris Jackson and Gary Hampson, are gratefully thanked to have helped me and supported me continuously and patiently throughout the last three years. Thank you very much to Andrew Morton to have kindly carried out the garnet provenance analyses (Chapter 3).

I need to thank Imperial College to have funded my research and my subsistence through the Janet Watson studentship. Without this vital financial help, nothing would have been possible.

Statoil is acknowledged for providing some of the Sognefjord Formation data to this study. Particularly, I wish to express my gratitude to Tom Dreyer, Paul Whipp and Theresa Melanie Lloyd-Llodden, to have been so helpful and actively involved in my work.

I also would like to extend my sincerest thanks to all my colleagues and friends at Imperial College, and particularly to Nick Holgate, for all the pleasant and hilarious time we spent together in Norway, U.S., Ireland and elsewhere. This three year voyage would have been much more tedious without you.

Last but not certainly least, my warmest gratitude goes to my family for their truly precious psychological and financial support. In particular, a huge thanks to my remarkable wife, Ioulietta, who had to bear the brunt of various PhD-related 'crises' and 'panic attacks' and who kept me in love, content and well throughout these years. A hug to my grand mum Elide, my dog Nala, my sister Sara, my little brother Luca, my little sisters Valentina, Martina and Stella, my mother Virginia and my father Domenico, back in Italy. They are all thanked from the bottom of my heart, and my thoughts are always with them. My parents are also thanked to have strained their personal finances throughout these hard years in order to support my long university studies. Without their support, I would have never managed to start this PhD, let alone finishing it.

Thanks to you all, this desert has been crossed. The journey has just begun.

TABLE OF CONTENTS

LIST OF CHAPTERS **Page No.**

LIST OF TABLES

Page No.

LIST OF FIGURES

Page No.

CHAPTER 1

Introduction

CHAPTER 1: INTRODUCTION

1.1 CHRONOSTRATIGRAPHIC ARCHITECTURAL METHODS

In continental shelf successions, the recognition of stratigraphic units bounded by chronostratigraphic surfaces underpins our understanding of geometric and genetic relationships between adjacent lithofacies. Lithostratigraphic units are time-transgressive packages (McKee, 1949) of limited lateral extent; a key observation is that more geological time is typically represented by hiatal surfaces than by preserved rocks (c.f., Sadler, 1981; Miall, 2012). As a consequence, the most helpful way to correlate different stratigraphic sections is via chronostratigraphic rather than lithostratigrahic correlations, based on the recognition of surfaces that approximate time lines.

1.1.1 Sequence stratigraphic methods

Sequence stratigraphic methods were developed to aid chronostratigraphic correlations between different depositional environments, based on direct observational criteria. Sequence stratigraphy aims to break down sedimentary successions into age-calibrated hierarchies of relatively conformable, genetically-related units. These are defined by a characteristic stratigraphic architecture (i.e., facies associations, vertical stacking patterns, stratal geometries and stratal terminations) and are bounded by key time-line surfaces (Fig. 1.1), reflecting successions of accommodation creation and sediment fill (e.g. Van Wagoner et al., 1990; Catuneanu et al., 2009; Abreu et al., 2010).

'Parasequences' (*sensu* Van Wagoner et al., 1990) are the highest-frequency, thinnest (usually, ca. 1-50 m) and most objectively-defined sequence stratigraphic units. These are shallowing upwards, broadly conformable successions of genetically-related beds bounded by marine flooding surfaces, which become progressively thinner

towards an offshore direction. In the "classical Exxonian" model (Vail et al., 1977; Mitchum et al., 1977; Van Wagoner et al., 1990; Mitchum & Van Wagoner, 1991), sequence stratigraphic units formed by groups of parasequences are bounded by two key time-line surfaces associated to a particular stage of the relative sea level curve. This is controlled by the interplay between rates of accommodation creation and sediment accumulation. These surfaces occur at points where facies associations, parasequence stacking patterns and stratal geometries show discontinuities that do not obey Walther's Law and, on seismic reflection data, are defined by seismic-scale stratal terminations at angular unconformities and/or by their correlative conformities (Van Wagoner et al., 1987, 1988, 1990; Abreu et al., 2010; Figs. 1.1, 1.2). Key stratal surfaces include:

- TS - Transgressive surfaces (or maximum regressive surfaces) correspond to ravinement surfaces at the top of a progradational package. Across this surface, parasequence stacking pattern changes from progradational to retrogradational.
- MFS - maximum flooding surfaces (or maximum transgressive surfaces) corresponds to downlap surfaces at the top of a retrogradational package. Across this surface the parasequence stacking pattern changes from retrogradational to progradational.
- SB - Sequence boundaries correspond to sharp, erosional surfaces of subaerial exposure and correlative conformities. These surfaces may be found in the upper portion of progradational packages, and are identified in seismic cross-sections by the presence of toplap and erosional truncation below, and onlap stratal terminations above.

These bounding surfaces are expected to form when the shoreline reaches its most basinward position (at the point of maximum regression; stratal units capped by a transgressive surface) or its most landward position (at the point of maximum transgression; stratal units capped by maximum flooding surface), or following times of abrupt basinward shift of coastal onlap (sequence boundaries) (Fig. 1.2). Subsequently, time-line-equivalent bounding surfaces tend to be associated with sediment condensation, starvation, nondeposition or erosion, which may cause early cementation and/or concentration of glauconite, faecal pellets and shell fragments in their proximity (Stewart et al., 1995). The stratigraphic stacking of hiatus-bounded units is assumed to be ultimately driven by predictable, sinusoidal changes in relative sea level that occurred over various temporal scales (Mitchum et al., 1977; Vail et al., 1977; Vail & Todd, 1981; Posamentier & Vail, 1988; Fig. 1.2).

The delineation of genetically-related, time-equivalent assemblages of different facies formed in adjacent depositional environments allows prediction of sandbody distribution and connectivity in shallow-marine strata,

potential delivery of deep-marine sands to the slope and basin-floor and, ultimately, reservoir presence, quality and behaviour (Posamentier et al., 1991; Catuneanu et al., 2009).

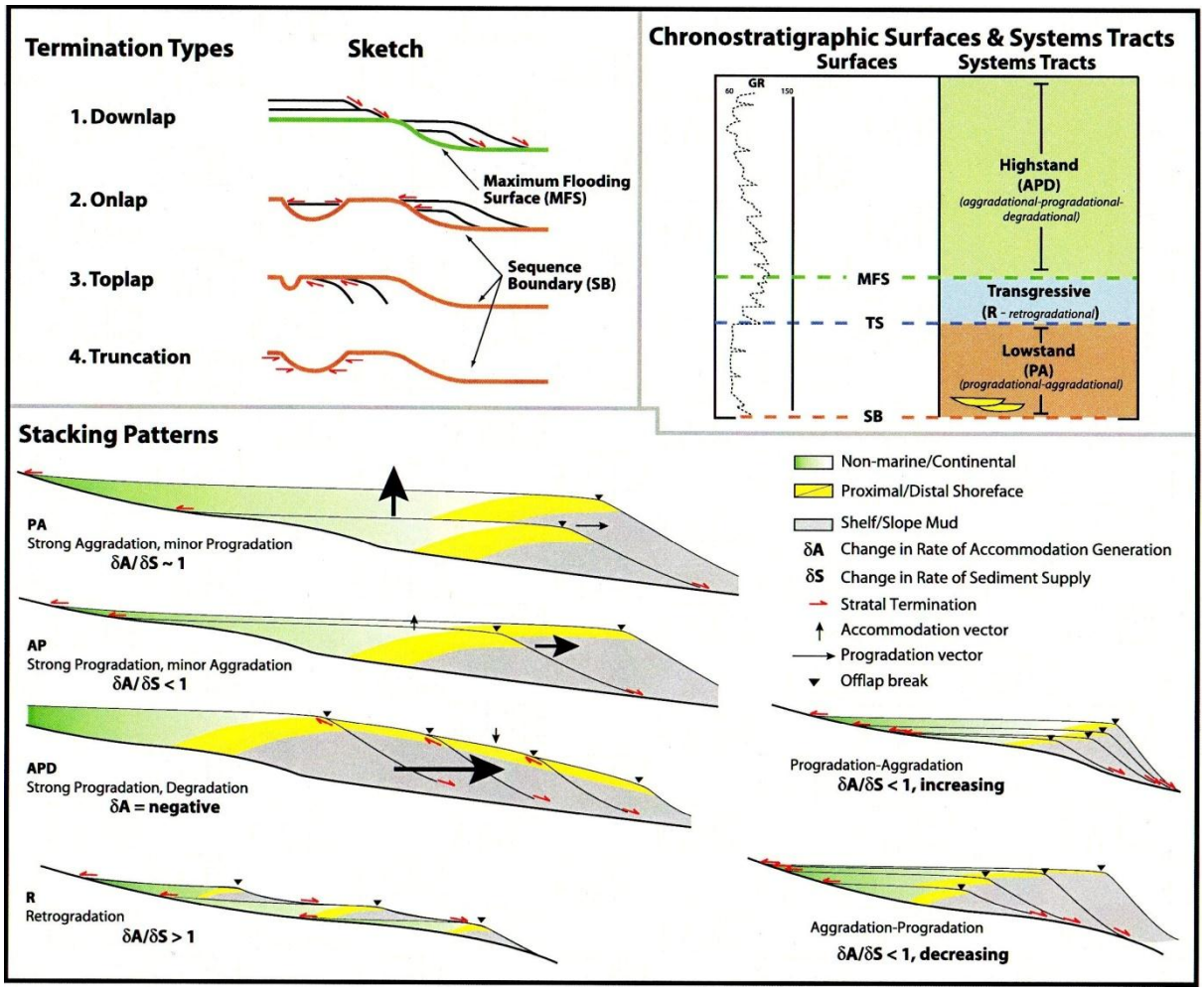

Figure 1.1. *Typical facies, stacking patterns, stratal geometries, stratal termination characteristics of sequence stratigraphic units. From: Abreu et al. (2010).*

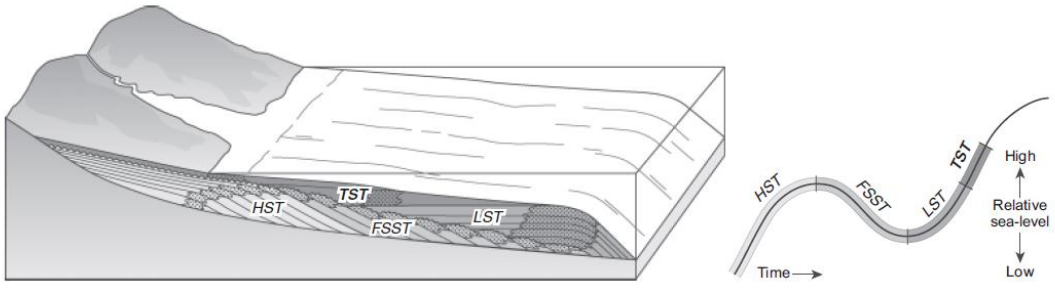

***Figure 1.2**. Typical sequence stratigraphic model, showing the sub-division of a sequence into: highstand system tract (HST); falling stage system-tract (FSST); lowstand system tract (LST); and transgressive system tract (TST). System tracts are bounded by the following time-line surfaces: maximum flooding surfaces; basal surface of forced regression (sensu Hunt & Tucker, 1992); sequence boundary; transgressive surface. From: Helland-Hansen & Hampson (2009).*

1.1.2 Shoreline and shelf-edge trajectory methods

Trajectory or 'aggradation angle' analysis is a practical stratigraphic tool which seeks to describe the style and architecture of the migration through time of palaeoseaward-dipping depositional surfaces (or 'clinoforms' sensu Rich, 1951). These record the morphology of shorelines and shelves (e.g. Mitchum et al., 1977), and often contain mappable geomorphological breaks-in-slope (Fig. 1.1) that can be linked with facies belt boundaries (Fig. 1.4; MacDonald & Aasen, 1994; Helland-Hansen & Gjelberg, 1994; Helland-Hansen & Martinsen, 1996; Steel & Olsen, 2002; Johannessen & Steel, 2005; Howell et al., 2008; Helland-Hansen & Hampson, 2009; Hampson et al., 2009; Henriksen et al., 2009).

Clinoform trajectory methodologies have been applied to describe the cross-sectional pathway taken by the shelf-edge break during the accretion of shelf-slope-basin clinoforms (Fig. 1.3; Mellere et al., 2002; Steel & Olsen, 2002; Johannessen & Steel, 2005), or to constrain the cross-sectional path of the 'depositional shoreline break-in-slope' (sensu Posamentier & Vail, 1988) of prograding, delta-scale clinoforms (Helland-Hansen & Gjelberg, 1994; Helland-Hansen & Martinsen, 1996). The latter trajectory type, or 'shoreline trajectories' (Fig. 1.4), can describe either the solitary shoreline transit across a shelf (i.e., trajectories internal to a parasequence), or the 'stacked shoreline transits' (sensu Helland-Hansen & Hampson, 2009; Hampson et al., 2009) across successive shoreline progradational phases punctuated by transgressive episodes (cf. 'parasequence sets' and 'parasequence stacking pattern' of Van Wagoner et al., 1990). This technique focuses on the direction of shoreline and shelf-edge migration. The type and angle of this migration is determined by the interplay between relative sea-level changes of various frequencies, sediment supply, subsidence from compaction, basin physiography and bathymetry (Helland-Hansen & Martinsen, 1996; Henriksen et al., 2009).

Trajectory angles determined by both solitary shoreline transits and shelf-edge migration are characteristically between -2° and +2° relative to a palaeo-horizontal datum (e.g., Bullimore et al., 2005; Johannessen & Steel, 2005; Carvajal & Steel, 2006; Løseth et al., 2006; Helland-Hansen & Hampson, 2009); however, 'stacked shoreline

transits' exhibit a significantly larger range of trajectory angles (between at least -50° and +179.9°; Hampson et al., 2009; Helland-Hansen & Hampson, 2009). This disparity reflects the prevalence of horizontal progradational or retrogradational translations during single clinoformal migration episodes. Much of the overall aggradational 'stratigraphic climbs' or its down-stepping equivalent seems to be generated at the transgressive-to-regressive and regressive-to-transgressive turnarounds between consecutive parasequences (Bullimore et al., 2008; Helland-Hansen & Hampson, 2009), and thus will impact mainly on the longer-term shoreline transits that result in stacked stratigraphic packages. A major difference between trajectory styles resulting from single or stacked shoreline transits and those recorded by shelf-edge migration is that the former can be either seaward-accreting (i.e., progradational) or landward-pointing (i.e., retrogradational), whereas the shelf-slope-basin clinoforms are typically only seaward-accreting or remain fixed through time (Helland-Hansen & Hampson, 2009).

Shoreline and shelf-edge trajectories can be calculated directly from successive positions of the clinoform rollover points relative to a palaeo-horizontal datum in outcrops and high-resolution seismic cross-sections oriented parallel to the clinoform depositional dip (Fig. 1.3). In addition, facies boundaries and erosional surfaces typically associated with a particular position along the depositional profile can be used as proxies for specified morphological breaks-in-slope, and used to track shoreline or shelf-edge trajectories in those datasets where clinoforms cannot be directly observed (e.g., well-log correlation panels) (Hampson et al., 2009; Fig. 1.4).

Based on the relationship between angle and direction of trajectories, and gradient and morphology of the pre-existing depositional topography, four main migratory classes of shoreline trajectory are distinguished (Helland-Hansen & Gjelberg, 1994; Helland-Hansen & Martinsen, 1996; Helland-Hansen & Hampson, 2009): (a) ascending regressive (c.f., 'normal regression' of Posamentier et al., 1992); (b1 and b2) accretionary and nonaccretionary descending regressive (c.f., 'forced regression' of Posamentier et al., 1992); (c1 and c2) accretionary and nonaccretionary transgressive and (d) stationary (i.e., nonmigratory) trajectories. In contrast, transgressive trajectories do not occur during shelf-edge migration, and thus only three main migratory classes of shelf-edge trajectories are recognized (cf., Johannessen & Steel, 2005; Deibert et al., 2003; Ryan et al., 2009) (Fig. 1.5).

Unlike discrete sequence-stratigraphic units, migratory classes switch from one to another at various scales and frequencies. Subsequently, trajectory analysis avoids 'pigeon-holing' the depositional history of continental shelves into discrete units driven by *a priori* driving mechanisms; the use of trajectory analysis therefore allows identification of subtle changes occurring between maximum and minimum relative sea level stands (Helland-Hansen & Hampson, 2009). However, trajectory analysis is also useful when integrated with standard sequence stratigraphic techniques, as major shifts in the horizontal movement of the shoreline take place along the three key bounding sequence stratigraphic surfaces discussed above (i.e. transgressive surface, maximum flooding

surface and sequence boundary). As a consequence, sequence stratigraphic units are also constrained by a characteristic depositional architecture and shoreline trajectory style. Backstepping shoreline trends are associated with stratigraphic intervals between a transgressive surface and a maximum flooding surface, whereas a strongly progradational to descending shoreline trajectory immediately underlies a sequence boundary (Catuneanu et al., 2009; Abreu et al., 2010).

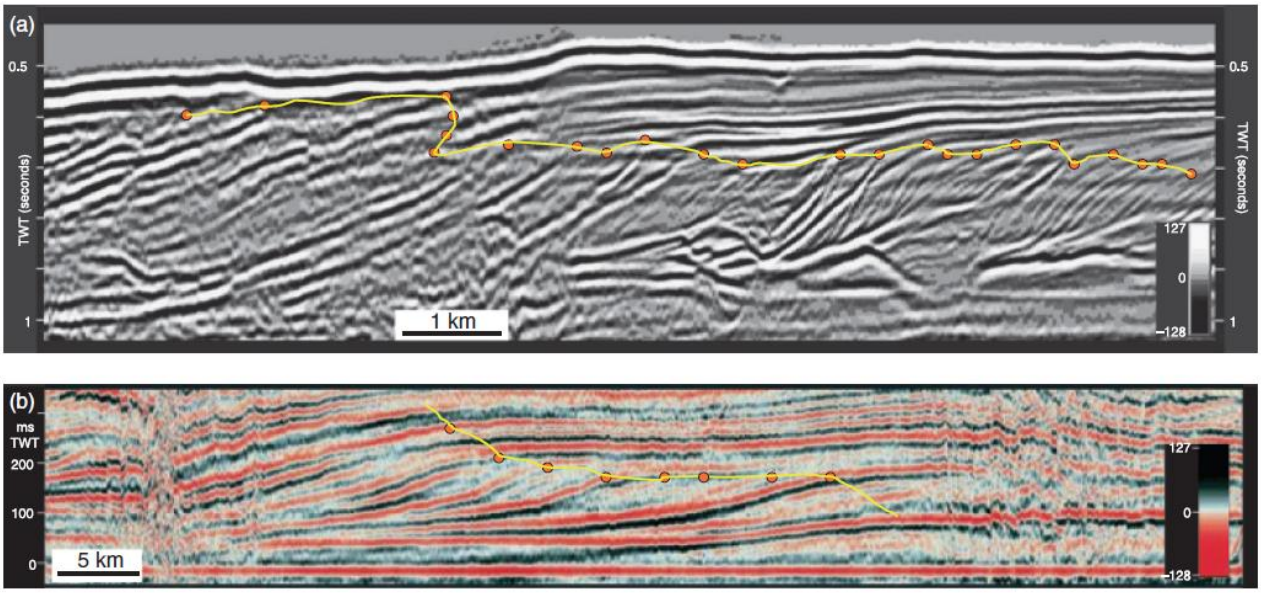

Figure 1.3. *Examples of seismic cross-sections oriented parallel to the depositional dip, showing shelf-edge clinoforms, their rollover points and their inferred trajectories (from Helland-Hansen & Hampson, 2009). (a) Oligo-Miocene, mid-Norwegian shelf; (b) Triassic Barents shelf.*

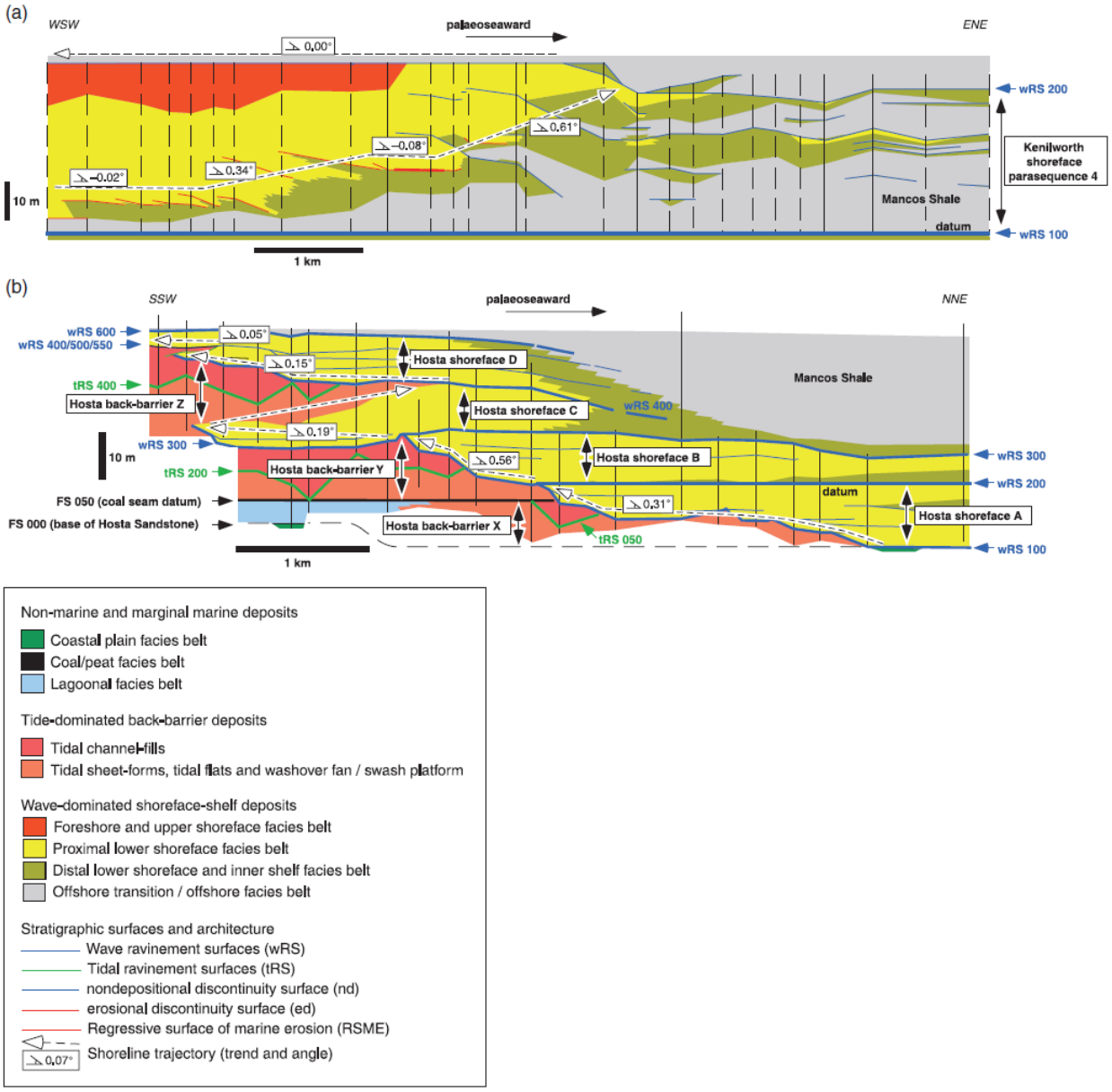

***Figure 1.4**. Examples of shoreline trajectories inferred from outcrop datasets and arranged in dip-oriented facies panels (from Helland-Hansen & Hampson, 2009). (a) Kenilworth K4 tongue, a wave-dominated shoreline; (b) Hosta Sandstones, a mixed wave/tide-dominated barrier shoreline.*

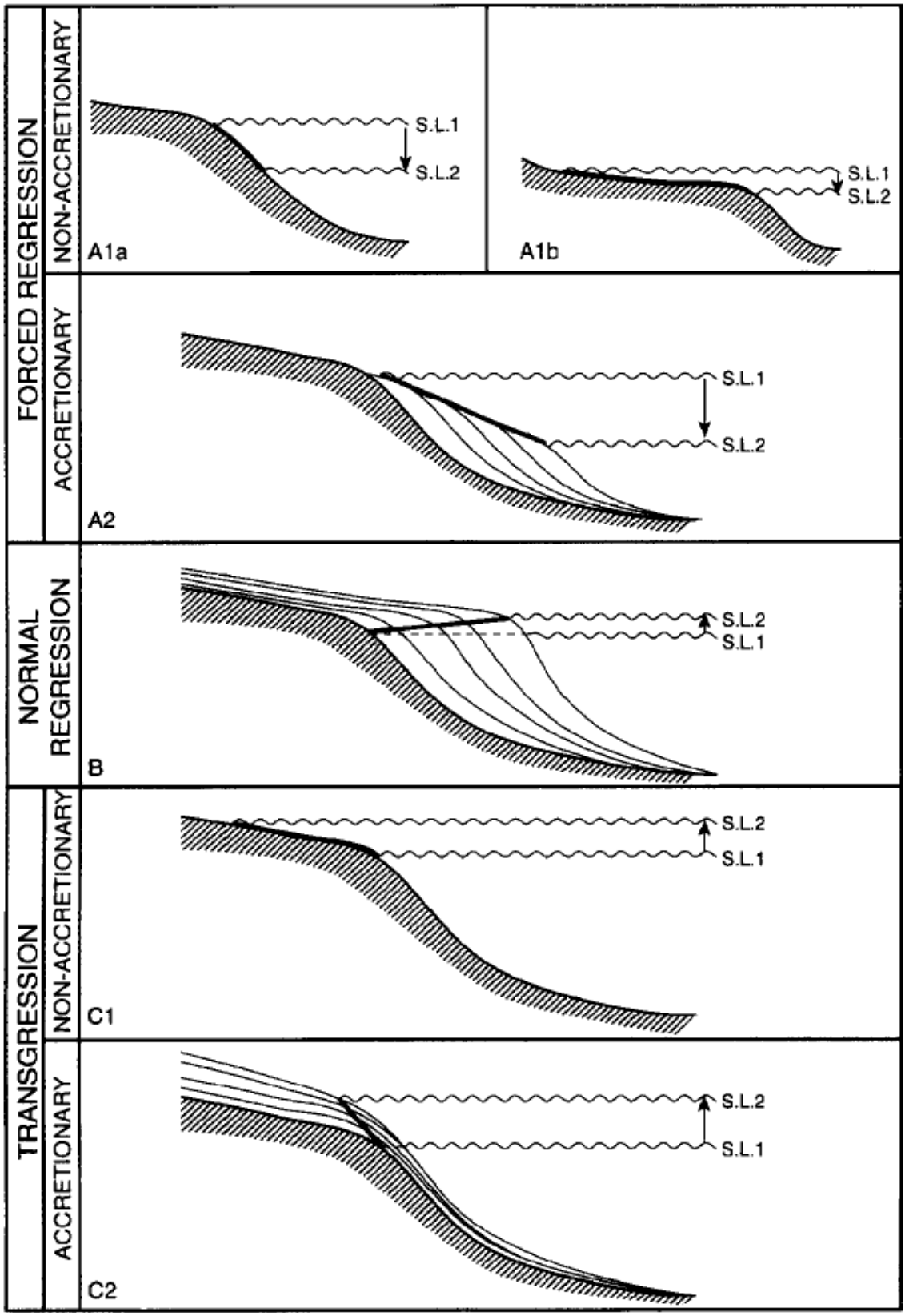

Figure 1.5*. The various clinoform trajectory classes (from Helland-Hansen & Martinsen, 1996). Black heavy lines designate the shoreline trajectories.*

1.2 SEDIMENT DISPERSAL PROCESSES ACROSS SHELF-SLOPE-BASIN TRANSECTS AND CONTROLLING MECHANISMS

The repeated, regressive-transgressive, cross-shelf transit of deltas and shorelines is the key process responsible for the construction of continental shelf successions (Johannessen & Steel, 2005). This process is controlled mainly by the interplay between: (a) relative sea level changes; (b) rates of river-fed sediment supply; (c) alongshore and shore-perpendicular marine transport rates; (d) dominant depositional processes on the shelf and at the shoreline; (e) initial shelf volume; and (f) length, gradient and physiography (including degree of channelling) of shoreline, shelf and slope (Burgess & Hovius, 1989; Steel & Olsen, 2002; Johannessen & Steel, 2005; Steel et al., 2008; Helland-Hansen & Hampson, 2009). Sediment types, climatic conditions and fluvial drainage type are other, minor variables (Burgess & Hovius, 1998; Johannessen & Steel, 2005). These factors fundamentally determine: (1) the possibility for a shoreline or delta to reach the shelf edge and establish a shelf-edge delta during any particular transit; (2) the time needed for that to happen ('shelf transit time'); and (3) the degree of sand/mud budget partitioning along the different segments of the shoreline-shelf-slope-basin delivery systems (e.g., Burgess & Hovius, 1998; Steel & Olsen, 2002; Muto & Steel, 2002; Johannessen & Steel, 2005; Porebski & Steel, 2003). If a shelf-edge delta fronts an oversteepened slope, its establishment is usually followed by cessation of shoreline progradation and subsequent en-masse sediment bypass down the slope, with subsequent delivery of sand to the basin floor by a variety sediment gravity-flows (cf., 'erosional margin' of Ross et al., 1994; 'self-regulated' shelf edges of Burgess & Steel, 2008; 'nonmigratory shoreline trajectory' class of Helland-Hansen & Hampson, 2009; see also Morton & Suter, 1996; McCave, 1972; Burgess & Hovius, 1998; Porebski & Steel, 2003, 2006; Dalrymple, 2005; Burgess & Steel, 2008). However, fixed shelf-edge positions could alternatively signify condensed outer-shelf sedimentation, with the inner shelf being the main locus of sediment accumulation (Helland-Hansen & Hampson, 2009).

Relative modern shelf volumes and magnitudes of sediment input from major riverine feeders suggest estimated shelf transit times below 0.15 Myr, which would mean a likely establishment of shelf-edge deltas and significant delivery of sand to the basin floor during 1 Myr-duration, 'third-order' highstands (Burgess & Hovius, 1998). However, alongshore marine transport on wave-dominated shelves may increase shelf transit times; if shore-parallel marine transport rates outpace the rates of fluvial input, the establishment of a shelf-edge delta and sediment delivery to the basin floor will be precluded (Burgess & Hovius, 1998; Liu et al., 2006). In fact, waves,

tides and alongshore currents that do not interact with an antecedent, shelf-indenting submarine canyon typically result in limited incision of the shelf edge and in a lack of sediment bypass to deep water; these sediments are trapped along the coastline (Carvajal & Steel, 2009).

In contrast, shelf bypass and the transfer of large amounts of sand to deep-water is favoured by the prevalence of across-shelf transport (e.g., Flemming, 1981; Traykovski et al., 2000; Wright et al., 2001), by the presence of river-dominated deltas and by submarine canyons cutting through the shelf until reaching the shoreline, intercepting the sediment flux carried by shore-parallel longshore drifts or shelf currents and diverting it off the shelf (e.g., Nittrouer et al., 1986; Posamentier et al., 1991; Johnson & Baldwin, 1996; Covault et al., 2007). In extreme cases, canyons and gullies directly outboard of river mouths may capture much of the fluvial sediment supply and deliver sediment direct to the slope and basin-floor (e.g., Milliman et al., 1984).

A recurring premise of sequence stratigraphic and shelf-edge trajectory studies prescribes that the primary control is eventually exerted by relative sea-level changes, and by the type and magnitude of shelf-edge and shoreline trajectory (e.g., Vail et al., 1977; Mitchum, 1985; Mutti, 1985; Damuth et al., 1988; Posamentier & Vail, 1988; Posamentier et al., 1988, 1991; Steel & Olsen, 2002; Johannessen & Steel, 2005; Helland-Hansen & Hampson, 2009; Fig. 1.6).

Rising trajectories are often associated with strongly-aggradational, shoreline-shelf successions in which deposition is dominated by storm, waves and alongshore currents. These are usually associated with linear shorelines and a shelf-edge morphology that lacks evidence (e.g. channelling) for focused sediment dispersal and bypass; these systems thus favour enhanced sand storage on the shelf and coastal plain (e.g., stacked, thick shoreline deposits), low deltaic progradation rate and negligible, sheet-like sand accumulation on the slope (c.f., Mitchum et al., 1994; Milton & Dyce, 1995; Deibert et al., 2003; Johannessen & Steel, 2005; Fig. 1.6). If shallow marine accommodation is coupled with highly energetic waves, currents and tides, delta-scale subaqueous clinoforms may actively grow on the shelf, below the fairweather wave base (e.g., Nittrouer et al., 1996; Pirmez et al., 1998; Hernández-Molina et al., 2000a; Cattaneo et al., 2003, 2007; Neil & Allison, 2004; Liu et al., 2006, 2007; Mitchell et al., 2012). In many highstand deltas, these subaqueous clinoforms are associated with prograding 'subaerial delta' clinoforms at the shoreline break, forming 'compound clinoform' systems (Swenson et al., 2005; Fig. 1.7).

In contrast, flat or descending shelf-edge and/or clinoform trajectories, even in presence of low sediment supply and wide shelves, tend to favour the establishment of the oceanographic and morphological factors that lead to efficient shelf bypass, rapid (<0.1 Myr) sand transport beyond the shelf-edge break and accelerated growth of

basin-floor fans. These oceanographic and morphological factors include: high progradation/aggradation rate, headward erosion of submarine canyons, predominance of fluvial processes in deltas, less storage potential on the shelf culminating in the subaerial exposure and fluvial entrenchment on the shelf and subsequent establishment of channelized shelf-slope pathways characterized by focused, long-lived sediment transport (cf., Mougenot et al., 1983; Kolla et al., 2000; Steel & Olsen, 2002; Ritchie et al., 2004; Bullimore et al., 2005; Johannessen & Steel, 2005; Porebski & Steel, 2006; Carvajal & Steel, 2009; Fig. 1.6).

Despite models suggesting sediment bypass during falling-stage to lowstand condition, delta progradation, turbidite deposition and significant deep-sea fan growth continued throughout the Holocene transgression and highstand in several modern delta-shelf-slope-basin systems, such as the Zaire, Mississippi, Amazon, Indus, Bengal and Californian Borderland fans (e.g., Heezen et al., 1964; Milliman et al., 1984; Kolla & Macurda, 1988; Flood et al., 1991; Kolla & Perlmutter, 1993; Weber et al., 1997; Burgess & Hovius, 1998; Khiripounoff et al., 2003; Carvajal & Steel, 2006; Covault et al., 2007). The establishment of shelf-edge deltas due to extremely high sediment supply relative to both initial shelf volume and the capacity for shelf-parallel marine transport is often invoked as the main cause leading to deep-marine deposition during phases of relative sea-level rise and highstand (e.g., Ito & Masuda, 1988; Weber et al., 1997; Burgess & Hovius, 1998; Traykovski et al., 2000; Wright et al., 2001; Piper & Normark, 2001; Muto & Steel, 2002; Carvajal & Steel, 2006, 2009; Covault et al., 2007). Furthermore, the action of marine currents perpendicular to the orientation of the shelf edge (e.g., Flemming, 1981), and/or the occurrence of canyons that extend far into the shelf and the shoreface during phases of highstand or rising relative sea level are often sufficient to allow continuous shelf bypass and sand transport to the slope and basin floor throughout relative sea-level cycles (e.g., Milliman et al., 1984; Burgess & Hovius, 1998; Posamentier et al., 1991; Covault et al., 2007). In contrast, the absence of these conditions sometimes prevents deposition of deep-marine sandstones even after the establishment of a shelf-edge delta (Henriksen et al., 2009).

It should be finally noted that the occurrence of significant, fault-related, differential tectonic subsidence and uplift during continental rifting may profoundly impact the style, location and magnitude of morphological gradients, drainage catchments and depositional processes, and often gives rise to distinctly complex trends of sediment dispersal, lithological distributions and stratigraphic architecture (e.g., Gawthorpe et al., 1994; Gawthorpe & Leeder, 2000; Fig. 1.8).

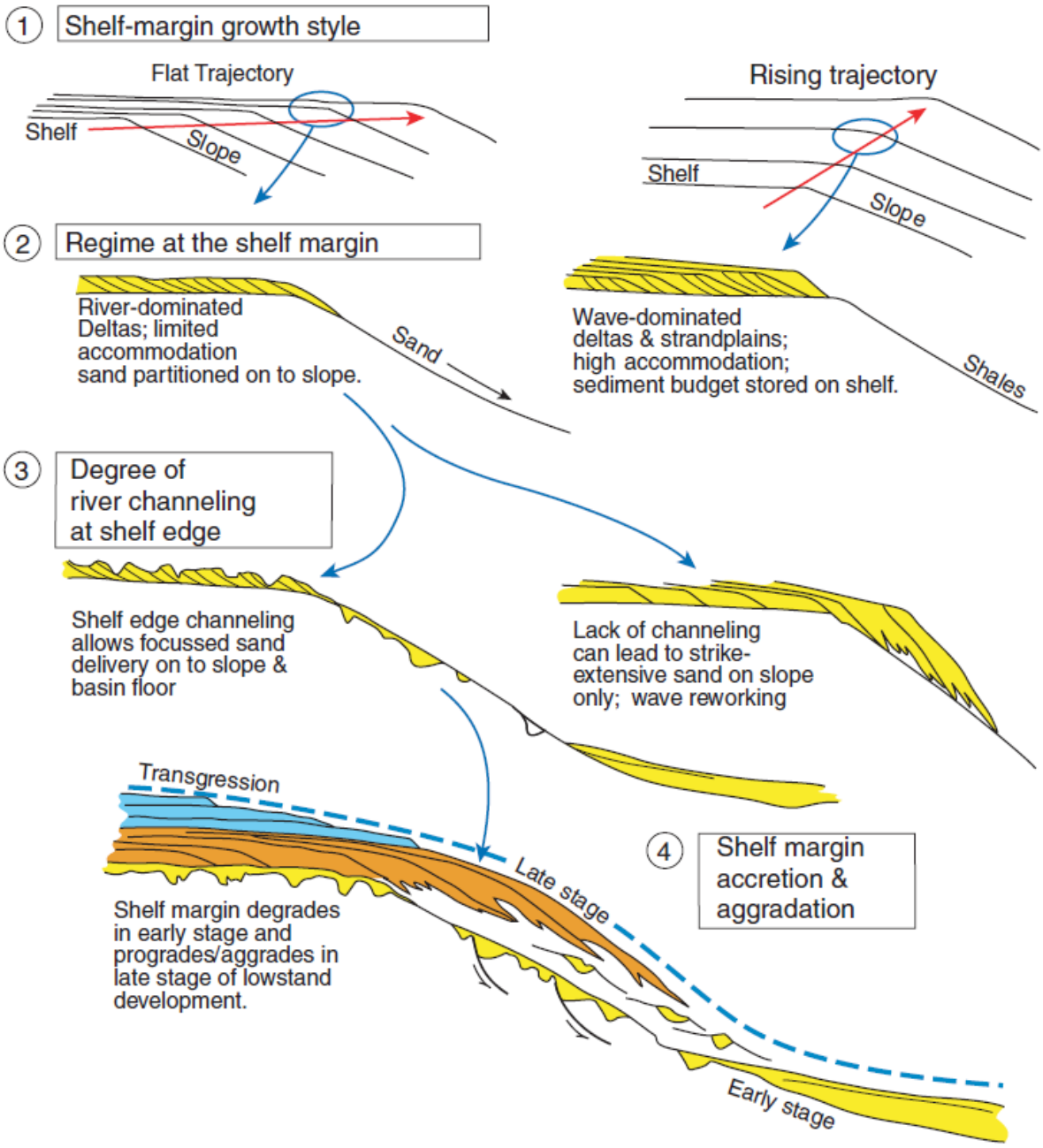

***Figure 1.6**. Facies distributions determined by different types of shelf-edge clinoform trajectories, process regime and degree of river channelling at the shelf margin (from Johannessen & Steel, 2005).*

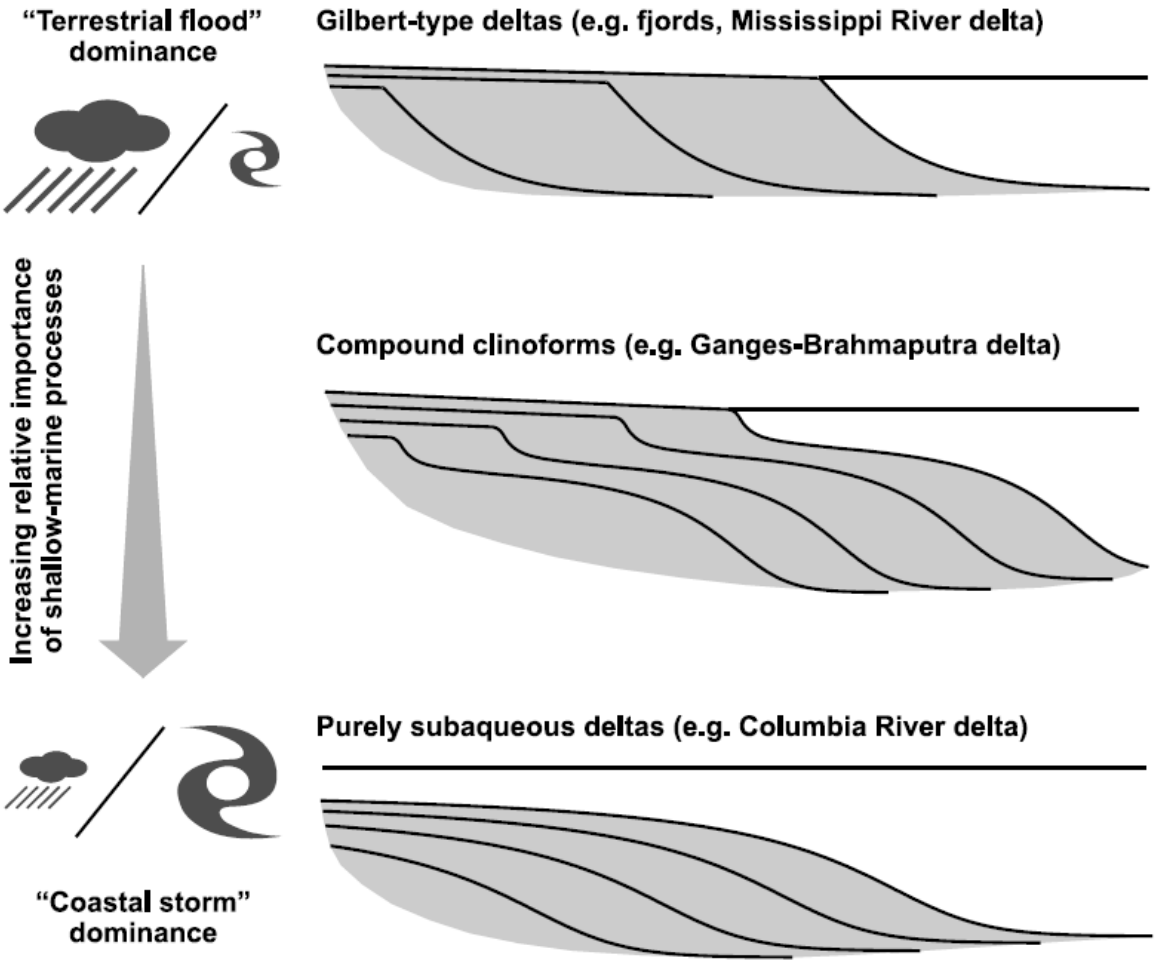

Figure 1.7. *Increasing the relative power of marine processes determines the transition from subaerial delta clinoforms to compound clinoforms and to purely subaqueous delta clinoforms (from Swenson et al., 2005).*

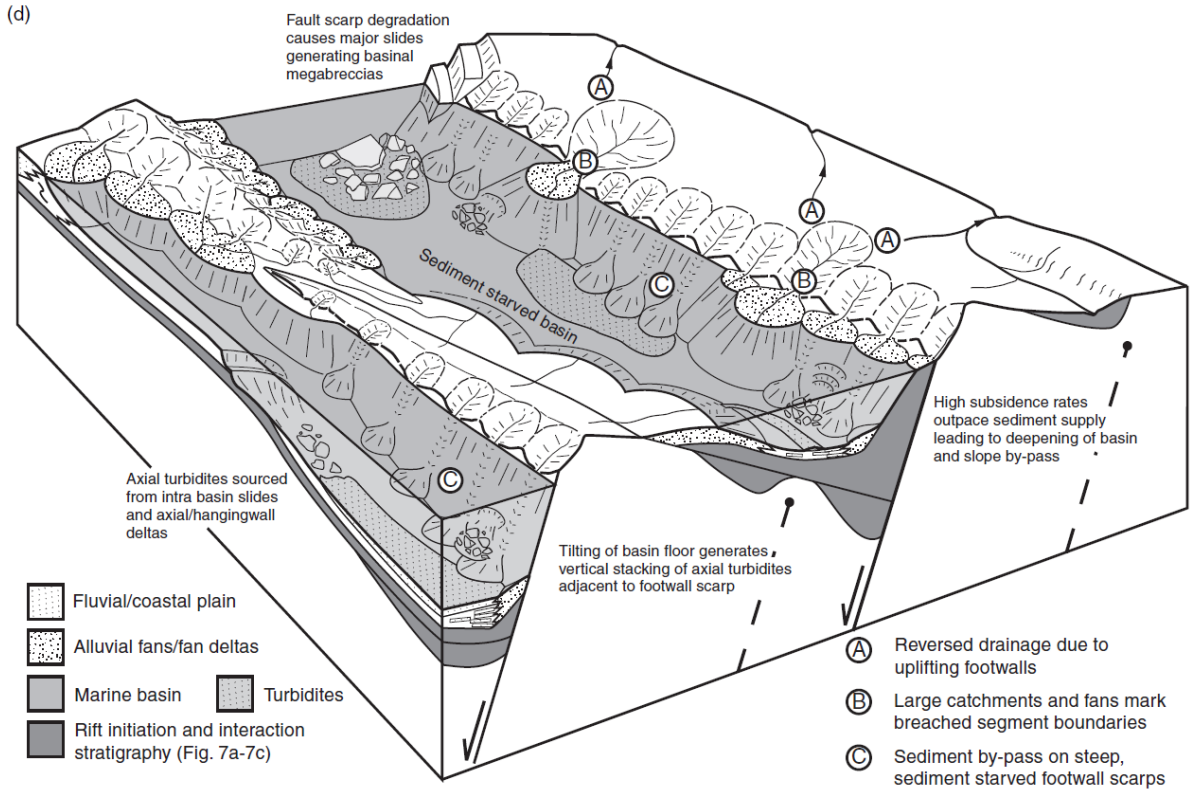

Figure 1.8*. Interactions between sedimentation patterns and fault block tectonics in different segments of a typical marine rift basin (from Gawthorpe & Leeder, 2000).*

1.3. REGIONAL GEOLOGICAL FRAMEWORK

1.3.1 The northern North Sea Basin

The northern North Sea Basin is a 170-200 km wide, fault-bounded, north-south trending zone of extended Mesozoic crust, flanked by the Norwegian mainland to the east and by the Shetland Platform to the west (Fig. 1.9). The basin represents the northern arm of the trilete, North Sea rift system, and is focused on a central low ('Viking Graben'), around which 10-50 km wide fault-bounded tilted blocks are arranged (Christiansson et al.,

2000; Zanella & Coward, 2003). The shallow water Horda Platform is the easternmost and most stable of the structural elements of this area, and is separated from the Viking Graben by tilted half-graben (transitional 'terraces', Fig. 1.9).

The Triassic-Jurassic stratigraphy of the Northern North Sea Basin is divided into nine "megasequences" bounded by retrogradational maxima (Steel, 1993). These megasequences range in thickness from 100-1200 m, and duration for each of these regressive-to-transgressive alluvial and marine clastic wedges is 6-18 Myr. The Middle-Late Jurassic Viking Group (Vollset & Doré, 1984) comprises the Krossfjord and Sognefjord megasequences; these comprise mudstone-dominated, shelfal deposits in the basin centre (Heather Formation) and shallow marine sandstone tongues on the Horda Platform towards the eastern basin margin (Krossfjord, Fensfjord, Sognefjord formations) (Steel, 1993; Fraser et al., 2003). Above these Triassic-to-lower Upper Jurassic megasequences, the uppermost unit of the Viking Group is represented by deep-marine shales of the Draupne Formation.

The Northern North Sea Basin was affected by rifting both in the Permo-Triassic and in the Middle-Late Jurassic. The present structural configuration reflects the effects of the Jurassic rift phase on the pre-existing Permo-Triassic framework (Nøttvedt et al., 2000; Zanella & Coward, 2003).

The Permian to Early Triassic rift event was followed by minor extensional tectonics ("proto-rift" sensu Færseth & Ravnås, 1998). This is reflected by more uniform thickness and facies distributions in Lower Jurassic strata (Steel, 1993). During the Middle-to-Late Jurassic rift phase, growth of major N-S striking fault arrays resulted in the formation of N-S-trending graben and fault blocks; this rift-related basin physiography controlled sediment dispersal patterns, which were largely rift-normal during the syn-rift period, compared to the rift-parallel patterns that characterised the pre-rift period (i.e. during deposition of the Brent Group; Ravnås et al., 1997). Thus, easterly-sourced nearshore and shelf, sand-rich wedges prograded westwards across the rift-marginal Horda Platform; in this location, sediment accumulation rates in these shallow-water systems kept pace with subsidence rates due to progressive diminution of fault-driven subsidence away from the axis of the Viking Graben. Near the steep basin margins, deep-water gravity-flow facies became locally important, whilst the basin axis remained shale prone (Steel, 1993).

The Middle-to-Late Jurassic main rift phase comprises longer periods of relative tectonic quiescence interrupted by five distinct basin-wide phases of increased fault-driven subsidence and footwall uplift. Each of the latter phases lasted 4-6 Myrs and corresponds to the transgressive retreat of a specific clastic wedge (Færseth & Ravnås, 1998; Nøttvedt et al., 2000):

1) Late Bajocian to Early Bathonian (flooding of the Brent Group);
2) Middle to Late Bathonian (flooding of the Krossfjord Formation);
3) Late Callovian (flooding of the Fensfjord Formation);
4) Late Oxfordian to Kimmeridgian (flooding of the Sognefjord Formation);
5) Middle Volgian (intra-Draupne Formation flooding).

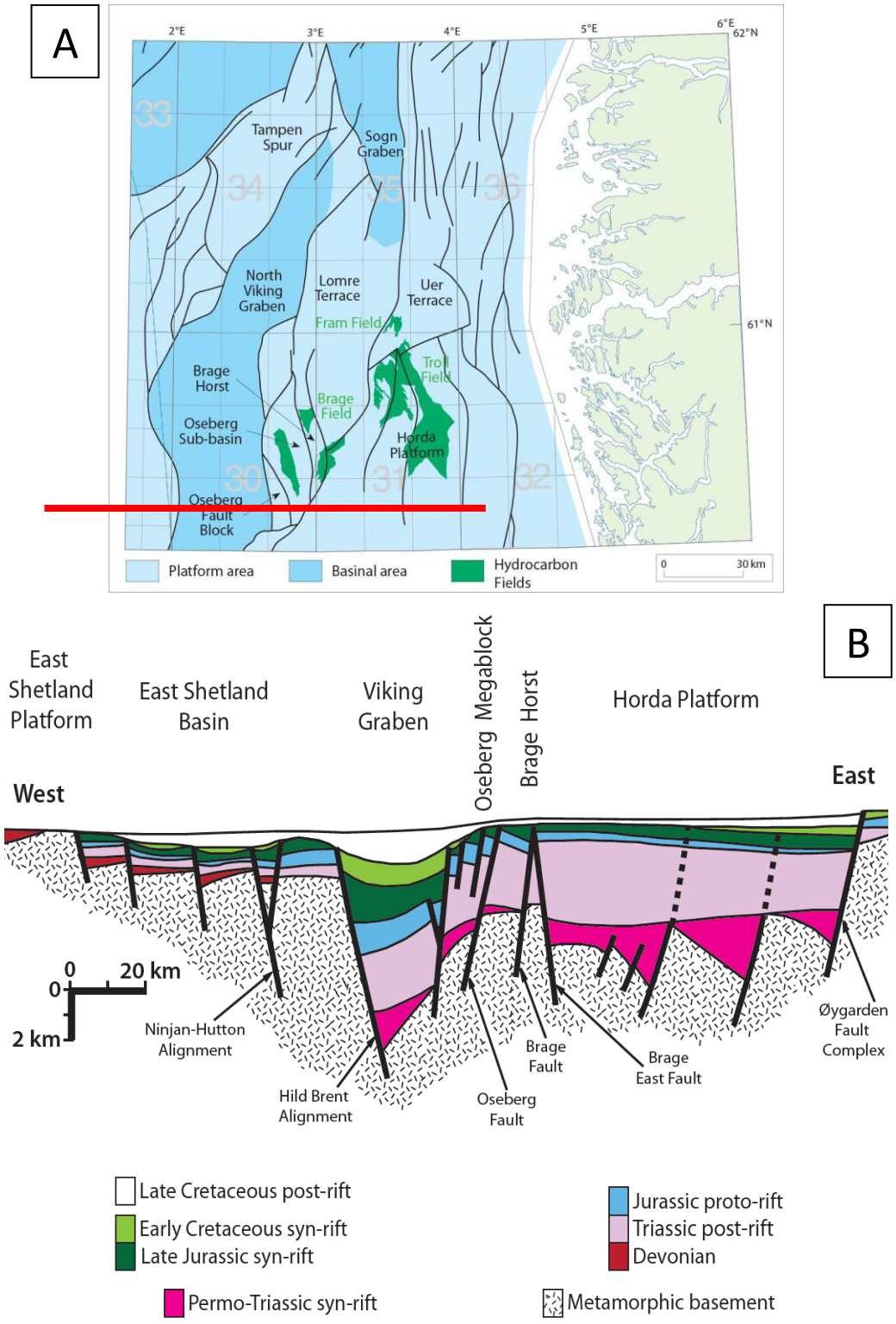

Figure 1.9. *(A) Structural map of the NW Horda Platform and surrounding areas (Modified after: Fraser et al., 2002). (B) Geological cross-section across the Northern North Sea Basin at end Cretaceous time (after Færseth, 1996). Notice the interference between Permo-Triassic (East-dipping) and Middle-Late Jurassic (West-dipping) fault arrays in the Oseberg Field area.*

1.3.2 The 'Troll Delta'

The Troll field is one of the world's largest offshore oil and gas fields (ca. 1,500 km^2). It is located on the Horda Platform, and is buried some 1,000-1,300 m below the present seabed, ca. 60-100 km to the west of Bergen. The main reservoir is Middle-to-Late Jurassic in age and consists of deltaic sandstones that were fed by a major basin-margin sediment input points (Stewart et al., 1995). The Troll Delta is imaged by 3D seismic reflection data and is penetrated by hundreds of wells, resulting in >5,000 m of cores and a wealth of lithological, biostratigraphic and geophysical data.

1.3.3 Sequence stratigraphic context of the Sognefjord Formation

The series of regressions and transgressions associated with the 'Troll Delta' outbuilding led to the accumulation of numerous, stacked, sandstone-prone, shallow-marine wedges (Krossfjord, Fensfjord and Sognefjord formations). Clinothems within each of these three 10-230 m thick formations are arranged in a north-south trend, parallel to the overall structural grain of the Viking Graben, and offlap and pinch out to the west (Stewart et al., 1995).

Three mudstone-siltstone tongues belonging to the Heather Formation separate the sandstone-prone formations, recording condensed intervals associated with five major transgressions. The Heather Formation tongues thicken westwards, until they amalgamate beyond the pinchouts of the sandstone formations (Fig. 1.10). The five transgressive maxima are defined by switching of the stacking pattern from backward-stepping to forward-stepping, and they roughly correspond with the onset of the five main rift pulses. These high-magnitude maximum flooding surfaces define the boundaries of 100-300 m thick megasequences (Steel, 1993, Dreyer et al., 2005). The Sognefjord Megasequence (sensu Steel, 1993) comprises the Sognefjord Formation and the underlying Heather B unit, and is subdivided into two genetic composite sequences, namely the Lower Sognefjord Composite Series (Series 2 and 3) and the Upper Sognefjord Composite Series (Series 4 and 5) (Dreyer et al., 2005). These are

separated by an intra-Sognefjord Formation composite MFS, associated with the Middle Oxfordian rift stage (Fig. 1.10).

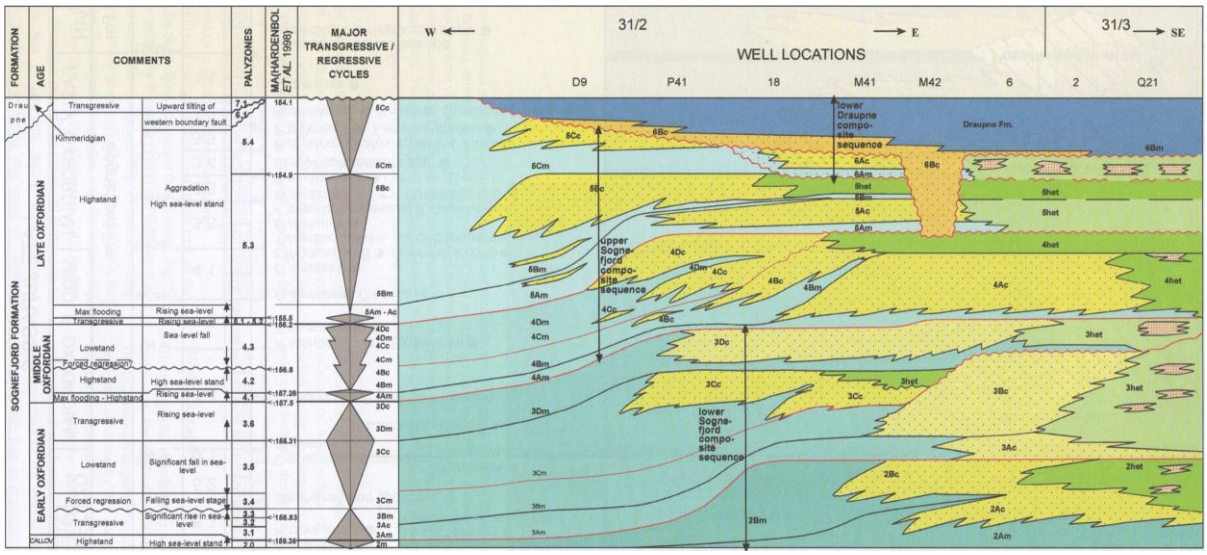

Figure 1.10. *Sequence stratigraphic model of the Sognefjord reservoir interval in Troll West (from Dreyer et al., 2005)*

1.3.4 Depositional model of the Sognefjord Formation

The Sognefjord Formation contains the majority of hydrocarbons in the Troll Field. This lithostratigraphic unit comprises a complex shallow marine, wave- and tide-influenced deltaic system that was deposited over ca. 8 Myr. It contains westwards-dipping clinothems that normally show a highstand-type, normal regression style (Stewart et al., 1995; Dreyer et al., 2005).

Early studies of the shallow-marine Sognefjord Formation interpreted most of the coarse-grained reservoir bodies as thick offshore bars derived by the transgressive reworking of shallower facies (Whitaker, 1984; Hellem et al., 1986; Osborn & Evans, 1987). The depositional architecture of the Sognefjord Formation was successively re-interpreted as a largely regressive, North-South elongated shoreface (Stewart et al., 1995) or coastal spit system (Dreyer et al., 2005), which prograded for tens of kilometres westwards, through downlapping clinoform "increments" that are clearly resolved on seismic data. Sediment was supplied by a major feeder located in the northeast and distributed southwards by persistent longshore currents. The spit was attached to the coast in the

north and flanked to the east by a tidal/riverine brackish backbasin (Fig. 1.11, Dreyer et al., 2005). The greatest part of the clinothems in the upper part of the formation became dominated by tidal facies, due to an inferred increase in tidal range. These include high energy tidal inlet shoals and sand-ridges with bi-directional cross strata, together with lower-energy tidal estuaries and lagoons (Dreyer et al., 2005). This overall depositional model is still used in field development.

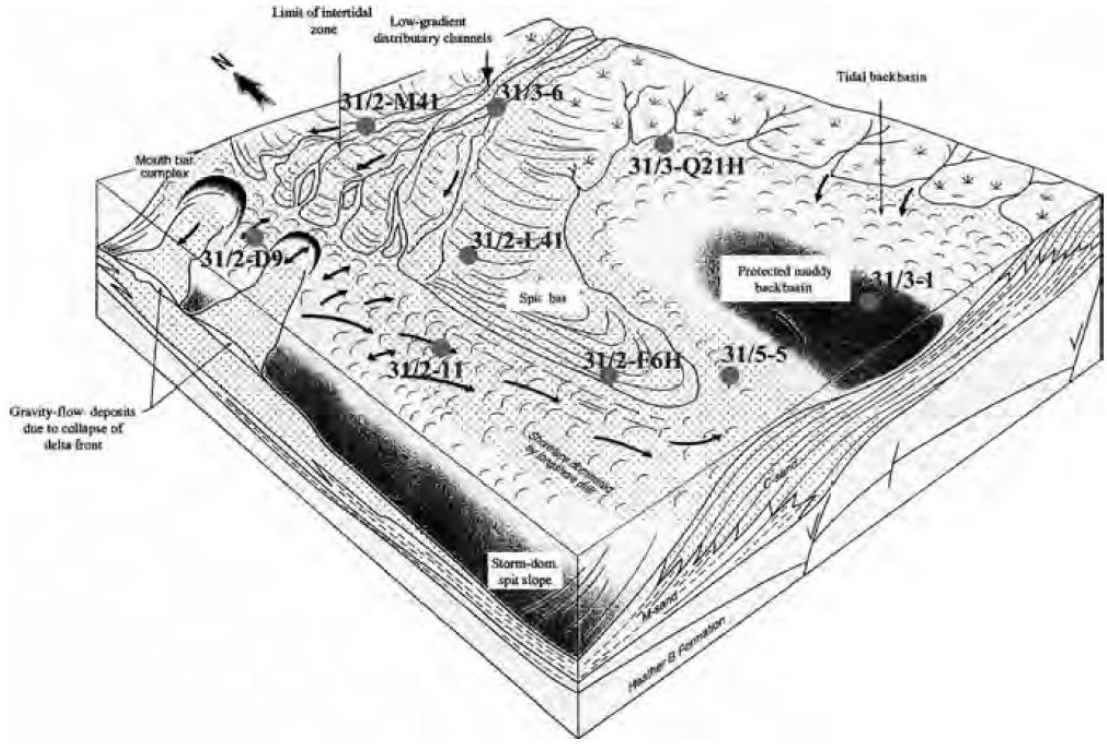

Figure 1.11. *Depositional model (not to scale) for the Sognefjord Formation in Troll West (From Dreyer et al., 2005).*

1.3.5 Tectonic influence on Sognefjord Formation deposition

Three NNW-SSE striking, easterly-rotated normal fault blocks define the Troll Field area today. These blocks are further dissected by three minor fault systems that strike NW-SE, NNW-SSE and WNW-ESE.

Stewart et al. (1995) argued that activity of the main fault blocks controlled the Troll Delta architecture. These authors assumed that the growth of north-south ribbons of shallow-marine sandbodies was promoted by the

presence of bathymetric highs onto the footwall highs. However, Dreyer et al. (2005) and Whipp et al. (in press) interpreted fault activity in the Troll West field to have been predominantly post-Oxfordian in age (i.e. late-to-post Sognefjord Fm age). Post-depositional erosion due to rift-related fault block rotation and uplift would explain thinning of the formation towards the fault-block crests.

However, Dreyer et al. (2005) also associate the most regionally-extensive flooding surfaces with active faulting along the western margin of the Horda Platform in the Late Callovian or in the Kimmeridgian. In particular, the Kimmeridgian event caused the major eastwards tilting and the final flooding of the "Troll Delta". This is shown by the deposition of a thick Draupne Formation in the eastern areas of the field, and by its absence or condensation towards the west (Stewart et al. 1995). The subaerial exposure of some footwall crests gave rise to footwall islands feeding localized hangingwall shorelines through the erosional reworking of the upper portion of the Sognefjord sandstones (Dreyer et al., 2005). Hence, the Oxfordian Sognefjord Formation is unconformably overlain by Lower Kimmeridgian, rift-climax sandstones. Crestal subaerial exposure sometimes persisted for as long as 50 Myrs, and the Sognefjord sandstones are erosively overlain by Cretaceous or Early Tertiary deposits (Dreyer et al., 2005; Whipp et al., in press).

1.4. KEY OUTSTANDING RESEARCH QUESTIONS

1.4.1 Clinoform rollovers as a palaeo-shoreline proxy?

Ancient clinoforms can be either directly observed in seismic reflection profiles or inferred from stratigraphic correlation panels based on outcrop and/or borehole data. However, in the absence of a full quantitative analysis of recent clinoforms on the basis of geometrical, sedimentological and/or stratigraphical observations, our ability to recognise and understand the palaeoenvironmental interpretation of ancient clinoforms is currently limited. In particular, a critical foundation of shoreline trajectory analyses is that rollover-points of delta-scale (i.e., ≤100 m

height) clinoforms are palaeo-shoreline proxies. As a consequence, rollover points in (seismic) cross-sections can be utilized to portray the cross-sectional pathway of the relative shoreline movements. However, shoreline-detached, delta-scale progradational clinoforms have been the focus of recent research (e.g., Swenson et al., 2005; Mitchell et al., 2012). These mud- to sand-prone 'subaqueous delta clinoforms' are formed during relative sea-level stillstands on several shallow-marine shelves, and their rollover point is usually situated at the depth of the fairweather wave base. The existence of these clinoforms, and particularly of sand-prone delta-scale subaqueous clinoforms, suggests that the rollover points of delta-scale clinoforms may not always mirror the palaeo-shoreline break. If delta-scale clinoforms are to be used for shoreline trajectory analyses or palaeo-sea level inferences, uncertainties in their location need to be reduced by facies and/or geomorphological characterization.

1.4.2 Chronostratigraphically-constrained rates and shoreline trajectory analysis

Sequence stratigraphy and shoreline trajectory analyses are effective tools to describe geometry and style of stratigraphic architectural features within a chronostratigraphic framework. Both techniques aim to reconstruct the evolution of relative sea-level changes and shoreline movements; from an applied perspective, they can help exploration geoscientists to predict reservoir presence and architecture. However, sequence stratigraphy and shoreline trajectory do not deal with the rate of the vertical and horizontal migration of the clinoform reference point (e.g., the shoreline break). Thus there is a relatively large gap in the predictive potential of these methods. In fact, vastly different estimates of architectural parameters, formative mechanisms, and near-field sandbody distribution can be formulated whether, for example: (a) the shoreline migration from a certain point to another occurred in tens of years or in millions of years; or (b) the progradation rate of basinward-stepping shoreline clinoforms is increasing or decreasing as they approach the shelf-edge.

Constraining the timing and rate at which deltas or the shorelines transits the shelf during progradational episodes is possible only by assigning ages to multiple clinoforms belonging to the same progradational set. The integration of these data with more 'traditional' seismic-stratigraphic and sedimentological observations is potentially a crucial constraint in order to understand or predict the precise distribution of shallow-marine sandbodies, the timing of sand delivery to the slope and basin-floor, and the spatial and temporal relationships between tectonic subsidence, bathymetry, basin hydrodynamics and sediment supply (Fig. 1.12). In particular:

- the likelihood of a delta or shoreline reaching the shelf edge is greater if progradation rates do not decrease during shoreline regression across the shelf;
- the likelihood of delta auto-retreat is greater if progradation rates decline as the shoreline builds out;
- nonmigratory shoreline trajectories at the shelf edge are likely associated with high-magnitude sediment bypass to basin floor fans if the clinoform progradation rate does not decrease towards the shelf edge;
- greater along-shore currents, waves and tides relative to river-driven constructive processes tend to decrease net-progradational rates, as they transport a larger amount of sediment parallel to the clinoform strike;
- Periods of rift-related normal faulting are mirrored by local spatial and temporal anomalies in the distribution and/or magnitude of progradation and aggradation rates.

Eventually, a greater knowledge of timing and rates of progradation will provide a tool to improve reservoir characterisation and near-field exploration by enhancing prediction of reservoir distribution and character. As a consequence, a data-driven method to systematically track the progradation rates of shoreline-shelf systems and their changes through time would be a useful tool for quantitative analysis of stratigraphic architectures.

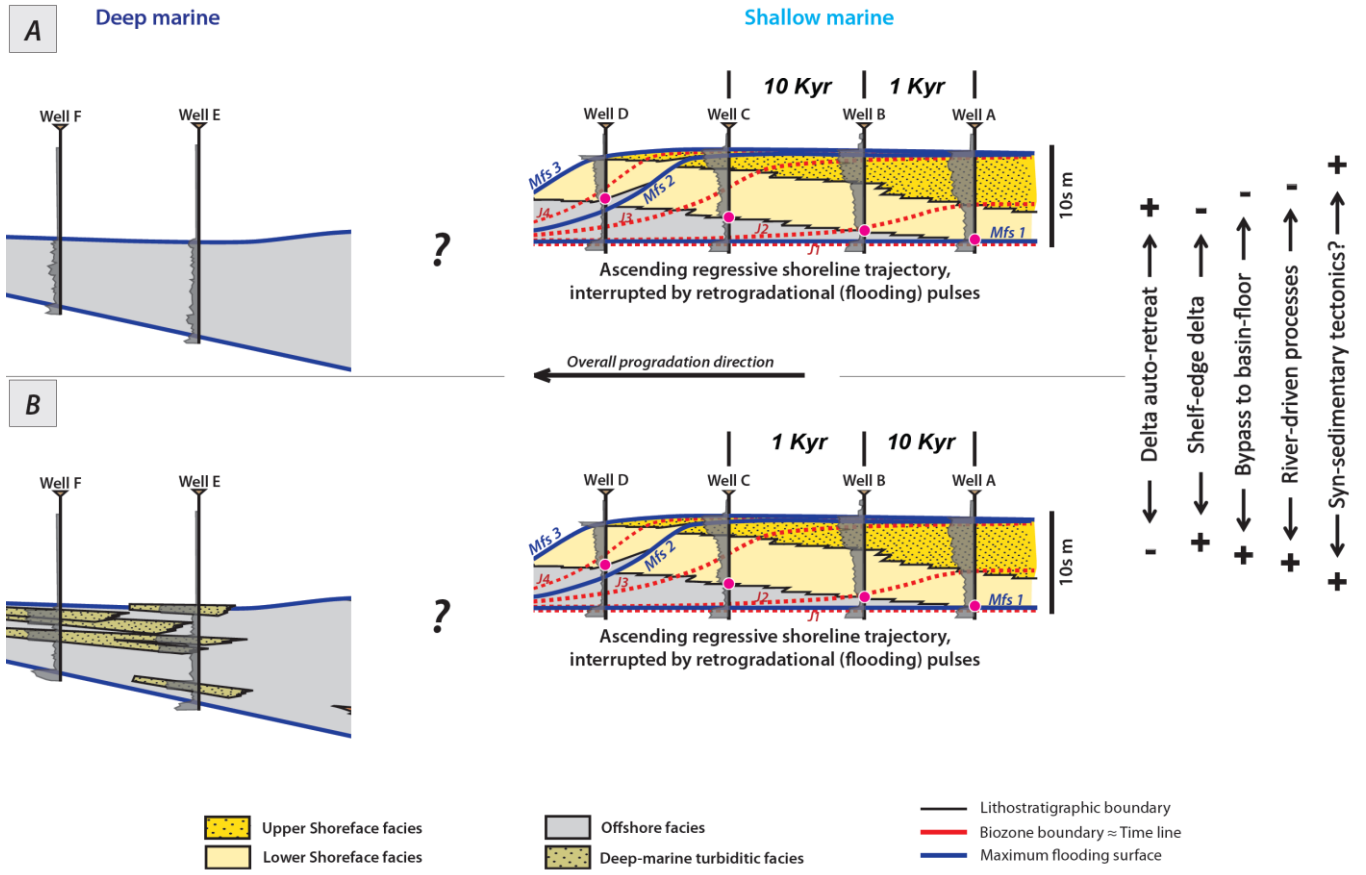

Figure 1.12. *This cartoon shows two shallow marine successions belonging to the same system tracts and migratory classes, but characterized by vastly different stratigraphic architecture, formative mechanisms and sandbody distribution. This is because sequence stratigraphy and shoreline trajectory methods currently fail to take into account the time variable, which controls pace and rate of the shallow-water clinoform migration. A progressively lower shallow-marine clinoform progradation rate as the shoreline approaches the shelf edge (A) will result in likely delta auto-retreats, is likely to hinder sediment bypass to basin-floor and shelf-edge delta creations, and is associated to dominant wave- and tide-processes over river-driven processes. Opposite conditions are associated to increasingly faster shallow-marine clinoform progradations (B). Localized anomalies in the distribution of chronostratigraphically-constrained rates may highlight even low-magnitude syn-sedimentary tectonics.*

1.4.3 Lack of subaerial facies in the Sognefjord Formation clinoforms

If Sognefjord Formation sandstone tongues were formed by the deposition of progradational shoreface or coastal spit successions, as postulated by Stewart et al. (1995) and Dreyer et al. (2005), clinoform topset areas should consists of coastal plain facies, or at least contain evidence of subaerial exposure (e.g., palaeosols or erosional

features). Yet, core- and seismic-based facies and architectural analyses of these sandbodies seem to show the lack of both unequivocal erosional features and subaerial facies, and the simultaneous presence of delta-scale clinoforms with well-developed topset areas (c.f., Dreyer et al., 2005). These features suggest that the Sognefjord Formation sandstone tongues may resemble delta-scale subaqueous clinoforms that have been observed in Quaternary successions, rather than spit or shoreface successions.

1.4.4 Sognefjord Formation: pre- or syn-rift deposition?

The Sognejord Formation is an overall isopachous clastic unit deposited on a rift-marginal shallow-water platform during a time of widespread rift-related fault-block rotation and differential subsidence in the basin depocentres. Localisation of fault-driven subsidence in the basin depocentres early in the rift event (i.e. Bathonian-to-Oxfordian), followed by migration of active faulting to the periphery of the rift system later on (Kimmeridgian-to-Ryazanian) is quite counterintuitive, and openly contradicts the general models of evolution and propagation of rifting (e.g., Cowie, 1998; Gawthorpe & Leeder, 2000; McLeod et al., 2000). However, episodes of low-magnitude fault-block rotations during the deposition of the Middle and Upper Jurassic sand-prone nearshore units on the Horda Platform were merely hypothesized (but not proven) by all the authors working on this area (Stewart et al., 1995; Fraser et al., 2003; Dreyer et al., 2005). If these low-magnitude rotational pulses actually occurred, they probably were below minimum vertical seismic resolution, which makes their recognition challenging.

1.5 THESIS OUTLINE

In Chapter 2 of this thesis, core sedimentology, stratigraphic architecture and 3D seismic geomorphology are integrated in order to present a refined depositional model of the Upper Jurassic Sognefjord Formation and to demonstrate the criteria for interpretation of delta-scale sand-prone subaqueous clinoforms within the unit. An

improved characterisation of the Sognefjord Formation is also of economic importance, since this unit forms the main reservoir in the giant Troll oil and gas field.

Chapter 3 develops a new method to extract progradation rates from ancient shallow-marine clinoforms in order to: (a) constrain sediment accumulation, progradation and sediment supply rates of the Sognefjord Formation; and (b) recognize potential rift pulses below vertical seismic resolution during the Late Callovian and Oxfordian.

In Chapter 4, the analysis of a large dataset of recent and ancient shallow-marine clinoforms highlights potential diagnostic criteria to assist in the recognition of ancient delta-scale sand-prone subaqueous clinoforms by exploiting seismic, sedimentological and/or stratigraphic data. This framework is also useful in order to envisage a realistic architectural and depositional model tied to modern examples once a delta-scale subaqueous clinoform interpretation has been made.

Each of the three main chapters has been written in the form of a scientific article. Article contents and structures, as well as the technical work underpinning them, were almost exclusively carried out by their lead author, Stefano Patruno. Co-author contributions have been limited to improving article structure, presentation and vocabulary and to discussing and refining some of the ideas originally conceived in the first drafts by the lead author. Chapters 2 and 3 are intended for submission to the journals Sedimentology and Basin Research, respectively. Presently (April 2013), the Troll licence partners did not grant approval for journal submission of either manuscript, due to confidentiality issues. Chapter 4 is intended for submission to Earth Science Reviews.

CHAPTER 2

Geomorphology, facies character and stratigraphic architecture of an ancient sand-prone subaqueous delta: Upper Jurassic Sognefjord Formation, Troll Field, Offshore Norway

Running head:

Ancient sand-prone subaqueous delta

Title:

Geomorphology, facies character and stratigraphic architecture of an ancient sand-prone subaqueous delta: Upper Jurassic Sognefjord Formation, Troll Field, Offshore Norway

Authors:

STEFANO PATRUNO, GARY J. HAMPSON, CHRISTOPHER A-L. JACKSON

Department of Earth Science & Engineering, Imperial College, London, SW7 2BP, UK

**Email: s.patruno09@imperial.ac.uk*

Key words:

Compound clinoform, Subaqueous delta, Seismic geomorphology, Sognefjord Formation, Troll Field

Word count: 291 (abstract) + 11,115 (main text)

Number of Figures: 15

Number of Tables: 1

Number of references: 123

CHAPTER 2: GEOMORPHOLOGY, FACIES CHARACTER AND STRATIGRAPHIC ARCHITECTURE OF AN ANCIENT SAND-PRONE SUBAQUEOUS DELTA: UPPER JURASSIC SOGNEFJORD FORMATION, TROLL FIELD, OFFSHORE NORWAY

2.1 ABSTRACT

The integration of core sedimentology, seismic stratigraphy and seismic geomorphology has enabled interpretation of a sand-prone subaqueous delta in the Upper Jurassic Sognefjord Formation of the Troll Field, Horda Platform, offshore Norway. Mud-prone subaqueous deltas characterised by a compound clinoform morphology are common in many modern tide- and wave-influenced settings, but ancient examples are rarely reported. The Sognefjord Formation data therefore demonstrate the criteria for recognition of subaqueous deltas in the stratigraphic record, as well as refining the depositional model of the main reservoir in the super-giant Troll oil and gas field.

Two 10-60 m thick, wave-dominated, regressive-transgressive packages bounded by major marine flooding surfaces are distinguished in the lower Sognefjord Formation. Each regressive-transgressive package corresponds to a set of seismically resolved, westerly-dipping clinoforms, and its bounding surfaces form the seismic "envelope" of a clinoform set. The packages thicken westwards, until they reach a maximum where the clinoform "envelope" rolls over to define a topset-foreset-toeset geometry at the position of maximum regression. Both individual clinoforms and reflections bounding the clinoform sets are oriented sub-parallel to the edge of the Horda Platform (N005-N030). In the eastern half of the field, individual clinoforms are relatively gently dipping (1°-6°) and bound thin (10-30 m) clinothems dominated by fine-grained, hummocky cross-stratified sandstones. Towards the west, clinoforms gradually become steeper (5°-14°) and bound thicker (15-60 m) clinothems that comprise medium-grained, cross-bedded sandstones in their upper parts. Topsets are consistently well developed, except in the westernmost area, where some clinoform foresets are top-truncated. No evidence of subaerial exposure is observed.

Deposition occurred by fully subaqueous, near-linear clinoforms that prograded westwards across the Horda Platform. Subaqueous clinoforms were fed by a river outlet at the north-east and sculpted by the action of currents sub-parallel to the clinoform strike.

[end of abstract]

2.2 INTRODUCTION

Clinoforms are inclined stratal surfaces (Rich, 1951) that occur over various spatial scales, ranging from delta-front foresets that are metres to tens of metres in height (e.g. Gilbert, 1885) to continental margin slopes that are thousands of metres in height (e.g. Steel & Olsen, 2002; Helland-Hansen & Hampson, 2009). Stratal packages bounded by clinoform surfaces are called clinothems, and represent the building blocks of many coastal and shelfal successions. Clinothem geometry and stacking patterns determine the overall stratigraphic architecture (e.g. Mitchum et al., 1977).

Typically, one or two breaks in slope ("rollover points") separate low gradient topsets and bottomsets from a steeper foreset zone (e.g. Mitchum et al., 1977; Pirmez et al., 1998). Most clinoforms display three basic cross-sectional morphologies (Sangree & Widmier, 1977; Adams & Schlager, 2000): (1) planar profiles, interpreted to represent clinoforms at the angle of repose; (2) oblique or concave-upward profiles, which have an abrupt transition between the gently-dipping (< 0.5°) topset and steeply-gently (1-15°) foreset, and a more gradual transition from the foreset to the gently-dipping (< 0.5°) bottomset; and (3) sigmoidal profiles, characterized by more gradual breaks in slope between topset, gently dipping (< 1°) foreset and bottomset. There is no simple relationship between water depth and clinoform morphology. Instead the different cross-sectional geometries are the expression of the complex interaction between basin physiography, mean grain size, shoreline or shelf-edge trajectory, and the dominant sediment dispersal processes (Sangree & Widmier, 1977; Orton & Reading, 1993; Pirmez et al., 1998; Driscoll & Karner, 1999; Adams & Schlager, 2000). Oblique clinoforms are typically associated with progradation over increasingly deep depositional substrates (e.g., Pirmez et al., 1998; Mortimer et al., 2005), coarse-grained sediment (e.g., Kenter, 1990; Orton & Reading, 1993), horizontal or descending regressive trajectories, sediment bypass or erosion, and weak sediment reworking by waves and basinal currents

(Pirmez et al., 1998; Driscoll & Karner, 1999; Adams & Schlager, 2000; Cattaneo et al., 2003; Swenson et al., 2005). Opposing conditions (e.g. fine grain size, ascending trajectories) favour the development of sigmoidal clinoforms.

Modern deltas in high-energy marine settings frequently exhibit a subaerial clinoform (coastal plain delta) and a subaqueous clinoform (subaqueous delta), which are separated by a subaqueous platform (Fig. 2.1A). This configuration has been termed a "compound clinoform" (e.g., Pirmez et al., 1998; Driscoll & Karner, 1999; Swenson et al., 2005). Examples of compound clinoform deltaic systems are those sourced by major rivers, such as the Amazon River Delta (Kuehl et al., 1986; Nittrouer et al., 1986), Ganges-Brahmaputra Delta (Michels et al., 1998; Kuehl et al., 1997, 2005), the Huanghe (Yellow) River Delta (Bornhold et al., 1986; Alexander et al., 1991); Yangtze River Delta (Hori et al., 2001; Liu et al., 2006, 2007) and the Fly River Delta (Walsh et al., 2004). Smaller-scale compound clinoform systems are also found offshore of several western Mediterranean deltas, such as the Rhône, Tiber, Po river deltas and adjoining shelves (Hernández- Molina et al., 2000; Amorosi & Milli, 2001; Cattaneo et al., 2003, 2007; Labaune et al., 2005), and have even been described from very shallow water settings in the Gulf of Mexico (Neill & Allison, 2005). Unlike shelf-edge clinoforms, compound clinoforms are typically characterized by a total vertical relief of less than 100 m (Helland-Hansen & Hampson, 2009). The upper clinoform rollover point of the subaerial delta lies in close proximity to the shoreline break, such that the topset is composed of subaerial, coastal-plain deposits that are prone to erosion. This often gives rise to top-truncated or oblique clinoform geometries (e.g. Ta et al., 2002; Correggiari et al., 2005). In contrast, the topset-foreset rollover point of the subaqueous clinoform is situated at variable distances from the shoreline and in water depths ranging from 5 m to the shelf break (Pirmez et al., 1998; Swenson et al., 2005). Subaqueous clinoforms typically exhibit a sigmoidal geometry with a broad topset, which is normally situated below mean fairweather wave base (e.g., Kuehl et al., 1986; 1997; Hernández- Molina et al., 2000; Cattaneo et al., 2003, 2007; Walsh et al., 2004; Swenson et al., 2005; Liu et al., 2007).

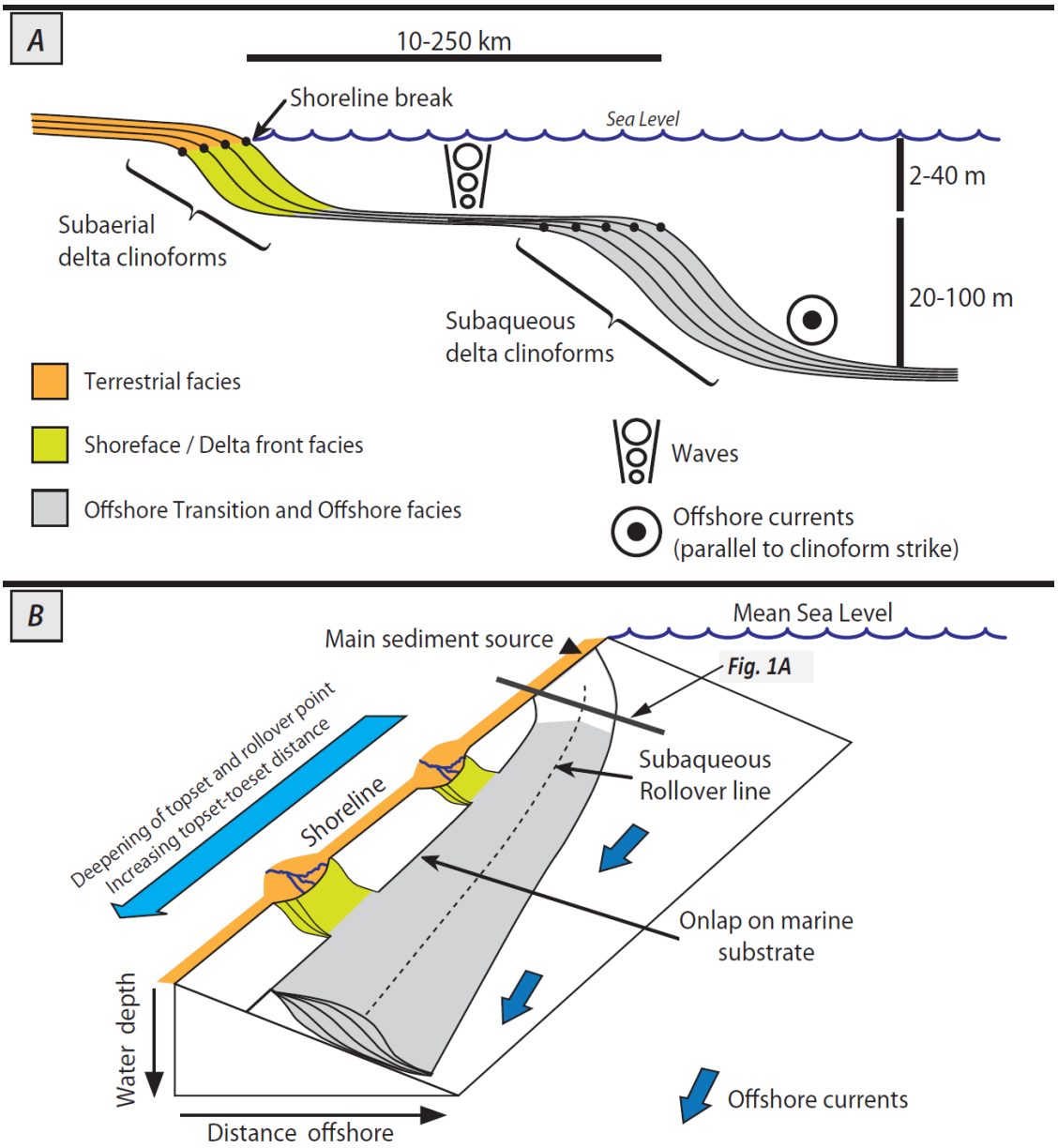

Figure 2.1. *(**A**) Facies and geometrical characteristics of a deltaic compound clinoform system in shoreline-normal cross-section (modified after Cattaneo et al., 2007 and Helland-Hansen & Hampson, 2009). (**B**) 3D sketch illustrating an advection-dominated subaqueous clinoform on the shelf, characterised by a shore-parallel geometry in which the depth of the rollover point becomes progressively deeper down current (modified after Cattaneo et al., 2007).*

High wave-current shear stress in shoreface environments ensures that topsets of subaqueous deltas are regions of dominant sediment bypass through lateral advection, resuspension and redistribution, and limit sediment accumulation at the bottomset of subaerial deltas (Cattaneo et al., 2007). Foreset areas of subaqueous clinoforms are situated below the point where the near-bed shear stress is attenuated, and are therefore characterized by

maximum accumulation rate (Kuehl et al., 1986; Alexander et al., 1991; Pirmez et al., 1998; Driscoll & Karner, 1999). Thus, the position of the topset-to-foreset rollover point of subaqueous clinoforms reflects the depth to the base of the wave-current traction field, which may vary from a few metres up to 40 m (Pirmez et al., 1998; Hernández- Molina et al., 2000; Pomar & Tropeano, 2001; Cattaneo et al., 2003, 2007). In addition, in some well-documented modern subaqueous deltas, the position of the foreset-to-bottomset transition is controlled by advective offshore currents that flow parallel to the clinoform strike along the bottomset (e.g. Cattaneo et al., 2003, 2007; Liu et al., 2007).

The partitioning of sediment between subaerial and subaqueous delta clinoforms is determined by the spatial and temporal interplay between river processes and basin hydrodynamics (Pirmez et al., 1998; Driscoll & Karner, 1999; Cattaneo et al., 2003, 2007; Swenson et al., 2005). The portion of sediment delivered to the subaqueous clinoform increases with: (1) greater frequency and/or magnitude of coastal storms, (2) lower river flood discharge; and (3) relatively fine mean sediment grain size (Swenson et al., 2005). Correspondingly, the depth of the subaqueous clinoform rollover and its distance from the shoreline increase with increasing depositional energy, which in turn may be related to the basin physiography (Pirmez et al., 1998). Due to the relatively constant and sustained hydrodynamic conditions that occur on many modern shelves, subaqueous deltas tend to show more uniform along-strike clinoform geometries than their subaerial counterparts, which are typically highly variable due to autocyclic delta lobe switching, erosion and delta retreat (Driscoll & Karner, 1999; Cattaneo et al., 2003; Correggiari et al., 2005).

In modern subaqueous deltas, sediment transport is often dominated by strong shore-parallel hydrodynamic advection resulting from high-energy geostrophic coastal currents and storms (Orton & Reading, 1993; Driscoll & Karner, 1999; Cattaneo et al., 2003, 2007). These deltaic bodies are characterized by shore-parallel geometries in which the depth of the rollover point becomes progressively deeper down current (Fig. 2.1B). As a consequence, oblique clinoform profiles, which are typical of subaerial deltas, are gradually replaced along-strike and/or down-dip by subaqueous deltas with distinctive sigmoidal geometries (e.g., Michels et al., 1998; Driscoll & Karner, 1999; Cattaneo et al., 2003, 2007; Fig. 2.1). Cattaneo et al. (2003) point out that a continuous suite of genetically related depocentres on the inner shelf exists between: (1) more localised, supply-dominated deltas, which are oriented normal to radial to the direction of net-sediment transport and progradation; (2) hybrid deltas with compound clinoforms, in which shore-parallel unidirectional currents cause the progradation direction to become normal to sediment transport in the prodelta region; and (3) shore-parallel subaqueous deltas, which are distant from direct river inputs and dominated by basinal storm waves and shelf currents.

Modern subaqueous delta clinoforms are typically mud-rich (Fig. 2.1); for this reason, they have been rarely recognized in the geological record (e.g. Hampson, 2010). Regressive, sand-rich clinoforms are generally assumed to be related to prograding shorelines or subaerial deltas, and clinoform rollover points are subsequently treated as proxies for the shoreline break. However, a few studies have identified modern subaqueous clinoforms with a noticeable amount of sand in their topsets (e.g., Hernández-Molina et al., 2000; Walsh et al., 2004) and ancient coarse-grained clinoforms containing cross-beds that were deposited below wave base by tractional currents oriented parallel to the shoreline (e.g. Pomar & Tropeano, 2001; Pomar et al., 2002).

This paper has three aims: (1) to demonstrate that reservoir forming sandstones were deposited below the fairweather wave base in an ancient subaqueous delta context; (2) to highlight similarities and differences between this ancient system and modern-day subaqueous deltas; and (3) to investigate how this interpretation impacts on facies predictions in delta successions. In order to address these research questions, data from the Upper Jurassic Sognefjord Formation in the supergiant Troll Gas and Oil Field, offshore Norway have been used. Clinoform topsets from this unit were previously interpreted to have been deposited in subaerial delta system fronted by a wave-dominated spit (Dreyer et al., 2005).

2.3 STUDY AREA AND TECTONO-STRATIGRAPHIC CONTEXT

The study area is located on the Horda Platform, on the eastern flank of the North Viking Graben (Fig. 2.2A), which is one of the failed arms of the trilete North Sea rift basin (Badley et al., 1988; Coward et al., 2002; Zanella & Coward, 2002). The Horda Platform is an up to 50 km wide, north-south trending, normal fault-bounded block (Fig. 2.2C). The Horda Platform, North Viking Graben and intermediate fault terrace formed in their present configuration during Late Jurassic rifting, which consisted of five extensional pulses separated by phases of quiescence (Færseth & Ravnås, 1998; Ravnås et al., 2000; Coward et al., 2002). However, the Horda Platform seems to have been affected by only negligible fault-related tectonic subsidence for much of the pre-Kimmeridgian time (e.g., Dreyer et al., 2005).

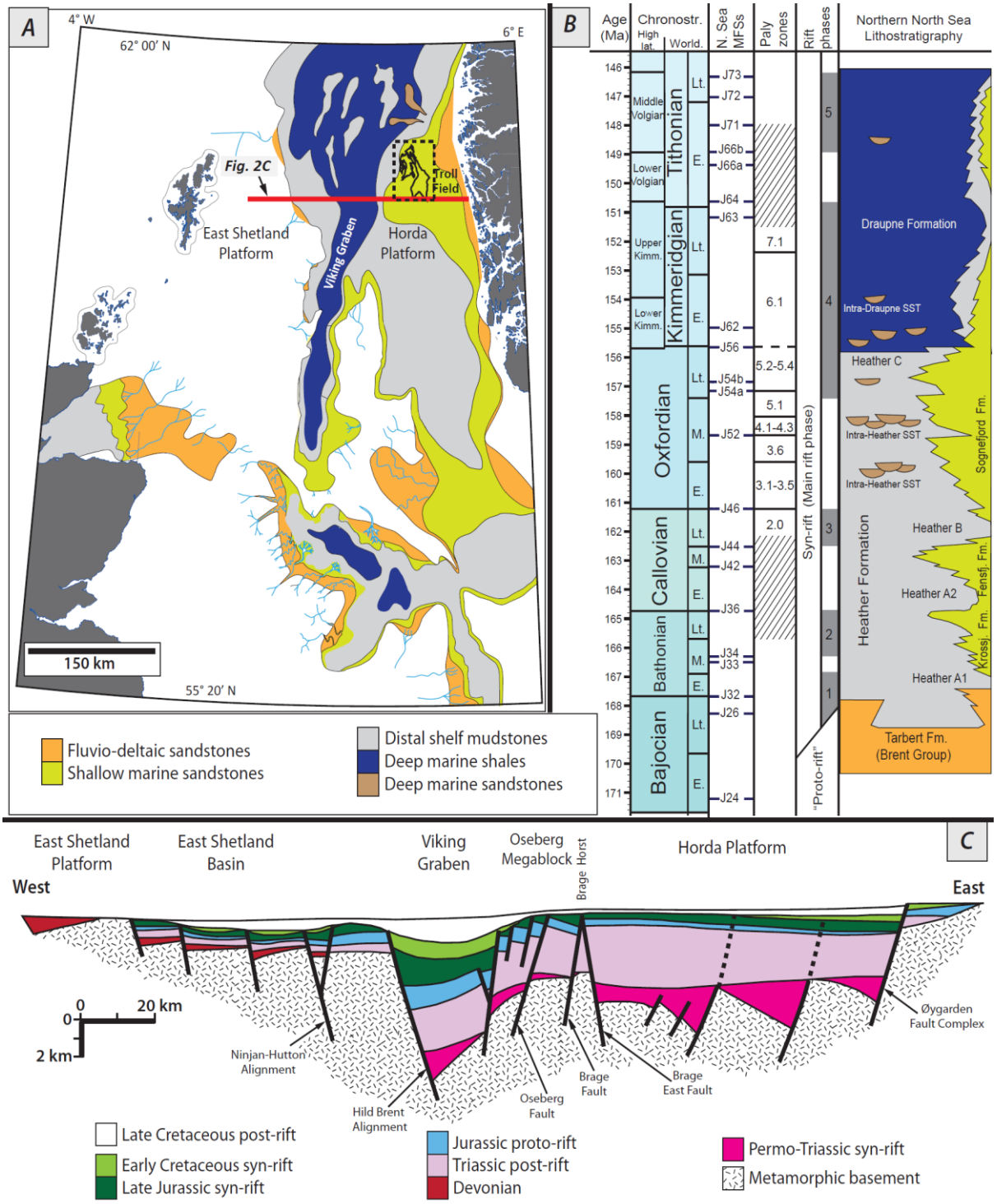

Figure 2.2. *(**A**) Palaeogeographic map of the North Sea area during the Early-Middle Oxfordian (modified after Fraser et al., 2002); (**B**) Late Jurassic stratigraphy developed on the eastern flank of the North Viking Graben and (**C**) regional cross section across the Northern North Sea Basin (modified after Faerseth, 1996). Chronostr. = standard chronostratigraphy; High lat. = high latitude (boreal and sub-boreal) nomenclature; World. = worldwide (Tethys-based) nomenclature; N. Sea MFSs = North Sea basin-wide maximum flooding surfaces; Paly. zones = palynostratigraphic zones. Position of stage boundaries and absolute ages is based on Ogg et al. (2008). Names and stratigraphic positions of the basin-wide, North Sea maximum*

flooding surfaces are from Partington et al. (1993); names and positions of the palynological zones are those proposed by Dreyer et al. (2005). The five rift phases indicated are based on the studies of Færseth & Ravnås (1998) and Ravnås et al. (2000).

The Late Jurassic stratigraphy of the Horda Platform contains three shallow marine, coarse-grained siliciclastic wedges that were deposited by westwards-prograding deltas sourced from the Norwegian mainland; these wedges correspond to the Krossfjord, Fensfjord and Sognefjord formations (Vollset & Doré, 1984; Steel, 1993; Stewart et al., 1995) (Fig. 2.2B). These formations each span 3-6 Myr and are separated by incursions of the offshore Heather Formation that represent transgressive maxima (Steel, 1993; Fraser et al., 2002). The internal architecture of these clastic wedges is defined by multiple regressive-transgressive tongues (e.g. Stewart et al., 1995; Fraser et al., 2002; Dreyer et al., 2005).

The Oxfordian Sognefjord Formation, which is the youngest of the three shallow marine wedges sourced from the Norwegian mainland, forms the main reservoir in the super-giant Troll oil and gas Field (Fig. 2.3A-B), which is located on the northern margin of the Horda Platform. The field initially hosted about 40% of the total gas reserves on the Norwegian continental shelf, and it still contains ca. 10^{12} Sm^3 (3.5 X 10^{13} Scf) of gas (Norwegian Petroleum Directorate, 2011). The earliest studies of the Sognefjord Formation interpreted most of the thick, coarse-grained reservoir sandstone bodies as offshore bars, derived by transgressive reworking of older regressive deposits (Whitaker, 1984; Hellem et al., 1986). Stewart et al. (1995) and Dreyer et al. (2005) reinterpreted the large-scale depositional architecture of the Sognefjord Formation in terms of a predominantly regressive, north-south-elongate, shallow marine shoreline-to-shelf system. In particular, the formation was interpreted by Dreyer et al. (2005) as the deposits of a coastal spit system, bordered to the east by a tidal backbasin. The spit system prograded for tens of kilometres westward, through incremental deposition of westerly-dipping clinothems. Dreyer et al. (2005) interpreted that clastic sediment was supplied to the system by a major feeder river located in the northeast of the Troll Field and that this sediment was distributed southwards by persistent longshore currents flowing parallel to the strike of the spit body.

This work is focused on the lower part of the Sognefjord Megasequence (*sensu* Steel, 1993), which is bounded below by the top of the Fensfjord Formation and above by the middle Oxfordian, J52 maximum flooding surface (*sensu* Partington et al., 1993). Hence, the studied stratigraphic interval is Late Callovian and Early to Middle Oxfordian in age (Fig. 2.2B).

2.4 DATA AND METHODS

Core, wireline log, biostratigraphic, biofacies, dipmeter and three dimensional (3D) seismic reflection data have been utilised to characterise the Sognefjord Formation. Data from 45 wells are used, including complete suites of wireline logs and biostratigraphic data (Fig. 2.3). Sedimentological interpretation is based on detailed (1:50 scale) logging of lithology, grain size and texture, sedimentary structures, and body-fossil and trace-fossil characteristics from 833 m of core from 12 wells distributed across both the western and the eastern parts of the Field area (Fig. 2.3; appendix). Dipmeter data were collected by 4-arm, 4-electrode or by 4-arm, 8-electrode sondes in 1988-1993 and interpreted by Nilsen et al. (1993). Their analysis involved data processing and comparison of the resulting arrow plots and microresistivity curves with wireline logs, core logs and core photos. The mean of several inferred, dune-scale cross-bedding dip clusters, which were characterised by fairly consistent dip azimuths, was used to constrain each single palaeocurrent direction (Nilsen et al., 1993). The palynofacies analyses used here are based on industry-sourced reports (Whitaker, 1981, 1982a, 1982b, 1983, 1985; Bell et al., 1984a, 1984b; Duxbury et al., 1984a, 1984b), which are now publically available. A biostratigraphic age framework has been constructed from the raw occurrence data of key palynostratigraphic markers and from published biostratigraphic schemes for the northern North Sea (e.g., Poulsen & Riding, 2003; Dreyer et al., 2005). Two 3D seismic reflection surveys that cover 3,320 km^2 supplement our well and biostratigraphic dataset. The line spacing in these surveys is 12.50-25 m in both inline and crossline directions, and the vertical record length is 2.4-3.0 seconds two-way time (s TWT).

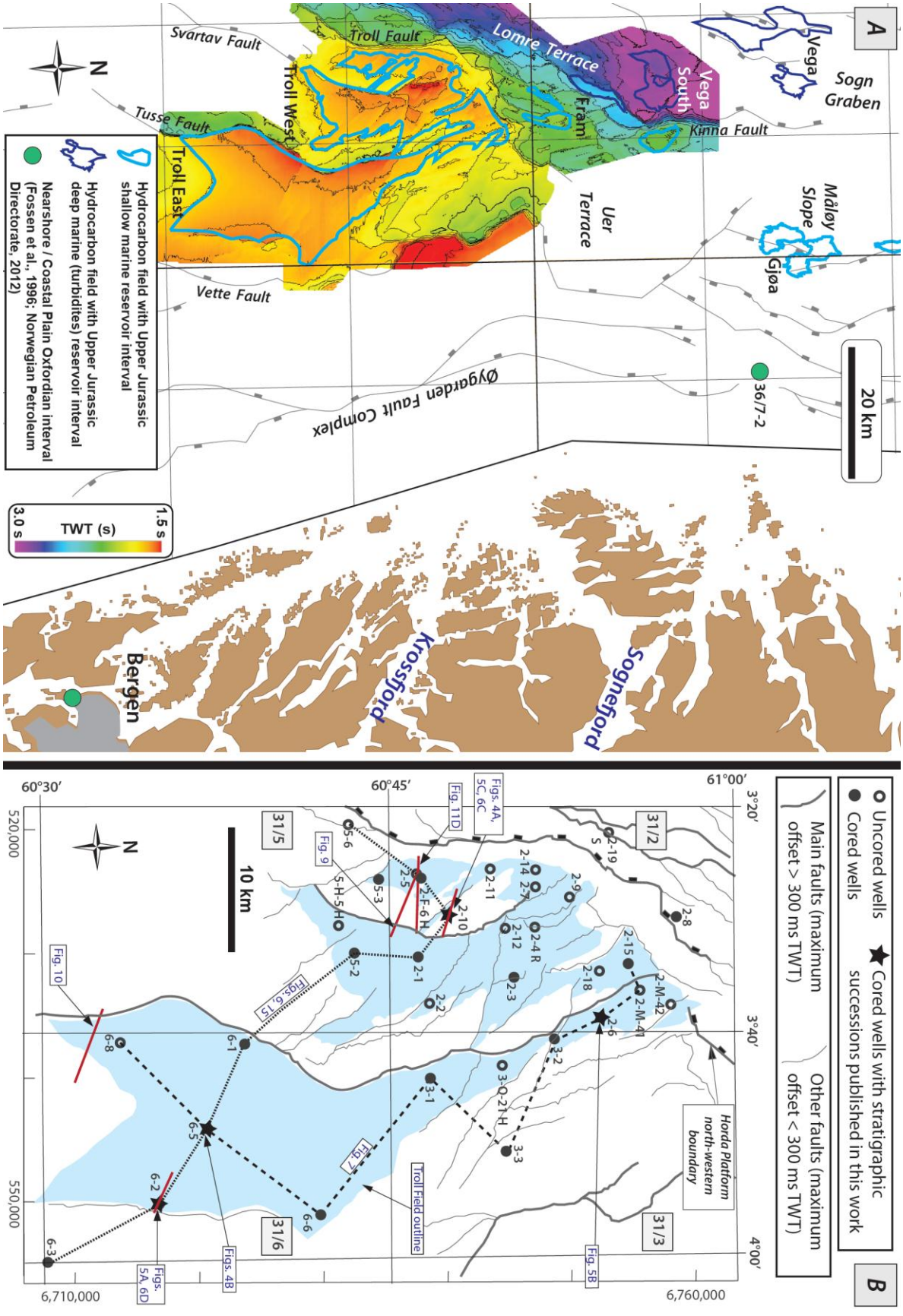
A
Svartav Fault
Troll Fault
Lomre Terrace
Vega South
Vega
Sogn Graben
Tusse Fault
Troll West
Fram
Kinna Fault
Troll East
Uer Terrace
Måløy Slope
Gjøa
Vette Fault
Øygarden Fault Complex
36/7-2
20 km
N
Hydrocarbon field with Upper Jurassic shallow marine reservoir interval
Hydrocarbon field with Upper Jurassic deep marine (turbidites) reservoir interval
Nearshore / Coastal Plain Oxfordian interval (Fossen et al., 1996; Norwegian Petroleum Directorate, 2012)
3.0 s
TWT (s)
1.5 s
Bergen
Krossfjord
Sognefjord
B
Uncored wells
Cored wells
Cored wells with stratigraphic successions published in this work
Main faults (maximum offset > 300 ms TWT)
Other faults (maximum offset < 300 ms TWT)
60°30′
60°45′
61°00′
3°20′
3°40′
4°00′
520,000
550,000
6,710,000
6,760,000
10 km
31/5
31/2
31/6
31/3
Fig. 11D
Figs. 4A, 5C, 6C
Fig. 9
Fig. 10
Figs. 6, 15
Fig. 7
Figs. 4B
Figs. 5A, 6D
Fig. 5B
Horda Platform north-western boundary
Troll Field outline
2-F-6 H
5-H-5 H
3-Q-21 H
2-M-42
2-M-41
2-4 R

Figure 2.3. *Map of the present-day Norwegian shelf between 60°20' and 61°30' latitude North, with superimposed time-structure map of the top of the Fensfjord Formation. This map also shows the location of the main hydrocarbon fields with Upper Jurassic reservoir intervals, their gross palaeoenvironments, and the position of Callovian to Oxfordian age deposits containing abundant coal beds. (**B**) Map of the Troll Field area, showing faults and studied wells. Wells whose cores have been logged are indicated by black closed circles; the core logs presented herein (Fig. 5) are indicated on the map by stars.*

Our data analysis comprises the following five steps: (1) combination of core-based sedimentology, wireline logs and palynofacies characteristics in order to interpret a depositional facies framework; (2) the occurrences of selected palynostratigraphic markers are used to constrain the precise age of the stratigraphic succession; (3) a sequence stratigraphic framework is then interpreted by integrating vertical facies successions with biostratigraphically constrained ages; (4) the stratigraphic succession is tied to the seismic reflection data by using checkshot data and synthetic seismograms (e.g. Fig. 4); and (5) the sequence stratigraphic interpretations derived from well data analysis are integrated with seismic observations and the palaeocurrent directions inferred from dipmeter data, in order to develop an integrated depositional and sequence stratigraphic model.

Almost all of the wells used in this paper are completely cored, and thus correlations presented here are constrained by very high core coverage. Qualitative and quantitative wireline log characteristics of the facies associations observed in cored intervals have been used to guide interpretations of the main facies associations in uncored intervals and wells. Palaeocurrent trends are used to determine the local sediment transport directions. Seismic data provide us with the geometrical framework with which to confidently interpret clinoform occurrence in the lower Sognefjord Formation, and they also enable placement of the wells in their appropriate geomorphological position (e.g. "seismic geomorphology" concept of Posamentier et al., 2007). Synthetic seismograms (e.g. Fig. 2.4) indicate that a vertical distance of 10 ms TWT equates to 10-17 m of vertical rock succession (13 m on average). Vertical seismic resolution for the studied strata is 7-16 ms TWT, which equates to 7-26 m.

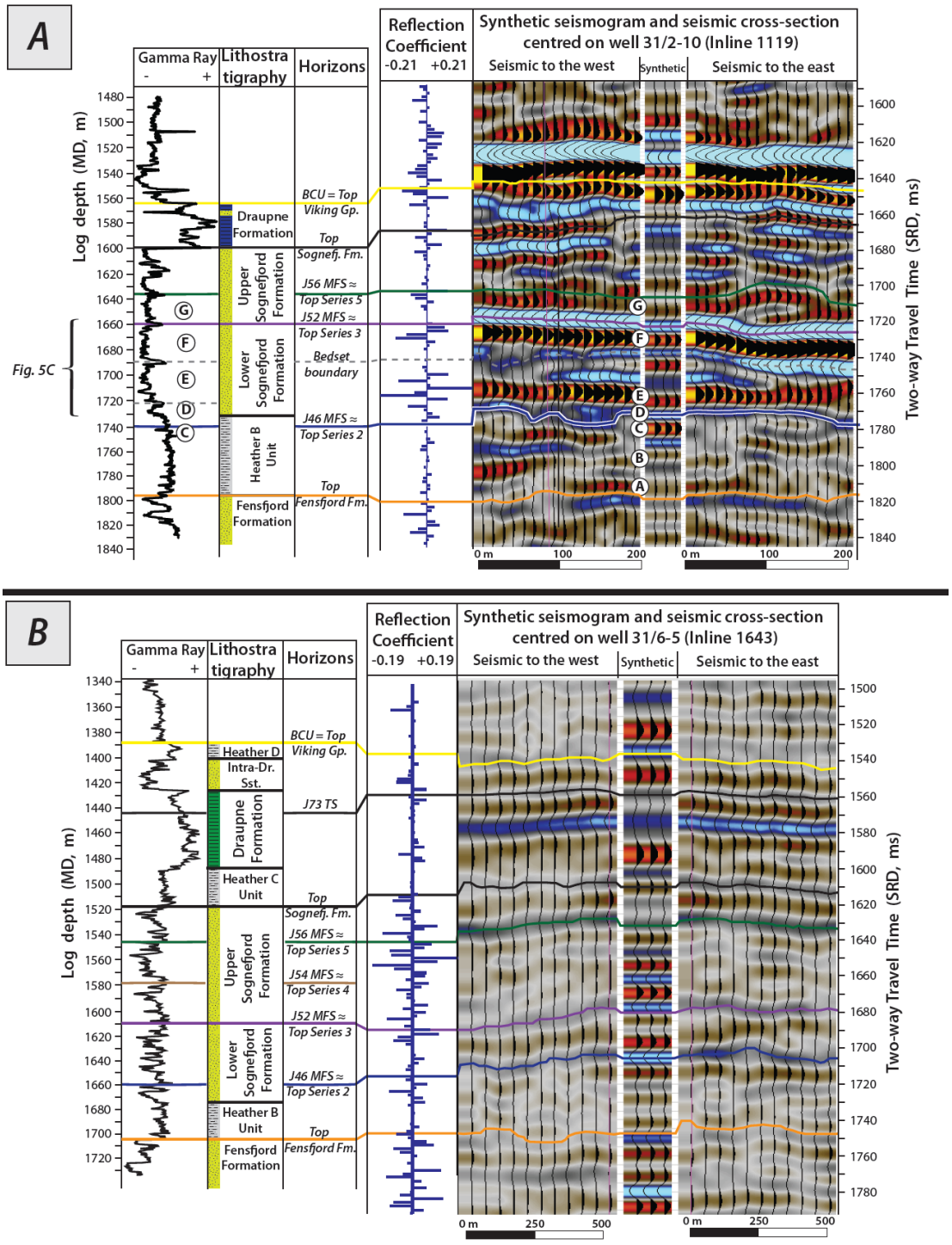

Figure 2.4. *Synthetic seismograms tying stratigraphic successions and seismic reflections for (**A**) well 31/2-10, and (**B**) well 31/6-5 (Fig. 3B). Regional maximum flooding surfaces (labelled J46, J52, J54 and J56 MFS) correspond to continuous negative (blue) reflections, which envelop sand-prone packages generally corresponding to positive (red) reflection events. Sandstone-rich bedsets in the lower Sognefjord Formation of well 31/2-10 are labelled A to G, in order to facilitate a direct correlation between the stratigraphic succession and its seismic expression (c.f., Figs. 5-6). Vertical seismic resolution for the studied strata is 7-16 ms TWT, which equates to 7-26 m.*

2.5 FACIES ANALYSIS

Dreyer et al. (2005) published a detailed facies analysis of the Sognefjord Formation in the western part of the Troll Field. Here this existing facies scheme has been modified and extended based on logging of cores from the lower Sognefjord Formation in both the western and eastern parts of the Troll Field. The Bioturbation Index (BI) scheme of Taylor & Goldring (1993) is used to describe bioturbation intensity, which ranges from 0 (no bioturbation) to 6 (completely bioturbated).

2.5.1 Facies Association 1 (Bioturbated Siltstones)

2.5.1.1 Description

Facies Association 1 (FA1) constitutes most of the Heather B unit (Fig. 2.2B) throughout the study area and part of the Sognefjord Formation (e.g. Figs. 2.5-2.7). It occurs in successions 0.2-70 m, with particularly thick successions (40-70 m) developed towards the western limit of the Troll Field area (Fig. 2.6). In the western part of the Troll Field, FA1 is typically underlain by FA4, FA5 or FA6. Towards the east, FA1 tends to be underlain by successions composed of FA2 or FA3. The basal contact between the underlying facies associations and FA1 is usually sharp to erosional. FA1 is overlain by FA2 or FA3 across a gradational to sharp transition throughout the study area. FA1 is equivalent to Facies 1 and 2 of Dreyer et al. (2005).

The bulk of FA1 is comprised of micaceous siltstones and very fine-grained sandstones that contain abundant marine fossils (e.g. belemnites and small, thin-shelled bivalves) (Facies 1a). These deposits are moderately to intensely bioturbated (BI of 3-6) by a diverse trace fossil assemblage (including *Terebellina*, *Chondrites, Planolites*) that constitutes the archetypal Cruziana ichnofacies (cf. Pemberton et al., 1992; MacEachern & Bann, 2008). Facies 1a is interbedded with rare (< 5% of FA1) sharp-based, planar-parallel laminated, very-fine grained sandstone beds (Facies 1b). The basal part of successions of FA1 may contain thin (< 1.5 m) sharp-based, upward-

fining beds that contain poorly-sorted, matrix-supported and coarse-grained sandstones at their bases (Facies 1c). Beds of Facies 1c contain anomalously high concentrations of randomly oriented bioclasts (e.g. fragments or intact specimens of bivalves and belemnites), intraclasts, granules and pebbles, glauconite, chamosite and/or heavy mineral grains. These beds are most commonly carbonate cemented.

2.5.1.2 Interpretation

Facies association 1 documents settling of mud and silt by suspension from river-fed plumes (e.g. Nemec, 1995), and subsequent bioturbation under conditions of low hydrodynamic energy below mean storm wave base (MSWB) in an offshore environment (*sensu* Hunter et al., 1979; Howard & Reineck, 1981; Van Wagoner et al., 1990). Planar-parallel laminated sandstone beds record deposition from unidirectional currents under upper flow regime conditions, and represent the distal expression of major event beds generated by large storms and/or flood-generated hyperpycnal flows (e.g. Goldring & Bridges, 1973; Dott & Bourgeois, 1982; Mulder & Syvitski 1995; Kassem & Imran, 2001). Sharp-based, poorly sorted sandstones at the base of successions of FA1 (Facies 1c) are interpreted as lags formed by the erosion and reworking of underlying sediments by waves and currents. Their context at the base of offshore successions, which record less energetic, deeper water conditions, implies that they are transgressive in origin.

2.5.1.3 Palynofacies

Facies association 1 is characterised by a palynofacies that suggests deposition in an overall low energy, uniform, shelfal marine setting. In particular, “lower offshore” markers dominate in a palaeo-seaward direction (e.g. 31/2-5 and 31/2-8 in Fig. 2.8A; Whitaker 1982b, 1985). In the central part of the study area, lower–to-upper offshore palynomacerals, which indicate a weak fluvial influence, are documented (e.g., well 31/2-3 Fig. 2.8A; Whitaker, 1981, 1982a). Finally, palynofacies in the east and south-east of the study area (e.g., wells 31/3-1 and 31/6-2 in Fig. 2.8; Duxbury et al., 1984a, 1984b) are indicative of a moderate terrestrial influence. Throughout the study area, palynomacerals that indicate brackish and terrestrial influence and higher depositional energies increase upwards in abundance within successions of FA1, mirroring an overall shallowing-upwards trend interpreted from sedimentological analysis of cores.

2.5.2 Facies Association 2 (Bioturbated Siltsones and 'Event Bed' Sandstones) and Facies Association 3 (Amalgamated 'Event Bed' Sandstones)

2.5.2.1 Description

Facies Associations 2 and 3 (FA2 and FA3) are developed throughout much of the study area, and in combination form upward-coarsening successions ranging from 1 to 50 m in thickness (Figs. 2.5-2.7). FA2 and FA3 are not distinguished by the types of facies they contain, but by the relative abundance of these facies (c.f. Fig. 2.5), such that FA2 comprises >50% siltstone (Facies 2a) and FA3 contains <50% siltstone (Facies 3a). FA2 is typically underlain by FA1 across a gradual or sharp contact, and passes gradationally upward into FA3. FA3 is gradationally or sharply overlain by FA4 and FA6 in the western part of the study area, and sharply or erosionally overlain by FA1 towards the east. FA2 and FA3 are equivalent to Facies 2 and 3 of Dreyer et al. (2005).

Most of FA2 and FA3 comprises bioturbated siltstones with rare thin-shelled bivalves (Facies 2a and 3a, equivalent to Facies 1a) and bioturbated fine-grained sandstones with fragments of carbonaceous debris (Facies 2b and 3b). Bioturbation is high to complete (BI of 4-6). Trace fossil suites contain vertical, *Skolithos*-like burrows and various horizontal burrows (*Planolites*, *Ophiomorpha*, *Terebellina*). These suites are characteristic of either a proximal Cruziana or distal Skolithos ichnofacies (*sensu* MacEachern & Bann, 2008). Bioturbated deposits are interbedded with three types of sharp-based beds that contain well-preserved primary structures. Well-sorted, parallel-laminated and hummocky cross-stratified, fine-grained sandstones (Facies 2c and 3c) occur as beds that contain micaceous and carbonaceous laminae, and display variable erosional amalgamation. Beds are generally well laminated and only sparsely bioturbated (BI of 0-2). Where preserved, bed tops have similar grain-size and sorting characteristics, but are moderately to completely bioturbated (BI of 3-6). Moderately to poorly sorted, coarse-grained to pebbly sandstones occur in sharp to erosionally based beds whose thickness ranges from centimetres to tens of centimetres (Facies 2d and 3d) up to metres (Facies 2e and 3e). Beds of Facies 2e/3d are variably amalgamated, and may from packages up to several metres in thickness. Individual beds are structureless, normally graded and/or planar-parallel laminated, and their base may contain particularly coarse-grained, poorly-sorted, matrix-supported intervals of subangular-to-rounded granules, pebbles, lithoclasts and bioclasts. Body and trace fossils are usually absent. The basal interval of FA2-FA3 successions is locally composed

of poorly sorted, upward-fining sandstones up to 2 m thick (Facies 2f and 3f, similar to Facies 1c). Carbonate-cemented layers are common in all of the facies components of FA2 and FA3.

2.5.2.2 Interpretation

FA2 and FA3 were deposited in a fully marine environment that was subject to intermittent high-energy events, most likely in a storm-dominated offshore transition setting, between mean fairweather wave base (MFWB) and mean storm wave base (MSWB). In this setting, bioturbated siltstones (Facies 2a and 3a) are interpreted to be the result of bioturbation during fairweather periods of fine-grained sediment that may have settling from suspension or been transported by gravity flows generated by river floods and/or storms (e.g. Bentley, 2003). Deposition of bioturbated, fine-grained sandstones (Facies 2b and 3b) indicates fairweather bioturbation of sand deposited by a range of depositional processes, including storm waves and suspension settling from hypopycnal jets (cf. Drake et al., 1985; Nemec, 1995). Hummocky cross-laminated fine-grained sandstones (Facies 2c and 3c) were deposited by simultaneous fallout from suspension and lateral tractive flow due to storm-wave oscillation (Goldring & Bridges, 1973; Dott & Bourgeois, 1982; Duke, 1985). Episodic processes of particularly high-energy may have transported sand and fine gravel offshore and deposited sharp-based, coarse-grained event beds (Facies 2d, 3d, 2e and 3e). These beds were deposited either from high-density turbidity currents and debris flows in which high sediment concentrations suppressed turbulence, resulting in structureless beds, or by turbulent deposition under strong unidirectional currents, resulting in fining-upwards beds containing planar-parallel lamination (Middleton & Hampton, 1976; Clifton, 1976; Lowe, 1982; Kneller & Branney, 1995). Sediment-laden, gravity flows of this type may be triggered by slope failure (Lowe, 1982; Field & Roy, 1984; Van den Berg et al., 2002), river flood-generated hyperpycnal flows (Wright et al., 1986; Mulder & Syvitski, 1995; Kassem & Imran, 2001; Parsons et al., 2001; Plink-Bjorklund & Steel 2004), and or major storms (cf. Kumar & Sanders, 1976; Myrow & Southard, 1996) and associated rip currents (Shepard, 1941; Bowen & Inman 1969; Hunter et al., 1979; Gruszczyński et al., 1993). Sharp-based, poorly sorted, coarse-grained sandstones of Facies 2f and 3f are interpreted as transgressive lags (cf. Facies 1c).

2.5.2.3 Palynofacies

FA2 is characterised by a marine palynofacies that contains a minor and moderate brackish influence respectively in western (palaeoseaward) and eastern (palaeolandward) parts of the study area. High-energy conditions are interpreted in the western part of the Troll Field (e.g. well 31/2-4 R in Fig. 2.8; Whitaker, 1981, 1982a), whereas towards the east and south-east (e.g. wells 31/3-1 and 31/6-6; Duxbury et al., 1984a, Bell et al., 1984b) FA2 is characterised by low-to-moderate energy, offshore marine palynofacies, with evidence that depositional energies slightly increase up-section. Throughout the study area, Facies Association 3 generally corresponds to a shallow marine palynofacies that is characterized by moderate or high depositional energies, and normal marine salinity and oxygenation level. Duxbury et al. (1984a,b) suggest prolonged sediment transport and deposition via storm-induced currents that were derived from more proximal locations. Furthermore, in the western part of the Troll Field (e.g. wells 31/2-2 and 31/2-4 R in Fig. 2.8; Whitaker, 1982a), the general paucity of terrestrial debris in FA2 and FA3 suggest a significant distance from the shoreline and riverine input. In the eastern part of the study area (e.g. well 31/6-2 in Fig. 2.8; Duxbury et al., 1984a,1984b), moderate terrestrial input is interpreted.

2.5.3 Facies Association 4 (Cross-Bedded Sandstones)

2.5.3.1 Description

Facies Association 4 (FA4) only occurs in the western part of the study area, where it comprises successions up to 40 m thick (Figs. 2.5-2.7). FA4 is underlain by FA2 or FA3 across a gradational to sharp contact. It is gradationally or sharply overlain by FA5 or FA6, or by FA1, FA2 or FA3 across a sharp to erosional boundary surface that is locally lined by a coarse-grained sandstone lag (Facies 1c, 2f or 3f). FA4 is equivalent to Facies 4 of Dreyer et al. (2005).

FA4 is dominated by cross-bedded to planar-parallel stratified, well- to moderately sorted, fine- to coarse-grained sandstones (Facies 4a). Facies 4a is interbedded with erosionally based packages of amalgamated, poorly sorted, fine- to very coarse-grained sandstones that are bedded at centimetre scale (Facies 4b, equivalent to Facies 2d and 3d) and metre scale (Facies 4C, equivalent to Facies 2e and 3e). Individual beds are structureless or normally graded with planar-parallel lamination. Trace fossil assemblages comprise rare *Ophiomorpha* and vertical, *Skolithos*-like burrows (BI of 0-3), which are indicative of the archetypal Skolithos Ichnofacies (*sensu* MacEachern

& Bann, 2008). Marine fossils are lower in abundance and diversity, comprising only bivalves, than in FA1, FA2 and FA3 (Fig. 2.5).

2.5.3.2 Interpretation

The predominance of cross-bedded sandstones (Facies 4a) in FA4 indicates that it was deposited under the near-continuous action of strong currents, which caused migration and accumulation of sand in dunes. Intermittent periods of higher velocity, and upper flow regime conditions, are recorded by planar-parallel stratified intervals. Sharp-based packages of structureless to planar-parallel laminated sandstones (Facies 4b and 4c) are inferred to represent stacked gravity flows infilling rip channels (cf. Gruszczyński et al., 1993) or hyperpycnal flows generated by exceptional river floods (cf. Mulder et al., 2003). The range of depositional processes recorded by FA4 is consistent with a range of high-energy nearshore environments, including the upper shoreface surf zone (e.g. Hunter et al., 1979; Howard & Reineck, 1981; Van Wagoner et al., 1990; Walker & Plint, 1992), longshore swash bars developed above or below fairweather wave base in subaqueous spit platforms (*sensu* Meistrell, 1972; e.g. Nielsen et al., 1988; Nielsen & Johannessen 2001, 2009) and offshore sand bars (e.g. Short, 1975). Stability diagrams indicate that dunes are formed by bottm currents flowing faster than 40 cm/s, whereas upper plane regime is reached at >75 cm/s. Mitchell (2012) and Mitchell et al. (2012) show that shallow-marine shore-parallel storm-induced bottom currents commonly reach 20-80 cm/s. A more specific interpretation of depositional environment for FA4 requires consideration of seismic geomorphological and stratigraphic context, as below.

2.5.3.3 Palynofacies

In well 31/2-4R, which is located in the western part of the Troll Field (Fig. 2.8B), palynofacies markers indicate that deposition under high-energy conditions in a strongly oxidizing environment (Whitaker, 1982a). A lack of terrestrial organic material suggests that this well was either distant from or axial to direct fluvial input; Whitaker (1982a) suggests that the most likely setting was a linear, “non-deltaic” shoreline. Further east (palaeolandward), in well 31/2-3 (Fig. 2.8B), Whitaker (1981) interpreted that the palynofacies markers suggest deposition of FA4 under high-energy marine conditions, with some degree of brackish influence relatively close to a river mouth.

2.5.4 Facies Association 5 (Planar-Parallel Laminated Sandstones)

2.5.4.1 Description

Facies Association 5 (FA5) is only identified in the western part of the study area (e.g. well 31/2-10, Figs. 2.3B, 2.5C) in successions 1-8 m thick. In general, FA5 gradationally overlies FA4. It is overlain by FA1, FA2 and FA3 across a sharp or erosional boundary, or by FA4 across a gradational to sharp boundary.

FA5 is composed of planar-parallel laminated, low-angle cross-stratified and structureless beds of medium- to coarse-grained sandstone with rare cross-bedding (Facies 5a). Bioturbation is absent to low in intensity (BI=0-2) and marine body fossils are absent.

2.5.4.2 Interpretation

FA5 is interpreted to record deposition under conditions of high flux of coarse-grained sand and high near-bed shear stress in response to the action of upper flow regime, unidirectional currents in a subaqueous environment. These conditions are similar to those represented by FA4, but the overall hydrodynamic energy is greater in FA5. Such conditions are common in modern beaches, where swash-backwash processes formed by breaking waves are dominant (cf., Clifton, 1969; Howard & Reineck, 1981), but they are not restricted to such environments. As for FA4, the seismic geomorphological and stratigraphic context of FA5, outlined below, has been used to interpret a specific depositional environment. FA5 is equivalent to Facies 5 of Dreyer et al. (2005).

2.5.4.3 Palynofacies

No palynological data are available for FA5.

2.5.5 Facies Association 6 (Massive to Cross-Bedded Coarse-Grained Sandstones)

2.5.5.1 Description

Facies Association 6 (FA6) is only developed in the north-eastern part of the study area (e.g. wells 31/3-2 and 31/2-6, Figs. 2.3B, 2.5B). FA6 occurs in successions up to 10 m thick. It is typically underlain by FA4 across a sharp contact, or by FA2 and FA3 across sharp to erosional contacts, and is sharply or erosionally overlain by FA1, FA2 or FA3. FA6 is equivalent to Facies 6 and 7 of Dreyer et al. (2005).

FA6 comprises three facies (Facies 6a, 6b, 6c). Facies 6a typically comprises moderately to poorly sorted beds of structureless or planar-parallel laminated, coarse-grained sandstone with occasional sub-rounded to sub-angular gravel clasts. These coarse-grained sandstone beds (Facies 6a) occur in intervals up to 5 m thick, and are usually amalgamated or separated by intervals of planar-parallel laminated, fine-grained, carbonaceous sandstones (Facies 6b), similar to beds within Facies 4b. Facies 6c comprises cross-bedded, medium to very coarse-grained sandstones (cf. Facies 4a).Trace fossils are absent to sparse (BI of 0-2) and are dominated by *Skolithos*. Body fossils are rare, and consist of large bivalve shells (oysters?) in life position.

2.5.5.2 Interpretation

FA6 is interpreted to document the interaction between marine and riverine processes within an overall delta front to nearshore environment. This interpretation is based on: (1) variable sorting and grain sphericity, suggesting localised influx of fluvial sediment, (2) the paucity of body and trace fossils, which implies freshwater dilution of marine salinites and/or high sedimentation rates (e.g. Mac Eachern & Bann, 2008), (3) the proximal and upward-shallowing character of the underlying facies, which implies that FA6 represents a near-shoreline setting, and (4) the occurrence of brackish palynofacies markers that suggest proximity to a point of fresh-water discharge (Bell et al., 1984a; Whitaker, 1981; Dreyer et al., 2005). The structureless, poorly sorted, coarse-grained character and sharp bases and tops of many beds (Facies 6a) are similar to beds in Facies 2e, 3e and 4d, and therefore Facies 6a was interpreted to have been deposited by sediment-laden gravity flows (e.g. Nemec, 1995; Van den Berg et al., 2002; Mulder et al., 2003; Plink-Bjorklund & Steel 2004), perhaps as hyperpycnal flows in a distal mouth bar or delta front environment. In this context, Facies 6b corresponds to parallel-laminated siltstone

intervals deposited between individual mouth bar deposits (cf. Olariu et al., 2010), and Facies 6c was generated by the occasional action of waves or tractional currents.

2.5.5.3 Palynofacies

Palynofacies data from well 31/3-2 (Fig. 2.8) contains palynomorphs that are suggestive of high fresh-water influx within an overall deltaic or inner marginal marine-to-nearshore depositional environment (Bell et al., 1984a).

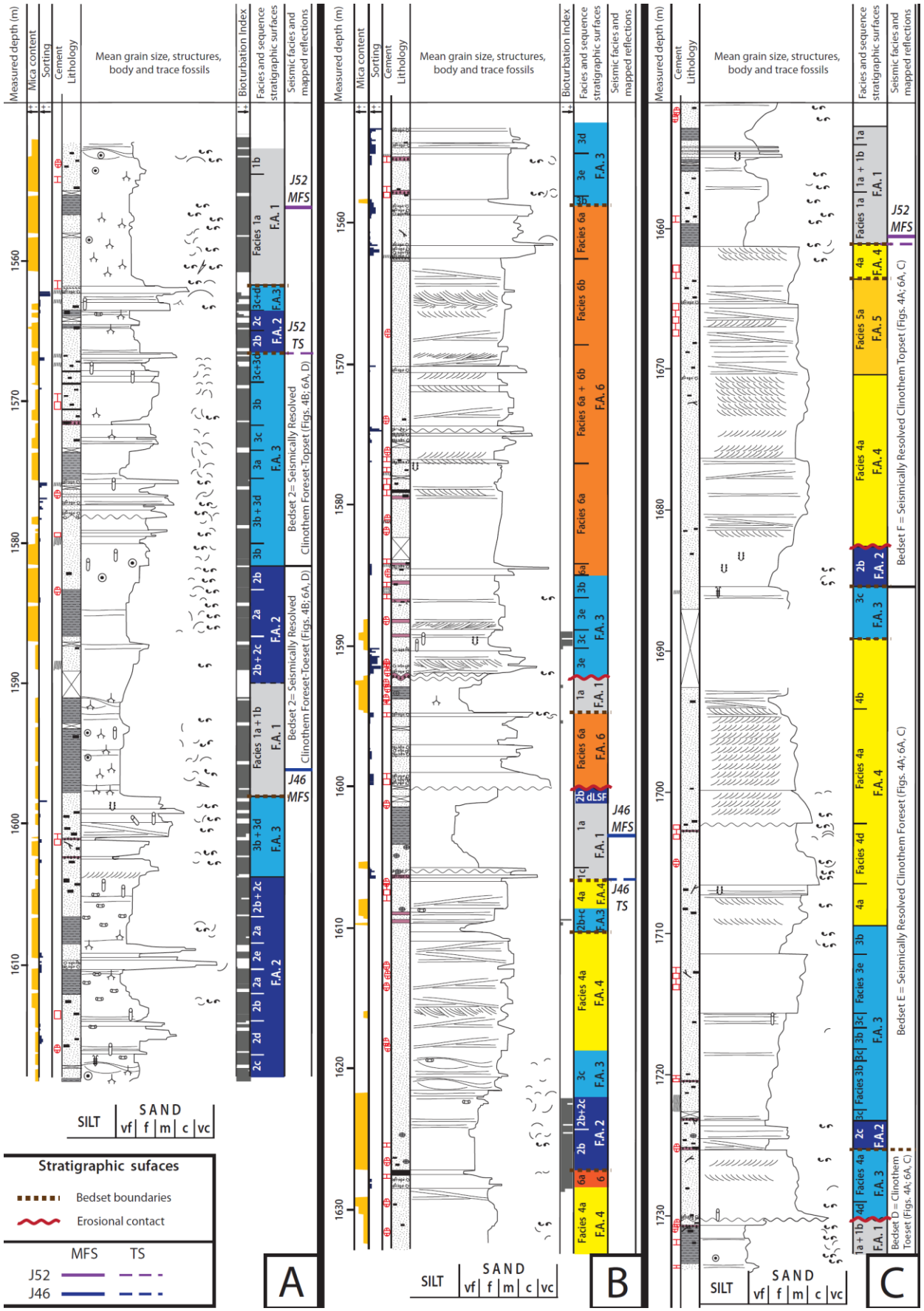
Measured depth (m)
Mica content
Sorting
Cement
Lithology
Mean grain size, structures, body and trace fossils
Bioturbation Index
Facies and sequence stratigraphic surfaces
Seismic facies and mapped reflections
J52 MFS
J52 TS
J46 MFS
J46 TS
Bedset 2= Seismically Resolved Clinothem Foreset-Toeset (Figs. 4B; 6A, D)
Bedset 2= Seismically Resolved Clinothem Foreset-Topset (Figs. 4B; 6A, D)
Bedset D = Clinothem Toeset (Figs. 4A; 6A, C)
Bedset E = Seismically Resolved Clinothem Foreset (Figs. 4A; 6A, C)
Bedset F = Seismically Resolved Clinothem Topset (Figs. 4A; 6A, C)
SILT
SAND
vf f m c vc
Stratigraphic sufaces
Bedset boundaries
Erosional contact
MFS TS
J52
J46
A
B
C

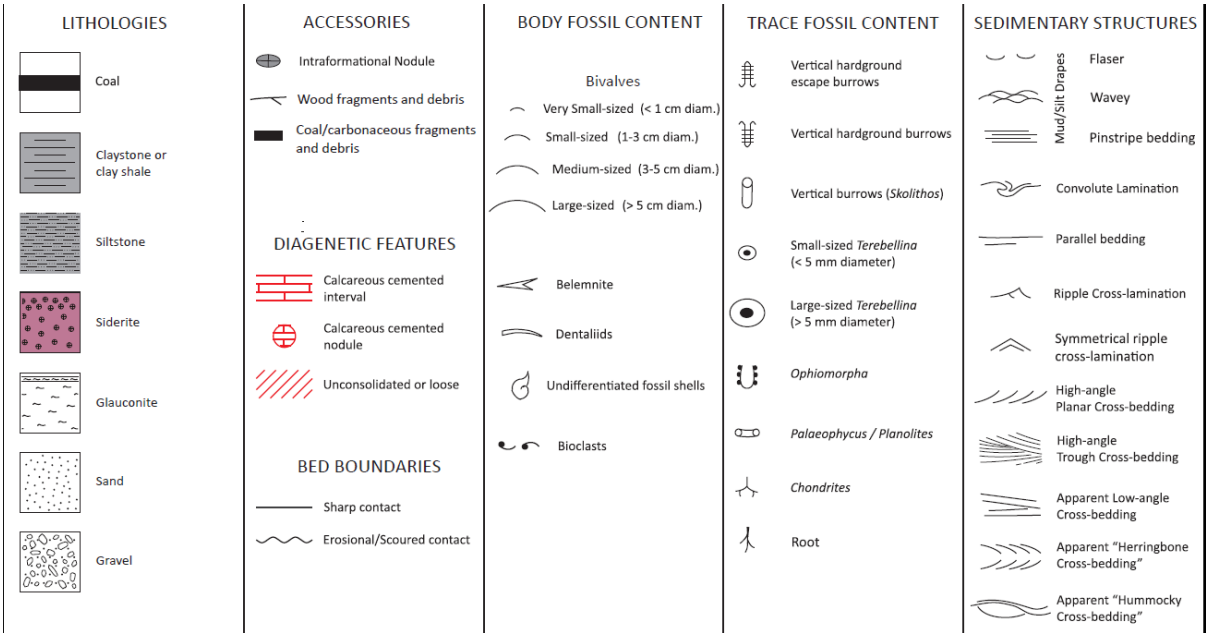

Figure 2.5. *Representative stratigraphic successions through the lower Sognefjord Formation, from various parts of the Troll Field (Fig. 2.3): (**A**) South-east (well 31/6-2); (**B**) North-east (well 31/2-6); and (**C**) West well (31/2-10). Sandstone-rich bedsets labelled D-F in well 31/2-10 correspond to those bounded by seismically resolvable clinoforms in Figures 4 and 6.*

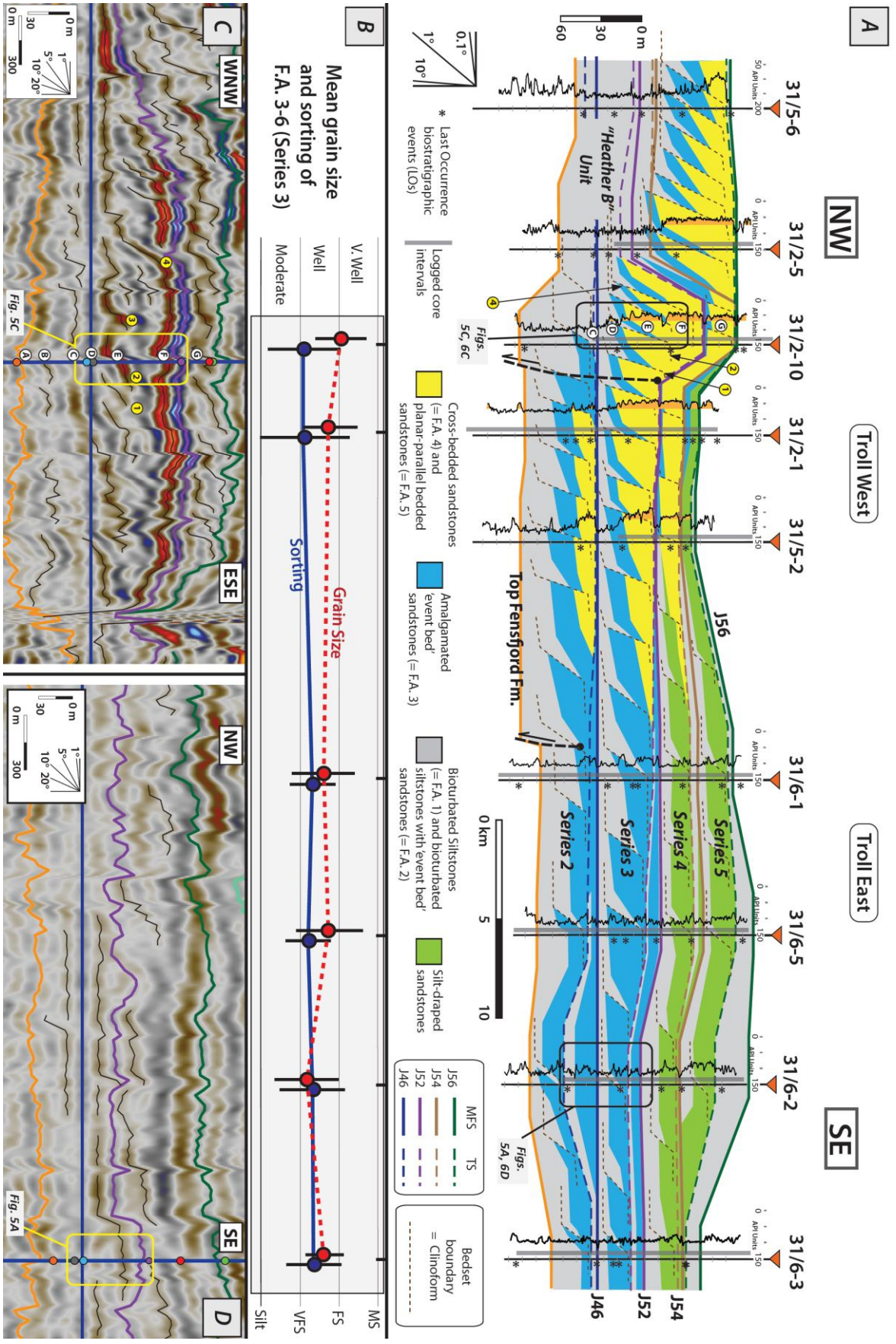
A
NW
Troll West
Troll East
SE
31/5-6
31/2-5
31/2-10
31/2-1
31/5-2
31/6-1
31/6-5
31/6-2
31/6-3
"Heather B" Unit
Top Fensfjord Fm.
J56
J54
J52
J46
Series 2
Series 3
Series 4
Series 5
Figs. 5C, 6C
Figs. 5A, 6D
0 km 5 10
* Last Occurrence biostratigraphic events (LOs)
Logged core intervals
Cross-bedded sandstones (= F.A. 4) and planar-parallel bedded sandstones (= F.A. 5)
Amalgamated 'event bed' sandstones (= F.A. 3)
Bioturbated Siltstones (= F.A. 1) and bioturbated siltstones with 'event bed' sandstones (= F.A. 2)
Silt-draped sandstones
MFS
TS
Bedset boundary = Clinoform
B
Mean grain size and sorting of F.A. 3-6 (Series 3)
V. Well
Well
Moderate
Grain Size
Sorting
MS
FS
VFS
Silt
C
WNW
ESE
Fig. 5C
D
NW
SE
Fig. 5A

Figure 2.6. *(**A**) SE-NW trending well correlation panel through the Sognefjord Formation in the Troll Field (Figs. 2.3B, 2.14A). A gamma ray curve is shown for each well, with sandstones (<70 API) highlighted in orange. "Series 2-5" bounded by regional maximum flooding surfaces ("J surfaces" of Partington et al., 1993) are identified, each corresponding to a set of westerly dipping clinoforms. "Series 2" and "Series 3" are discussed in this paper. The panel is flattened on the J46 maximum flooding surface, and oriented approximately parallel to the dip of the studied clinoforms (cf. Figs. 2.9-2.11). Sandstone-rich, clinoform-bounded bedsets in Well 31/2-10 are labelled C-G (cf. Figs. 2.4, 2,5, 2.6C). (**B**) Mean grain size and sorting of sandstone-rich deposits (Facies Associations 2-5) of "Series 3" along the same well correlation panel as Figure 2.6A. Bars about mean values represent the standard deviation. Grain size and sorting values are derived from hand-lens observation of cores, repeated at 5 cm intervals. VFS = very fine-grained sand; FS = fine-grained sand; MS = medium-grained sand; CS = coarse-grained sand; VCS = very coarse-grained sand. (**C**) and (**D**) Seismic cross-sections intersecting wells 31/2-10 and 31/6-2, and oriented sub-parallel to the correlation transect (Figs. 2.3B, 2.14A). Both cross-sections have been flattened on the J46 maximum flooding surface. Sandstone-rich, clinoform-bounded bedsets in Well 31/2-10 are labelled C-G (cf. Figs. 2.4, 2.5, 2.6C).*

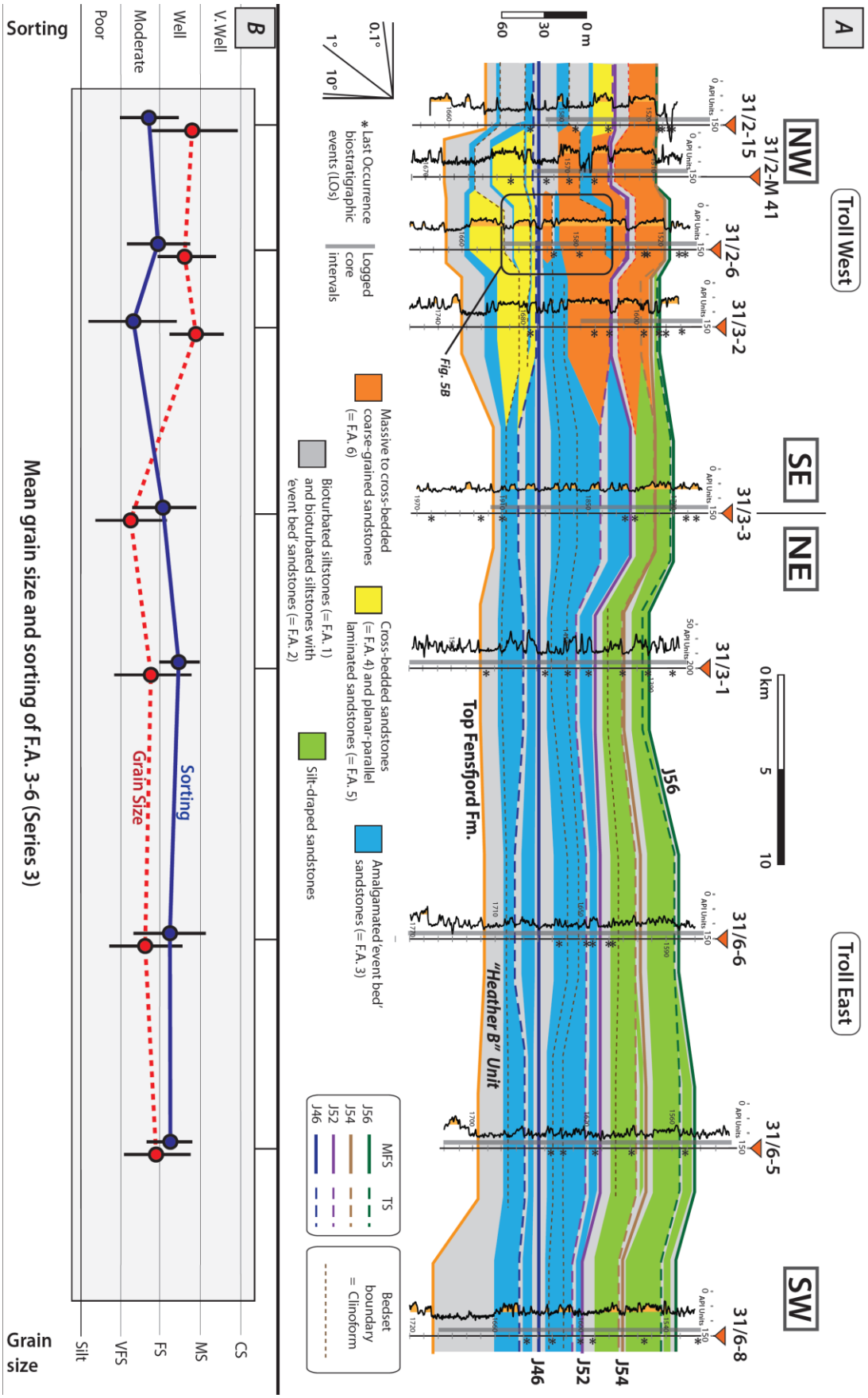
A
Troll West
Troll East
NW
SE
NE
SW
31/2-15
31/2-M 41
31/2-6
31/3-2
31/3-3
31/3-1
31/6-6
31/6-5
31/6-8
Fig. 5B
0 km
5
10
0 m
30
60
0.1°
1°
10°
* Last Occurrence biostratigraphic events (LOs)
Logged core intervals
Massive to cross-bedded coarse-grained sandstones (= F.A. 6)
Cross-bedded sandstones (= F.A. 4) and planar-parallel laminated sandstones (= F.A. 5)
Amalgamated 'event bed' sandstones (= F.A. 3)
Bioturbated siltstones (= F.A. 1) and bioturbated siltstones with 'event bed' sandstones (= F.A. 2)
Silt-draped sandstones
Top Fensfjord Fm.
"Heather B" Unit
J56
J54
J52
J46
MFS
TS
Bedset boundary = Clinoform
B
Sorting
V. Well
Well
Moderate
Poor
Grain Size
Sorting
CS
MS
FS
VFS
Silt
Grain size
Mean grain size and sorting of F.A. 3-6 (Series 3)

Figure 2.7. *(**A**) NE-SW trending well correlation panel through the Sognefjord Formation in the eastern portion of the Troll Field (Figs. 2.3B, 2.14A). The panel is flattened on the J46 maximum flooding surface, and oriented along the strike of the studied clinoforms (cf. Figs. 9-11). (**B**) Mean grain size and sorting of sandstone-rich deposits (Facies associations 2-5) of "Series 3" along the same well correlation panel as Figure 2.7A (cf. Fig. 2.6B).*

2.6 FACIES DISTRIBUTIONS AND STRATIGRAPHIC ARCHITECTURE

In this section, the distribution in cores and well logs of the facies associations documented above is described. These facies association are then related to distributions to stratigraphic architectures observed in cores, well logs and 3D seismic data.

2.6.1 Vertical Facies Successions

The facies associations described above are stacked into a series of 3-40 m thick, upward-coarsening successions that each records an upward increase in hydrodynamic energy (e.g. bedsets labelled in Fig. 2.5). From base to top, a complete upward-coarsening succession is composed of the following facies associations: bioturbated siltstones (FA1), bioturbated siltstones and 'event bed' sandstones (FA2), amalgamated 'event bed' sandstones (FA3), cross-bedded sandstones (FA4) and planar parallel-laminated sandstones (FA5). Cross-bedded sandstones (FA4) and planar parallel-laminated sandstones (FA5) are thin or absent in the south-east of the study area, and they are replaced by massive to cross-bedded coarse-grained sandstones (FA6) in the north-east of the study area (Figs. 2.5-2.7). The upward-coarsening facies successions described above are foreshortened in some wells by abrupt but minor facies dislocations across sharp-based intervals of FA3, FA4 and FA6 (e.g. FA3 abruptly overlies FA1 at 1593 m in Fig. 2.5B and 1730 m in Fig. 2.5C; FA4 abruptly overlies FA2 at 1683 m in Fig. 2.5C; FA6 abruptly overlies FA2 at 1600 m in Fig. 2.5B), recording localised, abrupt increases in hydrodynamic energy. Upward-coarsening successions are typically bounded by a sharp or erosional surface that is locally lined by a lag (Facies 1c, 2f, 3f) (Fig. 2.5).

The upward-coarsening successions may record increasing hydrodynamic energy in response to progressive shallowing of water depth, such that the successions are parasequences bounded by marine flooding surfaces (*sensu* Van Wagoner et al., 1990). However, in the absence of independent indicators of shoreline position and water depth, the successions may equally reflect conditions of progressively more energetic storm waves and/or currents driven by variations in climate, oceanographic circulation or shoreline palaeogeography (e.g. Storms & Hampson, 2005; Sømme et al., 2008), such that the successions constitute bedsets that formed without relative changes in sea level (cf. Hampson et al., 2008). Similarly, the abrupt, minor facies dislocations occurring locally within the upward-coarsening successions may reflect relative falls in sea-level (cf. Plint, 1988), increases in storm wave and/or current energy, or increased sand influx (e.g. Storms & Hampson, 2005). Distinguishing the potential origin(s) of the upward-coarsening successions from one dimensional (1D) core and well-log data is essentially impossible without consideration of the geometry, extent and associated shoreline position of the surfaces that bound the successions (Storms & Hampson, 2005), which in this case requires analysis of stratigraphic architecture in 3D seismic data. However, evidence for subaerial exposure as a proxy for shoreline position, in the form of rootlets, palaeosols and *Scoyenia* Ichnofacies (*sensu* Pemberton et al., 1992) at the top of the upward-coarsening successions, is noticeably absent throughout the Sognefjord Formation in the Troll Field area. Lower Oxfordian coal-bearing coastal plain deposits occur in the Bjorøy Formation near Bergen, onshore Norway (Fossen et al., 1996) and in the Sognefjord Formation in well 36/7-2 (Norwegian Petroleum Directorate, 2011), respectively situated 75 km to the south-east and 50 km to the north-east of the Troll Field (Fig. 2.3B). Evidences of palaeosols and rootlets in cores are missing everywhere but in well 32/4-1, situated ca. 10 km to the east of Troll East. There is no direct evidence that the shoreline lay within the Troll Field area at any point during Sognefjord Formation deposition, and therefore there is also no evidence in our dataset for shoreline retreat associated with the boundaries of the upward-coarsening successions.

Regional correlations constrained by biostratigraphic data indicate that several major flooding surfaces recognised throughout the northern North Sea occur within the Sognefjord Formation (J46, J52, J54 and J56 regional maximum flooding surfaces of Partington et al., 1993; Fig. 2.2B). These major flooding surfaces coincide approximately with the major subdivisions of the Sognefjord Formation reservoir in the Troll Field into “Series 2-6” (Figs. 2.4-2.7; Dreyer et al., 2005), and they also coincide with mappable seismic reflections (Figs. 2.4, 2.9, 2.10). The lower part of the Sognefjord Formation considered herein contains the J46 (top Callovian) and J52 (middle Oxfordian) regional maximum flooding surfaces, which coincide with the upper boundaries of “Series 2” and “Series 3” (Figs. 2.4-2.7). In core, both regional maximum flooding surfaces are characterised by concentrations of glauconite, faecal pellets, belemnites and shell fragments, indicating condensed sedimentation (Fig. 2.5). “Series 2” and “Series 3” are both up to 60 m thick, and each contains between one and four upward-

coarsening successions in any particular core or well-log section (Figs. 2.5-2.7). In sections where multiple upward-coarsening successions are stacked vertically within a "series", the successions are progressively thicker and more sandstone-rich from the base to the upper part of the "series" (e.g. Fig. 2.5C). The uppermost part of the "series" is marked by several metres of bioturbated siltstones (Facies 1a) (e.g. below J46 maximum flooding surface in Fig. 2.5A-B) and/or by a thinner, less sandstone-rich upward-coarsening succession (e.g. below J52 maximum flooding surface in Fig. 2.5A).

2.6.2 Areal Distributions of Facies Associations

In the south-eastern (palaeolandward) part of the Troll Field, upward-coarsening successions in both "Series 2" and "Series 3" consist mainly of FA2 and FA3, and are characterised by offshore-to-shoreface palynofacies that indicate low-to-moderate reworking (e.g. Figs. 2.5A, 2.6, 2.8). In contrast, upward-coarsening successions further west (palaeoseaward) are dominated by FA4 and FA5 in their upper part, whilst intervals of FA2 and FA3 are thin (Figs. 2.5-2.8). Palynofacies indicate prolonged and/or high-energy reworking (Fig. 2.8). In "Series 2", these successions pass westward into the shales of the Heather B unit (Fig. 2.6A). FA6 and deltaic or estuarine palynofacies occur only in the upper part of upward-coarsening successions in the north-east of the Troll Field (e.g., Figs. 2.5B, 2.6, 2.8). We follow Stewart et al. (1995) and Dreyer et al. (2005) in interpreting this areal distribution of facies associations to record deposition of each "series" in a mixed-process delta, which is internally subdivided into wave-dominated (FA2-5) and fluvial-dominated (FA6) environments. The detailed spatial distribution of these facies associations varies between "Series 2" and "Series 3" (Figs. 2.6-2.8), and potentially between the upward-coarsening successions of which the "series" are composed, reflecting the spatial variations in depositional process inherent to a mixed-process delta (e.g. Bhattacharya & Giosan, 2003; Ainsworth et al., 2011). Additional facies associations that display evidence of marked tidal influence occur in the upper part of the Sognefjord Formation (Figs. 2.6-2.7; Dreyer et al., 2005); these facies associations are not documented in this paper.

In "Series 2" and "Series 3", palaeocurrents are generally oriented towards the west or south-south-west, although more diverse palaeocurrent directions occur in FA6 in the north-eastern part of the Troll Field (Fig. 2.8; Nilsen et al., 1993). Handspecimen observations of cores, taken at 5 cm intervals from "Series 3", show that grain size and sorting trends of sandstones reflect the lateral distributions of facies associations described above (Figs.

6B, 7B). Sandstones in the south-eastern part of the Troll Field are fine-grained on average; medium- and coarse-grained sandstones are rare and restricted to thin event beds. In the west, however, the average grain size is distinctly coarser and dominated by medium-grained sandstone, although the overall range of grain sizes is larger. The presence of coarser, more poorly-sorted sandstones in the north-east is interpreted to indicate greater proximity to a fluvial sediment input point (e.g. Dreyer et al., 2005). Sandstone grains are generally sub-rounded throughout the study area, but gravel clasts are sub-angular to rounded.

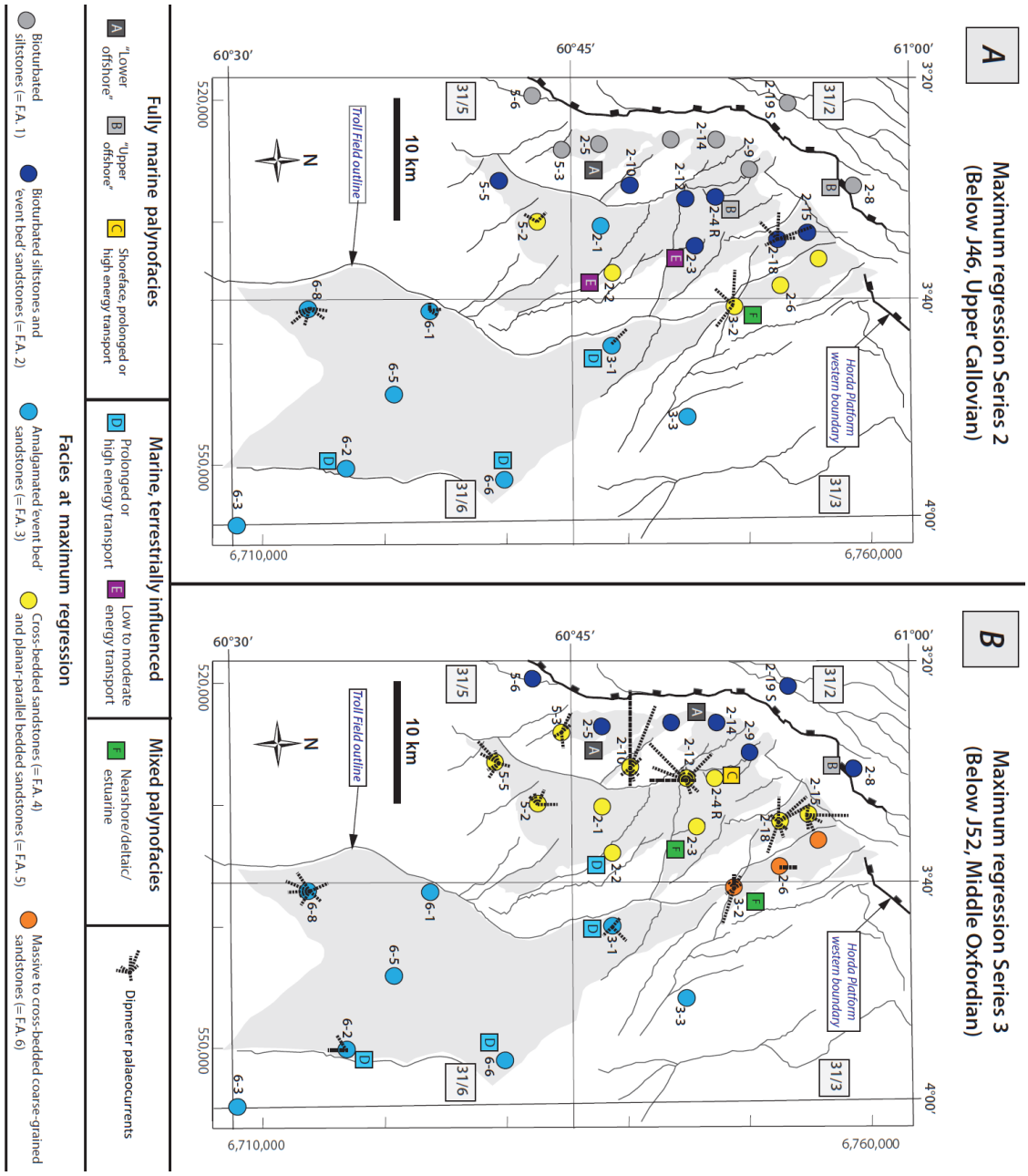

Figure 2.8. *Maps showing the main palaeocurrents, palynofacies and maximum regression facies across the Troll Field area in (**A**) "Series 2" and (**B**) "Series 3" (Figs. 2.4, 2.6, 2.7). Major faults are shown. Palaeocurrent interpretation of dipmeter data from Nilsen et al. (1993); each oriented line indicating a palaeocurrent represents the mean of several measurements, with the length of each line depending on the quality and quantity of data, and vertical extent over which the measurements are consistent. Facies data are from direct core observations, or by observations of core photos available online (NPD website, 2012). Qualitative and quantitative wireline log characteristics of the facies associations observed in cored intervals have been used to guide interpretations of the main facies associations in uncored intervals and wells. Palynofacies data and interpretations are from Whitaker (1981, 1982a, 1982b, 1983, 1985), Bell et al. (1984a, 1984b) and Duxbury et al. (1984a, 1984b).*

2.6.3 Seismic-Stratigraphic Architecture

Mapping of reflections in 3D seismic data shows that "Series 2" and "Series 3" each comprise a set of westerly prograding clinoforms (Figs. 2.6, 2.7, 2.9, 2.10). The top of each clinoform set is marked by a regional maximum flooding surface (labelled J46 and J52 in Figs. 2.6, 2.7, 2.9, 2.10). Upward-coarsening successions (or 'bedsets') within each "series" correspond to stratal packages bounded by clinoforms (i.e. clinothems *sensu* Rich, 1951), some of which are seismically resolved (Figs. 2.6C-D, 2.9, 2.10). The contrast in acoustic properties of facies associations juxtaposed across some clinoform surfaces is presumably sufficient to generate a seismic reflection, although core and well-log data contain additional upward-coarsening successions that are not seismically imaged. At the resolution of the seismic data, successive clinothems are stacked laterally with little or no vertical aggradation, indicating implying near-horizontal regressive trajectories (*sensu* Helland-Hansen & Hampson, 2009), implying that their bounding clinoforms are not linked to episodic rises in relative sea-level (or a proxy for relative sea-level represented by the clinoform topsets). As discussed previously, the clinoforms can also not be demonstrably linked to landward migration of the shoreline across flooding surfaces, because preserved shoreline deposits only lie outside of the study area.

Thus, the observed seismic-stratigraphic architecture favours interpretation of the clinothems as bedsets that formed independently of relative changes in sea-level. From this interpretation, it follows that each clinoform set represents a single episode of regression, with each clinothem representing an increment of regression. Seismically imaged clinoforms represent geomorphological "snapshots" of the ancient depositional surface, taken when regression was temporarily interrupted. Regional maximum flooding surfaces (e.g. J46 and J52 in Figs. 2.6C-

D, 2.9, 2.10) define the "seismic envelopes" of clinoform sets. In cores and well-logs, each regressive clinoform set is represented by vertically stacked upward-coarsening successions that are progressively thicker and more sandstone-rich. Corresponding transgressive deposits are too thin to be seismically resolved, but are probably represented in cores and well-logs by intervals of bioturbated siltstones and thin, sandstone-poor upward-coarsening successions that cap regressive successions and underlie maximum flooding surfaces (e.g. below J46 and J52 maximum flooding surfaces in Fig. 2.5A-B). Each "series" therefore represents a regressive-transgressive cycle (or genetic sequence *sensu* Galloway, 1989) in which the regressive clinoform set and overlying transgressive deposits are separated by a surface of maximum regression (*sensu* Helland-Hansen & Gjelberg, 1994, equivalent to a transgressive surface *sensu* Van Wagoner et al., 1990 and Embry, 1995).

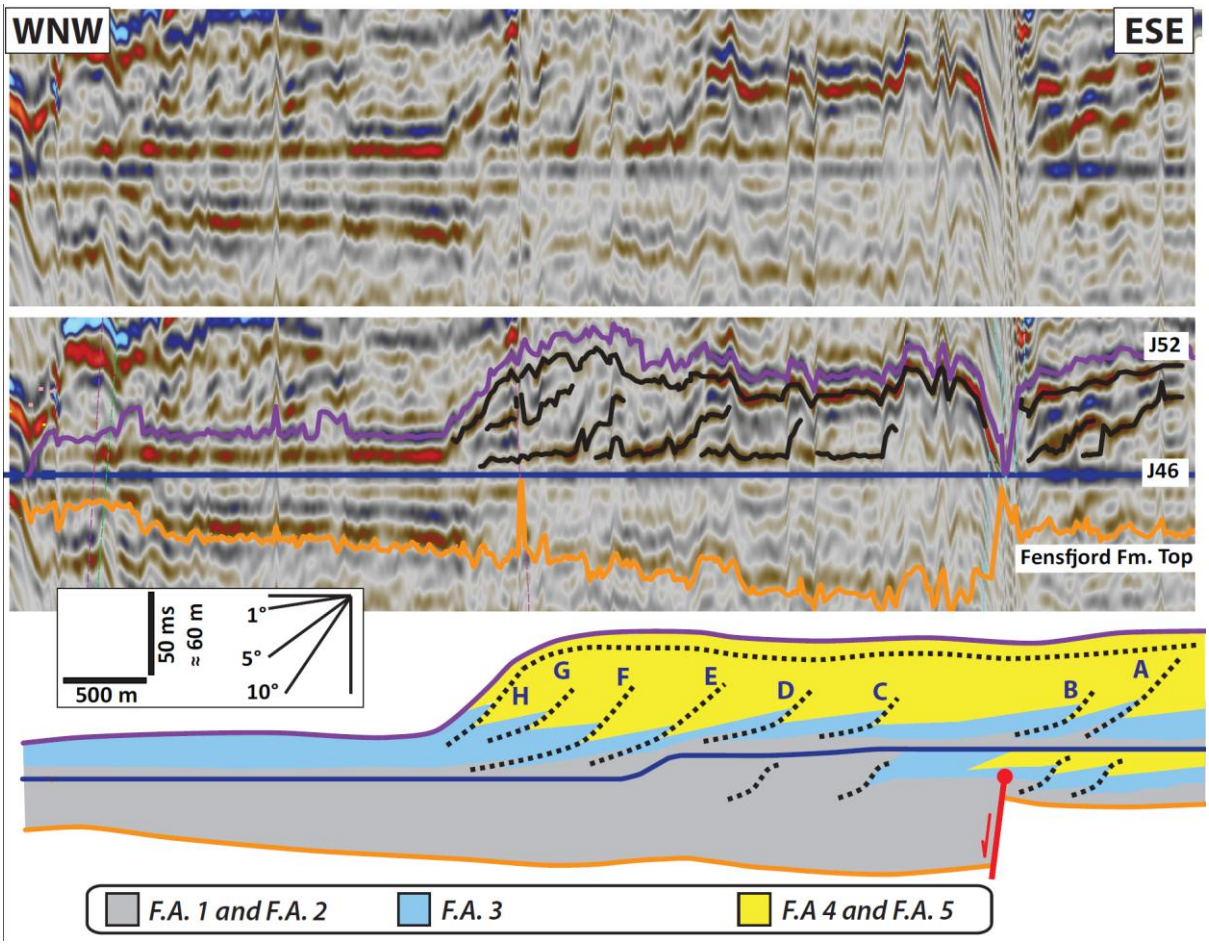

Figure 2.9. *(**A**) Uninterpreted and (**B**) interpreted, representative seismic cross-section showing clinoforms in the western part of the Troll field (Figs. 2.3B, 2.14A). The cross-section is flattened along the interpreted J46 maximum flooding surface. Westerly-dipping oblique clinoforms with narrow or absent topsets and steep foreset are observed in "Series 3", between reflections labelled J46 and J52. Calculated foreset dip angles and heights of clinoforms A-H are shown in Figure 2.10. (**C**)*

Interpretation of the seismic cross-section with J46 datum surface assigned geomorphological shape based on height and distribution of underlying clinoforms, and facies associations inferred by extrapolation from nearby cored wells 31/5-2 and 31/2-1. This interpretation implies fault-related thickening during the deposition of the Late Callovian "Heather B" unit (Series 2); however, fault activity ceased by the time that the sandstones of the lower Sognefjord Formation started to be deposited.

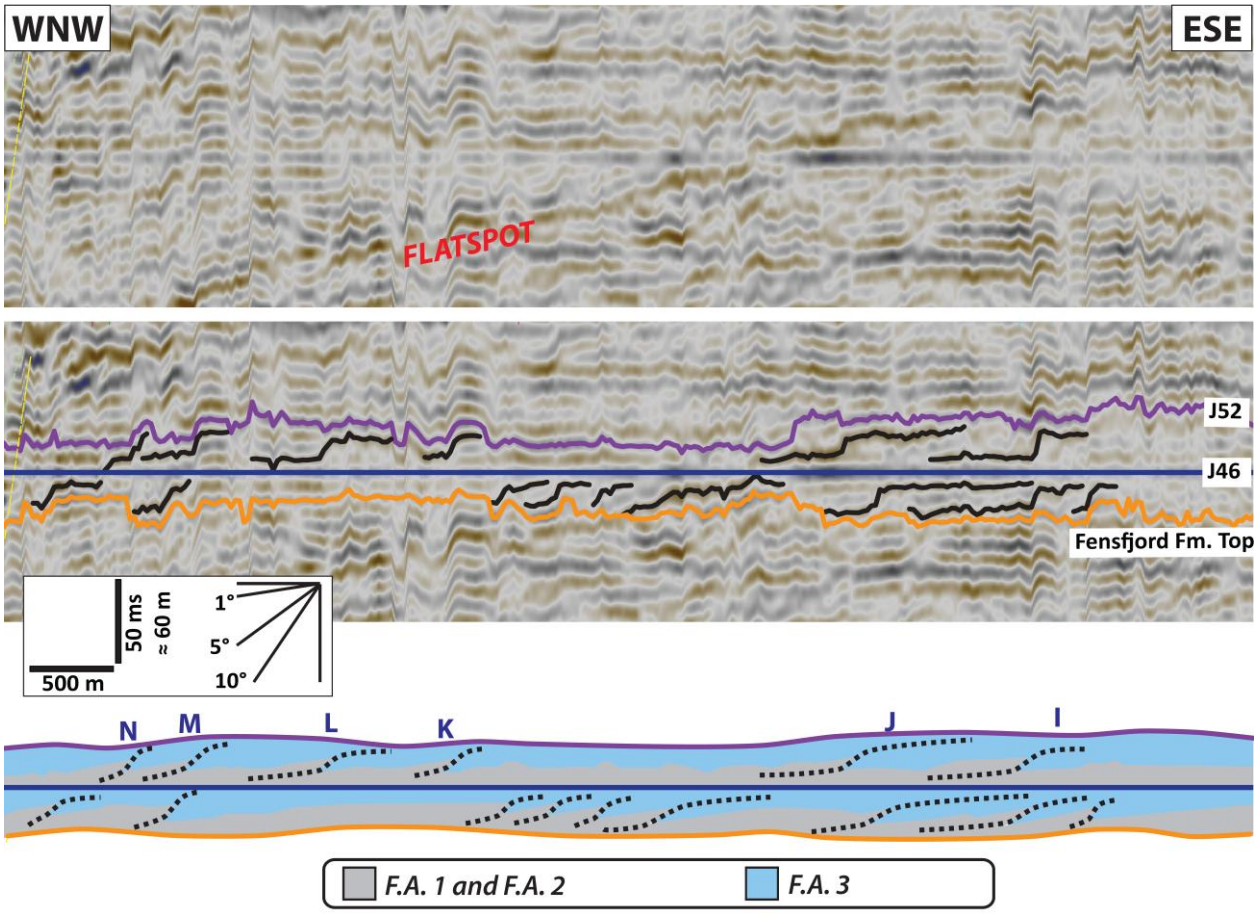

Figure 2.10. *(**A**) Uninterpreted and (**B**) interpreted, representative seismic cross-section showing clinoforms in the south-eastern part of the Troll field (Figs. 2.3B, 2.14A). The cross-section is flattened along the interpreted J46 maximum flooding surface. Westerly-dipping sigmoidal clinoforms with well-developed topsets and relatively gentle foreset dips are observed in both "Series 2", between reflections labelled Fensfjord Formation top and J46, and "Series 3", between reflections labelled J46 and J52. Calculated foreset dip angles and heights of clinoforms I-N in "Series 3" are shown in Figure 2.10. (**C**) Interpretation of the seismic cross-section with facies associations inferred by extrapolation from nearby cored wells 31/6-8, 31/6-1, 31/6-5 and 31/6-2.*

2.6.4 Clinoform Geometry

Well correlation panels and seismic cross-sections oriented west-east, from palaeoseaward to palaeolandward (Stewart et al., 1995; Dreyer et al., 2005), show that ”Series 2” and “Series 3” both thicken westwards. At the point of maximum thickness the maximum flooding surface at the top of the “series” rolls over to define a topset-foreset-toeset clinoform geometry at the position of maximum regression (Figs. 2.6C, 2.9). Furthermore, an isochron of the lower Sognefjord Formation indicates that the clinoform rollover and associated thinning at maximum regression of the “Series 3” clinoform set is linear, strikes NNE-SSW and is laterally extensive for at least 30 km along depositional strike (Fig. 2.11A). The clinoform-set rollover of this, and all, “series” is situated near and trends sub-parallel to the western edge of the Horda Platform (Fig. 2.11).

Maximum amplitude attribute maps extracted from ”windows” within the lower Sognefjord Formation show that a series of NNE-SSW oriented, laterally extensive, linear to slightly curvilinear anomalies occur throughout the Troll Field (Fig. 2.11B-C). Seismic cross-sections perpendicular to these linear anomalies show that they are situated at the intersection of the seismic attribute extraction windows with the foresets of individual clinoforms and with the roll-over positions of clinoform sets at maximum regression (Fig. 2.11D). In particular, the upper extraction window (Fig. 2.11B) defines the foresets of the clinoforms, whilst the lower window (Fig. 2.11C) defines the rollover position of the “Series 3” clinoform set. The map-view amplitude patterns shown by the attribute extractions conform to the NNE-SSW strike direction of the ”Series 3” clinoform set rollover (Fig. 2.11A). Therefore, all of the individual clinoforms and the major flooding surfaces that bound the clinoform sets are oriented parallel to each other, and share an overall NNE-SSW strike (Figs. 2.11, 2.12). This strike orientation is nearly uniform throughout the study area (Fig. 13A); it is sub-parallel to the overall structural grain (Figs. 2.11, 2.12) and the dominant palaeocurrent directions are either sub-parallel or orthogonal to it (Fig. 2.8).

Individual clinoforms form near-linear segments of 1-13 km strike extent (Fig. 2.12). In the eastern part of the Troll Field, clinoforms have small heights (10-30 m), large dip extents (1-3 km) and gentle foreset dips (1°-6°, measured relative to the flattened top-Fensfjord datum surface in Figs. 2.6C-D, 2.9, 2.10, 2.11D, 2.13B-C). Towards the west, the clinoforms gradually become higher (15-55 m), narrower (0.2-1.5 km) and steeper (5°-14°) (Figs. 2.12, 2.13B-C), resulting in an increasingly well-defined oblique profile. Clinoform topsets are well developed in the southeast of the study area, but are narrow or absent in the westernmost part, such that clinoform foresets may be top-truncated. As previously suggested by Dreyer et al. (2005), these steeply sloping clinoform foresets would create the geomorphological gradient necessary to trigger and sustain the episodic

sediment gravity flows and storm-related combined flows recorded by coarse-grained event beds in FA2 and FA3 (Facies 2d, 2e, 3d and 3e).

The topset-to-foreset portion of clinoforms in the southeast of the Troll Field area is composed largely of well-sorted, hummocky cross-stratified, fine-grained sandstones (FA2 and FA3), whereas the foreset-to-bottomset portion is composed of offshore siltstones (FA1) (Fig. 2.10). An important inference derived from this facies composition is that these clinothems accumulated below fairweather wave base. Towards the west, however, the whole clinoform foreset is composed of well-sorted, cross-bedded, fine- to coarse-grained, upper shoreface sandstones (FA4) (Fig. 2.9). This suggests that they accumulated in an environment that was continuously reworked by strong currents, either above or below fairweather wave base.

A
B
C
D
Figs. 4A, 5C, 6C
Clinoform set rollover line (Series 3)
Clinoform set rollover line (Series 5)
Fig. 9
Fig. 10
Fig. 11D
Troll Field outline
TWT (s)
0.12
0
10 km
N
60°30′
60°45′
61°00′
3°20′
3°40′
4°00′
520,000
550,000
6,710,000
6,760,000
Figs. 5A, 6D
Flatspot
Horda Platform western boundary
25,000
W
E
31/2-5
31/2-F6H
20-40 ms
40-60 ms
Top Fensfjord Fm.
J46
J52
500 m
60 ms

Figure 2.11. *Seismically derived maps illustrating the plan-view geometry of clinoforms identified in cross-section (Figs. 2.9, 2.10) and the stratigraphic intervals that contain them. (**A**) Time thickness map of the lower Sognefjord Formation (from the top of the Fensfjord Formation to the J52 transgression). (**B**, **C**) Maximum amplitude attribute maps extracted from windows placed (**B**) 20-40 ms and (**C**) 40-60 ms above the top of the Fensfjord Formation (constructed with the seismic volume flattened on the Fensfjord Formation top surface). (**D**) Uninterpreted (upper) and interpreted (lower) seismic cross section (Figs. 2.3B, 2.11A-C) oriented approximately perpendicular to the thickness trends in Figure 2.11A, the linear amplitude anomalies in Figure 2.11B-C, and clinoforms in Figure 2.12.*

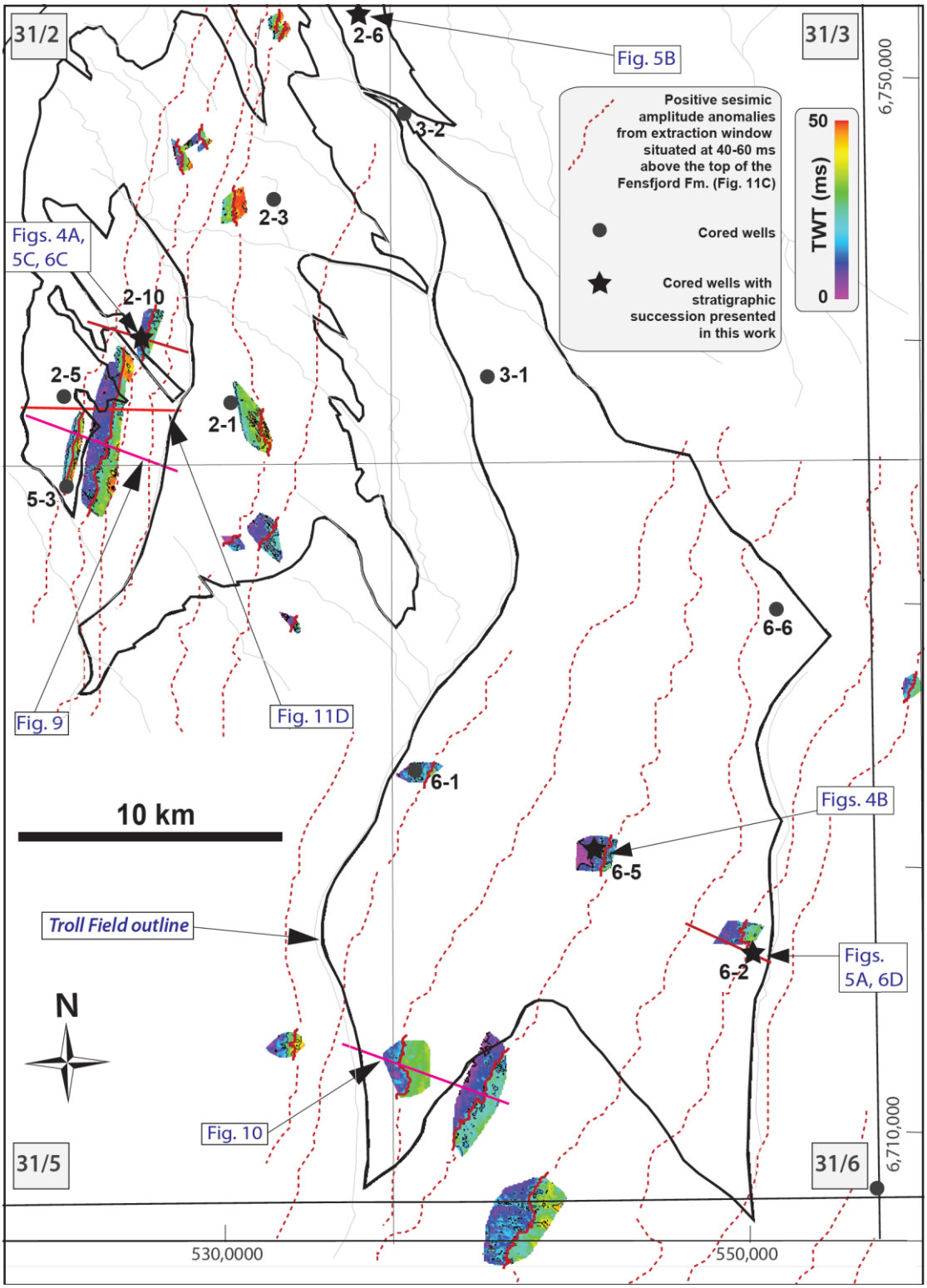

Figure 2.12. *Time-thickness map of selected clinoforms within "Series 3", with their thickness shown relative to the underlying J46 surface as an approximation of clinoform height. Individual clinoforms form near-linear segments of 1-13 km strike extent, all showing a consistent NNE-SSW strike direction and westerly dips. The clinoforms generally tend to become narrower and steeper towards the west.*

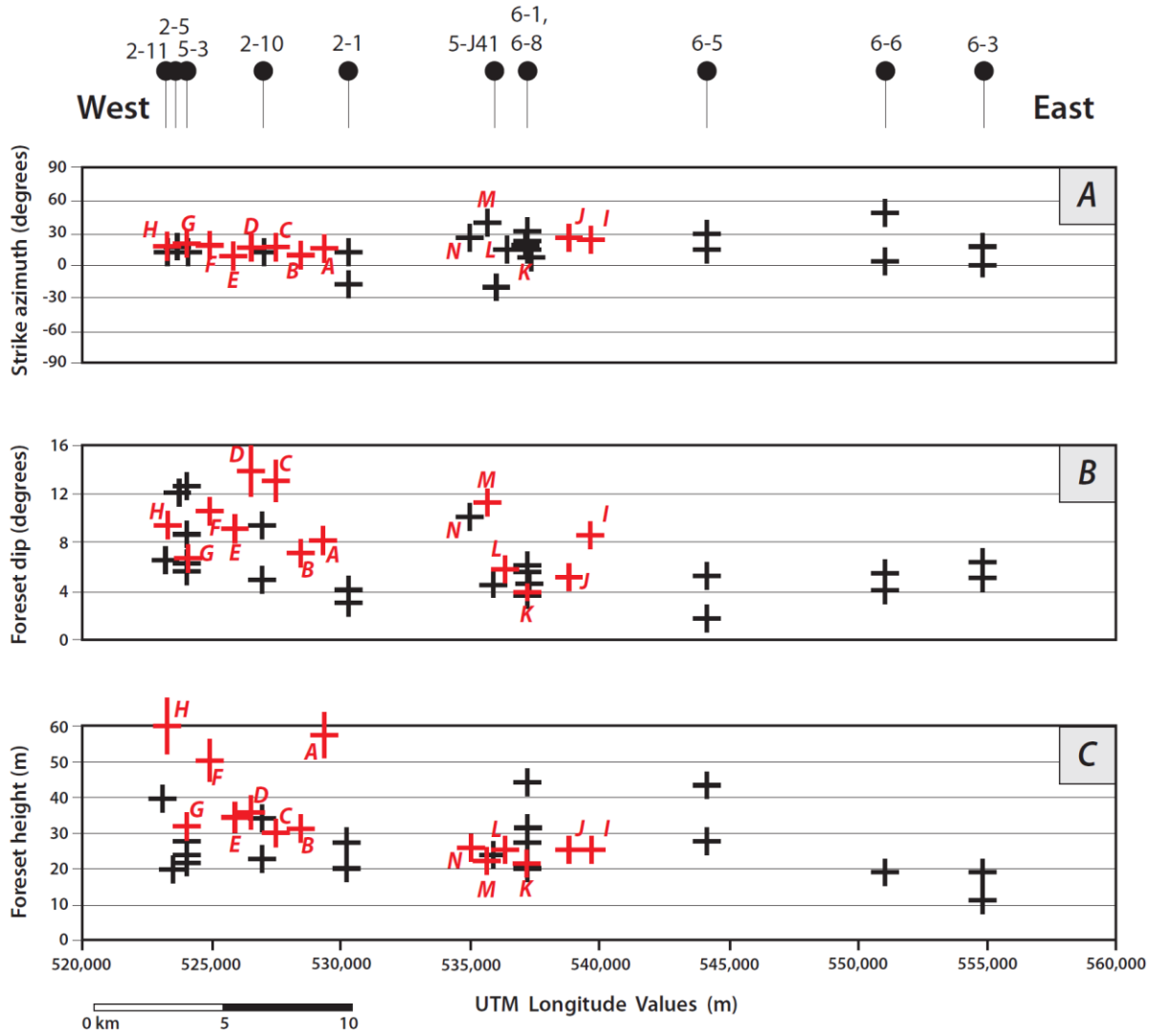

Figure 2.13. *Graphs showing morphological parameters of selected, clearly resolved clinoforms following depth conversion of seismic profiles oriented perpendicular to clinoform strike: (**A**) clinoform strike azimuth relative to north; (**B**) clinoform foreset dip; and (**C**) clinoform foreset height averaged along their strike. The data are arranged according to the approximate UTM longitude values of the clinoforms. Clinoforms shown in red and labelled A-N are shown in Figures 2.9 and 2.10. In the east, clinoforms generally have small heights (10-30 m) and relatively gentle westerly dips (1˚-6˚). Towards the west, clinoforms become thicker (20-50 m) and steeper (4˚-14˚). However, the NNE-SSW strike azimuth is constant throughout the study area.*

2.7 DEPOSITIONAL MODELS FOR THE LOWER SOGNEFJORD FORMATION

The facies characteristics and distributions, stratigraphic architecture and palaeocurrent distributions of the lower Sognefjord Formation suggest that each regressive-transgressive "series" consists principally of a clinoform set that prograded consistently towards the west through the accretion of successive clinothems. Clinoforms share the same strike direction, but their cross-sectional geometry evolves from sigmoidal in the east to more oblique and steeper towards the west, concomitant with changes in grain size and facies character that record increased hydrodynamic energy towards the west (Figs. 2.9-2.13). The parts of the depositional system represented in the study area were fully subaqueous and sand-prone, with local fluvial sediment influx in the northeast and a high degree of sediment reworking by waves and currents towards the south and southwest (Fig. 2.14). These characteristics are consistent with deposition in a delta with significant wave influence, as interpreted previously for the lower Sognefjord Formation (Stewart et al., 1995; Dreyer et al., 2005), but delta plain deposits and the deltaic shoreline are only preserved east of the Troll Field (Figs. 2.3A, 2.14). Four depositional models that may account for the key features summarised above are discussed below. The key elements of each model are first outlined, and then compared against observations that either support or refute the model.

A
Maximum regression Series 3 (below J52)
B
Early progradation Series 3
C
Late progradation Series 3
Wells with cores logged
Wells
Dipmeter palaeocurrents
Troll Field outline
10 km
N
Boundary of seismic surveys
Figs. 4A, 5C, 6C
Fig. 11D
Fig. 9
Fig. 10
Fig. 6-15
Fig. 7
Fig. 4B
Figs. 4A-B
Figs. 5A, 6D
Break in slope at rollover of "series 2" maximum regressive clinoform
Figs. 6, 15B-C
Fig. 15A
Subaqueous delta slope
Subaerial delta slope
Onlap on marine substrate ?
Bypassed submarine platform
Shoreline break
Subaqueous delta slope = Shelf edge break = J52 rollover line
Figs. 6, 15E
Marine currents
Clinoform rollover; Break in slope
Clinoform progradation direction
SUBAERIAL DELTA
Delta top and terrestrial facies
Delta front (= F.A. 6)
SUBAQUEOUS DELTA
Bioturbated siltstones and HCS fine-grained sandstones with coarse-grained 'event beds' (= F.A. 2-3)
SUBAERIAL OR SUBAQUEOUS DELTA
Cross-stratified to planar parallel stratified sandstones (= F.A. 4-5)
MEDIUM-OUTER SHELF
Prodelta and Offshore (= F.A. 1)

Figure 2.14. *(**A**) Map showing distribution of facies associations directly below surface of maximum regression in "Series 3", based on the maximum amplitude attribute map extracted from a window situated 40-60 ms above the top of the Fensfjord Formation (Fig. 2.11C). (**B, C**) Interpretive palaeogeographic maps relating clinoform geometry to facies character and depositional environments during (**B**) early and (**C**) late stages of clinoform-set regression in "Series 3". The inferred shoreline position is drawn to the east of the study area. Changes in facies character and clinoform geometry towards the west are interpreted to reflect: (1) increased wave energy , resulting in deepening of mean fairweather wave and current base (MFWCB); and (2) increased coarse-grained sediment flux, due to greater proximity to a river outlet and/or greater efficiency of marine sediment transport.*

2.7.1 Spit Fronting a Tidal Back-basin

The first model interprets a spit system to the west that sheltered a coeval embayment or back-basin to the east (Fig. 14 of Dreyer et al., 2005). The top of the spit was probably elevated above the mean low tide (cf. Evans, 1942), and may have comprised aeolian dunes and beach ridges (cf. Nielsen et al., 1988; Zecchin et al., 2010). Comparison with Pleistocene-to-Recent spits indicates that the subaerially exposed spit top was probably underlain by a more areally extensive subaqueous spit platform constructed by accretion of sand dunes that were transported by longshore currents (cf. FA4 and FA5) (Nielsen et al., 1988; Nielsen & Johannessen, 2009). The subaqueous spit platform has a greater volume and higher preservation potential than the subaerially exposed spit top (Nielsen & Johannessen, 2001, 2009). The back-basin lying to the east of the spit was sheltered from wave energy and was thus probably muddy. However, it may have been locally supplied with sand by a combination of: (1) storm washover from the spit to the west; (2) tidal currents entering the southern entrance of the embayed back-basin; and (3) fluvially fed bay-head deltas from the coastal plain to the east.

The spit model explains some of the spatial variability in facies associations across the study area, in particular the occurrence of a shoreline-parallel belt of cross-bedded sandstones (FA4 and FA5) in the west of the study area (Fig. 2.14A), where the model was first proposed (Dreyer et al., 2005). It also accounts for southward- and southwestward-directed palaeocurrents in these sandstones (Fig. 2.8), which can be attributed to the action of longshore currents. However, the spit model does not explain three key observations. Firstly, seismic data indicate a simple geomorphology of near-linear clinoforms that dip consistently to the west (Figs. 2.11B-C, 2.12, 2.13), rather than the more complex geometries that characterise Recent-to-modern spits (e.g. recurved tips in

plan view, with clinoforms locally dipping perpendicular to the shoreline trend; Nielsen et al., 1988; Nielsen & Johannessen, 2009) and sheltered back-basins (e.g. embayed margins in plan view, with clinoforms dipping towards the centre of the back-basin), Secondly, there are no preserved remnants of organic-rich mud and peat deposits, such as those developed at the top and behind Recent-to-modern spits (e.g., Redfield, 1965; Nielsen & Johannessen, 2001, 2009; Baily & Pearson, 2007). Thirdly, the interpretation of a sheltered back-basin in the east of the study area is contradicted by the abundance here of high-energy event beds (Facies 2d, 2e, 3d and 3e, within FA2 and FA3 in Figs. 2.5A, 2.6A, 2.10) and strongly reworked marine palynofacies (Fig. 2.8).

2.7.2 Subaqueous Clinoforms of a Compound-Clinoform Delta

This second model interprets that clinoforms throughout the southern part of the study area were formed as part of a sand-prone subaqueous deltas, fed from a river outlet situated to the northeast and sculpted by the action of southward-flowing marine currents (Figs. 2.14B-C, 2.15). The increase in clinoform height towards the west (Fig. 2.10C) suggests that clinoform progradation occurred across a westward-sloping seafloor. The increase in grain size and change from sigmoidal to oblique clinoform geometry towards the west imply that clinothems were fed by a progressively greater coarse-grained sediment flux, due to: (1) increased proximity to, and/or volume of, riverine sediment input; and (2) increased wave and/or current energy, related to a deeper mean fairweather wave and current base, within a fully subaqueous environment (Figs. 2.14B-C, 2.15B-D). In the context of the subaqueous clinoform model, deposits of FA4 and FA5 in the west of the study area (Fig. 2.14C) reflect the establishment of continuous, high near-bed shear stress conditions due to strong unidirectional currents. Such currents may have sculpted offshore sand ridges of a size below seismic resolution, as suggested in some previous interpretations of the Sognefjord Formation (Whitaker, 1984; Hellem et al., 1986). Deposits of FA6 in the northeast of the study area are interpreted as the delta-front deposits of a subaerial delta, which formed at the river outlet that supplied sediment to the entire delta system (Figs. 2.14B-C, 2.15A). No subaerial clinothems are observed in seismic data in this portion of the study area, probably because they are too small or too uniform in their internal acoustic properties to be resolved. The relatively localised subaerial delta is inferred to pass along depositional strike into a current-dominated subaqueous delta (Figs. 2.14B-C, 2.15A-B).

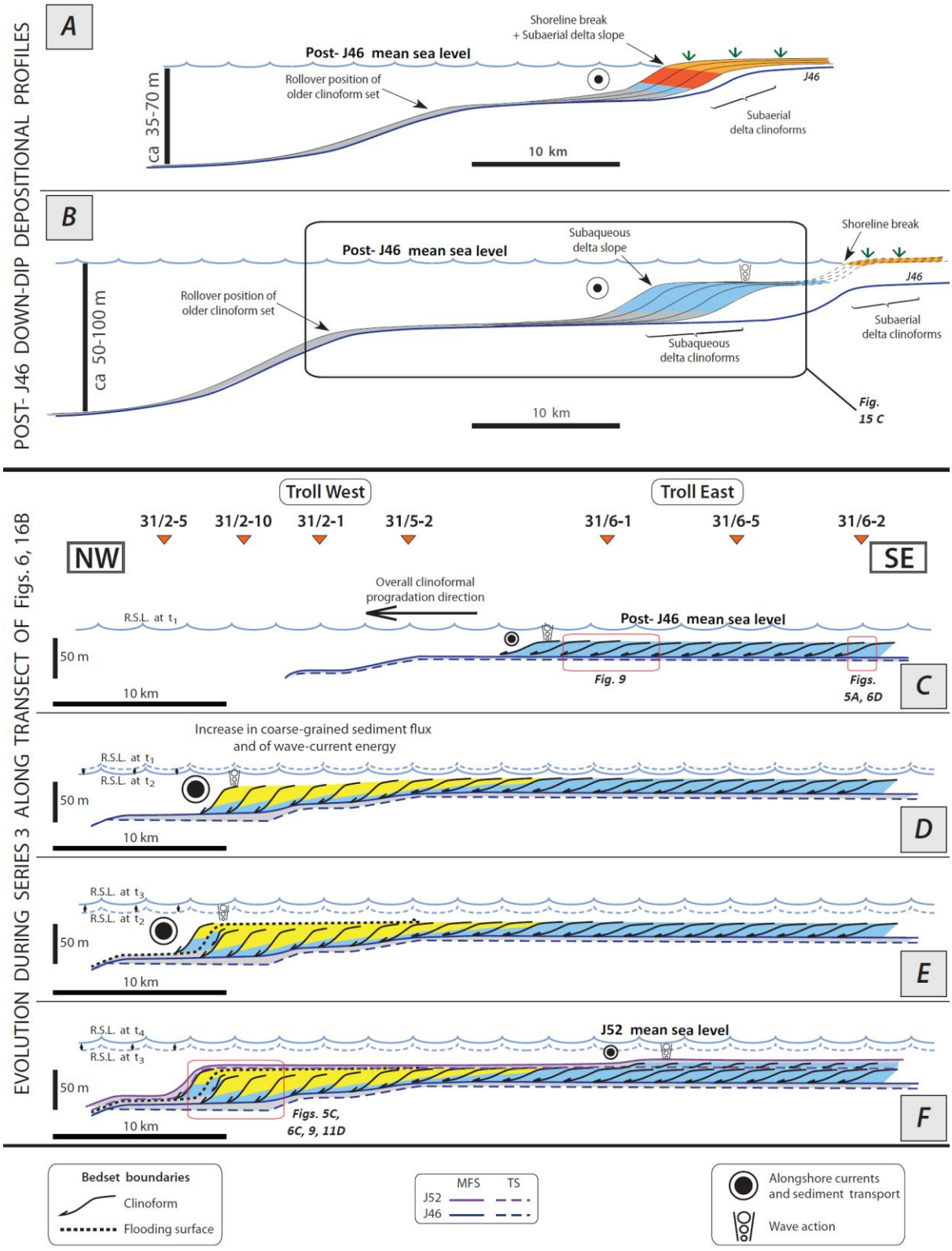

Figure 2.15. *(**A, B**) Idealized cross-sections oriented along depositional dip through the (**A**) northern and (**B**) southern parts of the Troll Field and adjoining areas (Fig. 2.14B), illustrating the compound clinoform delta model during early progradational of "Series 3". (**C-F**) Idealized depositional-dip-oriented cross-sections illustrating the temporal evolution of the "Series 3"*

*subaqueous clinoform set using the compound clinoform delta model (Figs. 2.15B). The model envisions westward-prograding clinoforms fed by currents flowing parallel to the clinoform strike. (**C**) During early progradation, subaqueous clinoforms prograded across the eastern part of the Troll Field (Fig. 2.14B). (**D**) Subsequently, the clinoforms continued their westwards progradation onto a sloping seafloor, synchronous with increases in coarse-grained sediment flux and alongshore current energy (Fig. 2.14C). (**E**) Transgression is marked by abandonment of the clinoform set, and localised development of thin, upward-coarsening successions that may contain sub-seismic clinoforms in the southeast (interval between surfaces labelled J52 TS and J52 MFS in Fig. 2.5A).*

The majority of the diagnostic features proposed by Cattaneo et al. (2003) for the recognition of ancient subaqueous deltas can be identified in the Troll Field area, especially in its eastern part (Table 2.1). The subaqueous clinoform interpretation explains the occurrence of well-developed, fully submarine clinoform topsets (Figs. 2.9, 2.10, 2.14A) and absence of subaerial deposits. This model also accounts for the occurrence of near-linear clinoforms and facies association belts that are consistently oriented sub-parallel to the inferred shoreline and to many palaeocurrents (Figs. 2.8, 2.12, 2.14). A similar stratigraphic architecture is observed in most modern compound-clinoform deltas, which contain subaqueous clinoforms that strike parallel to the alongshore currents that feed them (e.g., Driscoll & Karner, 1999; Cattaneo et al., 2003, 2007; Liu et al., 2007). The subaqueous clinoform model can readily explain the westward changes in clinoform cross-sectional geometry and grain size (Figs. 2.6, 2.7, 2.9, 2.10, 2.13), as these features are attributable to progradation across a basinward-sloping sea floor (Pirmez et al., 1998; Mortimer et al., 2005), an increase in average sediment calibre (Kenter, 1990; Orton & Reading, 1993) and an increase in sediment supply through time (Pirmez et al., 1998; Driscoll & Karner, 1999; Adams & Schlager, 2000; Swenson et al., 2005). Increased efficiency of alongshore sediment transport during westward progradation, as reflected in the occurrence of FA4 and FA5 in the west of the study area (Figs. 2.6, 2.9, 2.14A), may be due to focussing of waves and/or currents along the north-south trending break of slope formed by the rollover of older clinoform sets (e.g. break in slope at rollover of “Series 2” clinoform set in Fig. 2.14). Similar focussing of modern shelfal geostrophic currents is caused by bathymetric reliefs due to the impact of flow confinement and acceleration (e.g. Liu et al., 2007; Cattaneo et al., 2007). Strong shelfal bottom currents in the west may have slowed westward progradation of the clinoform bottomset and thus contributed to steepening of the clinoform foreset gradient (Fig. 2.13B) (cf. Cattaneo et al., 2003).

Some aspects of the lower Sognefjord Formation differ from those of modern subaqueous deltaic clinoforms (Table 2.1). Wide, gently dipping, sigmoidal clinoforms, which characterise many subaqueous deltas, are not observed across much of the study area (e.g. Figs. 2.6C, 2.9). However, the observed steep geometry of clinoform

foresets in the western part of the study area may be unrelated to the subaqueous origin of the clinoform and instead reflect the coarse grain size of the sand-rich Lower Sognefjord delta (cf. Kenter, 1990; Orton & Reading, 1993) in combination with high wave and/or current energy (Fig. 2.14C). Other subaqueous clinoforms that prograded onto a basinward-sloping sea floor are also observed to evolve through time from gently dipping, sigmoidal to steeper, more oblique geometries (e.g. Hernandez-Molina et al., 2000). The subaqueous clinoform model is our preferred interpretation, because it can explain all key observations; the differences between the interpreted Sognefjord Formation delta and modern compound clinoform deltas (Table 2.1) are explored further in a later section.

Diagnostic features of subaqueous deltas	Occurrence in lower Sognefjord Formation
1. Low-angle (< 1°) clinoform foresets arranged within regressive clinoform set	Clinoform foresets are steeper, particularly in western part of Troll Field
2. Shore-detached offlap breaks	Present
3. Internal architecture more uniform than that of subaerial deltas	Present
4. Exclusive occurrence of marine lithofacies and benthic fauna in clinoform topset	Present
5. Relatively uniform grain size, due to long-distance transport processes on the shelf	Absent in the west of the study area, present in the southeast
6. Irregular coastline containing morphological barriers or embayments, which may help to nucleate subaqueous delta clinoforms	Coastline is inferred to lie to the east of the Troll Field, and its configuration is unknown

Table 2.1. *Comparison of interpreted depositional systems in the lower Sognefjord Formation with criteria for identifying ancient subaqueous deltas (as proposed by Cattaneo et al., 2003).*

2.7.3 Forced Regressive, Subaqueous-to-Subaerial Deltaic Clinoforms

In the third model, clinothems in the east are also interpreted to be deposited by a subaqueous delta. However, the transition towards more sandstone rich deposits (FA4 and FA5) and steeper, oblique clinoform geometries towards the west (Figs. 2.6, 2.7, 2.9, 2.10, 2.14A) is interpreted to result from a downstepping, forced regressive

trajectory produced by falling relative sea level (i.e. falling stage systems tract *sensu* Plint & Nummedal, 2000), which juxtaposes subaqueous deltaic clinothems in the east against subaerial deltaic clinothems in the west. The observed increase in clinoform-foreset slope and associated decrease in topset width during westward progradation is consistent with progradation along a descending, forced regressive trajectory (cf. Pirmez et al., 1998; Driscoll & Karner, 1999; Adams & Schlager, 2000). The forced regression model implies that during the later stages of progradation, when deposition of the western clinothems was taking place, the eastern part of the Troll Field underwent subaerial exposure and erosion of any deposits that had accumulated above fairweather wave base, such that only subaqueous clinothems are preserved here. During subsequent transgression, clinoform topsets across the whole study area were subject to erosion (ravinement *sensu* Swift, 1968) that removed any coastal plain deposits that had accumulated during regression.

Although the model outlined above explains the areal distribution of facies associations (Fig. 2.14A), there is little evidence to support the strongly descending, forced regressive trajectory that it implies. The widespread occurrence of well-developed subaqueous topsets and sigmoidal foresets in clinoforms in the eastern Troll Field (Figs. 2.6D, 2.10) contradicts the interpretation of erosional truncation here, and there is a paucity of regressive fluvial or marine erosion surfaces developed during falling relative sea-level (e.g. at the base of incised valleys or sharp-based shorefaces *sensu* Plint, 1988) (Fig. 2.5). Such forced regressive trajectories are typically characterised by offlapping clinothems that thin progressively in a proximal-to-distal direction (Posamentier & Morris, 2000), but the opposite trend of proximal-to-distal clinothem thickening is observed in the Troll Field (Figs. 2.6, 2.9, 2.10).

2.7.4 Coeval Subaerial and Subaqueous Deltas in Separate Structural Domains

The fourth model envisages a delta with a subaerial topset in the western part of the Troll Field, and a separate but coeval subaqueous delta in the east. The two deltas were separated by one or more active extensional faults that created a bathymetric barrier on the sea floor. The subaerial and subaqueous deltas were fed by different sediment input points that were situated respectively to the northeast and east of the Troll Field area. The model requires that the subaerial deposits which capped the western delta were subsequently removed by transgressive erosion, and that the subaqueous delta situated in the east was part of a compound clinoform system whose subaerial component was located outside of the study area.

This model can in principle account for the lateral facies variability observed in the lower Sognefjord Formation (Fig. 2.14), and active rifting has previously been inferred to have influenced facies distributions in this interval, based on the observation that facies association belts trend sub-parallel to the structural grain of the northern Horda Platform (Stewart et al., 1995). However, isopach maps of the lower Sognefjord Formation reveal only minor thickness variations across the study area (Fig. 2.11A), implying that major faults defining present-day reservoir structure (Fig. 2.2) were largely inactive during deposition of this interval. Clinoform sets and their component facies association belts in "Series 2" and "Series 3" are observed to extend across major faults (Fig. 2.9). The proposed structural control on sedimentation therefore appears unlikely.

2.8 DISCUSSION: COMPARISON BETWEEN INTERPRETED SOGNEFJORD FORMATION AND MODERN SUBAQUEOUS DELTAS

The subaqueous clinoforms interpreted in the lower Sognefjord Formation in our preferred model (Figs. 2.14B-C, 2.15) are compared below to modern subaqueous deltaic clinoforms (Table 2.1), in order to identify the formative conditions for sand-prone subaqueous deltas in the former. Facies analysis reveals that subaqueous clinothems in the lower Sognefjord Formation in the south-eastern portion of the Troll Field area were deposited below the base of the fairweather wave-current traction field (FA2 and FA3), as commonly occurs in modern subaqueous deltas (e.g. Kuehl et al., 1986, 1997; Pirmez et al., 1998; Hernández-Molina et al., 2000; Cattaneo et al., 2007). Subaqueous clinoforms developed in modern deltas and those in the "Sognefjord Delta" share many geometrical characteristics; well-developed topsets, shoreline-detached offlap breaks, linear to gently curvilinear plan-view geometry, and a total vertical relief of <100 m (cf. Kuehl et al., 1986; 1997; Cattaneo et al., 2003, 2007; Walsh et al., 2004; Swenson et al., 2005; Liu et al., 2007). However, the foresets of the "Sognefjord Delta" subaqueous clinoforms are much narrower and steeper than the broad, low angle, sigmoidal profiles developed in most modern deltas (e.g., Kuehl et al., 1986, 1997, 2005; Liu et al., 2006, 2007; Cattaneo et al., 2003, 2007), particularly in the southwestern part of the Troll Field, where the foresets may exhibit a top-truncated, less sigmoidal geometry.

The steeper foresets in the "Sognefjord Delta" subaqueous clinoforms are attributed to their coarse grain size and sandstone-prone character, in contrast to most modern subaqueous deltas which are mud-dominated (e.g. the "along-shelf mud belt" of Liu et al., 2006, 2007). Most modern deltas with compound clinoforms are fed by river outlets that discharge a sediment load dominated by mud and silt (Orton & Reading, 1993; Pirmez et al., 1998; Driscoll & Karner, 1999), which accounts for the mud-dominated character of their subaqueous clinoforms. However, modern subaqueous deltaic clinoforms developed offshore Spain (Hernández-Molina et al., 2000) and Papua New-Guinea (Walsh et al., 2004) have topsets comprising up to 50% storm-reworked sand. Furthermore, examples of ancient distally steepened carbonate ramps of similar geometry to subaqueous clinoforms are documented to contain coarse-grained, cross-bedded, carbonate sandstones deposited below wave base in their steepened outer parts (Pomar & Tropeano, 2001; Pomar et al., 2002), in a context comparable to subaqueous clinoform foresets. Thus, there are analogues for steep, coarse-grained subaqueous foresets developed below fairweather wave base, although these analogues are not modern deltas with compound clinoforms. In addition, the slopes of both subaerial delta fronts and carbonate platforms become steeper with increasing grain size (Kenter, 1990; Orton & Reading, 1993); the steep (up to 16˚) clinoform foresets of the "Sognefjord Delta" are typical of coarse-grained subaerial deltas (Orton & Reading, 1993).

Since the partitioning of sediment between subaerial and subaqueous delta clinoforms is determined by the spatial and temporal interplay between river processes and basin hydrodynamics (cf. Pirmez et al., 1998; Driscoll & Karner, 1999; Cattaneo et al., 2003, 2007; Swenson et al., 2005), we suggest that the formation of coarse-grained subaqueous deltas requires that rivers discharge predominantly sand-to-gravel grade sediment into a high-energy marine basin. Unlike in many modern settings, these two conditions were met in the "Sognefjord Delta", as discussed below.

Firstly, modern subaerial deltas of similar grain size and foreset slope are generally characterised by relatively small catchment areas (≤10,000 km^2) of steep relief, although a minority are sourced by larger catchments situated in cold climatic settings (e.g. Colville Delta) or with particularly erratic discharge patterns (e.g. Burdekin Delta) (Orton & Reading, 1993). Given the rift-margin location (e.g. Ravnås et al., 2000; Fraser et al., 2002) and probable temperate climate (50°N palaeolatitude in Jurassic Greenhouse conditions; Torsvik et al., 2002; Mutterlose, 2003) of the "Sognefjord Delta", it was likely supplied with coarse-grained sediment from a steep, high relief catchment area that may have been subject to erratic fluvial discharge.

The large volume of sand in the "Sognefjord Delta" subaqueous clinoform implies either that the source catchment was relatively large, or that several small catchments supplied the subaqueous delta with coarse-grained sediment (e.g. as in the multiple subaerial deltas that supply mud-prone sediment to the modern

Gargano Delta subaqueous clinoform; Cattaneo et al., 2003). The low degree of rounding of gravel-grade clasts in FA6 in the northeastern part of the Troll Field area, which is interpreted to contain subaerial clinoforms in the most proximal part of the "Sognefjord Delta", further suggests a short fluvial transport distance (<25 km for angular and subangular quartz-rich gravel clasts; Pettijohn, 1976). High sediment discharge, a small delta plain and/or the confinement of feeder rivers within valleys are typically required for river-fed gravel to be delivered directly to the foresets of subaerial delta clinoforms (Orton & Reading, 1993).

Secondly, the Late Jurassic paleogeography of the northern North Sea Basin is compatible with the action of strong marine currents flowing from north to south in a high-energy marine basin. These currents may have been promoted by the open connection between the Boreal Ocean in the north and the warmer Tethys Ocean in the south (e.g. Doré, 1992; Torsvik et al., 2002; Mutterlose, 2003), and by funnelling through the narrow corridor of the Greenland-Norwegian Seaway (*sensu* Mutterlose, 2003). Delivery of sediment from the subaerial delta clinoform to the subaqueous clinoform may also have been enhanced by a high-energy storm wave climate (cf. Swenson et al., 2005).

2.9 CONCLUSIONS

The stratigraphic architecture of the lower Sognefjord Formation in the Troll Field consists of two regressive-transgressive packages ("series") bounded by regionally extensive maximum flooding surfaces. Each "series" gradually thickens towards the west until it reaches a maximum, beyond which the upper bounding surface rolls over to define an overall topset-foreset-bottomset geometry. The seismically resolved internal architecture of each "series" consists of a regressive clinoform set of westward-dipping clinoforms that prograded towards the west across a westward-deepening sea floor. Clinoforms bound upward-coarsening successions imaged in cores and wireline logs. Clinoforms are linear to gently curvilinear in plan-view, with a uniform NNE-SSW strike direction throughout the Troll Field. However, the cross-sectional geometry of the clinoforms varies across the field, in the three palaeogeographic domains summarised below.

(1) Low relief (10-30 m), relatively low gradient (1-6˚) sigmoidal clinoforms with broad topsets occur in the southeast of the field, and are characterised by bottomsets of bioturbated siltstones (Facies Association 1) and

foresets and topsets of hummocky cross-stratified, well-sorted, fine-grained sandstones (Facies Associations 2-3). Coarser-grained event beds resulting from intense storms and/or river floods also occur in the foresets and topsets. The various bottomset, foreset and topset facies were deposited below mean fairweather wave base. Despite the sandstone-rich character of the clinoforms, their interpreted setting and overall geometry resemble those of mud-dominated subaqueous clinoforms in modern wave- and tide-influenced deltas.

(2) Further west, clinoforms exhibit progressively greater relief (up to 60 m), steeper foresets (up to 16°), and oblique and top-truncated geometries with narrow or absent topsets. The foresets of these clinofoms are dominated by cross-bedded, well-sorted, fine- to coarse-grained sandstones (Facies Associations 4-5), which reflect the continuous action of strong currents and abundant coarse-grained sediment supply. Coastal plain deposits and palaeosols indicating subaerial exposure are absent. These clinoforms are interpreted as subaqueous deltaic clinoforms developed in an area of increased marine current activity and greater proximity to riverine sediment influx than the southeast of the field.

(3) In the northeast of the field, clinoforms and other geomorphological features are below seismic resolution. However, both “series” are dominated by cross-bedded, well-sorted, fine- to coarse-grained sandstones (Facies Associations 4-5) and poorly sorted, very coarse-grained gravity flow sandstones (Facies Association 6), which are interpreted as proximal delta front deposits within subaerial delta clinoforms. However, evidence of subaerial exposure is again absent.

Synthesising data from all parts of the Troll Field, deposition of each regressive-transgressive “series” was interpreted by fully subaqueous, NNE-SSW striking, elongated clinoforms that built westwards across the shallow-marine Horda Platform. These subaqueous clinoforms are interpreted to have formed part of deltas with an overall compound clinoform morphology; corresponding subaerial clinoforms are inferred to lie beyond the eastern boundary of the Troll Field. Subaqueous clinoform sets were supplied with sand-rich sediment by a river outlet near the north-east of the Troll Field, and sculpted by the action of alongshore advective currents that flowed sub-parallel to clinoform strike. The direction of clinoform progradation is approximately perpendicular to the inferred sediment transport direction, as in many modern subaqueous deltas. Clinoforms in each “series” became progressively coarser grained with higher, steeper foresets and narrower topsets as the subaqueous delta prograded from the inner (eastern), sheltered part of the Horda Platform to its outer (western) limit, which was open to direct wave and storm approach. The change in clinfororm morphology may also have been enhanced by forced regression. The complete absence of coastal plain deposits and evidence of subaerial exposure supports the interpretation of subaqueous clinoforms, although their removal from the top of each clinoform set by transgressive erosion cannot be discounted.

The resulting model of a coarse-grained subaqueous delta provides a new interpretative template that may be applicable to other clinoform-bearing shallow-marine sandstones in the ancient stratigraphic record. It also emphasises that sediment distribution and clinoform architecture in deltaic settings are controlled by the dynamic interplay between the bathymetric configuration of the receiving basin, the volume and grain size of sediment input, and the direction and power of basinal processes such as waves, tides, and surface and bottom currents, in addition to relative sea-level changes. An important implication is that, in the absence of a full facies and geomorphological characterisation to provide context, the use of the clinoform rollover point as a proxy for the palaeoshoreline may lead to erroneous predictions of relative sea level history and related facies distributions.

2.10 ACKNOWLEDGEMENTS

The authors thank Statoil ASA for providing data for this study, and Tom Dreyer (Statoil), Paul Whipp (Statoil), Theresa Lloyd-Lodden (Statoil), Prof. Howard Johnson (Imperial College London), Nicholas Holgate (Imperial College London) and Adam McCarthy (Statoil) for help, insightful discussions and comments. We also acknowledge the Troll Field partners, Statoil ASA, Petoro AS, A/S Norske Shell, Total E&P Norge AS and ConocoPhillips Skandinavia AS, for permission to publish this paper. Thanks also to Schlumberger Limited for provision of Petrel seismic and well interpretation software via an academic software donation.

CHAPTER 3

Estimation of progradation rates in ancient shallow-marine clinoform sets: a new method and its application to the Upper Jurassic Sognefjord Formation, Troll Field, offshore Norway

Running head:

Estimation of progradation rates

Title:

Estimation of progradation rates in ancient shallow-marine clinoform sets: a new method and its application to the Upper Jurassic Sognefjord Formation, Troll Field, offshore Norway

Authors:

STEFANO PATRUNO*, GARY J. HAMPSON*, CHRISTOPHER A-L. JACKSON* and ANDREW C. MORTON†

**Department of Earth Science & Engineering, Imperial College, London, SW7 2BP, UK*

†*HM Research Associates, 2 Clive Road, Balsall Common, West Midlands CV7 7DW, UK*

Email for correspondence: s.patruno09@imperial.ac.uk

Key words:

progradation rates, sediment flux, stratigraphic architecture, clinoform, trajectory analysis

Word count: 294 (abstract) + 11,662 (main text)

Number of Figures: 17

Number of Tables: 2

Number of references: 72

CHAPTER 3: ESTIMATION OF PROGRADATION RATES IN ANCIENT SHALLOW-MARINE CLINOFORM SETS: A NEW METHOD AND ITS APPLICATION TO THE UPPER JURASSIC SOGNEFJORD FORMATION, TROLL FIELD, OFFSHORE NORWAY

3.1 ABSTRACT

This paper presents a new method to estimate progradation rates in ancient shallow-marine clinoform sets, which is then used to refine the tectono-stratigraphic and depositional model for the Upper Jurassic Sognefjord Formation reservoir in the super-giant Troll Field, offshore Norway. The Sognefjord Formation is a 10-200 m thick, coarse-grained clastic wedge, deposited in ca. 6 Myr by a fully marine, westward-prograding, subaqueous delta system sourced from the Norwegian mainland. The formation comprises four, 10-60 m thick, westerly-dipping, regressive subaqueous clinoform sets, which can be mapped as near-linear features for several tens of kilometres along strike. Horizontal trajectories are observed in each clinoform set, and the sets are stacked vertically. Clinoform age and progradation rates are constrained by: (1) regionally correlatable bioevents, which are tied to seismically mapped clinoforms and clinoform-set boundaries that intersect wells, (2) exponential age-depth interpolations between bioevent-dated surfaces and a distinctive foreset-to-bottomset facies transition within each well, and (3) distances between wells along seismic transects that are oriented perpendicular to the clinoform strike and tied to well-based stratigraphic correlations. Our results indicate a fall in progradation rate (from 500 to 30 km/Myr) and net sediment flux (from 90 to 10 km^2/Myr) westwards towards the basin, which is synchronous with a rise in sediment accumulation rate (from 15 to 70 m/Myr). These variations are attributed to progradation of the subaqueous delta into progressively deeper waters, and a concomitant increase in the strength of along-shore currents that transported sediment out of the study area. Local spatial and temporal deviations from these overall trends are interpreted to reflect a subtle structural control on sedimentation. Detrital-garnet provenance data provide an independent verification of the proposed depositional model. This method provides a tool to improve the predictive potential of sequence stratigraphic and clinoform trajectory analyses.

(END OF ABSTRACT)

3.2 INTRODUCTION

The establishment of a robust stratigraphic framework that incorporates stratal geometries and time relationships is essential in sequence stratigraphic analysis. Palaeoseaward-dipping surfaces, or clinoforms (*sensu* Rich 1951), are a ubiquitous geometrical feature of shallow-marine strata, and record the morphology of shorelines and shelves (e.g. Mitchum et al., 1977). Shoreline-scale clinoforms are arranged in sets, each of which records the regressive transit of a shoreline across a coeval shelf. The spatial arrangement of these regressive clinoform sets and of the thin transgressive intervals that bound them is key in constructing continental shelf successions (e.g. Johannessen & Steel, 2005). Mapping the successive positions, or trajectory, of breaks-in-slope associated with clinoforms ("trajectory analysis" *sensu* Helland-Hansen & Martinsen, 1996; Helland-Hansen & Hampson, 2009) is a descriptive means of characterising stratigraphic architecture. Such geomorphological breaks-in-slopes are usually associated with facies-belt boundaries (e.g. shorelines), which allow stratal geometries to be linked to lithology distribution (Helland-Hansen & Gjelberg, 1994; Helland-Hansen & Martinsen, 1996; Helland-Hansen & Hampson, 2009). Thus, trajectory analysis of shelfal strata allows prediction of the distribution of shallow-marine sandstones, and timing of sand delivery to the slope and basin-floor (e.g. Steel & Olsen, 2002; Johannessen & Steel, 2005). The precision and detail of such predictions are limited by the degree to which ages can be assigned to stratal surfaces and units. Ages are typically assigned to condensed surfaces within the transgressive intervals that bound clinoform sets, based on the occurrence of biostratigraphic markers (e.g. Loutit et al., 1988), but not to individual clinoforms within sets. Such use of biostratigraphic data permits only the gross estimation of an average progradation rate for a clinoform set. Assigning ages to multiple different clinoforms within the same set would help to better constrain: (1) variations in shoreline progradation rate; (2) the time needed for a shoreline to prograde across a shelf and reach the shelf edge ("shelf transit time" *sensu* Steel & Olsen, 2002); (3) reservoir distribution and architecture within shallow-marine depositional systems; (4) the spatial and temporal relationships between tectonic subsidence, bathymetry, basin hydrodynamics and sediment supply, which combine to control the overall stratigraphic architecture; and (5) partitioning of sediment budget between the different segments of the linked shoreline-shelf-slope-basin-floor system.

Volumes and rates from modern examples suggest that the shelf transit times for many large, fluvial-dominated deltas are <0.15 Myr (Burgess & Hovius, 1998). Even in areas of lower sediment flux, flat or descending shoreline trajectories caused by steady or falling relative sea-level may lead to short shelf transit times (<0.1 Myr; Porebski & Steel, 2006). Alongshore sediment transport by waves and tides increases shelf transit time, and the shoreline may never reach the shelf edge if alongshore transport rate outpaces fluvial input rate (Steel et al., 2008). These estimates of shelf transit times indicate that a method of assigning ages to shoreline-scale clinoforms with a precision of at least c. 0.1 Myr is required to make useful estimates of progradation rates within a clinoform set.

The aims of this paper are: (1) to present a simple, data-driven method to systematically track the progradation rates of shoreline-scale clinoforms within a clinoform set, and (2) to apply the method to the Upper Jurassic Sognefjord Formation, Troll Field, offshore Norway in order to demonstrate its capacity to enhance the predictive potential of sequence stratigraphic models. When integrated with subsidence history reconstructed from sediment decompaction and backstripping and with trajectory-based analysis of clinoforms and detrital-garnet provenance data, estimation of clinoform progradation rate in the Sognefjord Formation allows us to assess the influence on stratigraphic architecture of various internal (autogenic) and external (allogenic) forcing mechanisms, including minor phases of rift-related uplift and subsidence that are not evident in seismically-resolved stratal geometries. A refined characterisation of the Sognefjord Formation is also of economic importance, because this unit forms the main reservoir in the super-giant Troll oil and gas field.

3.3 GEOLOGICAL CONTEXT OF SOGNEFJORD FORMATION

The study area is located on the Horda Platform, on the eastern flank of the N-S-trending North Viking Graben (Fig. 3.1A-B), which forms the northern arm of the trilete, failed North Sea rift system (Badley et al., 1988; Christiansson et al., 2000; Coward et al., 2003; Zanella & Coward, 2003). The Horda Platform is up to 60 km wide, and it is bound and dissected by a series of predominantly N-S-striking normal fault systems, which have up to 1 km of displacement (Fig. 3.1B) (Zanella & Coward, 2003; Whipp et al., in press). It is flanked to the east by the Norwegian mainland and to the west by several 10-50 km wide, fault-bounded, tilted blocks, which step down towards the axis of the North Viking Graben (Figs. 3.1B). These main structural elements formed in their current

configuration during Permo-Triassic and Late-Jurassic-to-Early Cretaceous rifting (Steel, 1993; Badley et al., 1988; Zanella & Coward, 2003; Whipp et al., in press). Færseth & Ravnås (1998) and Ravnås et al. (2000) defined five distinct rift pulses during the Late Jurassic-to-Early Cretaceous based on their analysis of seismic and well data from the nearby Oseberg Field. Four of these rift pulses correspond approximately with, and are probably genetically related to, the maximum flooding surfaces that bound the regressive-transgressive Krossfjord (Bathonian-Callovian) and Sognefjord (Oxfordian) megasequences of Steel (1993), and the formations that they contain (Fig. 3.1D).

The overall geometry of the North Viking Graben was controlled by the growth of major N-S-striking fault systems, which influenced the development of transverse sediment transport paths from the Norwegian mainland to the graben axis (Ravnås & Bondevik, 1997; Færseth & Ravnås, 1998; Whipp et al., in press). One or several of these fluvial drainages supplied large quantities of sediment to the "Troll Delta", which deposited the Krossfjord, Fensfjord and Sognefjord formations on the northern part of the Horda Platform and the southern part of the Måløy Slope (Stewart et al., 1995; Dreyer et al., 2005; Fraser et al., 2003). Færseth & Ravnås (1998) suggested that the switch from tectonic quiescence to rotational tilting during a rift pulse determined the transition from the regression to transgression in the constituent clastic wedges of the megasequences of Steel (1993) (Fig. 3.1D), with transgression accompanied by enhanced tidal activity. It is generally considered that the rift-marginal Horda Platform underwent little internal deformation in the Jurassic prior to the Kimmeridgian (Færseth, 1996), such that most of the faults in the study area (Fig. 3.1C) formed during or after deposition of the upper part of the Sognefjord Formation (Dreyer et al., 2005; Whipp et al., in press). However, it has been argued that active fault block rotation and associated bathymetric changes might have exerted a subtle control on facies-belt distributions in the Sognefjord Formation (Stewart et al., 1995). Today, a total of five N-S-trending, easterly-rotated fault blocks, which experienced both Permo-Triassic and Late-Jurassic-to-Early-Cretaceous activity, define the main structure of the study area (Whipp et al., in press; Fig. 3.1C). These fault blocks are internally deformed by a series of broadly NW-SE-striking, relatively low displacement (<200 m) normal faults, which also formed after deposition of the Sognefjord Formation (Dreyer et al., 2005; Whipp et al., in press). The Troll Fault (Fig. 3.1C) defines the western edge of the Horda Platform.

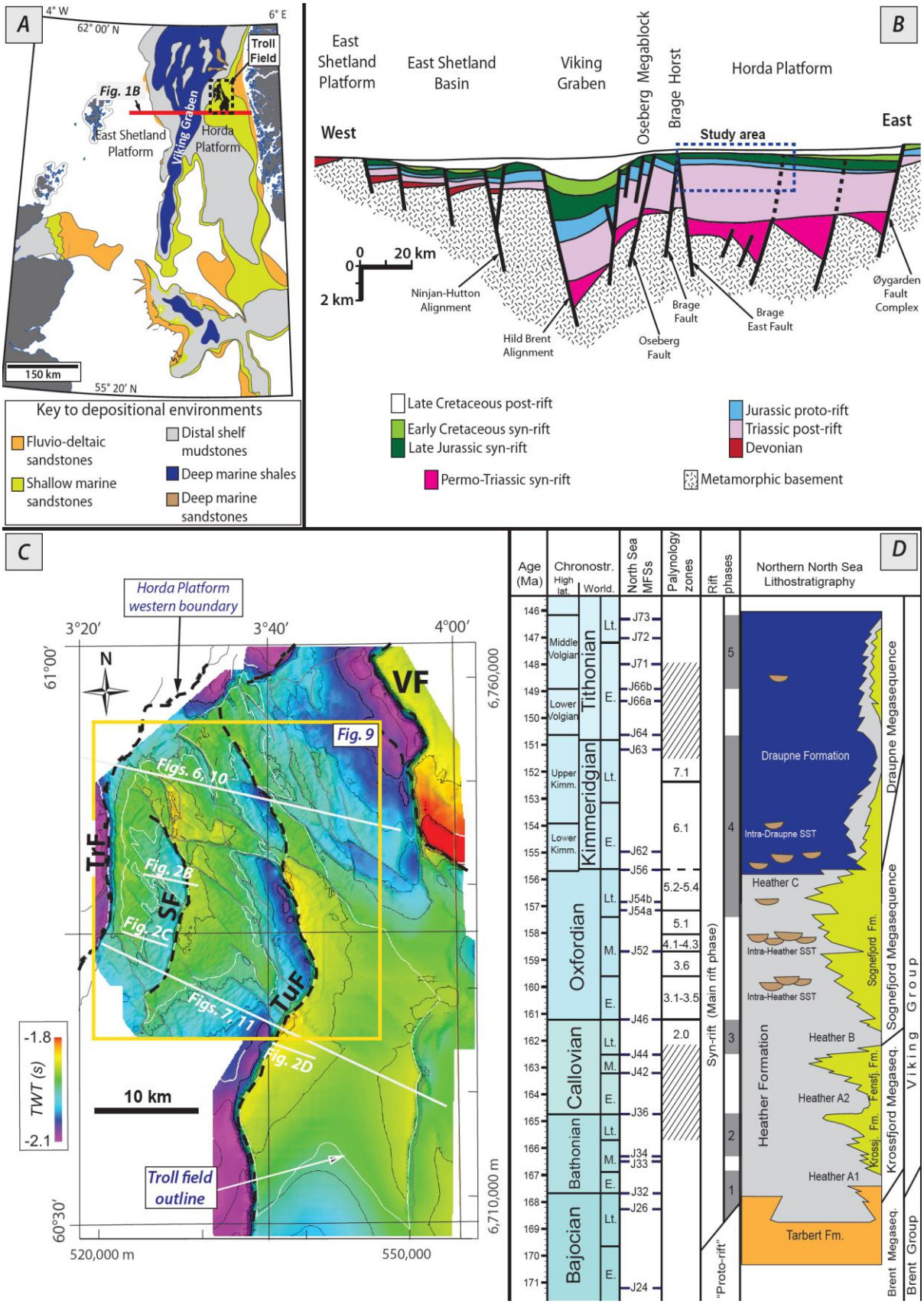
A
4° W
6° E
62° 00′ N
55° 20′ N
Troll Field
Fig. 1B
East Shetland Platform
Viking Graben
Horda Platform
150 km
B
East Shetland Platform
East Shetland Basin
Viking Graben
Oseberg Megablock
Brage Horst
Horda Platform
West
East
Study area
0
20 km
0
2 km
Ninjan-Hutton Alignment
Hild Brent Alignment
Oseberg Fault
Brage Fault
Brage East Fault
Øygarden Fault Complex
Key to depositional environments
Fluvio-deltaic sandstones
Shallow marine sandstones
Distal shelf mudstones
Deep marine shales
Deep marine sandstones
Late Cretaceous post-rift
Early Cretaceous syn-rift
Late Jurassic syn-rift
Permo-Triassic syn-rift
Jurassic proto-rift
Triassic post-rift
Devonian
Metamorphic basement
C
Horda Platform western boundary
3°20′
3°40′
4°00′
61°00′
60°30′
N
VF
Fig. 9
Figs. 6, 10
TrF
Fig. 2B
SF
Fig. 2C
Figs. 7, 11
TuF
Fig. 2D
-1.8
TWT (s)
-2.1
10 km
Troll field outline
6,760,000
6,710,000 m
520,000 m
550,000
D
Age (Ma)
Chronostr.
High lat.
World.
North Sea MFSs
Palynology zones
Rift phases
Northern North Sea Lithostratigraphy
Middle Volgian
Lower Volgian
Upper Kimm.
Lower Kimm.
Tithonian
Kimmeridgian
Oxfordian
Callovian
Bathonian
Bajocian
Lt.
E.
M.
J73
J72
J71
J66b
J66a
J64
J63
J62
J56
J54b
J54a
J52
J46
J44
J42
J36
J34
J33
J32
J26
J24
7.1
6.1
5.2-5.4
5.1
4.1-4.3
3.6
3.1-3.5
2.0
Syn-rift (Main rift phase)
"Proto-rift"
Draupne Formation
Intra-Draupne SST
Heather C
Intra-Heather SST
Intra-Heather SST
Heather B
Heather A2
Heather A1
Heather Formation
Tarbert Fm.
Sognefjord Fm.
Fensfj. Fm.
Krossfj. Fm.
Draupne Megasequence
Sognefjord Megasequence
Krossfjord Megaseq.
Brent Megaseq.
Viking Group
Brent Group

***Figure 3.1**. (**A**) Early-Middle Oxfordian palaeogeography of the North Sea area (modified after Fraser et al., 2002); (**B**) Regional cross section across the Northern North Sea Basin, perpendicular to the axis of the North Viking Graben (modified after Faerseth, 1996); (**C**) Time structure map of top-Fensfjord Formation surface in the Troll Field area, showing faults and cross-sections analysed in this study (Figs. 2, 4-6, 10, 12). Troll Fault (TrF); Svartav Fault (SF); Tusse Fault (TuF); Vette Fault (VF); (**D**) Late Jurassic stratigraphy developed on the eastern flank of the North Viking Graben (Fig. 3.1A). Columns in Figure 3.1D show, from left to right: age and standard chronostratigraphy (after Ogg et al., 2008), including high latitude (boreal and sub-boreal) and worldwide (Tethys-based) nomenclature; North Sea basin-wide maximum flooding surfaces (MFSs) (Partington et al., 1993); palynostratigraphic zones (Dreyer et al. (2005); rift phases in the North Viking Graben, including rift pulses 1-5 on the Horda Platform (shaded in grey; Færseth & Ravnås, 1998; Ravnås et al., 2000); and lithostratigraphy, including the megasequence nomenclature of Steel (1993). The biostratigraphic zonation is not the official Statoil's or Troll licence, but has been devised by us based on the raw microfossil occurrence data.*

The Sognefjord Formation is mainly of Late Callovian-to-Kimmeridgian age, and forms the upper of three shallow-marine-to-shelf clastic wedges within the Viking Group on the Horda Platform (Fig. 3.1D) (Vollset & Doré, 1984; Steel, 1993; Stewart et al., 1995). The formation ranges in thickness from a few metres to up to 250 m (Stewart et al., 1995; Dreyer et al., 2005), and consists of five, vertically stacked clinoform sets ("series 2, 3, 4, 5 and 6-7" of Dreyer et al., 2005), each recording a cycle of regression and transgression within the overall wedge (Dreyer et al., 2005; Chapter 2). Each clinoform set or series is bounded wholly or partly by regional maximum flooding surfaces ('J MFSs' of Partington et al., 1993; Fig. 3.1D), as outlined below: Series 2 (top-Fensfjord Formation MFS to J46 MFS); Series 3 (J46 MFS to J52 MFS); Series 4 (J52 MFS to J54 MFS); Series 5 (J54 MFS to J56 MFS); and Series 6-7 (J56 MFS to top-Sognefjord Formation MFS). The Sognefjord Formation represents ca. 6 Myr of deposition, and each clinoform set is estimated to represent 0.5-3.0 Myr (Stewart et al., 1995; Dreyer et al., 2005). Each clinoform set is 10-70 m thick, and thickens westwards to the point of maximum clinoform-topset regression (Dreyer et al., 2005; Chapter 2). Clinoforms and clinoform set foresets dip westwards and have a consistent north-northeast to south-southwest strike, which can be mapped in seismic data for several tens of kilometres along strike (Chapter 2) (Fig. 3.2). In each clinoform set, clinoform height and dip both increase from east to west, and clinoform dip extent decreases from east to west (Chapter 2). Clinoforms generally exhibit well-developed topsets, which lack evidence of subaerial exposure, and their foresets are represented by sandstone-rich bedsets (Chapter 2). Foreset sandstones are primarily wave- and current-dominated in Series 2-4 and tide-influenced in Series 5-7) (Dreyer et al., 2005; Chapter 2).

The consistent westward dip and north-northeast to south-southwest strike of the clinoforms, the prevalence of facies deposited below fair-weather wave base, and the absence of subaerial exposure at the clinoform topsets

imply deposition in a subaqueous delta setting (Chapter 2). Previous interpretations of a wave-dominated shoreface (Stewart et al., 1995) or wave-dominated spit fronting a tidal back-basin (Dreyer et al., 2005) are based solely on data from the western part of the Horda Platform, and are inconsistent with the three key observations listed above from both the western and eastern parts of the field. In the interpretation of Chapter 2, subaqueous clinoforms and their topsets were fed by a river outlet situated at the north-east of the study area and sculpted by currents directed sub-parallel (i.e. NNE-to-SSW) to the strike of the clinoforms (Fig. 3.2). Subaerial clinoforms marking the coeval shoreline are inferred to have been present beyond the eastern limit of the Troll Field study area, giving rise to a "compound clinoform" geometry that is common in many modern deltas (e.g. Swenson et al., 2005). Upstream controls on subaqueous delta development are poorly constrained because the coeval subaerial delta occurs in an area lacking data. Furthermore, the alluvial hinterland which provided sediment to the delta has been removed by later erosion of onshore Norway.

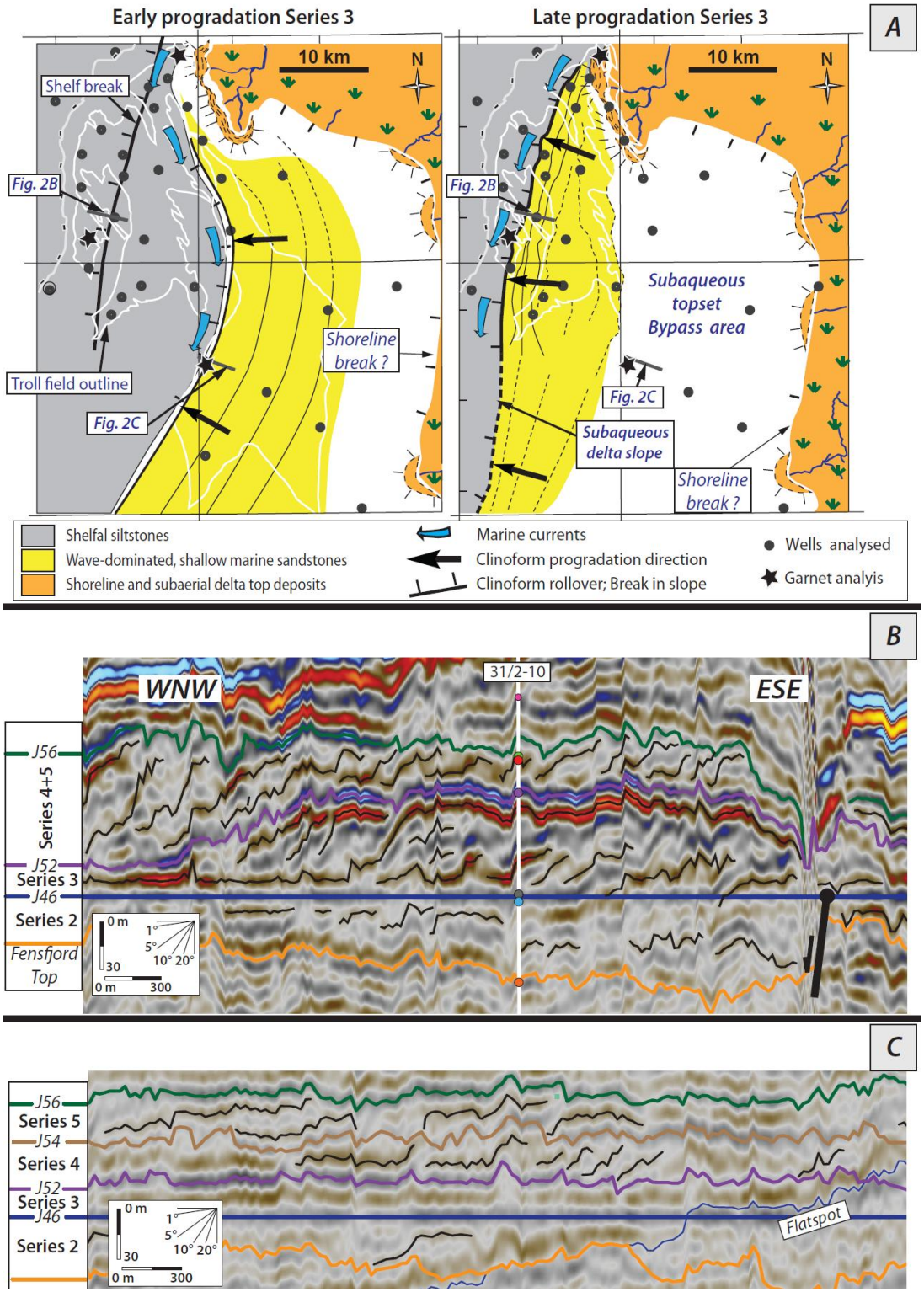

Figure 3.2. ***(A)*** *Interpreted palaeogeography of the Troll Field area, showing the distribution of depositional environments and clinoform geometry in plan view during early (left) and late (right) progradation of the Series 3 clinoform set (after Chapter 2);* ***(B-C)*** *Interpreted seismic cross-sections oriented perpendicular to clinoform strike (Fig. 3.2A) and sub-parallel to well correlation transects (Figs. 3.4-3.5, 3.10) (after Chapter 2). Cross-sections are flattened along the interpreted J46 maximum*

flooding surface. Each series corresponds to a set of westerly-dipping clinoforms; all clinoforms and clinoform sets share a NNE-SSW strike direction.

3.4 DATASET AND METHODOLOGY

Our methodology uses a five-step workflow that consists of: (1) construction of a chronostratigraphic framework; (2) sediment decompaction and backstripping to reconstruct subsidence history and depositional geometries; (3) measurement of clinoform trajectories; (4) assignment of ages to clinoform-trajectory reference points; and (5) estimation of progradation rates and other key parameters. The dataset used in this study and the five workflow steps are outlined below, using the Sognefjord Formation as a worked example.

3.4.1 Dataset review and construction of chronostratigraphic framework

3.4.1.1 General method

Our method to constrain shallow-marine clinoform ages requires a dataset that comprises stratigraphic and sedimentological data from a network of wells or stratigraphic sections. An important requirement is to be able to construct transects aligned parallel to the dip of the depositional system using wells or sections. High-quality, preferably 3D seismic reflection data, albeit not essential, also help to constrain the stratigraphic framework and architecture (i.e. clinoforms).

The succession needs to be subdivided into clinoform sets bounded by approximately isochronous surfaces, such as maximum flooding surfaces (cf., 'genetic sequences' of Galloway, 1989). These units need to contain a series of

dated stratigraphic points (e.g., micropalaeontological bioevents), including at least one dated point within each clinoform set.

3.4.1.2 Dataset for the Sognefjord Formation case study

The Sognefjord Formation case study uses several pre-stack time-migrated 3D seismic reflection datasets that together cover 3,320 km^2 of the Troll Field and surrounding region. The vertical record length in each of the constituent surveys varies from 2.4-3.0 seconds two-way time (s TWT). Line spacing is 25 m and 12.5 m in the crossline and inline direction, respectively. Seismic velocity values estimated from the checkshot survey in the study interval generally range from 0.90 to 1.02 m/ms. Synthetic seismograms indicate that vertical seismic resolution for the studied strata is 7-22 ms TWT, which equates to 6-22 m (Chapter 2). Estimations of geometric features inferred from seismic data (e.g. clinoform dips) are affected by both vertical seismic resolution and time-migration of the seismic data.

Core, wireline log and biostratigraphic data from 37 wells (Fig. 3.2A-B) have been used to develop sedimentological and stratigraphic interpretations (Chapter 2), which are consistent with interpretations based on many more wells (Dreyer et al., 2005). A subset of 14 wells was used to construct linear transects aligned parallel to clinoform dip in the northern and southern parts of the study area (Figs. 3.1C, 3.2A). Wells are projected into these two transects along local clinoform strike, which is constrained by seismic amplitude maps (Chapter 2). Projection distances are small (generally <2 km, but up to 4.5 km) relative to the along-strike continuity of clinoforms (Chapter 2). The 14 wells are extensively cored, and our sedimentological interpretations utilize the facies schemes of Chapter 2 and Dreyer et al. (2005) for the lower and upper parts of the formation, respectively.

We use palynological events and basin-wide maximum flooding surfaces (Partington et al., 1993) to construct a consistent age model, which is not the same as the biostratigraphic zonation devised by Statoil and the other partners of the Troll Field. Raw occurrence data of palynostratigraphic markers in all wells in the Troll Field and nearby areas have been analysed to determine 14 isochronous palynological events through the Callovian to Volgian interval (Table 3.1). We use only last occurrence events (LOs) and last common occurrence events (LCOs) in order to nullify potential contamination by caving and sloughing of the borehole wall whilst drilling. The chosen events occur in the same relative stratigraphic order in >95% of the wells. Furthermore, all of these events are used in biostratigraphic schemes at the basin scale (Hardenbol et al., 1998; Poulsen & Riding, 2003) or at more local scales, and via these schemes the events are associated with a specific sub-boreal and boreal ammonoid

zone that has been previously assigned an absolute age (Gradstein et al., 2004; Ogg et al., 2008) (Table 3.1). Once a consistent framework of dated palynological events was established in each well, this framework was then used to relate flooding surfaces bounding clinoform sets in each well to the basin-wide maximum flooding surfaces of Partington et al. (1993), which were each originally defined with reference to a single sub-boreal or boreal ammonoid zone. The absolute ages of the ammonoid zones (Gradstein et al., 2004; Ogg et al., 2008) can therefore be assigned to the various maximum flooding surfaces (Table 3.1). This approach can only be applied to Series 2 to 5 of Dreyer et al. (2005) (Upper Callovian to Upper Oxfordian), because Series 6-7 (Kimmeridgian) lack reliable biostratigraphic markers. The resulting chronostratigraphic framework allows the duration of each clinoform set to be estimated: Series 2 (Upper Callovian) was deposited in 0.7-0.8 Myr; Series 3 (Early to Middle Oxfordian) in 2.5 Myr; Series 4 (Middle to Upper Oxfordian) in 1.7 Myr; and Series 5 (Upper Oxfordian) in 1.4 Myr.

In order to test timing and pathways of the depositional model inferred by the method presented here with further evidences, provenance analysis was carried out on detrital garnets from six sandstone samples collected from the foresets and topsets of the Series 4 clinoform set. Three samples were collected from both the western and eastern parts of the Troll Field (from wells 31/2-M42, 31/2-F6H, and 31/6-1; Fig. 2A). Samples were analysed using the methodology of Morton et al. (2004).

Maximum flooding surface or palynological event	Ammonoid Zone	Source reference	Stage	Age (Ma)
J74	*Subcraspeditus preplicomphalus*	Partington et al. (1993)	Late Volgian	144.50 ± 4.00
LO Egmontodinium polyplacophorum	*Paracraspedites oppressus*	This study	Top Middle Volgian	146.15 ± 4.00
J73	*Titanites anguiformis*	Partington et al. (1993)	Top Middle Volgian	146.30 ± 4.00
LO Glossodinium dimorphum; LO *Senoniasphaera jurassica*		Poulsen & Riding (2003); This study		
J72	*Galbanites okusensis*	Partington et al. (1993)	Middle Volgian	147.00 ± 4.00
J71	*Virgatopavlovia fittoni*	Partington et al. (1993)	Middle Volgian	148.00 ± 4.00
J66b	*Pectinatites pectinatus*	Partington et al. (1993)	Top Early Volgian	148.90 ± 4.00
J66a	*Pectinatites hudlestoni*	Partington et al. (1993)	Early Volgian	149.35 ± 4.00
LCO Oligosphaeridium patulum		Poulsen & Riding (2003); This study		
J64	*Aulacostephanus autissiodorensis*	Partington et al. (1993)	Kimmeridgian / Volgian boundary	150.65 ± 4.00
LO Endoscrinium luridum		Poulsen & Riding (2003); This study		
J63	*Aulacostephanus eudoxus*	Partington et al. (1993)	Late Kimmeridgian	151.20 ± 4.00
J62	*Pictonia baylei*	Partington et al. (1993)	Early Kimmeridgian	155.00 ± 4.00
LO Scriniodinium crystallinum		Poulsen & Riding (2003); This study		
J56	*Amoeboceras rosenkrantzi*	Partington et al. (1993)	Oxfordian / Kimmeridgian boundary	155.65 ± 4.00
LO Endoscrinium galeritum	*Amoeboceras regulare*	This study	Late Oxfordian	156.30 ± 4.00
J54b	*Prionodoceras serratum*	Partington et al. (1993)	Late Oxfordian	156.85 ± 4.00
J54a	*Amoeboceras glosense*	Partington et al. (1993)	Late Oxfordian	157.15 ± 4.00
LO Gonyaulacysta jurassica longicornis; LO Rigaudella aemula	*Cardioceras tenuiserratum*	Poulsen & Riding (2003); This study	Middle Oxfordian	158.05 ± 4.00
J52	*Cardioceras densiplicatum*	Partington et al. (1993)	Middle Oxfordian	158.70 ± 4.00
LO Trichodinium scarburghensis		This study		
LO Wanaea fimbriata; LCO Trichodinium scarburghensis	*Cardioceras cordatum*	This study	Top Early Oxfordian	159.60 ± 4.00

J46	*Quenstedtoceras lamberti*	Partington et al. (1993)	Callovian / Oxfordian boundary	161.20 ± 4.00
LAO Mendicodinium groenlandicum; LO Lithodinia jurassica		This study		
LO Wanaea acollaris	*Peltoceras athleta*	This study	Late Callovian	162.00 ± 4.00
J44	*Erymnoceras coronatum*	Partington et al. (1993)	Top Middle Callovian	162.50 ± 4.00

Table 3.1. *Dated maximum flooding surfaces and palynological events used in this study, linked to Mid-to-Late Jurassic ammonoid zonation (Hardenbol et al., 1998; Poulsen & Riding, 2003). The biostratigraphic zonation is not the official Statoil's or Troll licence, but has been devised by us based on the raw microfossil occurrence data, and corresponds perfectly to the published zonation (c.f., Figure 11.17 of Fraser et al., 2003 – The Millennium Atlas). Stages and estimated ages assigned to ammonoid zones are taken from Gradstein et al. (2004) and Ogg et al. (2008). Uncertainties in estimated ages correspond to the age error of the boundaries of the stages within which the surfaces and events occur (Gradstein et al., 2004), and they are reported with a precision of 50-100 kyr. Some of the palynostratigraphic bioevents used in this study were linked to a specific chronostratigraphic horizon, based on a review of the relative occurrence of these fossils and other taxa in >120 wells situated in the Troll Field area.*

3.4.2 Sediment decompaction and backstripping to reconstruct subsidence history and depositional geometries

3.4.2.1 General method

Availability of accurate, pre-compaction stratigraphic geometries is necessary to interpret clinoform architectures and trajectories, and to infer the magnitude of relative sea level changes. In order to reconstruct, as far as possible, the depositional sediment thicknesses and stratal geometries for our quantitative stratigraphic analysis, we chose to decompact and backstrip the interval of interest and its overburden (Equations 1-3 in Appendix). Sediment decompaction and backstripping is performed on one-dimensional stratigraphic columns taken from well data which have been corrected to account for any deviation of the well path from vertical.

The change of porosity due to burial-related compaction is approximated by a negative exponential function, which is mostly dependent on the gross lithology (Athy, 1930; Hedberg, 1936; Sclater & Christie, 1980; Baldwin & Butler, 1985). Herein, we use the decompaction relationship defined by Allen & Allen (2005) (Equation 3.1 in Appendix).

In the second step, the cumulative tectonic subsidence or uplift that operated on the studied stratigraphic horizon during and before the time interval under consideration is extracted by removing the isostatic effects of the excess weight of the overlying sediment and water load, following the principles of Airy isostasy ('backstripping' *sensu* Watts & Ryan, 1976; Steckler & Watts, 1978; Sclater & Christie, 1980). The total subsidence (y) and tectonic subsidence (Y) accumulated on the basal surface of a given stratigraphic unit (S) prior to and during its deposition are assumed to be equal to the depth below a fixed reference surface of the decompacted horizon, and are quantified at the time interval of the reconstruction as a function of three factors: the palaeobathymetry of the depositional surface at the end of deposition of unit S (*wd*); eustatic sea level (Δ_{SL}) and the decompacted or partly decompacted thickness of the layer deposited on top of the stratigraphic horizon of interest (t_S) (Equations 2 and 3 in Appendix). Palaeobathymetry (*wd*) can be estimated from micropalaeontological data or from constraints provided by the geometry of depositional profiles such as clinoforms (e.g., Fig. 3.3A, Equation 4 in Appendix).

Once the values of tectonic subsidence in wells and well-correlation transects oriented perpendicular to structural grain have been estimated, then spatial variations in tectonic subsidence can be determined. For example, in a rift basin setting, if backstripping-derived subsidence variations are consistent with patterns of subsidence due to fault block rotation (e.g., progressive diminution of tectonic subsidence with increasing proximity to the footwall crest of a fault block), then they may be attributed to this mechanism, rather than to regional thermal subsidence trends. By tracing cross-sectional patterns of tectonic subsidence and their interpreted cut-offs across active faults, fault slip rates can be estimated in the plane of the well-correlation transects. In addition, tectonic tilting of the substrate during deposition of any given layer, $\kappa(x)$, can be calculated from trends of tectonic subsidence along cross-sections oriented perpendicular to the structural grain of the area (Equation 5 in Appendix; Fig. 3.3B).

Estimates of fault slip rates and tectonic tilting derived by backstripping analysis can be considered as potential indicators of tectonic activity or quiescence, and should be compared to similar parameters calculated by analysis of seismic cross-sections and seismically-derived sediment thickness maps. Active faults are interpreted in seismic data by observation of diagnostic stratal geometries, which in rift basins include wedge-shaped thickening across fault-bounded rotated blocks and onlap onto the hangingwall dipslope of such blocks. The amount of fault slip can be estimated in such data from the difference in the thickness of strata in the hangingwall and footwall of a fault. Subsidence analysis constrained by sediment backstripping may enable interpretation of low-magnitude fault slip (<30 m) and fault-block rotation (<0.10°), which are generally below vertical seismic resolution.

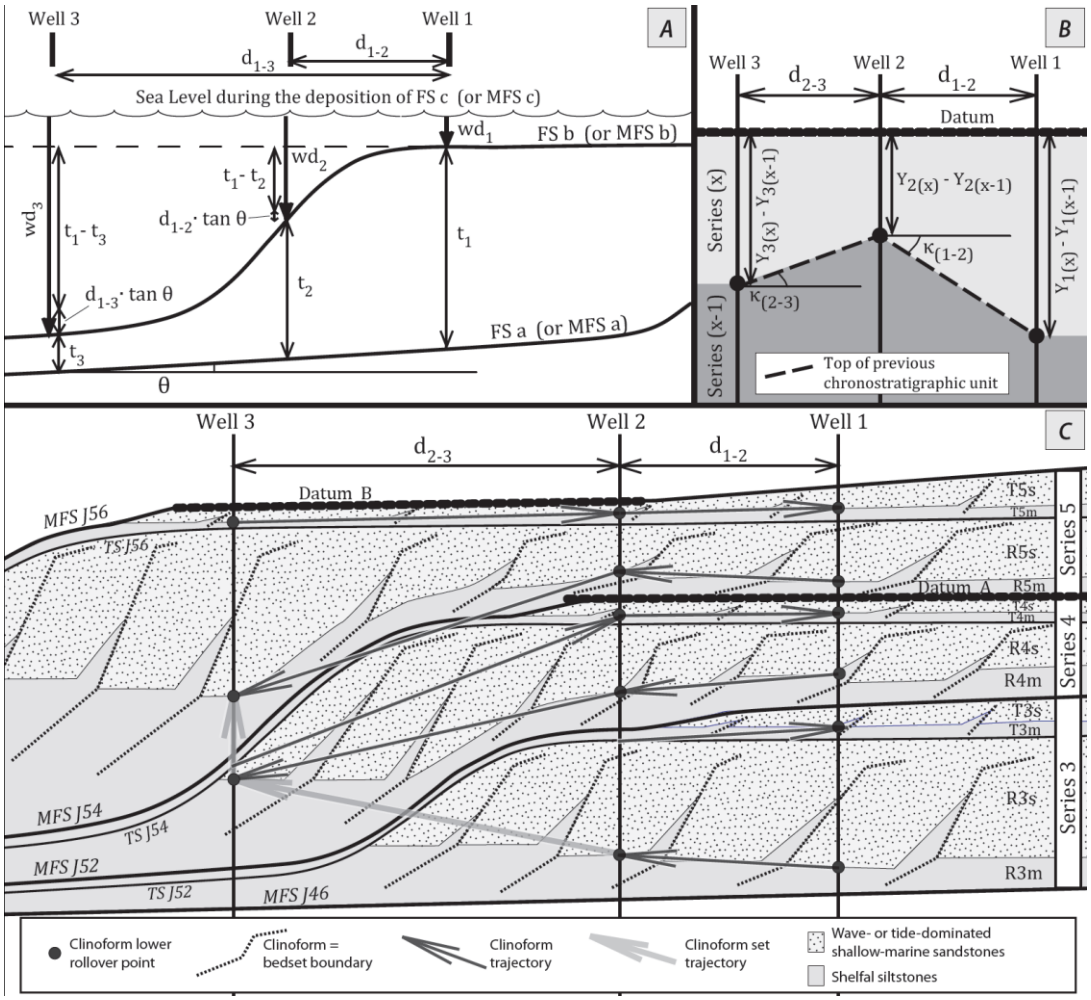

Figure 3.3*. Cartoon cross-sections illustrating geometrical relationships used to estimate various parameters. (**A**) Water depth of the depositional clinoform surface, after sediment thickness has been decompacted and water depth of the clinoform topset has been assigned. Parameters are explained in Equation 4 and associated text in Appendix. (**B**)Tectonic tilting of the substrate (κ), after tectonic subsidence has been calculated at each well. Parameters are explained in Equation 5 and associated text in Appendix. (**C**) Clinoform trajectories, measured within clinoform sets using a facies-belt boundary, and for stacked clinoform sets using the down-dip pinchout of the same facies-belt boundary in successive sets. Maximum regression positions and the main facies breaks, are approximations that are heavily dependant on the spacing between wells (cf., discussion of Hampson et al., 2009). Trajectories are calculated using the procedures outlined in Hampson et al. (2009) and Helland-Hansen & Hampson (2009) and by Equations 6 and 7 in the Appendix of this paper. R3m, R3s = thickness of respectively the mud-rich and the sand-prone parts of the regressive portion of Series 3; T3m, T3s = thickness of respectively the mud-rich and the sand-prone parts of the transgressive portion of Series 3, following the established nomenclature for the Sognefjord Formation reservoir (e.g. Dreyer et al., 2005). The distance between wells is the main source of error in the calculated trajectories, with large inter-well distances tending to decrease regressive trajectory angles and to increase transgressive trajectory angles.*

3.4.2.2 Decompaction and backstripping of the Sognefjord Formation

In the absence of palaeontologically-based, palaeobathymetric estimates of water depth for the Sognefjord Formation, we reconstruct the water depth of the depositional surface of interest from the geometrical constraints of our subaqueous delta interpretation (Fig. 3.3A). The topsets of modern, sand-rich subaqueous deltas, which are analogous to the "Troll Delta", occur at a water depth of ca. 20 m (±20 m; e.g., Pirmez et al., 1998; Hernández-Molina et al., 2000; Pomar et al., 2002; Walsh et al., 2004). Hence, clinoform topsets have been assigned a water depth of 20 m in the backstripping procedure (Equations 2 and 3 in Appendix) where they are intersected by wells. For wells intersecting the corresponding clinoform foreset or toeset, the water depth (wd_2) was estimated to be a function of topset water depth (wd_1), the distance down depositional dip between the well of interest and the topset-to-foreset rollover position (d), the difference in decompacted or partly compacted clinoform-set thickness between these two points (t_1-t_2), and the estimated shelfal bathymetric gradient (θ), according to Equation 4 in the Appendix (Fig. 3.3A).

In the shallow marine system under investigation, the shelfal bathymetric gradient (θ) is assigned a value of 0.02°, which is typical of modern shelves (Helland-Hansen & Hampson, 2009; Hampson et al., 2009). The timing and magnitude of eustatic sea-level variations during the Late Jurassic is too uncertain to be used for reliable adjustment of the subsidence profile in our backstripping of the Sognefjord Formation (e.g. see contrasting estimates of Pitman, 1978; Kominz, 1984; Haq et al., 1988). Instead, the late Oxfordian sea-level highstand is used as a datum horizon below which all backstripped depths are calculated (e.g., Fig. 3.3A).

In our backstripping of the Sognefjord Formation and its overburden, the values of φ_0 and c assigned to each layer are taken from Sclater & Christie (1980). Reasonable uncertainties of 25% for the compaction coefficient, c, (c.f. Steckler et al., 1999) could give rise to maximum errors of 6% in the calculated decompacted thicknesses. Using Equations 2, 3 and 4 in the Appendix, for typical values of t_1 (60 m), t_2 (20 m), d (2000 m), ρ_s (1,800 kg/m^3) and potential errors in θ of ±0.15° (cf. Olariu & Steel, 2009), we obtain relatively large errors in estimated total and tectonic subsidence for wells intersecting the clinoform topset (ca. 45 m), and even larger errors for wells intersecting the clinoform foreset (ca. 81 m). A large component of these errors (>20 m) is associated with uncertainties in estimates of eustatic sea-level and palaeobathymetry. However, such errors are systematic, and impact equally on all wells situated either landward or seaward of the underlying clinoform set rollover, with larger errors placed seaward of the rollover position. Conversely, errors associated with layer thickness in each well are small (<5 m). As a consequence, estimated relative changes of subsidence are still broadly reliable (e.g., in calculations of fault block tilting and slip rates – see later).

3.4.3 Clinoform trajectories

3.4.3.1 General method

Trajectories are derived by tracking the position of a reference point in successive clinoforms, relative to a palaeo-horizontal datum (Helland-Hansen & Hampson, 2009). This reference point is typically a break in slope, such as the topset-to-foreset rollover position ("depositional shoreline break-in-slope" *sensu* Posamentier & Vail, 1988; "offlap break" *sensu* Vail et al., 1991), but facies boundaries associated with a particular position along the clinoform profile can also be used in datasets where clinoform geometries are not directly observed (Hampson et al., 2009; Helland-Hansen & Hampson, 2009) (cf. Fig. 3.3C; Equations 6 and 7 in Appendix). Trajectories may be studied at a variety of scales, depending on data type and resolution, but most commonly are used to characterise migration of the shoreline and shelf edge (e.g. Henriksen et al., 2009). Trajectories for shoreline-scale clinoforms have been characterised within individual clinoform sets (to characterise architectures within parasequences, *sensu* Van Wagoner et al., 1990) and from the stacking of clinoform sets (cf. 'parasequence stacking pattern' of Van Wagoner et al., 1990). Trajectories within clinoform sets are small (<2° from palaeo-horizontal; Helland-Hansen & Hampson, 2009), while a wide range of angles is documented for stacking of clinoform sets (up to 90° from palaeo-horizontal for aggradationally stacked sets; Hampson et al., 2009; Helland-Hansen & Hampson, 2009).

Quantitative estimates of trajectory may be affected by five potential sources of error (Hampson et al., 2009; Helland-Hansen & Hampson, 2009): (1) data distribution and quality, including seismic resolution, time-depth conversion and well spacing; (2) choice of reference point to track between clinoforms; (3) morphology of the datum surface, which should be laterally extensive and approximately palaeo-horizontal; (4) post-depositional compaction; and (5) orientation of two dimensional (2D) transects used to calculate trajectory, relative to depositional dip.

3.4.3.2 Clinoform trajectory analysis of the Sognefjord Formation

In the Sognefjord Formation case study, clinoform trajectory is calculated at two scales; within individual clinoform sets, and the stacking of multiple clinoform sets. Although well spacing is large in the dataset (ca. 5 km,

but ranging from 1.3 to 10.3 km, Fig. 3.2A), errors associated with data distribution (error source 1 listed above) are likely to be small for both scales of investigation, because the geometry of clinoforms and clinoform sets is tightly constrained by 3D seismic data.

For trajectories within clinoform sets, a facies-belt boundary marked by a transition from siltstones to sandstones is used as a reference point (error source 2 listed above, Fig. 3.3C). Facies analysis indicates that this transition marks storm wave base (Chapter 2); although storm wave base is likely to be subject to some variation in water depth, the transition also coincides with the position of clinoform foreset-to-toeset rollover, which can be observed and mapped on 3D seismic data. Trajectories of stacked clinoform sets are calculated by tracing the down-dip pinchout of shallow-marine sandstones in each set, which is similar to the facies-belt transition used as a reference point within each clinoform set, and is subject to the same small degree of error.

The J54 and J56 maximum flooding surfaces are used as datum surfaces (error source 3 listed above) in the eastern and western parts of the study area, respectively (cf. Fig. 3.3C). Both flooding surfaces are laterally extensive and readily identifiable in seismic and well data. The J54 maximum flooding surface overlies the topset of the Series 4 clinoform set (Figs. 3.4-3.5), and thus approximates a palaeo-horizontal surface in the eastern part of the study area. The J56 surface overlies the topset of the Series 5 clinoform set (Figs. 3.4-3.5) in a similar way, although backstripping analysis indicates that the J56 surface underwent post-depositional tectonic rotation in the eastern part of the study area (Equations 6 and 7 in Appendix are used to take this rotation into account; Fig. 3.3C). Both datum surfaces are assigned a palaeo-seaward dip of 0.02° for trajectory calculations, consistent with values of θ used in Equation 4 in the Appendix (Fig. 3.3A) (cf. modern shelves; Hampson et al., 2009; Helland-Hansen & Hampson, 2009). Modern shelves are however steeper (ca. 0.1°) in regions out-of-axis of rivers supplying large volumes of sand (Olariu & Steel, 2009). As a result, our calculations may systematically underestimate transgressive and descending regressive trajectories, and overestimate ascending regressive trajectories (*sensu* Helland-Hansen & Martinsen, 1996).

Post-depositional compaction (error source 4 listed above) is corrected for in our analysis of the Sognefjord Formation dataset by applying decompaction and backstripping techniques prior to calculation of clinoform trajectory. Furthermore, the 2D transects used to calculate trajectories are consistently oriented perpendicular to the strike of seismically resolved clinoforms, which varies little in the study area (error source 5 listed above; Fig. 3.2) (Chapter 2).

In summary, the high quality of the Sognefjord Formation dataset, which integrates geometrical information from 3D seismic data and sedimentological information from cores and well logs, and the use of decompaction and

backstripping techniques results in only small errors in calculated clinoform trajectories, even in this ancient (155-163 Ma) stratigraphic succession.

3.4.4 Assignment of ages to clinoform-trajectory reference points

There are three steps in the general methods to assign ages to clinoform-trajectory reference points (e.g. positions of the siltstone-sandstone facies-belt transition in studied wells, Fig. 3.3C). Each of these, together with the method to assign an error to the age calculation, is explained below. Once ages have been assigned to the clinoform-trajectory reference points in all wells, then progradation rates and other parameters can be calculated. The application of the method to the Sognefjord Formation is then presented.

3.4.4.1 Estimation of depth-dependent instantaneous sediment accumulation rates in each well

The first step is to identify and assign ages to the maximum flooding surfaces that define the base and top of a particular clinoform set in a given well. Table 1 outlines the ages of maximum flooding surfaces in the Sognefjord Formation. The well may also intersect additional reliable biostratigraphic events within the clinoform set (e.g. "point 1" in Fig. 3.4A, D). A second-order polynomial function is fitted to the three or more data points that correspond to the maximum flooding surfaces and biostratigraphic events penetrated in the well. The location of biostratigraphic events in either the upper or lower part of the clinoform set determines whether the function will have a convex-upward or concave-upward shape, respectively (Fig. 3.4B, E). The first derivative of the function is used to calculate depth-dependent instantaneous sediment accumulation rates in each clinoform set along the well (Fig. 3.4B, E). The maximum and minimum values of instantaneous sediment accumulation rate may differ markedly from the average sediment accumulation rate in the clinoform set.

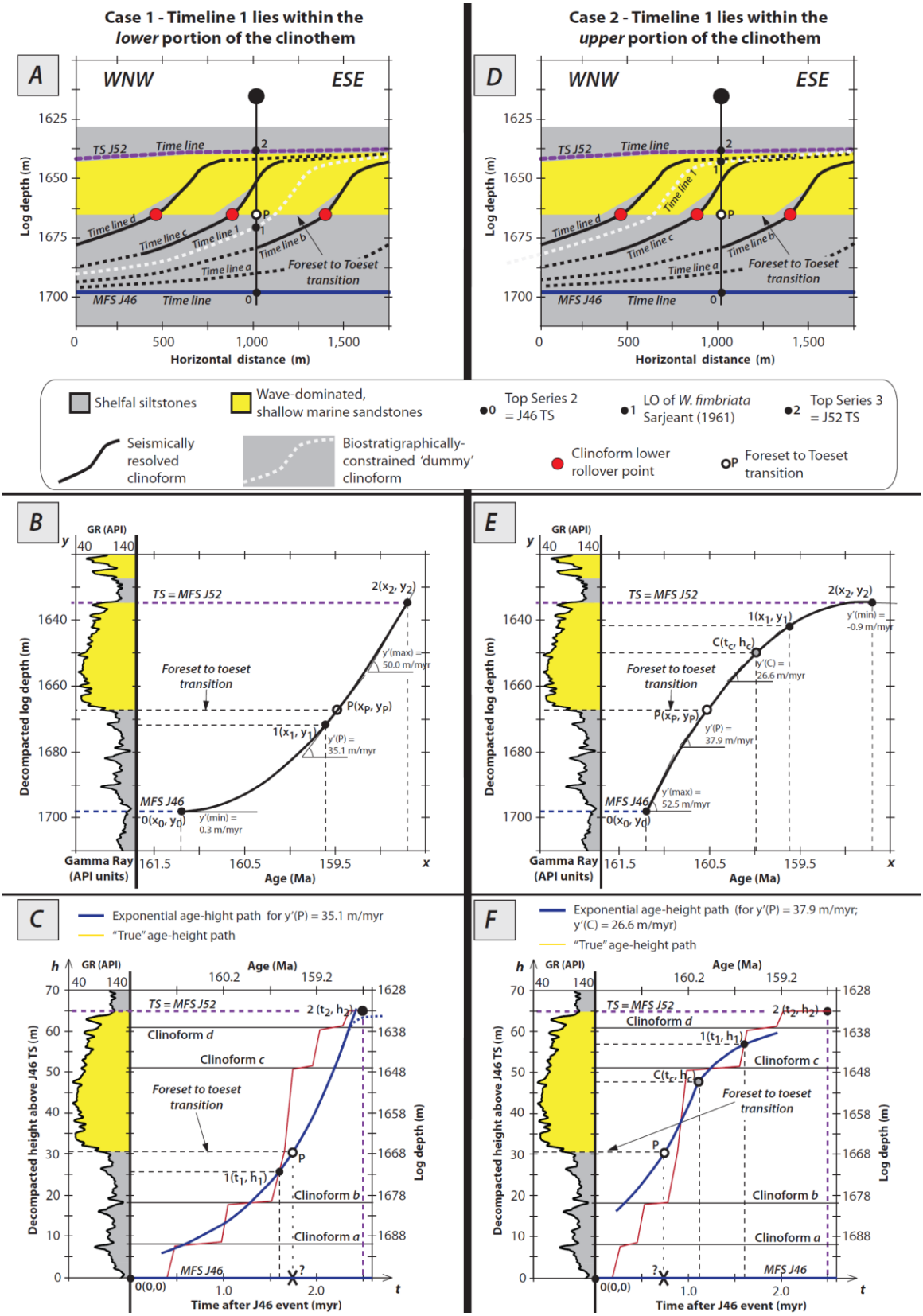

Figure 3.4*. Examples illustrating the method used to estimate the age of a clinoform in cases where a biostratigraphic event (point 1) lies within the lower (**A-C**) and upper (**D-F**) parts of a clinoform set. This example is synthesised from a real well (31/5-3); however the geoseismic cross-sections in parts A and D are schematic representations. (**A, D**) Geoseismic cross-*

*sections indicating stratal geomeries and relationships around a studied well. (**B, E**) Age-depth graphs showing the positions within a studied well of the maximum flooding surfaces defining the lower and upper boundaries of the clinoform set (points 0 and 2, respectively), and a biostratigraphic event occurring within the clinoform set (point 1). The three points are all dated. Point P marks a reference point for tracking clinoform trajectory in the well, in this case a facies-belt transition. (**C, F**) Exponential age-depth model applied to estimate the age of the sandstone-to-siltstone facies-belt transition in the well (t_P). See text and Equations 8-15 in Appendix for details.*

3.4.4.2 Estimation of age of clinoform-trajectory reference point in wells containing biostratigraphic events

The second step is to apply an age-depth model in order to derive an equation that calculates the age of the clinoform-trajectory reference point in the well (e.g. the facies transition between offshore siltstones and wave-dominated sandstones at "point P" in Fig. 3.4A, D). For horizontally-migrating, sigmoidal clinoforms, geometrical relationships dictate that vertical sediment accumulation rate is greatest in the foreset, where depositional dips are steepest, but decreases towards the underlying toeset and overlying topset (as also noted in Holocene subaqueous deltas; Kuehl et al., 1986; Alexander et al., 1991; Michels et al., 1998; Walsh et al., 2004; Cattaneo et al., 2007). The choice of equation to describe the age-depth model depends on whether the biostratigraphic events (e.g. "point 1" in Fig. 3.4A, D) lie in the lower or upper part of the clinoform set.

In the case when point 1 lies in the lower part of the clinoform (Equations 8-14 in Appendix), we apply an exponential age-depth interpolation model, which depends upon the values of four parameters: (1) age (t_1) and (2) height (h_1) above the basal maximum flooding surface of a dated biostratigraphic event within the clinothem; (3) height of the toeset-to-foreset transition (h_P) above the basal maximum flooding surface; (4) and sediment accumulation rate at the time of the deposition of the toeset/foreset transition (S_P). The parameter t_P in Figure 3.4, which is the age of the onset of sand-prone foreset deposition (i.e., of the facies break at the toeset-to-foreset transition) and the overall age model is given respectively by Equations 13 and 14 (see also Appendix):

$$t_P = [h_P \cdot (\ln h_P - \ln h_1) \cdot (S_P)^{-1}] + t_1 \qquad (13)$$

$$h(t) = K \cdot e^{\alpha t} = h_P \cdot \exp [(\ln h_P - \ln h_1) \cdot (t_P - t_1)^{-1} \cdot (t - t_P)] \qquad (14)$$

For a biostratigraphic event lying in the upper part of the clinoform set, it is first necessary to estimate the age of the point at the centre of a clinoform foreset (e.g. "point C" in Fig. 3.4D-F, with age t_C) in order to constrain age-depth relationships for the clinoform-trajectory reference point, where this lies in the bottom part of the clinoform set (i.e., the siltstone-sandstone facies-belt transition at "point P" in Fig. 3.4). In order to calculate t_C, we first need to estimate the age of the transgressive surface immediately overlying the topset of the clinoform set. This is considered to be equal to the age of maximum regression for the clinoform set (i.e., 'transgressive surface' *sensu* Van Wagoner et al., 1990), which predates the maximum flooding surface lying above it. This age is calculated by applying Equation 13 to wells situated towards the position of regional maximum regression of the given clinoform set, where the (bio)stratigraphic event (i.e., Point 1) is extremely likely to occur in the lower part of each clinoform set (see Fig. 3.4). The age of "point C" (t_C) is then calculated using a logarithmic interpolation based on Equation 13 that depends on the instantaneous sediment accumulation rate at the point C (i.e., S_C) and on the age-depth coordinates of the biostratigraphic event, "point 1" (t_1,h_1), as measured relative to the transgressive surface at the top of the clinoform set (Fig. 3.4E, Equation 15 in Appendix). Finally, we calculate the age of the clinoform-trajectory reference point, t_P, simply by utilizing the stratigraphic position and calculated age of "point C" (t_C,h_C) as substitute terms for t_1 and h_1 in equation 13 (Fig. 3.4E, F).

3.4.4.3 Estimation of age of clinoform-trajectory reference point in wells lacking biostratigraphic events

Ages of clinoform-trajectory reference points can also be estimated in wells that do not penetrate biostratigraphic events. A "dummy" clinoform, whose geometry is constrained by seismically-mapped clinoforms, is inserted into a neighbouring well that contains a biostratigraphic event (e.g. white line marked "time line 1" through "point 1" in Fig. 3.4A, D), and projected into the well of interest to define a "dummy" biostratigraphic event. The age of each "dummy" clinoform is thus constrained by biostratigraphic data in neighbouring wells, and its position in the well is constrained by seismic data.

3.4.4.4 Errors in estimated ages of clinoform-trajectory reference points

In the last step of our procedure, the cumulative error associated with estimated ages (Δt_P) of the clinoform-trajectory reference point, t_P, is calculated using the error propagation law (Equations 16 and 17 in Appendix), which is constrained by the errors associated with the four parameters required to calculate t_P through Equation 13 (i.e., Δt_1, Δh_1, Δh_P and ΔS_P, whose values are given by Equations 18 to 21 in Appendix).

Figure 3.5A shows how the relative error in the estimated age of the clinoform-trajectory reference point, t_P, varies according to relative errors in the four parameters (Δt_1, Δh_1, Δh_P, ΔS_P) upon which it depends (Equation 17 in Appendix). Relative errors in the stratigraphic position of the clinoform-trajectory reference point (Δh_P) have minimal effect on Δt_P. Relative errors in estimated instantaneous sediment accumulation rate at the clinoform-trajectory reference point (ΔS_P) and in the stratigraphic position of the biostratigraphic event (Δh_1) have only moderate impact, whereas Δt_P is most sensitive to relative errors in the age of biostratigraphic events within the clinoform set (Δt_1). However, errors in biostratigraphic event age (Δt_1) are systematic and apply equally in all wells, because they depend on uncertainties in the absolute ages of the maximum flooding surface at the base of the clinoform set (x_0; Fig. 3.4B,E) and of the biostratigraphic event within the clinoform set (x_1; Fig. 3.4B,E), as defined for the time scale in use. As a consequence, Δt_1 can be disregarded when used to calculate age-related parameters that are relative between wells (e.g. progradation rate between wells).

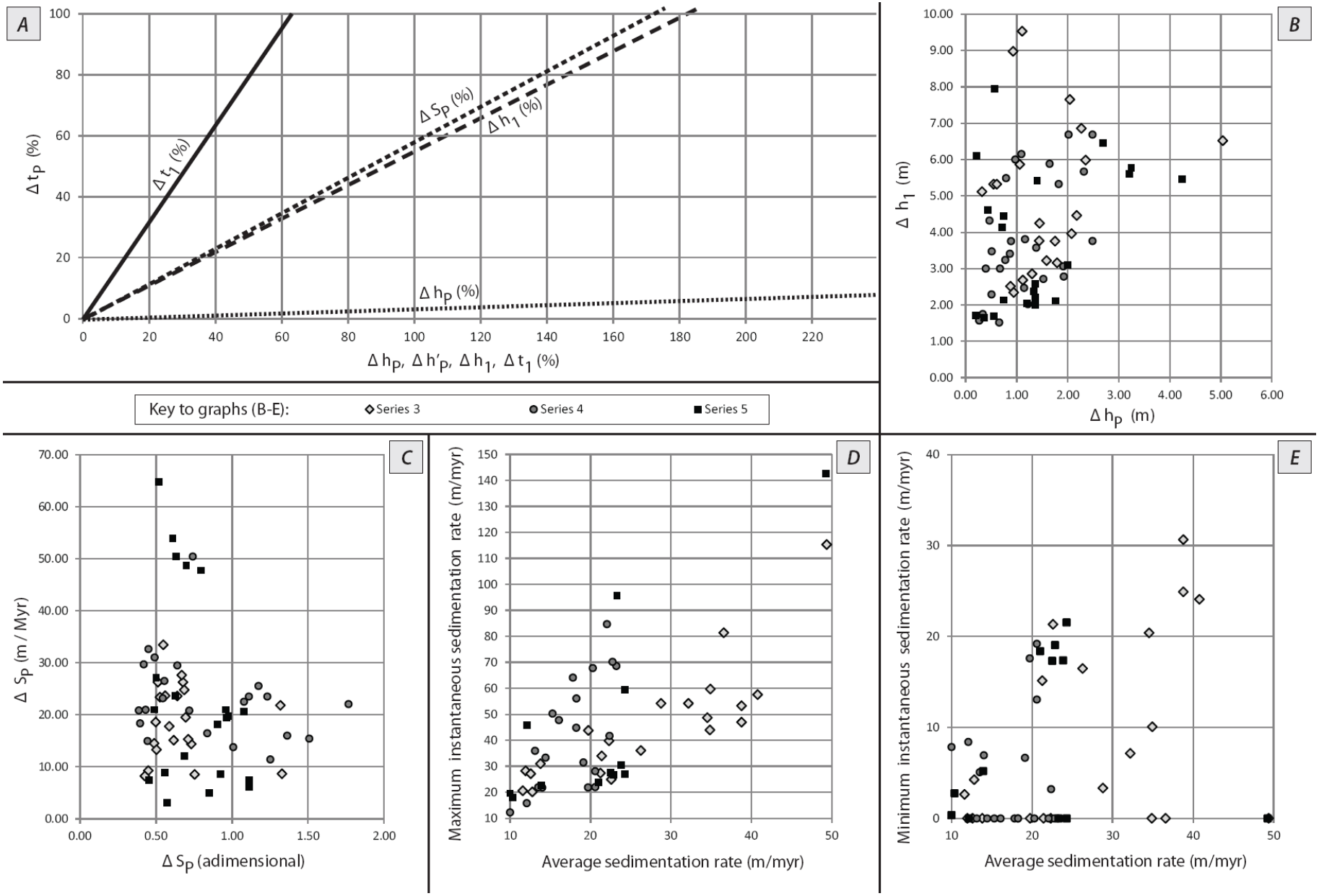
A
Δ tP (%)
Δ t1 (%)
Δ SP (%)
Δ h1 (%)
Δ hP (%)
Δ hP, Δ h'P, Δ h1, Δ t1 (%)
B
Δ h1 (m)
Δ hP (m)
Key to graphs (B-E):
Series 3
Series 4
Series 5
C
Δ SP (m / Myr)
Δ SP (adimensional)
D
Maximum instantaneous sedimentation rate (m/myr)
Average sedimentation rate (m/myr)
E
Minimum instantaneous sedimentation rate (m/myr)
Average sedimentation rate (m/myr)

***Figure 3.5**. (**A**) Plot showing how the relative errors in the age of the reference point used to track clinoform trajectory in a well (t_P; Fig. 3.4C, F) varies according to relative errors in the age of biostratigraphic events within the clinoform set (Δt_1), estimated instantaneous sedimentation rate at the reference point (ΔS_P), stratigraphic position of the biostratigraphic event (Δh_1), and stratigraphic position of the reference point (Δh_P) (calculated using Equations 16-21 in Appendix). (**B**) Plot of the relative error in stratigraphic height of the reference point above the base of the clinoform set (Δh_P) against the relative error in stratigraphic height of the biostratigraphic event above the base of the clinoform set (Δh_1). (**C**) Plot of the relative versus absolute error associated with the estimates of sedimentation rate during the deposition of the toeset-to-foreset transition. (**D-E**) Plots of average sedimentation rate versus minimum (**D**) and maximum (**E**) instantaneous sedimentation rate, calculated in each well and within each clinoform set using the method illustrated in Figure 3.4B.*

3.4.4.5 Application to the Sognefjord Formation

Availability of biostratigraphic range charts, core and wireline-log data allows a straightforward application of the method outlined above in order to estimate, in each well, the age of the facies break at the toeset-to-foreset transition (t_P). As a consequence, the age of the onset of sand-prone foreset deposition has been estimated in each the well-head location for each series.

In the case of the Late Jurassic Sognefjord Formation, errors in biostratigraphic event age (Δt_1) are high (± 4.00 Myr, after Gradstein et al., 2004; Table 3.1). Therefore, we disregard this parameter when we apply equation (17) in order to calculate error bars around the mean age of the foreset base at each well-head location.

3.4.5 Estimation of progradation rates, sediment accumulation rates and sediment fluxes

3.4.5.1 General method

Once the age of clinoforms (t_P) has been estimated at the position of well along one or more depositional-dip-oriented transects, four parameters that characterise temporal and spatial variations in sedimentation can be quantitatively assessed. (1) Progradation rate is calculated between each pair of wells along a depositional-dip-oriented transect (e.g. Figs. 3.6, 3.7, for the Sognefjord Formation example), by simply dividing the distance between the two wells by the relative age difference between clinoform-trajectory reference points in the two

wells. (2) Vertical sediment accumulation rate in each well is obtained by dividing the thickness of each clinoform set by its estimated duration. Volumetric sediment accumulation rates can be calculated in a similar way, by using sediment volumes in the study area rather than vertical thicknesses in wells for each clinoform set. Sediment volumes were obtained for each clinoform set by integrating their seismically-constrained, compacted time-thicknesses (i.e. isochrons) across their areal extent (within the limits of the 3D seismic dataset), and then converting time-thicknesses (ms TWT) to depth-thicknesses (in metres or other units of length) using interval velocities derived from checkshot surveys. (3) The ratio between vertical sediment accumulation rate and progradation rate is also calculated for each pair of wells along a depositional-dip-oriented transect. This ratio quantifies the amount of sediment that needs to accumulate in order for the clinoform to prograde of a single unit, and it represents a measure of the 'resistance' to clinoform progradation; it is termed herein the progradation resistance ratio. (4) Unit-width depositional flux along a depositional-dip-oriented transect is calculated as the product of estimated progradation rate and mean decompacted thickness of a given clinoform set. This parameter is a combination of riverine sediment input rate, which is predominantly oriented along depositional dip, and marine sediment transport rate, which is oriented alongshore and may transport sediment into or out of the plane of the transect (c.f. the 'deltaic and marine deposition/erosion rate' of Burgess & Hovius, 1998). When combined with sediment provenance analysis, estimates of depositional flux may be used to characterise sediment routing and budgets.

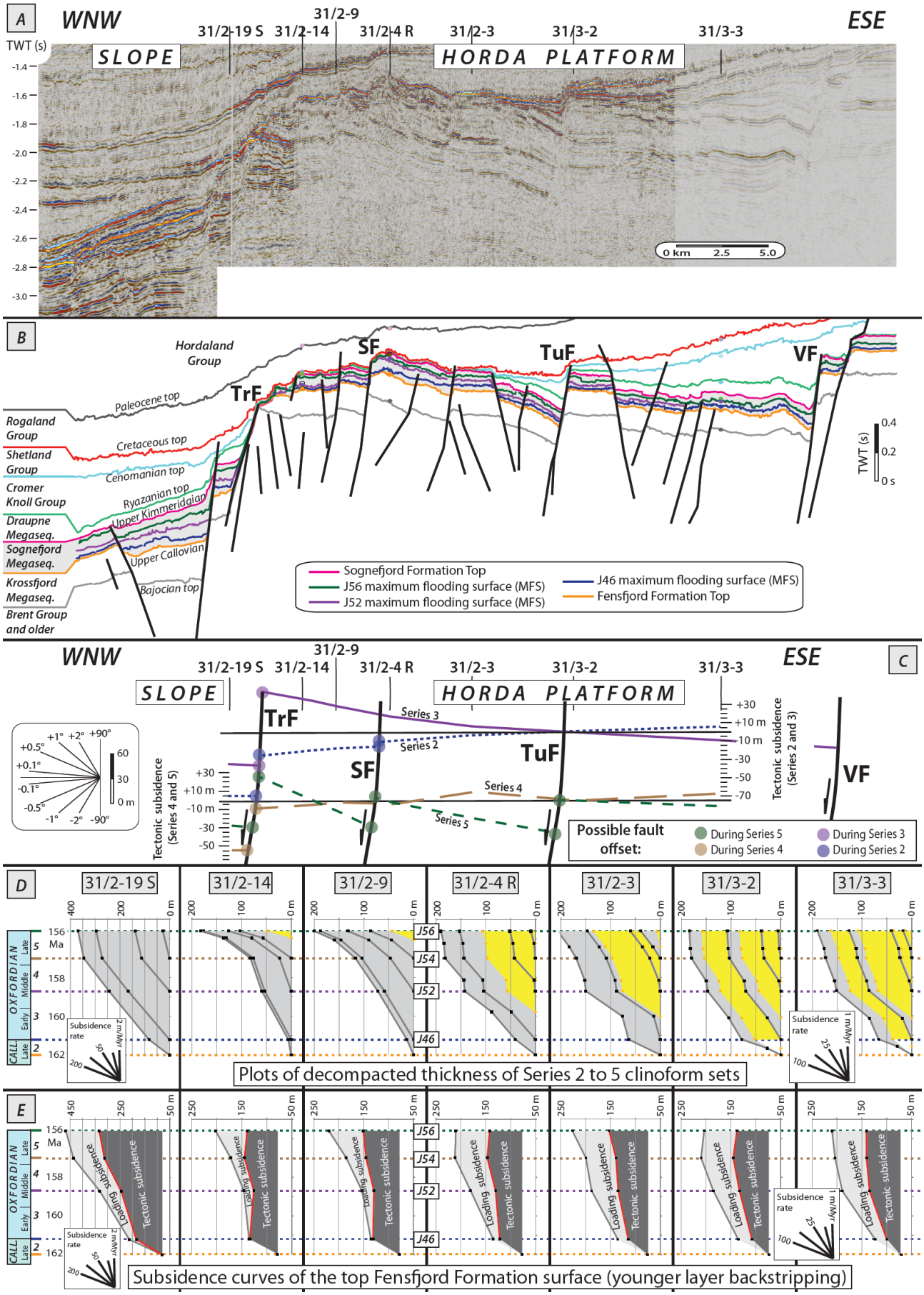
A
WNW
ESE
31/2-9
31/2-19 S
31/2-14
31/2-4 R
31/2-3
31/3-2
31/3-3
SLOPE
HORDA PLATFORM
TWT (s)
-1.4
-1.6
-1.8
-2.0
-2.2
-2.4
-2.6
-2.8
-3.0
0 km 2.5 5.0
B
Hordaland Group
SF
TuF
VF
TrF
Paleocene top
Rogaland Group
Cretaceous top
Shetland Group
Cenomanian top
Cromer Knoll Group
Ryazanian top
Upper Kimmeridgian
Draupne Megaseq.
Sognefjord Megaseq.
Upper Callovian
Krossfjord Megaseq.
Bajocian top
Brent Group and older
TWT (s)
0.4
0.2
0 s
Sognefjord Formation Top
J56 maximum flooding surface (MFS)
J52 maximum flooding surface (MFS)
J46 maximum flooding surface (MFS)
Fensfjord Formation Top
C
WNW
ESE
31/2-9
31/2-19 S
31/2-14
31/2-4 R
31/2-3
31/3-2
31/3-3
SLOPE
HORDA PLATFORM
TrF
SF
TuF
VF
Series 3
Series 2
Series 4
Series 5
+1° +2° +90°
+0.5°
+0.1°
-0.1°
-0.5°
-1° -2° -90°
60
30
0 m
Tectonic subsidence (Series 4 and 5)
+30
+10 m
-10 m
-30
-50
Tectonic subsidence (Series 2 and 3)
+30
+10 m
10 m
-30
-50
-70
Possible fault offset:
During Series 5
During Series 4
During Series 3
During Series 2
D
31/2-19 S
31/2-14
31/2-9
31/2-4 R
31/2-3
31/3-2
31/3-3
400
200
0 m
200
100
0 m
OXFORDIAN
CALL
Late
Middle
Early
Late
156
158
160
162
Ma
5
4
3
2
J56
J54
J52
J46
Subsidence rate
2 mm/yr
50
200
1 mm/yr
25
100
Plots of decompacted thickness of Series 2 to 5 clinoform sets
E
450
250
50 m
250
150
50 m
Loading subsidence
Tectonic subsidence
Subsidence curves of the top Fensfjord Formation surface (younger layer backstripping)

***Figure 3.6**. (**A**) Uninterpreted seismic cross-section and (**B**) geoseismic interpretation oriented approximately perpendicular to the depositional strike of clinoforms in the Sognefjord Formation across the northern part of the Troll Field (Figs. 3.1C, 3.2A). The main faults are labelled as in Figure 3.1C. (**C**) Tectonic subsidence calculated for each well along the correlation panel by backstripping analysis (Fig. 3.6D, E). Possible fault activity is indicated by differences in tectonic subsidence between wells situated in the hangingwall and footwall of the main faults, which are labelled as in Figure 3.1C. Interpreted stratal cut-offs at the faults are also shown. Similar trends are recognized as those shown in Figure 3.7C, and these trends are largely compatible with seismically derived thickness maps (e.g., Fig. 3.9, Table 3.2). (**D**) Plots of decompacted thicknesses of Series 2 to 5 clinoform sets for each well along the cross-sectional transect. The plots trace the Callovian-to-Oxfordian burial history of the maximum flooding surfaces that bound each clinoform set. The datum surface (0 m) is the seafloor at the time of the deposition of the studied layers. (**E**) Corresponding subsidence curves of the top Fensfjord Formation surface resulting from backstripping of younger layers in a water-filled basin. The datum surface (0 m) is the Top Oxfordian eustatic sea level stand of Hardenbol et al. (1998). The accumulation of subsidence due to both tectonic mechanisms and sediment loading is shown. Subsidence curves are corrected for eustacy and water depth.*

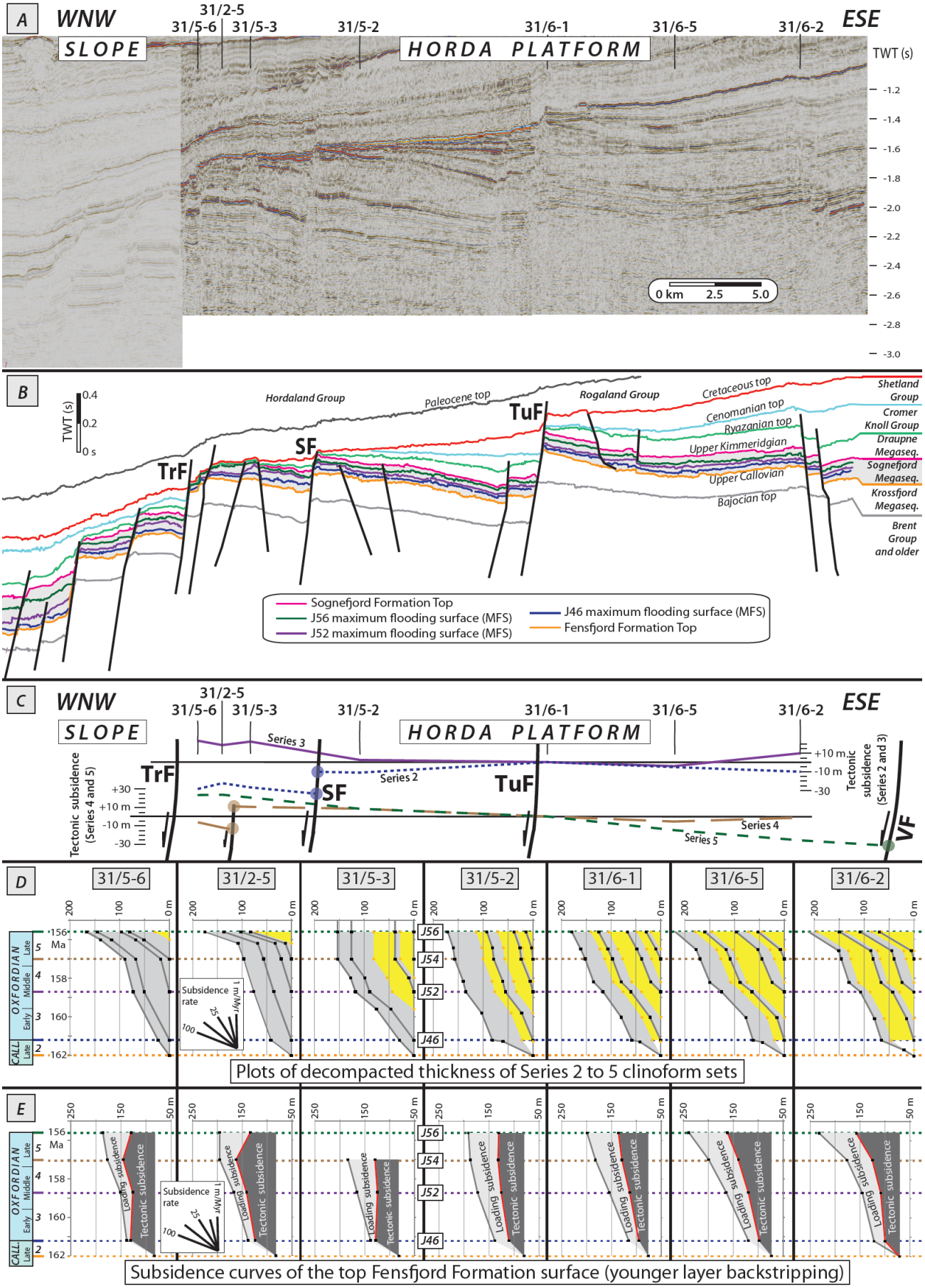
A
WNW
SLOPE
31/2-5
31/5-6
31/5-3
31/5-2
HORDA PLATFORM
31/6-1
31/6-5
31/6-2
ESE
TWT (s)
-1.2
-1.4
-1.6
-1.8
-2.0
-2.2
-2.4
-2.6
-2.8
-3.0
0 km 2.5 5.0
B
TWT (s)
0.4
0.2
0 s
Hordaland Group
Paleocene top
TuF
Rogaland Group
Cretaceous top
Cenomanian top
Ryazanian top
Upper Kimmeridgian
Upper Callovian
Bajocian top
SF
TrF
Shetland Group
Cromer Knoll Group
Draupne Megaseq.
Sognefjord Megaseq.
Krossfjord Megaseq.
Brent Group and older
Sognefjord Formation Top
J56 maximum flooding surface (MFS)
J52 maximum flooding surface (MFS)
J46 maximum flooding surface (MFS)
Fensfjord Formation Top
C
WNW
SLOPE
31/2-5
31/5-6
31/5-3
31/5-2
HORDA PLATFORM
31/6-1
31/6-5
31/6-2
ESE
Series 3
Series 2
Series 4
Series 5
TrF
SF
TuF
VF
Tectonic subsidence (Series 4 and 5)
+30
+10 m
-10 m
-30
+10 m
-10 m
-30
Tectonic subsidence (Series 2 and 3)
D
31/5-6
31/2-5
31/5-3
31/5-2
31/6-1
31/6-5
31/6-2
200
100
0 m
OXFORDIAN
CALL.
Late
Middle
Early
Late
156
Ma
158
160
162
5
4
3
2
Subsidence rate
1 m/Myr
25
100
J56
J54
J52
J46
Plots of decompacted thickness of Series 2 to 5 clinoform sets
E
250
150
50 m
Loading subsidence
Tectonic subsidence
Subsidence curves of the top Fensfjord Formation surface (younger layer backstripping)

Figure 3.7. *(**A**) Uninterpreted seismic cross-section and (**B**) geoseismic interpretation oriented approximately perpendicular to the depositional strike of clinoforms in the Sognefjord Formation across the southern part of the Troll Field (Figs. 3.1C, 3.2A). The main faults are labelled as in Figure 3.1C. (**C**) Tectonic subsidence calculated for each well along the correlation panel by backstripping analysis (Fig. 3.7D, E); see Figure 3.6C for key. Possible fault activity is indicated by differences in tectonic subsidence between wells situated in the hangingwall and footwall of the main faults, which are labelled as in Figure 3.1C. Interpreted stratal cut-offs are also shown. Similar trends are recognized as those shown in Figure 3.6C, and these trends are largely compatible with seismically derived thickness maps (e.g., Fig. 3.9, Table 3.2). (**D**) Plots of decompacted thicknesses of Series 2 to 5 clinoform sets for each well along the cross-sectional transect. The plots trace the Callovian-to-Oxfordian burial history of the maximum flooding surfaces that bound each clinoform set. The datum surface (0 m) is the seafloor at the time of the deposition of the studied layers. (**E**) Corresponding subsidence curves of the top Fensfjord Formation surface resulting from backstripping of younger layers in a water-filled basin. The datum surface (0 m) is the Top Oxfordian eustatic sea level stand of Hardenbol et al. (1998). The accumulation of subsidence due to both tectonic mechanisms and sediment loading is shown. Subsidence curves are corrected for eustacy and water depth.*

3.4.5.2 Application to the Sognefjord Formation

Progradation rate, sediment accumulation rate, volumetric sediment accumulation rate, progradation resistance ratio and depositional flux have been calculated in the study interval along two transects that integrate well and seismic data, and that are oriented parallel to the depositional dip of clinoforms in the Sognefjord Formation (Figs. 3.6, 3.7). The values of seismic velocity estimated from the checkshot survey (from 0.90 to 1.02 m/ms) were used to convert time-thickness (ms TWT) to true thickness (in metres), in order to calculate volumes of sediments and constrain volumetric sediment accumulation rates. Sediment volumes for the Series 4 and 5 clinoform sets are combined to give an average value, because the J54 maximum flooding surface cannot be resolved over the full area covered by the seismic dataset. Sediment volumes for each clinoform set are divided by the clinoform-set duration for each clinoform set to give volumetric sediment accumulation rates. Given the rift basin context of the Sognefjord Formation, the unit-width depositional flux is considered to consist of the initial river-fed sediment input supplied into the plane of the transect, plus any additional local contributions of sediment input (e.g. from the erosional reworking of fault block crests), minus the sediment removed from the transect plane by along-shelf transport (i.e., southwards or northwards) or cross-shelf (i.e. westwards) transport and transfer to the slope and basin floor.

In the following sections, we integrate our quantitative stratigraphic analysis of the Sognefjord Formation with provenance analysis, in order to constrain aspects of sediment routing. Six basement domains are recognised in onshore Norway based on detrital garnet composition, which is relatively unchanged by burial diagenesis (Morton

et al., 2004). These onshore basement domains provide a framework for provenance analyses of Middle Jurassic to Recent sandstones in the offshore North Sea, because these sandstones were supplied by erosional unroofing of the onshore domains but their garnet assemblages did not change significantly through time (Hurst & Morton, 1988; Morton et al., 2004).

3.5 RESULTS

The results presented below are based on applying the methods above to two well-correlation transects that are oriented broadly parallel to depositional dip (Figs. 3.6, 3.7).

3.5.1 Subsidence history reconstructed from sediment decompaction and backstripping

Estimates of total and tectonic subsidence derived by applying decompaction and backstripping techniques to the well-correlation transects reveal temporal and spatial variations in subsidence (Figs. 3.6C-E, 3.7C-E), which are summarised in Table 3.2. During deposition of Series 2, a relatively high tectonic subsidence rate is calculated, although rates are markedly lower in the footwall (ca. 28-47 m/Myr) than in the hangingwall (ca. 54-67 m/Myr) of the Svartav Fault. During deposition of Series 3 and 4, the tectonic subsidence rate was relatively uniform throughout the study area, but lower (ca. 0-20 m/Myr) than during deposition of Series 2. During deposition of Series 5, tectonic subsidence was spatially more variable, and was characterised by slow subsidence and possibly uplift area in the footwalls of block-bounding normal faults in the western part of the study area (i.e. an uplift rate of ca. 12 m/Myr in well 31/2-5) and increasingly rapid subsidence away from the crests of the fault-bounded blocks, down the adjacent hangingwall dip slopes (i.e. up to ca. 23 m/Myr in well 31/6-2). The only well situated in the hangingwall of the Troll Fault, well 31/2-19S, underwent more rapid subsidence (from ca. 60 m /Myr in Series 2 to ca. 15 m /Myr in Series 5) than wells in the footwall of this fault, such as 31/2-9, 31/2-14 and 31/2-4R (Figs. 3.6C-E).

These estimates of spatial and temporal variations in subsidence are partly supported by seismically-derived isochron maps of the Series 2, 3, and 4-5 clinoform sets (Fig. 3.8). In particular, a minor change in time-thickness across the Svartav Fault is evident in Series 2, which is ca. 20 ms TWT thicker in the hangingwall of this fault than on its footwall (Fig. 3.8A). In addition, Whipp et al. (in press) determined that the Sognefjord Formation is ca. 70 ms TWT thicker in the hangingwall of the Troll Fault than in its footwall. This is indicative of low-magnitude normal fault activity at the westernmost edge of the Horda Platform during the deposition of the Sognefjord Formation. However, many subtle thickness variations across faults that are interpreted from backstripping of well data are not resolved in the seismic data; we suggest that this is due to a combination of the inability of the seismic data to image relatively subtle thickness changes and the pronounced gas-water contact-related 'flat spot' that cuts across stratigraphy and distorts stratal thicknesses in the Troll Field.

The Troll Fault, which defines the edge of the Horda Platform, is inferred to have been active throughout deposition of the Sognefjord Formation; we estimate slip rates ranging from ca. 15 to ca. 60 m/Myr using the data and interpretations presented in Figs. 3.6C, 3.7C. Other faults exhibit episodic activity, which generated small displacements during deposition of the Series 2 and Series 5 clinoform sets. These periods of fault activity are separated by longer phases of tectonic quiescence; During deposition of Series 2, slip rates of ca. 60 m/Myr and 30 m/Myr are inferred respectively for the Troll and Svartav faults, whereas a slip rate of ca. 25 m/Myr is inferred during deposition of Series 5 for the Troll, Svartav, Tusse and Vette faults (Figs. 3.6C, 3.7C). Using Equation 5 (Appendix) in conjunction with well data within each fault-bounded block, tectonic tilting rates of the substrate in the Horda Platform is estimated to have been very low, ranging from 0.01 to 0.21°/Myr for Series 2-4, and up to 0.33°/Myr for Series 5 (Figs. 3.6C, 3.7C). Tilting associated with the Troll Fault was remarkably higher, ranging from tilting rates of 0.24 to 0.80°/Myr) (Fig. 3.9C-D). Regional seismic cross-sections indicate that most of the rift-related faulting occurred after deposition of the Sognefjord Formation, during deposition of the uppermost Jurassic and Cretaceous units (uppermost Draupne Formation, Cromer Knoll Group and Shetland Group; Figs. 3.6A-B, 3.7A-B) (see also Whipp et al., in press).

Fault	Methods	Series 2 (0.8 Myr)	Series 3 (2.5 Myr)	Series 4 (1.7 Myr)	Series 5 (1.4 Myr)
northern part of Troll Fault	Seismic interpretation	Active, ca. 50 ms slip	Active, ca. 50 ms slip	Active, ca. 75 ms of overall slip	
	Subsidence analysis	Active, ca. 50 m slip (63 m/Myr)	Active, ca. 70 m slip (28 m/Myr)	Active, ca. 50 m slip (29 m/Myr)	Active, ca. 25 m slip (18 m/Myr)
Svartav Fault	Seismic interpretation	Active, ca. 30 ms slip	Quiescent	Mostly quiescent, but potentially subtle activity of northern splay	
	Subsidence analysis	Active, ca. 25 m slip (31 m/Myr)	Quiescent		Northern splay active, ca. 30 m slip (21 m/Myr)
northern part of Tusse Fault	Seismic interpretation	Quiescent		Quiescent? (distorted by "flat spot")	
	Subsidence analysis	Quiescent			Active, ca. 35 m slip (25 m/Myr)
southern part of Tusse Fault	Seismic interpretation	Quiescent		Quiescent? (distorted by "flat spot")	
	Subsidence analysis	Potentially subtle activity, ca. 20 m slip (25 m/Myr)	Potentially subtle activity, ca. 20 m slip (8 m/Myr)	Quiescent	
northern part of Vette Fault and/or Øygarden Fault Complex	Seismic interpretation	Quiescent	Active, ca. 40 ms slip	Quiescent	
	Subsidence analysis	Quiescent	Active, ca. 30 m slip (12 m/Myr)	Quiescent	
southern part of Vette Fault and/or Øygarden Fault Complex	Subsidence analysis	Quiescent			Active, ca. 35 m slip (25 m/Myr)

Table 3.2. *Comparison of fault activity resolved by seismic interpretation (Fig. 3.8) and analysis of subsidence using sediment decompaction and backstripping (Figs. 3.6C, 3.7C).*

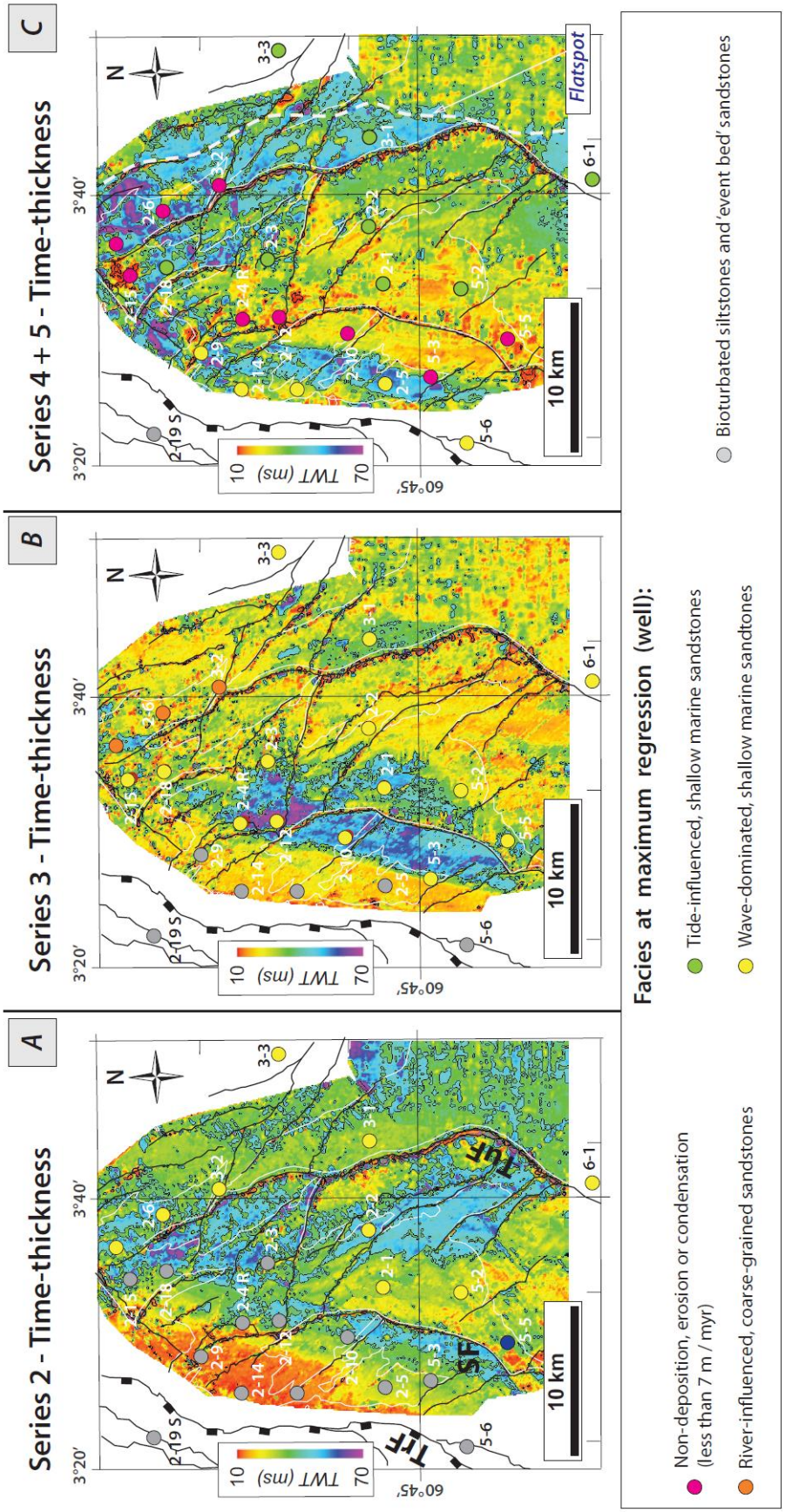

Figure 3.8. *Time-thickness seismic maps of (**A**) Series 2 clinoform set (Late Callovian), (**B**) Series 3 clinoform set (Early to Middle Oxfordian), and (**C**) Series 4 and Series 5 clinoform sets (Middle to Late Oxfordian).*

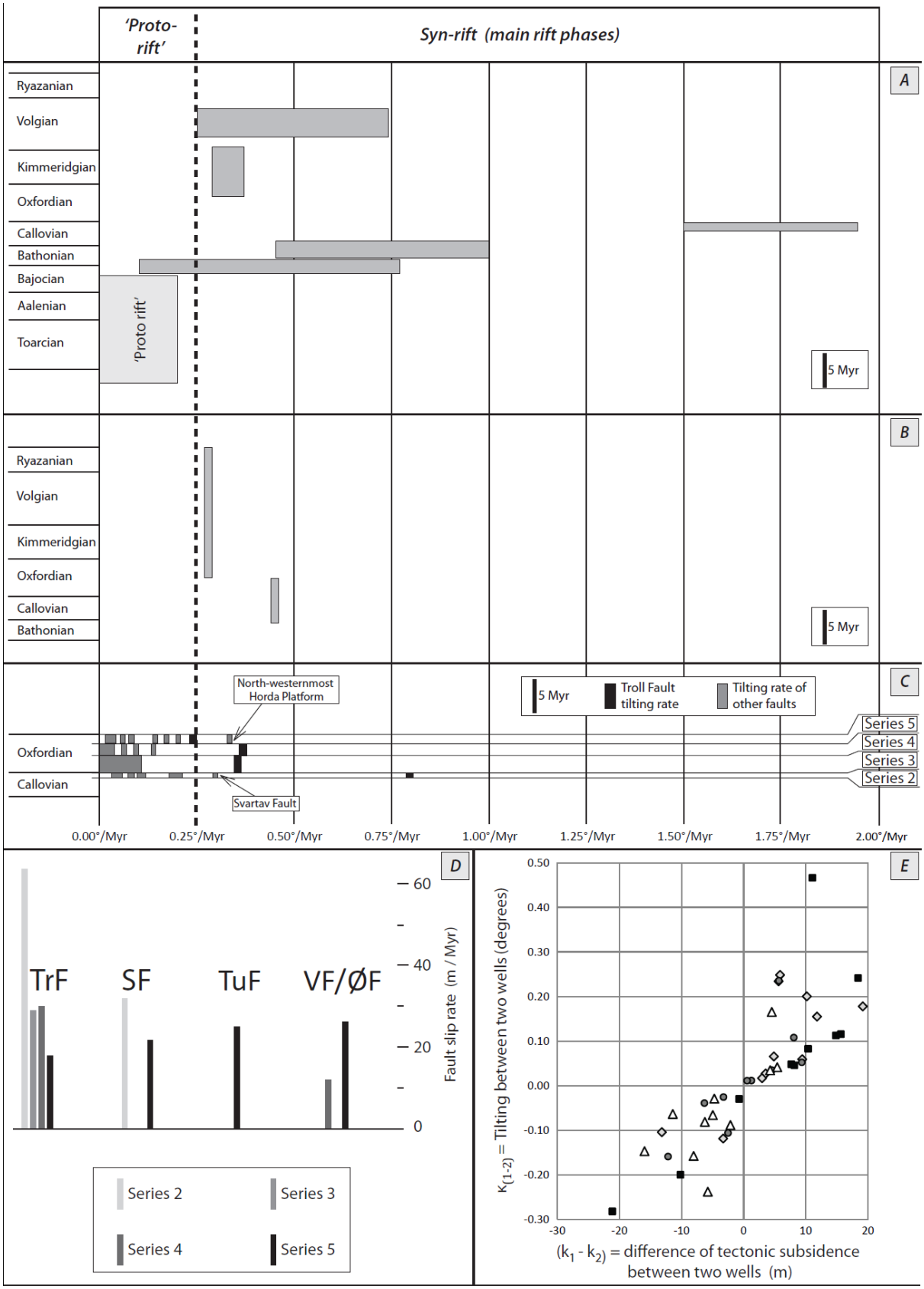
'Proto-rift'
Syn-rift (main rift phases)
A
Ryazanian
Volgian
Kimmeridgian
Oxfordian
Callovian
Bathonian
Bajocian
Aalenian
Toarcian
'Proto rift'
5 Myr
B
Ryazanian
Volgian
Kimmeridgian
Oxfordian
Callovian
Bathonian
5 Myr
C
North-westernmost Horda Platform
5 Myr
Troll Fault tilting rate
Tilting rate of other faults
Series 5
Series 4
Series 3
Series 2
Oxfordian
Callovian
Svartav Fault
0.00°/Myr
0.25°/Myr
0.50°/Myr
0.75°/Myr
1.00°/Myr
1.25°/Myr
1.50°/Myr
1.75°/Myr
2.00°/Myr
D
TrF
SF
TuF
VF/ØF
Fault slip rate (m / Myr)
60
40
20
0
Series 2
Series 3
Series 4
Series 5
E
κ(1-2) = Tilting between two wells (degrees)
0.50
0.40
0.30
0.20
0.10
0.00
-0.10
-0.20
-0.30
-30
-20
-10
0
10
20
(k1 - k2) = difference of tectonic subsidence between two wells (m)

***Figure 3.9**. (**A-C**) Plots of fault block tilting rates (in degrees per million years) during the Late Jurassic rifting event in (**A**) the Oseberg Fault Block (after Færseth & Ravnas, 1998), (**B**) in the Snorre-H Fault Block (after Nøttvedt et al., 2000) and (**C**) the north-western Horda Platform (this study). A threshold value of 0.25°/Myr which separates 'proto-rift' and 'main-rift' phases can be established. (**D**) Slip rate for each of the major faults, as constrained by the differences of tectonic subsidence in wells situated in their footwalls and hangingwalls. Tectonic subsidence values are calculated by backstripping analysis (Figs. 3.6D-E, 3.7D-E); (**E**) Plot of the difference in tectonic subsidence between two neighbouring wells along the studied transects (Figs. 1-2, 4-5, 10) and the basement tilting subsequently calculated, following the method described by Figure 3.33B. During the deposition of each series, the fault blocks underwent little or negligible rotations (usually <0.3°). The highest values of tilting are recorded during the deposition of the Series 5 clinoform set (up to 0.5°).*

3.5.2 Clinoform trajectories

Along both transects, trajectories within each clinoform set indicate regression towards the west, and show low angles that are close to palaeo-horizontal (-0.5° to +0.2°) in the east, and which descend sharply (to -2° to -3°) towards the west. This transition to steeper, descending trajectories occurs where clinoforms step basinward of the point of maximum regression (and maximum thickness) of the underlying clinoform set (indicated by red dots within each clinoform set in Figs. 3.10, 3.11). The steeply descending trajectories are associated with abrupt increases in clinoform-foreset height and sandstone thickness (to >40 m). Variations in these three geometrical and lithological parameters are attributed to clinoform progradation into abruptly deeper water characterized by an abruptly deeper wave base, reflecting antecedent palaeobathymetry formed by the morphology and stacking of older clinoform sets. This geometry is reminiscent of the architecture displayed by shelf-edge deltas (e.g., Porębski & Steel, 2003), and also accounts for the descending trajectories of the clinoform referece point (which is a proxy for the storm base).

Longer-term trajectories, as defined by the stacking pattern of successive clinoform sets, can be classified as ascending-regressive, with a progressive increase in the upward angle of trajectory between Series 2 and 3 (+0.2 to +0.5°), and Series 3 and Series 4 (ca. +90°) (indicated by thick, black dashed line in Figs. 3.10B, 3.11B). The trajectory between Series 4 and 5 indicates regression with a near-horizontal to slightly descending angle (<0.1°), which indicates renewed progradation, perhaps in response to decreased accommodation above normal faults that were initiating within the Troll Field during deposition of Series 5. An alternative interpretation is that there was an increase in unit-width depositional flux during deposition of Series 5 (as described below), which could

have occurred in concert with the onset of extension-related normal faulting. It is also noted that the vertical component of clinoform-set-stacking trajectory is greater along the northern transect (ca. 110 m between series 2 and 5) than along the southern transect (ca. 60 m).

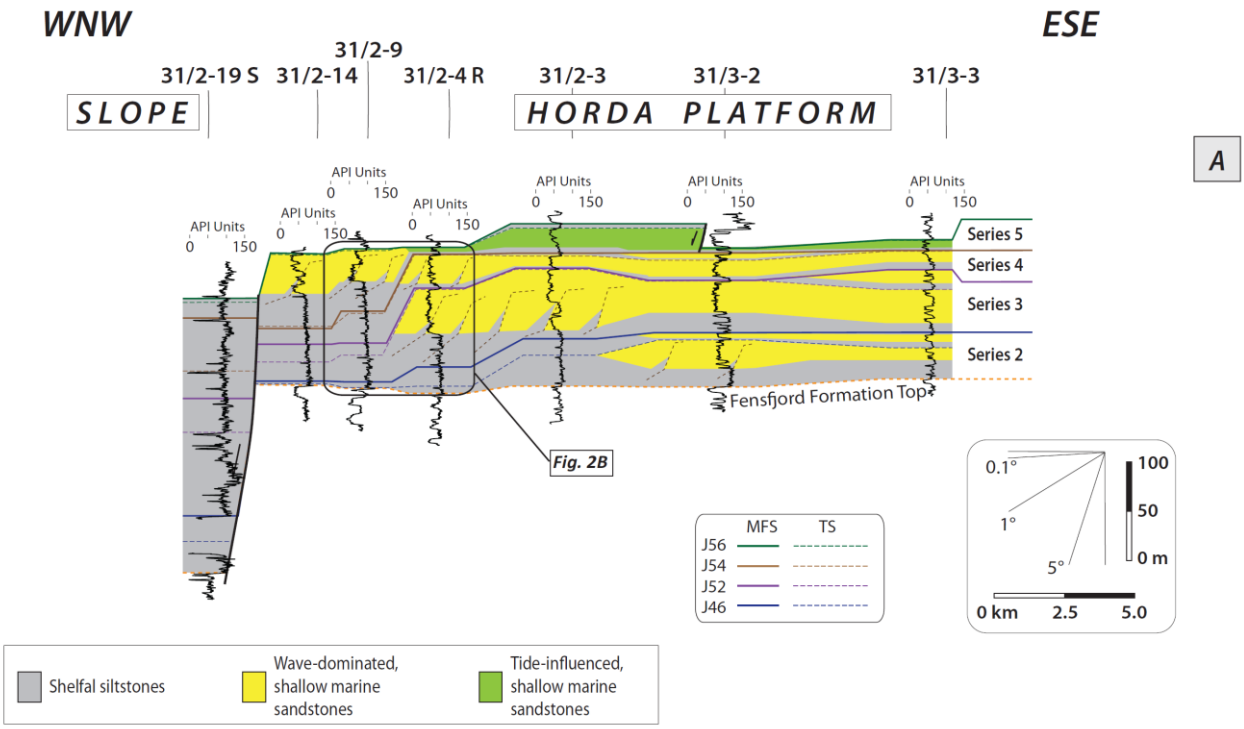
WNW
ESE
31/2-19 S
31/2-14
31/2-9
31/2-4 R
31/2-3
31/3-2
31/3-3
SLOPE
HORDA PLATFORM
A
API Units
0
150
Series 5
Series 4
Series 3
Series 2
Fensfjord Formation Top
Fig. 2B
MFS
TS
J56
J54
J52
J46
0.1°
1°
5°
100
50
0 m
0 km
2.5
5.0
Shelfal siltstones
Wave-dominated, shallow marine sandstones
Tide-influenced, shallow marine sandstones

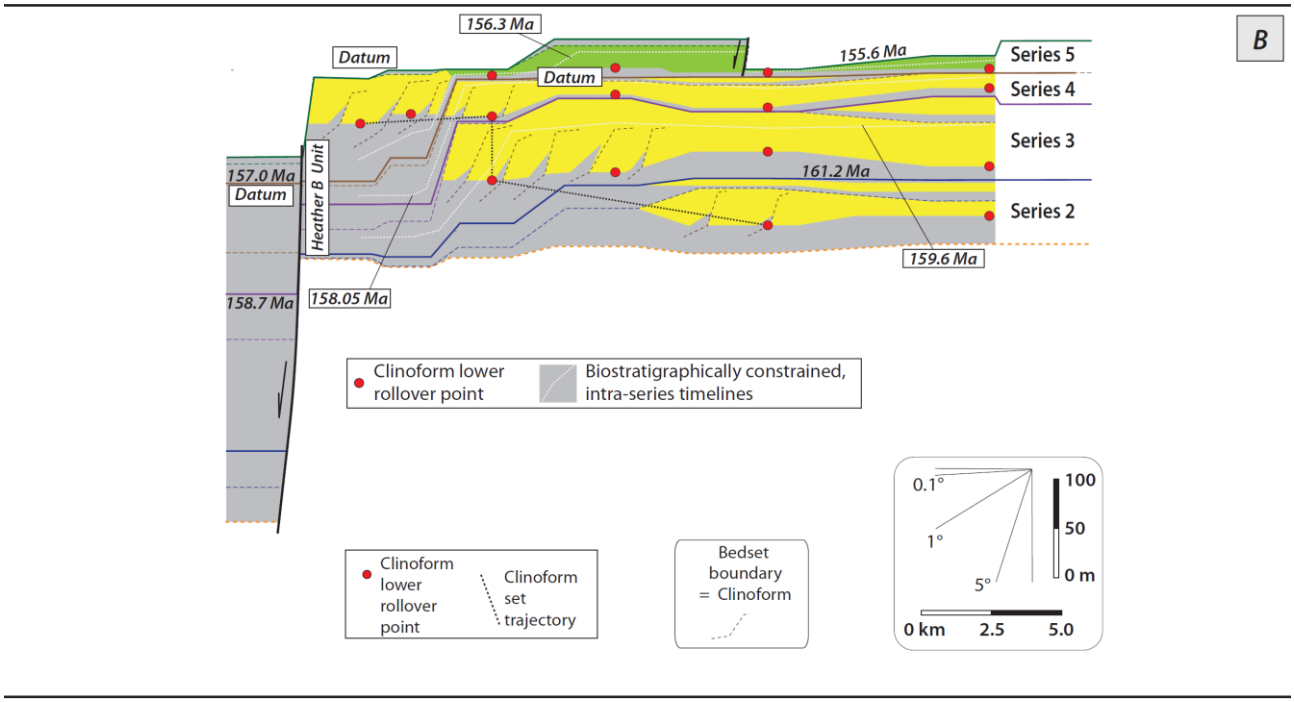
B
156.3 Ma
Datum
155.6 Ma
Series 5
Series 4
Series 3
Series 2
161.2 Ma
157.0 Ma
Datum
Heather B Unit
158.7 Ma
158.05 Ma
159.6 Ma
Clinoform lower rollover point
Biostratigraphically constrained, intra-series timelines
Clinoform lower rollover point
Clinoform set trajectory
Bedset boundary = Clinoform
0.1°
1°
5°
100
50
0 m
0 km
2.5
5.0

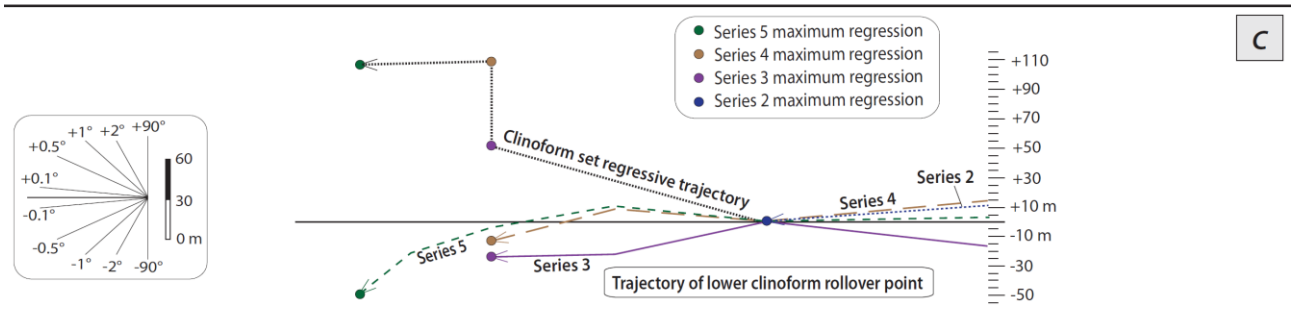
C
Series 5 maximum regression
Series 4 maximum regression
Series 3 maximum regression
Series 2 maximum regression
Clinoform set regressive trajectory
Series 2
Series 4
Series 5
Series 3
Trajectory of lower clinoform rollover point
+110
+90
+70
+50
+30
+10 m
-10 m
-30
-50
+0.5°
+1°
+2°
+90°
+0.1°
-0.1°
-0.5°
-1°
-2°
-90°
60
30
0 m

***Figure 3.10**. (**A**) Depositional-dip-oriented well-log correlation panel through the Sognefjord Formation and (**B**) its decompacted equivalent, highlighting the stratigraphic architecture of Series 2 to 5 clinoform sets. The transect line is the same as in Figure 3.6, in the northern part of the Troll Field area (Fig. 3.1C). The J54 and J56 maximum flooding surfaces are used as local datum surfaces for the correlation panel. This uncompacted correlation panel displays stratal thicknesses during deposition of the surface at the top of Series 5; as a consequence, Series 5 is totally decompacted, whilst Series 4, 3 and 2 are increasingly 'partly compacted' due to the weight of the overlying units. Selected clinoforms mapped in seismic data (thin, black dashed lines) and biostratigraphically constrained "dummy" clinoforms (thin, white dashed lines; cf. Fig. 3.4A, D) are shown in each clinoform set. (**C**) Reconstructions of clinoform trajectories within each clinoform set (constructed using the red reference points shown in Fig. 3.10B) and between stacked clinoform sets (thick, black dashed lines in Fig. 3.10B).*

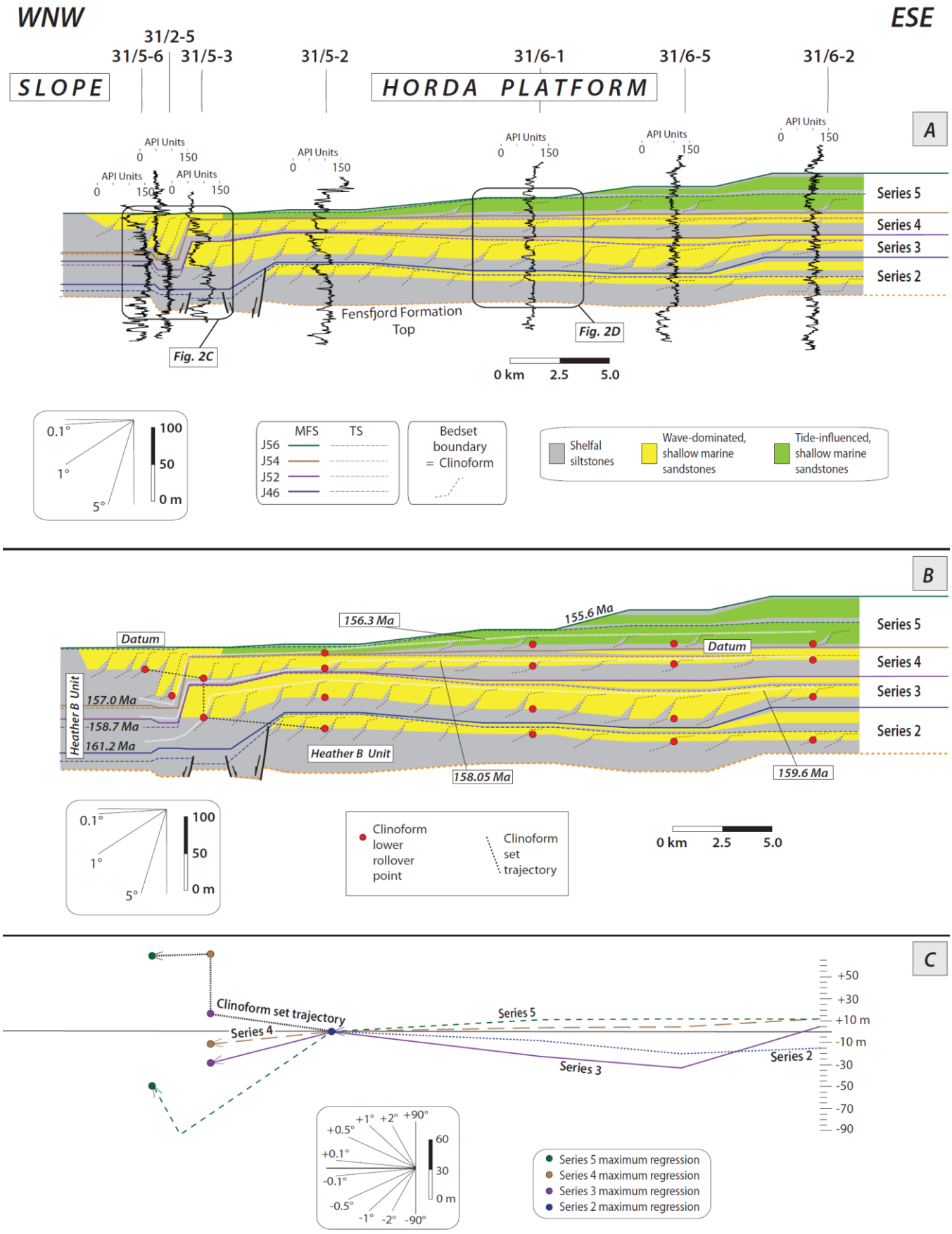
WNW
ESE
31/2-5
31/5-6
31/5-3
31/5-2
31/6-1
31/6-5
31/6-2
SLOPE
HORDA PLATFORM
A
API Units
0
150
Series 5
Series 4
Series 3
Series 2
Fensfjord Formation Top
Fig. 2C
Fig. 2D
0 km
2.5
5.0
0.1°
1°
5°
100
50
0 m
MFS
TS
J56
J54
J52
J46
Bedset boundary = Clinoform
Shelfal siltstones
Wave-dominated, shallow marine sandstones
Tide-influenced, shallow marine sandstones
B
Datum
156.3 Ma
155.6 Ma
157.0 Ma
158.7 Ma
161.2 Ma
Heather B Unit
158.05 Ma
159.6 Ma
Clinoform lower rollover point
Clinoform set trajectory
C
Clinoform set trajectory
+50
+30
+10 m
-10 m
-30
-50
-70
-90
+1°
+2°
+90°
+0.5°
+0.1°
-0.1°
-0.5°
-1°
-2°
-90°
60
30
Series 5 maximum regression
Series 4 maximum regression
Series 3 maximum regression
Series 2 maximum regression

***Figure 3.11**. (**A**) Depositional-dip-oriented well-log correlation panel through the Sognefjord Formation and (**B**) its decompacted equivalent, highlighting the stratigraphic architecture of Series 2 to 5 clinoform sets. The transect line is the same as in Figure 3.7, in the southern part of the Troll Field area (Fig. 3.1C). The J54 and J56 maximum flooding surfaces are used as local datum surfaces for the correlation panel. This uncompacted correlation panel displays stratal thicknesses during deposition of the surface at the top of Series 5; as a consequence, Series 5 is totally decompacted, whilst Series 4, 3 and 2 are increasingly 'partly compacted' due to the weight of the overlying units. Selected clinoforms mapped in seismic data (thin, black dashed lines) and biostratigraphically constrained "dummy" clinoforms (thin, white dashed lines; cf. Fig. 3.4A, 3.D) are shown in each clinoform set. (**C**) Reconstructions of clinoform trajectories within each clinoform set (constructed using the red reference points shown in Fig. 11B) and between stacked clinoform sets (thick, black dashed lines in Fig. 3.11B.*

3.5.3 Progradation rates

Within each clinoform set, the age of the facies-belt transition from wave-dominated shallow-marine sandstones to shelfal siltstones, which is used as the clinoform-trajectory reference point, tends to be progressively younger towards the west, consistent with westward progradation (Figs. 3.12A, 3.13A). For each clinoform set, the ages of the sandstone-to-siltstone facies-belt transition have been interpolated between 42 wells situated across the Troll Field area (Fig. 3.2A), including those located along the two well correlation panels (Figs. 3.12A, 3.13A). This interpolation has allowed us to generate contour maps of estimated clinoform age that provide a visual representation of the map-view evolution of the depositional system (Fig. 3.14). The resulting clinoform-age contours mirror the strike orientations of clinoforms that are seismically-resolved in each clinoform set (Chapter 2; cf. Fig. 3.2A). Furthermore, the clinoform-age contours become more closely-spaced from east to west, indicating a progressive decrease in progradation rate through time within each clinoform set (Figs. 3.12B, 3.13B).

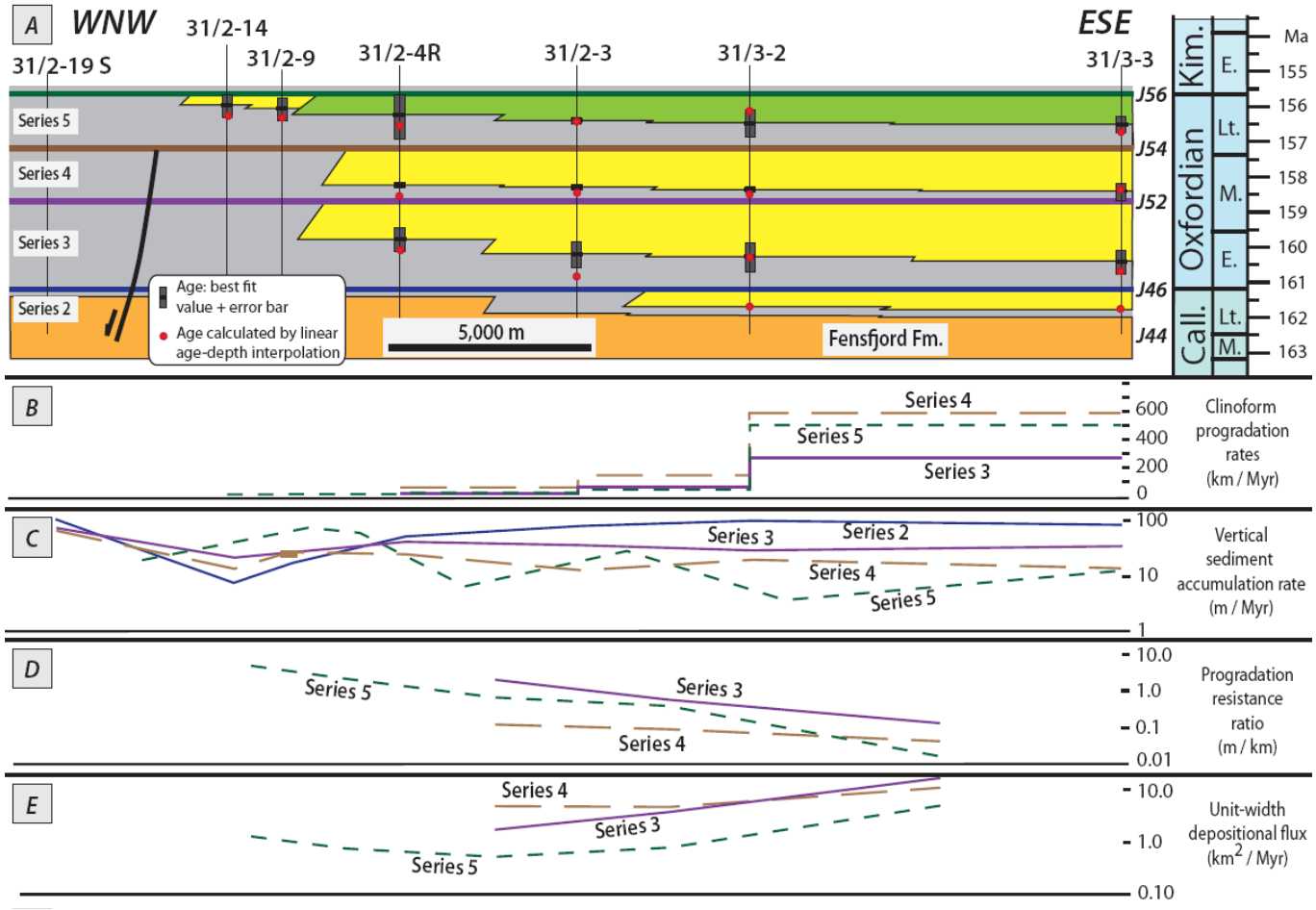

Figure 3.12. *(**A**) Chronostratigraphic chart along the northern well-correlation transect (Figs. 3.6, 3.10), which is oriented along depositional dip. The age of the siltstone-to-sandstone facies-belt transition for each clinoform set in each well is calculated through the method illustrated in Figure 3.4, with error bars derived by the law of error propagation (Equations 15 and 16 in Appendix). The red dots mirror the age of the siltstone-to-sandstone facies break calculated with a simple linear interpolation, and shows how our exponential interpolation method gives a more reliable and geologically reasonable estimate. (**B**) Progradation rates calculated for each clinoform set between pairs of wells along the transect. (**C**) Vertical sedimentation rates calculated for each clinoform set at each well along the transect reflect the difference between sedimentation rate measured in the siltstone-rich toeset and sandstone-rich foreset and topset. (**D**) Progradation resistance ratio calculated for each clinoform set between pairs of wells along the transect. (**E**) Unit-width depositional flux calculated for each clinoform set between pairs of wells along the transect. Colours for facies associations and surfaces follow the convention of Figures 3.2A and 3.6.*

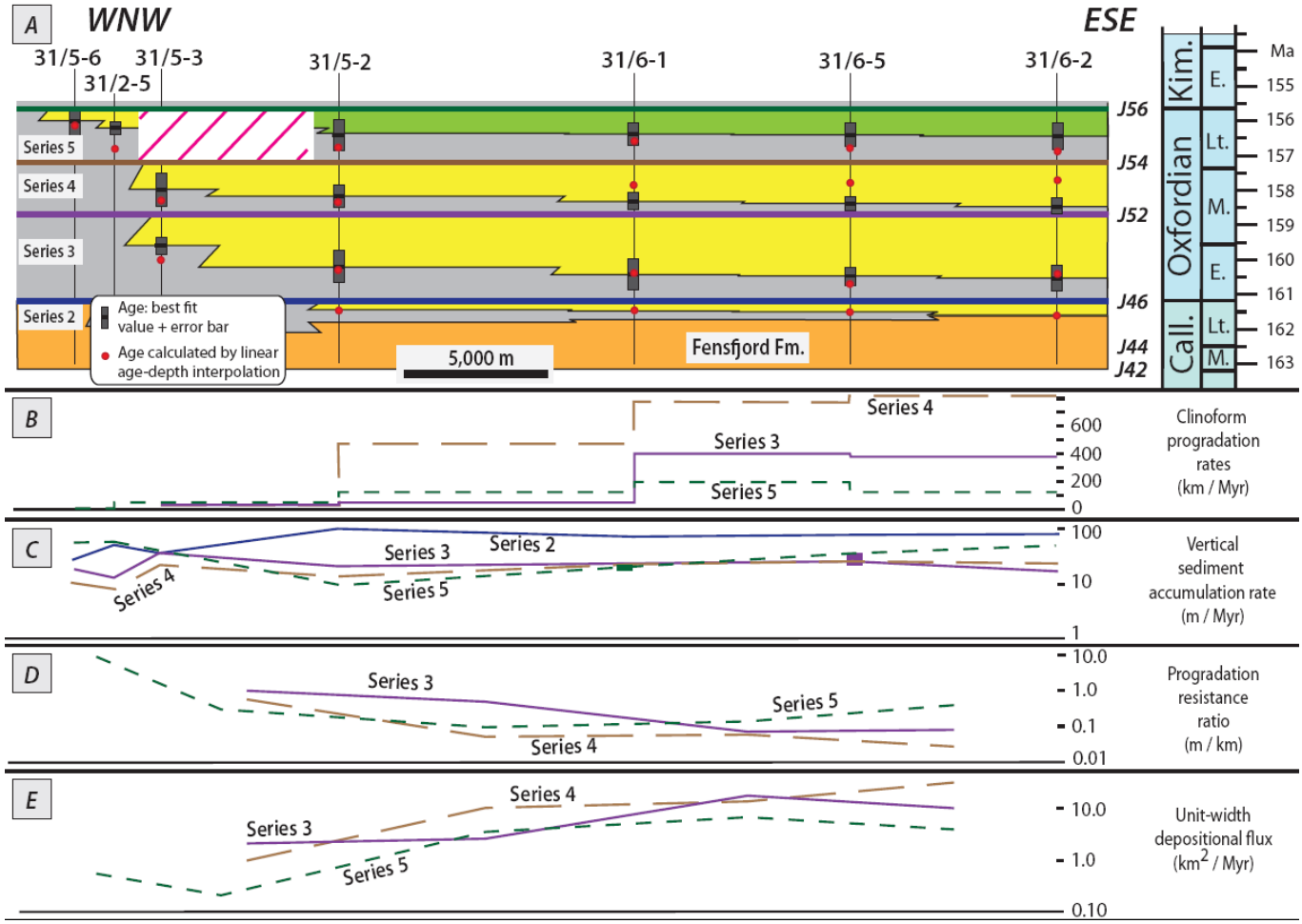

Figure 3.13. *(**A**) Chronostratigraphic chart along the southern well-correlation transect (Figs. 3.7, 3.11), which is oriented along depositional dip. The age of the siltstone-to-sandstone facies-belt transition for each clinoform set in each well is calculated through the method illustrated in Figure 3.4, with error bars derived by the law of error propagation (Equations 15 and 16 in Appendix). The red dots mirror the age of the siltstone-to-sandstone facies break calculated with a simple linear interpolation, and shows how our exponential interpolation method gives a more reliable and geologically reasonable estimate. (**B**) Progradation rates calculated for each clinoform set between pairs of wells along the transect. (**C**) Vertical sedimentation rates calculated for each clinoform set at each wells along the transect reflect the difference between sedimentation rate measured in the siltstone-rich toeset and sandstone-rich foreset and topset. (**D**) Progradation resistance ratio calculated for each clinoform set between pairs of wells along the transect. (**E**) Unit-width depositional flux calculated for each clinoform set between pairs of wells along the transect. Colours for facies associations and surfaces follow the convention of Figures 3.2A and 3.6.*

3.5.4 Sediment accumulation rates

Lateral trends in vertical sediment accumulation rate are more variable than progradation rate in each clinoform set (Fig. 3.12C, 3.13C); accumulation rate either decreases basinwards, from east to west (i.e. Series 2), remains relatively uniform across the transects (i.e. Series 3 and 4), or increases basinwards (i.e. Series 5). The peak in sediment accumulation rate within each clinoform set generally coincides with the position of maximum regression and associated down-dip pinchout of sandstone (e.g. compare Figs. 3.10A-B and 3.12C, and Figs. 3.11A-B and 3.13C). This pattern is modified in the northern transect, where vertical sediment accumulation rates increase markedly from the footwall to the hangingwall of the Troll Fault in Series 2-4 (Fig. 3.9C). Vertical sediment accumulation rates are generally highest in Series 2 (ca. 65 m/Myr, averaged across the two transects), have intermediate values in Series 5 (ca. 31 m/Myr), and are lowest in Series 3 and 4 (ca. 20 m/Myr) (Figs. 3.12C, 3.13C). Volumetric sediment accumulation rates in the study area show a similar pattern, with a peak in Series 2 (ca. 28 km^3/Myr) followed by consistently lower values in Series 3, 4 and 5 (ca. 13-15 km^3/Myr) (Fig. 3.15A). However, mean vertical and volumetric sediment accumulation rates for Series 5 may be underestimated as a result of syn- to post-depositional erosion, which removed all or part of the Series 5 clinoform set from the footwall crests of fault blocks in the western part of the Troll Field (e.g. Figs. 3.6A, 3.7A; regions shaded pink in Figs. 3.13A, 3.14D). Movement of these fault blocks may have initiated during deposition of Series 5, resulting in local condensation and non-deposition (Dreyer et al., 2005), which may have caused the horizontal to slightly descending trajectory observed within Series 4 to Series 5 clinoform sets (as described above, and indicated by thick, black dashed line in Figs. 3.10, 3.11).

3.5.5 Progradation resistance ratios and unit-width depositional flux

Progradation resistance ratios increase westwards in each clinoform set (Figs. 3.12D, 3.13D), reflecting lower rates of progradation and higher rates of sediment accumulation towards the basin. Cross-sectional, unit-width depositional flux decreases basinwards in each clinoform set (from ca. 3-90 to 0.2-10 km^2/Myr, for different clinoform sets), except in the western part of Series 5, where depositional flux increases basinwards (Figs. 3.12E, 3.13E). The descending clinoform trajectory and seaward-decreasing progradation rate may be at least partly accounted for by a basinward increase in water depth controlled by antecedent palaeobathymetry. However, this cannot possibly explain the basinwards-decrease in depositional flux, which may instead point out to a reduction in riverine sediment influx and/or an increase in alongshore sediment export by marine currents. The latter

mechanism appears more likely, because the facies character of each clinoform set exhibits increasing alongshore-current activity with progradation into deeper waters to the west (Dreyer et al., 2005; Chapter 2). Alongshore sediment transport by strong marine currents is a common characteristic of Holocene-to-modern subaqueous deltas (e.g. in the Adriatic Sea; Cattaneo et al., 2003, 2007, and the Yangtze Delta in the South China Sea; Liu et al., 2006).

Average values of unit-width depositional flux for each clinoform set were greatest during deposition of Series 2 (ca. 80 km^2/Myr), lowest during deposition of Series 3 and 4 (ca. 20 km^2/Myr), and intermediate during deposition of Series 5 (ca. 40 km^2/Myr), although there is much scatter around these estimates (Fig. 3.15C). The increase in depositional flux from Series 4 to Series 5 is consistent with the slightly descending trajectory between these two clinoform sets (as described above, and indicated by thick, black dashed line in Figs. 3.12, 3.13), and implies accelerated export of sediment from the hinterland.

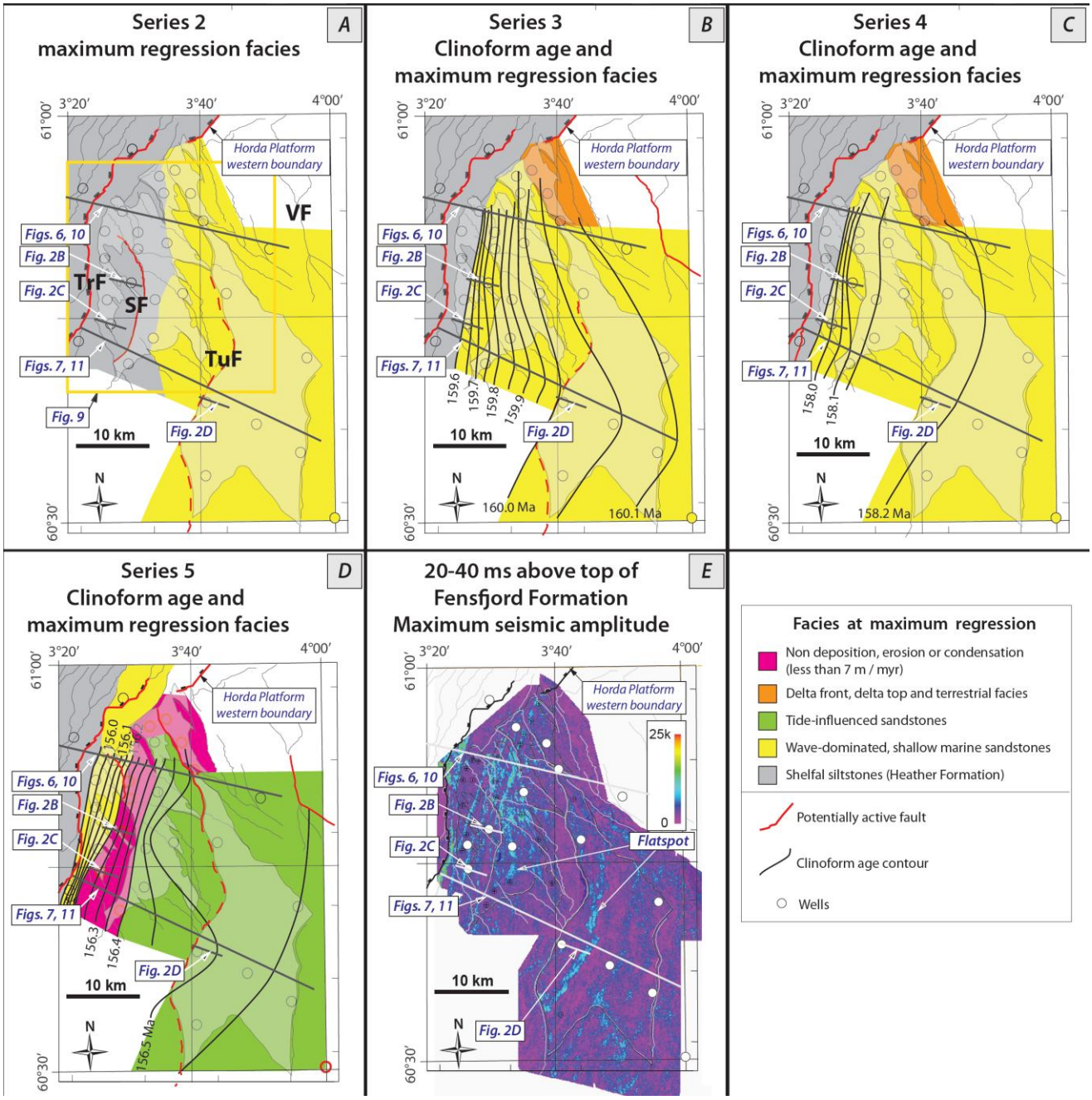

Figure 3.14. *(**A**-**D**) Maps showing clinoform-age contours and facies-association distributions at maximum regression for each clinoform set: (**A**) Series 2; (**B**) Series 3; (**C**) Series 4; and (**D**) Series 5. Clinoform ages are estimated in each well using the method illustrated in Figure 3.4, and then interpolated between wells to generate contours. (**E**) Maximum amplitude seismic attribute map, extracted from a window in the lower part of the Sognefjord Formation situated 20-40 ms above the top of the underlying Fensfjord Formation (after Chapter 2). Amplitude anomalies forming linear features oriented parallel to the NNE-SSW-striking age contours represent the strike orientation of clinoforms imaged in cross-section within the seismic data volume (Chapter 2).*

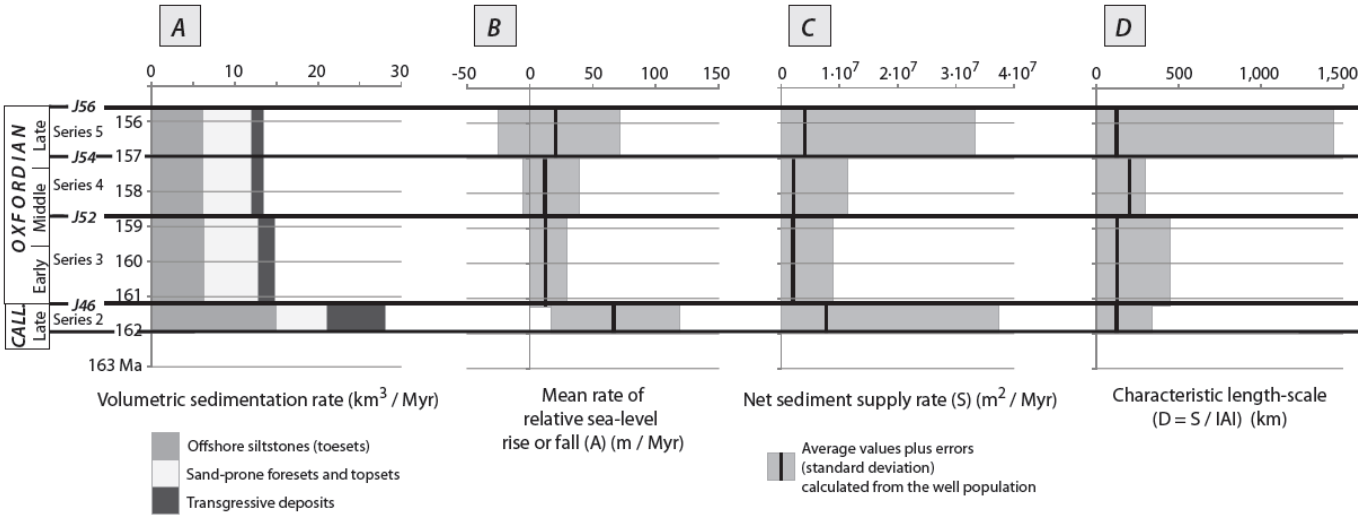

***Figure 3.15**. Plots comparing estimates of key parameters in the Series 2-5 clinoform sets: (**A**) volumetric sedimentation rate and the proportion of siltstone-rich toesets, sandstone-rich foresets and topsets, and transgressive deposits. Sediment volumes were estimated by using the values of seismic velocity of the checkshot survey (from 0.90 to 1.02 m/ms) to convert measurement thicknesses TWT to depth, and integrating thicknesses over the study area; (**B**) mean rate of relative sea level rise or fall during deposition of the clinoform set, which corresponds to the spatially averaged value of tectonic subsidence calculated via backstripping analysis of the studied well dataset (Figs. 3.6E, 3.7E); (**C**) average net sediment supply rate calculated for the studied well dataset (it equals to the well-constrained averaged vertical sediment accumulation rate times the dip extent of the system); and (**D**) characteristic length of the genetically linked coastal-to-shelfal depositional system (after Muto, 2001). Series 4 and 5 are combined, because the J54 maximum flooding surface that separates them could not be mapped in seismic data over the full extent of the study area (see also Fig. 12A).*

3.5.6 Provenance and sediment routing

The compositions of garnets in sandstones from the foresets and topsets of the Series 4 clinoform set were compared to those of modern rivers draining the basement terrains of onshore Norway (Morton et al., 2004), and were found to be nearly identical to that of the calcium- and magnesium-enriched garnets that characterise the N4 terrain (Fig. 3.16A, B). These data constrain the provenance of sediment in the Sognefjord Formation, and are compared below with parameters derived from our quantitative stratigraphic analysis.

The characteristic length scale (*D*) of the Sognefjord Formation coastal-to-shelfal depositional system (*sensu* Muto, 2001) was calculated for each clinoform set, based on estimates of depositional flux (*S*) (Fig. 3.15C) and the

rate of relative sea-level rise or fall (*A*) (Fig. 3.15B), which corresponds to the spatially averaged value of tectonic subsidence calculated via backstripping analysis (Figs. 3.6E, 3.7E; Muto, 2001):

$$D = S / A \qquad (22)$$

D corresponds to the dip extent at maximum regression of the genetically linked coastal-to-shelfal depositional system under conditions of steady external forcing (i.e. constant rates of net sediment supply and relative sea-level rise or fall). Under such conditions, the depositional system will start to retreat once it has prograded sufficiently far to reach its characteristic length scale ("autoretreat" *sensu* Muto & Steel, 1992; Muto, 2001), because all supplied sediment is deposited on the coastal plain and subaqueous delta topset, and none is available for progradation of the delta foreset. The landward limit of *D* is shown in Figure 3.16C, based on using the positions of maximum regression of the Series 2-5 clinoform sets as its seaward limit. The landward limit represents the position at which the coastal plain of the Sognefjord Formation coastal-to-shelfal depositional system would have onlapped against basement rocks.

Our estimates of the characteristic length scale (*D*) of the Sognefjord Formation coastal-to-shelfal depositional system, although associated with large errors (Fig. 3.15D), are consistent with the onshore distribution of Oxfordian shallow-marine deposits (Fossen et al., 1997) and with the extent of the N4 basement terrain (Morton et al., 2004) (Fig. 3.16C). In this context, the concave-landward trajectory of the stacked Series 2-4 clinoform sets (indicated by thick, black dashed line in Figs. 3.6C-E, 3.7C-E) and the long-term decrease in sediment accumulation rate from Series 2 to Series 5 (Figs. 3.15A), indicate decreased progradation and increased aggradation, which mimics stratal architectures produced by autoretreat (Muto & Steel, 1992; Muto, 2001; Muto et al., 2007). Strong along-shore marine transport may also favour the onset of large-scale autoretreat dynamics (Muto, 2001). The horizontal to slightly descending trajectory between Series 4 and Series 5 is not consistent with autoretreat, and implies a change in external forcing (e.g. more rapid export of sediment from the hinterland, or slower tectonic subsidence rate in parts of the Troll Field).

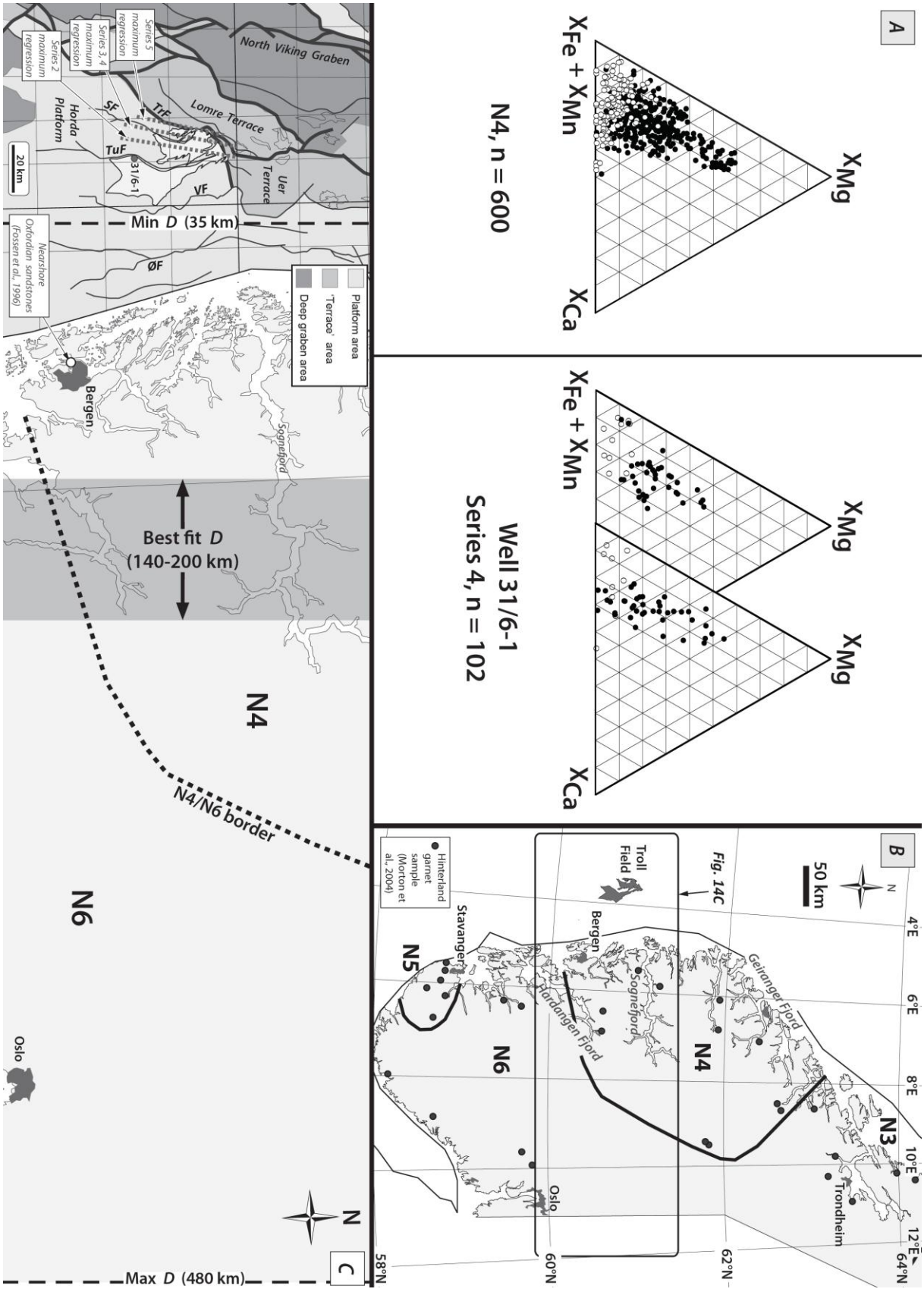

Figure 3.16. *(**A**) Detrital garnet composition of six sandstone samples from the Series 4 clinoform set in the Troll Field, and from the N4 basement terrain of onshore Norway (after Morton et al., 2004). X_{Fe}+X_{Mn}, X_{Mg} and X_{Ca} are molecular proportions*

*of Fe + Mn, Mg and Ca, with all Fe determined as Fe^{2+}. Filled circles: X_{Mn} <5%, open circles: X_{Mn} >5%. (**B**) Map of Norway indicating the distribution of onshore basement terrains N3-N6 (after Morton et al., 2004) and the location of the Troll Field. (**C**) Detailed map (located in Fig. 3.16B) showing calculated estimates of the 'characteristic length' scale of the Sognefjord Formation genetically linked coastal-to-shelfal depositional system (after Muto, 2001), the onshore distribution of Oxfordian shallow-marine deposits (Fossen et al., 1997), the boundary of the N4 basement terrain (Morton et al., 2004), and the position of maximum regression of the Series 2-5 clinoform sets within the Troll Field. In combination, these features constrain the sediment routing system that fed the "Troll Delta" during deposition of the Sognefjord Formation.*

3.6 DISCUSSION

3.6.1 Robustness, reproducibility and wider application of the method

Clinoform ages obtained by applying the method outlined herein define a chronostratigraphic model that is more geologically robust than that derived, for example, by calculating clinoform ages based on a linear age-depth model based on the depth and age of the two bounding maximum flooding surfaces (i.e., red dots in Figs. 3.12A, 3.13A). Furthermore, the proposed method is readily applicable to any clinoform-bearing, shallow-marine succession for which at least three vertical sections roughly positioned along a cross-section perpendicular to the depositional dip of the shallow-marine system are available, provided that a network of reliably isochronous, (bio)stratigraphic events is present within each clinothem.

The error analysis shown in Fig. 3.5 indicates that the overall error in the age of the clinoform-trajectory reference point (Δt_P) depends on small errors associated with the stratigraphic position (Δh_1) and, more significantly, the age (Δt_1) of (bio)stratigraphic events within the clinoform set. Therefore, to minimise the errors in the method outlined herein, effort should be focussed on reducing the uncertainties in these two parameters. Uncertainty in Δh_1 can be reduced by decreasing the vertical spacing of biostratigraphic sample points. The degree of uncertainty associated with Δt_1 depends on the time-scale employed, and is systematic in that it applies equally to all the samples within a particular dataset. As a consequence, whilst it is not possible to reduce this error, Δt_1 can be

disregarded when calculating relative changes along individual transects, even if it is larger than Δt_P,. In most Cenozoic successions, Δt_1 (<0.1 Myr) is smaller than typical values of Δt_P, such that estimates of Δt_1 be reliably used to calculate the cumulative, absolute error in t_p.

The exponential age-model employed here is consistent with the accumulation and magnitude of stratigraphic layers and intervening gaps through time, which is approximated by the 'Devil's staircase' profile in which hiatuses of shorter duration become evident for shorter periods of observation (Sadler, 1981; Plotnick, 1986), because the exponential interpolation approximates the shape of the specific segment of the 'Devil's staircase' for which it is calculated (e.g., the two stepped, red curves in Fig. 3.4C, 3.4F). This arises because the shape of the time-depth curve derived from Equations 13 and 14 (Appendix) depends on the coordinates of two points on the age-depth graph (i.e., Point 1 and Point P in Fig. 3.4C, 3.4F) and on the exponential interpolation of sediment accumulation rate between these two points. Low-resolution erosional or hiatal surfaces occurring above or below the analysed portion of clinoform set (e.g., maximum flooding surfaces at the base of regressive-transgressive cycles) do not affect the age calculation.

It is possible that the facies-belt transition from wave-dominated, shallow-marine sandstones to shelfal siltstones, which corresponds to the clinoform foreset-to-toeset transition and inferred storm wave base, may not have formed at a uniform water depth and is, therefore, not a reliable reference point for the calculation of clinoform trajectories. For example, the abrupt lowering of the clinoform trajectory angles observed in this study occurs when the subaqueous delta progrades beyond the point of maximum regression attained by the underlying series. This may have therefore been caused by the sudden clinoform encroachment into deep, antecedent bathymetry, and/or by deepening of wave base caused by an increase in alongshore current energy rather than by variations in the balance between sediment supply rate and relative sea level changes. This interpretation is strengthened by the observation of trajectories constrained by mapping the upper rollover points of clinoforms observed in seismic cross-sections aligned along depositional-dip, which appear to be overall flat to slightly concave-landward (Figs. 3.2B-D). Another evidence of the unreliability of the lower clinoform rollover point as a relative sea level reference point is the unusual association of regressive descending 'trajectories' with 'overthickened' sandstone beds in proximity of the clinothem maximum regression position (Figs. 3.11-3.12). This association is a suspect one, because forced regressions should cause deposition of foreshortened and/or missing facies belts instead (c.f., Cant, 1991; Howell et al., 2008; Helland-Hansen & Hampson, 2009).

Although the likely unreliability of the lower clinoform rollover as a clinoform-trajectory reference point impacts upon some aspects of the Sognefjord Formation case study presented here, alternative reference points may be used to measure clinoform trajectory in many other datasets. The facies-belt transition representing the

shoreline, and corresponding to the topset-to-foreset transition of subaerial clinoforms, is likely to be most robust (Hampson et al., 2009; Helland-Hansen & Hampson, 2009).

3.6.2 Tectonic evolution of the Horda Platform

Our analysis of the clinoform progradation rates in the Sognefjord Formation also provides important insights in the tectonic evolution of the Horda Platform. The Late Jurassic was a key time in the development of the North Sea rift basin, characterised by complex, diachronous extension (Nøttvedt et al., 1995, 2000; Færseth & Råvnas, 1998; Råvnas et al., 2000; Coward et al., 2003; Fraser et al., 2003; Whipp et al., in prep.). Areas surrounding the Horda Platform were markedly affected by rift-related fault activity. For example, the Snorre-H fault block (Nøttvedt et al., 2000) and the Oseberg fault block (Færseth & Råvnas, 1998) experienced a tilting rate greater than 0.25°/Myr during discrete rift phases, with maximum values approaching 2.00°/Myr (Fig. 3.9A, B). In contrast, the values of tilting rate that we deduce on the Horda Platform during the deposition of the Sognefjord Formation are consistently lower than 0.25°/Myr, with particularly low values (<0.13°/Myr) recorded during deposition of Series 3 and 4 clinoform sets (Table 3.2; Fig. 3.9C). Furthermore, the differential stratal thicknesses in the hangingwall and footwall of faults in the Troll field is markedly smaller (<30 m, Figs. 3.10D-E) than for faults in the surrounding areas affected by rift-related fault activity, where differential stratal thicknesses exceed several hundred metres. Similarly low values of fault slip and tilting rates were recorded during the Early-to-Middle Jurassic, 'proto-rift' phase in the Oseberg Fault Block (Færseth & Råvnas, 1998).

Although at seismic scale the Sognefjord Formation appears tabular, high-resolution seismic mapping reveals minor thickening across faults, development of wedge-shaped stratal geometries, and onlap onto hangingwall dipslopes (e.g. across the Svartav Fault in Series 2; Figs. 3.2B, 3.8A, 3.11), which implies low-magnitude active faulting. In addition, the backstripped-subsidence analysis presented herein reveals two periods of fault activity during deposition of Series 2 and Series 5 that generated small displacements and local maxima in tilting rates and slip rates (occasionally exceeding values of 0.25 m/Myr and 20 m/Myr, respectively) on several of the major, N-S-striking faults that dissect the platform (Table 3.2; Fig. 3.9C-E). These two episodes of active rotational faulting are separated by longer periods of tectonic quiescence (e.g., during deposition of Series 3 and 4; Table 2). This pattern of low-intensity tectonic pulses typifies a 'proto-rift' or 'rift initiation' (*sensu* Prosser, 1993) setting (c.f., Nøttvedt et al., 1995; Færseth & Ravnås, 1998), and is reminiscent of larger-magnitude pulsed rifting interpreted in nearby areas along the eastern margin of the North Viking Graben (e.g. Færseth & Ravnås, 1998; Ravnås et al.,

2000). The periods of faulting identified on the Horda Platform are Late Callovian and Late Oxfordian in age, and correspond to two of the five Late Jurassic rift phases described on the nearby Oseberg Fault Block (Fig. 3.1D) by Færseth & Råvnas (1998) and Råvnas et al. (2000). During the Late Oxfordian (time of deposition of Series 5), low-magnitude fault activity may have caused erosion or bypass of sediment on fault-block crests in the west of the Troll Field (Figs. 3.10, 3.11, 3.14D), and increased tidal influence in the east of the field, due to localised amplification of tidal currents and damping of wave energy here.

Backstripped-subsidence analysis (Figs. 3.6C, E, 3.7C, E) and seismic mapping (Fig. 3.8) suggest that the Troll Fault, which bounds the western edge of the Horda Platfrom, was active throughout much of the deposition of the Sognefjord Formation, with slip rates of 15-60 m/Myr and tilting rates greater than 0.25°/Myr, particularly during the deposition of Series 2 (ca. 0.80°/Myr) (Table 3.2; Figs. 3.6C, 3.7C). These relatively high rates are consistent with the deposition of wedge-shaped stratal packages in the fault hangingwall (Whipp et al., in press) and by a greater vertical component of clinoform-set stacking trajectory in the northern transect (Fig. 3.7), which lies closer to the Troll Fault. During deposition of the Sognefjord Formation, the Troll Fault underwent activity comparable in magnitude to that taking place on other faults in the Northern North Sea during the main rift phases, as suggested by Whipp et al. (in press).

3.6.3 Spatial and temporal evolution of the Sognefjord Formation

The integration of detailed observations of stratigraphic architecture with temporal and spatial variations in progradation, sediment accumulation and unit-width depositional flux improves our understanding of Sognefjord Formation sedimentation. In particular, it places quantitative constrains on: (1) the shelf transit time; (2) the partitioning of sediment volumes between the different segments of the shoreline-shelf-slope profile; and (3) the relationships between tectonic subsidence, bathymetry, basin hydrodynamics and sediment supply. It also provides stratigraphic-architectural evidence to support the timing of phases of tectonic evolution that are suggested by backstripped-subsidence analysis but that lie below seismic resolution.

Volumetric sediment accumulation rates were highest during deposition of Series 2 (28 km^3/Myr) and then decreased during deposition of Series 3, 4 and 5 (ca. 13-15 km^3/Myr) (Fig. 3.15A). This upward decrease in sediment accumulation rates from Series 2 to Series 5 did not result in the occurrence of 'underfilled' basin conditions and clinoform-set retrogradation as a result of decreased sediment supply, but instead reflects slower rates of accommodation creation in the younger strata. During and/or prior to deposition of the Series 2

clinoform set, therefore, the rate of accommodation creation was greater than in the three overlying clinoform sets. Some of this anomalous accommodation may reflect antecedent topography created, for example, during the drowning of the deltaic system formed by the Fensfjord Formation, and/or the creation of differential topography during the deposition of the Upper Callovian Series 2 itself via active faulting. During deposition of the Series 3 and 4 clinoform sets, both progradation rate and depositional flux decreased towards the west (Fig. 3.12, 3.13), because the subaqueous delta that prograded onto and across the shelf was subject to increased interaction with shore-parallel marine currents that are interpreted to have transported a significant proportion of river-fed sediments along-shelf and out of the study area (Fig. 3.17A-C), as in many modern subaqueous delta systems (cf, Cattaneo et al., 2003, 2007; Liu et al., 2006). Decreasing progradation rates towards the west are noted in the Series 2, 3 and 4 clinoform sets, and may be attributed to a combination of shelf bathymetry, with water depth increasing towards the west, and increased energy of the alongshore marine currents marine currents. The pattern of westward-decreasing progradation rate differs in Series 5 (Fig. 3.17D), as explained below. Our chronostratigraphic analysis implies that the subaqueous "Troll Delta" reached its position of maximum regression relatively rapidly for each clinoform set (i.e., within 30-70% of the time span of the regressive-transgressive cycle that corresponds to the clinoform set; Figs. 3.12A, 3.13A). Therefore, much time is inferred to be represented by condensed sedimentation, non-deposition and erosion during transgression.

The transition from Series 4 to Series 5 clinoform sets is marked by an abrupt change in long-term, clinoform-set-stacking trajectory, from nearly vertical (Series 3 to Series 4) to nearly horizontal (Series 4 to Series 5) (Figs. 3.10, 3.11), indicating renewed progradation. Series 5 is thin or absent (<15 m) over fault blocks in the central-to-western part of the Troll Field and anomalously thick (>40 m) towards the east (Figs. 3.10, 3.11, 3.14D), such that sediment accumulation rates and depositional flux are greatest in two locations, at the position of maximum regression and on the hangingwall dip-slope of the Tusse Fault (Figs. 3.12, 3.13, 3.17D). We interpret these local spatial and temporal anomalies in stratal thicknesses and sedimentation rates to reflect a period of rift-related normal faulting and footwall uplift (Table 3.2). This interpretation is further constrained by subsidence analysis (Figs. 3.6C, E, 3.7C, E) and seismic isochron maps (Fig. 3.8C), which suggests that the Troll, Svartav and Tusse faults, and either the Vette Fault or Øygarden Fault, were active during deposition of Series 5, and that the western Horda Platform underwent minor (< 0.15°) eastward rotation (Fig. 3.17D). In this context, the increase in unit-width depositional flux towards the west of the Horda Platform likely resulted from bypass across uplifting fault blocks in the western parts of the Troll Field (Fig. 3.17D). Renewed progradation from Series 4 to Series 5 clinoform sets may also be attributed to more rapid export of sediment from the hinterland and/or reduction of accommodation creation at the footwall of the main fault blocks (i.e., towards the west), which is consistent with a period of rift activity on the Horda Platform after a previous period of relative tectonic quiescence.

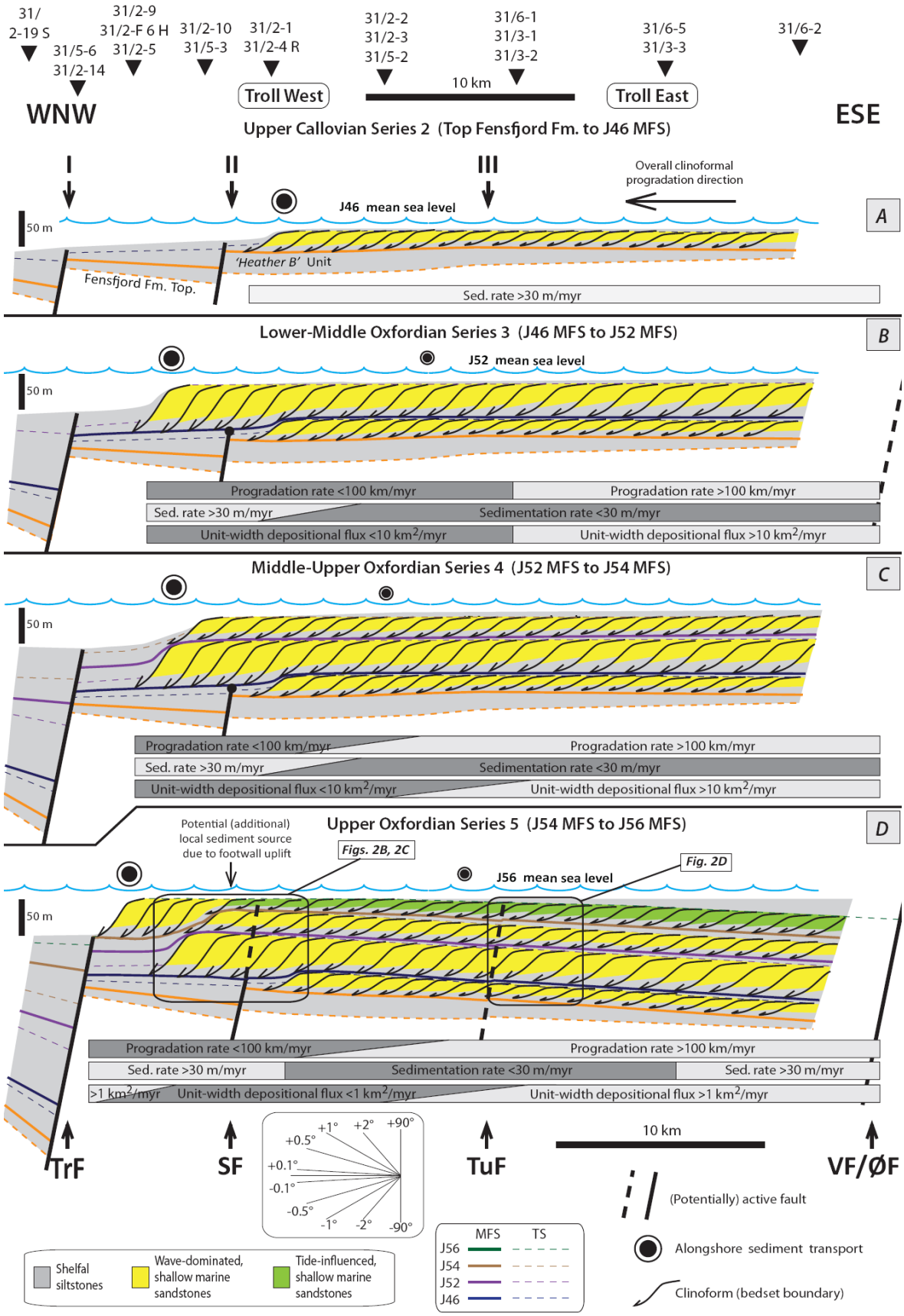

Figure 3.17. *Schematic cross-sections oriented along depositional dip in the Troll Field and adjoining areas, illustrating the temporal evolution of the Sognefjord Formation (cf. Table 3.2, Figs. 3.6, 3.7, 3.10, 3.11, 3.12B, 3.13B): (**A**) Series 2 clinoform*

*set, during which the Troll and Svartav faults were both active; (**B**) Series 3 during which the Troll Fault and either the Vette or Øygarden faults were active; (**C**) Series 4, during which only the Troll Fault was active; and (**D**) Series 5, during which the Troll, Svartav and Tusse Faults and either the Vette or Øygarden faults were active, and the western Horda Platform underwent minor rotation (<0.15°). Volumetric sedimentation rates were highest during deposition of Series 2 (28 km^3/Myr) and then decreased in Series 3, 4 and 5 (ca. 13-15 km^3/Myr) (Fig. 3.15A). During deposition of Series 3 and 4, progradation rate and depositional flux decreased towards the west, due to progradation into progressively deeper water in which marine currents transported sediment alongshore. During deposition of Series 5, progradation rate decreased towards the west, but depositional flux decreased and then increased in this direction; this latter reflects more rapid export of sediment from the hinterland and bypass across slowly subsiding fault blocks in localised parts of the Troll Field. Progradation rates and depositional flux could not be calculated for Series 2 because of the absence of biostratigraphic events.*

3.7 CONCLUSIONS

We propose a new method to estimate ages and progradation rates within sets of shallow-marine clinoforms that are bounded by flooding surfaces, based on integrated, quantitative analysis of subsurface and/or outcrop data. This analysis requires the availability of a dense stratigraphic and sedimentological dataset, and involves four steps: (1) sediment decompaction and backstripping; (2) measurement of clinoform trajectories; (3) assignment of clinoform ages; and (4) calculation of progradation rate, sediment accumulation rate and depositional flux. Since sediment accumulation rate decreases steeply from the foreset to the toeset and topset of a clinoform, we use an exponential age-depth model in the third step of the method, to derive an equation for the age in a vertical section of the reference point chosen to measure clinoform trajectory. This equation is a function of four parameters: (1) age and (2) height above the basal flooding surface of a dated (bio)stratigraphic event within the clinoform set; (3) height of the clinoform-trajectory reference point above the basal flooding surface; and (4) instantaneous sediment accumulation rate at the time of deposition of the clinoform-trajectory reference point. Progradation rate, sediment accumulation rate and unit-width depositional flux are constrained along 2D transects that intersect multiple vertical sections and that are aligned parallel to clinoform dip, but may also be interpolated between transects. The results of the analysis enhance the predictive potential of sequence stratigraphic and clinoform trajectory analyses.

This method is applied to the Upper Jurassic Sognefjord Formation in the Norwegian North Sea, a 10-200 m thick clastic wedge deposited in ca. 6 Myr by a fully marine, westward-prograding subaqueous delta system. The internal architecture of this unit comprises four 10-60 m thick, westerly-dipping subaqueous clinoform sets

(Series 2 to 5) that can be mapped as nearly linear features for several tens of kilometres along strike. Horizontal trajectories are observed in each clinoform set, and the sets are stacked vertically. Within each series, clinoforms progressively increase their height, foreset slope and along-strike length, and decrease their down-dip extent in a basinward direction. Each clinoform set is characterised by a fall in progradation rate (from 500 to 30 km/Myr) and net sediment flux (from 90 to 10 km^2/Myr), synchronous with increased sediment accumulation rate (from 15 to 70 m/Myr) towards the basin. Within each clinoform set, the subaqueous delta was subject to increased interaction with shore-parallel marine currents as it advanced across the open shelf, and these currents probably transported a significant proportion of river-fed sediments along the shelf and out of the study area. In the Series 2 and 5 clinoform sets, localised spatial and temporal departures from the trends in rates described above are attributed to the effects of rift-related normal faulting during deposition, as supported by backstripping analysis and seismic isochron mapping.

The stacking pattern of the Series 2 to 4 clinoform sets defines an overall regressive, concave-landward trajectory, which is nearly vertical between Series 3 and 4. This clinoform-set-stacking trajectory implies autoretreat, resulting from an increase in sediment storage on the clinoform topset and associated coastal plain and a corresponding decrease in sediment delivery to the clinoform foreset as the delta system prograded to reach its characteristic length. The trajectory may also reflect strong shore-parallel sediment transport, which hindered further progradation. The concave-landward trajectory changed abruptly to nearly horizontal between Series 4 and 5, and internally the Series 5 clinoform set exhibits a minor, renewed rise in depositional flux in the westernmost part of the study area. The westward increase in depositional flux is attributed to a combination of sediment bypass across uplifting fault blocks in the western parts of the Troll Field, and to more rapid export of sediment from the hinterland in western onshore Norway, both of which are consistent with a period of rift activity during deposition of Series 5.

3.8 ACKNOWLEDGEMENTS

The mathematical effort that underpins this work has greatly benefited from the insightful collaboration of Ms. Giovanna Cisternino (Scientific High School of Chieti, Italy) and Sonia Anzellotti (University of Pisa, Italy) who are gratefully thanked. The authors also thank Statoil ASA for providing data for this study, Dr. Paul Whipp (Statoil ASA), Prof. Philip Allen (Imperial College) and Prof. Peter Sadler (University of California, Riverside) for stimulating

discussions and comments, and Dr. Amandine Prelat (Imperial College) for reviewing a previous version of this manuscript. We acknowledge the Troll Field partners, Statoil ASA, Petoro AS, A/S Norske Shell, Total E&P Norge AS and ConocoPhillips Skandinavia AS, for permission to publish this paper, and Schlumberger for provision of Petrel seismic and well interpretation software via an academic software donation.

APPENDIX: EQUATIONS AND ALGORITHM

Decompaction and backstripping

The decompaction equation is modified from Allen & Allen (2005):

$$y_A' - y_B' = y_A - y_B - (\varphi_0/c)\cdot\{e^{-cyB} - e^{-cyA}\} + (\varphi_0/c)\cdot\{e^{-cy'B} - e^{-cy'A}\} \quad (1)$$

where y_A = bottom of stratigraphic unit 'A' at the present day; y_B = top of stratigraphic unit 'B' at the present day; y'_A = bottom of stratigraphic unit 'A' at the decompacted or partly decompacted depth; y'_B = top of stratigraphic unit 'B' at the decompacted or partly decompacted depth; φ_0 = porosity of the decompacted lithology; and c = exponential decay constant of the given lithology.

In the second step of our decompaction and backstripping procedure, we calculate the total subsidence (y) and tectonic subsidence (Y) accumulated in a water-filled basin on the basal surface of a given stratigraphic unit (S) before and during deposition of the unit itself. These are given by the following equations (after Watts & Ryan, 1976; Steckler & Watts, 1978):

$$y = t_S - \{\Delta_{SL}\cdot [\rho_m / (\rho_m-\rho_w)]\} + w_d \quad (2)$$

$$Y = \{t_S \cdot [(\rho_m-\rho_s) / (\rho_m-\rho_w)]\} - \{\Delta_{SL}\cdot [\rho_m / (\rho_m-\rho_w)]\} + w_d \quad (3)$$

where ρ_m = mantle density (ca. 3,300 kg/m^3); ρ_w = seawater density (ca. 1,030 kg/m^3); ρ_s = water-filled density of unit S at the time under consideration, calculated from porosity estimated using equation 1; and t_S = decompacted thickness of unit S at the time under consideration, calculated from equation 1.

Water depths in wells intersecting a clinoform foreset or toeset (wd_2) has been estimated as a function of topset water depth (wd_1), the distance down depositional dip between the well of interest and the topset-to-foreset rollover position ($d_{1\text{-}2}$), the difference in decompacted or partly compacted clinoform-set thickness between these two points (t_1-t_2), and the estimated shelfal bathymetric gradient (θ) (Fig. 3.3A):

$$wd_2 = wd_1 + (t_1-t_2) + (d_{1\text{-}2} \cdot \tan\theta) \quad (4)$$

Once the values of tectonic subsidence in wells and well-correlation transects oriented perpendicular to structural grain have been estimated, tectonic tilting of the substrate during deposition of a given layer, $\kappa(x)$, can be calculated (Fig. 3.3B):

$$\kappa_{1\text{-}2}(x) = atan \{[(Y_{1(x)}\text{-}Y_{1(x\text{-}1)})\text{-}(Y_{2(x)}\text{-}Y_{2(x\text{-}1)})]/d_{1\text{-}2}\} \quad (5)$$

where: $d_{1\text{-}2}$ = distance between Well 1 and Well 2; $Y_{1(x)}$, $Y_{2(x)}$ = tectonic subsidence accumulated during and before deposition of layer x, measured at the top of this layer, in Well 1 and Well 2, which are respectively located in proximal and distal locations relative to the shoreline; $Y_{1(x\text{-}1)}$, $Y_{2(x\text{-}1)}$ = tectonic subsidence accumulated during and before deposition of layer (x-1), measured at the top of this layer, respectively in Well 1 and 2. [$Y_{i(x)}$-$Y_{i(x\text{-}1)}$] is the tectonic subsidence accumulated during the deposition of layer x, in well *i*. Positive vaues of $\kappa(x)$ indicate landward tilting of the substrate, and negative values indicate seaward tilting.

Calculation of trajectory angles

In order to calculate clinoform trajectories, the lower clinoform rollover point is traced as a reference point (rather the the shoreline break) relative to datum surfaces situated both above and below the studied clinoform sets (e.g. Fig. 3.3C). We then apply the mathematical method outlined in Figure 10 of Helland-Hansen & Hampson (2009) in a modified form in order to account for active tectonic rotation during the deposition of the clinoform set. The resulting equations 6 and 7 enable calculation of clinoform trajectories in stratigraphic intervals that underwent active tectonic modification (e.g., between wells 2 and 3 in Series 5, Fig. 3.3C). Clinoform trajectory for the regressive part of a regressive-transgressive cycle is given by the following equation, with parameters labelled acording to the example illustrated in Figure 3.3C:

$$[T5s_2 + T5m_2 + R5s_2] - [T5s_3 + T5m_3 + R5s_3] - [(d_{2\text{-}3} \cdot \tan \vartheta)] - [(d_{2\text{-}3} \cdot \tan \kappa_{2\text{-}3}(5))] \quad (6)$$

Clinoform trajectory for the transgressive part of a regressive-transgressive cycle is given by the following equation, with parameters labelled acording to the example illustrated in Figure 3.3C:

$$[T5s_3] - [T5s_2] + [(d_{2\text{-}3} \cdot \tan \vartheta)] + [(d_{2\text{-}3} \cdot \tan \kappa_{2\text{-}3}(5))] \quad (7)$$

where: $d_{2\text{-}3}$ = distance between Well 2 and Well 3 (Fig. 3.3C); θ = seafloor bathymetric gradient ; $\kappa_{2\text{-}3}(x)$ = tectonic tilting of datum surface between Well 2 and Well 3 (i.e. datum surface B at the top of Series 5 Fig. 3.3C), as calculated from equation 5; RXm_i, RXs_i, = decompacted or partly decompacted thickness of respectively the mud-rich and sand-rich portions of the regressive part (R) of regressive-transgressive cycle.

in well *i*; TXm_i, TXs_i = decompacted or partly decompacted thickness of respectively the mud-rich and sand-rich portions of the transgressive part (T) of regressive-transgressive cycle X in well *i* (c.f., Fig. 3.3C).

Clinoform age estimation

For a biostratigraphic event lying in the lower part of the clinoform set, the vertical trend in sedimentation rate across the foreset-toeset transition is approximated by an exponential function (Fig. 3.4C):

$$h(t) = W e^{\alpha t} \quad (8)$$

where *h(t)* is the stratigraphic height above the maximum flooding surface at the base of the clinoform set, *t* is the duration of the time period since this basal maximum flooding event, and *W* and α are coefficients that depend on the age-depth coordinates of the biostratigraphic event, "point 1" (t_1,h_1), and the clinoform-trajectory reference point, "point P" (t_P,h_P) (Fig. 3.4):

$$K = h_P \cdot e^{-\alpha t_P} = h_P \cdot exp\,[-(ln\, h_P - ln\, h_1) \cdot (t_P - t_1)^{-1} \cdot t_P] \quad (9)$$

$$\alpha = (ln\, h_P - ln\, h_1) \cdot (t_P - t_1)^{-1} \quad (10)$$

In order to determine the value of t_P, the age of the clinoform-trajectory reference point in the studied well (Fig. 3.4C), let us impose the following condition:

$$h'(t_P) = K \cdot \alpha \cdot e^{\alpha t_P} \quad (11)$$

By replacing *K* and α in Equation 11 with their explicit values, as determined by Equations 9 and 10, we obtain the following equation:

$$h'(t_P) = S_P = h_P \cdot (ln\, h_P - ln\, h_1) \cdot (t_P - t_1)^{-1} \quad (12)$$

where S_P is the instantaneous sedimentation rate at "point P". All of the terms in Equation 12 are known except t_P. The equation can be re-arranged as follows to allow derivation of t_P:

$$t_P = [h_P \cdot (ln\, h_P - ln\, h_1) \cdot (S_P)^{-1}] + t_1 \quad (13)$$

Once the value of t_P has been calculated from Equation 13, the coordinates of "point 1" (t_1,h_1) and "point P" (t_P,h_P) can be used in conjunction with Equations 8, 9 and 10 to determine an exponential function that tracks changes in stratigraphic height (h) as a function of variations in age (t). This exponential function describes the age-depth model:

$$h(t) = K \cdot e^{\alpha t} = h_P \cdot exp\,[(ln\, h_P - ln\, h_1) \cdot (t_P - t_1)^{-1} \cdot (t - t_P)] \quad (14)$$

"Point C" is the stratigraphic middle point of the sand-rich foreset package (Fig. 3.4E-F). The age of "point C" is needed in order to calculate the age of "point P" in cases where the known timeline (i.e., "point 1") is situated in the upper portion of the clinothem (Fig. 3.4D-F). The age of "point C" is calculated using a logarithmic interpolation based on Equation 14 that depends on the age-depth coordinates of the biostratigraphic event, "point 1" (t_1,h_1), and "point C" (t_C,h_C) as measured relative to the transgressive surface at the top of the clinoform set:

$$t_C = [h_C \cdot (ln\, h_C - ln\, h_1) \cdot (S_C)^{-1}] + t_1 \quad (15)$$

Once the age and position of "point C" are known, the age of "point P" is calculated by applying Equation 14 once more, but using the values of h_C and t_C as substitute terms for h_1 and t_1.

Calculation of the error in estimated age of a clinoform

The error propagation law is given by the following equation:

$$\Delta t_P = |\partial f/\partial t_1| \cdot \Delta t_1 + |\partial f/\partial h_1| \cdot \Delta h_1 + |\partial f/\partial h_P| \cdot \Delta h_P + |\partial f/\partial S_P| \cdot \Delta S_P \quad (16)$$

which in this method can be expressed as:

$$\Delta t_P = \Delta t_1 + [|h_P/(S_P \cdot h_1)| \cdot \Delta h_1] + \{|[ln(h_1/h_P) + 1]/S_P| \cdot \Delta h_P\} + \{|[h_P \cdot ln(h_1/h_P)]/(S_P^2)| \cdot \Delta S_P\} \quad (17)$$

Where Δt_1, Δh_1, Δh_P and ΔS_P are the errors associated with the four parameters required to calculate t_P through Equation 13, and Δt_P is the cumulative error in t_P. The value of Δt_1 is estimated as follows:

$$\Delta t_1 = \Delta x_0 + \Delta x_1 \quad (18)$$

where Δx_0 and Δx_1 are the respective uncertainties in the absolute ages of the maximum flooding surface at the base of the clinoform set (x_0; Fig. 3.4B, E) and of the biostratigraphic event within the clinoform set (x_1; Fig. 3.4B, E), as defined for the time scale in use. This parameter can be disregarded in calculations of age-related parameters that are relative between wells (e.g. progradational rates between wells), as in this study. Consequently, the following equations are used to calculate Δh_P, Δh_1 and ΔS_P:

$$\Delta h_P = [(L/2)/(1-\mu)] + [(\Delta\mu \cdot h_P)/(\mu-1)^2] \quad (19)$$

$$\Delta h_1 = \{[(b/2)+(L/2)] / (1-\mu)\} + [(\Delta\mu \cdot h_1)/(\mu-1)^2] \quad (20)$$

$$\Delta S_P = S_P \cdot \{ |[(S_{mean} \cdot \Gamma_{min}) - S_P]/ S_P | + |[(S_{mean} \cdot \Gamma_{max}) - S_P]/ S_P | \ / 2 \} \quad (21)$$

where b is the average biostratigraphic sampling resolution, L is the core-to-log shift (to be considered only if the studied dataset comprises both log depth and driller's depth values), μ is the compaction coefficient that measures the thickness difference between compacted and uncompacted units (μ = I(compaced-decompacted)/decompactedI), and Δμ is the average error in the compaction coefficient (equals to the standard deviation of the statistical population formed by all the μ values). Within a single clinoform set, Δα is considered to be equal to the standard deviation of the statistical population formed by all values of α for that set in the studied wells. S_{mean} is the average sedimentation rate, calculated by dividing the decompacted clinoform-set thickness by the clinoform-set duration; Γ_{min} and Γ_{max} represent, for a given clinoform set, the mean deviations of average sedimentation rate from respectively minimum and maximum instantaneous sedimentation rates, calculated for a given clinoform set from the entire population of studied well.

Equations (20) and (21) have been obtained by applying once more the error propagation law. In fact Δh_P and Δh_1 have been derived from the same errors in the case of a compacted succession (Δh^*_P and Δh^*_1), and from the compaction coefficient (μ), assuming that:

$$h_P \approx [h^*_P / (1-\mu)] \quad (22)$$

$$h_1 \approx [h^*_1 / (1-\mu)] \quad (23)$$

$$\Delta h_P \approx L/2 \quad (24)$$

$$\Delta h_1 \approx [(b/2) + (L/2)] \quad (25)$$

Equation (21), conversely, gives an approximate error bar around values of SP. The terms $(S_{mean} \cdot \Gamma_{min})$ and $(S_{mean} \cdot \Gamma_{max})$ used in this equation represent respectively 'averaged' minimum and maximum sedimentation rates, which are dependent on the distribution of minima and maxima in each series.

CHAPTER 4

Quantitative characterisation of delta-scale subaqueous clinoforms

Running head:

Delta-scale subaqueous clinoforms

Title:

Quantitative characterisation of delta-scale subaqueous clinoforms

Authors:

STEFANO PATRUNO, GARY J. HAMPSON, CHRISTOPHER A-L. JACKSON

Department of Earth Science & Engineering, Imperial College, London, SW7 2BP, UK

Email for correspondence: s.patruno09@imperial.ac.uk

Key words:

Clinoform, subaerial delta, subaqueous delta, compound clinoform

Word count: 451 (abstract) + 12,733 (main text)

Number of Figures: 19

Number of Tables: 8

CHAPTER 4: QUANTITATIVE CHARACTERISATION OF DELTA-SCALE SUBAQUEOUS CLINOFORMS

4.1 ABSTRACT

Subaqueous clinoforms are common in modern deltas, and constitute a hitherto overlooked depositional model for modern and ancient shallow marine sandbodies. The topset-to-foreset rollovers of subaqueous deltas are developed in significant (up to 60 m) water depths, such that delta-scale clinoforms recognised in the rock record or in seismic reflection data should not be assumed to record the position and morphology of ancient shorelines, even if they are sand- or sandstone-rich. In this study, qualitative observations and quantitative data from delta-, shelf edge- and continental margin-scale clinoforms are analysed using a large dataset compiled from published stratigraphic architectures. Comparative analysis allows us to establish diagnostic criteria to recognize different clinoform types, including fine- and coarse-grained, delta-scale subaqueous clinoforms, in both subsurface and outcrop datasets.

Recent, delta-scale (foreset height <50 m), sand-prone subaqueous clinoforms occur on steep (≥0.26°) and narrow (<35 km) shelves, where they strike parallel to the shoreline at distances typically <8 km from the shoreline break. These sand-rich clinoforms started prograding after the attainment of the Late Holocene sea-level highstand (ca. 6-7 Ka), and may form compound clinoform systems with associated subaerial-deltaic shorelines. Shoreline or subaerial-delta clinoforms are characterised by heights and slopes that are ca. 20-90% and 50-500%, respectively, of those of subaqueous-delta clinoforms. Topset (0.4-5°), foreset (0.7°-40°) and bottomset (0.4-5°) gradients of delta-scale sand-prone subaqueous clinoforms are steep, and their foresets have dip extents that are approximately 10 times smaller than those of other delta-scale clinoforms (typically <2 km). However, all delta-scale subaqueous clinoforms, whether sand-rich or not, tend to be sigmoidal in cross-section, in contrast to the markedly oblique cross-sectional geometries of subaerial deltas.

Due to their distal position from direct fluvial sediment input and to the sporadic nature of depositional episodes at time scales below Milankovitch cyclicity (≤20 kyr), delta-scale sand-prone subaqueous clinoform deposits have average progradation rates and unit-width depositional flux (respectively, 1-5 x 10^2 km/Myr and 1-15 km^2/Myr) that are up to 3-4 orders of magnitude lower than in equivalent subaerial deltas. These lower rates of

progradation, relative to coeval aggradation, are reflected in a larger spread of progradational clinoform trajectory values (from -0.5° to +2° relative to horizontal) than the very low angles (<0.1°) displayed by progradational subaerial-delta clinoforms.

Our analysis therefore indicates that slowly prograding, steep, sigmoidal clinoforms are strongly suggestive of sand-prone subaqueous deltas. Subsequently, the shallow-marine Sognefjord Formation (Upper Jurassic, offshore Norway) and Bridport Sand (Lower Jurassic, onshore southern UK) subsurface reservoirs were most likely deposited by delta-scale sand-prone subaqueous clinoforms types, the Blackhawk Formation (Upper Cretaceous, Utah, USA) is a probable outcrop example of delta-scale compound clinoforms with a muddy, subaqueous component.

4.2 INTRODUCTION

4.2.1 Shallow-marine compound clinoforms

Clinoforms are basinward-dipping, chronostratigraphic stratal surfaces that constitute the dominant architectural component of most deltaic to deep-marine successions (e.g., Gilbert, 1885; Rich, 1951; Bates, 1953; Mitchum et al., 1977; Pirmez et al., 1998; Adams & Schlager, 2000). Clinoform cross-sectional profiles vary from planar to sigmoidal to concave-upward (or 'oblique') (Sangree & Windmier, 1977), in response to environmental forcing and average sediment grain-size (e.g., Pirmez et al., 1998; Driscoll & Karner, 1999; Adams & Schlager, 2000). The cross-sectional geometry of clinoforms have therefore been used to characterise the environment conditions occurring in ancient depositional environments.

Clinoforms and inclined, clinoform-bounded stratal packages (clinothems *sensu* Rich, 1951) occur over a range of vertical scales (tens to thousands of metres). In certain cases, up to four types of progressively larger-scale clinoforms prograde synchronously along shoreline-to-abyssal plain transects, albeit at very different rates (Fig. 4.1A). These 'compound clinoforms' are genetically and morphologically linked, such that the bottomset of one

clinoform in an up-dip location corresponds to the topset of a larger-scale clinoform in a down-dip location (Swenson et al., 2005; Helland-Hansen & Hampson, 2009; Fig. 4.2). From the most proximal to the most distal, these clinoforms are: (1) subaerial deltas (or shorelines); (2) subaqueous deltas; (3) shelf-edge breaks; and (4) continental margins (Figs. 4.1-4.2).

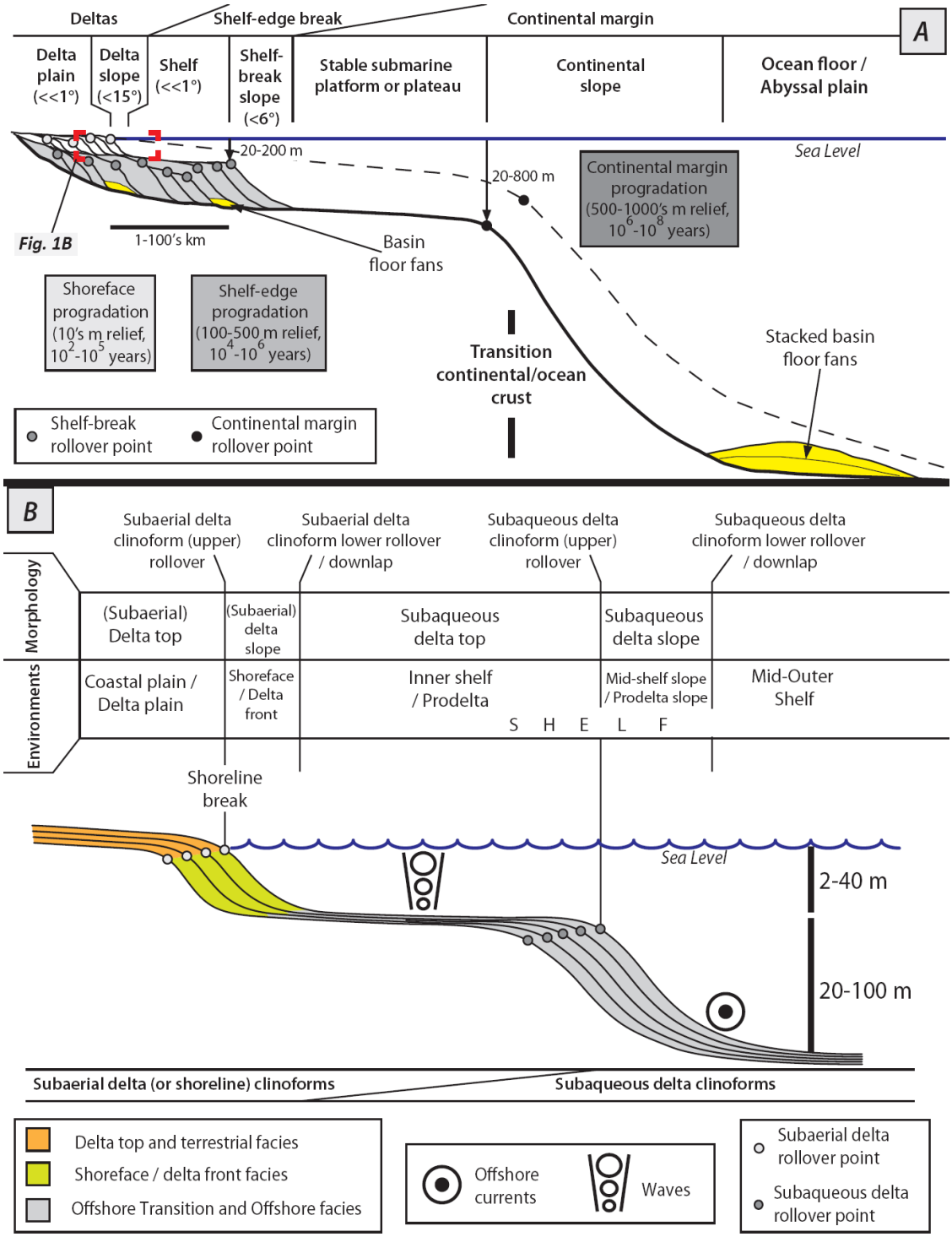

Figure 4.1. *Compound clinoform systems at different scales. (A) Idealized regional cross-section parallel to regional depositional dip, showing three actively growing clinoforms systems: delta, shelf-edge and continental margin clinoforms*

(modified after Henriksen et al., 2009). (B) Cross-sectional profile parallel to depositional dip showing a typical delta-scale compound clinoform system (located in Fig. 4.1A), comprising subaerial delta and subaqueous delta clinoforms (modified after Helland-Hansen & Hampson, 2009).

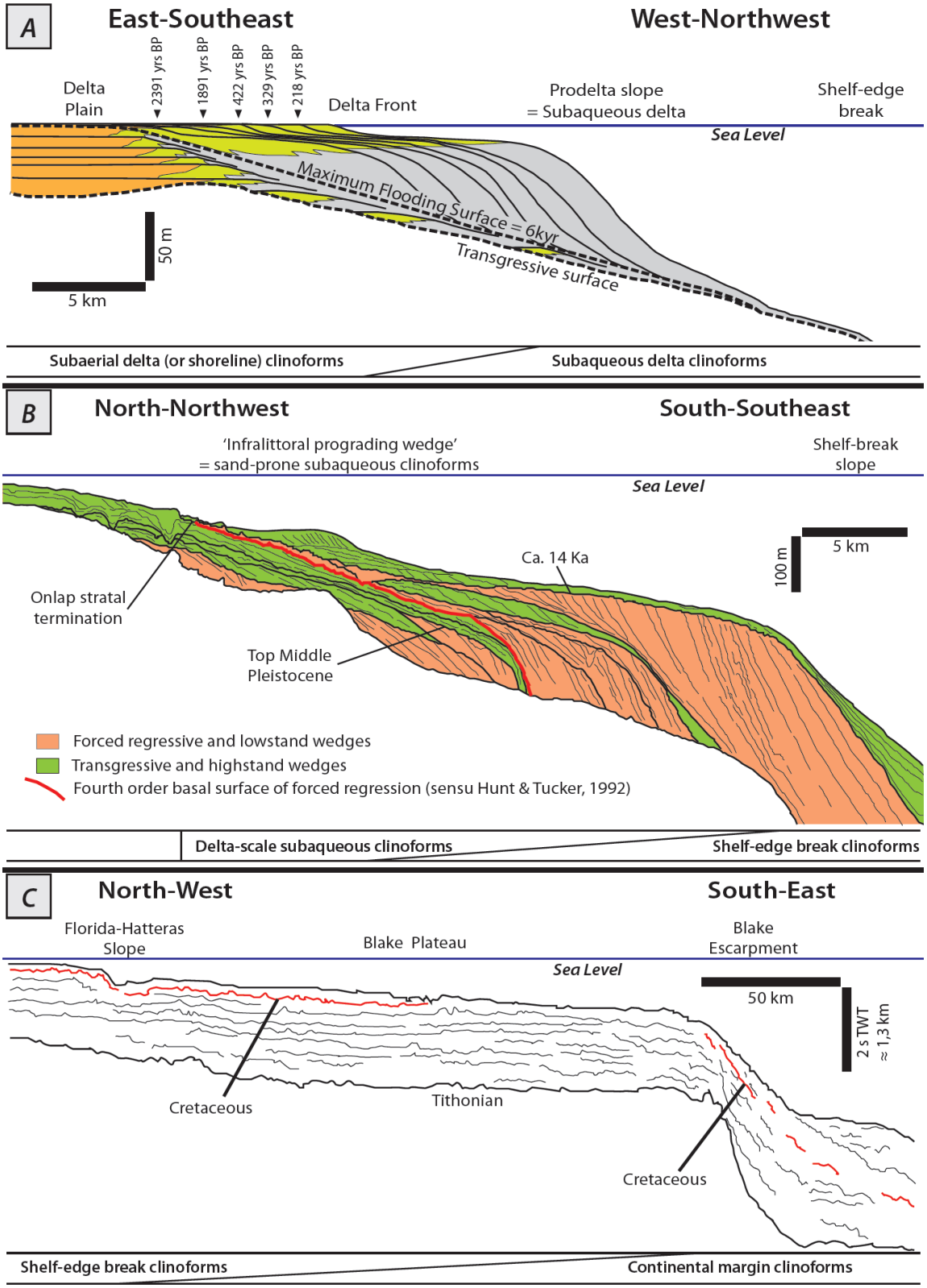

Figure 4.2. *Examples of compound clinoform systems at different scales. (A) Upper Holocene delta-scale compound clinoforms at the mouth of the present-day Tiber River (modified after Amorosi & Milli, 2001); (B) Cross-section oriented perpendicular to the southern Portugal shelf, showing the transition between an isolated Quaternary delta-scale sand-prone subaqueous clinoform and its associated, time-equivalent shelf-edge clinoform. The uppermost unit ('Seismic Unit 12' of Hernández-Molina et al., 2000a) is interpreted to have formed during the overall latest-Pleistocene-to-earliest-Holocene transgression, with the regressive delta-scale compound clinoform body deposited during the 'Younger Dryas' relative sea level stillstand (modified after Line 1-Figure 2 of Hernández-Molina et al., 2000b); (C) Regional cross-section showing a continental shelf-slope profile, including Tertiary shelf-edge clinoforms (Florida-Hatteras Slope) and their associated, time-equivalent continental margin clinoforms (Blake Escarpment) (modified after Schlee et al., 1979, their reflection profile FCB).*

Both subaerial and subaqueous delta-scale clinoforms are characterised by vertical relief of tens of metres, and typically occur within progradational-retrogradational cycles of 0.1-100 kyr duration (e.g., Burgess & Hovius, 1998; Hampson & Storms, 2003). The height of shelf-break clinoforms is ca. 100-500 m, and they generally occur in progradational-retrogradational units that represent 10-1,000 kyr (e.g., Steel & Olsen, 2002; Helland-Hansen & Hampson, 2009). Clinoforms that construct continental margins can approach several thousands of metres in relief, and their progradational-retrogradational cycles typically occur over 1-100 Myr (Henriksen et al., 2009).

Both autogenic controls and high-frequency allogenic controls exert progressively less influence on the architecture of clinoforms developed at increasingly larger spatial and temporal scales. As a result, larger-scale clinoforms are characterised by increasingly simpler clinoform trajectories. In particular, only delta-scale clinoforms occur in units that translate both seawards (i.e., progradation) and landwards (i.e., retrogradation). In contrast, shelf-edge and continental-margin clinoforms only accrete basinwards or remain fixed through time (Helland-Hansen & Hampson, 2009). Nonetheless, fundamental aspects of the style and dynamics of clinoform outbuilding are scale-invariant, despite their markedly different magnitudes. For example, both delta-scale clinoforms (Kuehl et al., 1986; Michels et al., 1998; Friedrichs & Wright, 2004; Walsh et al., 2004; Cattaneo et al., 2007) and shelf-edge clinoforms (e.g., Pratson et al., 1994) record maximum sedimentation rates in the upper part of their foresets (Nittrouer & Wright, 1994; Pirmez et al., 1998). An abrupt increase of depositional rates seaward of the topset-to-foreset rollover serves to maintain the clinoform shape over time, and suggests that topset-to-foreset rollovers mirror critical, time-averaged bed shear stress conditions (Walsh et al., 2004; Mitchell et al., 2012). Laterally extensive, alongshore clinoform geometries, with little along-strike variability and only minor protuberances that correspond to the position(s) of feeder rivers, are characteristic of subaqueous delta-scale clinoforms (Cattaneo et al., 2003, 2007; Mitchell et al., 2012; Chapter 2) and are also common in both shoreline clinoforms and shelf-edge clinoforms that accumulated during times of ascending clinoform trajectories and/or in locations lacking focused fluvial input(s) and dominated by basinal processes (e.g., Suter & Berryhill,

1985; Johannessen & Steel, 2005; Olariu & Steel, 2009). Furthermore, the range of progradational clinoform trajectory angles of both delta-scale and shelf-edge clinoforms are similar within a single progradational clinoform set, typically between -2° and +2°(e.g., Bullimore et al., 2005; Johannessen & Steel, 2005; Carvajal & Steel, 2006; Løseth et al., 2006). Overall aggradation of shelfal strata is therefore generated by vertical stacking of successive deltaic and shoreline clinothem sets (Bullimore et al., 2008; Helland-Hansen & Hampson, 2009). The repeated, regressive-transgressive transit of deltas and shorelines across the shelf is the process responsible for the outbuilding of continental shelf successions (Johannessen & Steel, 2005), and can, through time, contribute to the basinward accretion and morphological evolution of the larger-scale, shelf-margin clinoforms (e.g., via the establishment of shelf-edge deltas; Burgess & Hovius, 1998; Olariu & Steel, 2009; Helland-Hansen & Hampson, 2009).

4.2 2 Controls on the evolution of delta-scale subaqueous clinoforms

Two types of delta-scale clinoforms exist (Figs. 4.1B, 4.2A-B). In subaerial deltas (or shorelines), the clinoform topset is composed of subaerial delta top or coastal plain deposits, the topset-to-foreset rollover approximates the shoreline-break position, the foreset corresponds to the shoreface or delta slope, and the bottomset is contiguous with the inner shelf. In contrast, subaqueous delta clinoforms occur within regressive subtidal wedges. They are characterised by a subaqueous topset dominated by sediment bypass across the inner shelf, a shoreline-detached, topset-to-foreset rollover situated in water-depths approximating fairweather-wave base, a subaqueous delta slope (or prodelta slope), and a bottomset that is contiguous with the mid-to-outer shelf (Kuehl et al., 1986; Alexander et al., 1991; Pirmez et al., 1998; Driscoll & Karner, 1999; Hernández- Molina et al., 2000a; Cattaneo et al., 2003, 2007; Swanson et al., 2005; Helland-Hansen & Hampson, 2009; Mitchell et al., 2012; Chapter 2). Subaqueous deltas have been so far recognized mostly on present-day shelves. Only a few ancient delta-scale subaqueous clinoform systems have been identified, based on detailed sedimentological and geomorphological characterisation (e.g., Hampson, 2010; Chapter 2; Hampson et al., in review).

Recent delta-scale subaerial and subaqueous clinoforms either occur in isolation or are dynamically linked to each other along-strike or down-depositional dip, thus forming compound clinoform systems (Fig. 4.3). Sediment bodies containing delta-scale subaqueous clinoforms tend to be deposited during relative stillstands of sea level on near-shore areas between fairweather and storm wave bases (e.g., Hernández-Molina et al., 2000a,b; Cattaneo et al., 2003), and often exhibit along-shore-elongated to convex-seawards plan-view morphologies (Field & Roy, 1984; Driscoll & Karner, 1999; Hernández-Molina et al., 2000a; Cattaneo et al., 2003; Lobo et al.,

2005; Mitchell et al., 2012; Chapter 2). Delta-scale subaqueous clinoforms can be either mud-rich or sand-prone (e.g., in the 'infra-littoral prograding wedges' of Hernández-Molina et al., 2000a). Recent delta-scale sand-prone subaqueous clinoform bodies are usually composed of fine-grained sands, but their average grain-size may range from very fine-grained (e.g., New Zealand) to medium-grained (e.g., southern Iberia, south-east Australia, Monterey Bay) (Mitchell et al., 2012). In previous case studies, mud- and sand-rich subaqueous clinoforms have been treated in isolation (e.g., Hernández-Molina et al., 2000a; Cattaneo et al., 2003), even though their morphological and environmental similarities outnumber their differences. Herein, all delta-scale subaqueous clinoforms are systematically compared, irrespective of their grain size.

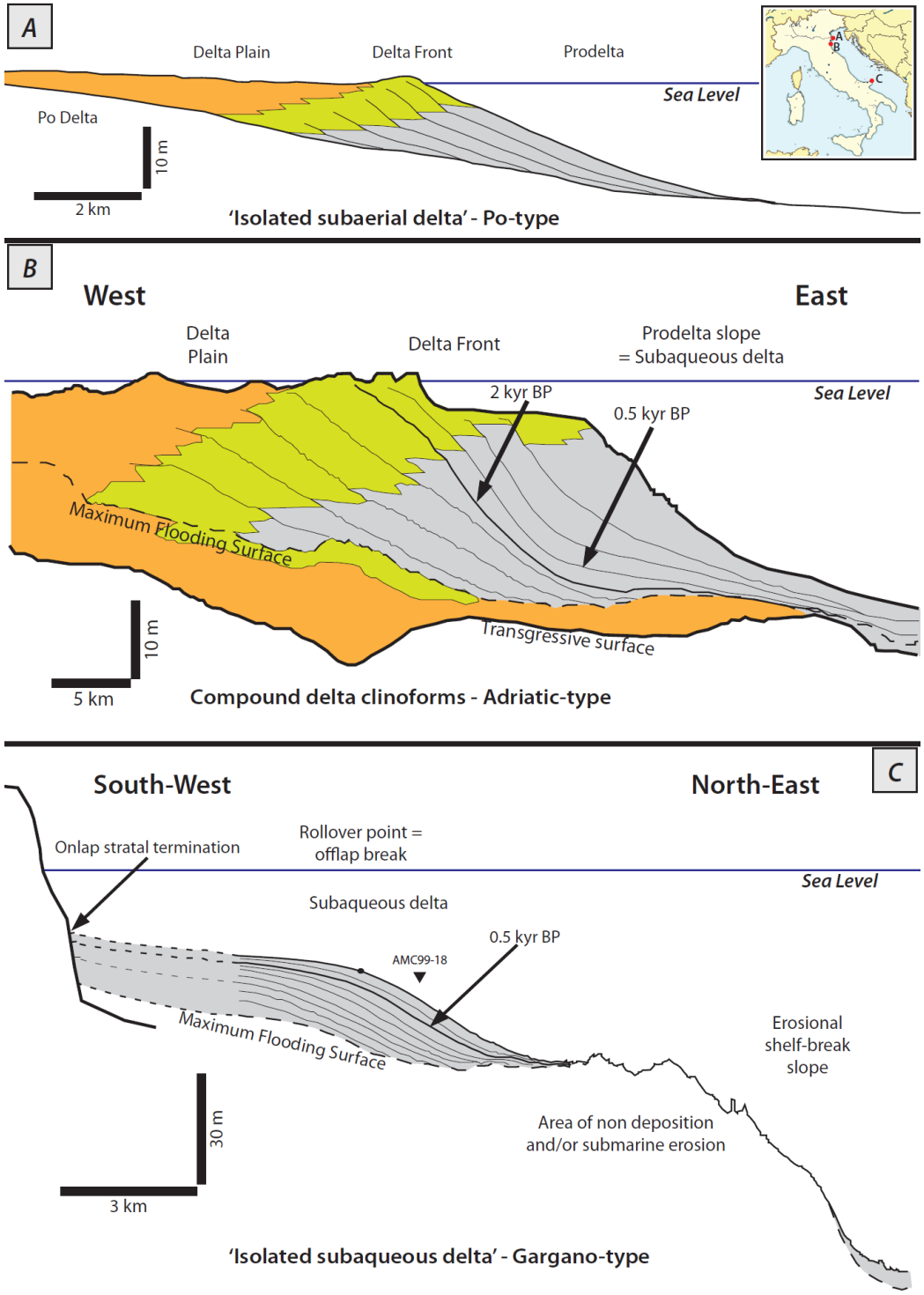

Figure 4.3. *The three main types of delta-scale clinoform configurations, with reference to their characteristic depositional profiles on the western Adriatic shelf (Cattaneo et al., 2003, 2007; Correggiari et al., 2005). (A) Isolated subaerial delta clinoforms, such as at the mouth of the present-day Po River; (B) delta-scale compound clinoforms, comprising a shoreline or subaerial delta clinoform and a time-equivalent subaqueous delta clinoform, formed along the western Adriatic shelf to the south of the Po River mouth; (C) isolated subaqueous delta clinoform offshore of the Gargano peninsula on the south-western Adriatic shelf, onlapping onto a pre-existing erosional substrate.*

Subaerial deltas are actively affected by river input, whereas subaqueous clinoforms are formed in shallow marine environments where sediment advection driven by basin dynamics (e.g., waves, tides and currents), rather than river discharge, is the principal mechanism by which sediment dispersal and deposition occurs (e.g., Pirmez et al., 1998; Driscoll & Karner, 1999; Adams & Schlager, 2000; Cattaneo et al., 2003; 2007; Hernández-Molina et al., 2000a; Swenson et al., 2005; Mitchell, 2012; Mitchell et al., 2012). As a consequence, subaerial clinoforms are oriented normal or radial to the sediment input direction at a river-mouth point source (Barrell, 1912; Bates, 1953; Bhattacharya, 2006). In contrast, the elongated plan-view geometries typical of delta-scale subaqueous clinoforms strike parallel to the alongshore advective transport belt that feeds and sculpts them (Fig. 4.4). As shown schematically in Figure 4.4, significant near-bed shear stresses in shallow-marine areas marked by high-energy waves, tides and/or currents often prevent deposition along subaqueous clinoform topsets, causing topographic flattening and bypass of these areas through lateral advection and resuspension of sediment (Pirmez et al., 1998; Driscoll & Karner, 1999; Swenson et al., 2005; Cattaneo et al., 2007). Time-averaged deposition occurs preferentially just seaward of the topset-to-foreset rollover point, where wave- and current-induced, near-bed agitation declines below the threshold of sediment motion (Mitchell, 2012; Mitchell et al., 2012), causing maximum sediment accumulation rates in the upper foreset region of most clinoforms. The along-strike uniformity of subaqueous deltas is due to the energetic hydrodynamic forces active on the shelf, whereas in their subaerial counterparts, high-frequency allogenic forcing and autogenic behaviours result in very rapid episodes of local progradation that alternate with periods of abandonment, erosion and retreat (Cattaneo et al., 2003; Correggiari et al., 2005).

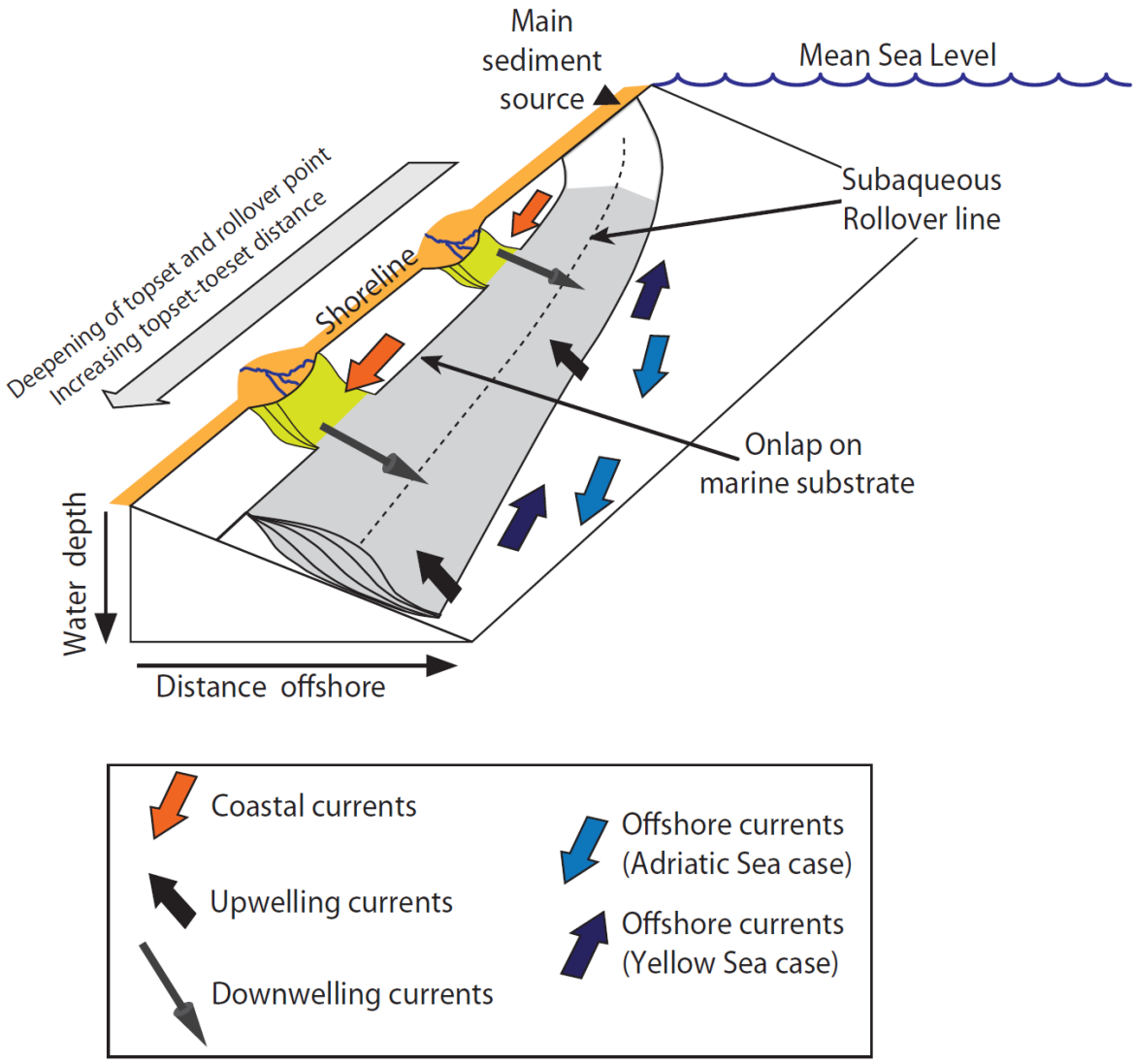

Figure 4.4. *Three-dimensional scheme portraying the main architectural features and the typical oceanographic environment of present-day delta-scale compound clinoforms, such as the western Adriatic shelf (Cattaneo et al., 2003, 2007) and the western Yellow Sea (Liu et al., 2006, 2007). Shore-parallel coastal currents contribute to the uniform growth of the subaqueous clinoform, by along-shelf redistribution of sediments fed by fluvial input points. Offshore currents influence the overall shore-parallel strike-direction of the subaqueous clinoforms. Downwelling currents transport shoreface sediments offshore, thereby sustaining the overall growth and progradation of the subaqueous clinoform perpendicular to the alongshore currents that feed it. In well-documented modern examples, the position of clinoform bottomsets is controlled by seafloor-hugging offshore currents flowing parallel to the clinoform strike and/or by upwelling processes, which force sediment transport along clinoform strike rather than offshore (e.g., Cattaneo et al., 2003, 2007; Liu et al., 2006, 2007).*

4.2.3 Aims

The model of delta-scale sand-prone subaqueous clinoforms proposed by Hernández-Molina et al. (2000a), Mitchell et al. (2012) and Chapter 2 provides an interpretative template that may be applicable to other ancient shallow-marine strata. Their existence indicates that delta-scale clinoforms in the rock record or in seismic reflection data should not be automatically linked to ancient shoreline positions, even if they are sand-rich, as their toeset-to-foreset rollovers may have formed at up to 60 m water depth (Mitchell et al., 2012). However, in the absence of sedimentological characterisation, it is at present impossible to distinguish whether an ancient delta-scale clinoform was formed at the shoreline or in a subaqueous setting.

In order to improve our understanding of these different clinoform types, this study analyses a large architectural and chronological dataset of modern and ancient clinoforms in order to: (1) test the existence of geomorphological proxies to constrain the depositional water depth of clinoforms; (2) characterise diagnostic architectural, sedimentological and stratigraphic features of compound clinoform systems, and particularly of delta-scale subaqueous clinoforms; (3) construct a data-driven interpretation methodology that allows delta-scale subaqueous clinoforms to be interpreted in seismic reflection, sedimentological and/or stratigraphical data; and (4) elucidate the impact of this hitherto underappreciated depositional system on existing sequence stratigraphic models.

4.3 DEFINITION OF TERMS AND PARAMETERS

The term ‘shelf’ is often used ambiguously (Vanney & Stanley, 1983; Helland-Hansen et al., 2012). Here the term is utilized to refer to the ‘subaqueous marine shelf’ (*sensu* Burgess & Steel, 2008; Olariu & Steel, 2009), which has a low overall gradient (typically 0.01-0.02°, but as steep as 0.7°; Asquith, 1970; Olariu & Steel, 2009) and is located between the shoreline break and shelf-edge break. The shelf-edge break is identified at the first change in bathymetric gradient occurring at water depths of 50-300 m (Shepard, 1959; Wear et al., 1974; Southard & Stanley, 1976; Olariu & Steel, 2009) and with a minimum total bathymetric relief of 100 m (Henriksen et al., 2009; Helland-Hansen & Hampson, 2009; Helland-Hansen et al., 2012; Figs. 4.1A-B). This definition implies that non-erosional shelves correspond to the topset component of shelf-edge clinoforms and to the bottomset of delta and shoreline clinoforms (Burgess & Steel, 2008), and that shelf-edge trajectories demarcate neritic and bathyal subaqueous environments (Henriksen et al., 2009).

Shelf-edge clinoforms and continental margin clinoforms (Figs. 4.1A; 4.2C) are here differentiated because, in certain cases, the seaward termination of a shelf-break slope is not situated at oceanic depths, but lies above another sub-horizontal, bathyal platform (e.g., Florida Hatteras Slope to Blake Escarpment system, Fig. 4.2C, Schlee et al., 1979; the 'combined structural-sedimentary' shelf of the Gulf of Corinth, Helland-Hansen et al., 2012). In these cases, the continental margin is situated seaward of this submarine plateau or platform, and may be marked by a further clinoform whose position is primarily controlled by the transition between continental and oceanic crust. However, in many present-day shelves, shelf-break and continental margin clinoforms are coincident.

In this work, several clinoform architectural and geochronological parameters have been measured from published cross-sections, maps and other data (Fig. 4.6, Tables 4.1-4.2). Below, and in Figure 4.5, these parameters are briefly defined. On the cross-sectional profile of a clinoform surface, two points of maximum curvature ('rollover points') are usually located landward and basinward of the point of maximum slope ('inflection point'; Fig. 4.5). Upper and lower rollover points are centred respectively on the upward-convex topset-to-foreset transition of a clinoform surface (e.g., Figs. 4.1A-B) and on the upward-concave foreset-to-bottomset transition of a clinoform surface. The positions of these two prominent breaks-in-slope subdivide the clinoform surface into a steeper central area ('foreset') and two gently-sloping areas, respectively landward ('topset') and basinward ('bottomset' or 'toeset') of the inflection point (Barrell, 1912; Mitchum et al., 1977; Pirmez et al., 1998; Fig. 4.5). Bottomsets and topsets are here subdivided into inner and outer parts, based on the positions of the points where bottomset and topset become horizontal or conformable with the underlying surface (clinoform 'toe point' and 'head point', respectively; Pirmez et al., 1998; Fig. 4.5). The height and dip extent of a foreset (*Fh*, *Fd*), outer topset (*Th*,*Td*) and inner bottomset (*Bh*, *Bd*) are determined by the vertical and horizontal distances between the toe point, the two rollover points and the head point of the clinoform (Fig. 4.5). The elevation of the inflection point (*Ih*) is measured from the toe point, whereas the 'total clinoform relief' (*H*) corresponds to the vertical distance from the toe point to the head point of a horizontal topset or to the shallowest point at the mouth of the river in the case of a sloping topset (Pirmez et al., 1998; Fig. 4.5). A parameter named 'shape ratio' (c.f., Fig. 4.5) or 'normalized elevation of the inflection point' (*h/H*) was defined by Pirmez et al. (1998) as the height of the inflection point (*Ih*) divided by the clinoform total relief (*Hh*). This parameter was proposed to quantitatively distinguish symmetrical, sigmoidal clinoforms ($h/H < 0.4$) from asymmetrical, oblique clinoforms ($h/H \geq 0.4$).

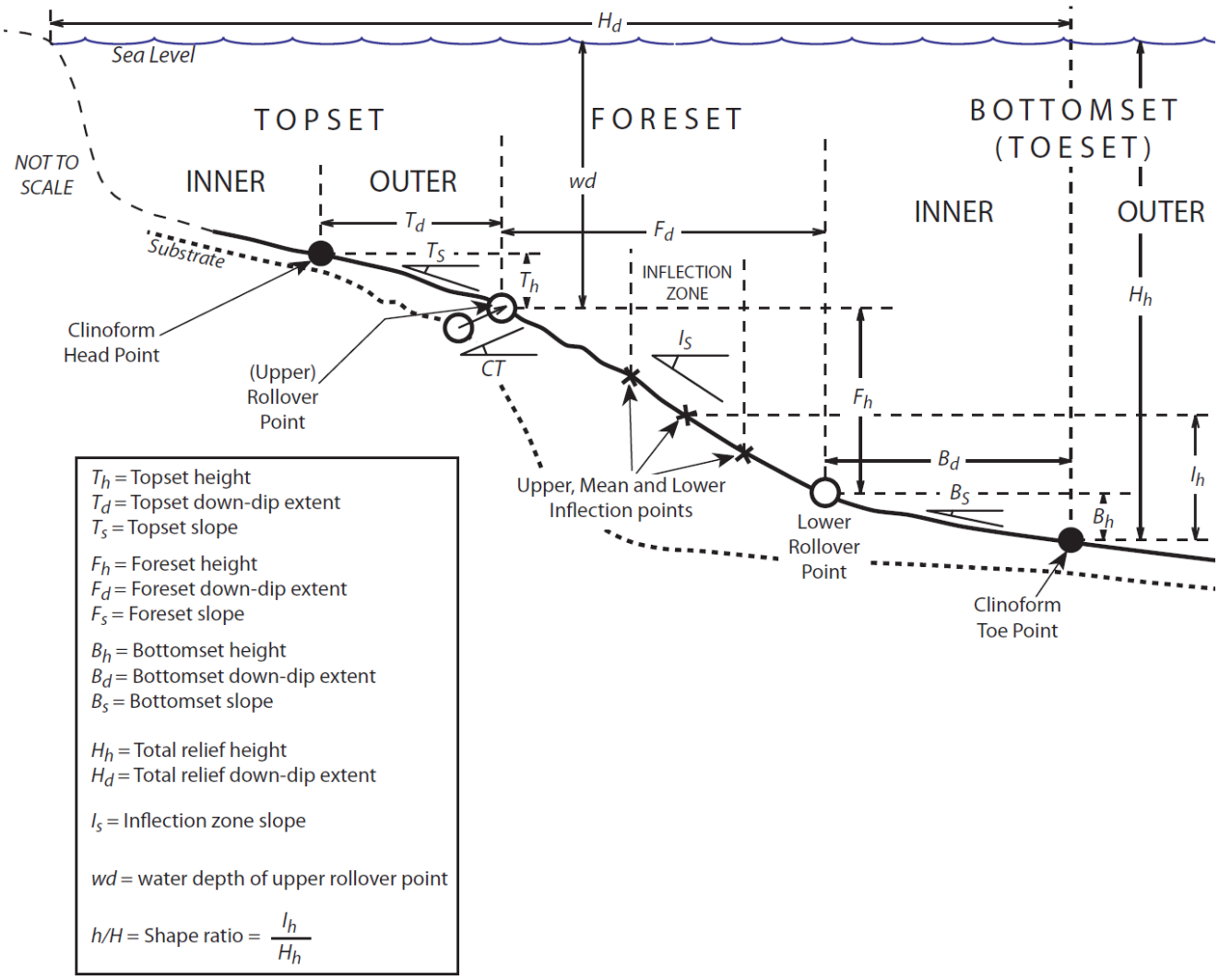

Figure 4.5. *Summary of clinoform nomenclature, illustrated for a delta-scale subaqueous clinoform (Fig. 4.1B). The clinoform inflection point (or inflection zone) is the point (or area) where the gradient reaches maximum values. The rollover points are the two points of maximum curvature located landward and seaward of the inflection point. The rollover points separate a foreset of steeper gradient from the landward-lying topset and seaward-lying bottomset, which both have gentler gradients. The toe of the clinoform occurs in the bottomset, where the clinoform becomes conformable with the underlying substrate. The clinoform height (H) is the difference in elevation between the clinoform toe point and the clinoform head point, where the topset becomes conformable with the underlying substrate. Additional parameters are described in the text.*

The points of stratal termination associated with clinoforms in seismic cross-sections partly reflect imperfect resolution of progressive stratal pinchouts occurring landward of the upper rollover point ('offlap' or 'toplap') and basinward of the lower rollover point ('downlap'). In particular, seismic data suggest that: (1) the downlap point occurs between the lower rollover point and clinoform toe point; (2) the toplap point occurs in close proximity to

the upper rollover point in oblique clinoforms with narrow topsets; and (3) in strongly progradational clinoform successions, the offlap point occurs at the clinoform head point, although in reality it may lie landward of this point.

Vertical sediment accumulation rate is considered to be the maximum vertical thickness of a clinothem divided by the age difference between the basal and top clinoform surface, which usually correspond to flooding surfaces. Progradation rate is measured as the horizontal distance between the inflection point positions of two dated clinoforms divided by their age difference (e.g., following the method proposed in Chapter 3). Progradation resistance ratio is a dimensionless number corresponding to the ratio between mean vertical sediment accumulation rate and progradation rate calculated along a cross-section parallel to the clinoform dip (cf., Chapter 3). This ratio reflects the amount of sediment that needs to accumulate in order for the clinothem foreset to prograde of a single unit. The cross-sectional net sediment flux is the product of progradation rate and mean thickness of a clinothem, both measured along a cross-section parallel to the depositional dip. This parameter was defined by Burgess & Hovius (1998) and Chapter 3), and is equal to the initial river-fed sediment input rate, minus the sum of the rates of sediment addition by deposition and removal by erosion down depositional dip (e.g., by gravity flows) and the rate of sediment addition or removal by out-of-plane transport (e.g., by alongshore currents).

4.4 RECENT DELTA-SCALE SUBAQUEOUS CLINOFORMS

Plan views and cross-sections oriented parallel to the depositional dip of twenty recent delta-scale subaqueous clinoforms and compound clinoforms are located in Figure 4.6 and Tables 4.1-4.2 and presented in Figures 4.7-4.10 and in Table 4.3. These systems are either formed by deltaic systems (e.g., off the mouth of the Yangtze, Yellow-Shandong, Ganges-Brahmaputra, Amazon, Fly, Orinoco, Shoalhaven, Atchafalaya, Salinas, San Diego, Manawatu, Rhone, Tiber, Arno-Cecina and Italian Adriatic rivers), or are not directly related to river mouths (e.g., mid-shelf clinoforms off the coast of southern Spain, southern Portugal, south-eastern Australia, western Ascension Island). Detailed cross-sections of modern delta-scale subaqueous clinoforms, based on interpretations of seismic reflection profiles, are shown in Figure 4.11.

A wealth of publications exists for many recent delta-scale subaqueous clinoforms and associated compound clinoforms. The reader is referred to Hori et al. (2001) and Liu et al. (2006, 2007) (Yangtze River delta); Bornhold et al. (1986), Alexander et al. (1991), Liu et al. (2004) and Yang & Liu (2007) (Yellow River delta and subaqueous Shandong delta); Kuehl et al. (1997, 2005), Michels et al. (1998), and Palamenghi et al. (2011) (Ganges-Brahmaputra River subaqueous delta); Kuehl et al. (1986), Nittrouer et al. (1986, 1996) and Methling et al. (1996) (Amazon River delta); Walsh et al. (2004) (Fly River delta); Warne et al. (2002) (Orinoco River delta); Neill & Allison (2005) (Atchafalaya delta); Amorosi & Milli (2001) and Correggiari et al. (2005) (Tiber and Po River deltas); Cattaneo et al. (2003, 2004, 2007) (Adriatic subaqueous clinoforms); Dunbar & Barrett (2005) (Manawatu coastlines, New Zealand); Field & Roy (1984) (south-eastern Australia coastlines); Hernández- Molina et al. (2000a,b) and Lobo et al. (2005) (southern Spanish and Portuguese coastlines); and Chin et al. (1988) (Monterey Bay coastlines). Mitchell et al. (2012) provided a synthesis of delta-scale sand-prone subaqueous clinoforms (e.g., offshore of Manawatu, southern Spanish and Portuguese, and south-eastern Australia coastlines), as well as describing similar clinoforms off the coasts of western Ascension Island and Oceanside, USA. Some of the systems shown in Figures 4.7-4.10 have not been previously investigated, but they contain physiographic features typical of delta-scale subaqueous and compound clinoforms, and occur in close proximity to previously documented examples. For example, the Arno-Cecina (Italy), Shoalhaven (south-eastern Australia) and San Diego (USA) deltas are situated respectively along-strike of the Tiber, Port Jackson-Bate Bay-Botany Bay and the Oceanside subaqueous and compound clinoforms (c.f. Mitchell et al., 2012), even though they may not represent a unique, continuous subaqueous system. In the case of the Rhone delta, a compound clinoform interpretation is also supported by Holocene sediment isopach and grain-size maps published by Gensous & Tesson (1997), Tesson et al. (2000) and Labaune et al. (2005).

Bathymetric contours and cross-sections in Figures 4.7-4.10 have been drawn using the Global Multi-Resolution Topography dataset of Ryan et al. (2009), and areas of relatively steep gradient on the inner-to-mid shelf have been highlighted in the maps by grey shading. These areas of relatively steep gradient form shoreline-parallel belts that generally correspond to the foresets of actively accreting clinoforms, although in some cases they may correspond to steep erosional surfaces (e.g., south-eastern Australia coastlines; Field & Roy, 1984). In most examples, it is possible to distinguish a subaerial delta clinoform at the shoreline, a subaqueous delta clinoform in the middle of the shelf, and a clinoform marking the shelf edge. In most of the examples presented here, maps of Late Holocene sediment thickness support the interpretation of actively accreting clinoforms situated at the three present-day breaks in bathymetric gradient (e.g., Nittrouer et al., 1986; Gensous & Tesson, 1997; Micheals et al., 1998; Cattaneo et al., 2003, 2007; Liu et al., 2004, 2007; Lobo et al., 2005; Yang & Liu, 2007; Le Dantec et al., 2010). Below, we summarise four representative and particularly well-documented examples of recent delta-scale subaqueous clinoforms and compound clinoforms, before drawing general observations from comparisons between the associated maps and cross-sections (Fig. 4.13).

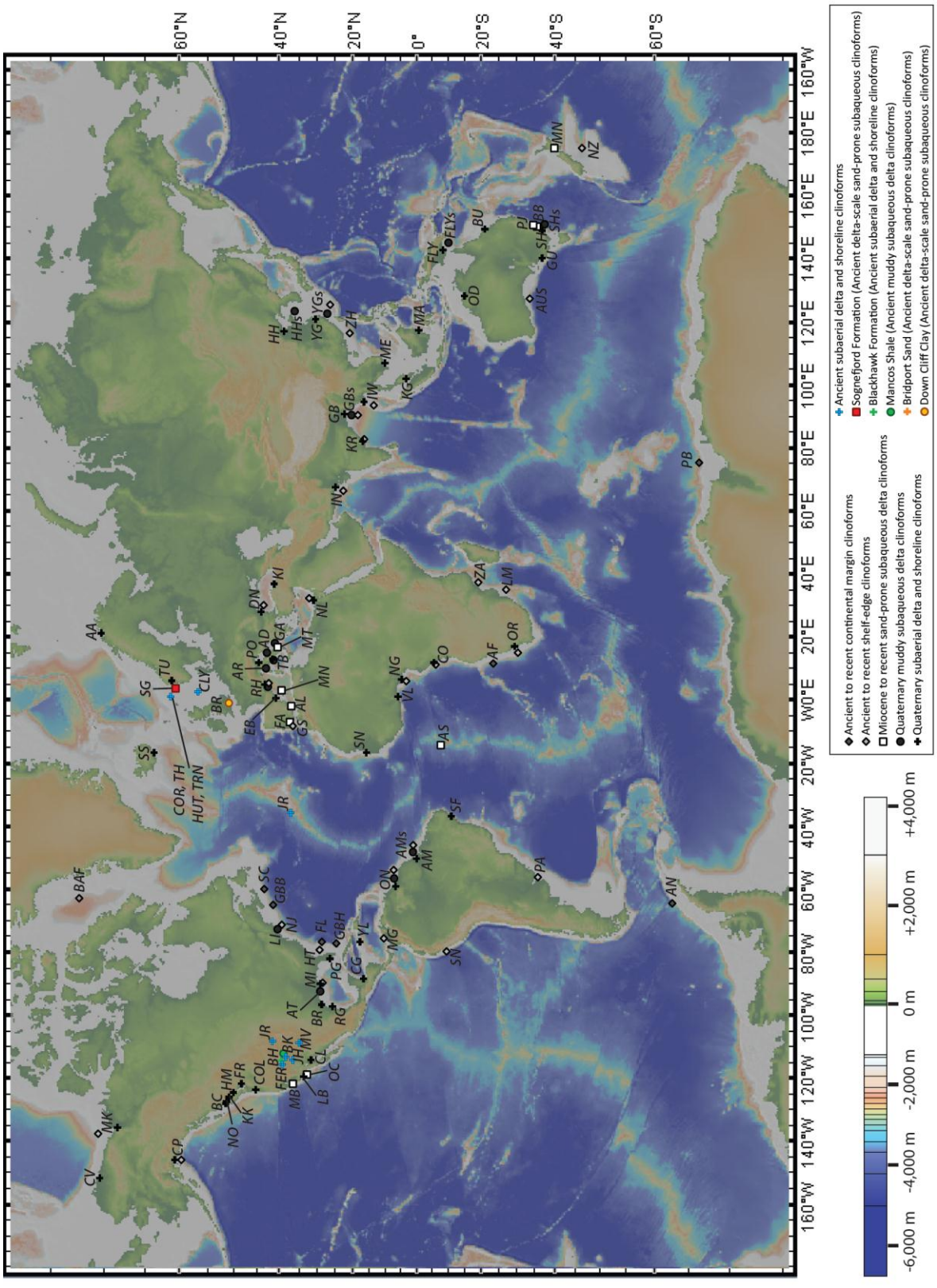

Figure 4.6. *Location of recent and ancient clinoforms and clinoform sets analysed in this study. Bathymetry and topography are derived from the Global Multi-Resolution Topography dataset of Ryan et al. (2009), and are plotted using GeoMapApp freeware. Abbreviations for clinoforms and clinoform sets are given in Tables 4.1 and 4.2.*

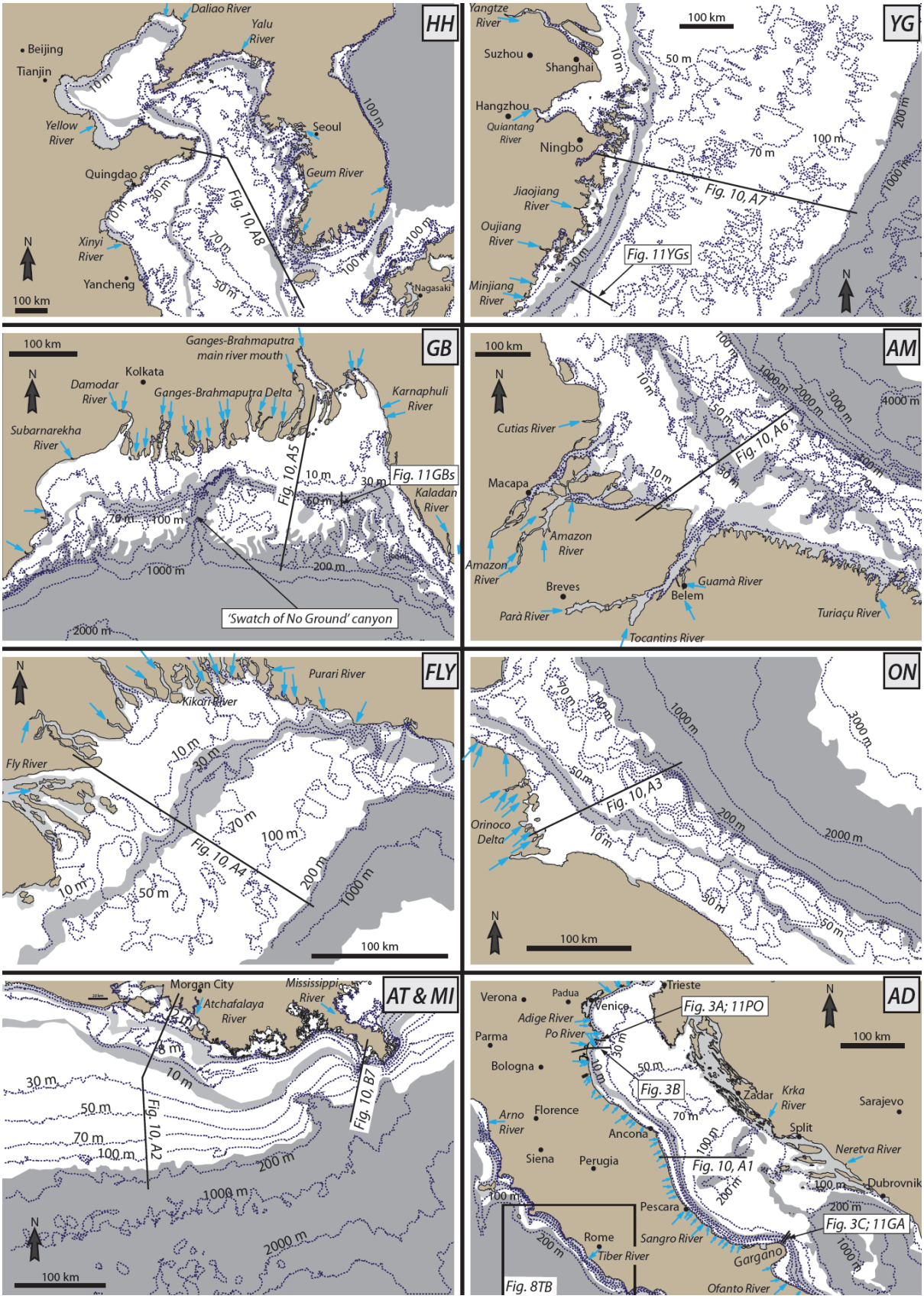

Figure 4.7. *Maps showing plan-view features of present-day macro-scale shelfal settings where delta-scale compound clinoforms and/or subaqueous clinoforms are actively prograding. Maps and contours are taken from the Global Multi-Resolution Topography dataset of Ryan et al. (2009). Steeper subaqueous areas on the inner-to-mid shelf (with respect to the*

surrounding low-gradient shelf) are highlighted by grey shading. The majority of these areas of steeper shelf gradient correspond to the foresets of actively growing clinoforms, whereas in other cases they may correspond to steep erosional surfaces. Cross-sectional profiles shown in Figures 4.3, 4.14 and 4.16 are located. (HH) Northern Yellow Sea shelf (North-east China and Korea), including the mouth of the Yellow River; (YG) Southern Yellow Sea shelf (eastern China), including the mouth of the Yangtze River; (GB) Indian Ocean shelf off the mouth of the Ganges-Brahmaputra River system (eastern India and Bangladesh) (AM) Western Southern Atlantic Ocean shelf, off the Amazon River mouth (north-eastern Brazil); (FLY) shelf off the southern coasts of Papua New Guinea, including off the Fly River mouth; (ON) Western Southern Atlantic Ocean shelf, off the Orinoco River mouth (eastern Venezuela); (AT & MI) Northern Gulf of Mexico shelf, off the mouth of the Mississippi and Atchafalaya rivers (southern Louisiana, U.S.); (AD) Adriatic Sea shelf, Italy, including the cross-sectional profiles of Po-, Adriatic- and Gargano-type clinoforms in Figure 4.3 and the Adriatic Shelf bathymetric profile in Figure 4.14.

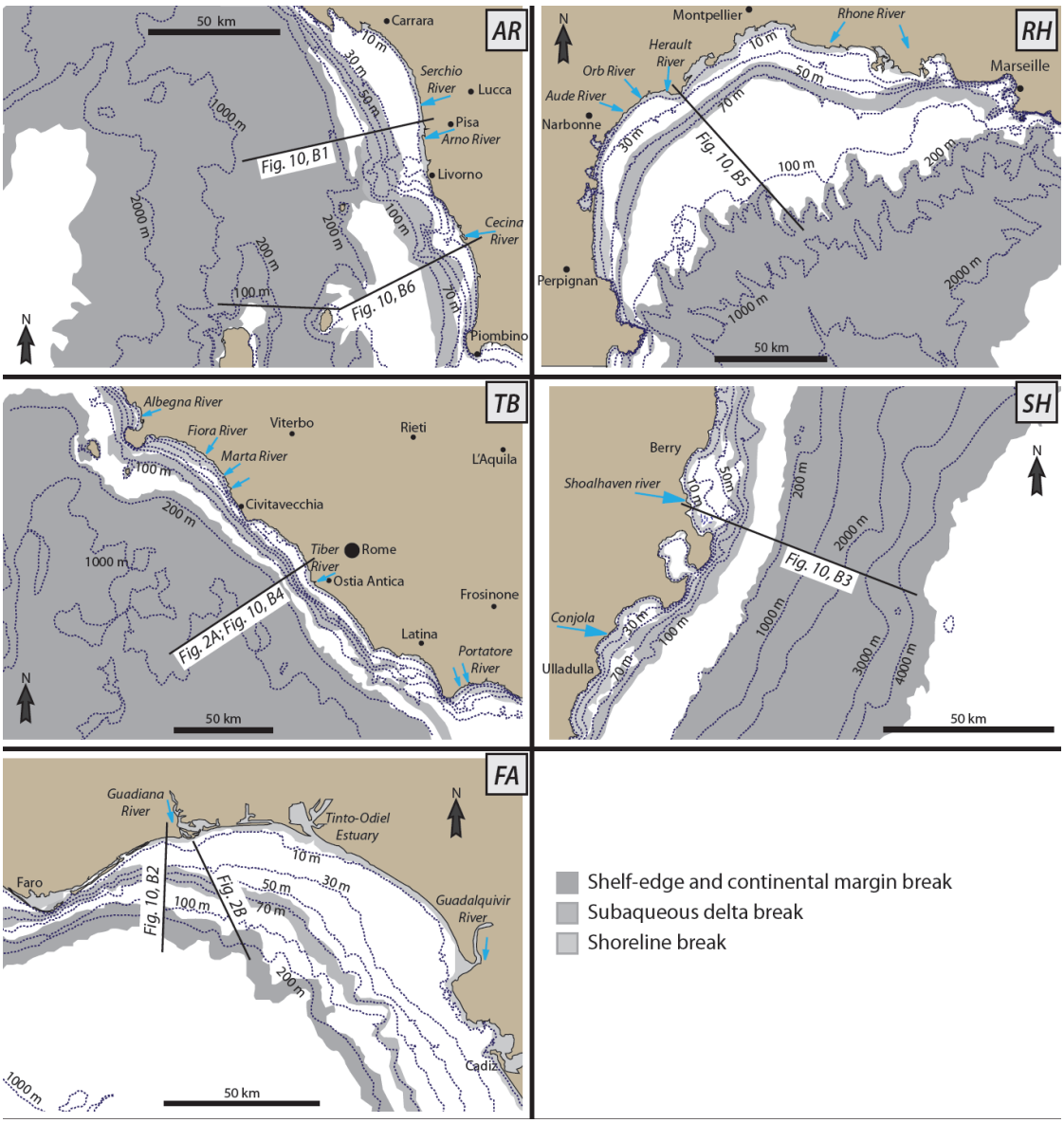

Figure 4.8. *Maps showing plan-view features of present-day meso-scale shelfal settings where delta-scale compound clinoforms and/or subaqueous clinoforms are actively prograding. Maps and contours are taken from the Global Multi-*

Resolution Topography dataset of Ryan et al. (2009). Steeper subaqueous areas on the inner-to-mid shelf (with respect to the surrounding low-gradient shelf) are highlighted by grey shading. The majority of these higher-gradient areas correspond to the foresets of actively growing clinoforms, whereas in other cases they may correspond to steep erosional surfaces. Cross-sectional profiles shown in Figures 4.2, 4.14 and 4.16 are located. (AR) Tuscany coastlines (Tyrrhenian Sea, north-western Italy), including the profiles off the mouths of Cecina and Arno rivers; (RH) Languedoc shelf (southern France, Western Mediterranean) off the Rhone River mouth; (TB) Tyrrhenian Sea Shelf off the Tiber River mouth (central-western Italy, Western Mediterranean); (SH) shelf off the Shoalhaven River mouth (south-eastern Australia coast); (FA) Eastern North Atlantic Ocean shelf off the coasts of southern Spain and Portugal (Faro-Guadiana).

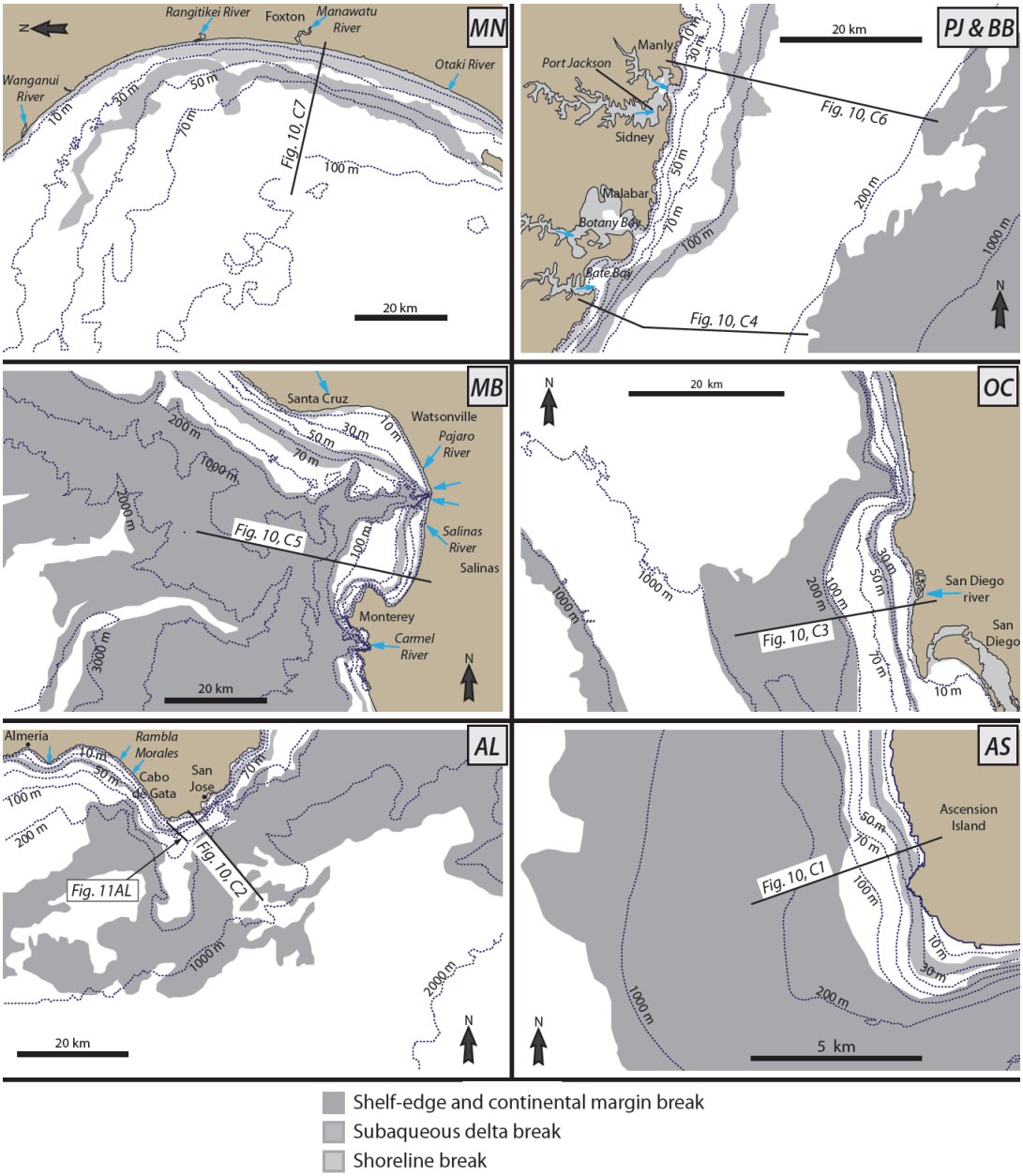

Figure 4.9. *Maps showing plan-view features of present-day micro-scale shelfal settings where delta-scale compound clinoforms and/or subaqueous clinoforms are actively prograding. Maps and contours are taken from the Global Multi-Resolution Topography dataset of Ryan et al. (2009). Steeper subaqueous areas on the inner-to-mid shelf (with respect to the surrounding low-gradient shelf) are highlighted by grey shading. The majority of these higher-gradient areas correspond to the foresets of actively growing clinoforms, whereas in other cases they may correspond to steep erosional surfaces. Cross-sectional profiles shown in Figures 4.14 and 4.15 are located. (MN) Manawatu coast (New Zealand); (PJ & BB) South-eastern Australia shelf, including Port Jackson and Bate Bay profiles; (MB) shelf off Monterey Bay, near the Salinas River mouth (California, U.S.A.); (OC) shelf off Oceanside, near the Sand Diego river mouth (California, U.S.A.); (AL) Western Mediterranean Shelf off the Cabo de Gata promontory (Almeria, southern Spain); (AS) Atlantic ocean off the western coastlines of Ascension Island.*

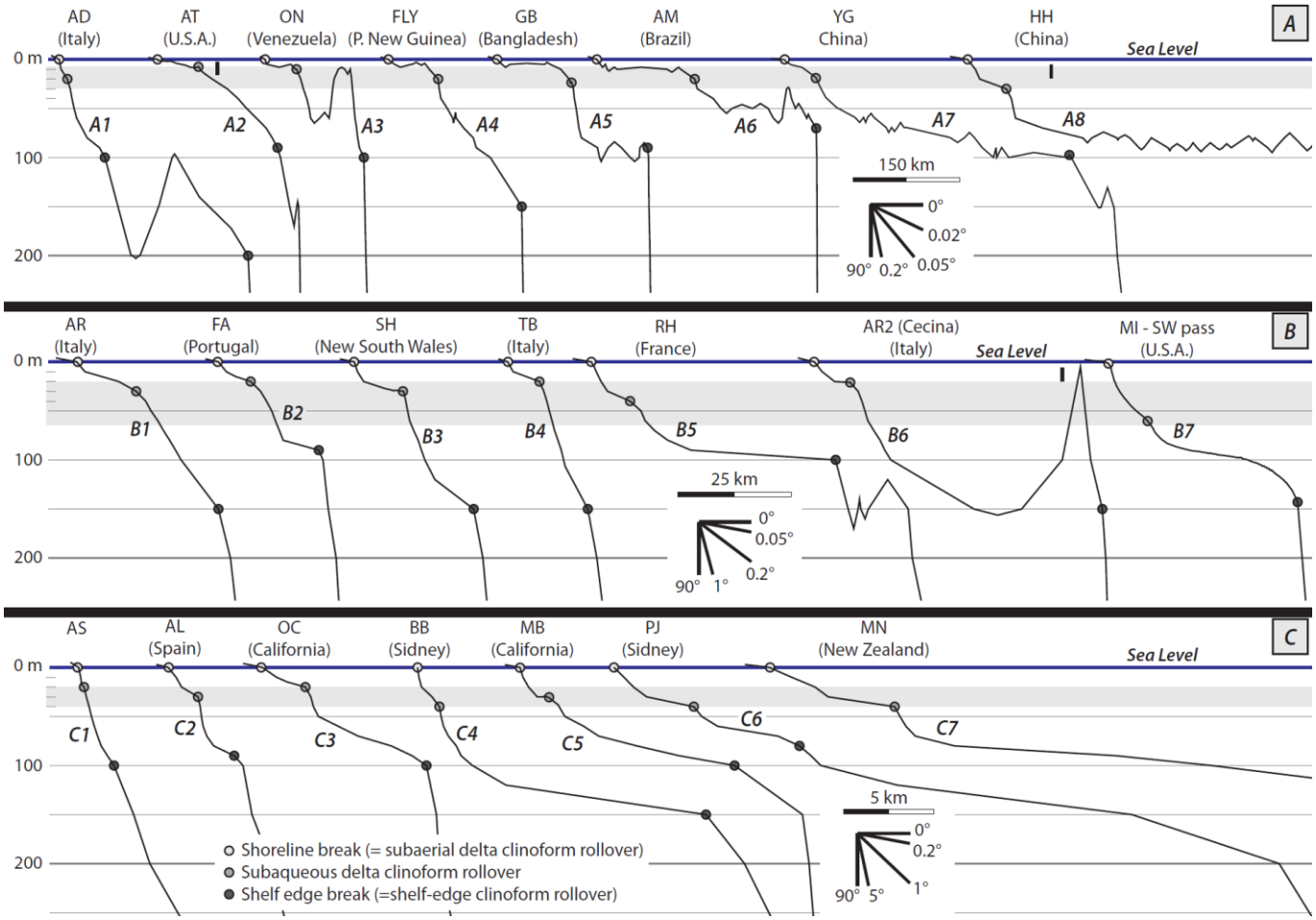

Figure 4.10. *Bathymetric profiles of typical present-day delta-scale subaqueous clinoforms and compound clinoforms, drawn by utilizing the Global Multi-Resolution Topography dataset of Ryan et al. (2009): (A) macro-scale systems (Fig. 4.7); (B) meso-scale systems (Fig. 4.8); and (C) micro-scale systems (Fig. 4.9).*

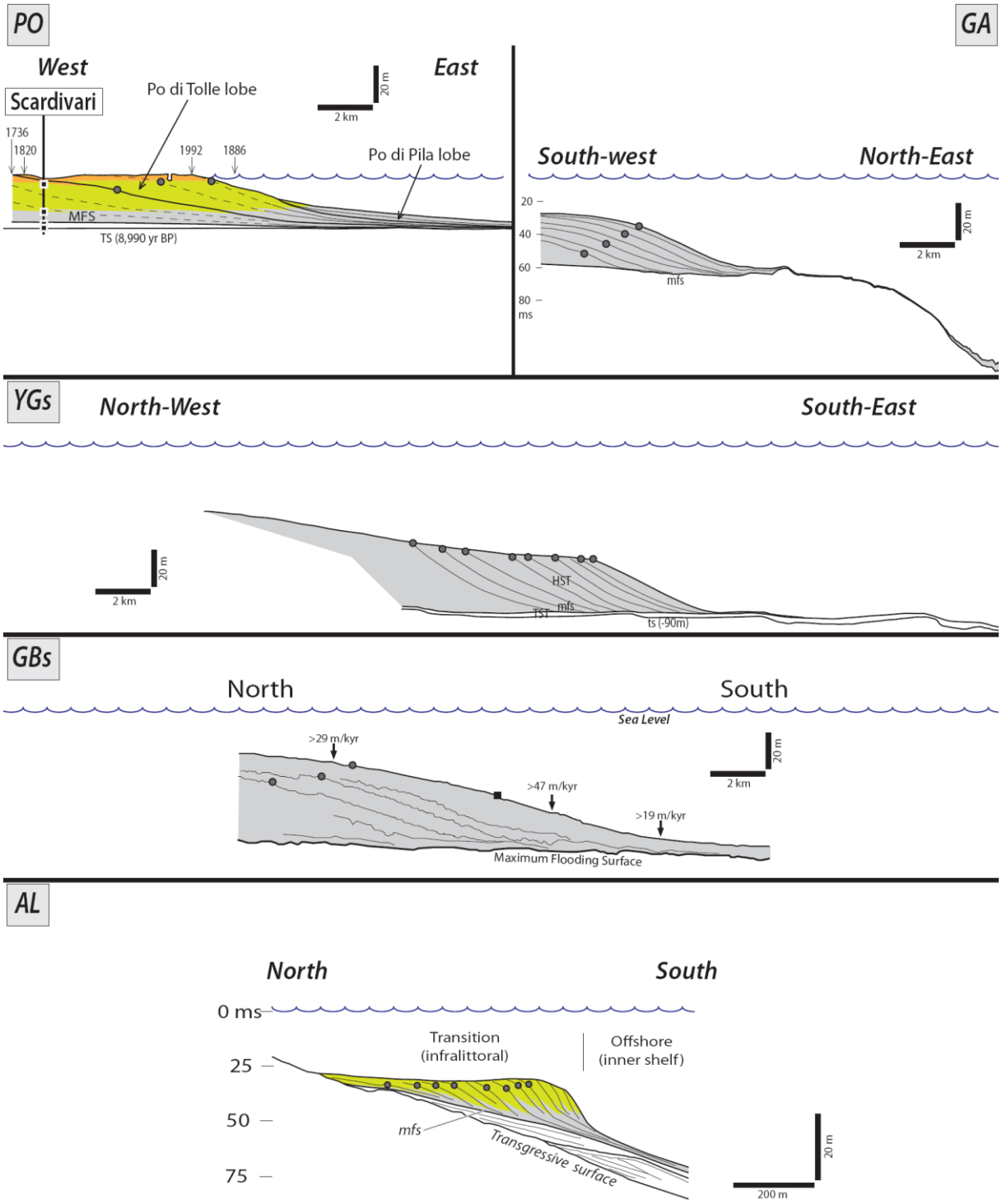

Figure 4.11. *Depositional-dip profiles across recent delta-scale subaqueous clinoforms: (AL) subaqueous clinoform off Cabo de Gata shoreline, southern Spain (after Hernández-Molina et al., 2000a); (PO) Po subaerial delta clinoform and linked (GA) Gargano subaqueous delta clinoform (after Correggiari et al., 2005; Cattaneo et al., 2003; 2007); (YGs) subaqueous clinoform off the Yangtze River delta (after Liu et al., 2007); (GBs) subaqueous clinoform off the Ganges-Brahmaputra River delta (after Palamenghi et al., 2011).*

4.4.1 Example 1: Po subaerial delta and Adriatic subaqueous delta clinoforms

Cattaneo et al. (2003, 2007) used high-resolution CHIRP sonar profiles and bathymetric data to constrain the architecture of Late Holocene muddy subaqueous clinoforms that are actively accreting on the western Adriatic shelf margin, offshore eastern Italy (Figs. 4.3, 4.7AD, 4.10A1, 4.11PO-GA). Biostratigraphic and chronostratigraphic data from cores were used to define a high-resolution chronology for the clinoform-bearing strata. The Adriatic subaqueous clinoform set is a laterally extensive (ca. 600 km), mud-rich belt that strikes parallel to the current Italian coastline, from the Po Delta in the north to the Gargano peninsula in the south. It is up to 35 m thick and clinoform foresets dip up to 0.5°. Adriatic shelf clinoforms started to form after the attainment of the Holocene sea-level highstand (6.5-5.5 ka), and are still prograding perpendicular to the north-to-south flowing Western Adriatic Coastal Current that drives shore-parallel advective sediment transport from the Po river and numerous other, smaller Adriatic rivers. The clinoform is compound in the north (Fig. 3B) and has a subaqueous clinoform topset-to-foreset rollover at a water depth of 8 m. In contrast, an isolated subaqueous clinoform is developed in the south (Fig. 3C) with a subaqueous clinoform topset-to-foreset rollover at a water depth of 30 m. Despite the absence of direct river supply in the southern portion of the clinoform set, the subaqueous delta accounts for up to 14% of the total volume (180 km^3) of the mud belt. Southward-flowing, bottom-hugging shelf currents play an important role in redistributing the sediment southwards and in limiting sedimentation in the bottomset region, by trapping most of the sediment on the inner shelf and forcing it along-shore rather than across-shelf. Lead isotope dates from several cores document a maximum sedimentation rate of up to 1.5 cm/y in the clinoform foreset, and discrete episodes of active clinothem outbuilding separated by periods of condensed sedimentation. The onset of the most recent subaqueous clinothem-building phase is coeval with the initiation of major progradation of the subaerial Po Delta at the beginning of the Little Ice Age, about 500 years ago (Cattaneo et al., 2003; Correggiari et al., 2005).

4.4.2 Example 2: Yangtze subaqueous delta clinoforms

Since the Holocene relative sea-level highstand at 6-7 ka BP, the Yangtze (Changjiang) River has delivered ca. 1.7 $x10^{12}$ t of sediment to the coastline and submarine shelf, forming a broad tide-dominated subaerial delta (Hori et

al., 2001) and an associated muddy subaqueous delta (Liu et al., 2006, 2007; Figs. 4.7YG, 4.10A7, 4.11YG). Interlaminated sand-mud couplets and bidirectional ripple cross-laminations in the sediments of the subaerial delta indicate a strong tidal influence (Hori et al., 2001). The subaqueous delta forms a silt-to-clay-rich, sigmoidal clinothem oriented parallel to the coastline. This stretches along-shelf from the river mouth for 800 km, and extends across-shelf for up to nearly 100 km (Liu et al., 2006, 2007). Holocene subaqueous-delta clinoforms downlap onto a sub-horizontal, post-glacial, sandy transgressive layer (Fig. 4.7YG), and form a mud wedge encompassing a total volume of 4.5×10^{11} m^3; this accounts for approximately half the current annual sediment discharge of the Yangtze (Liu et al., 2007). Subaqueous clinoform foresets are situated between the 20 and 30 m isobaths, corresponding to the main clinothem depocentre, which exhibits a maximum thickness of ca. 40 m. Bottomsets reach distances of up to 100 km offshore and terminate in water depths of 60-90 m (Liu et al., 2006, 2007). ^{14}C chronology indicates that average progradation rate of the subaerial delta since 5 ka BP was ca. 50 km/year, but after 2 ka BP it abruptly increased to ca. 80 km/year, possibly due to anthropogenic or climatic forcing; maximum sediment accumulation rate in the subaerial delta front has been ca. 3.5 m/kyr (Hori et al., 2001). ^{210}Pb data show that maximum sedimentation rates of 430 m/kyr occur in the portion of the subaqueous delta adjacent to the Yangtze subaqueous delta, and decrease both offshore and to the south (Liu et al., 2006, 2007). Mineralogical, geochemical and grain-size analyses suggest that subaqueous deposits have been fed by the alongshore Chinese Coastal Current, which has redistributed sediments sourced predominantly by the Yangtze River towards the south, with minor inputs from smaller local rivers (Liu et al., 2006). Interaction of strong tides, waves, upwelling and alongshore currents have created an oceanographic setting that has trapped most Yangtze-fed sediment on the inner shelf, forcing it to be transported alongshore rather than across-shelf. This formed a shelfal sediment wedge striking parallel to the shore and precluded sediment escape towards the deep-marine Okinawa Through (Liu et al., 2006).

4.4.3 Example 3: Ganges-Brahmaputra subaqueous delta clinoforms

The Ganges-Brahmaputra is the world's third largest river feeder in terms of sediment load (Kuehl et al., 1997). Kuehl et al. (1997), Michels et al. (1998) and Palamenghi et al. (2011) utilized seismic reflection profiles and piston and gravity cores in order to study the Ganges-Brahmaputra sandy-silty subaqueous deltas, and estimated sediment accumulation rates using ^{210}Pb and ^{137}Cs gamma spectrometry. The sigmoidal clinoform formed by the subaqueous delta comprises a very gently-dipping topset and bottomset (0.02-0.04°), and a slightly steeper foreset (ca. 0.19°) (Figs. 4.7GB, 4.10A5, 4.11GB). The topset is located in <20 m water depth, whereas the bottomset is located in ca. 80 m water depth, where it overlies an Upper Pleistocene transgressive surface (Kuehl

et al., 1997). Below this depth, no Holocene sediment is preserved (Michels et al., 1998). About 20% of the total sediment load of the Ganges-Brahamaputra river mouth is deposited on the foreset of the subaqueous clinoform, which is therefore characterised by higher sediment accumulation rates (ca. 50-100 m/kyr) than the bottomset (ca. 30 m/kyr). These interpretations are also supported by seismic-reflection profiles showing clinoform reflection surfaces progressively diverging from the topset to the foreset and converging again towards the bottomset (Kuehl et al., 1997). The clinoform foreset is formed by graded sandy-silty laminae interbedded with clay laminae. The coarsest-grained layers are presumably deposited by sediment-laden underflows generated during tropical storms, with up to 8 m thick mass flows created in the subaqueous delta front area by episodic earthquakes or storms (Michels et al., 1998). These last deposits are imaged in seismic reflection profiles as transparent units (Palamenghi et al., 2011). The subaqueous clinoform is actively prograding every year by ca. 12-17 m across the Bengal Shelf. Sediment becomes increasingly finer-grained offshore and westwards, which in combination with analyses of seabed palaeocurrent indicators, suggests that subaqueous clinoforms have been fed by westward-flowing cyclonic currents that transport sediment fed by the Ganges-Brahamaputra river mouth alongshore and offshore (Kuehl et al., 1997). A large canyon, known as 'Swatch of No Ground', deeply dissects the shelf and the subaqueous delta front (Fig. 4.7GB). This canyon captures most of the sediment load carried by the westward-flowing cyclonic currents, allowing shelf bypass of >35% of the fluviatile sediment load towards the deep-marine Bengal Fan. This oceanographic configuration has caused off-shelf sediment transport and turbidite deposition to the slope and basin-floor during the Holocene highstand, together with growth faults, slumping and high Holocene sedimentation rate (ca. 500 m/kyr) near the canyon head (Kuehl et al., 1986, 1997; Weber et al., 1997; Michels et al., 1998). Palamenghi et al (2011) suggest that sediment deposition towards the western part of the subaqueous delta has increased in the last few centuries, with subsequent higher sediment export to the deep-water fan through the 'Swatch of No Ground' canyon.

4.4.4 Example 4: Southern Iberia subaqueous clinoforms

Sand-prone subaqueous clinoforms dipping sub-parallel to the present-day seabed and striking parallel to the modern shoreline are situated south of the promontory of Capo de Gata (southern Spain, Mediterranean Iberia) and in the proximity of Faro (Portugal, Atlantic Iberia) (Figs. 4.9AL, 4.10C2, 4.11AL). These sandbodies have been described by Hernández-Molina et al. (2000a) and Lobo et al. (2005) through the use of boomer seismic profiles. The clinoform wedge started to prograde during the Late Holocene sea-level highstand (from ca. 6.5 ka) and it downlaps older transgressive units. The seafloor over which this prograding wedge developed dips relatively steeply offshore (up to 0.50°) and the clinoform foresets within it become progressively steeper seawards. Mean

grain sizes of medium-grained and fine-grained sands were described from surface grab samples located respectively 1 km seaward and 1 km landward of the clinoform topset-to-foreset rollover (Hernández-Molina et al., 2000a). The clinoform set is interpreted to have been generated by storm-related downwelling currents, with associated seawards sediment transport and deposition below fairweather wave base (Hernández-Molina et al., 2000a). The subaqueous clinoforms offshore southern Spain consist of a series on *en-échelon* bodies in plan-view (Fernández-Salas et al., 2009), suggesting that there was also a significant component of alongshore sediment transport.

4.4.5 Comparison and general observations

Map views confirm that all of the identified delta-scale subaqueous clinoforms strike parallel to the adjacent coastline, particularly in systems dominated by waves and currents (Figs. 4.7-4.9; Table 4.2). On subaqueous shelves where tides are an important component of the overall hydrodynamic regime (e.g., Amazon and Orinoco systems), the plan-view geometry of delta-scale subaqueous clinoform bodies is less regular (Figs. 4.7AM, ON).

Cross-sections oriented parallel to depositional dip (Fig. 4.10) show overall subaqueous clinoform heights of 10-100 m, whilst the dip extent of the subaqueous clinoforms is extremely variable (1-100 km). The water depth of the topset-to-foreset rollover point is relatively shallow in macro-scale, muddy subaqueous systems linked to major subaerial deltas (ca. 10-30 m depth; Fig. 4.10A), but relatively deep in meso- and micro-scale, sandier systems (ca. 20-60 m water depth; Fig. 4.10B-C). A likely explanation for this is that the position of the topset-to-foreset rollover point directly reflects the maximum entrainment depth of the upper 10-percentile wave-current traction field (cf., Pirmez et al., 1998; Hernández- Molina et al., 2000a; Cattaneo et al., 2003, 2007; Mitchell, 2012; Mitchell et al., 2012), and progressively stronger mean waves are required to transport increasingly coarser-grained sediments. In the transition from macro-scale, muddy deltaic systems towards meso- and micro-scale, sandier deltaic and shoreline systems, the associated subaqueous clinoforms and shelves become steeper and narrower (Fig. 4.10).

The average foreset slopes of both subaerial and subaqueous components of recent delta-scale compound clinoforms are ≤0.76° in muddy systems and ≥0.39° in sandy systems, with minimum and maximum values of 0.03° and 6° respectively (Fig. 4.13A). Sand-prone systems are also characterised by distinctly higher ratios between the gradients of subaerial and subaqueous clinoform foresets (ranging from 53-445%) than those for muddy compound clinoform systems (39-246%). As shown in Figure 4.13B, the height of the subaerial clinoform

foreset is often more than 20% greater than its subaqueous counterpart in sand-prone compound clinoforms. Values of this ratio in muddy compound clinoforms are generally less than 20% (Fig. 4.13B). The topset-to-foreset rollovers of sand-prone and muddy, delta-scale subaqueous clinoforms occur at distances from the present-day shoreline of 0.6-7.2 km and 7.5-125 km, respectively (Fig. 4.13C). Furthermore, mud-prone, subaqueous delta clinoforms are situated on gently-sloping (0.01-0.38°), wide (23-376 km) shelves, whereas sand-prone, subaqueous clinoforms are situated on steep (≥0.26°), narrow (5-32 km) shelves (Fig. 4.13B-C; Table 4.3).

Modern, delta-scale, sand-prone subaqueous clinoforms tend to occur on steep, wave-dominated, inner shelves where mean wave heights and periods are typically 1-2.5 m and 6-11 s respectively, with a maximum of 2-4.5 m and 8-13 s (Mitchell et al., 2012), and where a relatively high sediment supply is provided by longshore and/or storm-related downwelling currents (Hernández-Molina et al., 2000a; Xing & Davies, 2002). Numerical modelling suggests that strong seafloor agitation produced by the combined action of large waves and alongshore and downwelling bottom currents during the rising stage of storms result in net-seaward export of shoreface-derived sand (Mitchell, 2012; Mitchell et al., 2012). The availability of large volumes of reworked sand permits active subtidal accretion of sand-rich clinoforms by deposition along their foresets. In particular, upper-10 percentile waves are able to entrain sand-grade sediment at the topset-to-foreset rollover depth, and therefore clinoform rollover depth primarily reflects the upper-10 percentile wave base depth. Strong surface winds generate alongshore and seaward-directed (i.e., downwelling) advective bottom currents that may affect sites deeper than 60 m at distances of up to 15 km away from the shoreline. Currents and waves interact in a nonlinear pattern, and comparatively modest increases in current velocities result in much higher combined stresses at the seafloor (Mitchell, 2012; Mitchell et al., 2012). Furthermore, Friedrichs & Wright (2004) described how the hyperpycnal outflow of certain rivers may be modulated by wave action. This process may potentially aid bypass of riverine sediment across the inner shelf and the generation of delta-scale sand-prone subaqueous clinoforms seaward of the mouth of a river (e.g., Monterey Bay clinoforms, off the mouth of the River Salinas; Mitchell et al., 2012). This type of subaqueous clinoform is composed of sands that are more poorly-sorted than those derived from adjacent shorefaces (e.g., southern Iberia subaqueous clinoforms; Hernández-Molina et al., 2000a).

4.5 ANCIENT DELTA-SCALE SUBAQUEOUS CLINOFORMS

Compared to their modern equivalents, there are relatively few documented examples of ancient delta-scale subaqueous clinoforms. Each of these examples is summarised below, with the aid of cross-sections showing the clinoforms and their associated stratigraphic architecture (Figure 4.12).

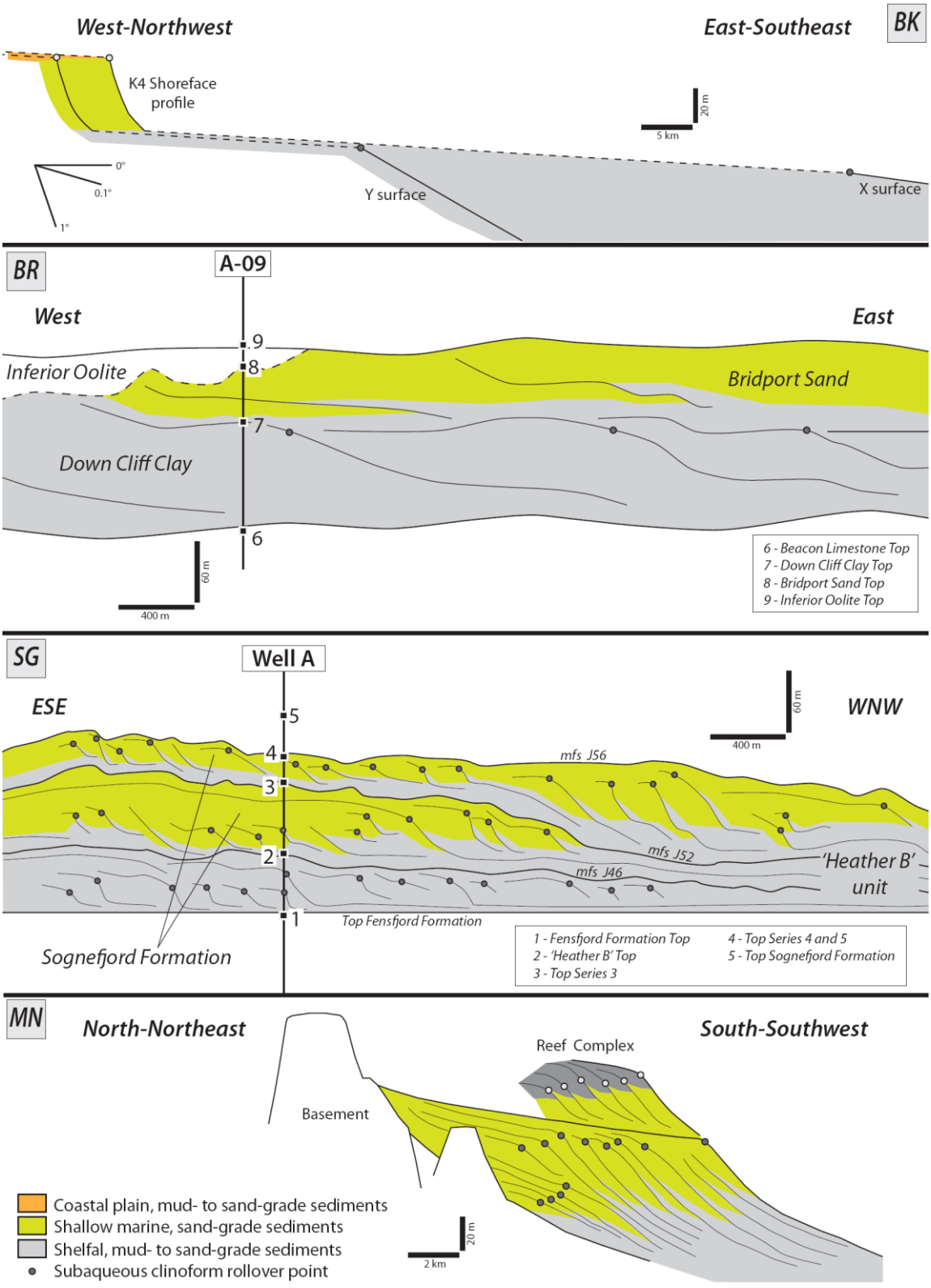

Figure 4.12. *Depositional-dip profiles across ancient delta-scale subaqueous clinoforms: (SG) Upper Jurassic Sognefjord Formation subaqueous delta clinoforms, North Sea Basin, offshore Norway (after Patruno et al., 2013b); (BR) Lower Jurassic Bridport Sand Formation subaerial delta clinoforms and linked Down Cliff Clay subaqueous delta clinoforms, Wessex Basin, onshore UK (after Morris et al., 2006; Hampson et al., in review); (MN) Upper Miocene calcareous grainstones, Menorcan platform (Spain), Mediterranean Basin (after Pomar et al., 2002); (BK) Upper Cretaceous Blackhawk Formation subaerial delta*

clinoforms and linked Mancos Shale subaqueous delta clinoforms, Western Interior Basin, onshore USA (after Hampson, 2010).

4.5.1 Example 1: Blackhawk Formation subaerial delta and Mancos Shale subaqueous delta clinoforms

Hampson (2010) used large outcrop transects (ca. 200-300 km wide) and a large well dataset (ca. 2,800 wells) to reconstruct the sedimentology and stratigraphic architecture of ca. 60,000 km^2 of the Santonian-Campanian, sub-tropical shelf of the Western Interior Seaway (Utah, USA) within a high-resolution (ca. 0.1 to 0.5 Myr) sequence stratigraphic framework. A wave-dominated delta with a compound clinoform morphology was interpreted for the Lower Campanian 'K4' shoreface-shelf tongue of the Blackhawk Formation and coeval Mancos Shale (Fig. 4.12BK). This deltaic shelf is characterised by a relatively high sediment accumulation rate (ca. 270 m/Myr) and by a concave-landward, net-regressive shoreline trajectory (>0.1°). The compound clinoform interpretation was suggested by Hampson (2010) because the 'X', 'Y' and 'Z' middle shelf gravity flow intervals of the Prairie Canyon Member, Mancos Shale dip palaeoseaward of 0.1-0.2° relative to the underlying flooding surfaces, and correlate with the 'K4' shoreface-shelf 'subaerial delta' clinoform (Fig. 4.12BK). The wave-dominated shoreline clinoform is sandstone-prone, and is separated by a 2 to 22 km wide belt of nearshore, storm-reworked sandstones from a gently-dipping subaqueous clinoform on the middle shelf. The subaqueous clinoforms in this stratigraphic interval comprise a muddy topset and a foreset composed of gravity-flow siltstones and sandstones, and is part of a >250 km wide, offshore mudstone belt. Decompacted subaqueous clinoforms were inferred to have been low gradient (ca. 0.2-0.4°), and have a topset depth that implies a storm wave-base at ca. 50-80 m water depth. These geomorphological and facies characteristics are comparable to modern-day subaqueous deltas. Hampson (2010) noted that, in the case of the delta-scale compound clinoform system formed by the sandy 'K4' shoreline clinoforms and by the 'X' to 'Y' subaqueous clinoforms, shoreline progradation distance (9 km) was approximately three times smaller than the coeval subaqueous delta progradation (ca. 20-30 km), thus resulting in a progressive lengthening of the subaqueous clinoform topset during this particular time interval.

4.5.2 Example 2: Bridport Sand Formation subaerial delta and Down Cliff Clay Member subaqueous delta clinoforms

The Lower Jurassic Bridport Sand Formation and coeval Down Cliff Clay Member were deposited in ca. 2 Myr in the Wessex Basin, southern UK, in a linked shoreface-to-shelf depositional system. The Bridport Sand Formation is dominated by bioturbated storm-event beds with calcite-cemented bioclastic lag horizons, which were deposited in an offshore transition to lower shoreface environment. These strata form 10-40 m thick, upward-shallowing units that overlie laterally-extensive, mudstone-rich horizons (Morris et al., 2006). The Down Cliff Clay Member comprises calcareous bioturbated mudstones that record deposition in an offshore transition to offshore environment (Morris et al., 2006). 2D and 3D seismic data calibrated with wells from the onshore Wytch Farm Field indicate that each upward-shallowing, shoreface-to-shelf unit of the Bridport Sand Formation corresponds to a steeply-dipping (2-3°), delta-scale, progradational clinoform set that downlaps onto the topset of a similar progradational clinoform set in the Down Cliff Clay Member (Morris et al., 2006; Hampson et al., in review; Fig. 4.12BR). Each clinoform set represents a duration of ca. 0.5 Myr, downlaps onto a basal maximum flooding surface and is likely arranged into a compound clinoform system (Hampson et al., in review). According to this interpretation, these systems comprise a subaerial delta clinoform composed by shoreface sediments (Bridport Sand Formation), grading seawards into an outer finer-grained, middle shelf clinoform (Down Cliff Clay unit) that displays a nearly linear plan-view geometry.

4.5.3 Example 3: Sognefjord Formation subaqueous delta clinoforms

The Upper Jurassic Sognefjord Formation forms a 100-300 m thick, coarse-grained, regressive-transgressive clastic wedge of ca. 6 Myr duration, developed on the eastern flank of the Northern North Sea rift system, offshore Norway (Vollset & Doré, 1984; Steel, 1993; Stewart et al., 1995; Fraser et al., 2002). Offshore shales of the Heather Formation occur above and below this sandstone-rich wedge and they represent periods of tectonically-driven transgression (Steel, 1993; Ravnås et al., 2000; Fraser et al., 2002). The internal stratigraphic architecture of the Sognefjord Formation is dominated by the progradational-to-aggradational stacking of sandstone-prone clinoform sets, which are separated by basin-wide flooding surfaces (Chapter 2; Fig. 4.12SG). Clinoform sets in the lower part of the Sognefjord Formation are linear in map view, strike parallel to the rift-margin fault (NNE-SSW), and are laterally extensive for at least 30 km along depositional strike (Dreyer et al., 2005; Chapter 2). Within each clinoform set, there is a progressive basinward increase in clinoform height (from 10-30 m to 60-70 m), foreset slope angle (from 1-6° to 16°) and along-strike length (from 1 km to 6 km), and a basinward decrease in clinoform dip extent (from 3000 m to 200 m) (Chapter 2). Clinoform foresets also exhibit distinct facies changes down depositional dip, becoming coarser-grained and more dominated by current-driven tractional structures in a basinward direction (Dreyer et al., 2005; Chapter 2).

The Sognefjord Formation was deposited by a deltaic system sourced from the Norwegian mainland that prograded westwards across a stable rift-margin platform for tens of kilometres, through incremental deposition of west-dipping clinothems (Stewart et al., 1995; Dreyer et al., 2005; Chapter 2). The thicknesses of clinoform sets (10-60 m), clinoform foreset slope angle (1°-16°) and inferred clinoform progradation rates (15-500 km/Myr) are compatible with those of modern coarse-grained deltas with small catchment areas (Dreyer et al., 2005; Chapter 2). Based on analysis of sedimentological facies in cores and stratigraphic relationships in 3D seismic reflection data from the Troll Field, Chapter 2) interpret that the clinoforms were deposited in a fully subaqueous delta. This interpretation is based on the following evidence: (a) absence of subaerial facies in cores; (b) presence of well-developed topsets in most the clinoforms observed; and (c) laterally-extensive, plan-view geometry orientated parallel to the shelf-edge break and to the alongshore currents that are inferred to have fed them.

4.5.4 Example 4: Calcarenite di Gravina subaqueous clinoforms

The progradational units in the lower member of the Pliocene-Pleistocene Calcarenite di Gravina unit are exposed in outcrops near the city of Matera (southern Italy), and comprise wave-dominated shoreline to offshore calcirudite and calcarenite facies (Pomar & Tropeano, 2001). These deposits form laterally extensive clinothems that strike parallel to the palaeo-shoreline and prograded seawards below wave base. High-angle (up to 35°) foresets are composed of offshore-transition sediments that downlap onto fine-grained offshore deposits. These sandbodies are interpreted by Pomar & Tropeano (2001) to represent avalanches of shoreface sand- to gravel-grade sediments, transported along shoreface-shelf depositional slopes by wind-driven storm waves and currents and subsequently emplaced in a subaqueous shelfal setting below wave base. Progradational clinoform sets correspond to upward-shallowing parasequences formed during relative sea-level stillstands or during falling relative sea-level, and are underlain by flooding surfaces and/or transgressive lag deposits. Evidence of subaerial exposure is absent in each offshore-transition-dominated delta-scale subaqueous clinothem, although a subaerial erosional surface may have formed above the beachface deposits of the coeval, thin, subaerial delta clinothems during forced regression. The overall parasequence stacking pattern is retrogradational, with clinoforms onlapping onto a Cretaceous limestone substrate, reflecting tectonically forced transgression (cf., Pomar & Tropeano, 2001).

4.5.5 Example 5: Calcareous Grainstone subaqueous clinoforms, Miocene, Menorca

Pomar et al (2002) analysed the facies belts and depositional profile of the distally-steepened, Tortonian carbonate ramp outcropping along the sea cliffs of Menorca (Balearic Islands, Spain). Palaeoshoreline-detached, cross-bedded, coarse-grained grainstones, were deposited below wave base on the Lower Tortonian carbonate ramp (Fig. 4.12MN). Fan deltas and beach deposits at the palaeoshoreline (subaerial delta) pass down-slope into 5 km-wide, gently-dipping topset strata in the inner-middle ramp, then into 12-20° foreset beds on the ramp slope and, eventually, into sub-horizontal bottomset strata in the outer ramp (subaqueous clinoform). The fan deltas and beaches at the palaeoshoreline contain continental conglomerates and red sandstones, structureless conglomerates, pebbly sandstones and beach face deposits. The subaqueous topset area is composed of bioturbated dolo-packstone; the subaqueous foreset strata contain dolo-grainstone/rudstone and, lower on the slope, are dominated by turbiditic and debris flow deposits and by sediment reworking by shore-parallel bottom currents. The bottomset basinal area contains mostly fine-grained dolo-packstone to dolo-wackestone, interbedded with distal turbidites and alongshore-transported grainstones at the toe of the slope. Coarse-grained carbonates are widespread on this ancient shallow-marine ramp, which are not subject to the usual decrease in grain-size with water depth along the ramp depositional profile (Fig. 4.12MN). Coarse-grained deposits occur: (1) on the beach/palaeoshoreline; (2) at 40-70 m water depth on the subaqueous topset, where medium-scale coarse-grained grainstone bedforms are oriented parallel to the palaeoshoreline; (3) on the subaqueous foreset area, as *in-situ* rhodoliths and small-scale subaqueous dunes migrating parallel to the slope; (4) at the transition between the subaqueous foreset and bottomset, as rudstone-grainstone slide/slump scar infills; and (5) at ca. 150 m of estimated water depth at the toe of the bottomset, as coarse skeletal grainstone bedforms migrating parallel to the clinoform strike. Sediments in settings deeper than the inner ramp were continuously reworked by ubiquitous, westward-flowing, shore-parallel bottom currents, and by likely upwelling currents. Pomar et al. (2002) indicate that, without three-dimensional facies and bathymetric reconstructions, a similar succession may be interpreted as a shoal-rimmed carbonate shelf.

Type	Location	Age	Abbrev.	Reference
Continental margin clinoforms	Western Florida escarpment + continental margin (Blake escarpment) (passive margin)	Units I/II = Miocene-Recent; from Top Tithonian (Blake Escarpment)	FL	Mullins et al 1988, Profile 40-42; Schlee et al. 1979, Fig.13, Profile FC8
	Antarctic pacific margin (passive margin)	Cenozoic and Pliocene	AN	Adams & Schlager 2000, Figs. 4A, 8A
	Western Great Bahama Bank (passive margin)	Cenozoic	GBH	Adams & Schlager 2000, Fig. 6C
	Prydz Bay, Antarctica (passive margin)	Unit PS1 = Post-Middle Miocene	PB	Adams & Schlager 2000, Fig. 6B
	SW Africa (passive margin)	Post-surface D (Upper Paleocene)	AF	Adams &Schlager, 2000, Fig. 7C
	Baffin Bay, West Greenland (passive margin)	Cenozoic	BAF	Adams &Schlager 2000, Fig. 7B
	Georges Bank Basin, U.S.A. (passive margin)	Cenozoic	GBB	Adams &Schlager 2000, Fig. 7A
	Scotian Slope, Canada (passive margin)	Cenozoic	SC	Adams &Schlager 2000, Fig. 4B
Shelf-edge clinoforms	Backstripped New Jersey (passive margin)	Oligocene-Miocene	NJ	Steckler et al. 1999, 7 clinofoms labelled: m2.3, m 2.5, m3, m4, m5, m5.4, m6
	Shelf edge off Guadiana River (active margin?)	Pleistocene	GS	Hernandez-Molina et al. 2000b, Fig. 2
	SE south island, New Zealand (active margin)	Cenozoic, Post-'reflector 4'	NZ	Adams &Schlager, Fig. 6A
	Florida Hatteras slope (passive margin)	Post-Top Tithonian	HT	Schlee et al. 1979, Profile FC8, Fig.13
	Carbonate shelf edge Australia (passive margin)	Upper Miocene arrow reflection	AUS	Adams &Schlager, Fig. 8B, Line-45
Mud-rich subaqueous delta clinoforms	Amazon Delta (passive margin)	Holocene-Recent	AMs	Nittrouer et al. 1986, Figs. 9, 13, Profiles F. G, M; Nittrouer et al. 1996, Figs. 9a, 9b
	Ganges-Brahmaputra (active margin)	Holocene-Recent	GBs	Michels et al. 1998, Fig. 4, Profiles 1, 2, 3; Palamenghi et al. 2011, Figs. 4-5
	Yangtze Delta (intracratonic seaway)	Holocene-Recent	YGs	Liu et al 2007, Profiles 1-2, 4-6
	Adriatic and Gargano clinoforms (active margin)	Holocene-Recent; post 1500 AD; from 1886 to 1959	AD and GA	Cattaneo et al. 2003, 2004, Figs. 6, 8, Profiles A-C, YD5-8, AMC167-175; Cattaneo et al., 2007, Fig.2, Profiles A-F; Friedrichs & Scully 2007, Fig.8a
	Gulf of Papua, New Guinea (active margin)	Holocene-Recent	FLYs	Walsh et al., 2004, Profile I, G, F, D
	Atchafalaya subaqueous delta (passive margin)	Holocene-Recent	AT	Neill & Allison, 2005, lines A, B, C, D
	Yellow River Subaqueous Delta (known as Shandong Delta) (intracratonic seaway)	Holocene-Recent	HHs	Liu et al. 2004, Figs. 8, 9, 10, 11, 13; Yang & Liu, 2007, Figs. 2A, 2B, 2D
	Tiber subaqueous delta (rift basin)	Holocene-Recent; Post 422 BP	TBs	Amorosi & Milli, 2001 (subaqueous delta), Fig.3
	Rhone (active margin / rift basin)	Pleistocene-Holocene	RHs	Tesson et al. 2000, clinoforms around IUc', RPUd, dIUc' surfaces in Figs. 13, 15; clinoforms in unit from 5'' to 6 in Fig. 10; post-glacial inner clinoforms in Profile F of Fig.5
subaqueous delta	Almeria prograding clastic wedge (active margin)	Holocene-Recent	AL	Hernandez-Molina et al 2000a, Fig.3; Mitchell et al 2012, Fig. 3 + Table 1
	Manawatu, New Zealand (active margin)	Holocene-Recent	MN	Dunbar & Barrett 2005, Fig. 2, Lines 27-29;

				Mitchell et al 2012, Fig. 3 + Table 1
	Port Jackson (Sidney) subaqueous sandbodies, SE Australia (intracratonic seaway)	Late Holocene-Recent	PJ	Field & Roy 1984, Fig.1, Profiles 11, 18, 23, 29
	Bate Bay-Malabar subaqueous sandbodies, SE Australia (intracratonic seaway)	Late Holocene-Recent	BB	Field & Roy 1984, Fig.2, Profiles D, K, N, R
	Faro and Tavira depocentre (active margin)	Late Holocene-Recent	FA	Lobo et al 2005, Figs. 5, 8; Hernandez-Molina et al 2000a, Fig.4; Mitchell et al 2012, Fig. 3 + Table 1 (10 ms = 7.5 m)
	Monterey Bay, La Jolla, California (active margin)	Holocene	MB	Le Dantec et al. 2010; Chin et al. 1988; Fig. 10
	Oceanside, San Diego, California (active margin)	Holocene-Recent	OC	Mitchell et al 2012, Fig. 3 + Table 1
	Ascension Island (mid-Atlantic ridge)	Holocene?	AS	Mitchell et al 2012, Fig. 3
	Menorca (Spain) carbonatic clinoforms (active margin)	Tortonian-age outcrops	MN	Pomar et al., 2002
	Matera, southern Italy (active margin)	Plio-Pleistocene-age outcrops	MT	Pomar & Tropeano, 2001
Subaerial delta / shoreline clinoforms	Mississippi subaerial and shelf-edge delta (passive margin)	Post-1550 profiles of years 1838, 1874, 1921, 1947	MI	Kenyon & Turcotte1985
	Amazon subaerial delta (passive margin)	Holocene-Recent	AM	Nittrouer et a 96, subaerial delta = Rio Fleshal sandflat (Fig.4)
	Yangtze subaerial delta (intracratonic seaways)	Late Holocene (3.31 Ka) - Recent	YG	Hori et al., 2001, present (subaerial delta)
	Po Delta (active margin)	Post-1500 AD profiles, until year 2002	PO	Correggiari et al 2005, Figs. 3, 4, 5, 8, profiles A-B, C-D-E; Cattaneo et al., 2003, Fig.6, profile A-C; Friedrichs & Scully 2007, Figs. 8a, 8b
	Mekong Subaerial Delta (intracratonic seaways)	Post 5 Ka BP to Recent	ME	Ta et al., 2002, Fig.2, profiles X-Y, A-B
	Tiber subaerial delta (rift basin)	Holocene-Recent; Post 422 BP	TB	Amorosi & Milli 2001 (subaerial delta), Fig.3
	Long beach and Willapa Bay spit (active margin)	Recent (80 years)	LB	Jol et al., 2002, Fig.5C
Ancient subaqueous clinoforms	Blackhawk Fm. - Mancos shale, K4 shoreface and X-Y associated subaqueous clinoforms	F100 to F150 surfaces – Lower Campanian-age	BH	Hampson, 2010, Fig. 13
	Sognefjord Formation (rift basin)	Upper Callovian to Oxfordian	SG	Patruno et al. 2013a,b; Figs. 1-5
	Bridport Sand (subaerial clinoform?) and Down Cliff Clay (subaqueous clinoform) (rift basin)	Toarcian-?Aalenian-age	BRD	Morris et al. 2006, Fig. 14

Table 4.1. *Clinoforms and clinoform sets analysed using direct measurements from published cross-sections, thickness and facies maps. Abbreviations are used in Figures 4.6, 4.11-4.13.*

Type	Location	Age	Abbrev.	Average quantitative parameters														
				Subaerial delta type	Shelf-edge *wd* (m)	Shelf-edge *Fs* (°)	shelf-edge *Ts* (°)	% Sand in delta front	Subaerial delta *Fh*(m)	Subaerial delta *Ts* (°)	Subaerial delta *Fs* (°)	Duration (Myr)	*Sv* (m/Myr)	*P* (km/Myr)	*F* (km^2/Myr)	*R* (adim.)	Shoreline *CT* (°)
				a	Mean *b + c*	*c*	*c*	*b; d*	After *d*	*a*	*a; e; d*	After *b; d*	After *b; c; d*	After *b; d; e*	After *b; d*	After *d*	*d*
Present-day shelf-edge clinoforms	Limpopo	Holocene	LM		87	1.04	0.27										
	Magdalena	Holocene	MG		99.6	1.89	0.36										
	Parana	Holocene	PA		98.3	2.75	0.07										
	Pearl (Zhujiang)	Holocene	ZH		189	0.59	0.03										
	Santa	Holocene	SN		173	1.05	0.18										
	Yangtze	Holocene	YG	MS it	180	0.78	0.01										
	Zambese	Holocene	ZA		92.3	1.55	0.10										
Present-day subaerial delta/shoreline clinoforms and associated shelf-edge clinoforms	Amazon	Recent	AM	Msti	94	2.63	0.02	16		0.001	0.315	$1.16{\cdot}10^{-2}$	$8.13{\cdot}10^{3}$	$2.77{\cdot}10^{4}$	$1.19{\cdot}10^{3}$	$3.07{\cdot}10^{-4}$	
	Copper	Recent	CP	FS wt	193	2.58	0.13	98		0.034	0.401	$8.52{\cdot}10^{-3}$	$2.27{\cdot}10^{4}$	$9.98{\cdot}10^{3}$	4.99E+02	$4.54{\cdot}10^{-3}$	
	Danube	Recent	DN		107	2.30	0.16					$1.08{\cdot}10^{-2}$	$9.94{\cdot}10^{3}$	$1.04{\cdot}10^{4}$	$1.56{\cdot}10^{2}$	$1.91{\cdot}10^{-3}$	
	Ganges-Brahmaputra	Recent	GB	FS t	150	1.42	0.09	45		0.006	0.010	$4\ 10^{-2}$	$4.\cdot10^{3}$	$4.64{\cdot}10^{3}$	$4.20{\cdot}10^{2}$	$1.05{\cdot}10^{-3}$	
	Indus	Recent	IN		126	2.156	0.07	2				$1.55{\cdot}10^{-2}$	$8.20{\cdot}10^{3}$	$7.44{\cdot}10^{3}$	$2.97{\cdot}10^{2}$	$1.38{\cdot}10^{-3}$	
	Irrawady (and Salween)	Recent	IW	MS m	146	1.21	0.32			0.003	0.034	$3.11{\cdot}10^{-2}$	$4.70{\cdot}10^{3}$	$5.94{\cdot}10^{3}$	$2.88{\cdot}10^{2}$	$9.79{\cdot}10^{-4}$	
	Krishna (and Godavari)	Recent	KR		95.7	3.79	0.22	42				$8.70{\cdot}10^{-3}$	$1.10{\cdot}10^{4}$	$5.52{\cdot}10^{3}$	$1.10{\cdot}10^{2}$	$3.99{\cdot}10^{-3}$	
	Mackenzie* (McKenzie)	Recent	MK	FS i	112	1.02	0.03	5		0.003	0.017	$1.16\ 10^{-1}$	$9.64{\cdot}10^{2}$	$1.72{\cdot}10^{3}$	$1.03{\cdot}10^{2}$	$9.35{\cdot}10^{-4}$	
	Mississippi	Recent	MI	MS i	127	0.75	0.05	2		0.001	0.516	$1.31{\cdot}10^{-2}$	$9.73{\cdot}10^{3}$	$8.79{\cdot}10^{3}$	$5.00{\cdot}10^{2}$	$1.26{\cdot}10^{-3}$	
	Niger	Recent	NG	FS m	95.5	1.44	0.11				0.115						
	Nile	Recent	NL	FS wi	152	1.97	0.34	20		0.005	0.015	$2.80{\cdot}10^{-2}$	$5.44{\cdot}10^{3}$	$1.79{\cdot}10^{3}$	$1.34{\cdot}10^{2}$	$5.08{\cdot}10^{-3}$	
	Orange	Recent	OR		174	0.41	0.17					$3.35{\cdot}10^{-2}$	$5.19{\cdot}10^{3}$	$5.37{\cdot}10^{3}$	$2.95{\cdot}10^{2}$	$1.93{\cdot}10^{-3}$	
	Orinoco*	Recent	ON	MS m	83.6	1.48	0.04	7		0.004	0.026	$2.33{\cdot}10^{-2}$	$3.59{\cdot}10^{3}$	$4.50{\cdot}10^{3}$	$1.35{\cdot}10^{2}$	$1.20{\cdot}10^{-3}$	

	Rhone	Recent	RH	FS wi	142	3.18	0.43				0.195	1.02 10^{-2}	1.40·1 0^{4}	4.72·1 0^{3}	1.53·1 0^{2}	5.93·1 0^{-3}	
	Zaire (Congo)*	Recent	CO		140	1.14	0.10	2				4.18 10^{-2}	3.35·1 0^{3}	1.67·1 0^{3}	8.37E +01	4.00E-03	
Present-day subaerial delta/shoreline clinoforms	Alta	Recent	AA	GS i						0.086	20.06						
	Bella Coola	Recent	BC	GS iw						0.127	9.589						
	Brazos	Recent	BR		100			10				3.16 ·10^{-2}	3.16·1 0^{3}	4.43·1 0^{3}	1.11·1 0^{2}	1.43·1 0^{-3}	
	Burdekin	Recent	BU	FS/GS m													
	Chachaguala	Recent	CG	GR w						0.057	2.291						
	Colorado	Recent	CL		200			15				1.13·1 0^{-1}	1.77·1 0^{3}	9.29·1 0^{2}	4.64E +01	3.81·1 0^{-3}	
	Columbia	Recent	COL		165							7.77· 10^{-2}	2.12·1 0^{3}	1.08·1 0^{3}	4.46E +01	3.93·1 0^{-3}	
	Colville	Recent	CV	GS													
	Ebro	Recent	EB	FS iw	125					0.022	0.498	2.04 10^{-2}	6.13·1 0^{3}	3.43·1 0^{3}	1.07·1 0^{2}	3.57·1 0^{-3}	
	Fly	Recent	FLY		65							1.32·1 0^{-2}	4.92·1 0^{3}	1.1 ·10^{4}	1.79 ·10^{2}	8.97 ·10^{-4}	
	Fraser	Recent	FR	FS it							1.432						
	Guichen Bay	Recent	*GU*								5.20			7.80·1 0^{3}			
	Homathko	Recent	HM	GS it						0.063	3.712						
	Huanghe (Yellow River)	Recent	HH	MS i						0.001	0.344						
	Kizil Irmak	Recent	KI		100							2.78·1 0^{-2}	3.60·1 0^{3}	1.26·1 0^{3}	3.15·1 0^{1}	5.71·1 0^{-3}	
	Klang	Recent	KG	FS t						0.003							
	Klinaklini	Recent	KK	GS i						0.083	2.860						
	Mahakam*	Recent	MA	FS it	130			30			0.372	5.46·1 0^{-2}	2.38·1 0^{3}	7.33·1 0^{2}	2.38·1 0^{1}	6.50·1 0^{-3}	
	Mekong	Recent	ME	FS m						0.001	0.029						
	Noeick	Recent	NO	GS i							5.426						
	Po	Recent	PO	FS i	120			23		0.003	0.189	1.12·1 0^{-1}	1.07·1 0^{3}	2.14·1 0^{3}	6.43E +01	1.00·1 0^{-3}	
	Punta Gorda	Recent	PG	GR w						0.802	2.291						
	Rio Grande	Recent	RG		200			4				3.73 10^{-2}	5.36·1 0^{3}	2.14·1 0^{3}	1.07·1 0^{2}	5.00·1 0^{-3}	
	Sao Francisco	Recent	SF	FS w							0.246						
	Senegal	Recent	SN	FS w							0.401						

	Shoalhaven	Recent	SH	FS m							0.802						
	Skeidararsandur	Recent	SS	GS w						0.115	0.917						
	Tiber	Recent	TB	FS w							0.687						
	Tunsberg Dalbre	Recent	TU	GR i						1.489	5.711						
	Volta	Recent	VL		200							$2.36\ 10^{-2}$	$8.48{\cdot}1\ 0^{3}$	$1.70{\cdot}1\ 0^{3}$	$8.48{\cdot}1\ 0^{1}$	$1.00{\cdot}1\ 0^{-2}$	
	Yallahs	Recent	YL	GR wi						0.859	10.2						
Ancient subaerial delta/shoreline clinoforms (Howell et al., 2008)	Panther Tongue		BK (Book Cliffs, U.S.)					41	30		2.1	0.5	10	$3.17{\cdot}1\ 0^{4}$	0.16	$3.15{\cdot}1\ 0^{-4}$	0.07
	Spring Canyon Mb.							16	19		0.27	0.5	20	$9.26{\cdot}1\ 0^{3}$	0.09	$2.16{\cdot}1\ 0^{-3}$	0.21
	Kenilworth Mb.							12	21		0.04	0.5	20	$3.76{\cdot}1\ 0^{4}$	0.38	$5.32{\cdot}1\ 0^{-4}$	0.04
	Sunnyside Mb.							31	22		0.22	0.5	20	$2.46{\cdot}1\ 0^{4}$	0.25	$8.14{\cdot}1\ 0^{-4}$	0.10
	Grassy Mb.							24	25		0.06	0.5	20	$2.55{\cdot}1\ 0^{4}$	0.26	$7.83{\cdot}1\ 0^{-4}$	0.13
	Ferron Sst., USA (1)		FER					22	26		5.2	0.8	35	$1.31{\cdot}1\ 0^{4}$	0.37	$2.67{\cdot}1\ 0^{-3}$	1.90
	Ferron Sst., USA (2)							16	26		6.4	0.8	35	$1.53{\cdot}1\ 0^{4}$	0.43	$2.30{\cdot}1\ 0^{-3}$	1.10
	John Henry Mb., USA		JH					23	70			1	30				
	Judith River Fm., USA		JR					23	16			4	30				
	Mesaverde, USA		MV						16			6.5	35				
	Clyde Field, North Sea		CLY						21			1	120				
	Cormorant Field, Shetland Basin		COR						22			1.5	5				
	Thistle Field, Viking Graben		TH						26			3	5				
	Hutton Field, Shetland Basin		HUT						14			3	5				
	Tern Field, Shetland Basin		TRN						4			3	5				

Table 4.2. *Clinoforms and clinoform sets analysed using measurements taken from published literature compilations. Abbreviations are used in Figures 4.6, 4.11-4.13. Clinoform topset and foreset slopes are assumed to equate to the parameters 'average delta plain gradient' and 'average upper delta slope gradient' of Orton & Reading (1993). Delta bottomset slopes are assumed to equate to average shelf gradient (e.g., Olariu & Steel, 2009). Classification of subaerial delta type is after Orton & Reading (1993), and is based on both dominant grain size (GR = gravelly sand; FS = fine-grained sand; MS = mud-silt) and dominant depositional processes (i = input; w = wave; t = tide). References are cited as follows: (a) Orton & Reading (1993); (b) Burgess & Hovius (1998); (c) Olariu & Steel (2009); (d) Howell et al. (2008); (e) Bristow & Pucillo (2006).*

	Muddy delta-scale subaqueous clinoforms	Sand-prone delta-scale subaqueous clinoforms
Water depth of rollover points of delta-scale subaqueous clinoforms (m)	6-59 m	21-57 m
Distance from shoreline to rollover point of delta-scale subaqueous clinoforms (m)	7,500-126,000 m	610-7,200 m
Distance from subaqueous rollover to shelf-edge-break (m)	15,000-308,000 m	3,700-32,500 m
Distance from shoreline to shelf-edge break (m)	23,000-376,000 m	5,000-32,500 m
Shelf average gradient (°)	0.01-0.38°	0.26-2.12°
Subaerial foreset gradient (°)	0.03-0.62°	0.40-5.67°
Subaqueous foreset gradient (°)	0.03-0.76°	0.39-3.49°
Ratio subaerial / subaqueous gradient (non-dimensional)	0.39-2.46	0.53-4.45
Ratio subaerial / subaqueous foreset heights (non-dimensional)	0.11-0.73	0.20-0.91

Table 4.3. *Parameters extracted from the Global Multi-Resolution Topography bathymetric dataset (Ryan et al., 2009), for present-day delta-scale compound clinoform systems (Figures 4.7-4.10). The range refers to the 5- to 95-percentile of the statistical distribution.*

4.6 DATASET AND METHODOLOGY FOR QUANTITATIVE COMPARATIVE ANALYSIS OF CLINOFORMS

Quantitative comparative analysis of parameters measured from published cross-sections oriented parallel to clinoform dip was carried out for 47 clinoform systems belonging to continental margin, shelf-edge, subaqueous delta, and subaerial delta categories (Table 4.1). Quantitative data describing a further 44 recent subaerial delta and shelf-edge clinoform sets and 15 ancient subaerial delta clinoform sets was extracted from published compilations (Orton & Reading, 1993; Burgess & Hovius, 1998; Bristow & Pucillo, 2006; Howell et al., 2008; Olariu & Steel, 2009) and utilized in the analysis (Table 4.2). The resulting global dataset characterises modern and ancient clinoforms developed in various environmental and climatic settings (Fig. 4.6).

For each clinoform that has been directly measured from published seismic cross-sections and maps (Table 4.1), the geometrical parameters described in Figure 4.5 were systematically recorded. Furthermore, where possible, the water depth of the rollover point (*wd*) was measured, and if chronological data were available, average vertical sediment accumulation rate (*Sv*), clinoform progradation rate (*P*), cross-sectional net sediment flux (*F*)

and progradation resistance ratio (*R*) were also estimated. The parameter 'duration' (*Age*) represents the time span over which these average measurements have been calculated, based on the available chronological data. Published quantitative data for additional clinoforms (Table 4.2) were used to extract the following parameters: foreset slope (*Fs*), bottomset slope (*Bs*), topset slope (*Ts*), water depth of the rollover point (*Wd*), average vertical sediment accumulation rate (*Sv*), clinoform progradation rate (*P*), cross-sectional net sediment flux (*F*), progradation resistance ratio (*R*), duration (*Age*), and clinoform trajectory as defined by successive positions of the upper rollover point (*CT*; only for ancient systems). Given the limitations imposed by seismic data resolution discussed earlier, parameters that describe bottomsets and topsets essentially refer to 'inner bottomsets' (between lower rollover point and clinoform toe point; Fig. 4.5) and 'outer topsets' (between clinoform head point and upper rollover point; Fig. 4.5).

4.7 RESULTS OF QUANTITATIVE COMPARATIVE ANALYSIS OF CLINOFORMS

Delta-scale, shelf-edge and continental-margin clinoform types are characterised by different geomorphological and stratigraphic parameters, and tend to occupy different fields of graphs were parameter pairs are plotted against each other (Figs. 4.13-4.16). For each clinoform type, ranges formed by the 5- to 95-percentile of the values of each geometric and chronostratigraphic parameter are summarised in Table 4.4**.** Relationships between these parameters are investigated in a series of cross-plots, which show best-fit lines generated by least-square regression methods for moderate or strong correlations (coefficient of determination, R^2 = 0.5-0.8 and 0.8-1.0, respectively) (Figs. 4.15-4.16; Tables 4.5-4.6). The equations describing best-fit lines between parameter pairs showing a moderate-to-strong correlation are shown in Tables 4.7-4.8. Best-fit lines have been plotted by utilizing either linear, power-law or second-degree polynomial functions. The function type that shows the best fit to the data (i.e., characterized by the highest R^2 value) has generally been selected for each parameter pair. The only exceptions are polynomial functions that give tightly curved best-fit lines with minima that are poorly contrained by data control, which are considered to be geologically unreasonable. In these cases, the second best-fit function type has been chosen (e.g., Fig. 4.16I-K).

Two types of relationships between parameters are observed. The first type comprises positive and negative correlations between parameters from the same dimensional domain (e.g., heights of the different portions of a clinoform) or from related dimensional domains (e.g., height versus down-dip extent of a certain clinoform

portion). The second type comprises positive and negative correlations between parameters from different dimensional domains that were not derived from each other (e.g., slope of a certain clinoform portion versus height of another clinoform portion; duration versus water depth of rollover points). This second type of relationship is perhaps more meaningful, because it highlights potential links between parameters that are not directly related.

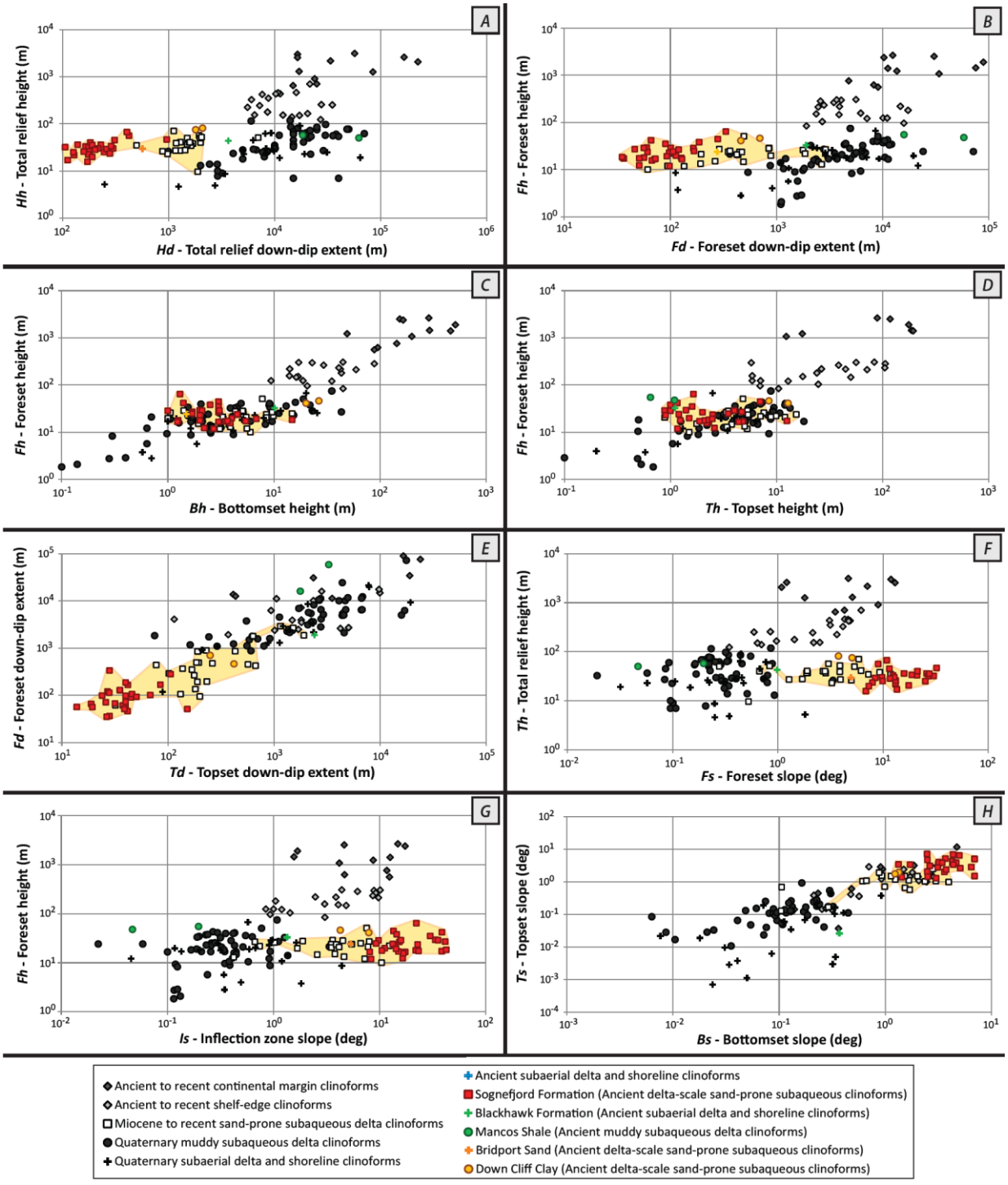

Figure 4.13. *Plots of clinoform morphological parameters. Different clinoform types tend to plot in different, but overlapping, fields.*

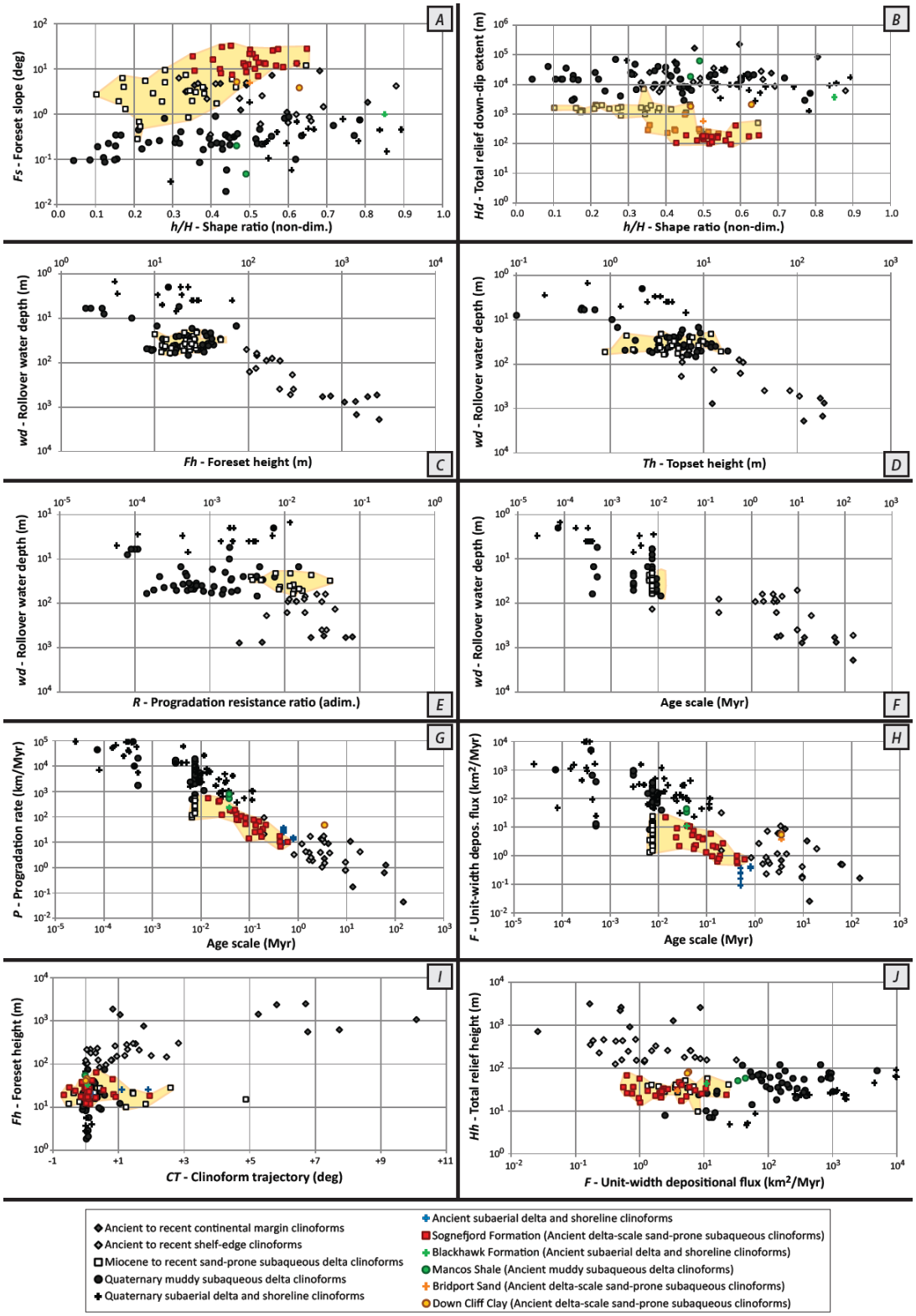

Figure 4.14. *Plots of clinoform morphological, architectural and chronostratigraphic parameters. Different clinoform types tend to plot in different, but overlapping, fields.*

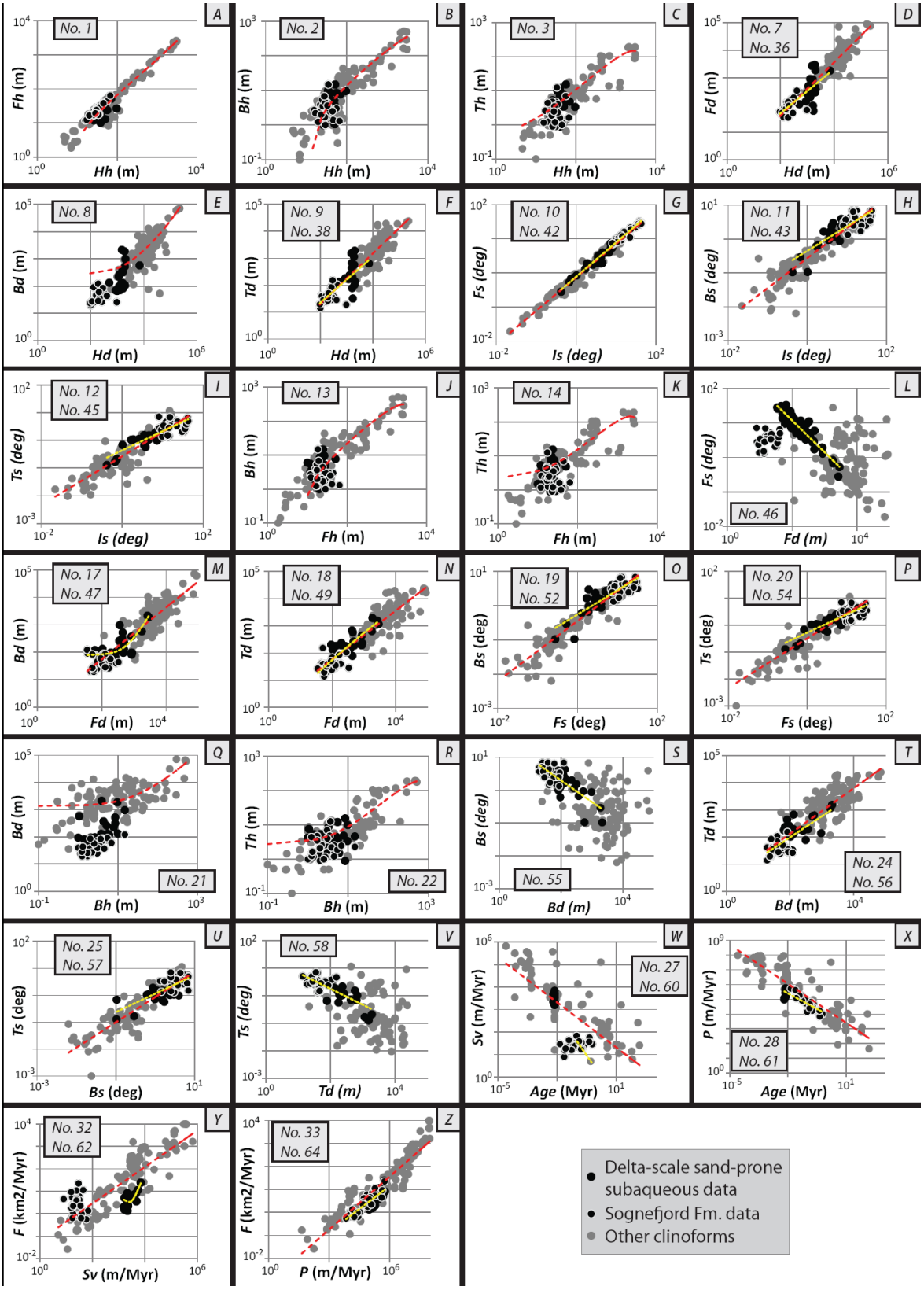

Figure 4.15. *Plots of parameter pairs showing moderate-to-strong (R^2>0.5) statistical correlations. Red and yellow best-fit lines correspond to correlations for all clinoforms and sand-prone subaqueous delta clinoforms, respectively. Equations for the*

best-fit lines are numbered in the grey boxes in each plot; these equations and values of the coefficient of determination (R^2) describing each best-fit line are given in Tables 4.5-4.7.

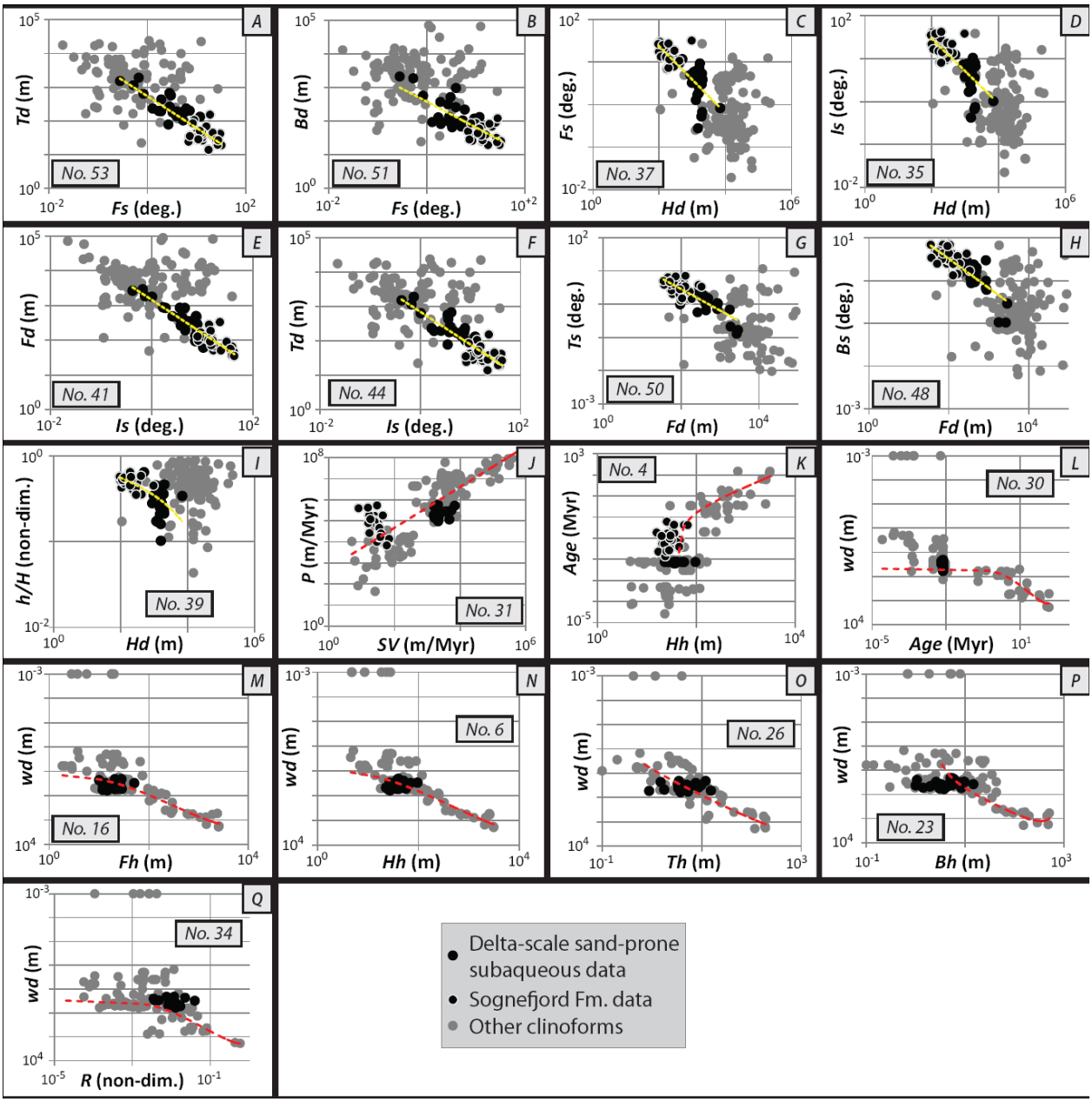

Figure 4.16. *Plots of parameter pairs showing moderate-to-strong (R^2>0.5) statistical correlations. Red and yellow best-fit lines correspond to correlations for all clinoforms and sand-prone subaqueous delta clinoforms, respectively. Equations for the best-fit lines are numbered in the grey boxes in each plot; these equations and values of the coefficient of determination (R^2) describing each best-fit line are given in Tables 4.5-4.7.*

FEATURE			Continental margin clinoforms	Shelf-edge clinoforms	Muddy subaqueous deltas	Sand-prone subaqueous delta clinoforms		Subaerial deltas and shoreline clinoforms	
						≤10 kyr	>10 kyr	≤10 kyr	>10 kyr
			Values						
Total relief (H)	height (m)	*Hh*	670-3,050	140-460	9-103 m	20-62 m		5-67 m	
	down-dip extent (m)	*Hd*	15,700-195,500	6,100-33,900	2,700-42,800	110-2,000 m		1,150-34,440 m	
Inflection zone slope (°)		*Is*	1.6-16.2°	0.9-9.8°	0.1-1.2°	0.7-10°	0.9-38.5°	0.1-1.9°	
Foreset	height (m)	*Fh*	590-2,570	97-300 m	3-46 m	12-43 m		5-38 m	
	down-dip extent (m)	*Fd*	6,540-82,300 m	2,400-17,200 m	1,000-11,800 m	96-2,550 m	49-1,800 m	118-19,600 m	
	slope (°)	*Fs*	1.1-12.5°	0.6-4.8°	0.1-0.9°	0.6-9°	0.7-27°	0.05-6.1°	
Inner Bottomset	height (m)	*Bh*	69-487 m	14-59 m	0-27 m	1-10 m		0.7-23 m	
	down-dip extent (m)	*Bd*	2,800-66,300 m	401-7,850 m	177-11,510 m	81-1,460 m	24-770 m	403-6,960 m	
	slope (°)	*Bs*	0.3-3.9°	0.2 -2.5°	0 -0.4°	0.1-3.9°	0.4-6.7°	0.02-0.42°	
Outer Topset	height (m)	*Th*	14-192 m	6-102 m	0.5-12 m	0.9-11 m		0.5-6 m	
	down-dip extent (m)	*Td*	420-22,500 m	456-9,940 m	260-12,740 m	69-1,800 m	22-885 m	165-12,500 m	
	slope (°)	*Ts*	0.2-9.0°	0 -2.4°	0-0.4°	0.2-2.65°	0.4-5.7°	0.01-0.6°	
Shape ratio (h/H; non-dim.)		*h/H*	0.38-0.76	0.33-0.69	0.11-0.68	0.16-0.46	0.17-0.60	0.44-0.86	
Net-to-gross (% sand+pebble)		*N-g*				36-89%		8-61%	
Age scale (Myr)		Age	3.71 to 123.30	0.20 to 17.60	$5{\cdot}10^{-4}$ to 0.01	0.01	0.01-0.42	$7{\cdot}10^{-5}$ to 0.006	0.01-1.62
Vertical sediment accumulation rate (m/Myr)		Sv	7.7 to $2.6{\cdot}10^{2}$	$2.5{\cdot}10^{1}$ to $2{\cdot}10^{3}$	$4.6{\cdot}10^{2}$ to 10^{5}	$1.6{\cdot}10^{3}$ to $5.7{\cdot}10^{3}$	$1.6{\cdot}10^{1}$ to $5{\cdot}10^{3}$	$3{\cdot}10^{3}$ to $3.5{\cdot}10^{5}$	10^{3} to $2{\cdot}10^{5}$
Clinoform progradation		P	$8.2{\cdot}10^{-2}$ to	$8{\cdot}10^{-1}$ to	$7{\cdot}10^{2}$ to	$1.1{\cdot}10^{2}$ to	10^{1} to	$5{\cdot}10^{3}$ to	10^{3} to

rate (km/Myr)		10^{1}	$8{\cdot}10^{1}$	$2{\cdot}10^{4}$	$5.4{\cdot}10^{2}$	$5{\cdot}10^{2}$	$9{\cdot}10^{4}$	$4{\cdot}10^{4}$
Unit-width depositional flux (km^2/Myr)	F	$7{\cdot}10^{-2}$ to $7.1{\cdot}10^{0}$	$2{\cdot}10^{-1}$ to $1.1{\cdot}10^{1}$	$1.1{\cdot}10^{1}$ to $9.4{\cdot}10^{2}$	1.5 to $1.5{\cdot}10^{1}$	$6{\cdot}10^{-1}$ to $1.1{\cdot}10^{1}$	$4{\cdot}10^{1}$ to 10^{4}	$2.6{\cdot}10^{1}$ to $3.4{\cdot}10^{3}$
Progradation resistance ratio (non-dimensional)	R	$3{\cdot}10^{-3}$ to $4.3{\cdot}10^{-1}$	10^{-2} to $8{\cdot}10^{-2}$	10^{-4} to $7.3{\cdot}10^{-3}$	$3.7{\cdot}10^{-3}$ to $2.7{\cdot}10^{-2}$	$6{\cdot}10^{-5}$ to $2{\cdot}10^{-2}$	10^{-4} to $7{\cdot}10^{-3}$	$4.6{\cdot}10^{-4}$ to $5{\cdot}10^{-3}$
Clinoform trajectory (°)	CT	+0.9° to +49.4°	0° to +2.4°	0° to +0.5°	-0.4° to +3.5°	-0.5° to +2°	0° to +0.13°	0° to +0.9°
Water depth of rollover point (m)	Wd	550-1,770 m	60-426 m	6-59 m	21-57 m		0-5 m	

Table 4.4. *Typical value ranges for the statistical parameters examined within the clinoform population shown by Tables 4.1-4.2. For each clinoform type, the value ranges refer to the 5- to 95-percentile of the parameter statistical distribution. In order to show chronostratigraphically-constrained rate values that can be readily compatible with the short-term (≤10Kyr) data obtained for muddy subaqueous clinoforms, both short-term (≤10 kyr) and longer term (>10 kyr) rates for the other delta-scale clinoforms are displayed in this table.*

Features			*Hh*	*Hd*	*Is*	*Fh*	*Fd*	*Fs*	*Bh*	*Bd*	*Bs*	*Th*	*Td*	*Ts*	*h/H*	Age	Sv	P	F	R	CT	Wd
Total relief (H)	height (m)	*Hh*	-			1			2			3				4				5		6
	down-dip extent (m)	*Hd*		-			7			8			9									
Inflection zone slope (°)		*Is*			-			10			11			12								
Foreset	height (m)	*Fh*	1			-			13			14								15		16
	down-dip extent (m)	*Fd*		7			-			17			18									
	slope (°)	*Fs*			10			-			19			20								
Inner Bottomset	height (m)	*Bh*	2			13			-	21		22										23
	down-dip extent (m)	*Bd*		8			17		21	-			24									
	slope (°)	*Bs*			11			19			-			25								
Outer Topset	height (m)	*Th*	3			14			22			-										26
	down-dip extent (m)	*Td*		9			18			24			-									
	slope (°)	*Ts*			12			20			25			-								
Shape ratio (h/H; non-dim.)		*h/H*													-							
Age scale (Myr)		Age	4													-	27	28		29		30
Vertical sediment accumulation rate (m/Myr)		Sv														27	-	31	32			
Clinoform progradation rate (m/Myr)		P														28	31	-	33			
Unit-width depositional flux (km^2/Myr)		F															32	33	-			

Progradation resistance ratio (non-dimensional)	R	**5**			**15**										**29**				**-**		**34**
Clinoform trajectory (°)	CT																			**-**	
Water depth of rollover point (m)	W d	**6**			**16**			**23**			**26**				**30**				**34**		**-**

Table 4.5. *Strength of correlation between each possible pair of statistical parameters within the global clinoform dataset. Weak-to-strong positive correlations (R^2>0.1) are shown by light grey boxes, and weak-to-strong negative correlations by dark grey boxes. Moderate-to-strong correlations (R^2>0.5) are indicated by numbers, each corresponding to an equation in Tables 4.6-4.7 and Figure 4.9-4.10.*

Features			*Hh*	*Hd*	*Is*	*Fh*	*Fd*	*Fs*	*Bh*	*Bd*	*Bs*	*Th*	*Td*	*Ts*	*h/H*	Age	Sv	P	F	R	CT	Wd
Total relief (H)	height (m)	*Hh*	-		**			**			*			*	*	*	**	*	*		*	**
	down-dip extent (m)	*Hd*		-	35	*	36	37					38		39	**	40 *	*			*	*
Inflection zone slope (°)		*Is*	**	35	-		41 *	42	*		43	*	44	45	*				*	*		*
Foreset	height (m)	*Fh*		*		-		*	*	*		*		*	*		*			*	*	*
	down-dip extent (m)	*Fd*		36	41 *		-	46	*	47	48		49	50	*	**	*	*			*	*
	slope (°)	*Fs*	**	37	42	*	46	-		51	52	*	53	54	*				*	*	*	*
Inner Bottomset	height (m)	*Bh*			*	*	*		-			*			*	*		*			*	*
	down-dip extent (m)	*Bd*				*	47	51		-	55		56		*	**		*			*	*
	slope (°)	*Bs*	*		43		48	52		55	-			57	*					*		*
Outer Topset	height (m)	*Th*			*	*		*	*			-		*	*	**	*	*			*	*
	down-dip extent (m)	*Td*		38	44		49	53		56			-	58	*	*	59	*	*			*
	slope (°)	*Ts*	*		45	*	50	54			57	*	58	-						*	*	*
Shape ratio (h/H; non-dim.)		*h/H*	*	39	*	*	*	*	*	*	*	*	*		-	*	*	*	*	*		
Age scale (Myr)		Age	*	**	**		**		*	**		**	*		*	-	60	61			*	
Vertical sediment accumulation rate (m/Myr)		Sv	**	40 *	*	*	*					*	59		*	60	-		62	63 *	*	**
Clinoform progradation rate (m/Myr)		P	*	*			*		*	*		*	*		*	61		-	64		*	*
Unit-width depositional flux (km^2/Myr)		F	*		*			*					*		*		62	64	-	*		*

Progradation resistance ratio (non-dimensional)	R			*	*		*			*			*	*		63 *		*	-	*	
Clinoform trajectory (°)	CT	*	*		*	*	*	*	*		*		*		*	*	*		*	-	*
Water depth of rollover point (m)	W d	**	*	*	*	*	*	*	*	*	*	*	*			**	*	*		*	-

Table 4.6. *Strength of correlation between each possible pair of statistical parameters within the dataset of sand-prone subaqueous delta clinoforms. Weak-to-strong positive correlations (R^2>0.1) are shown by light grey boxes, and weak-to-strong negative correlations by dark grey boxes. Moderate-to-strong correlations (R^2>0.5) correlations are indicated by numbers, each corresponding to an equation in Tables 4.6-4.7 and Figures 4.9-4.10. Parameter pairs characterized by absence of correlation whereas in the global dataset (Table 4.5) a correlation exist (and vice versa) are highlighted by an asterisk (*). A double asterisk (**) marks parameter pairs showing an opposite correlation type than in the global dataset (cf. Table 4.5).*

Correlations	All clinoforms			Sand-prone subaqueous delta clinoforms		
	No.	Type	Regression equation	No.	Type	Regression equation
Total relief height (*Hh*) – Foreset height (*Fh*)	1	Positive polynomial	$Fh = [4 \cdot 10^{-5}(Hh)^2 + 0.71\ (Hh) - 4.33]$ $(R^2 = 0.98)$	-	Positive weak correlation $(R^2 \leq 0.40)$	
Total relief height (*Hh*) – Bottomset height (*Bh*)	2	Positive polynomial	$Bh = [-10^{-5}(Hh)^2 + 0.16(Hh) - 2.10]$ $(R^2 = 0.80)$	-	Positive, weak correlation $(R^2 \leq 0.30)$	
Total relief height (*Hh*) – Topset height (*Fh*)	3	Positive polynomial	$Th = [-2 \cdot 10^{-5}(Hh)^2 + 0.11(Hh) + 0.47]$ $(R^2 = 0.7551)$	-	No correlations at all $(R^2 \leq 0.12)$	
Total relief down-dip extent (*Hd*) – Foreset down-dip extent (*Fd*)	7	Positive power	$Fd = [0.4789(Hd)^{0.9696}]$ $(R^2 = 0.8834)$	36	Positive power	$Fd = [1.2386(Hd)^{0.8049}$ $(R^2 = 0.62)$
Total relief down-dip extent (*Hd*) – Bottomset down-dip extent (*Bd*)	8	Positive polynomial	$Bd = [8 \cdot 10^{-7}(Hd)^2 + 1.72(Hd) + 275.94]$ $(R^2 = 0.91)$	-	Positive, weak correlation $(R^2 \leq 0.50)$	
Total relief down-dip extent (*Hd*) – Topset down-dip extent (*Td*)	9	Positive power	$Td = [0.271(Hd)^{0.94}]$ $(R^2 = 0.94)$	38	Positive power	$Td = [0.43(Hd)^{0.86}]$ $(R^2 = 0.63)$
Inflection zone slope (*Is*) – Foreset slope (*Fs*)	10	Positive power	$Fs = [0.74\ (Is)^{0.98}]$ $(R^2 = 0.98)$	42	Positive power	$Fs = [0.77(Is)^{1.005}]$ $(R^2 = 0.97)$
Inflection zone slope (*Is*) – Bottomset slope (*Bs*)	11	Positive power	$Bs = [0.27\ (Is)^{0.89}$ $(R^2 = 0.86)$	43	Positive power	$Bs = [0.45(Is)^{0.73}]$ $(R^2 = 0.695)$
Inflection zone slope (*Is*) – Topset slope (*Ts*)	12	Positive power	$Ts = [0.265(Is)^{0.88}]$ $(R^2 = 0.84)$	45	Positive power	$Ts = [0.43\ (Is)^{0.69}]$ $(R^2 = 0.72)$
Foreset height (*Fh*) – Bottomset height (*Bh*)	13	Positive power	$Bh = [0.19\ (Fh)^{0.96}]$ $(R^2 = 0.75)$	-	No correlations at all $(R^2 \leq 0.1)$	
Foreset height (*Fh*) – Topset height (*Th*)	14	Positive polynomial	$Th = [-3 \cdot 10^{-5}(Fh)^2 + 0.135(Fh) + 2.23]$ $(R^2 = 0.68)$	-	No correlations at all $(R^2 \leq 0.1)$	
Foreset down-dip extent (*Fd*) – Foreset	-	Negative, weak correlation $(R^2 \leq 0.38)$ (relationship breaks down at *Fd* >2,000 m)		46	Negative power	$Fs = [794.68(Fd)^{-0.92}]$ $(R^2 = 0.89)$

slope (*Fs*)						
Foreset down-dip extent (*Fd*) – Bottomset down-dip extent (*Bd*)	17	Positive power	$Bd = [0.71\ (Fd)^{0.94}]$ $(R^2 = 0.83)$	47	Positive polynomial	$Bd = [0.0002(Fd)^2 + 0.04(Fd) + 77.48]$ $(R^2 = 0.84)$
Foreset down-dip extent (*Fd*) – Topset down-dip extent (*Td*)	18	Positive power	$Td = [0.9062(Fd)^{0.90}]$ $(R^2 = 0.82)$	49	Positive polynomial	$Td = [-2\cdot10^{-5}(Fd)^2 + 0.58(Fd) – 2.17]$ $(R^2 = 0.745)$
Foreset slope (*Fs*) – Bottomset slope (*Bs*)	19	Positive power	$Bs = [0.3594(Fs)^{0.88}]$ $(R^2 = 0.875)$	52	Positive power	$Bs = [0.5559(Fs)^{0.71}]$ $(R^2 = 0.70)$
Foreset slope (*Fs*) – Topset slope (*Ts*)	20	Positive power	$Ts = [0.3237(Fs)^{0.92}]$ $(R^2 = 0.85)$	54	Positive power	$Ts = [0.528(Fs)^{0.68}]$ $(R^2 = 0.72)$
Bottomset height (*Bh*) – Bottomset down-dip extent (*Bd*)	21	Positive polynomial	$Bd = [0.0548(Bh)^2 + 74.57(Bh) + 1358.4]$ $(R^2 = 0.62)$	-	Positive, weak correlation $(R^2 \leq 0.33)$	
Bottomset height (*Bh*) – Topset height (*Th*)	22	Positive polynomial	$Th = [-5.15\cdot10^{-4}(Bh)^2 + 6.217(Bh) + 2.6869]$ $(R^2 = 0.78)$	-	No correlations at all $(R^2 \leq 0.1)$	
Bottomset down-dip extent (*Bd*) – Bottomset slope (*Bs*)	-	Negative, weak correlation $(R^2 \leq 0.33)$		55	Negative power	$Bs = [40.265(Bd)^{-0.654}]$ $(R^2 = 0.61)$
Bottomset down-dip extent (*Bd*) – Topset down-dip extent (*Td*)	24	Positive power	$Td = [2.7414(Bd)^{0.84}]$ $(R^2 = 0.7458)$	56	Positive polynomial	$Td = [0.0001(Bd)^2 + 0.40(Bd) + 78.35]$ $(R^2 = 0.76)$
Bottomset slope (*Bs*) – Topset slope (*Ts*)	25	Positive power	$Ts = [0.8655(Bs)^{0.94}]$ $(R^2 = 0.805)$	57	Positive power	$Ts = [1.1555(Bs)^{0.6864}]$ $(R^2 = 0.55)$
Topset down-dip extent (*Td*) – Topset slope (*Ts*)	-	Negative, weak correlation $(R^2 \leq 0.39)$		58	Negative power	$Ts = [25.949(Td)^{-0.58}]$ $(R^2 = 0.63)$
Age scale (*Age*) – Vertical sedimentation rate (*Sv*)	27	Negative power	$Sv = [95.827(Age)^{-0.669}]$ $(R^2 = 0.57)$	60	Negative power	$Sv = [2.1202(Age)^{-1.27}]$ $(R^2 = 0.63)$
Age scale (*Age*) – Progradation rate (*P*)	28	Negative power	$P = [19\ (Age)^{-0.88}]$ $(R^2 = 0.73)$	61	Negative power	$P = [9930.6(Age)^{-0.70}]$ $(R^2 = 0.73)$
Vertical sedimentation rate (*Sv*) – Sediment	32	Positive power	$F = [0.067(Sv)^{0.82}]$ $(R^2 = 0.72)$	62	Positive polynomial	$F = [10^{-6}(Sv)^2 - 0.0051\ (Sv) + 9.68]$

fluxes (*F*)						$(R^2 = 0.83)$
Vertical sedimentation rate (*Sv*) – Progradation resistance ratio (*R*)	-	Maximum point at $Sv \approx 200m/Myr; R \approx 0.6$		63	Positive power	$R = [3 \cdot 10^{-5}(Sv)^{0.745}]$ $(R^2 = 0.74)$
Progradation rate (*R)* – Sediment fluxes (*F*)	33	Positive power	$F = [8.95 \cdot 10^{-4}(R)^{0.77}]$ $(R^2 = 0.87)$	64	Positive power	$F = [0.0013(R)^{0.67}]$ $(R^2 = 0.71)$

Table 4.7. *Equations describing best-fit lines between parameter pairs showing a moderate-to-strong correlation (R^2>0.5). Graphical representations of data point distributions and best-fit lines are shown in Figure 4.9.*

Correlations	All clinoforms			Sand-prone subaqueous delta clinoforms		
	No.	Type	Regression equation	No.	Type	Regression equation
Total relief height (*Hh*) – Age scale (*Age*)	4	Positive linear*	*Age = [0.03(Hh) – 1.363]* *(R^2 = 0.57)*	-	No correlation at all *($R^2 \leq 0.10$)*	
Total relief height (*Hh*) – Progradation resistance ratio (*R*)	5	Positive polynomial	*$P = [5 \cdot 10^{-8}(Hh)^2 - 4 \cdot 10^{-0.5}(Hh) + 0.011]$* *($R^2$ = 0.60)*	-	Positive, weak correlation *($R^2 \leq 0.17$)*	
Total relief height (*Hh*) – Water depth of rollover (*Wd*)	6	Positive linear	*Wd = [0.48(Hh) +16.33]* *(R^2 = 0.83)*	-	Negative, weak correlation *($R^2 \leq 0.12$)*	
Total relief down-dip extent (*Hd*) – Inflection zone slope (*Is*)	-	Negative, weak correlation *($R^2 \leq 0.34$)* (relationship breaks down at *Hd >5,000 m)*		35	Negative power	*$Is = [935.31(Hd)^{-0.754}]$* *($R^2$ = 0.60)*
Total relief down-dip extent (*Hd*) – Foreset slope (*Fs*)	-	Negative, weak correlation *($R^2 \leq 0.3751$)* (relationship breaks down at *Hd >5,000 m)*		37	Negative power	*$Fs = [876.14(Hd)^{-0.784}]$* *($R^2$ = 0.63)*
Total relief down-dip extent (*Hd*) – Shape ratio (*h/H*)	-	No correlation at all *($R^2 \leq 0.1$)*		39	Negative logarithmic*	*$h/H = -0.09 \ln(Hd) + 0.97]$* *($R^2$ = 0.50)*
Total relief down-dip extent (*Hd*) – Vertical sedimentation rate (*Sv*)	-	Positive?, weak correlation *($R^2 \leq 0.18$)*		40	Positive power	*$Sv = [0.0021(Hd)^{1.8334}]$* *($R^2$ = 0.79)*
Inflection zone slope (*Is*) – Topset down-dip extent (*Td*)	-	Negative, weak correlation *($R^2 \leq 0.38$)* (relationship breaks down at *1°< Is <10°)*		44	Negative power	*$Td = [701.11(Is)^{-0.955}]$* *($R^2$ = 0.73)*
Inflection zone slope (*Is*) – Foreset down-dip extent (*Fd*)	-	Negative, weak correlation *($R^2 \leq 0.34$)* (relationship breaks down at *1°< Is <20°)*		41	Negative power	*$Fd = [1460.5(Is)^{-0.961}]$* *($R^2$ = 0.84)*
Foreset height (*Fh*) – Progradation resistance ratio (*P*)	15	Positive polynomial	*$P = [7 \cdot 10^{-8}(Fh)^2 - 4 \cdot 10^{-5}(Fh) + 0.0096]$* *($R^2$ = 0.60)*	-	No correlation at all *($R^2 \leq 0.1$)*	

Foreset height (*Fh*) – Water depth of rollover (*Wd*)	16	Positive polynomial	$Wd = [-1.08 \cdot 10^{-4}(Fh)^2 + 0.819(Fh) + 13.101]$ $(R^2 = 0.81)$	-	No correlation at all $(R^2 \leq 0.1)$	
Foreset down-dip extent (*Fd*) – Bottomset slope (*Bs*)	-	Negative, weak correlation $(R^2 \leq 0.38)$ (relationship breaks down at *Fd >2,000 m)*		48	Negative exponential	$Bs = [3.50e^{-0.001Fd}]$ $(R^2 = 0.70)$
Foreset down-dip extent (*Fd*) – Topset slope (*Ts*)	-	Negative, weak correlation $(R^2 \leq 0.33)$ (relationship breaks down at *Fd >2,000 m)*		50	Negative power	$Ts = [54.52(Fd)^{-0.642}]$ $(R^2 = 0.68)$
Foreset slope (*Fs*) – Bottomset down-dip extent (*Bd*)	-	Negative, weak correlation $(R^2 \leq 0.28)$		51	Negative power	$Bd = [377.49(Fs)^{-0.77}]$ $(R^2 = 0.57)$
Foreset slope (*Fs*) – Topset down-dip extent (*Td*)	-	Negative, weak correlation $(R^2 \leq 0.40)$		53	Negative power	$Td = [539.34(Fs)^{-0.94}]$ $(R^2 = 0.74)$
Bottomset height (*Bh*) – Water depth of rollover (*Wd*)	23	Positive polynomial	$Wd = [-0.011(Bh)^2 + 7.36(Bh) - 19.11]$ $(R^2 = 0.75)$	-	No correlation at all $(R^2 \leq 0.1)$	
Topset height (*Th*) – Water depth of rollover (*Wd*)	26	Positive polynomial	$Wd = [-0.0094(Th)^2 + 8.29(Th) - 1.52]$ $(R^2 = 0.70)$	-	No correlation at all $(R^2 \leq 0.1)$	
Topset down-dip extent (*Td*) – Vertical sedimentation rate (*Sv*)	-	Positive, weak correlation $(R^2 \leq 0.22)$		59	Positive power	$Sv = [0.096(Td)^{1.679}]$ $(R^2 = 0.69)$
Age scale (*Age*) – Progradation resistance ratio (*R*)	29	Positive polynomial	$R = [3 \cdot 10^{-5}(Age)^2 - 0.0009(Age) + 0.0095]$ $(R^2 = 0.88)$	-	Minimum point at $Age \approx 0.01$ Myr; $R \approx 5 \cdot 10^{-4}$	
Age scale (*Age*) – Water depth of rollover (*Wd*)	30	Positive polynomial	$Wd = [-0.073(Age)^2 + 19.49(Age) + 48.14]$ $(R^2 = 0.72)$	-	Positive, weak correlation $(R^2 \leq 0.11)$	
Vertical sedimentation rate (*Sv*) – Progradation rate (*P*)	31	Positive power*	$P = [521.81(Age)^{0.964}]$ $(R^2 = 0.68)$	-	Positive, weak correlation $(R^2 \leq 0.26)$	
Progradation resistance	34	Positive	$Wd = [-4785(R)^2 + 6050.3$	-	Positive, weak correlation	

ratio (*R*) – Water depth of rollover (*Wd*)		polynomial	*(R) + 30.23]* *(R^2 = 0.77)*		*($R^2 \leq 0.19$)*

Table 4.8. *Equations describing best-fit lines between parameters pairs showing a moderate-to-strong correlation (R^2>0.5). Graphical representations of data point distribution and best-fit lines are shown in Figure 4.10.*

4.7.1 Morphological parameters and correlation relationships

4.7.1.1 Clinoform heights

The examined dataset demonstrates that progressively larger scale clinoforms are deposited in increasingly deeper waters and over progressively larger time spans (Figs. 4.14F, 4.16K-L; Tables 4.4-4.8), as described by strong correlations between these parameters (Tables 4.7-4.8). Topset-to-foreset rollovers of subaerial delta clinoforms occur at <5 m water depth, whereas the corresponding rollovers in muddy and sandy delta-scale subaqueous clinoform rollovers are respectively at 6-59 m and 21-57 m. Topset-to-foreset rollovers of shelf-edge clinoforms (60-430 m) and continental margin clinoforms (440-1,770 m) occur at increasingly deeper water depths. Foreset height and total relief of delta-scale clinoforms are respectively <45 m and <100 m. Shelf-edge clinoforms and continental margin clinoforms are characterised by foreset heights of 97-300m and 590-2,700 m, and total relief of 140-460 and 670-3,050 m (Fig. 4.13A-D). In addition, the dataset comprising all the analysed clinoforms, regardless to their type, shows moderate-to-strong, positive correlations between water depths of topset-to-foreset rollover points and each of the following six parameters: total relief ($R^2 \approx 0.83$); foreset height ($R^2 \approx 0.77$); topset height ($R^2 \approx 0.81$); bottomset height ($R^2 \approx 0.74$); duration ($R^2 \approx 0.72$); progradation resistance ratio ($R^2 \approx 0.77$) (Figs. 4.16L-Q). The last two relationships are indirect consequences of the accumulation of hiatuses of different scales over increasingly longer time spans (Sadler, 1981). Each of these parameters can be generally used as a palaeobathymetry proxy, according to the correlations given in Table 4.7-4.8. However, none of these relationships seem to be valid for statistical populations formed only by delta-scale, sand-prone subaqueous clinoforms (Figs. 4.16L-Q; Tables 4.5, 4.7-4.8). The data-points relating to this clinoform type generally follow the trend for the global clinoform dataset but, presumably due to the low spread of water depth values, do not form a clearly define trend of their own (Figs. 4.16L-Q).

4.7.1.2 Clinoform dips

The slopes of clinoform inflection zones range from 0.1-1.9° for subaerial deltas and muddy subaqueous deltas, to 0.9-9.8° for shelf-edge clinoforms and 0.9-16.2° for continental margin clinoforms (Fig. 4.13F-G). These slope values indicate that larger clinoforms are characterized by steeper foresets, independent of depositional

environment. However, delta-scale sand-prone subaqueous clinoforms are typically characterised by inflection-point slope values of 0.7-10°, up to a maximum of 38°, similar to those of shelf-edge clinoforms (Fig. 4.13E-F). We propose that these anomalously steep values for foreset slope are a diagnostic criterion for identifying delta-scale sand-prone subaqueous clinoforms. The heights of delta-scale sand-prone subaqueous clinoforms (12-43 m) are similar to those of other delta-scale clinoforms, suggesting their greater slope values are due to much smaller dip extents of their foresets (<2,000 m, compared with values of <12,000 m for muddy subaqueous clinoforms and of <19,600 m for subaerial delta clinoforms; Fig. 4.13A-B). Similar trends are observed for the inner bottomset and the outer topset areas of the clinoforms, which are characterised by heights of <20 m for all delta-scale clinoforms, but smaller dip extents for sand-prone subaqueous clinoforms (20-800 m) than for other types of delta-scale clinoform (200-12,000 m) (Fig. 4.13C-F). This gives rise to very low topset and bottomset slopes for both muddy subaqueous and subaerial delta clinoforms (generally <0.4°), and to much steeper slopes for recent sand-prone subaqueous delta clinoforms (up to 4°; Fig. 4.13H). In particular, values of inner bottomset slope in sand-prone subaqueous delta clinoforms (0.1-4°) are greater than those in all the other clinoform types at every scale, except for continental margin clinoforms (0.3-3.9°, Table 4.1). These steep bottomset slopes are another diagnostic criterion of sand-prone subaqueous delta clinoforms.

4.7.1.3 Cross-sectional clinoform morphology

As shown in Figure 4.14A-B, the greatest values of shape ratio (h/H; Fig. 4.5) occur in subaerial delta clinoforms (0.44-0.86), with progressively lower values exhibited by continental margin clinoforms (0.38-0.76), shelf-edge clinoforms (0.33-0.69) and subaqueous delta clinoforms (0.10-0.65). Although the ranges of shape ratio show overlap between the different types of clinoforms, the cross-sectional morphology of subaerial and subaqueous delta clinoforms can be used to an extent as a feature to distinguish them, with subaerial delta clinoforms being more oblique and subaqueous delta clinoforms being more sigmoidal, irrespective of grain size.

4.7.1.4 Parameter correlations

Moderate-to-strong positive correlations are observed for morphological parameters in three groups: (1) between the total vertical relief of clinoforms and the heights of their constituent foresets, bottomsets and topsets (Figs. 4.15A-C, 4.15J-K, 4.15R); (2) between the dip extents of clinoforms and their constituent foresets, bottomsets and topsets (Figs. 4.15D-F, 4.15M-N, 4.15T); and (3) between the slopes of clinoform inflection zones, foresets, bottomsets and topsets (Figs. 4.15G-I, 4.15O-P, 4.15U). Values of bottomset height and down-dip extent

are weakly correlated (Fig. 4.15Q). Very strong correlations ($R^2 > 0.97$) are noted between slopes of foresets and inflection zones for all clinoforms (Fig. 4.15G), and between the total relief of all clinoforms and their foreset heights (Fig. 4.15A).

In the case of delta-scale sand-prone subaqueous clinoforms, strong negative correlations were observed between the dip extents and slopes of clinoforms, and between the same parameters for their constituent foresets, bottomsets, topsets and inflection zones (Figs. 4.15L,S,V, Figs. 4.16A-H). Furthermore, delta-scale sand-prone subaqueous clinoforms with narrower clinoform dip extents also show larger values of shape ratio (Fig. 4.16I). These correlations demonstrate the quantitative nature of the relationships between dip extents and slopes in delta-scale sand-prone subaqueous clinoforms, and reveal that narrower and steeper delta-scale subaqueous clinoforms are characterised by progressively more asymmetric, oblique geometries (Tables 4.7-4.8). Similar correlations do not occur in the dataset of all clinoform types, suggesting that they can be regarded as additional diagnostic criteria for recognition of delta-scale coarse-grained subaqueous clinoforms.

4.7.2 Chronostratigraphically-constrained parameters

4.7.2.1 Rates of progradation, vertical sedimentation, unit-width depositional flux

Clinothem outbuilding occurs over increasingly long time spans for delta-scale (<2.0 Myr), shelf-edge (0.2-17.6 Myr) and continental margin clinoforms (3.7-123.3 Myr). This pattern is reflected in positive correlations between clinoform set duration and the water depth of rollover points, the height of clinoform foresets, and total clinoform relief (Figs. 4.14F, 4.10). As a consequence, average vertical sedimentation rates, progradation rates and unit-width depositional flux of continental margin clinoforms are respectively up to four, six and five orders of magnitude lower than the typical values for delta-scale clinoforms, with intermediate values for shelf-edge clinoforms (Fig. 4.14F-H). In delta-scale clinoform sets deposited over time spans of less than 10 kyr, vertical sedimentation rates, progradation rates and unit-width depositional flux are greatest in subaerial deltas (respectively, 10^3-10^5 m/Myr, 10^3-10^5 km/Myr, 10^1-10^4 km^2/Myr), slightly lower in muddy subaqueous deltas (respectively, 10^2-10^5 m/Myr, 10^2-10^4 km/Myr, 11-950 km^2/Myr), and markedly lower in sand-prone subaqueous deltas (respectively, 1-5 x 10^3 m/Myr, 1-5 x 10^2 km/Myr, 1-15 km^2/Myr).

4.7.2.2 Clinoform trajectories and Progradation resistance ratio

Clinoform trajectories generally tend to be relatively low angle in deltaic clinoform sets (≤0.9°), increasing for shelf-edge (≤2.4°) and continental margin clinoform sets (0.9-49°). In concert with this trend, clinoform progradation resistance ratios increase from deltaic (10^{-4} to $7x10^{-3}$) to shelf-edge (1-8 x 10^{-2}) and continental margin clinoform sets (up to $4x10^{-1}$) (Fig. 4.14E, I). These trends reflect the dominance of short-term progradation and long-term aggradation in cycles of continental shelf outbuilding (Bullimore et al., 2008; Helland-Hansen & Hampson, 2009). However, sand-prone subaqueous delta clinoform sets contain a larger spread of trajectories (from -0.5° to +2°), even in the short term (<10 kyr). Furthermore, the values of clinoform progradation resistance ratio (≤3 x 10^{-2}) for sand-prone subaqueous delta clinoforms are up to two orders of magnitude higher than those typical of other delta-scale clinoforms, and are similar to those that characterise shelf-edge clinoform sets. Low rates of progradation relative to aggradation are therefore characteristic of the outbuilding of sand-prone subaqueous deltas.

4.7.2.3 Parameter correlations

Moderate to strong negative power correlations exist between age duration and both vertical mean sedimentation rates ($R^2 > 0.57$) and horizontal mean progradation rates ($R^2 > 0.73$) for clinoform sets (Figs. 4.15W-X; Fig. 4.16J). Such trends were first documented by Sadler (1981), and indicate that the net rate of sediment accumulation recorded by a sedimentary unit has a systematic inverse relation to the average time duration of the unit, due to the occurrence of gaps in deposition of various frequencies and durations. Cross-sectional net-sediment flux, which directly depends on values of progradation rate and vertical mean sedimentation rate ($R^2 > 0.70$, Figs. 4.15Y-Z), shows only a modest negative correlation with clinoform set duration ($R^2 \approx 0.55$). This phenomenon was highlighted by Sadler (2012), who argues that, for time intervals greater than 10^3 years, the product of aggradation and progradation rates (i.e., the cross-sectional sediment flux) is largely time scale-independent for siliciclastic passive margins.

4.8 DISCUSSION

In the preceding sections, examples of modern and ancient delta-scale subaqueous clinoforms have been summarized from the published literature, and their morphological and chronostratigraphic parameters have been quantitatively analysed in the context of other clinoform types. In this section, we return to the problems identified in the introduction to this paper: (1) how can delta-scale subaqueous clinoforms be recognized in the stratigraphic record using seismic reflection, sedimentological and/or stratigraphical data?; (2) what kind of depositional processes and settings are implied by clinoform morphology, lithology and internal facies character?; and (3) what are the implications of recognising this particular type of shallow-marine sediment body in ancient and modern environments for sequence stratigraphic models?

4.8.1 Diagnostic criteria for delta-scale subaqueous clinoforms

An interpretation of delta-scale subaqueous clinoform is likely whenever clinoforms encompassing heights of tens of metres are characterised by a relatively well-developed topset that lack evidences for subaerial exposure. In addition, the quantitative analysis presented herein indicates a series of diagnostic geomorphological, sedimentological and stratigraphic features for either muddy or sandy delta-scale subaqueous clinoforms (Figs. 4.13-4.16, Tables 4.3-4.8). Some of these quantitative characteristics can be recognised in high-resolution 3D seismic data, making it possible to propose a sandy or muddy delta-scale subaqueous clinoform interpretation even without detailed sedimentological data. All analysed delta-scale subaqueous clinoforms, irrespective of their dominant grain-size, share three common characteristics: (1) they have a shore-parallel, laterally extensive, near-linear, plan-view morphology (Fig. 4.17); (2)their stratigraphic architecture, geomorphology, sediment grain size and facies character are dominated by basinal processes (waves, currents, tides) and tend to be more uniform than those of their subaerial delta counterparts (Fig. 4.17); and (3) their nearly symmetrical, sigmoidal cross-sectional geometry (shape ratio of 0.10-0.65) contrasts with the oblique cross-sectional geometries that characterise subaerial deltas (Fig. 4.18).

Our analysis of recent clinoforms highlights three morphological differences that allow muddy and sandy delta-scale subaqueous clinoforms to be further differentiated (Figs. 4.18-4.19). Firstly, the dip extents of the topset, foreset and bottomset components of sand-prone delta-scale subaqueous clinoforms are ca. 1 order of magnitude smaller than in other delta-scale clinoforms (Figs. 4.13A-B; 4.14B; 4.15D-F, L-N; 4.16A-I). Secondly, steep topsets, foresets and bottomsets are diagnostic of sand-prone delta-scale subaqueous clinoforms, whereas

markedly gentler gradients are typical of their mud-prone counterparts (Figs. 4.13F-H; 4.14A; 4.15G-I, L, O-P, S, U-V; 4.16A-H). A foreset gradient threshold between the two systems is observed at ca. 0.3-0.5° (Fig. 4.19). Thirdly, delta-scale sand-prone subaqueous clinoforms show a moderate inverse correlation between the slope and dip extents of their foresets, topsets and bottomsets slopes, which is not observed in other types of clinoforms (Fig. 4.16A-I).

Values of short term (≤10 kyr) progradation rates and depositional flux for sand-prone subaqueous clinoforms (respectively, 1-5 x 10^2 km/Myr and 1-15 km^2/Myr) are up to 3-4 orders of magnitude lower than in equivalent subaerial deltas, and average vertical sediment accumulation rate values (1-5 x 10^3 m/Myr) can be up to two orders of magnitude lower than in other delta-scale clinoforms deposited over similar time spans (Fig. 4.15W-Y; Table 4.4). In addition, sand-prone systems are characterised by a larger spread of clinoform trajectory values (from -0.5° to +2°) than mud-prone delta-scale subaqueous clinoforms (0-0.5°), even in the Holocene (≤10 kyr duration). This is in marked contrast with the very low shoreline trajectory angles developed over similar timescales (<0.1°) (Figs. 4.14I, 4.18; Table 4.4).

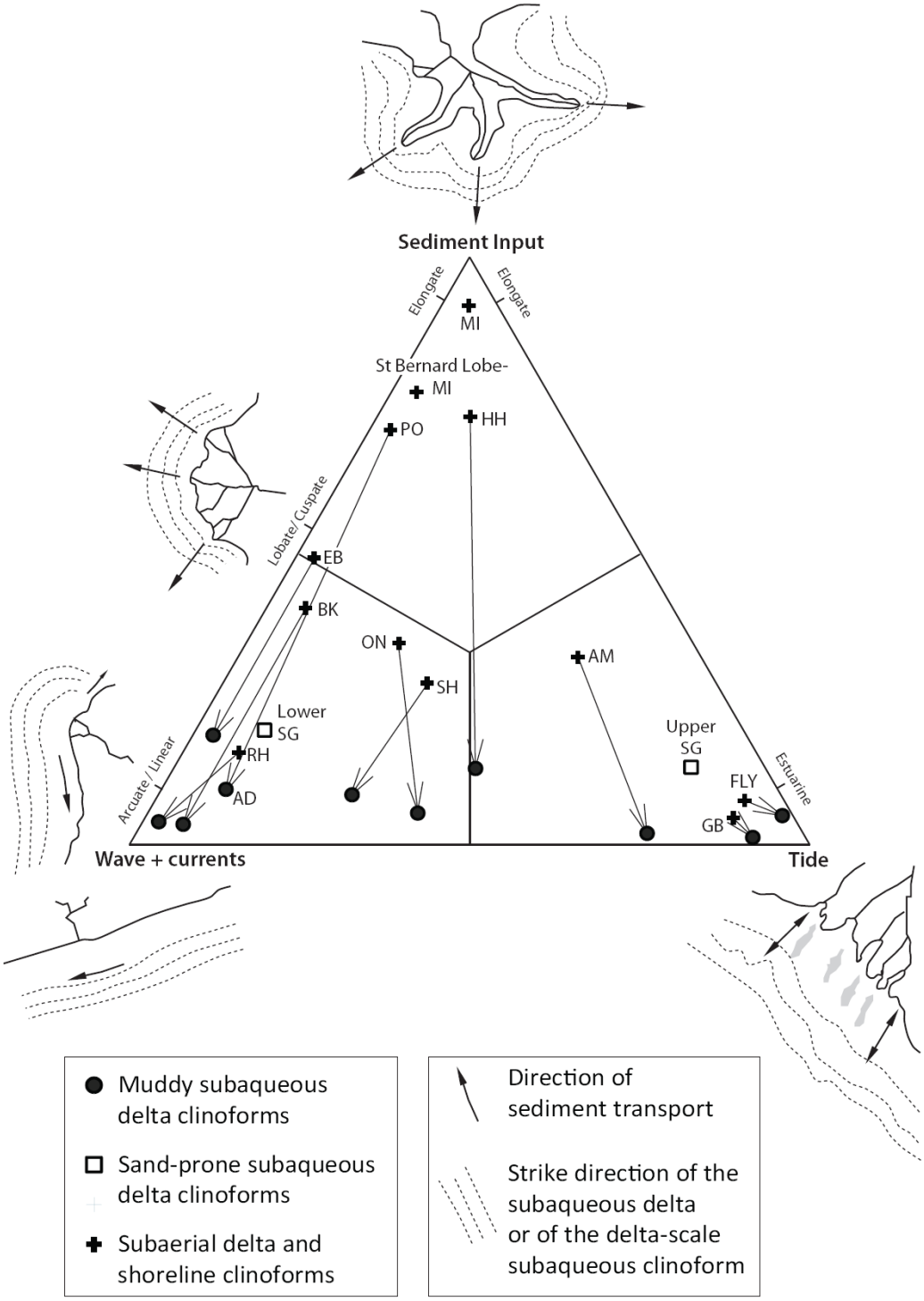

Figure 4.17 *Delta-scale compound clinoforms plotted on the tripartite classification scheme of Galloway (1975) for deltas. The positions of the subaerial delta clinoforms are derived from Orton & Reading (1993) and Galloway (1975). Approximate positions of the subaqueous delta clinoforms are inferred from the magnitude of waves and tides in the receiving basins for modern systems and from core-based facies analysis for ancient systems (supporting references listed in Tables 4.1-4.2). Qualitative changes in plan-view morphology of coeval subaerial and subaqueous delta clinoforms are also shown, and related to spatial changes in sedimentary processes.*

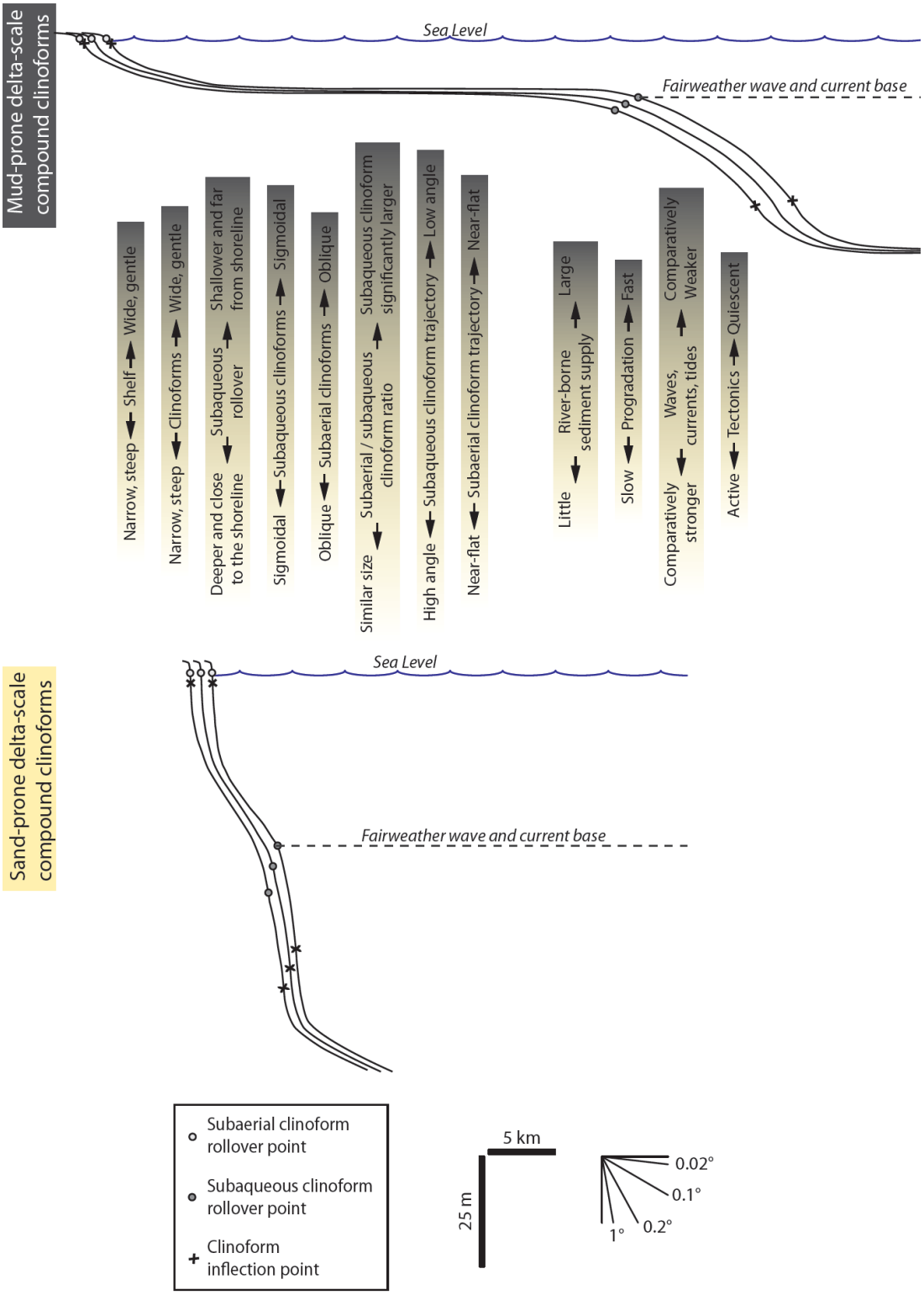

Figure 4.18 *Typical cross-sectional morphologies of mud- and sand-prone delta-scale compound clinoforms. The summarised differences between these two end-members is based on the analysis shown in Figures 4.13-4.16 and Tables 4.2-4.8, and discussed in the text. Both types of compound clinoform are characterised by oblique subaerial delta clinoform morphologies and sigmoidal subaqueous clinoform morphologies.*

4.8.2 Depositional processes and settings of delta-scale subaqueous clinoforms

4.8.2.1 Significance of plan-view clinoform morphology

Processes dispersing sediment away from river mouths range from fair-weather waves, storm waves and gravity flows, to hyperpycnal plumes, and tidal and oceanographic currents (e.g., Dreyer et al., 2005; Hampson, 2010). In the subaqueous portion of compound clinoforms, dispersal processes are dominated by persistent oceanographic currents, waves and tides that transport sediment alongshore. This shore-parallel marine transport belt, observed in many present-day mud-rich subaqueous deltas, causes a lateral deflection of sediment input beyond the river mouth, (e.g., Driscoll & Karner, 1999; Cattaneo et al., 2003, 2007; Liu et al., 2006; Mitchell et al., 2012; Fig. 4.17). As a consequence, delta-scale subaqueous clinoforms are predominantly controlled by basinal processes, and form laterally-extensive, near-linear, shore-parallel plan-view geometries (Fig. 4.17).

Field & Roy (1984) and Hernández-Molina et al. (2000a) in their initial interpretations of 'infralittoral prograding wedges' state that delta-scale sand-prone subaqueous clinoforms are formed by the action of storm-generated downwelling currents transporting shoreline sands seawards from the surf zone, and are unconnected to subaerial delta input points. Furthermore, they indicate that these systems onlap on underlying discontinuities and do not form compound clinoform systems (c.f., coarse-grained variant of 'Gargano-type' clinoforms; Fig. 4.3C). The uniform sediment texture that is generally associated with delta-scale subaqueous clinoforms, which often causes their internal architecture to be poorly imaged on seismic data (Mitchell et al., 2012), is consistent with this origin, since shoreface sands are normally well sorted by wave action in the surf zone or during alongshore transport from river mouths. The modelling studies of Mitchell (2012) and Mitchell et al. (2012) suggests that the alongshore components of storm-generated bottom currents are usually much stronger and longer lasting than the offshore-directed component, resulting in near-bed stresses above the sediment transport thresholds even in the absence of combined wave action. This potentially gives rise to sedimentation patterns dominated by intermittent, current-driven alongshore sediment transport belts (Mitchell et al., 2012), which resembles the sedimentation style of typical mud-rich subaqueous deltas (e.g., Driscoll & Karner, 1999; Cattaneo et al., 2003, 2007; Liu et al., 2006; Mitchell et al., 2012).

4.8.2.2 Significance of cross-sectional clinoform morphology

Previous analysis of seismic reflection profiles has identified two types of clinoform morphology and related them to different environmental variables (e.g. Sangree & Widmier, 1977; Pirmez et al., 1998; Driscoll & Karner 1999; Adams & Schlager, 2000). Oblique clinoforms exhibit asymmetrical morphologies produced by diffusion law (i.e. abrupt break in slope from topset-to-foreset and gradual break in slope from foreset-to-bottomset), have narrow topsets and steep foresets, and are associated with low angle, regressive clinoform trajectories that lack aggradation. In contrast, sigmoidal clinoforms exhibit symmetrical morphologies (i.e. gradual breaks in slope from topset-to-foreset and from foreset-to-bottomset), have broad topsets and gently dipping foresets, and are associated with regressive, aggradational clinoform trajectories. The 'shape ratio' values presented in our study indicate that both sandy and muddy delta-scale subaqueous clinoforms tend to show the most highly symmetrical, sigmoidal cross-sectional geometries, whereas subaerial delta clinoforms are oblique (Figs. 4.14A-B, Fig. 4.18).

Clinoform cross-sectional geometries are controlled by a complex spatial and temporal interplay between mean grain size, clinoform height, sediment dispersal processes and water column energy distribution, clinoform trajectory type and basin physiography (Kenter, 1990; Orton & Reading, 1993; Pirmez et al., 1998; Driscoll & Karner, 1999; Adams & Schlager, 2000; Swenson et al., 2005; Cattaneo et al., 2003, 2007). In particular, oblique clinoform profiles, characterised by steep equilibrium slopes, are favoured by coarse-grained sediments, high clinoform relief, low trajectory angles, close proximity to the shoreline, and predominance of river-driven over basinal processes (Pirmez et al., 1998). The opposite conditions favour development of sigmoidal clinoforms and gentler slopes (Fig. 4.18). When one or more of the controlling parameters vary through space or time, clinoform cross-sectional profiles change accordingly. For example, Pirmez et al. (1998) point out that when sigmoidal clinoforms prograde across a sloping basin floor towards greater water depths, their cross-sectional profile tends to become more oblique (height-induced changes). However the clinoforms change from oblique to sigmoidal geometries if the rate of sediment supply cannot keep pace with the rate of water depth rise (shoreline trajectory-induced changes; e.g., Mortimer et al., 2005). Due to the changes in shoreline trajectory implicit in a typical sinusoidal relative sea level cycle, clinoforms are predicted to evolve through time from oblique to sigmoidal in lowstand system tracts, and from sigmoidal to oblique in highstand system tracts (e.g., Mitchum et al., 1977; Vail et al., 1977; Mitchum & Van Wagoner, 1991).

The typical sigmoidal profile of large-scale, shelf-edge and continental-margin clinoforms is due to the predominance of basinal processes, their fine grain-size and generally high-angle trajectories. Although their relief is not high, subaerial-delta clinoforms are oblique because they are predominantly associated with river-driven sediment dispersal processes and low-angle clinoform trajectories. Delta-scale subaqueous clinoforms tend to be

sigmoidal due to the effects of strong wave, current and tidal processes and of higher-angle clinoform trajectories than in subaerial deltas (Fig. 4.18). The anomalously steep gradients typical of delta-scale sand-prone subaqueous clinoforms are more similar to the slopes of continental margin clinoforms than to those of other delta-scale clinoform types (Table 4.4; Figs. 4.13F-H), and are probably the result of the higher friction experienced in subaqueous environments below fairweather wave base, combined with the availability of well-sorted, coarse-grained sediment.

4.8.2.3 Significance of chronostratigraphically-constrained parameters for clinoform sets

Delta-scale sand-prone subaqueous clinoforms are characterised by a larger spread of clinoform trajectory values (from -0.5° to +2°) than mud-prone subaqueous systems (0-0.5°) and, above all, shoreline systems (<0.1°) (Figs. 4.14I, 4.18; Table 4.4). This characteristic, coupled with progradation resistance ratio values that in sand-prone subaqueous systems are up to two orders of magnitude higher ($\leq 3 \times 10^{-2}$) than in those typical of other delta-scale clinoform types deposited during similar time spans (Fig. 4.16Q; Table 4.4), shows that lower progradation relative to aggradation is characteristic of delta-scale sand-prone subaqueous clinoform sets (Fig. 4.18). Similar steep clinoform trajectory angles are displayed by larger-scale clinoforms, deposited in longer time spans (e.g., shelf-edge and continental-margin clinoform; cf. Fig. 4.14I, Table 4.4), reflecting the dominance of short-term progradation and long-term aggradation in cycles of continental shelf outbuilding (Bullimore et al., 2008; Helland-Hansen & Hampson, 2009).

Slow progradation and the very low values of unit-width depositional flux typical of delta-scale sand-prone subaqueous clinoform systems may reflect the distance of many sand-prone subaqueous clinoform foreset from river sediment input points (Figs. 4.7-4.9, 4.17) and/or the sporadic nature of sediment supply and depositional episodes by basinal processes in these settings (c.f., Mitchell, 2012; Mitchell et al., 2012). Higher sediment supply and progradation rate values in muddy subaqueous deltas are attributed to the association of these clinoform types with large feeder rivers and subaerial deltas (Fig. 4.7-4.9, 4.18). Subaerial deltas may prograde seawards very rapidly (e.g. the Po Delta has prograded at a rate of 45 km/kyr in the last 360 years, partly due to anthropogenic forcing), but at the same time may be subject to topset subaerial truncation and also to frontal erosion and retreat in between rapid episodes of progradation (e.g., Po di Tolle lobe of the Po Delta) (Correggiari et al., 2005; Friedrichs & Scully, 2007).

4.8.2.4 Depositional settings of delta-scale compound clinoforms

Holocene delta-scale sand-prone compound clinoforms form in different oceanographic and depositional settings than muddy compound clinoforms (Figs. 4.18-4.19): (1) in sandy systems, the water depth of the rollover point of the subaqueous clinoform (ca. 20-60 m) tends to be ca. 10-30 m deeper than in muddy subaqueous deltas; (2) delta-scale muddy and sandy subaqueous clinoforms are characterised by relatively wide and relatively narrow subaqueous topsets, respectively, with a threshold value between the two systems of ca. 9 km of distance between the subaqueous rollover point and the shoreline break; (3) delta-scale sand-prone subaqueous clinoforms are hosted by steep (≥0.26°) and narrow (<35 km) shelves, whereas muddy systems are found on broad and gently sloping shelves, with critical cut-off values between the two systems of ca. 30-70 km distance from the shoreline to the shelf-edge break and 0.2-0.5° average shelf-gradients; and (4) muddy and sandy compound clinoforms respectively contain a larger and smaller subaqueous clinoform relative to the associated subaerial clinoform, with a threshold value between the two systems for the ratio of subaerial foreset to subaqueous foreset height of ca. 17-30%.

The deeper clinoform rollovers for sand-prone systems are attributed to the greater wave and current velocities needed to transport sand- rather than mud-grade sediment. These greater velocities are mirrored by a deeper storm wave-base that, in turn, directly affects the depth of the delta-scale subaqueous rollover (e.g., Pirmez et al., 1998; Swenson et al., 2005; Mitchell et al., 2012). The wide, low-gradient shelves that typically host mud-rich subaqueous deltas, together with the greater distance of these clinoforms from the shoreline, are interpreted to reflect the lower angle of repose of fine-grained sediments, and the high rates of river-fed sediment supply and deltaic progradation that typify these systems.

Sand-prone delta-scale subaqueous clinoforms are particularly common in tectonically active settings, such as the periphery of rift basins (e.g., the Sognefjord Formation) or in the vicinity of compressional to transpressional plate boundaries (e.g., California Borderlands, southern Iberia) (Table 4.1; Figs. 4.6, 4.18). These contexts are effective in: (1) delivering coarse-grained clastic sediment to the shelf via short, steep subaerial drainages; (2) favouring the formation of narrow, steep shelves; and (3) triggering or enhancing strong oceanographic circulation (e.g., Færseth & Råvnas, 1998; Gawthorpe & Leeder, 2000). Conversely, muddy subaqueous deltas are particularly common on broad, low-gradient shelves situated in passive margin or cratonic basins (Table 4.1; Figs. 4.6, 4.18).

The amount of river-derived sediment delivered to the subaqueous clinoform relative to that retained in the subaerial clinoform is proportional to the predominance of basinal processes over fluvial processes (Swenson et al., 2005). As a consequence, the degree of relative growth and development of subaerial and subaqueous clinoforms tends to be inversely related to each other, with a negative correlation between width of coastal plain and the width of the shelfal mudstone belt (c.f., Swenson et al., 2005; Hampson, 2010). It is possible to distinguish

compound clinoform systems characterised by large subaqueous clinoforms with a clearly sigmoidal geometry (shape ratio <0.4) and a broad, well-developed subaqueous topset (e.g., muddy delta systems fed by large rivers and strongly influenced by waves or tides, such as the Amazon, Ganges-Brahmaputra, Fly, Yangtze River deltas) and other systems characterised by much larger subaerial delta or shoreline clinoforms with an oblique to top-truncated geometry (shape ratio ≥0.4), and a much reduced to absent subaqueous counterpart (e.g. sandy delta systems or muddy delta systems containing a strongly progradational subaerial delta, such as the Mississippi River delta) (cf., Figs. 4.17-4.18).

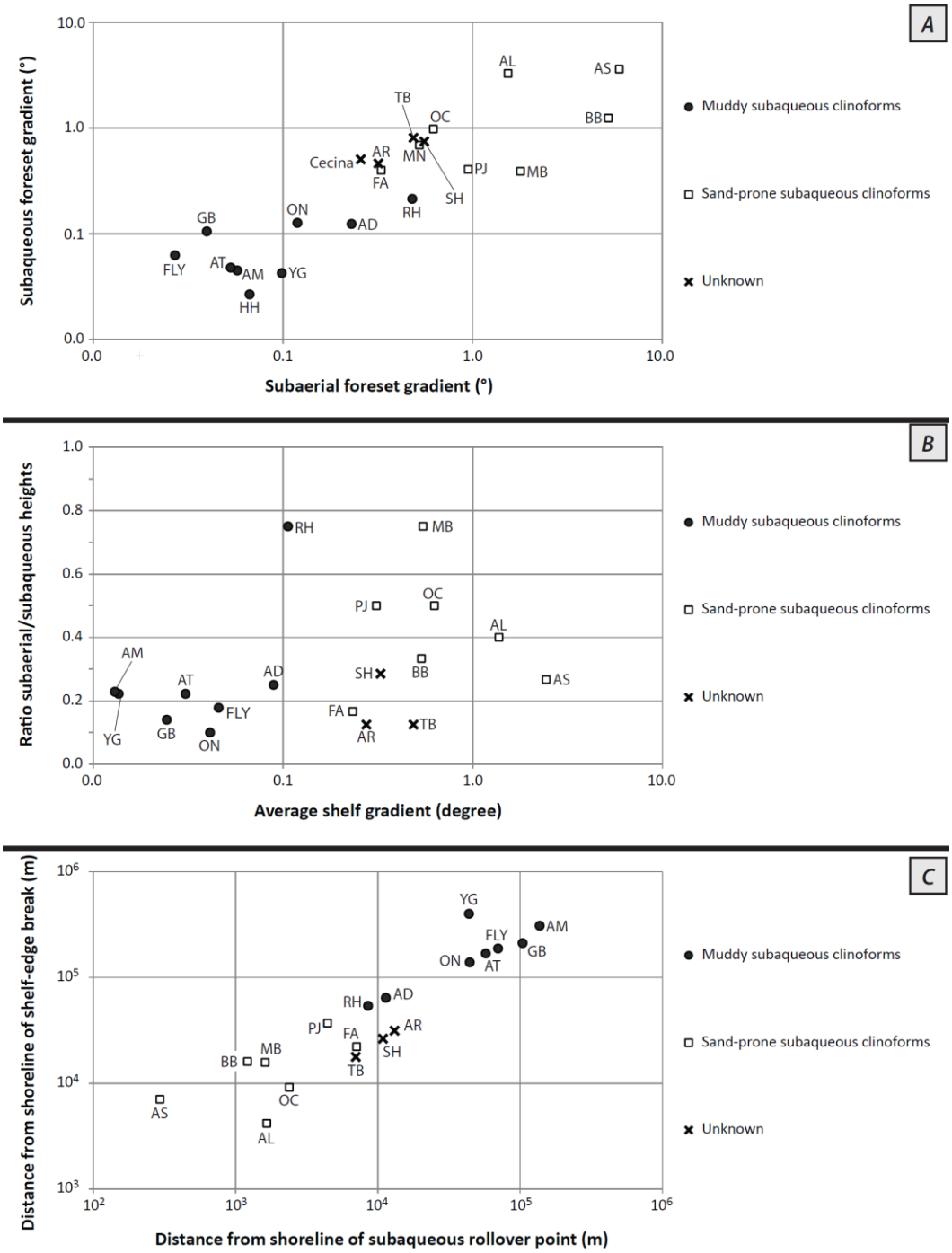

Figure 4.19. *Plots of morphological parameters of recent deltaic compound clinoforms and delta-scale subaqueous clinoforms (Figs. 4.11-4.14): (A) subaqueous clinoform foreset gradient versus subaerial clinoform foreset gradient; (B) ratio of subaerial to subaqueous clinoform heights versus average shelf gradient; and (C) distance from shoreline of shelf-edge break versus distance from shoreline of subaqueous rollover point. Abbreviations for clinoforms and clinoform sets are introduced in Tables 4.1-4.2.*

4.8.3 Implications for sequence stratigraphic models

The recognition of delta-scale subaqueous clinoforms in the stratigraphic record has profound implications for the interpretation of ancient clinoform-bearing strata, because topset-to-foreset rollovers in delta-scale clinoforms are near-universally interpreted as palaeo-shorelines and are thus treated as robust indicators of relative sea-level position. Vertical stacking of delta-scale clinoform sets in seismic data is typically used as evidence for repeated regression and transgression of a palaeo-shoreline (i.e. a subaerial delta) (e.g., Helland-Hansen & Hampson, 2009).

An alternative interpretation of delta-scale compound clinoform geometries is that their subaerial and subaqueous clinoforms were shoreline clinoforms deposited at different times under different relative sea-level conditions (e.g. highstand and lowstand delta clinoforms). This alternative interpretation is particularly troublesome in the case of Quaternary compound clinoforms, because a major sea-level rise (up to 120 m) occurred following the last de-glaciation, at about 7-8 Ka, such that modern subaqueous delta clinoforms superficially resemble Pleistocene subaerial delta clinoforms developed during the last glacial sea-level lowstand. However, direct dating of several mud- and sand-prone subaqueous clinoforms clearly indicates that they were initiated and grew after the attainment of the Late Holocene sea-level highstand (e.g. sand-prone subaqueous clinoforms off south-eastern Australia, southern Iberia, and California; Field & Roy, 1984; Roy et al., 1994; Hernández-Molina et al., 2000a; Le Dantec et al., 2010; muddy subaqueous clinoforms of the Adriatic shelf and Yangtze River delta; Cattaneo et al. 2003, 2007; Liu et al., 2006). Seismically resolved lap-out relationships also indicate development and progradation of subaqueous delta clinoforms after the Late Holocene sea-level highstand (e.g. subaqueous clinoforms off the Manawatu coast, New Zealand and the Tiber River mouth, Italy; Amorosi & Milli, 2001; Dunbar & Barrett, 2005). Thus, recent examples demonstrate that delta-scale compound clinoforms and subaqueous clinoforms are a viable template for interpretation of ancient strata. The diagnostic criteria presented above provide a tool to differentiate subaerial and subaqueous delta-scale clinoforms using subsurface data (cores, wireline logs, seismic data, biostratigraphic and other chronostratigraphic data), and also to indicate whether delta-scale subaqueous clinoforms are sand-prone or mud-prone. Delta-scale subaqueous clinoform trajectories within clinoform sets are likely to directly reflect changes in wave base, which in turn are modulated by variations in both relative sea level and wave climate. The stacking of consecutive delta-scale subaqueous clinoform sets is likely to reflect relative sea-level and sediment supply history, in the same way as stacking of subaerial delta clinoform sets.

The very different time scales over which delta-, shelf edge- and continental margin-scale clinoform systems prograde cause the formation of shelf-edge deltas in <0.15 Myr during relative sea-level stillstands, although shore-parallel marine sediment transport can result in significantly longer shelf-transit times, and may inhibit the

establishment of shelf-edge deltas if river sediment input rates are outpaced by the shelf transport rates (Burgess & Hovius, 1998; Yoshida et al., 2007; Burgess & Steel, 2008; Olariu & Steel, 2009; Helland-Hansen & Hampson, 2009) or even encourage delta autoretreat (*sensu* Muto & Steel, 1992, Muto et al., 2007). In the case of delta-scale subaqueous clinoforms, ascending normal-regressive clinoform trajectories and sediment transport by powerful alongshore currents are likely to cause progressive decrease of across-shelf net-sediment fluxes and progradation rates as the subaqueous delta approaches the shelf-edge. Much of the sediment budget in delta-scale subaqueous clinoform systems is redistributed alongshore rather than across the shelf and towards the shelf break. This pattern is commonly observed in present-day subaqueous deltas, which form laterally extensive (up to 10^2-10^3 km), shore-parallel traps for river-fed sediments on the shelf, at the expense of sediment bypass across the shelf to the basin floor (e.g., in the Yangtze River delta, Liu et al., 2006). As a consequence, the presence of delta-scale subaqueous clinoform sets on an ancient shelf may suggest that sediment storage on the shelf was greater than sediment bypass across the shelf, except where canyons are observed to extend across the shelf to the palaeoseaward limit of the subaqueous delta. Such canyons constitute efficient conduits for the transfer of sediment to the basin floor (e.g., Milliman et al., 1984; Nittrouer et al., 1986; Posamentier et al., 1991; Johnson & Baldwin, 1996; Covault et al., 2007), as observed in the present day Ganges-Brahamaputra subaqueous delta (Kuehl et al., 1997; Michels et al., 1998).

4.9 CONCLUSIONS

Delta-scale subaqueous clinoforms are common features of Holocene-to-modern shelves, but ancient examples are rarely interpreted. The analysis of a quantitative dataset comprising morphological and stratigraphic characteristics of recent and ancient clinoforms of different scales and types indicates that delta-scale subaqueous clinoforms may be distinguished from other clinoform types (e.g., subaerial delta or shoreline clinoforms, shelf-edge and continental margin clinoforms) using a combination of six diagnostic criteria: (1) delta-scale heights of topset (<20 m), foreset (<50 m) and bottomset (<20 m); (2) laterally extensive, shore-parallel plan-view morphology; (3) well-developed topset lacking evidence of subaerial exposures; (4) nearly symmetrical, sigmoidal cross-sectional geometry; (5) relatively uniform clinoform morphology, sediment grain-size, internal facies characteristics and stratigraphic architecture; and (6) predominance of basinal processes, such as waves, storms, tides or oceanographic currents, on sediment dispersal. In addition, strong positive correlations between the water depth of the clinoform topset-to-foreset rollover point and total clinoform relief, clinoform topset

height, clinoform foreset height, and clinoform bottomset height allow delta-scale, shelf edge-scale and continental margin-scale types of clinoform to be distinguished.

Sand-prone and muddy delta-scale subaqueous clinoforms can be further differentiated using morphological parameters. Clinoform topsets, foresets and bottomsets are steeper and tend to have narrower dip extents in sand-prone delta-scale subaqueous clinoforms (respectively 0.1-38° and <2 km) than those of other delta-scale clinoforms (0-1.2° and 1-25 km). The steep clinoform slopes are directly caused by their narrow dip extents. . Due to the stronger mean velocities needed to transport sand-grade sediment, the characteristic water depth of the topset-to-foreset rollover point in sand-prone delta-scale subaqueous clinoforms (ca. 20-60 m) tends to be ca. 10-30 m deeper than in muddy delta-scale subaqueous clinoforms. The distance of the topset-to-foreset rollover point from the shoreline break is about 15 times smaller for modern sand-prone delta-scale subaqueous clinoforms (0.6-7.2 km) than for modern muddy delta-scale subaqueous clinoforms, such that a shoreline-to-subaqueous-rollover distance of 9 km acts as a threshold value between the two types of clinoform. In compound clinoform systems that comprise a subaerial (or shoreline) clinoform and a subaqueous clinoform, the ratio of the foreset heights for the subaerial and subaqueous clinoforms may be used to diagnose the predominant grain size. Sand-prone delta-scale subaqueous clinoforms exhibit subaerial-to-subaqueous foreset height ratios of >0.17, while their muddy counterparts exhibit subaerial-to-subaqueous foreset height ratios of <0.30. There are also significant differences in the depositional settings of modern sand-prone and muddy delta-scale subaqueous clinoforms. Modern sand-prone delta-scale subaqueous clinoforms are situated on narrow (5-32 km) and steep (≥0.26°) shelves, which are up to two orders of magnitude narrower and steeper than shelves hosting muddy subaqueous deltas.

Chronostratigraphic parameters also allow different types of clinoform to be differentiated. Delta-scale, shelf edge-scale and continental margin-scale types of clinoform can be distinguished using strong positive correlations between: (1) the water depth of the clinoform topset-to-foreset rollover point and the time span of clinoform deposition; and (2) the water depth of the clinoform topset-to-foreset rollover point and progradation resistance ratio (ratio between mean vertical sediment accumulation rate and progradation rate, which reflects the amount of sediment that needs to accumulate in order for the clinoform foreset to prograde). Because of the large distance of sand-prone delta-scale subaqueous clinoforms from direct fluvial sediment input points and the sporadic nature of their depositional episodes, average vertical sediment accumulation rates in such clinoforms over short time spans (≤10 kyr) that correspond to progradation of a single clinoform set can be up to two orders of magnitude lower (1-5 x 10^3 m/Myr) than in other delta-scale clinoforms over similar durations. Both clinoform progradation rates (1-5 x 10^2 km/Myr) and unit-width depositional flux (1-15 km^2/Myr) are up to 10^3-10^4 times lower in sand-prone delta-scale subaqueous clinoforms than in subaerial delta clinoforms. Lower rates of progradation relative to aggradation thus typify the outbuilding of sand-prone delta-scale subaqueous systems,

and are reflected in a large spread of short term (<10 kyr) clinoform trajectories (from -0.5° to +2°) and in values of progradation resistance ratio that are up to two orders of magnitude higher (≤3 x 10^{-2}) than those typical of other delta-scale clinoforms.

Our analysis indicates that delta-scale compound clinoforms and subaqueous clinoforms are a viable template for interpretation of ancient strata. These clinoform types can be diagnosed using geomorphological, sedimentological and stratigraphic features that are readily applicable to subsurface data (cores, wireline logs, seismic data, biostratigraphic and other chronostratigraphic data). The capacity to recognise different clinoform types based on seismic geomorphological parameters is particularly important, since seismic data is the pre-eminent tool for analysis of many ancient sedimentary basins. Robust recognition of different clinoform types is significant, because they denote different palaeo-environmental conditions and require different sequence stratigraphic interpretations. For example, the presence of delta-scale subaqueous clinoform sets suggests predominant along-shore sediment transport and correspondingly little sediment bypass to the basin floor. Furthermore, sand-prone delta-scale subaqueous clinoforms are associated with active tectonic settings, whereas muddy delta-scale subaqueous clinoforms are generally associated with tectonic quiescence.

4.10 ACKNOWLEDGEMENTS

We would like to thank Clara Rodriguez Rondon (Imperial College) for valuable suggestions and observations, and Mr. Nicholas Holgate (Imperial College) for comments on a previous draft of this manuscript.

CHAPTER 5

Conclusions

CHAPTER 5: CONCLUSIONS

The Sognefjord Formation is a 10-200 m thick clastic wedge, deposited in ca. 6 Myr during the Callovian to Kimmerdigian, by a fully marine deltaic system that was sourced from the Norwegian mainland. The lower part of the unit comprises wave- and current-dominated, sandstone-rich bedsets, and the upper part is dominated by tide-influenced sandstones. Chapter 2 demonstrates that the lower Sognefjord Formation can be subdivided into a series of regressively-stacked, 10-60 m thick, regressive-transgressive sandstone-rich packages ("series"). These packages are bounded by regionally extensive maximum flooding surfaces, are devoid of subaerial facies and are separated by thin mudstone intervals. Each "series" gradually thickens towards the west until it reaches a maximum, beyond which the upper bounding surface rolls over to define an overall topset-foreset-bottomset geometry. The seismically resolved internal architecture of each "series" consists of a regressive set of westward-dipping subaqueous clinoforms that are linear to curvilinear in plan-view, and strike for several tens of kilometres parallel to the NNE-SSW-oriented Horda Platform edge. Within each clinoform set, near-horizontal trajectories are observed. The sets are stacked according to an overall regressive, concave-landward trajectory in the Middle-Late Oxfordian, whilst the clinoform set stacking patterns changed abruptly to nearly horizontal in the Late Oxfordian. In the eastern half of the field, individual clinoforms are relatively gently dipping (1-6°) and bound thin (10-30 m) clinothems dominated by fine-grained, hummocky cross-stratified sandstones. Towards the west, clinoforms gradually become steeper (5-16°) and bound thicker (15-60 m) clinothems that comprise medium-grained sandstones in their upper parts. Topsets are usually well-developed throughout the study area. Towards the north-east, the coarsest grain-size and the most proximal facies types of the whole Troll Field area have been recognized. These are dominated by cross-bedded, well-sorted, fine- to coarse-grained sandstones and poorly-sorted, very coarse-grained, gravity flow-deposited sandstones, which are interpreted as proximal delta front deposits within subaerial delta clinoforms.

Equations presented in Chapter 3 allow to calculate clinoform age and progradation rates in the Sognefjord Formation along 2D transects that intersect multiple vertical sections and that are aligned parallel to clinoform dip, together with clinoform trajectory and decompacted sediment accumulation and unit-width depositional flux. These equations are based on integrated, quantitative analyses of subsurface data that are constrained by regionally correlatable bioevents. Each clinoform set is characterised by a decrease in progradation rate (from 500 to 30 km/Myr) and net sediment flux (from 90 to 10 km^2/Myr), which is synchronous with increased sediment accumulation rate (from 15 to 70 m/Myr) towards the basin. A minor, renewed rise in depositional flux in the westernmost part of the study area has been identified in the Upper Oxfordian clinoform sets.

Delta-scale, sand-prone subaqueous clinoforms constitute a relatively new and overlooked depositional model for reservoir-forming shallow-marine sandbodies. Recent delta-scale sand-prone subaqueous clinoforms comprise

progradational-aggradational fully submarine clinoforms accumulated in inner shelves (20-60 m water depth at their upper rollover point) during the Late Holocene or Late Pleistocene (Younger Dryas) relative sea-level stillstands. These clinoform types may form compound systems with their subaerial delta clinoform counterparts, but most commonly they onlap onto older substrate material and do not show a direct connection with subaerial deltas and delta-fed sediment input points.

The analysis of a large dataset of recent and ancient shallow-marine clinoforms presented in Chapter 4 indicates that delta-scale sand-prone subaqueous clinoforms are usually elongated parallel to the coastline in plan-view, and are situated on steep (≥0.26°) and narrow (<35 km) submarine shelves, at <8 km from the shoreline itself. Although heights of delta-scale sand-prone subaqueous clinoform foresets (12-43 m), bottomsets and topsets (<20 m) is largely compatible with the values of muddy subaqueous deltas and shoreline/subaerial delta clinoforms, their down-dip extents are ca. 10 times smaller those of other delta-scale clinoforms (<2 km), and their topsets, foreset and bottomsets are steeper (respectively 0.4-5°, 0.7-35°, and 0.4-5°) than other delta-scale clinoform types. Nevertheless, all delta-scale subaqueous clinoforms (including those that are sand-prone) tend to be more sigmoidal than the classically oblique cross-sectional geometries of subaerial deltas. Furthermore, because of the distance from direct sediment input points and of the sporadic nature of depositional episodes, average progradation rates and unit-width depositional flux in sub-Milankovitch time spans are up to 3-4 orders of magnitude lower than in equivalent subaerial deltas.

These anomalies constitute potential diagnostic criteria to assist in the recognition of ancient delta-scale sand-prone subaqueous clinoforms by exploiting seismic, sedimentological and/or stratigraphical data, and to envisage a realistic architectural and depositional model tied to modern examples once this interpretation has been made. For example, the data presented in Chapter 4 suggest that the Jurassic shallow-marine Sognefjord Formation (offshore Norway) and Bridport Sand Formation (onshore UK) subsurface reservoirs most likely contain delta-scale sand-prone subaqueous clinoforms, whereas the Cretaceous Blackhawk Formation and Mancos Shale in Utah (U.S.) provides a probable outcrop example of delta-scale compound clinoforms with a muddy subaqueous component.

In particular, for the lower Sognefjord Formation (Chapter 2), it is inferred that fully-subaqueous, NNE-SSW-striking, elongated delta-scale subaqueous clinoforms prograded westwards across a westward-deepening, shallow sea-floor. As is common in most recent delta-scale subaqueous clinoforms, the direction of clinoform progradation is approximately perpendicular to the inferred sediment transport direction. Each clinoform set became coarser grained and was characterized by narrower topsets and taller, steeper foresets as the subaqueous delta prograded from the inner part of the Horda Platform towards its western limit, which was directly exposed to wave (and storm) attack. The absence of coastal plain deposits and evidence of subaerial

exposure supports the interpretation of subaqueous clinoforms, although their removal from the top of each clinoform set by transgressive erosion cannot be completely discounted. The time-equivalent shoreline lay beyond the eastern boundary of the study area. Sand-rich sediment was likely supplied to the subaqueous clinoform system by a river outlet situated at or beyond north-eastern part of the study area, and then transported by the action of alongshore advective currents that flowed sub-parallel to clinoform strike. Changes in progradation, sediment accumulation and unit-width depositional flux within each clinoform set (Chapter 3), suggest that the subaqueous delta was subject to increased interaction with shore-parallel marine currents as it advanced across the open shelf, and these currents probably transported a significant proportion of river-fed sediments along the shelf and out of the study area, as well as sculpting the linear, elongated clinoforms. In Series 2 and 5 clinoform sets, localised spatial and temporal departures from the trends in rates described above are attributed to the effects of rift-related normal faulting during deposition, as supported by backstripping analysis and seismic isochron mapping (Chapter 3).

The model of delta-scale coarse-grained subaqueous clinoforms provides a viable interpretative template that may be applicable to other ancient shallow-marine clinoforms with reservoir potential. The very existence of delta-scale sand-prone subaqueous clinoform sets indicates that delta-scale clinoforms in the rock record or in seismic reflection data, in the absence of a full facies and geomorphological characterisation to provide context, should not be automatically linked to ancient shoreline positions, even if they are sand-rich, as their rollovers may have actually formed at up to 60 m water depth. Furthermore, this depositional model emphasises that sediment distribution and clinoform architecture in deltaic settings are controlled by the dynamic interplay between the bathymetric configuration of the receiving basin, the volume and grain size of sediment input, and the direction and power of basinal processes such as waves, tides, and surface and bottom currents, in addition to relative sea-level changes.

Calculation of progradation rates provides a tool to improve reservoir characterisation and near-field exploration by enhancing prediction of reservoir distribution and character. For example, in the Sognefjord Formation case study, the progressive basinward decrease of both clinoform progradation and unit-width depositional flux within each Lower-Middle Oxfordian clinoform set, together with the concave-landward clinoform-set-stacking trajectory, suggest that long-term autoretreat mechanisms were likely governing the deposition of these delta-scale clinoforms, and may also reflect strong shore-parallel sediment transport, which hindered further progradation. In similar cases, delivery of delta-fed sediments to deep-marine settings is not likely, even in the presence of short-term descending clinoform trajectories, and most of these sediments should be sought along-strike rather than perpendicular to the shelf.

Localised anomalies in spatial and temporal progradation rates may indicate minor phases of rift-related normal faulting (even below seismic resolution). For example, the anomalous depositional flux and progradation rate peaks in the westernmost study area within the Upper Oxfordian Sognefjord Formation clinoform set, together with a sudden decrease of clinoform-set stacking trajectories, is attributed to a combination of sediment bypass across uplifted fault blocks in the western parts of the Troll Field, and to more rapid export of sediment from the hinterland in western onshore Norway. Both of these events are consistent with a period of rift activity during Late Oxfordian times, which has been documented in nearby areas.

5.1 Recommendations for future work

The research work presented in this thesis gives rise to new questions and opportunities to address in the future. These deal with both generic stratigraphic-sedimentological issues and with the North Sea basin evolution.

The framework provided by chapters 3 and 4 of this thesis allows exploiting seismic geomorphological, stratigraphic and sedimentological datasets in order to: (1) identify ancient examples of delta-scale subaqueous clinoform sets; and (2) estimate rates of progradation, aggradation and depositional flux of prograding shallow-water clinoform sets. This provides useful bases to work for the future (re-)assessments of other shallow-marine units throughout the globe as delta-scale subaqueous clinoforms, as well as highlighting their depositional rates and provenance. Revaluating depositional models of existing shallow-marine sand-prone reservoir units could mean very different predictions on shallow- and deep-marine sandstone distribution. This would be crucial for both hydrocarbon production in mature shallow-water provinces and exploration in shallow- and deep-marine areas surrounding them. Due to peaking oil production in the early 2010s (IEA, 2010), next decades are expected to be challenging years for hydrocarbon exploration and production, as well as for the global economy as a whole. The economic and scientific value for pursuing this kind of studies is hence self-evident.

Software that may automatize the implementation of the well-based chronostratigraphic method presented in Chapter 3 may be easily programmed. Any interested party possessing lithostratigraphic and chronostratigraphic well data along cross-sections oriented roughly parallel to the depositional dips of shallow-water clinothems, may easily type them into this piece of software and obtain estimates of the depositional rates as outputs, as well as plan-view and cross-sectional representations of them.

A possibility exists that the relative movement of delta-scale subaqueous clinoforms reflect variations of fair-weather wave base depths, which in turns are mostly controlled by changes of relative sea level and wave climate. Therefore, specific studies on the behaviour of modern and ancient delta-scale subaqueous clinoforms and their compounded shorelines are needed. In particular, how different the clinoform trajectories of the two clinoform systems are? Can trajectories of any delta-scale clinoforms be utilized as (direct or indirect) proxies of relative shoreline movement and sea-level changes? For this purpose, clinoform trajectories of systems with a wealth of seismic-stratigraphic, geomorphological, sedimentological and stratigraphic data exist (e.g., Po-Adriatic-Gargano clinoforms, Ganges-Brahmaputra, southern Iberia coastlines, Blackhawk Formation clinoforms) should be characterized both in their subaerial delta and subaqueous delta components. Oceanographic data associated with the modern systems should clarify what the driving forces behind the short-term and long-term clinoform migrations are.

Lastly, the data presented in Chapter 3 suggest that the Late Jurassic rifting in the Troll Field area comprises a succession of fault-block rotational pulses and longer quiescent phases. In the time-interval analysed, the age of the rotation pulses on the Horda Platform (Late Callovian, Late Oxfordian, Kimmeridgian) is consistent with the timing of higher-magnitude fault-block rotational stages in nearby tectonic 'terraces' (cf., Færseth & Ravnås, 1998; Nøttvedt et al., 2000; Ravnås et al., 2000). Additional studies are advised in order to test whether this timing is consistent with other Northern North Sea areas, and how it compares with the general models of evolution and propagation of rifting (e.g., Cowie, 1998; Gawthorpe & Leeder, 2000; McLeod et al., 2000). Recognition of rotational events below seismic resolution can be aided by estimating chronostratigraphically-constrained rates based on well data, following the method proposed in Chapter 3.

REFERENCE LIST

REFERENCES (total = 285)

Abreu, V., Neal, J., Blum, M., Marftin, J., 2010. Accommodation succession method and the meaning of sequence stratigraphic surfaces. American Association of Petroleum Geologists (AAPG) 2010 Annual Conention and Exhibition,Abstract volume, New Orleans, Louisiana (U.S.A.), 11-14 April 2010, 1-2.

Adams, E.W., Schlager, W., 2000. Basic types of submarine slope curvature. Journal of Sedimentary Research 70, 814-828.

Ainsworth, R.B., Vakarelov, B.K., Nanson, R.A., 2011. Dynamic spatial and temporal prediction of changes in depositional processes on clastic shorelines: Towards improved subsurface uncertainty reduction and management. AAPG Bulletin 95, 267–297.

Alexander, C.R., DeMaster, D.J., Nittrouer, C.A., 1991. Sediment accumulation in a modern epicontinental-shelf setting: the Yellow Sea. Marine Geology 998, 51-72.

Allen, P.H., Allen, J.R., 2005. Chapter 9 – Subsidence and thermal history. Basin Analysis, Principles and Applications, Second Edition, Blackwell Publishing, 349-395.

Amorosi, A., Milli, S., 2001. Late Quaternary depositional architecture of Po and Tevere river deltas (Italy) and worldwide comparison with deltaic successions. Sedimentary Geology 144, 357-375.

Asquith, D.O., 1970. Depositional topography and major marine environments, Late Cretaceous, Wyoming. AAPG Bulletin 54, 1184-1224.

Athy, L.F., 1930. Density, porosity and compaction of sedimentary rocks. Bulletin American Association of Petroleum Geologists 14, 1-24.

Austin, J.A., JR., Uchupi, E., 1982. Continental-oceanic crustal transition off Southwest Africa. American Association of Petroleum Geologists Bulletin 66, 1328–1347.

Badley, M. E., Price, J. D., Rambech Dahl, C., Agdestein, T., 1988. The structural evolution of the northern Viking Graben and its bearing upon extensional models of graben formation. Journal of the Geological Society, London, 145, 455-472.

Baily, B., Pearson, A.W., 2007. Change detection mapping and analysis of salt marsh areas of Central Southern England from Hurst Castle Spit to Pagham Harbour. Journal of Coastal Research 23, 1549-1564.

Baldwin, B., Butler, C.O., 1985. Compaction curves. AAPG Bulletin 69, 622-626.

Barrell, J., 1912. Criteria for the recognition of ancient delta deposits. Geological Society of America Bulletin, 23, 377-446.

Bates, C.C., 1953. Rational theory of delta formation. American Association of Petroleum Geologists Bulletin 37, 2119-2162.

Bell, D.G., Bjærkø, T., Selnes, H. and Skarbø, O., 1984a. Well 31/3-2: biostratigraphy kerogen analysis prepared for Norsk Hydro a.s., Stratlab a.s. stratigraphical laboratory consultants in stratigraphy. Available online on:

http://www.npd.no/engelsk/cwi/pbl/wellbore_documents/100_03_31_3_2_Biostrat._kerogen_analysis_by_Stratlab.pdf

Bell, D.G., Bjærkø, T., Selnes, H. and Skarbø, O., 1984b. Well 31/6-6: biostratigraphy kerogen analysis prepared for Statoil a.s., Stratlab a.s. stratigraphical laboratory consultants in stratigraphy. Available online on: http://www.npd.no/engelsk/cwi/pbl/wellbore_documents/127_03_31_6_6_Biostratigraphy_Kerogen_Analysis.pdf

Bentley, S.J., 2003. Wave-current dispersal of fine-grained fluvial sediments across continental shelves: the significance of hyperpycnal plumes. In: Scott, E.D., Bouma, A.H., Bryant, W.R. (Eds.), Siltstones, mudstones and shales: depositional processes and characteristics. SEPM/Gulf Coast Association of Geological Society Joint Publication, 35–48.

Bhattacharya, J.P., Giosan, L., 2003. Wave-influenced deltas: geomorphological implications for facies reconstruction. Sedimentology 50, 187-210.

Bhattacharya, J.P., 2006. Deltas. In: Walker, R.G., Posamentier, H. (Eds.), Facies Models Revisited. SEPM (Society for Sedimentary Geology) Special Publications, Tulsa (Oklahoma), 84, pp. 237-292.

Bornhold, B.D., Yang, Z.-S., Keller, G.H., Prior, D.B., Wiseman, W.J., Wright, L.D., 1986. The sedimentary framework of the modern Huanghe (Yellow River) Delta. Geo-Marine Letters 6, 77-83.

Bowen, A.J., Inman, D.L., 1969. Rip currents 2: laboratory and field evidence. Journal of Geophysical Research 74, 5479–5490.

Bristow, C.S., Pucillo, K., 2006. Quantifying rates of coastal progradation from sediment volume using GPR and OSL: the Holocene fill of Guichen Bay, south-east South Australia. Sedimentology 53, 769-788.

Bullimore, S., Henriksen, S., Liestøl, F., Helland-Hansen, W., 2005. Clinoform stacking patterns, shelf-edge trajectories and facies associations in theTertiary coastal deltas, offshoreNorway. implications for the prediction of lithology in prograding systems. Norwegian Journal of Geology 85, 169-187.

Bullimore, S.A., Helland-Hansen, W., Henriksen, S., Steel, R.J., 2008. Shoreline trajectory and its impact on coastal depositional environments: an example from the Upper Cretaceous Mesaverde Group, NW Colorado. In: Hampson, G.J., Steel, R.J., Burgess, P.M., Dalrymple, R.W. (Eds.), Recent Advances in Models of Siliciclastic Shallow-Marine Stratigraphy. SEPM Special Publication 90, pp. 209-236.

Burgess, P.M., Hovius, N., 1998. Rates of delta progradation during highstands; consequences for timing of deposition in deep-marine systems. Journal of Geological Society 155, 217-222.

Burgess, P.M., Lammers, H.,Van Oosterhout, C., Granjeon, D., 2006. Multivariate sequence stratigraphy. tackling complexity and uncertainty with stratigraphic forward modeling, multiple scenarios, and conditional frequency maps. AAPG Bulletin 90, 1883-1901.

Burgess, P.M., Steel, R.J., 2008. Stratigraphic forward modelling of delta auto-retreat and shelf width: implications for controls on shelf width and timing of formation of shelf-edge deltas. In: Hampson, G.J., Steel, R.J.,

Burgess, P.M., Dalrymple, R.W. (Eds.), Recent Advances in Models of Siliciclastic Shallow-Marine Stratigraphy. SEPM Special Publication 90, pp. 35-45.

Cant, D.J., 1991. Geometric modelling of facies migration: theoretical development of facies successions and local unconformities. Basin Research 3, 51-62.

Carter, R.M., 1988. Post-breakup stratigraphy of the Kaikoura Synthem (Cretaceous–Cenozoic), continental margin, southeastern New Zealand. New Zealand Journal of Geology and Geophysics 31, 405–429.

Carvajal, C., Steel, R.S., 2006. Thick turbidite successions from supply-dominated shelves during sea-level highstand. Geology 34, 665-668.

Carvajal, C., Steel, R.S., 2009. Shelf-edge architecture and bypass of sand to deep water: influence of shelf-edge processes, sea level and sediment supply. Journal of Sedimentary Research 79, 652-672.

Cattaneo, A., Correggiari, A., Langone, L., Trincardi, F., 2003. The late-Holocene Gargano subaqueous delta, Adriatic shelf: Sediment pathways and supply fluctuations. Marine Geology 193, 61-91.

Cattaneo, A., Trincardi, F., Langone, L., Asioli, A., Puig, P., 2004. Clinoform Generation on Mediterranean Margins. Oceanography 17, 4, 104-117.

Cattaneo, A., Trincardi, F., Asioli, A. and Correggiari, A., 2007. The western Adriatic shelf clinoform: energy-limited bottomset. Continental Shelf Research 27, 506-525.

Catuneanu, O., Abreu, V., Bhattacharya, J.P., Blum, M.D., Dalrymple, R.W., Eriksson, P.G., Fielding, C.R., Fisher, W.L., Galloway, W.E., Gibling, M.R., Giles, K.A., Holbrook, J.M., Jordan, R., Kendall, C.G.St.C., Macurda, B., Martinsen, O.J., Miall, A.D., Neal, J.E., Nummedal, D., Pomar, L., Posamentier, H.W., Pratt, B.R., Sard, J.F., Shanley, K.W., Steel, R.J., Strasser, A., Tucker, M.E., Winker, C., 2009. Towards the standardization of sequence stratigraphy. Earth-Science Reviews, 92:1-2, 1-33.

Charvin, K., Hampson, G.J., Gallagher, K.L., Labourdette, R., 2010. Intra-parasequence architecture of an interpreted asymmetrical wave-dominated delta. Sedimentology 57, 760-785.

Chin, J.L., Clifton, H.E., and Mullins, H.T., 1988. Seismic stratigraphy and late Quaternary shelf history, south-central Monterey Bay, California. Marine Geology 81, 137–157.

Christiansson, P., Faleide, J.I., Berge, A.M., 2000. Crustal structure in the northern North Sea: An integrated geophysical study. In: Nøttvedt, A. (Ed.), Dynamics of the Norwegian Margin. Geological Society, London, pp. 15-40.

Clifton, H.E., 1969. Beach lamination: Nature and origin. Marine Geology 7, 553-559.

Clifton, H.E., 1976. Wave-formed sedimentary structures – a conceptual model. In: Davis, R.A.J., Ethington, R.L. (Eds.), Beach and nearshore sedimentation. SEPM Special Publication 24, pp. 126–148.

Correggiari, A., Cattaneo, A., Trincardi, F., 2005. The modern Po Delta system: lobe switching and asymmetric prodelta growth. Marine Geology 222-223, 49-74.

Covault, J.A., Normark, W.R., Romans, B.W., Graham, S.A., 2007. Highstand fans in the California borderland: The

overlooked deep-water depositional systems. Geology, 35, 783-786.

Coward, M.P., Dewey, J., Hempton, M. and Holroyd, J., 2003. Tectonic evolution of the North Sea. In: Evans, D., Graham, C., Armour, A., Bathurst, P. (Eds.), The Millennium Atlas: petroleum geology of the central and northern North Sea. Geological Society of London, London, pp. 2,1-2,19.

Cowie, P.A., 1998. A healing-reloading feedback control on the growth rate of seismogenic faults. Journal of Structural Geology 20, 1075-1087.

Curray, J., 1964. Transgressions and regressions. In: Miller, R. (Ed.), Papers in Marine Geology. Macmillan, NewYork, pp. 175-203.

Dalrymple, R.W., 2005. The offshore transport of mud: why it doesn't happen and the stratigraphic implications (abstract). In: Salt Lake City Annual Meeting (October 16-19, 2005), 37, 403. GSA, Abstracts with Programs.

Damuth, J.E., Flood, R.D., Kowsmann, R.O., Belderson, R.H., Gorini, M.A., 1988. Anatomy and growth pattern of Amazon deep-sea fan as revealed by long-range side-scan sonar (GLORIA) and high-resolution seismic studies: American Association of Petroleum Geologists Bulletin, 72, 885–911.

Deibert, J.E., Benda, T., L_seth, T., Schellpeper, M., Steel, R.J., 2003. Eocene clinoform growth in front of a storm-wave-dominated shelf, Central Basin, Spitsbergen: no significant sand delivery to deepwater areas. Journal of Sedimentary Research, 73, 546-558.

Doré, A.G., 1992. Synoptic palaeogeography of the Northeast Atlantic Seaway: late Permian to Cretaceous. In: Parnell, J. (Ed.), Basins on the Atlantic Seaboard: Petroleum Geology, Sedimentology and Basin Evolution. Geological Society of London, Special Publications, 62, pp. 421-446.

Dott, R.H., Bourgeois, J., 1982. Hummocky stratification: Significance of its variable bedding sequences. Geological Society of America Bulletin 93, 663-680.

Drake, D.E., Cacchione, D.A., Karl, H.E., 1985. Bottom currents and sediment transport on the San Pedro shelf, California. Journal of Sedimentary Petrology 55, 15-28.

Dreyer, T., Whitaker, M., Dexter, J., Flesche, H., Larsen, E., 2005. From spit system to tide dominated delta: integrated reservoir model of the upper Jurassic Sognefjord Formation on the Troll West Field. In: Doré, A.G., Vining, B. (Eds.), Petroleum Geology of North-West Europe and Global Perspectives, Proceedings of the 6th Petroleum Geology Conference, Geological Society of London, London, pp. 1-26.

Driscoll, N.W., Karner, G.D., 1999. Three-dimensional quantitative modelling of clinoform development. Marine Geology 154, 383-398.

Duke, W.L., 1985. Hummocky cross-stratification, tropical hurricanes, and intense winter storms. Sedimentology 32, 167-194.

Duxbury, N., Fenton, J.P.G. and Tooby, K.M., 1984a. Statoil 31/3-1 Norwegian North Sea well: palynofacies and palynostratigraphy of the interval 1322.50m (SWC) – 1800.00m (SWC), Robertson Research Int. Ltd. Available online on:

http://www.npd.no/engelsk/cwi/pbl/wellbore_documents/20_31_3_1_Palynofacies_and_stratigraphy.pdf

Duxbury, N., Fenton, J.P.G., Tooby, K.M., Rich, B.E., 1984b. Statoil 31/6-2 Norwegian North Sea well: palynofacies and palynostratigraphy of the interval 1332.50m (SWC) – 1846.00m (SWC), Robertson Research Int. Ltd. Available online on: http://www.npd.no/engelsk/cwi/pbl/wellbore_documents/34_03_31_6_2_Palynofacies_and_Palynostratigraphy_interval_1332-1846m.pdf

Dunbar, G.B., Barrett, P.J., 2005. Estimating palaeobathymetry of wave-graded continental shelves from sediment texture. Sedimentology 52, 253–269.

Eberli, G.P., Swart, P.K., Malone, M.J., 1997. Proceedings of the Ocean Drilling Program, Initial Reports. College Station, Texas. Ocean Drilling Program, 166.

Embry, A., 1995. Sequence boundaries and sequence hierarchies: problems and proposals. In: Steel, R.J., Felt, V.F., Johannesson, E.P., Mathieu, C. (Eds.), Sequence Stratigraphy on the Northwest European Margin, Norwegian Petroleum Society Special Publication 5, pp. 1-11.

Evans, O.F.,1942. The origin of spits, bars, and related features. In: Schwarts, M.L. (Ed.), Spits and Bars. Dowden, Hutchinson and Ross, Stroudsburg, P.A., pp. 53-72.

Færseth, R.B., Ravnås, R., 1998. Evolution of the Oseberg Fault-Block in the context of the northern North Sea structural framework. Marine and Petroleum Geology 15, 467-490.

Færseth, R. B., 1996. Interaction of Permo-Triassic and Jurassic fault-blocks during the development of the northern North Sea. Journal of Geological Society, London 153, 931-944.

Fernández-Salas, L.M., Dabrio, C.J., Goy, J.L., Díaz Del Río, V., Zazo, C., Lobo, F.J., Sanz, J.L., Lario, J., 2009. Land-sea correlation between Late Holocene coastal and infralittoral deposits in the SE Iberian Peninsula (Western Mediterranean). Geomorphology 104, 4–11.

Field, M.E., Roy, P.S., 1984. Offshore transport and sand-body formation: evidence from a steep, high-energy shoreface, southeastern Australia. Journal of Sedimentary Petrology 54, 1292–1302.

Flemming, B.W., 1981. Factors controlling shelf sediment dispersal along the south- east African continental margin. Marine Geology, 42, 259-277.

Flood, R.C., Manley, P.L., Kowsmann, R.O., Appi, C.J., Pirmez, C., 1991. Seismic facies and late Quaternary growth of the Amazon submarine fan. In: Weimer, P. Links, M.H. (Eds), Seismic facies and sedimentary processes of modern and ancient submarine fans and turbidite systems. New York, Springer-Verlag, 247–272.

Fossen, H., Mangerud, G., Hesthammer, J., Bugge, T., Gabrielsen, R. H., 1997. The Bjorøy Formation: a newly discovered occurrence of Jurassic sediments in the Bergen Arc System. Norsk Geologisk Tidsskrift 77, 269-288.

Fraser, S.I., Robinson, A.M., Johnson, H.D., Underhill, J.R., Kadolski, D.G.A., Connell, R., Johannessen, P., Ravnås, R., 2003. Upper Jurassic. In: Evans, D., Graham, C., Armour, A., Bathurst, P. (Eds.), The Millennium Atlas:

petroleum geology of the central and northern North Sea. Geological Society of London, London, pp. 157-189.

Friedrichs, C.T., Scully, M.E., 2007. Modeling deposition by wave-supported gravity flows on the Po River prodelta: From seasonal floods to prograding clinoforms. Continental Shelf Research 27, 322-337.

Friedrichs, C.T., Wright, L.D., 2004. Gravity-driven sediment transport on the continental shelf: implications for equilibrium profiles near river mouths. Coastal Engineering 51, 795–811.

Galloway, W.E., 1975. Process framework for describing the morphologic and stratigraphic evolution of deltaic depositional systems. In: Broussard, M.L. (Ed.), Deltas: Models for exploration. Houston Geological Society, Houston, pp. 87-98.

Galloway, W.E., 1989. Genetic stratigraphic sequences in basin analysis 1: architecture and genesis of flooding-surface bounded depositional units. AAPG Bulletin 73, 125-142.

Galloway, W.E., 2001. Seismic expressions of deep- shelf depositional and erosional morphologies, Miocene Utsira Formation, North Sea Basin. Marine Geophysical Researches 22, 309-321.

Gawthorpe, R.L., Fraser, A.J., Collier, R.E.L., 1994. Sequence stratigraphy in active extensional basins: implications for the interpretation of ancient basin-fills. Marine Petroleum Geology 11, 642-658.

Gawthorpe, R.L., Leeder, M.R., 2000. Tectono-sedimentary evolution of active extensional basins. Basin Research 12, 195-218.

Gensous, B., M. Tesson, 1997. Les dépôts postglaciaires de la plate-forme rhodanienne. organisation stratigraphique et conditions de mise en place. Académie des Sciences de Paris, Comptes Rendus, Série 2, 325, 695–701.

Gilbert, G.K., 1885. The topographic feature of lake shores. U.S. Geological Survey, Annual Report 5, 104-108.

Gilbert, G. K., 1890. Lake Bonneville. U.S. Geological Survey Monograph 1, 1-438.

Goldring, R., Bridges, P., 1973. Sublittoral sheet sandstones. Journal of Sedimentary Petrology 43, 736-747.

Gradstein, F.G., Ogg, J.G., Smith, A.G., 2004. A Geological Time Scale 2004. Cambridge University Press, Cambridge UK, pp. 1-599.

Gruszczyński, M., Rudowski, S., Semil, J., Skominski, J., Zrobek, J., 1993. Rip currents as a geological tool. Sedimentology 40, 217-236.

Hampson, G.J., 2000. Discontinuity surfaces, clinoforms, and facies architecture in a wave-dominated, shoreface-shelf parasequence. Journal of Sedimentary Research 70, 325-340.

Hampson, G.J., 2010. Sediment dispersal and quantitative stratigraphic architecture across an ancient shelf. Sedimentology 57, 96-141.

Hampson, G.J., Rodriguez, A.B., Storms, J.E.A., Johnson, H.D., Meyer, G.T., 2008. Geomorphology and high-resolution stratigraphy of progradational wave-dominated shoreline deposits: impact on reservoir-scale

facies architecture. In: Hampson, G.J., Steel, R.J., Burgess, P.M., Darlymple, R.W. (Eds.), Recent advances in models of siliciclastic shallow-marine stratigraphy. SEPM Special Publication 90, 117-142.

Hampson, G.J., Storms, J.E.A., 2003. Geomorphological and sequence stratigraphic variability in wave-dominated, shoreface-shelf parasequences. Sedimentology 50, 667-701.

Hampson, G.J., Sixsmith, P.J., Kieft, R.L., Jackson, C.A.-L., Johnson, H.D., 2009. Quantitative analysis of net-transgressive shoreline trajectories and stratigraphic architectures: mid-to -late Jurassic of the North Sea Rift Basin. Basin Research 21, 528-588.

Haq, B.U., Hardenbol, J., Vail, P.R., 1988. Mesozoic and Cenozoic chronostratigraphy and cycles of sea-level change. In: Wilgus, C.K., Hastings, B.S., Kendall, C.G.St.C., Posamentier, H.W., Ross, C.A., Van Wagoner, J.C. (Eds.), Sea-Level Changes -An Integrated Approach. SEPM Special Publication 42, 71-108.

Hardenbol, J., Thierry, J., Farley, M. B., Jacquin, T., de Graciansky, P. C., Vail, P., 1998. Mesozoic and Cenozoic sequence chronostratigraphic framework of European basins. In: Graciansky, P.C.M Hardenbol, J., Jaquin, T., Vail, P.R. (Eds.), Mesozoic and Cenozoic Sequence Stratigraphy of European Basins. SEPM Special Publication 60, 3-13, charts 1-8.

Hedberg, H.G., 1936. Gravitational compaction of clays and shales. American Journal of Science 31, 241-287.

Heezen, B.C., Menzies, R.J., Schneider, E.D., Ewing, W.M., Granelli, N.C.L., 1964. Congo submarine canyon: American Association of Petroleum Geologists Bulletin, 48, 1126–1149.

Helland-Hansen, W., Gjelberg, J.G., 1994. Conceptual basis and variability in sequence stratigraphy: a different perspective. Sedimentary Geology 92, 31-52.

Helland-Hansen, W., Hampson, G.J., 2009. Trajectory analysis: concepts and applications. Basin Research 21, 454-483.

Helland-Hansen, W., Martinsen, O.J., 1996. Shoreline trajectories and sequences: description of variable depositional dip scenarios. Journal of Sedimentary Research B66, 670-688.

Helland-Hansen, W., Steel, R.J., Sømme, T.O., 2012. Shelf genesis revisited. Journal of Sedimentary Research, 82, 133-148.

Hellem, T., Kjemperud, A., Øvrebø, O.K., 1986. The Troll Field: A geological/geophysical model established by PL. 085. In: Spencer, A.M. (Ed.), Habitat of Hydrocarbons on the Norwegian Continental Shelf. Norwegian Petroleum Society and Graham & Trotman, London, pp. 217-238.

Henriksen S., Hampson, G.J., Helland-Hansen, W., Johannessen, E.P., Steel, R.J., 2009. Shelf edge and shoreline trajectories, a dynamic approach to stratigraphic analysis. Basin Research 21, 445-453.

Hernández-Molina, F.J., Fernández-Salas, L.M., Lobo, F., Somoza, L., Díaz-del-Río, V., Alveirinho Dias, J.M., 2000a. The infralittoral prograding wedge. a new large-scale progradational sedimentary body in shallow marine environments. Geo-Marine Letters 20, 109-117.

Hernández-Molina, F.J., Somoza, L., Lobo, F., 2000b. Seismic stratigraphy of the Gulf of Cadiz Continental Shelf: a model for Late Quaternary very high-resolution sequence stratigraphy and response to sea-level fall. In: Hunt, D., Gawthorpe, R.L. (Eds.), Sedimentary Responses to Forced Regression. Geological Society of London Special Publication 172, London, pp. 329-362.

Hogarth, L.J., Babcock, J., Driscoll, N.W., Dantec, N.L., Haas, J.K., Inman, D.L., Masters, P.M., 2007. Long-term tectonic control on Holocene shelf sedimentation offshore La Jolla, California. Geology 35, 275–278.

Hori, K., Saito, Y., Zhao, Q., Cheng, X., Wang, P., Sato, Y., Li, C., 2001. Sedimentary facies and Holocene progradation rates of the Cahngjiang (Yangtze) delta, China. Geomorphology 41, 233-248.

Howard, J.D., Reineck, H.-E., 1981. Depositional facies of high-energy beach-to-offshore sequence: comparison with low-energy sequence. AAPG Bulletin 65, 807-830.

Howell, J.A., Skorstad, A., MacDonald, A.C., Fordham, A., Flint, S.S., Fjellvoll, B., Manzocchi, T., 2008. Sedimentological parameterization of shallow-marine reservoirs. Petroleum Geoscience 14, 17-34.

Hunter, R.E., Clifton, H.E. Phillips, R.I., 1979. Depositional processes, sedimentary structures, and predicted vertical sequences in barred nearshore systems, southern Oregon coast. Journal of Sedimentary Petrology 49, 711-726.

Hunt, D., Tucker, M.E., 1992. Stranded parasequences and the forced regressive wedge systems tract: deposition during base-level fall. Sedimentary Geology 81, 1-9.

Hurst, A. R., Morton, A. C., 1988. An application of heavy-mineral analysis to lithostratigraphy and reservoir modelling in the Oseberg field, northern North Sea. Marine and Petroleum Geology 5, 157–169.

IAE (International Energy Agency), 2010. World Energy Outlook 2010. Available online on: http://www.worldenergyoutlook.org/

Ito, M., Masuda, F., 1988. Late Cenozoic deep-sea to fan-delta sedimentation in an arc-arc collision zone, central Honshu, Japan; sedimentary response to varying plate-tectonic regime. In: Nemec, W., Steel, R.J. (Eds.), Fan deltas: sedimentology and tectonic settings. Blackie and Son, Glasgow, UK, 400–418.

James, N.P., Von Der Borch, C.C., 1991. Carbonate shelf edge off southern Australia: A prograding open-platform margin. Geology 19, 1005–1008.

Jansa, L.F., 1991. Lithostratigraphy; 10, Carbonate buildup morphology. In: Bates, J.L. (Ed.), East Coast Basin Atlas Series, Scotian Shelf. Geological Society of Canada, Frontier Geoscience Program, pp. 69–70.

Jensen, M., Larsen, E., 2009. Shoreline trajectories on glacially influenced stable margin: insight from the Barents Sea Shelf, NW Russia. In: Henriksen, S., Hampson, G.J., Helland-Hansen, W., Johannessen, E.P., Steel, R.J. (Eds.), Trajectory Analysis in Stratigraphy. Basin Research 21(5), 759-779.

Johannessen, E.P., Steel, R.J., 2005. Shelf-margin clinoforms and prediction of deepwater sands. Basin Research 15, 521-550.

Johnson, H.D., Baldwin, C.T., 1996. Shallow clastic seas. In: Reading, H.G. (Ed.), Sedimentary environments: Processes, facies and stratigraphy. Blackwell Science, Oxford, 232–280.

Jol, H.M., Lawton, D.C., Smith, D.G., 2002. Ground penetrating radar: 2-D and 3-D subsurface imaging of a coastal barrier spit, Long Beach, WA, USA. Geomorphology 53, 165-181.

Kassem, A., Imran, J., 2001. Simulation of turbid underflows generated by the plunging of a river. Geology 29, 655-658.

Kenyon, P.M., Turcotte, D.L., 1985. Morphology of a delta by bulk sediment transport Geological Society of America Bulletin, 96, 1457-1465.

Kenter, J.A.M., 1990. Carbonate platform flanks: slope angle and sediment fabric. Sedimentology 37, 777-794.

Khripounoff, A., Vangriesheim, A., Babonneau, N., Crassous, P., Dennielou, B. , Savoye, B., 2003. Direct observation of intense turbidity current activity in the Zaire submarine valley at 4000 m water depth. Marine Geology 194, 151–158.

Kneller, B.C., Branney, M.J., 1995. Sustained high-density turbidity currents and the deposition of thick, massive beds. Sedimentology 42, 607–616.

Kolla, V., Biondi, P., Long, B., Fillon, R., 2000. Sequence stratigraphy and architecture of the Late Pleistocene Lagniappe Delta Complex, northeast Gulf of Mexico. In: Hunt, D., Gawthorpe, R.L. (Eds.), Sedimentary Responses to Forced Regression. Geological Society of London Special Publication 172, 291-327.

Kolla,V., Macurda,D.B. Jr., 1988. Sea-level changes and timing of turbidity- current events in deep-sea fan systems. In: Wilgus, C.K., Hastings, B.S., Kendall, C.G.St.C., Posamentier, H.W., Ross C.A., VanWagoner, J.C. (Eds.), Sea-Level Changes - An Integrated Approach. SEPM Special Publication 42, 71-108.

Kolla, V., Perlmutter, M.A., 1993. Timing of turbidite sedimentation on the Mississippi Fan. American Association of Petroluem Geologists Bulletin 77, 1129–1141

Kominz, M.A., 1984. Oceanic ridge volumes and sea level change: an error analysis. In: Schlee, J. (Ed.), Interregional Unconformities and Hydrocarbon Accumulation. American Association of Petroleum Geologists Memoir 36, 109-127.

Kuehl, S.A., Allison, M.A., Goodbred, S.L., Kudrass, H., 2005. The Ganges-Brahmaputra Delta. In: Giosan, L., Bhattacharya, J.P. (Eds.), River Deltas: Concepts, Models and Examples. SEPM Special Publication 83, pp. 413-434.

Kuehl, S.A., Levy, B.M., Moore, W.S., Allison, M.A., 1997. Subaqueous delta of the Ganges-Brahmaputra river system. Marine Geology 144, 81-96.

Kuehl, S.A., Nittrouer, C.A., DeMaster, D.J., 1986. Nature of sediment accumulation on the Amazon continental shelf. Continental Shelf Research 6, 209-225.

Kumar, N., Sanders, J.E., 1976. Characteristics of shoreface storm deposits: modern and ancient examples. Journal of Sedimentary Petrology 46, 145-162.

Labaune, C., Jouet, G., Berné, S., Gensous, B., Tesson, M., Delpeint, A., 2005. Seismic stratigraphy of the deglacial deposits of the Rhône prodelta and of the adjacent shelf. Marine Geology 222-223, 299-311.

Larter, R.D., Barker, P.F., 1989. Seismic stratigraphy of the Antarctic Peninsula Pacific margin: A record of Pliocene–Pleistocene ice volume and paleoclimate. Geology, 17, 731-734.

Le Dantec, N., Hogarth, L.J., Driscoll, N.W., Babcock, J.M., Barnhardt, W.A., Schwab, W.C., 2010. Tectonic controls on nearshore sediment accumulation and submarine canyon morphology offshore La Jolla, Southern California. Marine Geology 268, 115–128.

Liu, J.P., Milliman, J.D., Gao, S., Cheng, P., 2004. Holocene development of the Yellow River's subaqueous delta, North Yellow Sea. Marine Geology 209, 45-67.

Liu, J.P., Li, A.C., Xu, K.H., Velozzi, D.M., Yang, Z.S., Milliman, J.D., DeMaster, D.J., 2006. Sedimentary features of the Yangtze River-derived along-shelf clinoform deposit in the East China Sea. Continental Shelf Research 26, 2141-2156.

Liu, J.P., Xu, K.H., Li, A.C., Milliman, J.D., Velozzi, D.M., Xiao, S.B., Yang, Z.S., 2007. Flux and fate of Yangtze River sediment delivered to the East China Sea. Geomorphology, 85, 208-224.

Lobo, F.J., Fernández-Salas, L.M., Hernández-Molina, F.J., González, R., Dias, J.M.A., Díaz Del Río, G., Somoza, L., 2005. Holocene highstand deposits in the Gulf of Cadiz, SW Iberian Peninsula: a high-resolution record of hierarchical environmental changes. Marine Geology 219, 109–131.

Løseth, T.M., Steel, R.J.,Crabaugh, J.P., Schellpeper, M., 2006. Interplay between shoreline migration paths, architecture and pinchout distance for siliciclastic shoreline tongues: evidence from the rock record. Sedimentology 53, 735-767.

Loutit, T.S., Hardenbol, J., Vail, P.R., Baum, G.R., 1988. Condensed sections: the key to age determination and correlation of continental margin sequences. In: Wilgus, C.K., Hastings, B.S., Kendall, C.G.St.C., Posamentier, H.W., Ross, C.A., VanWagoner, J.C. (Eds.), Sea-Level Changes -An Integrated Approach. SEPM Special Publication 42, 183-213.

Lowe, D., 1982. Sediment gravity flows: II. Depositional models with special reference to the deposits of high-density turbidity currents. Journal of Sedimentary Petrology 52, 279-297.

MacDonald, A.C., Aasen, J.O., 1994. A prototype procedure for stochastic modelling of facies tract distribution in shoreface reservoirs. In: Yarus, J.M., Chambers, R.L. (Eds.), Stochastic Modelling and Geostatistics. AAPG Computer Applications in Geology 3, 91-108.

MacEachern, J.A., Bann, K.L., 2008. The role of ichnology in refining shallow marine facies models. In: Hampson, G.J., Steel, R.J., Burgess, P.M., Dalrymple, R.W. (Eds.), Recent advances in models of siliciclastic shallow-marine stratigraphy. SEPM Special Publication 90, 73-116.

Mandelbrot, B.B., 1983. The fractal geometry of nature. Freeman, New York, pp. 468.

McCave, I.N., 1972. Sediment transport and escape of fine-grained sediment in shelf areas. In: Swift, D.J.P., Pilkey, O.H. (Eds.), Shelf Sediment Transport, Process and Patterns. Dowden, Hutchinson & Ross, Stroudsburg, PA., pp. 215-248.

McKee, E.D., 1949. Facies changes in the Colorado Plateau. Geological Society of America Memoirs 39, 35-48.

McLeod, A.E., Dawers, N.H., Underhill, J.R., 2000. The propagation and linkage of normal faults: insights from the Strathspey-Brent-Statfjord fault array, northern North Sea. Basin Research 12, 263-284.

Meistrell, F.J., 1972. The spit-platform concept: laboratory observation of spit development. In: Schwartz, M.L. (Ed.), Spits and Bars. Dowden, Hutchinson and Ross, Stroudsberg, P. A., pp. 225-283.

Mellere, D., Breda, A., Steel, R.J., 2003. Fluvially incised shelf-edge deltas and linkage to upper- slope channels (Central Tertiary Basin, Spitsbergen). In: Roberts, N.C.R.H.H., Fillon, R.H., Anderson, J.B. (Eds.), Shelf-Margin Deltas and Linked Downslope Petroleum Systems (Cd-Rom). 23rd Annual Research Conference (Houston), GCS-SEPM, pp. 231-266.

Methling, D., Jaschinski, W., Narcisi, B., Stemberg, R. W., Cacchione, D. A., Paulson, B., Kineke, G. C., Drake, D. E., 1996. Observations of sediment transport on the subaqueous Amazon delta. Continental Shelf Research 16, 697-715.

Miall, A.D., 2012. A new uniformitarianism: stratigraphy as just a set of “frozen accidents”. Preprint in preparation for Geological Society of London, London, Symposium “Strata and Time”, September 2012, pp. 22.

Michels, K.H., Kudrass, H.R., Hübscher, C., Suckow, A., Wiedicke, M., 1998. The submarine delta of the Ganges-Brahmaputra: cyclone-dominated sedimentation patterns. Marine Geology 149, 133-154.

Middleton, C.V., Hampton, M.A., 1976. Subaqueous sediment transport and deposition by sediment gravity flows. In: Stanley, D.J., Swift, D.J.P. (Eds.), Marine Sediment Transport and environmental management. Wiley, New York, pp. 197-216.

Middleton, G.V., Plotnick, R.E., Rubin, D.M., 1995. Nonlinear dynamics and fractals; new numerical techniques for sedimentary data sets. Society for Sedimentary Geology, Tulsa, Oklahoma, Short Course 36, 174 pp.

Milliman, J.D., Quraishee, G.S., Beg, M.A.A., 1984. Sediment discharge from the Indus River to the ocean, past, present and future. In: Haq, B.U., Milliman, J.D. (Eds.), Marine geology and oceanography of the Arabian Sea and coastal Pakistan. Van Norstrand Rheinhold Co., New York, pp. 65–70.

Milton, N., Dyce, M., 1995. Systems tract geometries associated with Early Eocene lowstands, imaged on a 3D seismic dataset from the Bruce area, UK North Sea. In: Steel, R.J., Felt, V.L., Johannessen, E.P., Mathieu, C. (Eds.), Sequence stratigraphy on the Northwest European margin. Norwegian Petroleum Society Special Publications 5, pp. 429–442.

Mitchell, N.C., 2012. Modelling the rollovers of sandy clinoforms from the gravity effect on wave-agitated sand. Journal of Sedimentary Research 82, 464-468.

Mitchell, N.C., Masselink, G., Huthnance, J.M., Fernández-Salas, L.M., Lobo, F.J., 2012. Depths of Modern Coastal sand clinoforms. Journal of Sedimentary Research 82, 469-481.

Mitchum, R.M., Vail, P.R., Thompson, S. III, 1977. Seismic stratigraphy and global changes in sea level, part 2: the depositional sequence as the basic unit for stratigraphic analysis. In: Payton, C.E. (Ed.), Seismic Stratigraphy: applications to hydrocarbon exploration. AAPG Memoir 26, Tulsa, Oklahoma, pp. 53-62.

Mitchum, R.M., Van Wagoner, J.C., 1991. High frequency sequences and their stacking patterns: sequence-stratigraphic evidence of high-frequency eustatic cycles. Sedimentary Geology 70, 131-160.

Mitchum, R.M., Jr., 1985. Seismic stratigraphic expression of submarine fans. In: Berg, O.R., Wolverton, D.G. (Eds.), Seismic stratigraphy II. American Association of Petroleum Geologists Memoir 39, pp. 117–138.

Mitchum, R.M., Sangree, J.B., Vail, P.R., Wornardt, W.W., 1994. Recognizing sequences and systems tracts from well logs, seismic data and biostratigraphy: Examples from the Late Cenozoic of the Gulf of Mexico. In: Weimer, P., Posamentier, H.W. (Eds), Siliciclastic sequence stratigraphy: recent developments and applications. American Association of Petroleum Geologists Memoirs 58, pp. 163–197.

Morris, J.E., Hampson, G.J., Johnson, H.D., 2006. A sequence stratigraphic model for an intensely bioturbated shallow-marine sandstone: the Bridport Sand Formation, Wessex Basin, UK. Sedimentology 53, 1229-1263.

Mortimer, E., Gupta, S., Cowie, P., 2005. Clinoform nucleation and growth in coarse-grained deltas, Loreto basin, Baja California Sur, Mexico: a response to episodic accelerations in fault displacement. Basin Research 17, 337-359.

Morton, A., Hallsworth, C., Chalton, B., 2004. Garnet compositions in Scottish and Norwegian basement terrains: a framework for interpretation of North Sea sandstone provenance. Marine and Petroleum Geology 21, 393-410.

Morton, R.A., Suter, J.R., 1996. Sequence stratigraphy and composition of late Quaternary shelf-margin deltas, northern Gulf of Mexico. AAPG Bulletin 80, 505-530.

Mougenot, D.,Boillot, G., Rehault, J.P., 1983. Prograding shelfbreak types on passive continental margins: some European examples. In: Stanley, D.J., Moore, G.T. (Eds.), The Shelf break: Critical Interface on Continental Margins. SEPM Special Publication 33, 61-78.

Mulder, T., Syvitski, J.P.M., 1995. Turbidity currents generated at river mouths during exeptional discharges to world oceans. Journal of Geology 103, 285–299.

Mulder, T., Syvitski, J.P.M., Migeon, S., Faugères, J.-C., Savoye, B., 2003. Marine hyperpycnal flows: Initiation, behaviour and related deposits: A review. Marine and Petroleum Geology 20, 861-882.

Mullins, H.T., Gardulski, A.F., Hine, A.C., Melillo, A.J., Wise, S.W. Jr., Applegate, J., 1988. Three-dimensional framework of the carbonate ramp slope of central west Florida: A sequential seismic stratigraphic perspective. Geological Society of America Bulletin 100, 514-533.

Muto, T., Steel, R.J., 1992. Retreat of the front in a prograding delta. Geology, 20, 967–970.

Muto, T., Steel, R.J., 2002. In defence of shelf- edge delta development during falling and lowstand of relative sea level. Journal of Geology 110, 421-436.

Muto, T., Steel., R.J., Swenson, J.B., 2007. Autostratigraphy: a framework norm for genetic stratigraphy. Journal of Sedimentary Research 77, 2–12.

Muto, 2001. Shoreline autoretreat substantiated in flume experiments. Journal of Sedimentary Research 77, 2-12.

Mutterlose, J., 2003. The Greenland-Norwegian Seaway: a key area for understanding Late Jurassic to Early Cretaceous paleoenvironments. Paleoceanography 18, 10,1-10,26.

Mutti, E., 1985, Turbidite systems and their relations to depositional sequences. In: Zuffa, G.G. (Ed.), Provenance of arenites. NATO ASI Series C: Mathematical and Physical Sciences 148. Dordrecht, Boston, D. Reidel Publishing Company, 65-93.

Mutti, E., Davoli, G., Tinterri, R., Zavala, C., 1996. The importance of fluvio-deltaic systems dominated by catastrophic flooding in tectonically active basins. Memorie di Scienze Geologiche 48, 233-291.

Myrow, P.M., Southard, J.B., 1996. Tempestite deposition. Journal of Sedimentary Research 66, 875-887.

Neill, C.F., Allison, M.A., 2005. Subaqueous deltaic formation on the Atchafalaya Shelf, Louisiana. Marine Geology 214, 411-430.

Nemec, W., 1995. The dynamics of deltaic suspension plumes. In: Oti, M.N. (Ed.), The Geology of Deltas. Balkema, Rotterdam, pp. 31-93.

Nielsen, L.H., Johannessen, P.N., 2001. Accretionary, forced regressive shoreface sands of the Holocene–Recent Skagen Odde spit complex, Denmark – a possible outcrop analogue to fault-related shoreface sandstone reservoirs. In: Martinsen, O.J., Dreyer, T. (Eds.), Sedimentary environments offshore Norway – Palaeozoic to Recent. Norwegian Petroleum Society Special Publication, 10, Elsevier, Amsterdam, pp. 457–472.

Nielsen, L.H., Johannessen, P.N., 2009. Facies architecture and depositional processes of the Holocene-Recent accretionary forced regressive Skagen spit system, Denmark. Sedimentology 56, 935-968.

Nielsen, L.H., Johannessen, P.N., Surlyk, F., 1988. A Late Pleistocene coarse-grained spit-platform sequence in northern Jylland, Denmark. Sedimentology 35, 915-937.

Nilsen, D.E., Sundsbø, G., Skaug, M., Dreyer, T. Goodyear, P., 1993. Depositional Model of the Troll Field. NorskHydro report.

Nittrouer, C.A., Kuehl, S.A., DeMaster, D.J., Kowsmann, R.O., 1986. The deltaic nature of Amazon shelf sedimentation. GSA Bulletin 97, 444-458.

Nittrouer, C.A., Wright, L.D., 1994. Transport of particles across continental shelves. Review of Geophysics 32, 85-113.

Nittrouer, C.A., Kuehl, S.A., Figueiredo, A.G., Allison, M.A., Sommerfield, C.K., Rine, J.M., Faria, E.C., Silveira, O.M., 1996. The geological record preserved by Amazon shelf sedimentation. Continental Shelf Research 16, 817–841.

Nøttvedt, A., Gabrielsen, R. H., Steel, R. J., 1995. Tectonostratigraphy and sedimentary architecture of rift basins, with reference to the northern North Sea. Marine and Petroleum Geology 12, 8, 881-901.

Nøttvedt, A., Berge, A. M., Dawers, N. H., Færseth, R. B., Häger, K. O., Mangerud, G., Puigdefabregas, C., 2000. Syn-rift evolution and resulting play models in the Snorre-H area, northern North Sea. In: Nøttvedt, A., et al. (Eds.), Dynamics of the Norwegian Margin. Geological Society, London, Special Publications 167, 179-218.

Norwegian Petroleum Directorate, 2012. Available online on: http://npdmap1.npd.no/website/NPDGIS/viewer.htm

Ogg, J.G., Ogg, G., Gradstein, F.M., 2008. The concise geologic time scale. Cambridge University Press, 177 pp.

Olariu, C., Steel, R.J., 2009. Influence of point- source sediment- supply on modern shelf-break morphology: implications for interpretation of ancient shelf margins. Basin Research 21, 484-501

Olariu, C., Steel, R.J., Petter, A.L., 2010. Delta-front hyperpycnal bed geometry and implications for reservoir modelling: Cretaceous Panther Tongue delta, Book Cliffs, Utah. AAPG Bulletin 94, 819-845.

Orton, G.J., Reading, H.G., 1993. Variability of deltaic processes in terms of sediment supply, with particular emphasis on grain size. Sedimentology 40, 475-512.

Osborne, P. & Evans, S., 1987. The Troll Field: reservoir geology and field development planning. North Sea Oil and Gas Reservoirs, Norwegian Institute of Technology and Graham & Trotman, London, 457-472.

Palamenghi, L., Schwenk, T., Spiess, V., Kudrass, H.R., 2011. Seismostratigraphic analysis with centennial to decadal time resolution of the sediment sink in the Ganges-Brahmaputra subaqueous delta. Continental Shelf Research 31, 712-739.

Parsons, J.D., Bush, J.W.M., Syvitski, J.P.M., 2001. Hyperpycnal plume formation from riverine outflows with small sediment concentrations. Sedimentology 48, 465-478.

Partington, M.A., Copestake, P., Mitchener, B.C., Underhill, J.R., 1993. Biostratigraphic calibration of genetic stratigraphic sequences of the Jurassic-lowermost Cretaceous (Hettangian to Ryazanian) of the North Sea and adjacent areas. In: Parker, J.R. (Ed.), Petroleum Geology of North-West Europe. Proceedings of the 4th conference, Geological Society of London, London pp. 347-370.

Patruno, S., 2013. Geological characterization of sand-prone subaqueous delta systems: a case study of the Upper Jurassic Sognefjord Formation (Troll Field, Northern North Sea, offshore Norway) and global examples. Ph.D. thesis, Imperial College London, pp. xx.

Patruno, S., Hampson, G.J., Jackson, C. A-L., Whipp, P., 2013a. Geomorphology, Facies Character and Stratigraphic architecture of an ancient sand-prone subaqueous delta: Upper Jurassic Sognefjord Formation, Troll Field, Offshore Norway. Extended abstract 1554161, AAPG Conference, Pittsburgh, U.S., pp. xx.

Patruno, S., Jackson, C. A-L., Hampson, G.J., Whipp, P., 2013b. Quantitative stratigraphic architecture, depositional history and progradation rates of an ancient sand-prone subaqueous delta (Sognefjord Formation, Troll Field, Norwegian North Sea). Extended abstract 1554156, AAPG Conference, Pittsburgh,

U.S., pp. xx.

Pemberton, S.G., MacEachern, J.A., Frey, R.W., 1992. Trace fossil facies models: environmental and allostratigraphic significance. In: Walker, R.G., James, N.P. (Eds.), Facies Models: Responses to Sea Level Change. Geological Association of Canada, Waterloo, Ontario, pp. 47-72.

Pettijohn, F.J., 1976. Sedimentary Rocks. Harper & Row, New York, 628 pp.

Piper, D.J.W., Normark, W.R., 2001. Sandy fans; from Amazon to Hueneme and beyond. American Association of Petroleum Geologists Bulletin 85, 1407-1438.

Pirmez, C., Pratson, L.F., Steckler, M.S., 1998. Clinoform development by advection-diffusion of suspended sediment: modeling and comparison to natural systems. Journal of Geophysical Research 103, 24,141-24,157.

Pitman, W.C., 1978. Relationship between eustasy and stratigraphic sequences of passive margins. Bulletin Geological Society of America 89, 1389-1403.

Plink-Björklund, P., Steel, R.J., 2004. Initiation of turbidity currents: Outcrop evidence for Eocene hyperpycnal flow turbidites. Sedimentary Geology 165, 29-52.

Plint, A.G., 1988. Sharp-based shoreface sequences and “offshore bars” in the Cardium Formation of Alberta: their relationship to relative changes in sea level. In: Sea Level Changes – An Integrated Approach. SEPM Special Publication, pp. 357-370.

Plint, A.G., Nummedal, D., 2000. The falling stage system tract: recognition and importance in sequence stratigraphic analysis. In: Hunt, D., Gawthorpe, R.L. (Eds.), Sedimentary Responses to Forced Regressions. Geological Society of London, Special Publications 172, pp. 1-17.

Plotnick, R.E., 1986. A fractal model for the distribution of stratigraphic hiatuses. Journal of Geology 94, 885-890.

Pomar, L., Tropeano, M., 2001. The Calcarenite di Gravina Formation in Matera (southern Italy): new insights for coarse- grained, large-scale, cross-bedded bodies encased in offshore deposits. AAPG Bulletin 85, 661-689.

Pomar, L., Obrador, A., Westphal, H., 2002. Sub-wave base cross-bedded grainstones on a distally steepened carbonate ramp, Upper Miocene, Menorca, Spain. Sedimentology 49, 139-169.

Porębski, S.J., Steel, R.J., 2003. Shelf-margin deltas: their stratigraphic significance and relation to deepwater sands. Earth Science Reviews 62, 283-326.

Porębski S.J., Steel R.J., 2006. Deltas and sea-level change. Journal of Sedimentary Research 76, 390–403.

Posamentier, H.W., Morris, W.R., 2000. Aspects of the stratal architecture of forced regressive deposits. In: Hunts, D., Gawthorpe, R.L. (Eds.), Sedimentary Responses to Forced Regressions. 172Geological Society of London, Special Publications 172, pp. 19-46.

Posamentier, H.W., Davies, R.J., Cartwright, J.A., Wood, L., 2007. Seismic geomorphology, an overview. In: Davies, R.J., Posamentier, H.W., Wood, L.J., Cartwright, J.A. (Eds.), Seismic Geomorphology: Applications to Hydrocarbon Exploration and Production. Geological Society of London, Special Publication 277, pp. 1-14.

Posamentier, H.W., Vail, P.R., 1988. Eustatic controls on clastic deposition II - sequence and systems tract models. In: Wilgus, C.K., Hastings, B.S., Kendall, C.G.St.C., Posamentier, H.W., Ross, C.A., VanWagoner, J.C. (Eds.), Sea-Level Changes -An Integrated Approach. SEPM Special Publication 42, 125-154.

Posamentier, H.W, Allen, H.W, James, D.P., Tesson, M., 1992. Forced regressions in a sequence stratigraphic framework: concepts, examples and sequence stratigraphic significance. AAPG Bulletin 76, 1687-1709.

Posamentier, H.W., Erskin, R.D., Mitchum, R.M. Jr., 1991. Models for submarine fan deposition within a sequence stratigraphic framework. In: Weimer, P., Link, M.H. (Eds.), Seismic Facies and Sedimentary Processes of Submarine Fans and Turbidite Systems. Springer-Verlag, NewYork, 127-136.

Posamentier, H.W., Jervey, M.T., Vail, P.R., 1988. Eustatic controls on clastic deposition. In: Wilgus, C.K., Hastings, B.S., Ross, C.A., Posamentier, H.W., Van Wagoner, J., Kendall, C.G.St.C. (Eds.), Sea level change: an integrated approach. Society of Economic Paleontologists and Mineralogists Special Publication 42, 109–124.

Poulsen, N.E., Riding, J.B., 2003. The Jurassic dinoflagellate cyst zonation of Subboreal Northwest Europe. Geological Survey of Denmark and Greenland Bulletin 1, 115-144.

Pratson, L.F., Ryan, W.B.F., Mountain, G.S., Twichell, D.C., 1994. Submarine canyon initiation by downslope eroding sediment flows: evidence in Late Cenozoic strata on the New Jersey continental slope. Geological Society of America Bulletin 106, 395-412.

Prosser, S., 1993. Rift-related linked depositional systems and their seismic expression. Geological Society, London, Special Publications 71, 35-66.

Ravnås, R., Bondevik, K., 1997. Architecture and controls on Bathonian-Kimmeridgian shallow-marine syn-rift wedges of the Oseberg-Brage area, northern North Sea. Basin Research 9, 197-226.

Ravnås, R., Bondevik, K., Helland-Hansen, W., Lømo, L., Ryseth, A., Steel, R. J., 1997. Sedimentation history as an indicator of rift initiation and development: Late Bajocian-Bathonian evolution of the Oseberg area, northern North Sea. Norsk Geologisk Tidsskrift 77, 205-232.

Ravnås, R., Nøttvedt, A., Steel, R.J., Windelstad, J., 2000. Syn-rift sedimentary architectures in the Northern North Sea. In: Nøttvedt, A. (Ed.), Dynamics of the Norwegian Margin. Geological Society of London, Special Publications 167, London, pp. 133-177.

Redfield, A.C., 1965. Ontogeny of a Salt Marsh Estuary. Science 147, 50-55.

Rich, J.L., 1951. Three critical environments of deposition and criteria for recognition of rocks deposited in each of them. GSA Bulletin 62, 1-20.

Ritchie, B.D., Gawthorpe, R.L., Hardy, S., 2004. Three dimensional numerical modelling of deltaic depositional sequences 1: influence of the rate and magnitude of sea-level change. Journal of Sedimentary Research 74, 203-220.

Roy, P.S., Cowell, P.J., Ferland, M.A., Thom, B.G., 1994. Wave-dominated coasts. In: Carter, R.W.G., Woodroffe,

C.D. (Eds.), Coastal Evolution; Late QuaternaryShoreline Morphodynamics. Cambridge University Press, New York, pp. 121–186.

Rebesco, M., Camerlenghi, A., 1997. Sediment drifts on the continental rise of the Antarctic Peninsula. In: Davies, T.A., Bell, T., Cooper, A.K., Josenhans, H., Polyak, L., Solheim, A., Stoker, M.S., and Stravers, J.A. (Eds.), Glaciated Continental Margins: An Atlas of Acoustic Images. London, Chapman & Hall, pp. 294–296.

Rice, P.D., Shade, B.D., 1982. Reflection seismic interpretation and seafloor spreading history of Baffin Bay. In: Embry, A.F., Balkwill, H.R. (Eds.), Arctic Geology and Geophysics. Proceedings of the Third International Symposium on Arctic Geology. Canadian Society of Petroleum Geologists Memoir 8, pp. 245–265.

Ross, W.C.,Halliwell, B.A., May, J.A., Watts, D.E., Syvitski, J.P.M., 1994. Slope readjustment; a new model for the development of submarine fans and aprons. Geology 22, 511-514.

Ryan, M.C., Helland-Hansen, W., Johannessen, E.P., Steel, R.J., 2009. Erosional versus accretionary shelf margins: the influence of margin type on deepwater sedimentation - an example from the Porcupine Basin, offshore western Ireland. Basin Research 21, 676-703.

Sadler, P.M., 1981. Sedimentation rates and the completeness of stratigraphic sections. Journal of Geology 89, 569-584.

Sadler, P.M. 2012. Scaling Laws for Aggradation and Progradation of the Stratigraphic Record. In. William Smith Meeting 2012, Strata and Time; Probing the Gaps in our Understanding. Geological Society of London, London, 4-5 September 2012, Abstract Book, pp. 32.

Sangree, J.B., Widmier, J.M., 1977. Seismic stratigraphy and global changes in sea level; 9, Seismic interpretation of depositional facies. In: Payton, C.E. (Ed.), Seismic Stratigraphy: Applications to Hydrocarbon Exploration. American Association of Petroleum Geologists, Tulsa, Oklahoma, pp. 165-184.

Schlee, J.S., Dillon, W.P., Grow, J.A., 1979. Structure of the continental slope off the eastern United States. In: Doyle, L.J., Pilkey, O.H. (Eds.), Geology of Continental Slopes. Society of Economic Paleontologists and Mineralogists, Special Publication 27, pp. 95–117.

Sclater, J.G., Christie, P.A.F., 1980. Continental stretching: an explanation of the post-mid-Cretaceous subsidence of the Central North Sea Basin. Journal of Geophysical Research 85 B7, 3711-3739.

Shepard, F.P., 1959. The Earth Beneath the Sea. Johns Hopkins Press, Baltimore, MD, 275pp.

Shepard, F.P., Emery, K.O., La Fond, E.C., 1941. Rip currents: a process of geological importance. Journal of Geology 49, 337-369.

Short, A.D., 1975. Offshore bars along the Alaskan arctic coast. Journal of Geology 83, 209-221.

Southard, J.B., Stanley, D.J., 1976. Shelf-break processes and sedimentation. In: Stanley, D.J., Swift, D.J.P. (Eds.), Marine Sediment Transport and Environmental Management. Wiley-Interscience, New York, pp. 351-377.

Stagg, H.M.J., 1985. The structure and origin of Prydz Bay and MacRobertson Shelf, Antarctica. In: Husebye, E.S., Johnson, G.L., and Kristoffersen, Y. (Eds.), Geophysics of the Polar Regions. Tectonophysics, 114, pp. 315–

340.

Steckler, M.S., Mountain, G.S., Miller, K.G., Christie-Blick, N., 1999. Reconstructioonf Tertiary progradationa and clinoform development on the New Jersey margin by 2-D backstripping. Marine Geology 154, 399-420.

Steel, R.J., 1993. Triassic-Jurassic megasequence stratigraphy in the Northern North Sea: rift to post-rift evolution. In: Parker, J.R. (Ed.), Petroleum Geology of North-West Europe: Proceedings of the 4th Conference. Geological Society of London, London, pp. 299-315.

Steel, R.J., Carvajal, C., Petter, A.L., Uroza, C., 2008. Shelf and shelf-margin growth in scenarios of rising and falling sea level. In: Hampson, G.J., Steel, R.J., Burgess, P.M., Dalrymple, R.W. (Eds.), Recent advances in models of siliciclastic shallow-marine. SEPM Special Publication 90, pp. 47-71.

Steel, R.J., Olsen, T., 2002. Clinoforms, clinoform trajectory and deepwater sands. In: Armentrout, J.M., Rosen, N.C. (Eds.), Sequence Stratigraphic Models for Exploration and Production: evolving methodology, emerging models and application histories. GCS-SEPM Special Publication, pp. 367-381.

Steel, R.J., Carvajal, C., Petter, A., Uroza, C., 2008. Feature of prograding and aggrading clastic shelf platforms and margins. In: Hampson, G.J., Steel, R.J., Burgess, P.M., Dalrymple, R.W. (Eds.), Recent Advances in Models of Siliciclastic Shallow-Marine Stratigraphy. SEPM Special Publication 90, pp. 47-71.

Steel, R.J., 1993. Triassic-Jurassic megasequence stratigraphy in the Northern North Sea. rift to post-rift evolution. In: Parker, J.R. (Ed.), Petroleum Geology of North-West Europe. Proceedings of the 4th Conference, Geological Society of London, London, pp. 299-315.

Stewart, D.J., Schwander, M., Bolle, L., 1995. Jurassic depositional systems of the Horda Platform, Norwegian North Sea: practical consequences of applying sequence stratigraphic models. In. Steel, R.J., Felt, V.L., Johannessen, E.P., Mathieu, C. (Eds.), Sequence Stratigraphy on the Northwest European Margin. Norwegian Petroleum Society Special Publication 5, Elsevier, pp. 291-323.

Storms, J.E.A., Hampson, G.J., 2005. Mechanisms for forming discontinuity surfaces within shoreface-shelf parasequences: Sea level, sediment supply or wave regime? Journal of Sedimentary Research 75, 67-81.

Suter, J.R., Berryhill, H.L., 1985. Late Quaternary shelf margin deltas, northwest Gulf of Mexico. AAPG Bulletin 69, 77-91.

Swenson, J.B., Paola, C., Pratson, L., Voller, V.R., Murray, A.B., 2005. Fluvial and marine controls on combined subaerial and subaqueous delta progradation: morphodynamic modeling of compound-clinoform development. Journal of Geophysical Research 110, 1-16.

Swift, D.J.P., 1968. Coastal erosion and transgressive stratigraphy. Journal of Geology 76, 444-456.

Sømme, T.O., Howell, J.A., Hampson, G.J., Storms, J.E.A., 2008. Genesis, architecture, and numerical modelling of intra-parasequence discontinuity surfaces in wave-dominated deltaic deposits: Upper Cretaceous Sunnyside Member, Blackhawk Formation, Book Cliffs, Utah, U.S.A. In: Hampson, G.J., Steel, R.J., Burgess, P.M., Dalrymple, R.W. (Eds.), Recent Advances in Models of Siliciclastic Shallow-Marine Stratigraphy. SEPM

Special Publication 90, pp. 421–441.

Ta, T.K.O., Nguyen, V.L., Tateishi, M., Kobayashi, I., Tanabe, S., Saito, Y., 2002. Holocene delta evolution and sediment discharge of the Mekong River, southern Vietnam. Quaternary Science Reviews 21, 1807-1819.

Taylor, A.M., Goldring, R., 1993. Description and analysis of bioturbation and ichnofabric. Journal of the Geological Society, London, 150, 141-148.

Tesson, M., Posamentier, H.W., Gensous, B., 2000. Stratigraphic Organization of Late Pleistocene deposits of the western part of the Golfe du Lion Shelf (Languedoc Shelf), western Mediterranean Sea, using high-resolution seismic and core data. AAPG Bulletin 84, 1, 119–150.

Torsvik, T.H., Carlos, D., Mosar, J., Cocks, R.M., Malme, T.N., 2002. Global reconstructions and North Atlantic paleogeography 440 Ma to Recent. In: Eide, E.A. (Ed.), Batlas – Mid Norway plate reconstruction atlas with global and Atlantic perspectives. Geological Survey of Norway, Trondheim, pp. 18-39.

Traykovski, P., Geyer, W.R., Irish, J.D., Lynch, J.F., 2000. The role of wave-induced density-driven fluid mud flows for cross-shelf transport on the Eel River continental shelf. Continental Shelf Research **20**, 2113-2140.

Vail, P.R., Todd, R.G., 1981. Northern North Sea Jurassic unconformities, chronostratigraphy and sea-level changes from seismic stratigraphy. In: Illing L.V., Hobson, G.D. (Eds.), Petroleum Geology of the Continental Shelf of Northwest Europe. Proceedings of the Second Conference. Heyden, London, pp. 216-235.

Vail, P.R., Audemard, F., Bowman, S.A., Eisner, P.N., Perez-Cruz, C., 1991. The stratigraphic signatures of tectonics, eustasy and sedimentology – an overview. In: Einsele, G., Ricken, W., Seilacher, A. (Eds.), Cycles and events in stratigraphy. Springer-Verlag, Berlin, 617-659.

Vail, P.R., Mitchum, R.M. Jr., Todd, R.G., Widmeir, J.R., Thompsons, S. III, Sangree, J.R., Bubb, J.N., Hatlid, W.G., 1977. Sequence stratigraphy and global changes in sea level. In: Payton, C.E. (Ed.), Seismic Stratigraphy, Applications to Hydrocarbon Exploration. American Association of Petroleum Geology Memoirs 26, 49-205.

Vanney, J.R., Stanley, D.J., 1983. Shelfbreak physiography: an overview. In: Stanley, D.J., Moore, G.T. (Eds.), The Shelf break: critical Interface on Continental Margins. SEPM Special Publicaltion 33, pp. 1-24.

Van den Berg, J., Van Gelder, A., Mastbergen, D.R., 2002. The importance of breaching as a mechanism of subaqueous slope failure in fine sand. Sedimentology 49, 81-95.

Van Wagoner, J.C., Mitchum, R.M., Posamentier, H.W., Vail, P.R., 1987. Seismic stratigraphy interpretation using sequence stratigraphy: part 2, key definitions of sequence stratigraphy. In: Bally, A.W. (Ed.), Atlas of Seismic Stratigraphy, 1. AAPG Stud.Geol. 27, 11-14.

Van Wagoner, J.C., Posamentier, H.W., Mitchum, R.M.,Vail, P.R., Sarg, J.F., Loutit,T.S., Hardenbol, J., 1988. An overview of the fundamentals of sequence stratigraphy and key definitions. In: Wilgus, C.K., Hastings, B.S., Kendall, C.G.St.C., Posamentier, H.W., Ross C.A., VanWagoner J.C. (Eds.), Sea-Level Changes: An Integrated Approach. SEPM Special Publication 42, 39-45.

Van Wagoner, J.C., Mitchum, R.M., Campion, K.M., Rahmanian, V.D., 1990. Siliciclastic Sequence stratigraphy in well logs, cores, and outcrops: concepts for high resolution correlation of time and facies. AAPG Methods in Exploration, Series 7, 55pp.

Vollset, J., Doré, A.G., 1984. A revised Triassic and Jurassic lithostratigraphy nomenclature for the Norwegian North Sea, northern area. Norwegian Petroleum Directorate Bulletin 3, 1-53.

Walker, R.G., Plint, A.G., 1992. Wave and storm-dominated shallow marine systems. In: Walker, R.G., James, N.P. (Eds.), Facies Models: Responses to Sea Level Change. Geological Association of Canada, Waterloo, Ontario, pp. 219-238.

Walsh, J.P., Nittrouer, C.A., Palinkas, C.M., Ogston, A.S., Sternberg, R.W., Brunskill, G.J., 2004. Clinoform mechanics in the Gulf of Papua, New Guinea. Continental Shelf Research 24, 2487-2510.

Warne, A.G., Meade, R.H., White, W.A., Guevara, E.H., Gibeaut, J., Smyth, R.C., Aslan, A., Tremblay, T., 2002. Regional controls on geomorphology, hydrology and ecosystem integrity in the Orinoco Delta, Venezuela. Geomorphology 44, 273-307.

Watts, A.B., Ryan, W.B.F., 1976. Flexure of the lithosphere and continental margin basins. Tectonophysics 36, 25-44.

Wear, C.M., Stanley, D.J., Boula, J.E., 1974. Shelf break physiography between Wilmington and Norfolk canyons. Marine Technological Society Journal 8, 37-48.

Weber, M.E., Wiedicke, M.H., Kudrass, H.R., Hubsher, C., Erlenkueser, H., 1997. Active growth of the Bengal Fan during sea-level rise and highstand. Geology 25, 315-318.

Whipp, P.S., Jackson, C. A-L., Gawthorpe, R.L., Dreyer, T., Quinn, D., in press. Fault array evolution above a reactivated rift fabric; a subsurface example from the northern Horda Platform fault array, Norwegian North Sea. Basin Research.

Whitaker, M.F.,1981. Palynofacies investigation in the Jurassic interval of the Norske Shell well 31/2-3, Shell International Petroleum Maatschappij B.V. Available online on: http://www.npd.no/engelsk/cwi/pbl/wellbore_documents/236_31_2_3_Palynofacies_invest_on_the_Juras.pdf

Whitaker, M.F., 1982a. Palynofacies investigation in the Jurassic interval of the Norske Shell well 31/2-4, Shell International Petroleum Maatschappij B.V. Available online on: http://www.npd.no/engelsk/cwi/pbl/wellbore_documents/208_31_2_4_Palynofacies_investigation.pdf

Whitaker, M.F., 1982b. Palynofacies investigation in the Jurassic interval of the Norske Shell well 31/2-5, Shell International Petroleum Maatschappij B.V. Available online on: http://www.npd.no/engelsk/cwi/pbl/wellbore_documents/210_13_Palynofacies_Jurassic_investigation_by%20SHELL.pdf

Whitaker, M.F., 1983. Palynofacies investigation in the Jurassic interval of the Norske Shell well 31/2-8, Shell

International Petroleum Maatschappij B.V. Available online on: http://www.npd.no/engelsk/cwi/pbl/wellbore_documents/78_07_31_2_8_Palynofacies_invest_in_the_jura_by_Shell.pdf

Whitaker, M.F., 1984. The usage of palynostratigraphy and palynofacies in definition of Troll Field geology, offshore Northern Seas: Reduction of uncertainties by innovative reservoir geomodelling. In: Offshore Northern Seas Conference and Exhibition, 6, Paper G6, pp. 44. Norske Petroleumshorening, Stavanger.

Whitaker, M.F., 1985. Palynological results of well 31/2-14. A/S Norske Shell Exploration and Production. Available online on: http://www.npd.no/engelsk/cwi/pbl/wellbore_documents/106_03_31_2_14_Palynological_results_by_Shell.pdf

Wright, L.D., Yang, Z.-S., Bornhold, B.D., Keller, G.H., Prior, D.B., Wiseman, W.J., 1986. Hyperpycnal plumes and plume fronts over the Huanghe (Yellow River) delta front. Geo-Marine Letters 6, 97-105.

Wright, L.D., Friedrichs, C.T., Kim, S.C., Scully, M.E., 2001. The effects of ambient currents andwaves on the behaviour of turbid hyperpycnal plumes on continental shelves. Marine Geology 175, 25-45.

Xing, J., Davies, A.M., 2002. Influence of wind direction, wind waves, and density stratification upon sediment transport in shelf edge regions: the Iberian shelf. Journal of Geophysical Research 107, C8, 16.1-16.24.

Yang, Z. S., Liu, J. P., 2007. A unique Yellow River-derived distal subaqueous delta in the Yellow Sea. Marine Geology 240, 169-176.

Yoshida, S., Steel, R.J., Dalrymple, R.W., 2007. Changes in depositional processes: an ingredient in a new generation of sequence stratigraphic models. Journal of Sedimentary Research 77, 447-460.

Zanella, E., Coward, M.P., 2003. Structural Framework. In: Evans, D., Graham, C., Armour, A., Bathurst, P. (Eds.), The Millennium Atlas: petroleum geology of the central and northern North Sea. Geological Society of London, London, pp. 49-59.

Zecchin, M., Caffau, M., Civile, D., Roda, C., 2010. Anatomy of a Late Pleistocene clinoformal sedimentary body (Le Castella, Calabria, southern Italy): A case of prograding spit system? Sedimentary Geology 223, 291-309.

APPENDIX

Core logs

These include:

- Most cores have been logged 'from scratch' by Stefano Patruno in the core stores of Statoil (Bergen, Norway) and Weatherford (Stavanger, Norway) in 2010-2011
- For a few cores (31/2-3, 31/2-8, 31/3-2), the logs carried out in the 1970s-1990s by oil industry personnel and publicly released by the NPD website (www.npd.no/en/) were used as a 'base' over which new observations were collected by Stefano Patruno in the Statoil core store of Bergen (Norway) in 2010

31/2-1

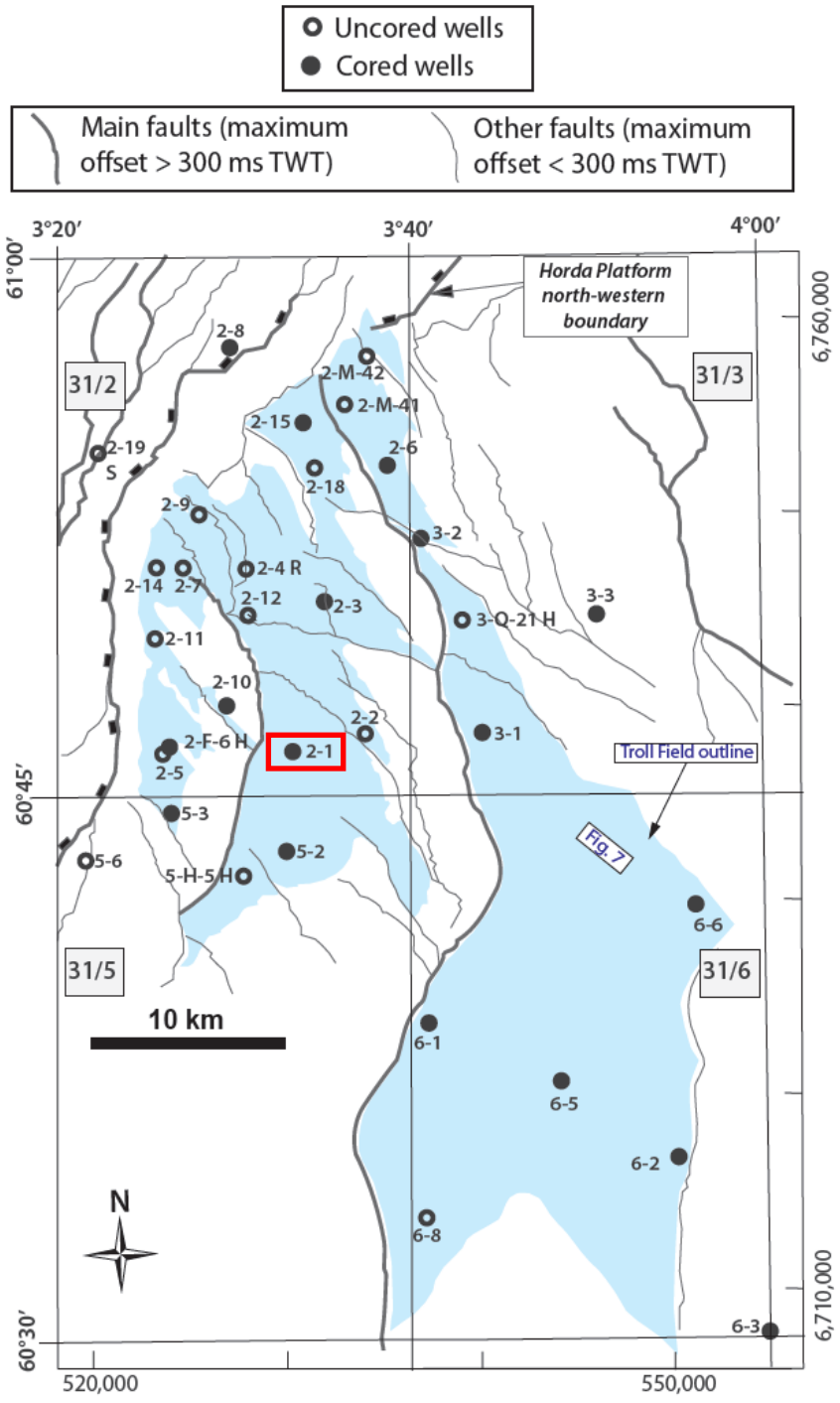
Uncored wells
Cored wells
Main faults (maximum offset > 300 ms TWT)
Other faults (maximum offset < 300 ms TWT)
3°20′
3°40′
4°00′
61°00′
60°45′
60°30′
6,760,000
6,710,000
520,000
550,000
Horda Platform north-western boundary
31/2
31/3
31/5
31/6
2-8
2-M-42
2-M-41
2-15
2-19 S
2-6
2-18
2-9
3-2
2-14
2-7
2-4 R
2-12
2-3
3-3
3-Q-21 H
2-11
2-10
2-2
3-1
2-F-6 H
2-5
2-1
Troll Field outline
Fig. 7
5-3
5-6
5-H-5 H
5-2
6-6
10 km
6-1
6-5
6-2
N
6-8
6-3

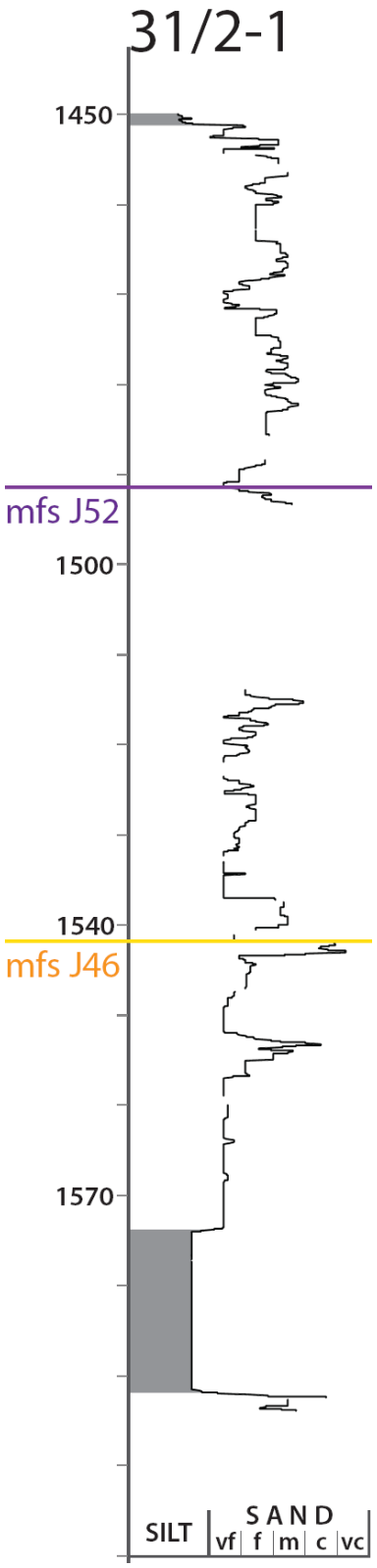
31/2-1
1450
mfs J52
1500
1540
mfs J46
1570
SILT
SAND
vf
f
m
c
vc

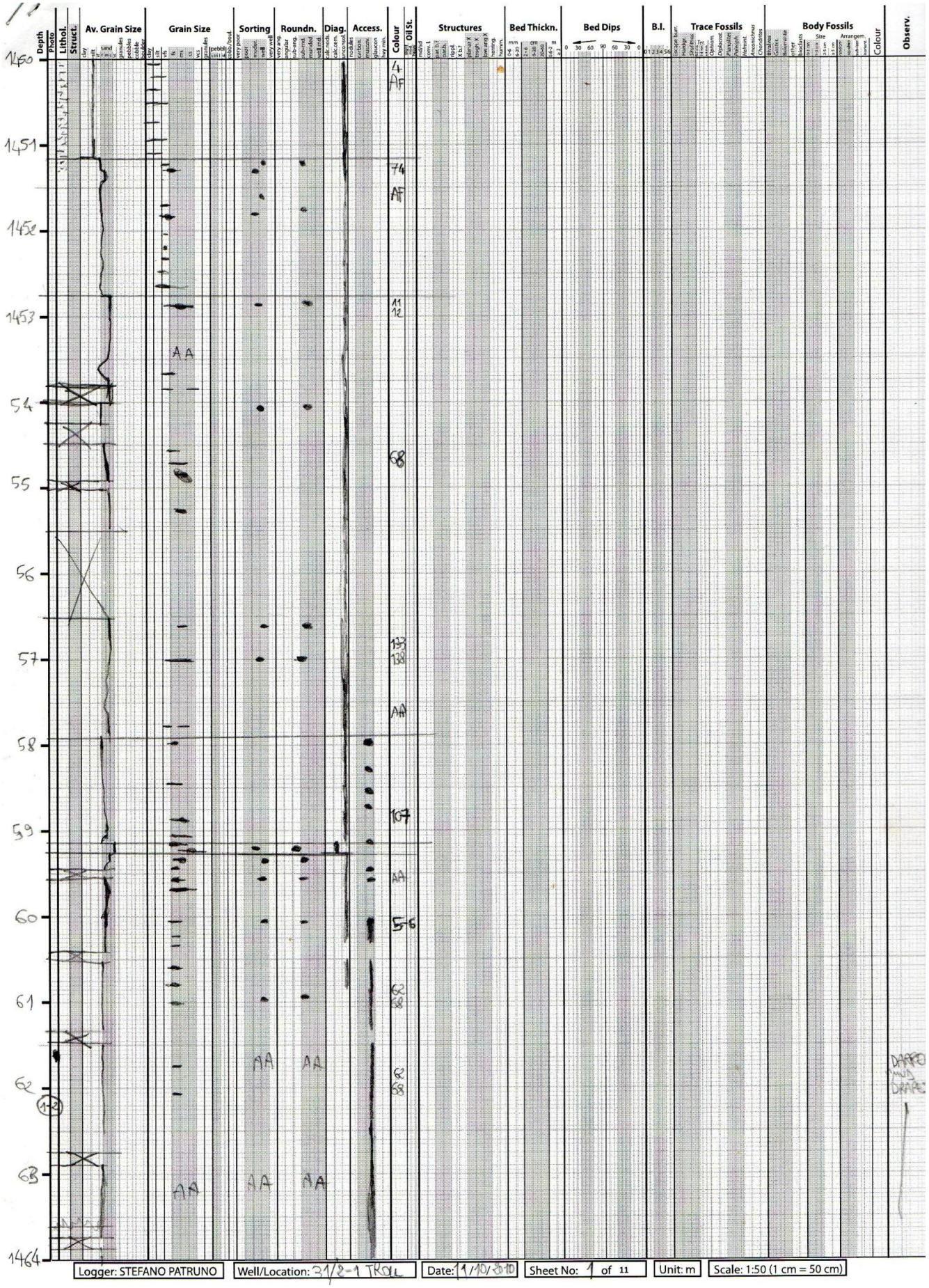
Depth
Photo
Lithol.
Struct.
Av. Grain Size
Grain Size
Sorting
Roundn.
Diag.
Access.
Colour
Oil St.
Structures
Bed Thickn.
Bed Dips
B.I.
Trace Fossils
Body Fossils
Observ.
1450
1451
1452
1453
54
55
56
57
58
59
60
61
62
63
1464
Logger: STEFANO PATRUNO
Well/Location: 31/8-1 TROLL
Date: 11/10/2010
Sheet No: 1 of 11
Unit: m
Scale: 1:50 (1 cm = 50 cm)

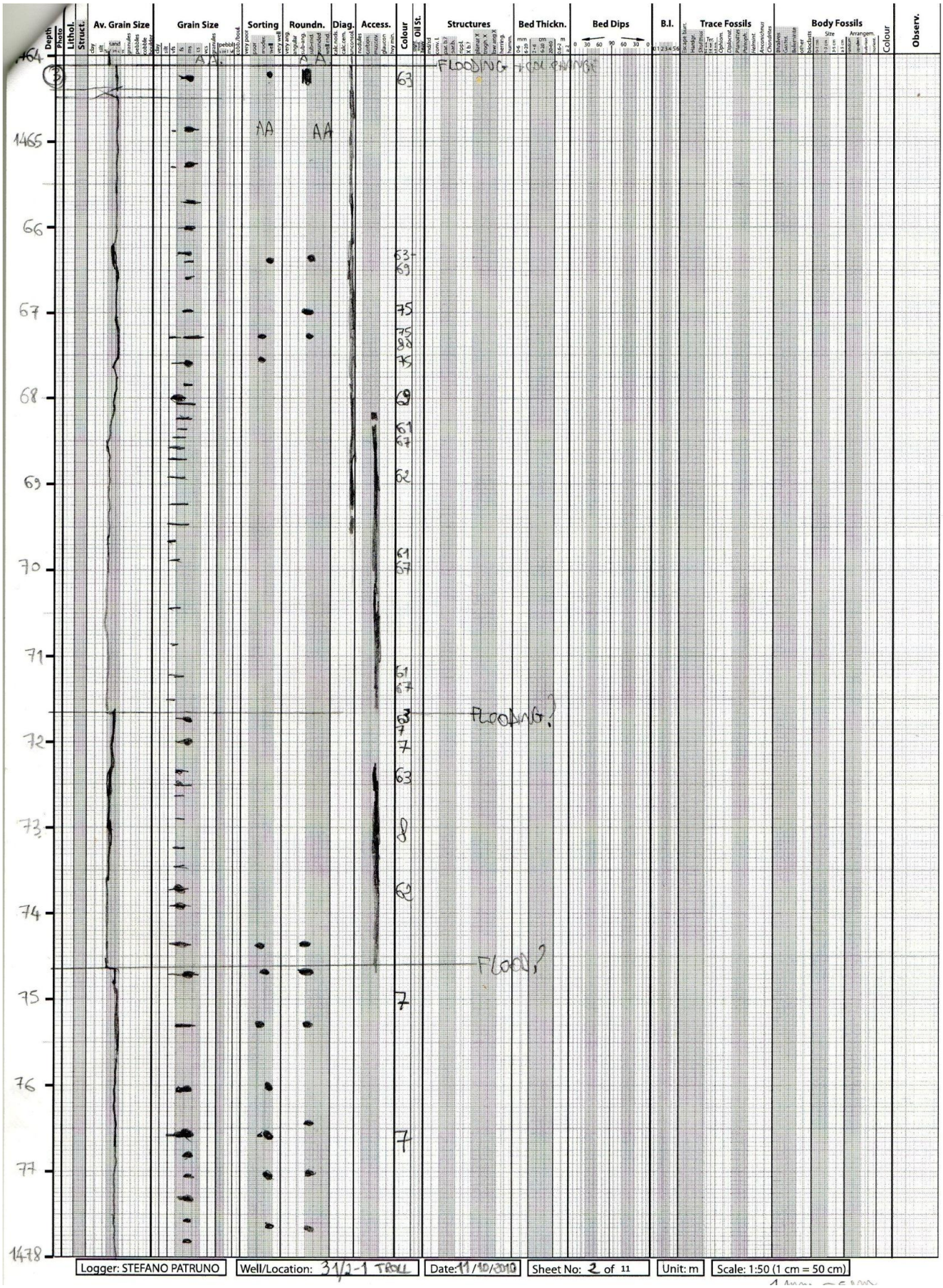
Depth
Photo
Lithol.
Struct.
Av. Grain Size
Grain Size
Sorting
Roundn.
Diag.
Access.
Colour
Oil St.
Structures
Bed Thickn.
Bed Dips
B.I.
Trace Fossils
Body Fossils
Observ.
1464
1465
66
67
68
69
70
71
72
73
74
75
76
77
1478
FLOODING
FLOODING?
FLOOD?
Logger: STEFANO PATRUNO
Well/Location: 31/2-1 TROLL
Date: 11/10/2010
Sheet No: 2 of 11
Unit: m
Scale: 1:50 (1 cm = 50 cm)

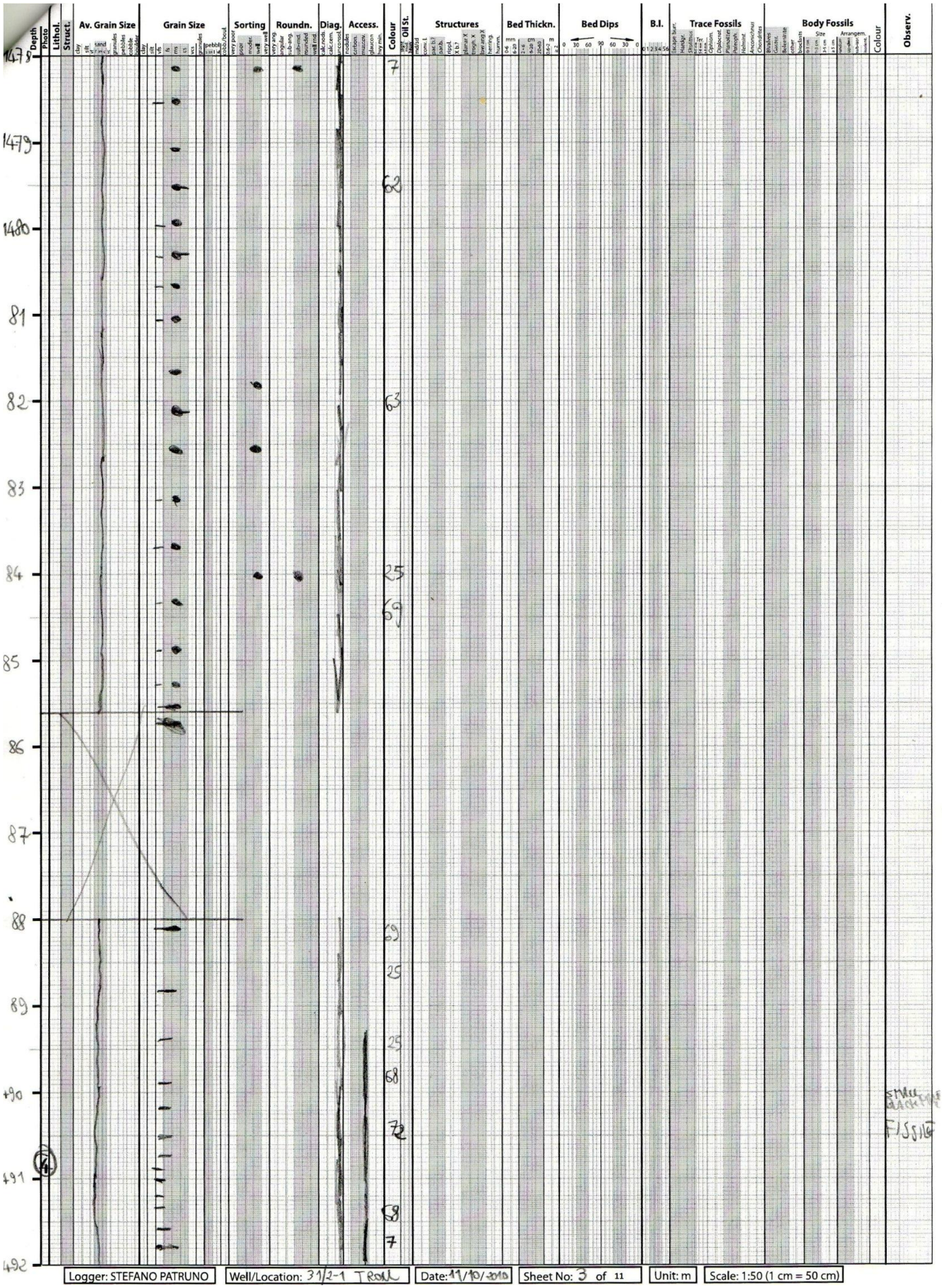
Depth
Photo
Lithol.
Struct.
Av. Grain Size
Grain Size
Sorting
Roundn.
Diag.
Access.
Colour
Oil St.
Structures
Bed Thickn.
Bed Dips
B.I.
Trace Fossils
Body Fossils
Observ.
Colour
1478
1479
1480
81
82
83
84
85
86
87
88
89
90
91
492
Logger: STEFANO PATRUNO
Well/Location: 31/2-1 T
Date: 11/10/2010
Sheet No: 3 of 11
Unit: m
Scale: 1:50 (1 cm = 50 cm)

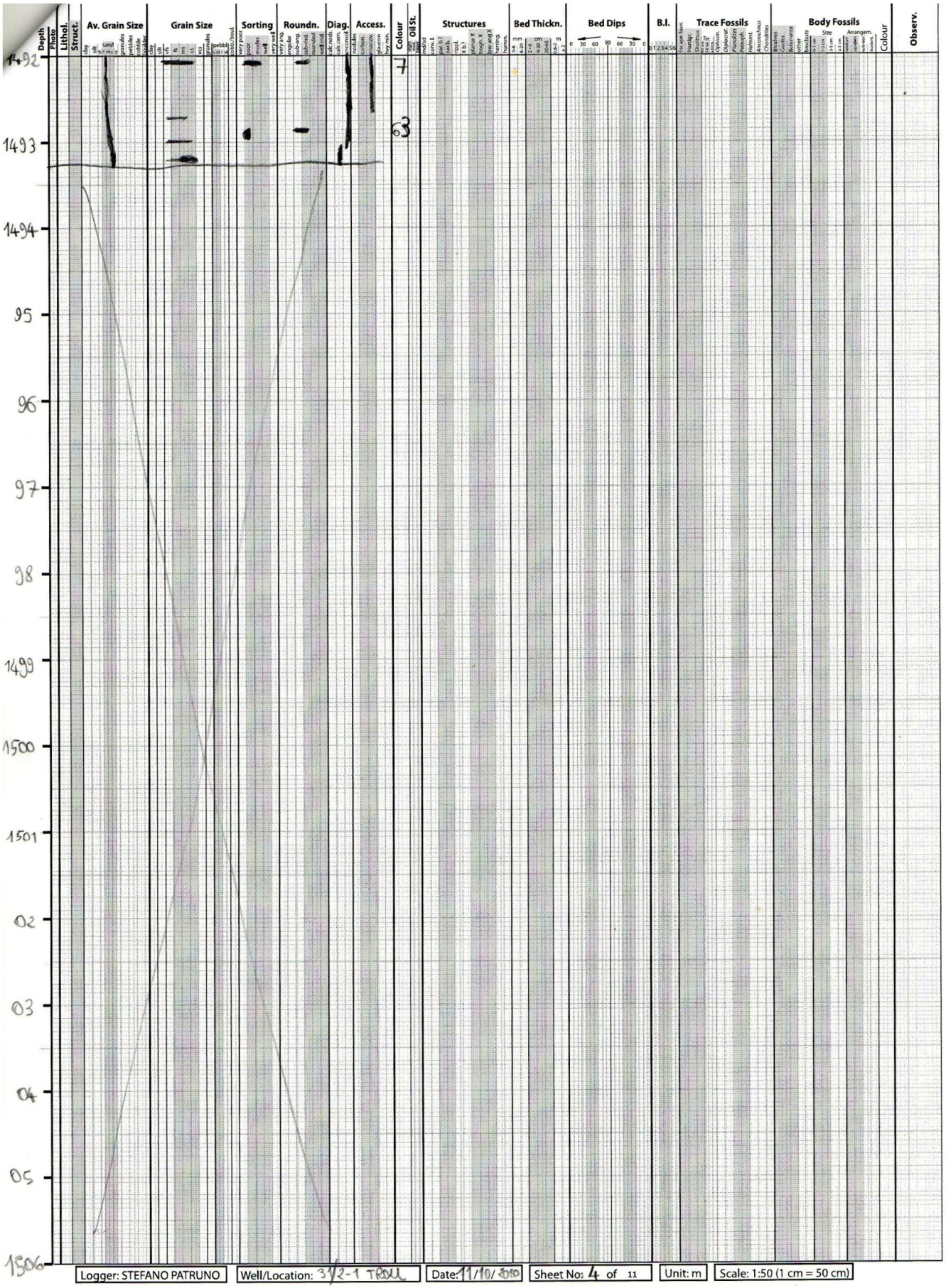
Depth
Photo
Lithol.
Struct.
Av. Grain Size
Grain Size
Sorting
Roundn.
Diag.
Access.
Colour
Oil St.
Structures
Bed Thickn.
Bed Dips
B.I.
Trace Fossils
Body Fossils
Observ.
1492
1493
1494
95
96
97
98
1499
1500
1501
02
03
04
05
1506
Logger: STEFANO PATRUNO
Well/Location: 3/2-1 TROLL
Date: 11/10/2010
Sheet No: 4 of 11
Unit: m
Scale: 1:50 (1 cm = 50 cm)

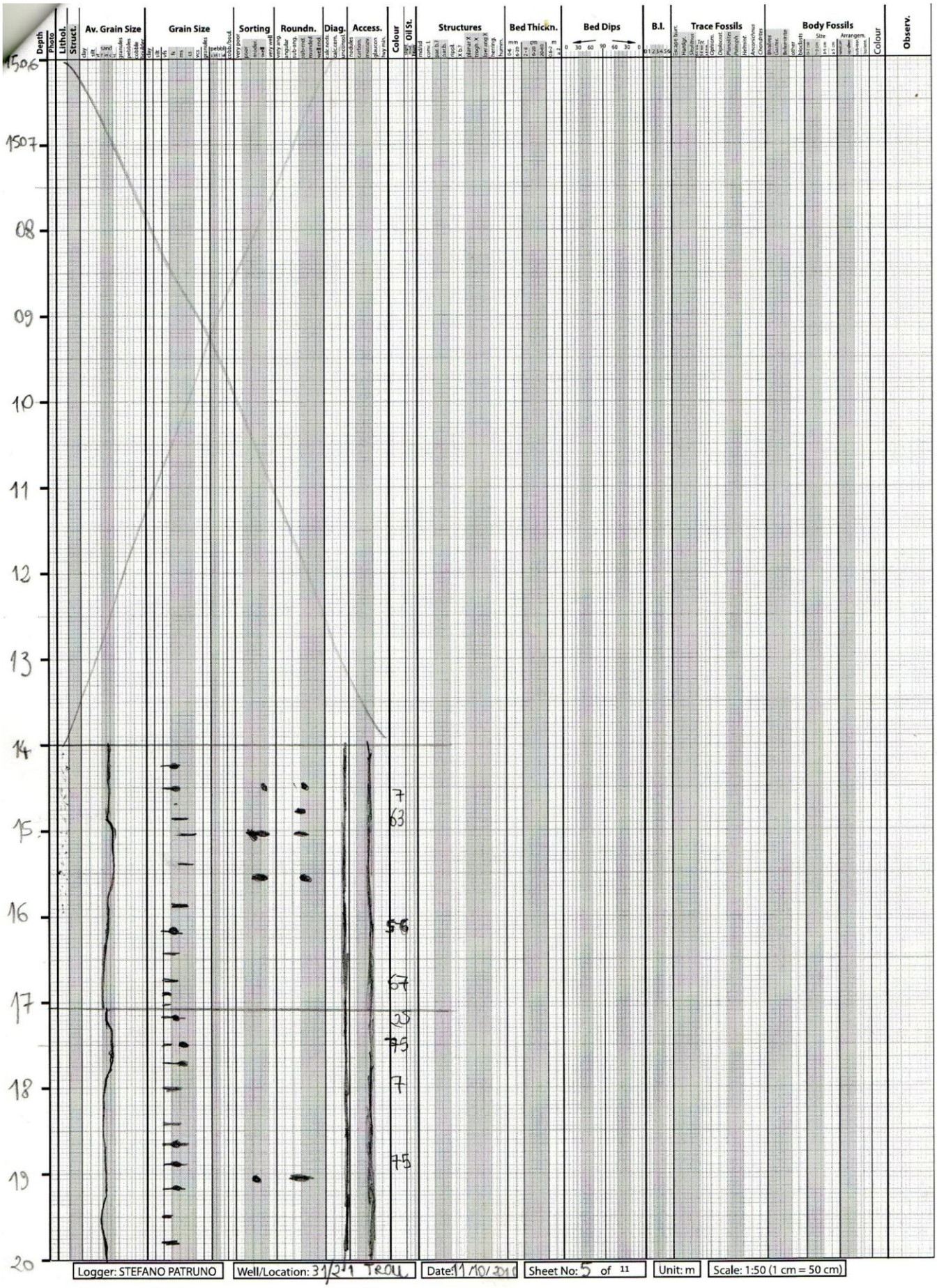
Depth
Photo
Lithol.
Struct.
Av. Grain Size
Grain Size
Sorting
Roundn.
Diag.
Access.
Colour
Oil St.
Structures
Bed Thickn.
Bed Dips
B.I.
Trace Fossils
Body Fossils
Observ.
1506
1507
08
09
10
11
12
13
14
15
16
17
18
19
20
63
56
67
25
75
7
75
Logger: STEFANO PATRUNO
Well/Location: 31/2-1 TROLL
Date: 11/10/2010
Sheet No: 5 of 11
Unit: m
Scale: 1:50 (1 cm = 50 cm)

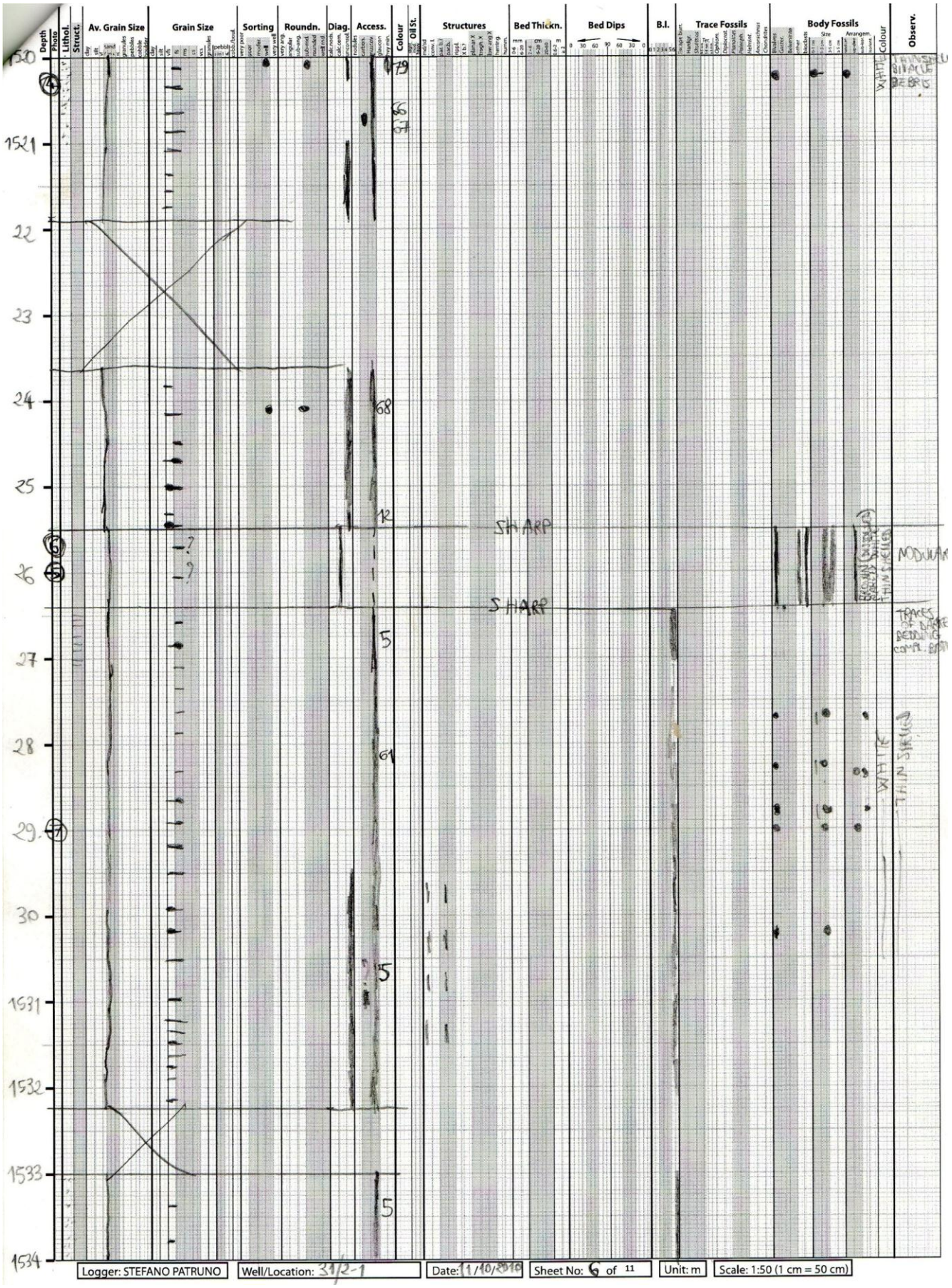
Depth
Photo
Lithol.
Struct.
Av. Grain Size
Grain Size
Sorting
Roundn.
Diag.
Access.
Colour
Oil St.
Structures
Bed Thickn.
Bed Dips
B.I.
Trace Fossils
Body Fossils
Observ.
1520
1521
22
23
24
25
26
27
28
29
30
1531
1532
1533
1534
SHARP
SHARP
MODULAR
TRACES OF PARA BEDDING
Logger: STEFANO PATRUNO
Well/Location: 31/2-1
Date: 11/10/2016
Sheet No: 6 of 11
Unit: m
Scale: 1:50 (1 cm = 50 cm)

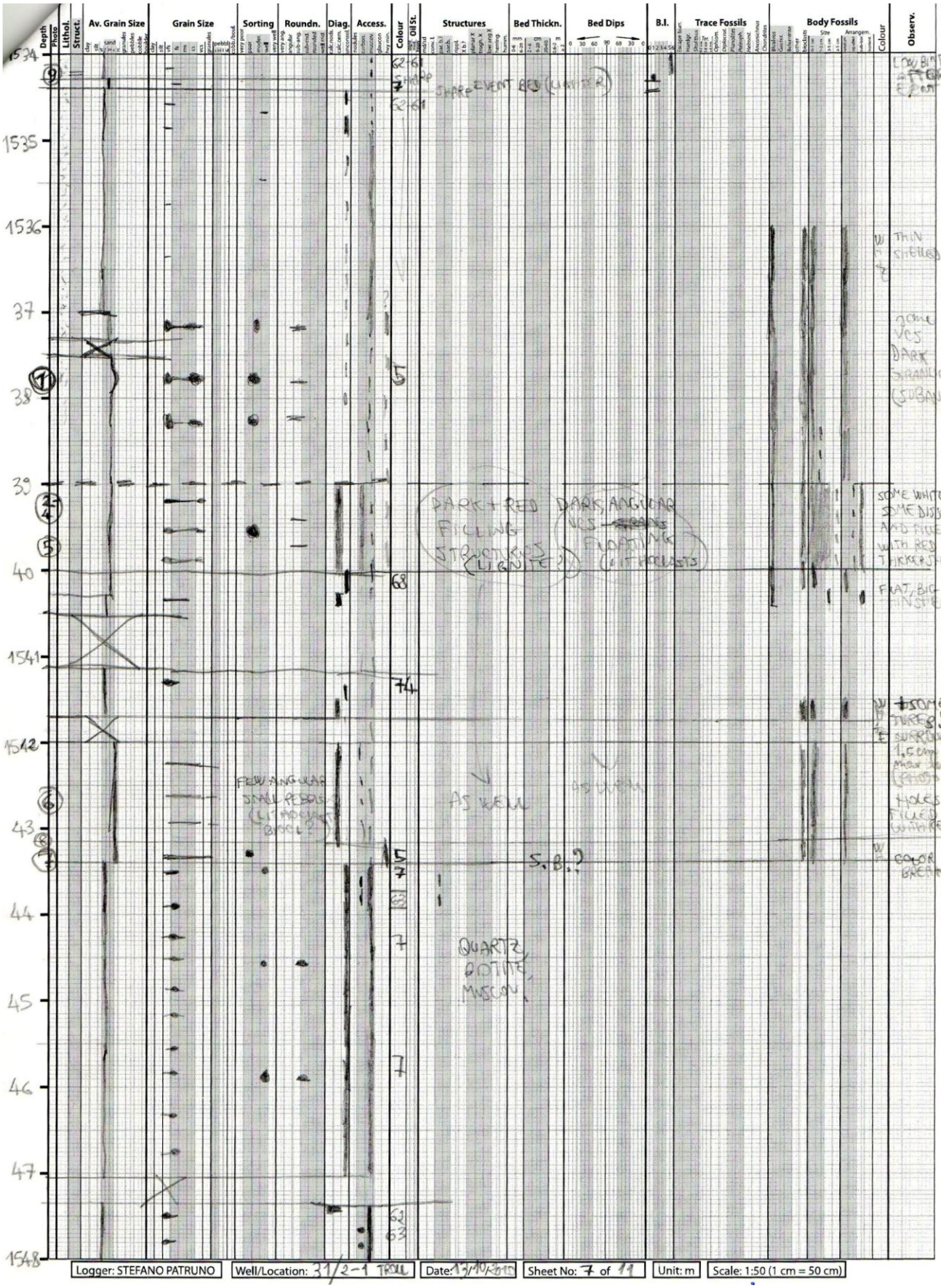
Depth
Photo
Lithol.
Struct.
Av. Grain Size
Grain Size
Sorting
Roundn.
Diag.
Access.
Colour
Oil St.
Structures
Bed Thickn.
Bed Dips
B.I.
Trace Fossils
Body Fossils
Observ.
1534
1535
1536
37
38
39
40
1541
1542
43
44
45
46
47
1548
THIN SHELLS
SOME WHITE
SOME DISSOLV
AND FILLED
WITH RED
FLAT, BIG
HOLES
FILLED
COLOR
BREAK
S.B.?
QUARTZ,
BIOTITE,
MUSCOV.
Logger: STEFANO PATRUNO
Well/Location: 31/2-1 TROLL
Date: 13/10/2015
Sheet No: 7 of 11
Unit: m
Scale: 1:50 (1 cm = 50 cm)

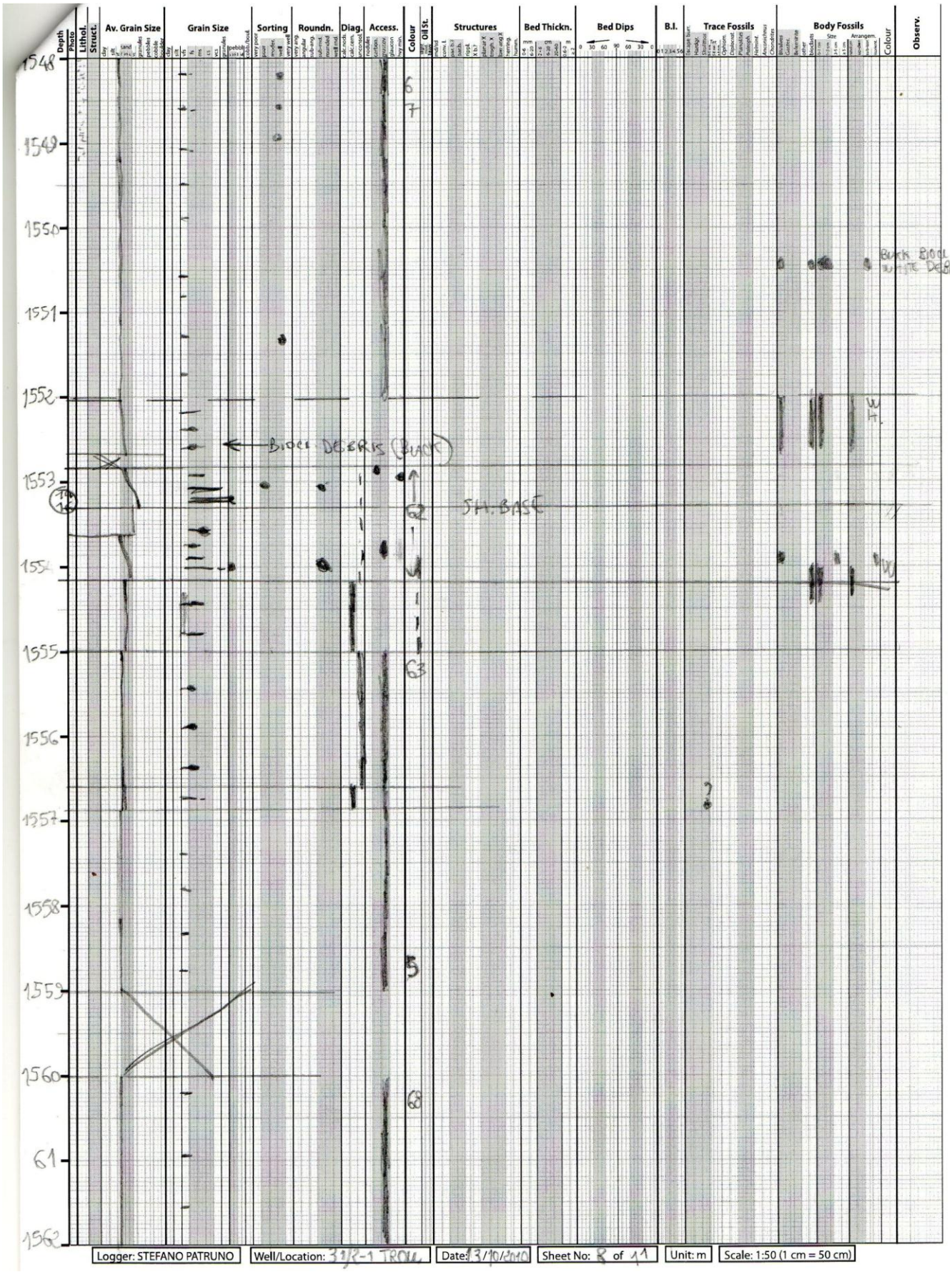
Depth
Photo
Lithol.
Struct.
Av. Grain Size
Grain Size
Sorting
Roundn.
Diag.
Access.
Colour
Oil St.
Structures
Bed Thickn.
Bed Dips
B.I.
Trace Fossils
Body Fossils
Observ.
1548
1549
1550
1551
1552
1553
1554
1555
1556
1557
1558
1559
1560
61
1562
BIOCL DEBRIS (BLACK)
SH. BASE
BLACK BIOCL
WHITE DEB
Logger: STEFANO PATRUNO
Well/Location: 31/2-1 TROLL
Date: 13/10/2010
Sheet No: 8 of 11
Unit: m
Scale: 1:50 (1 cm = 50 cm)

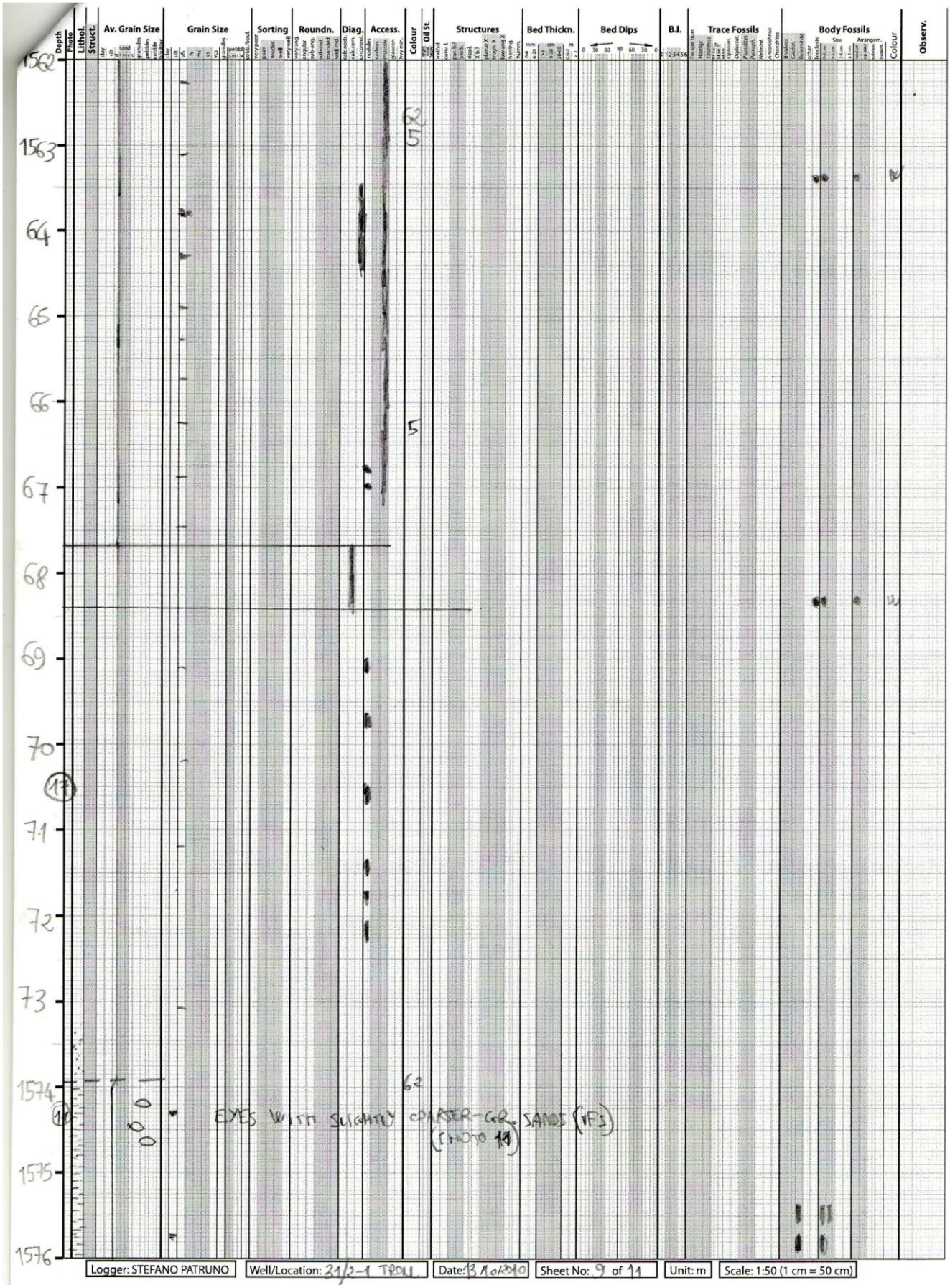
Depth
Photo
Lithol.
Struct.
Av. Grain Size
Grain Size
Sorting
Roundn.
Diag.
Access.
Colour
Oil St.
Structures
Bed Thickn.
Bed Dips
B.I.
Trace Fossils
Body Fossils
Observ.
1562
1563
64
65
66
67
68
69
70
71
72
73
1574
1575
1576
EYES WITH SLIGHTLY COARSER-GR. SANDS (VFS)
(PHOTO 19)
Logger: STEFANO PATRUNO
Well/Location: 31/2-1 TROLL
Date: 13 MAY 2010
Sheet No: 9 of 11
Unit: m
Scale: 1:50 (1 cm = 50 cm)

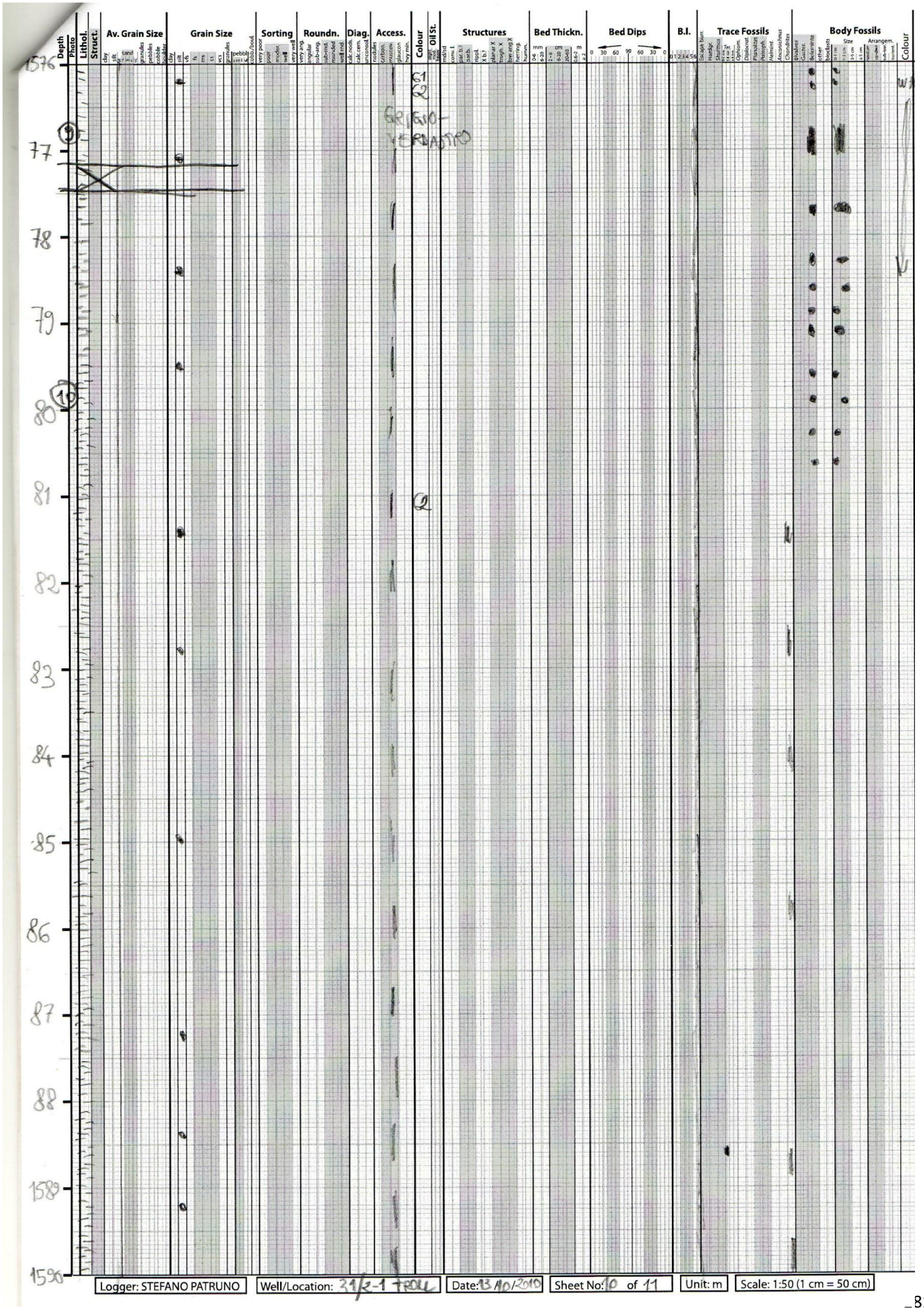
Depth
Phase
Lithol.
Struct.
Av. Grain Size
Grain Size
Sorting
Roundn.
Diag.
Access.
Colour
Oil St.
Structures
Bed Thickn.
Bed Dips
B.I.
Trace Fossils
Body Fossils
Size
Arrangem.
Colour
1576
77
78
79
80
81
82
83
84
85
86
87
88
1589
1596
Logger: STEFANO PATRUNO
Well/Location: 31/2-1 TROLL
Date: 13/10/2010
Sheet No: 10 of 11
Unit: m
Scale: 1:50 (1 cm = 50 cm)

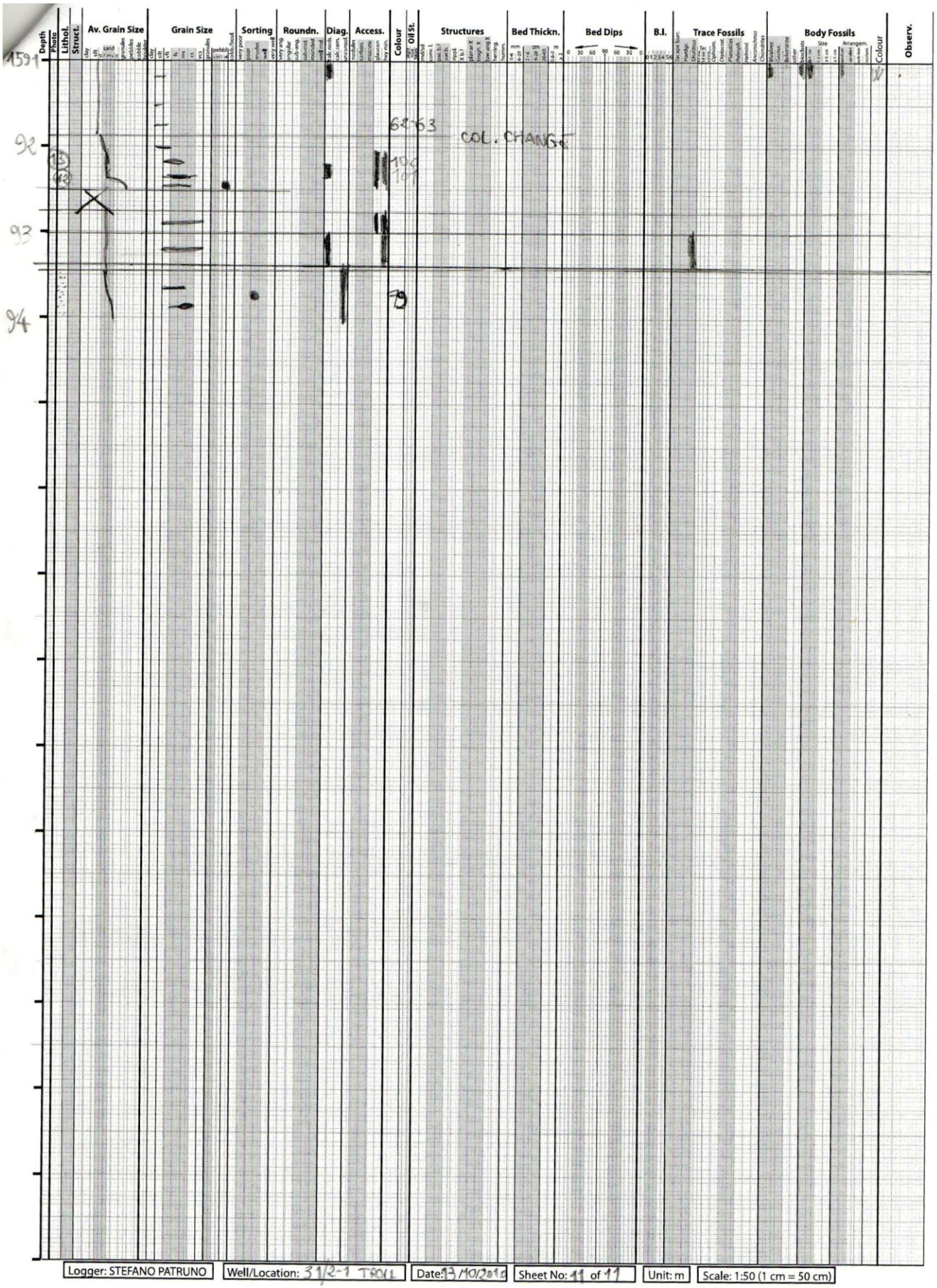
Depth
Photo
Lithol.
Struct.
Av. Grain Size
Grain Size
Sorting
Roundn.
Diag.
Access.
Colour
Oil St.
Structures
Bed Thickn.
Bed Dips
B.I.
Trace Fossils
Body Fossils
Observ.
1591
92
93
94
63-63
COL. CHANGE
Logger: STEFANO PATRUNO
Well/Location: 31/2-1 TROLL
Date: 13/10/2010
Sheet No: 11 of 11
Unit: m
Scale: 1:50 (1 cm = 50 cm)

31/2-3

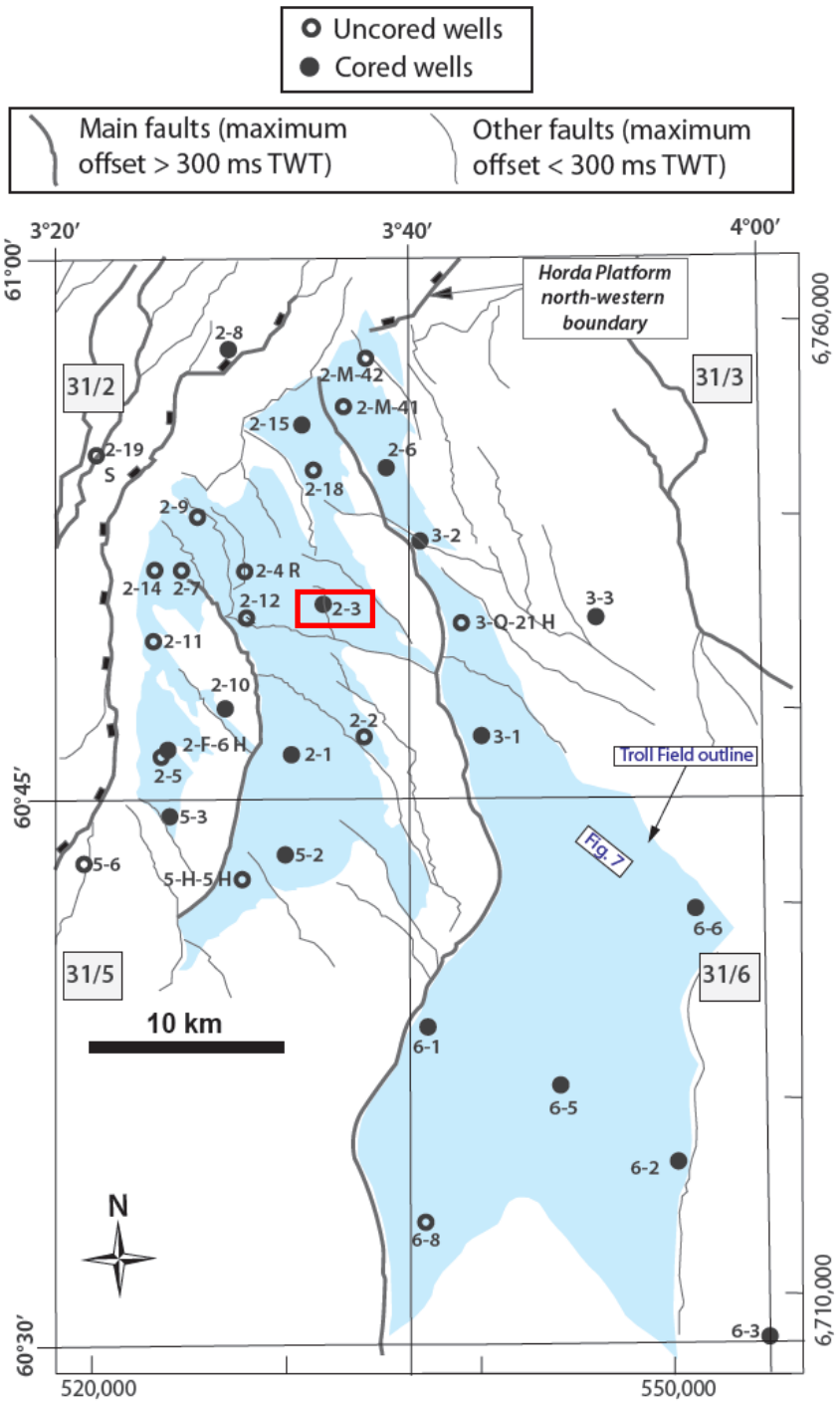
Uncored wells
Cored wells
Main faults (maximum offset > 300 ms TWT)
Other faults (maximum offset < 300 ms TWT)
3°20′
3°40′
4°00′
61°00′
60°45′
60°30′
6,760,000
6,710,000
520,000
550,000
Horda Platform north-western boundary
31/2
31/3
31/5
31/6
2-8
2-M-42
2-M-41
2-15
2-19 S
2-6
2-18
2-9
3-2
2-14
2-7
2-4 R
2-12
2-3
3-3
3-Q-21 H
2-11
2-10
2-2
3-1
2-F-6 H
2-5
2-1
Troll Field outline
Fig. 7
5-3
5-6
5-H-5 H
5-2
6-6
10 km
6-1
6-5
6-2
6-8
6-3
N

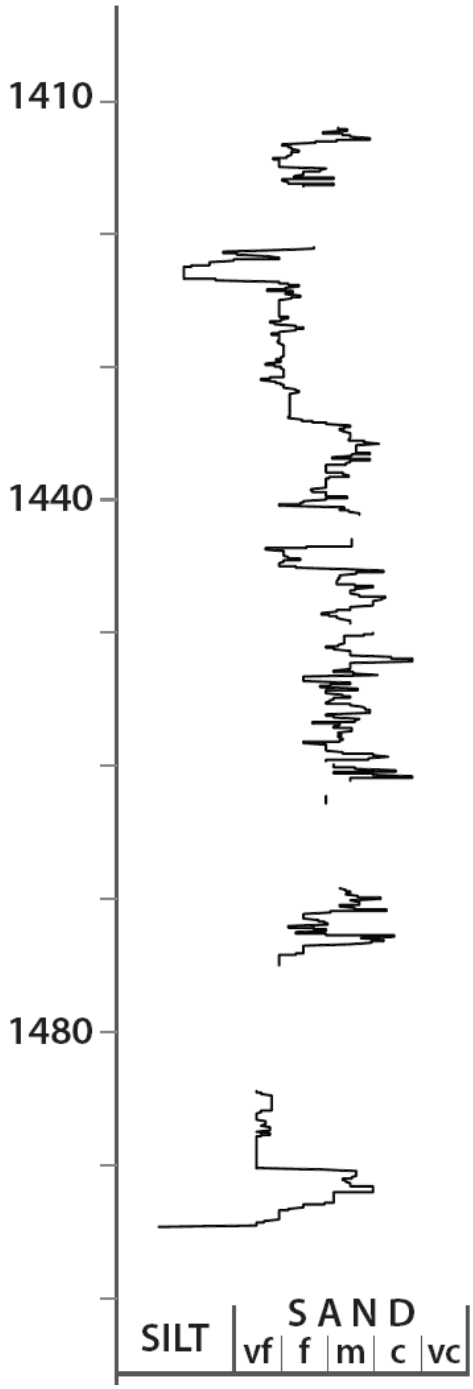
1410
1440
1480
SILT
SAND
vf
f
m
c
vc

A/S NORSKE SHELL | Well: 31/2-3 | Core No 1

CORE DESCRIPTION

Cored from 1412 to 1421M Recovered: 4.5M 50 % Core size: 4"

Formation: Date: 18/4/80 Described by: P. Stacher Corehead: Sheet: 1 of 1

DEPTH & SAMPLES	GRAPHIC LITHOLOGY	GRAIN SIZE (FINE / FINE / MED / CRS / CRS)	SEDIMENTARY STRUCTURES & FEATURES	COLOUR	COMPOSITION (& ACCESSORY MINERALS)	CMT	ESTIMATED %	HYDROCARBON INDICATIONS: SMPL FLU / CUT COL / CUT FLU	GAS %	REMARKS [OIL BLEED; DIPS; FRACTURES ETC.]
1412			(rnd)-(ang) (elong)-(sph)	gy blk	uncons arg cons (Mic)	((calc)) calc				
			srt	gy	uncons					
1413	mic		mod srt		uncons Mic cons (arg)	(calc)				
					uncons (Mic)					
			srt	gy	uncons-cons Mic					
			1413.80 mod srt		uncons					
1414	mic		srt-well srt		cons					
					uncons-cons					
					cons mod hd (Mic)					
			"Mud cracks" arg hor "tubes" wedging vertically	ltgy (brn)	cons, hd	calc	poor / mod - very good	none		none to very weak milky
1415			srt (rnd), (sph)	gy	(Mic)					
			1415.60		uncons	hon-calc	very good			
1416			srt-well srt (rnd)-(ang), (elong)-(sph)							
1416.5										

Drawing No. 13994

A/S NORSKE SHELL | Well: 31/2-3 | Core No 2

CORE DESCRIPTION

Cored from 1421 to 1425 M Recovered: 4 M gr. 100% % Core size: 4"

Formation: Date: 21/4/80 Described by: P. Stacher Corehead:

Sheet: 1 of 1

DEPTH & SAMPLES	GRAPHIC LITHOLOGY	GRAIN SIZE (FINE / FINE / MED / CRS / CRS)	SEDIMENTARY STRUCTURES & FEATURES	COLOUR	COMPOSITION (& ACCESSORY MINERALS)	CMT	ESTIMATED %	HYDROCARBON INDICATIONS: SMPL FLU / CUT COL / CUT FLU	GAS %	REMARKS [OIL BLEED; DIPS; FRACTURES ETC.]
1421			FS, slstone MS VFS/FS VFS/FS SILTST VFS lenses and "nodules" of: - MdstSh (yel), hd, ((chk)) SILTST SILTST - siliceous/calc nodules; CALCSTONE MARLSTONE - hd SH/clst nodules in diameter of up to 2cm MARLSTONE HARD SILICEOUS FS MULTI COLR MARLSTONE SHALE FS/VFS 1423.90 FS/some VFS FS (coarse) FS/VFS srt - srt VFS FS ang - (ang) FS/VFS (rnd) - rnd 1424.60 FS/VFS, fissile MS FS (coarse) FS/VFS	dkbrn to blk	UND — ARKIVET Nr.: 4					
1422					slt-(s)					
1423				dkbrn to blk	slt-s					
1424					mic					
				gy	uncons lse-fi		good	no dir Flu		
1425										

Drawing No. 13994

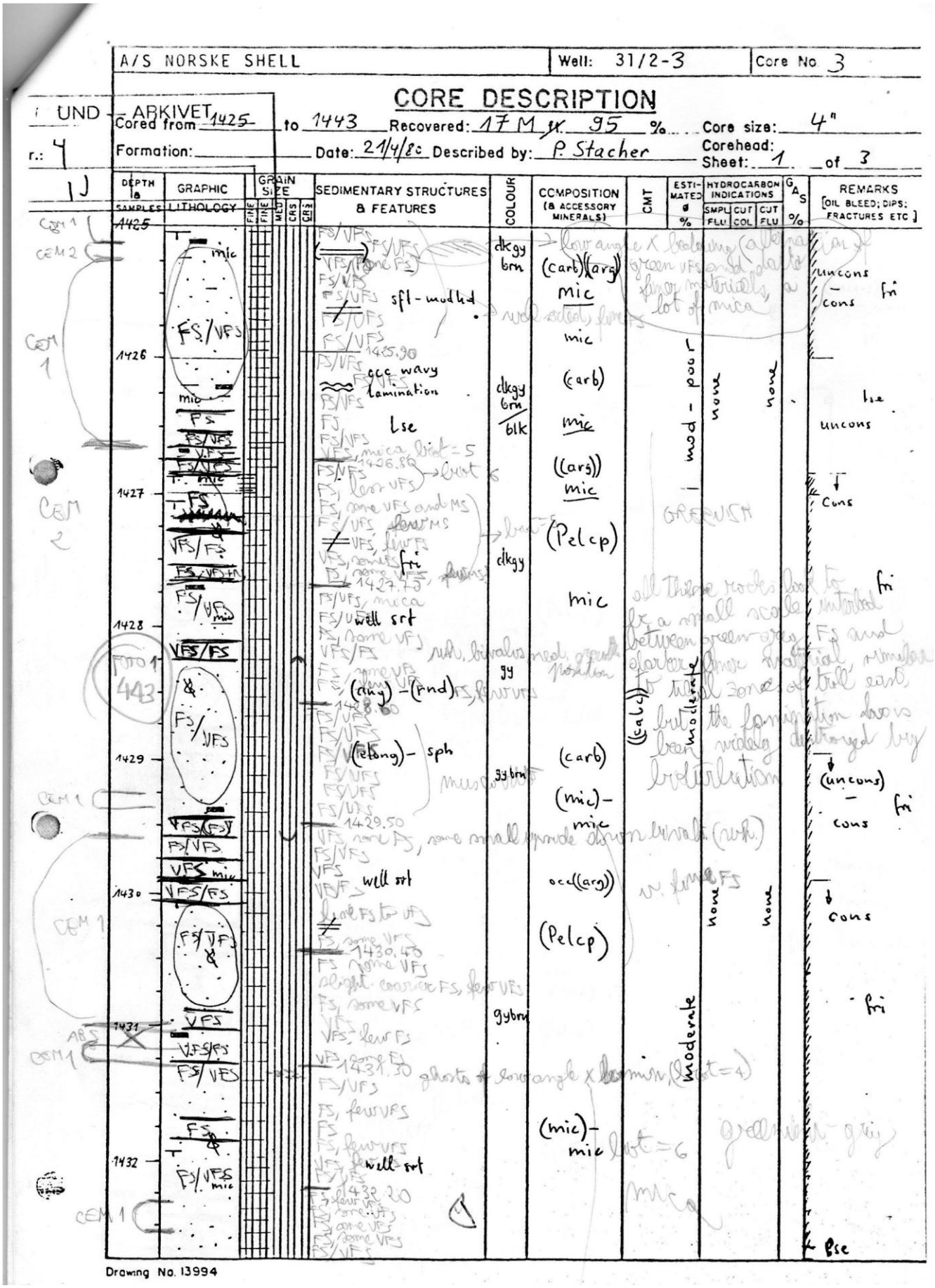
A/S NORSKE SHELL
Well: 31/2-3
Core No. 3
CORE DESCRIPTION
ARKIVET
Cored from 1425 to 1443 Recovered: 17 M 95 % Core size: 4"
Formation: Date: 21/4/80 Described by: P. Stacher
Corehead:
Sheet: 1 of 3
DEPTH m
SAMPLES
GRAPHIC LITHOLOGY
GRAIN SIZE
SEDIMENTARY STRUCTURES & FEATURES
COLOUR
COMPOSITION (& ACCESSORY MINERALS)
CMT
ESTIMATED %
HYDROCARBON INDICATIONS
SMPL FLU
CUT COL
CUT FLU
GAS %
REMARKS [OIL BLEED; DIPS; FRACTURES ETC.]
1425
1426
1427
1428
1429
1430
1431
1432
Drawing No. 13994

A/S NORSKE SHELL | Well: 31/2-3 | Core No 3

CORE DESCRIPTION

Cored from 1425 to 1443 Recovered: 17 M 95 % Core size: 4"

Formation: Date: 21/4/83 Described by: P. Stacher Corehead: Sheet: 2 of 3

DEPTH & SAMPLES	GRAPHIC LITHOLOGY	GRAIN SIZE (FINE / FINE / MED / CRS / CRS)	SEDIMENTARY STRUCTURES & FEATURES	COLOUR	COMPOSITION (& ACCESSORY MINERALS)	CMT	ESTIMATED %	HYDROCARBON INDICATIONS: SMPL FLU	CUT COL	CUT FLU	GAS %	REMARKS (OIL BLEED; DIPS; FRACTURES ETC.)
1433	(mic) FS/VFS		FS, very few VFS; FS, very few VFS; well srt; (ang)-(rnd); (elong)-(sph); FS/VFS; FS, some VFS; VFS, some FS; 1433.10	gy-brn	(mic)	((calc))	mod-good	none	none			(uncons) - cons fri
1434	VFS, FS; FS/MS, VFS; FS/CS, VCS, VFS; FS/MS, CS		FS/MS, few VFS; FS/MS, few VFS; FS/CS, few VCS and VFS; FS/CS, few VCS and VFS; FS/MS, few VCS; FS/MS, few CS; srt-well srt; 1434.90	Lt gy brn								
1435	FS/CS		FS/CS; FS/CS; FS/CS; MS, some CS and VFS; CS, some CS, some FS/VFS; 1435.80		occ (mic); (Pelsp)							lse
1436	FS/MS + CS; MS + CS; FS + MS		(ang)-(rnd); (elong)-sph; MS, some CS; FS/MS, some CS; MS, some FS and CS; FS/MS, some CS/VCS; MS, some CS; 1436.70				very good	none - occ very weak yellowish				(cons)
1437	FS/VCS; FS/CS; MS; FS/MS		FS, a few MS; FS/VCS; FS/CS; MS; FS, some MS; 1437.60 FS/MS	gy and Lt gy brn					very weak milky			uncons - (cons) lse parts (fri)
1438	FS/MS + CS; FS/MS		FS/MS some CS; MS, some FS, some CS; FS/MS; 1438.50 FS/MS; FS, some MS; FS/MS; FS/MS		occ (mic); (Pelsp)							
1439	FS/MS; FS/MS + CS		FS/MS some CS; srt-well srt; 1439.40 FS some MS; FS/MS; FS/MS, some CS; FS, some MS; FS		occ (carb) stks		very good					lse
1440	FS, MS; FS; VFS/FS; VFS/CS, VCS		1440.30 FS/some VFS; VFS/FS; VFS/CS some VCS									

Drawing No. 13994

A/S NORSKE SHELL | Well: 31/2-3 | Core No 3

CORE DESCRIPTION

Cored from 1425 to 1443 Recovered: 17 M 95 % Core size: 4"

Formation: _____ Date: 21/4/80 Described by: P. Stacher Corehead: Sheet: 3 of 3

DEPTH & SAMPLES	GRAPHIC LITHOLOGY	GRAIN SIZE (FINE / FINE / MED / CRS / CBS)	SEDIMENTARY STRUCTURES & FEATURES	COLOUR	COMPOSITION (& ACCESSORY MINERALS)	CMT	ESTIMATED Ø %	HYDROCARBON INDICATIONS: SMPL FLU	CUT COL	CUT FLU	GAS %	REMARKS [OIL BLEED; DIPS; FRACTURES ETC.]
1441	MS/CS, VCS; FS. MS; MS/CS; FS		≠ MS/CS common VCS; FS, few MS; MS/CS, few VCS srt - well srt (ang) - (rnd) (elong) - (sph)		(mic) occ (carb)		good	Very weak (yel)		very weak milky		lse,
1442												
1443												

Core 1 END CORE 3

Drawing No. 13994

A/S NORSKE SHELL | Well: 31/2-3 | Core No 4

CORE DESCRIPTION

Cored from 1443 to 1450 Recovered: 6.25 m ~~91~~ 90 % Core size: 4"

Formation: _____ Date: 22/4/80 Described by: P. Stacher Corehead:

Sheet: 1 of 1

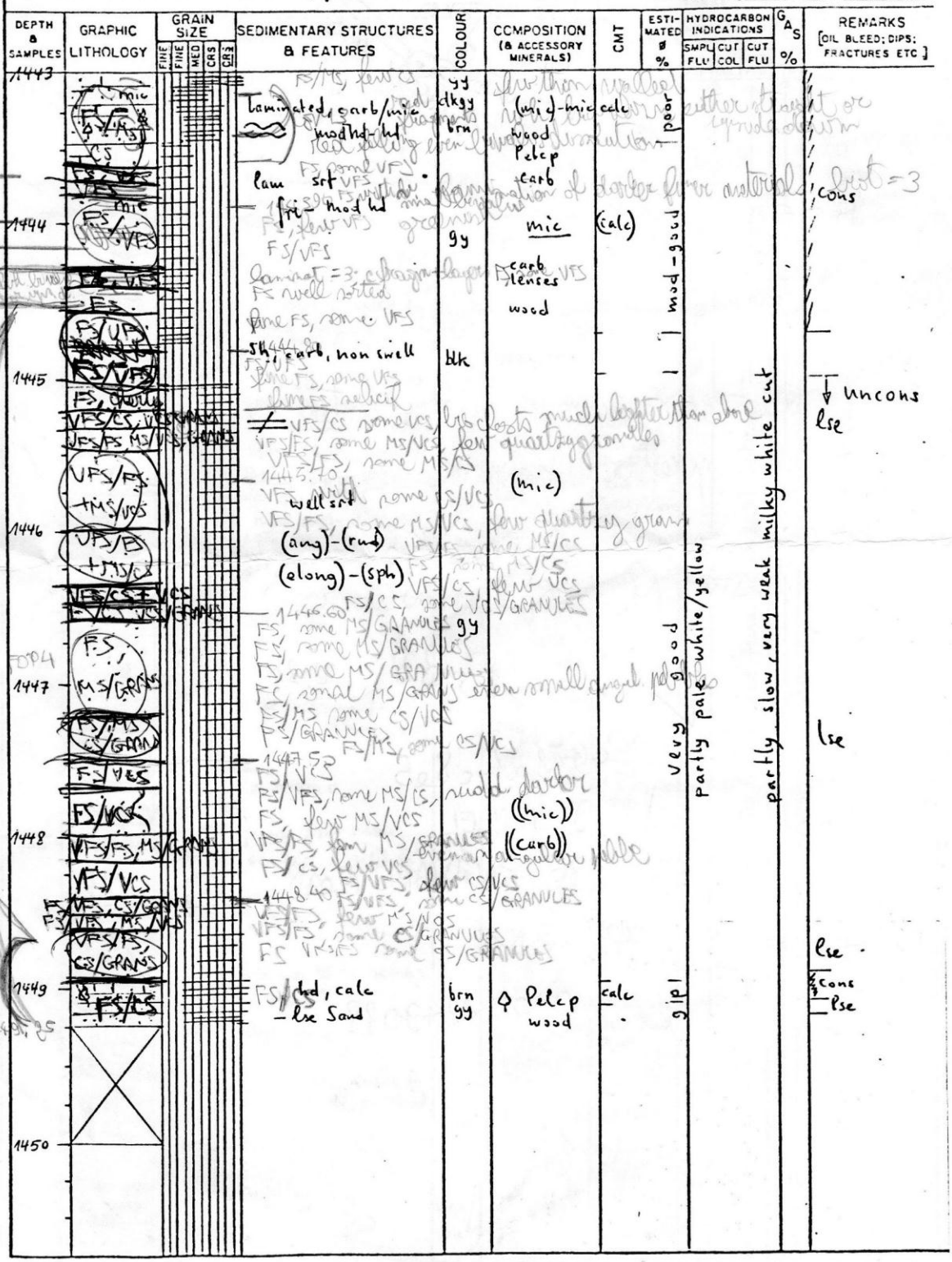

Drawing No. 13994

No.: 14

A/S NORSKE SHELL | Well: 31/2-3 | Core No. 5

CORE DESCRIPTION

Cored from 1450 m to 1462 m Recovered: 11·20 m 93 % Core size: 4"

Formation: J. Sst. Date: 22.4.80 Described by: S. Willis / A. Beecham Corehead: Sheet: 1 of 2

DEPTH & SAMPLES	GRAPHIC LITHOLOGY	SEDIMENTARY STRUCTURES & FEATURES	COLOUR	COMPOSITION (& ACCESSORY MINERALS)	CMT	HYDROCARBON INDICATIONS	GAS %	REMARKS [OIL BLEED; DIPS; FRACTURES ETC.]
1450	FS/VCS; MS/VFS; some VCS/GRANS; FS/MS	Ss, fsl-pbl ((svt)), md fri-uncons. Poss. erosion surface. Irregular cementation Calc. sst. hd. Shell debris.	Gy (bn); Ltgy	Quartz, feldspar, occ mica throughout. Tr. carb. mat. thr'out. Pyrite.	CALC.	NIL	0%	lower part of cm = 3 becomes a subrounded floating pit coquina (MS/FS) and some reddish beds are intercalating in limestone (FOTO 5-7)
1451	FS/CS; FS/MS, VFS	Generally unconsolidated to very friable. 1451.80		FS/CS; FS/MS, some CS, VFS; FS/CS, some VCS, VFS				
1452	VCS/CS; FS/MS, GRANS; FS/VFS, some CS/GRANS	Sst, gy-ltgy (bn). Occ rose coloured grs, fri-uncons., vwl, sph-(sph), mod. srt. Patchy calc cmt. fri (hd). 1452.70		VCS/CS, some FS/MS; same, some floating black grans; FS/VFS " some CS; FS/VFS, some CS GRAN; FS/VFS, few CS/CS	Patchy Calc cmt s/t, wh. (due to shell debris)	Trace pale, dull yellow cut fluo. in isolated samples		(FOTO 8)
1453	VFS/VCS; MS/CS, FS/VFS; FS/MS, CS; VFS/FS, CS/GRANS; VFS/MS	Pred msl-msu sst. occ cs. - (pbl). 1453.60		VFS/VCS; MS/CS, some FS/VFS; FS/MS, few CS; VFS/FS, some CS/GRANULES; VFS/MS; VFS/MS, some CS/VCS	Tr. coal fragments.			
1454	VFS/CS, V.CS; VFS/FS, CS; VFS/MS, CS/VCS; FS/MS/VCS	fsl-gran. (rnd) (sph) - (elong), ((srt)). 1454.50. PY NODULE		VFS/CS, some VCS; VFS/FS, some CS; VFS/MS, some CS/VCS; Qutz, (py) (mica) (carb) feldspar frag. Occ. gy litho frag. FS, some MS/CS, few VCS; FS, some CS, some VCS				
1455	VFS/FS, CS/VCS; FS/VCS, VFS; FS/MS; FS, CS/VCS; VFS/GRANS	pred fsl-msu. occ cs. (srt)-srt. 1455.40		VFS/FS, few CS/VCS; FS/VCS, few VFS; FS/MS; FS, some CS/VCS; VFS/VCS, few granules				
1456	FS/CS, GRANS; VFS/FS, CS; FS/CS; FS/MS, CS/GRANS; FS/CS	Appears to be lenses f-m sst, srt. More angular. 1456.30. Cl, slty, s/t, lenses f bm sst. Ripple x-bed	Dk gy	FS/VCS, few granules; FS/CS; FS/CS, few granules; VFS/FS, few CS; FS/CS; FS/MS, some CS/GRANULES; FS/CS	Local s/t Calc cmt a.a.			1.17
1457	VFS/FS, MS; VFS/MS, CS; MS/CS, VCS; VFS/MS, CS; FS, CS/VCS	Sst, fsl-msl (srt) - srt, (ang) - (rnd), slightly ang.	Ltgy/wh	VFS/FS, few MS; FS/CS; (mic) (py) VFS/MS, some CS; VFS/FS, some CS; MS/CS, few VCS; VFS/MS, few VCS CS; FS, some CS/GRANS; FS, some CS				

Margin notes: CEM 1; CEM 3; FOTO 8; CEM 1

Drawing No. 13994

A/S NORSKE SHELL | Well: 31/2-3 | Core No 5

CORE DESCRIPTION

Cored from 1450m to 1462m Recovered: 11.20m ± 93 % Core size: 4"

Formation: J. Sst. Date: 22/4/80 Described by: Willis / Beacham Corehead:

Sheet: 2 of 2

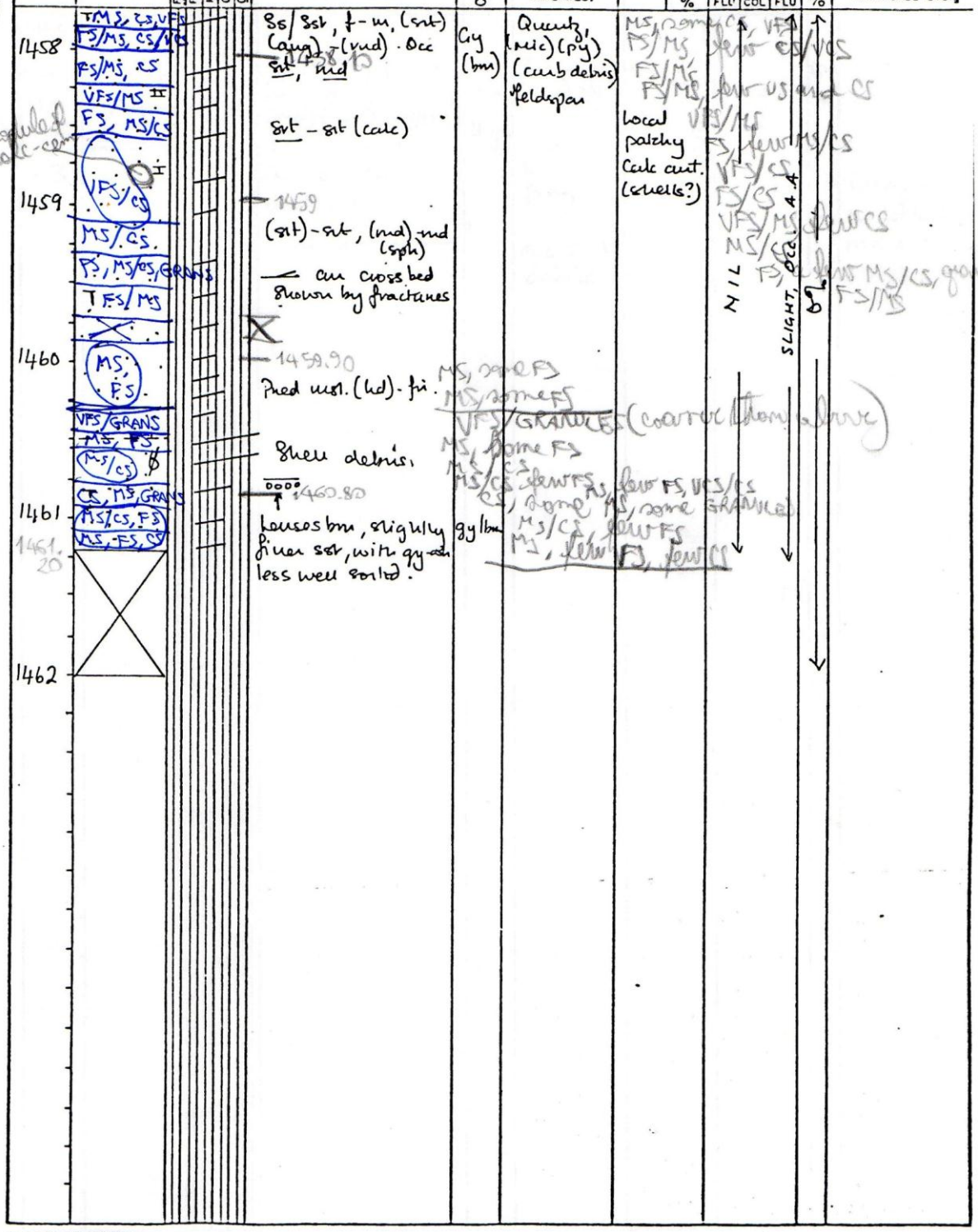

A/S NORSKE SHELL | Well: 31/2-3 | Core No 6

CORE DESCRIPTION

Cored from 1462·36 to 1462·85 Recovered: 40cm N. 80 % Core size: 4"

Formation: J. Sst Date: 22·4·80 Described by: S. Willis / A. Beacham Corehead: CB 17 Sheet: 1 of 1

DEPTH & SAMPLES	GRAPHIC LITHOLOGY	GRAIN SIZE (FINE / FINE / MED / CRS / CRS)	SEDIMENTARY STRUCTURES & FEATURES	COLOUR	COMPOSITION (& ACCESSORY MINERALS)	CMT	ESTIMATED %	HYDROCARBON INDICATIONS: SMPL FLU	CUT COL	CUT FLU	GAS %	REMARKS [OIL BLEED; DIPS; FRACTURES ETC.]
1462							Good					
1462.36			Ss/Sst, gy-brn fi-md, few-mod (md)(sph)(mic)(py) occ cs-pbl in calc cmt nodule. ⌐ in nodule?	Gy-brn 4.gy	Quenk (mic) (py) Carb frag. Occ shell detris.	FS/MS Calc	Nil	NIL			0 %	Core jammed on Lst/Sst nodule.
FS/MS .76												
1463												

Drawing No. 13994

A/S NORSKE SHELL | Well: 31/2-3 | Core No. 8

CORE DESCRIPTION

Cored from 1465.2 to 1473.0 Recovered: 3.8 m 11. 47 % Core size: 4"

Formation: Jurassic Sst. Date: 24/4/80 Described by: S. Willis A Beecham Corehead: CB17

Sheet: 1 of 1

DEPTH & SAMPLES	GRAPHIC LITHOLOGY	GRAIN SIZE (FINE FINE MED CRS CRS)	SEDIMENTARY STRUCTURES & FEATURES	COLOUR	COMPOSITION (& ACCESSORY MINERALS)	CMT	ESTIMATED %	HYDROCARBON INDICATIONS: SMPL FLU	CUT COL	CUT FLU	GAS %	REMARKS [OIL BLEED; DIPS; FRACTURES ETC.]
1466												FORMATION PROBABLY LSE SAND (as below), BUT TOP OF CORE WASHED OUT DURING RECOVERY.
1467												
1468												
1469												
1469.20	VFS/CS, VCS		Ss, F-CRS, occ M-CRS, scatt. PEB, (ANG)-(RND), (SPH), SRT-(SRT), LSR	lt gy	qz (tsp) ((carb)) (calc.qz.)	local (calc) cmt		NIL	CORE SAT. WITH WATER DURING PUMPING		0%	Ss, lse/ uncons washed out during pumping of core
1470	CS, VCS, MS		1470.10 FS/CS MS/CS, some FS									
1471	VFS/MS?		sandy top - irreg. contact - poss. erosion surface. Calc cmt. sst, F-PEB, (ANG) HD shell beds 2-4cm, lamellis (Rhynes?)	gy	qz, calc (tsp) (carb)	calc						
1472	VFS, MS		Ss, F-CRS, acc. PEB, (RND)-(ANG) SRT (SPH), LSR, lt gy		qz calc (tsp) (carb)	local calc. cmt						
1473	FS/CS, VCS, MS		1471.90 Cist, dk gy w/ wht-lt gy Silt-FSU ss lenses, acc. MSC (~7) (=mm)	dk gy/ wht-lt gy	qz calc. ((carb))	calc str. & lenses						

Drawing No. 13994

A/S NORSKE SHELL | Well: 31/2-3 | Core No 9

CORE DESCRIPTION

Cored from 1473 to 1484·4 Recovered: 2ms & 18 % Core size: 4"
Formation: J. Sst Date: 25·4·80 Described by: Willis / Beecham Corehead: CB 17
Sheet: 1 of 1

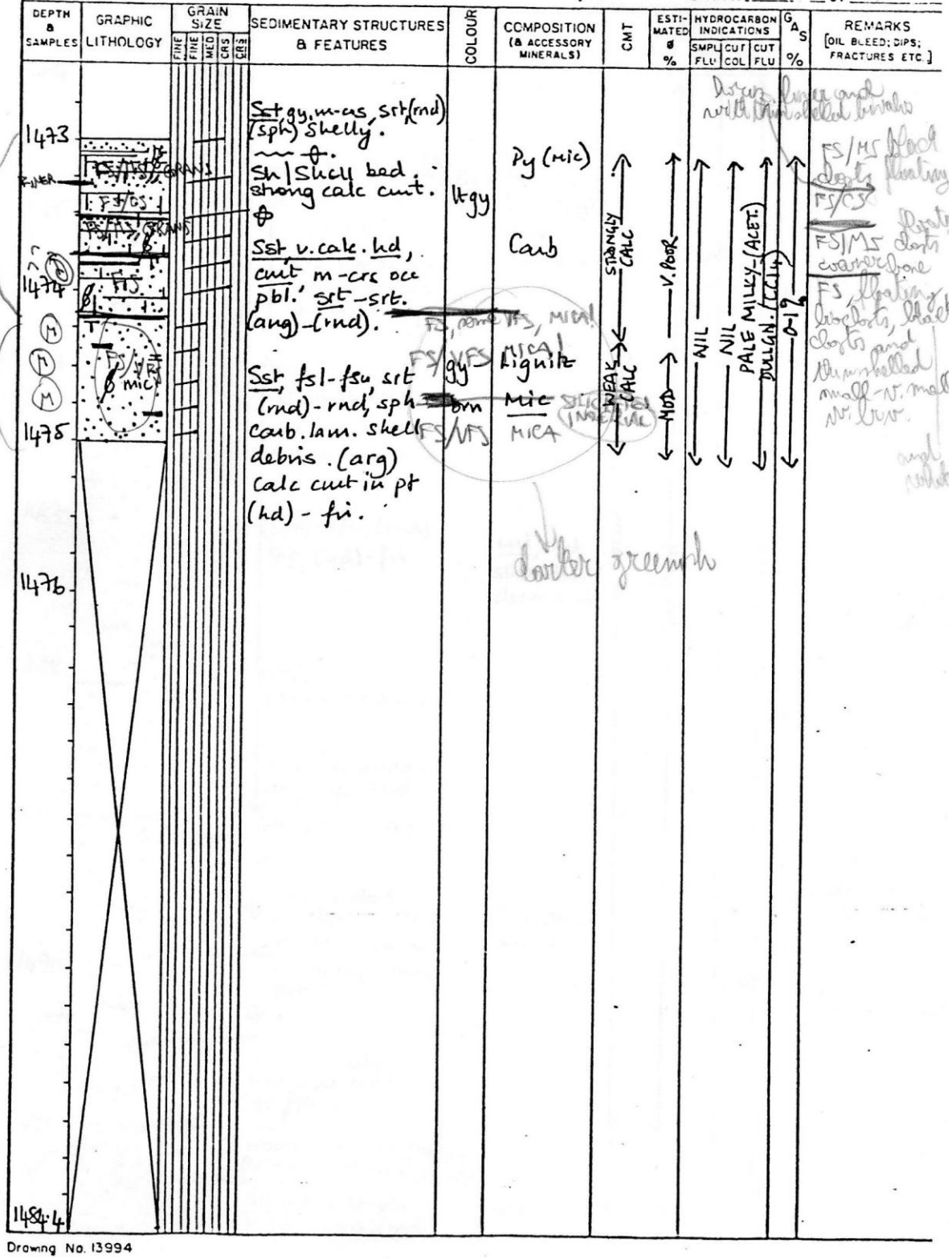

Drawing No. 13994

TO COMPLETE: cores 10-11

A/S NORSKE SHELL | Well: 31/2-3 | Core No. 10

CORE DESCRIPTION

Cored from 1484·45 to 1496·4m Recovered: 11·95m & 100 % Core size: 4"

Formation: J. Sst. Date: 25·4·80 Described by: S. Willis / A. Baecham Corehead: CB 17 Sheet: 1 of 2

DEPTH & SAMPLES	GRAPHIC LITHOLOGY	GRAIN SIZE (INF · FINE · MED · CRS · CGR)	SEDIMENTARY STRUCTURES & FEATURES	COLOUR	COMPOSITION (& ACCESSORY MINERALS)	CMT	ESTIMATED Ø %	HYDROCARBON INDICATIONS: SMPL FLU	CUT COL	CUT FLU	GAS %	REMARKS [OIL BLEED; DIPS; FRACTURES ETC.]
1484			occ. lithoclast/granules floating									
1484.45	T.		Sst, f, (sph) (rnd) srt (hd)-fri.	Gy-brn	Quartz-mic (py) carb shell deb.							
1485			Occ. carb/mic lam. vis. Pass x-bedding.									
1486	(I)		Bioturbated. Occ. carb. lenses occ. laminae.									
1487			(sph)-sph, (rnd) sst, (hd)-fri		mic, carb shell deb. decreasing	local calcite (slight)	Poor/Mod		NIL			
1488			WOOD FRAG. Mic laminae. arg. app. lnd.									
1489	T.	VFS	Silty clst. lenses.									
			lenses dark arg. looking fsst w/ ltgy cleaner v.slightly coarser sst.		Thin shell lamell.					Pa. milky yellow (Acetone) bec. stronger downward		low angle ripple-bed. an
1490			Calc. nodule. Irregular edge. VFS/FS, VCS, GRANS									
1491			WOOD FRAG. VFS/FS lt.gy occ whole shells VCS/GRANS			Calc	Nil					
			Sst, grdg sltst-pbl ((srt)) uncons, (rnd) FS/GRANS		mic							

Drawing No. 13994

A/S NORSKE SHELL | Well: 31/2- 3 | Core No 10

CORE DESCRIPTION

Cored from 1484·45 to 1496·4 Recovered: 11·95 mtr. 100 % Core size: 4"

Formation: J. Sst. Date: 25·4·80 Described by: S. Willis / A. Reedham Corehead: 2 B 17

Sheet: 2 of 2

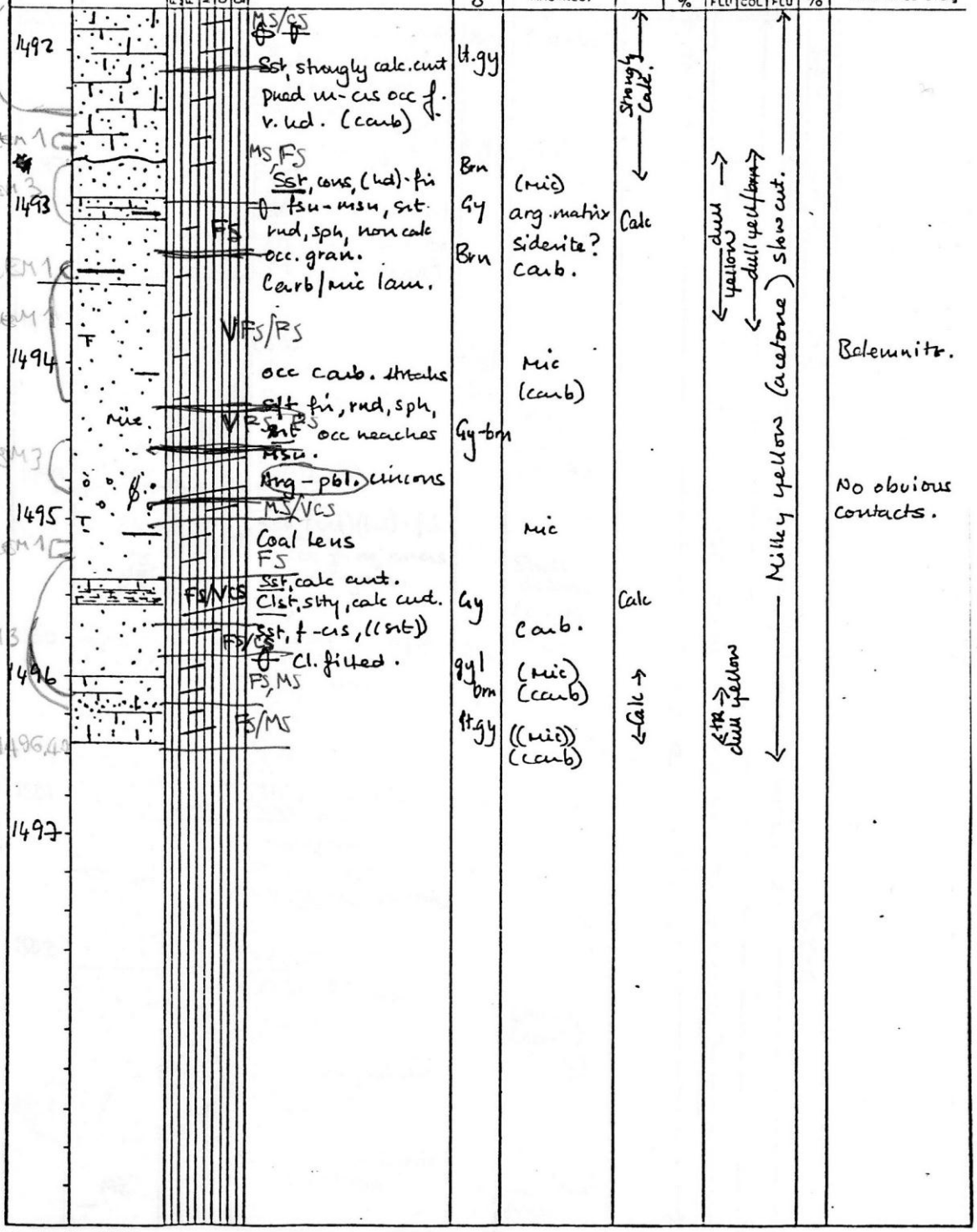

Drawing No. 13994

NB. 5.88m Stuck in barrel.

A/S NORSKE SHELL | Well: 31/2-3 | Core No 11

CORE DESCRIPTION

Cored from 1496·5 to 1514·5 Recovered: 12.14 m/ft ____ % Core size: 4"

Formation: J. Sst Date: 26·4·80 Described by: S. Willis / A. Beacham Corehead: CB 17 Sheet: 1 of 3

DEPTH & SAMPLES	GRAPHIC LITHOLOGY	GRAIN SIZE (FINE / FINE / MED / CRS / CBS)	SEDIMENTARY STRUCTURES & FEATURES	COLOUR	COMPOSITION (& ACCESSORY MINERALS)	CMT	ESTIMATED %	HYDROCARBON INDICATIONS: SMPL FLU	CUT COL	CUT FLU	GAS %	REMARKS (OIL BLEED; DIPS; FRACTURES ETC.)
1496		FS/CS	Sst, calc. cmt, GRANULE, srt w/ occ. crs gns.	ltgy	(carb)	←CMT	← NIL				1.5%	
1497		FS/VCS GRANS	Fred fst-fsu w/ crs - pbl. gns.	t.gy	(mic) (carb)						0.5%	
		FS/CS										
		FS/MS	Sst gy fs u-ms l occ crs, lse, uncons									
		FS/MS	Srt, (sph) (rnd)									
1498			(srt) FS, MS Srt, hd-fri.	Gy/ Brn	dissem. Py. (mic) (carb)						1.5%	
1499		PS/MS, VFS	MS, CS									
		FS/CS	Sst, (srt)(hd)-fri lenses f-m, m-cs occ pbl-gran.		Shell debris (carb) (Py)							
		MS, CS	MS, FS									
1500		FS/MS/VFS	Occ lens mica/f. Py w/ sand + (carg) mat.	Blk.								
		FS/MS	" aa.									
		FS/MS	" a.a.									
		MS										
1501		FS/MS/VFS	Structureless Sst: aa. uniform.									
		FS/MS/VFS	" a.a. (calc)									
		FS/MS/VFS	Clst, ss, (py)(mic)		lignite							
1502		FS/VCS/VFS										
		FS/CS/VFS	Cons, fri, non calc.		(mic) (carb) (Py)							
		FS/MS/VFS	f gnd, m gnd in Srt patches									
1503		FS/MS	(⇒) Occ carb/mic laminae		Mic							
	Mic	FS/MS			occ lithic frag.							

MODERATE TO GOOD — OCCASIONAL PA. YELL. SPECKLED. — NIL — PA YELLOW – MILKY (Acetone) — 0.2%

Drawing No. 13994

A/S NORSKE SHELL | Well: 31/2-3 | Core No. 11

CORE DESCRIPTION

Cored from 1496.5 to 1574.5 Recovered: ft. % Core size: 4"

Formation: J. Sst. Date: 26.4.80 Described by: Sue Willis, Ann Beecham Corehead: CB 17 Sheet: 2 of 3

DEPTH & SAMPLES	GRAPHIC LITHOLOGY	GRAIN SIZE (FINE / FINE / MED / CRS / CRS)	SEDIMENTARY STRUCTURES & FEATURES	COLOUR	COMPOSITION (& ACCESSORY MINERALS)	CMT	ESTIMATED Ø %	HYDROCARBON INDICATIONS: SMPL FLU	CUT COL	CUT FLU	GAS %	REMARKS (OIL BLEED; DIPS; FRACTURES ETC.)
1504	Mic	FS	Sst, pred f., loc. m, md-fn. Sst (sph) (rnd)	Gy/ Brn	Mic Carb (py) (calc)	loc (calc)	Moderate	Nil	dull yell (Acet)		0 %	
1505	Mic	FS/VFS, FS, FS/MS	burrows.									
1506												
1507			1505.84 – 1511.70 m STUCK IN CORE BARREL									
1508												
1509												
1510												
1511												

Drawing No. 13994

A/S NORSKE SHELL | Well: 31/2-3 | Core No 11

CORE DESCRIPTION

Cored from 1496·5 to 1514·5 Recovered: ____ ft. ____ % Core size: 4"

Formation: J. Sst Date: 26.4.80 Described by: Sue Willis, Ann Beecham Corehead: CB 17

Sheet: 3 of 3

DEPTH & SAMPLES	GRAPHIC LITHOLOGY	GRAIN SIZE (VFINE / FINE / MED / CRS / CRS)	SEDIMENTARY STRUCTURES & FEATURES	COLOUR	COMPOSITION (& ACCESSORY MINERALS)	CMT	ESTIMATED ø %	HYDROCARBON INDICATIONS: SMPL FLU	CUT COL	CUT FLU	GAS %	REMARKS [OIL BLEED; DIPS; FRACTURES ETC.]
1512	Mic		Bioturbated thro' (=) Carb/mic lam throughout. CEM 1 Sst, gy, cons, (hd) slt - fsl occ ± su srt (rnd) sph	dk gy	mic carb shell debris	loc. sl. calc.	Poor	Nil		Milky grey.	0%	
1513	Mic		Calc nodule. CEM 1									
1514			Occ Lgnite frag. (=)	gy	Lgnite							
1514.5			low angle ripple x-bed.									
1515												

NICK'S

NICK'S

Drawing No. 13994

31/2-6

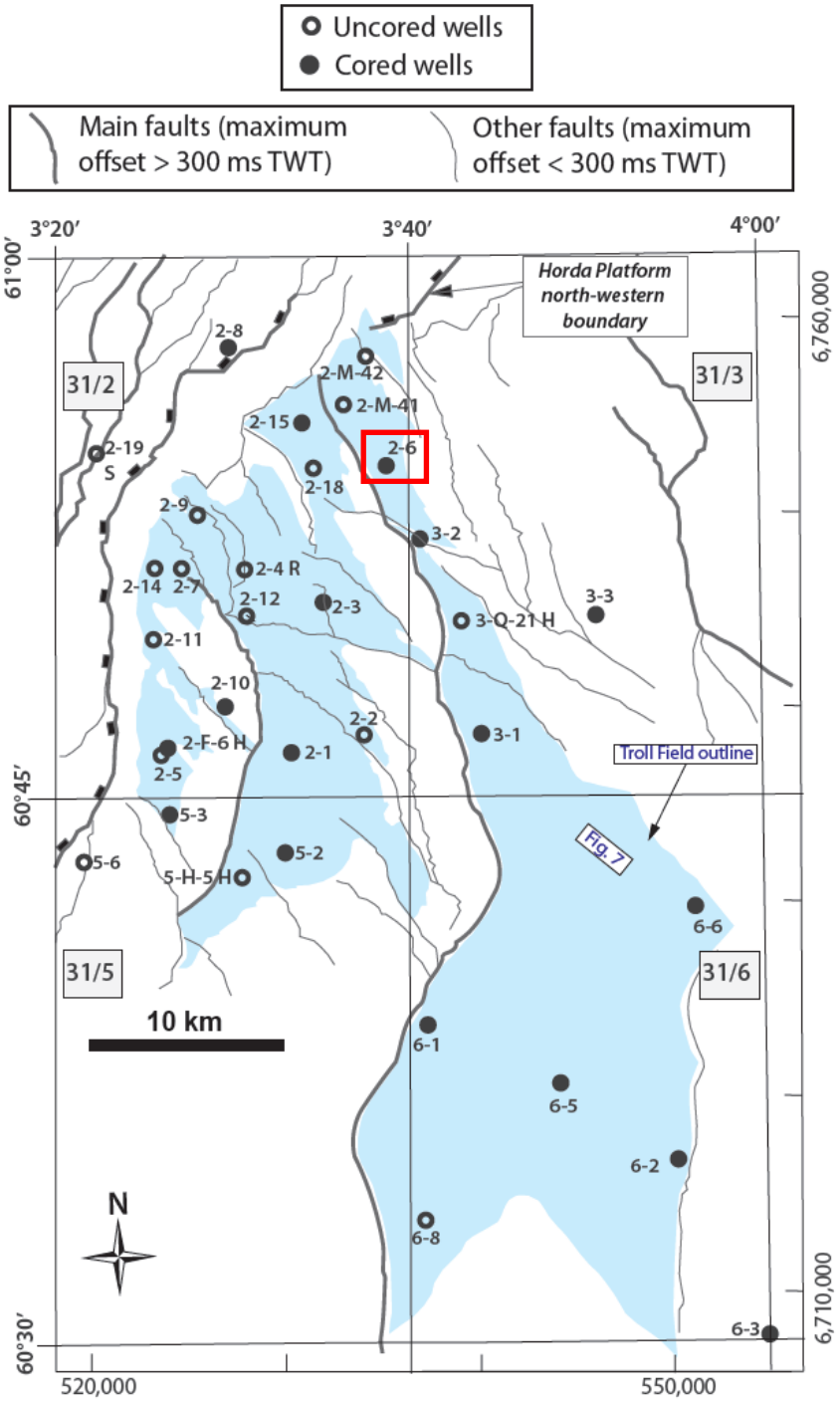
Uncored wells
Cored wells
Main faults (maximum offset > 300 ms TWT)
Other faults (maximum offset < 300 ms TWT)
3°20′
3°40′
4°00′
61°00′
60°45′
60°30′
6,760,000
6,710,000
520,000
550,000
Horda Platform north-western boundary
31/2
31/3
31/5
31/6
2-8
2-M-42
2-M-41
2-15
2-19 S
2-6
2-18
2-9
3-2
2-14
2-7
2-4 R
2-12
2-3
3-3
3-Q-21 H
2-11
2-10
2-2
3-1
2-F-6 H
2-5
2-1
Troll Field outline
Fig. 7
5-3
5-6
5-H-5 H
5-2
6-6
10 km
6-1
6-5
6-2
6-8
6-3
N

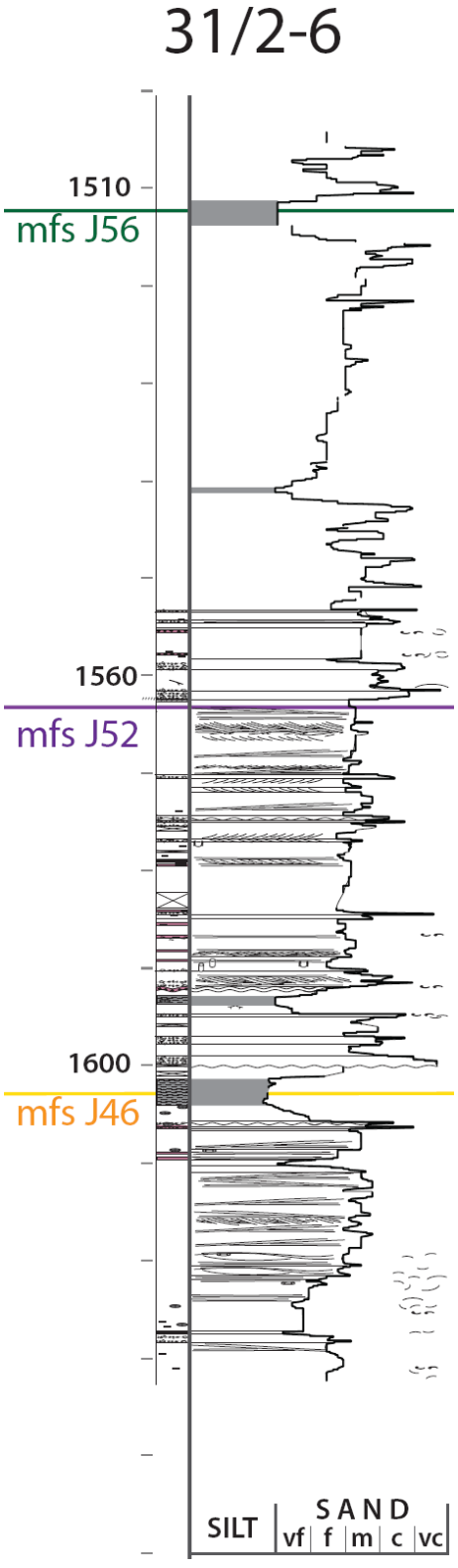
31/2-6
1510
mfs J56
1560
mfs J52
1600
mfs J46
SILT
SAND
vf
f
m
c
vc

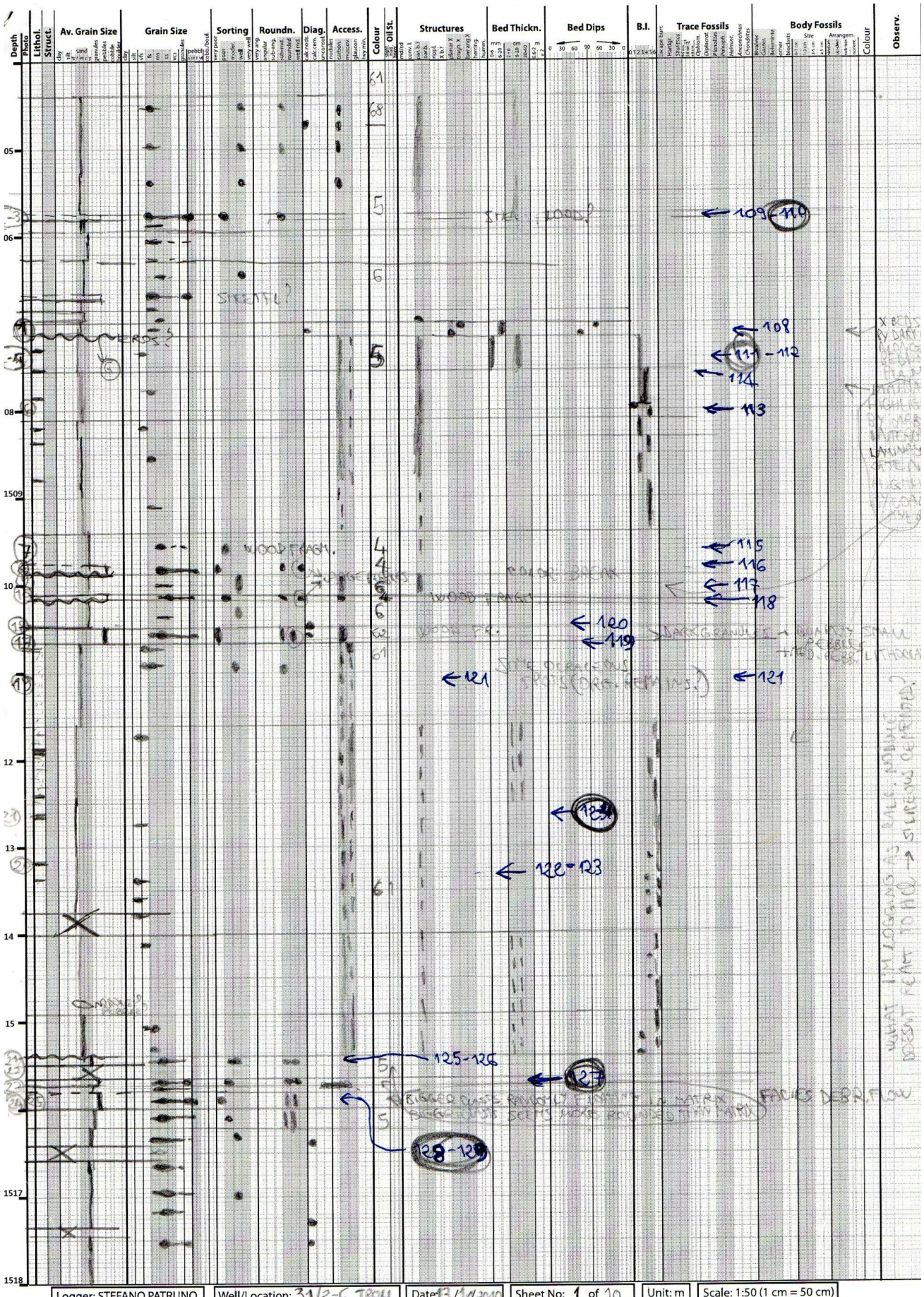
Depth
Photo
Lithol.
Struct.
Av. Grain Size
Grain Size
Sorting
Roundn.
Diag.
Access.
Colour
Oil St.
Structures
Bed Thickn.
Bed Dips
B.I.
Trace Fossils
Body Fossils
Observ.
STRUCT. LOAD?
WOOD TRASH
109-110
108
111-112
114
113
115
116
117
118
120
119
121
122-123
125-126
127
128-129
Logger: STEFANO PATRUNO
Well/Location: 31/2-6 TROLL
Date: 13/11/2010
Sheet No: 1 of 10
Unit: m
Scale: 1:50 (1 cm = 50 cm)

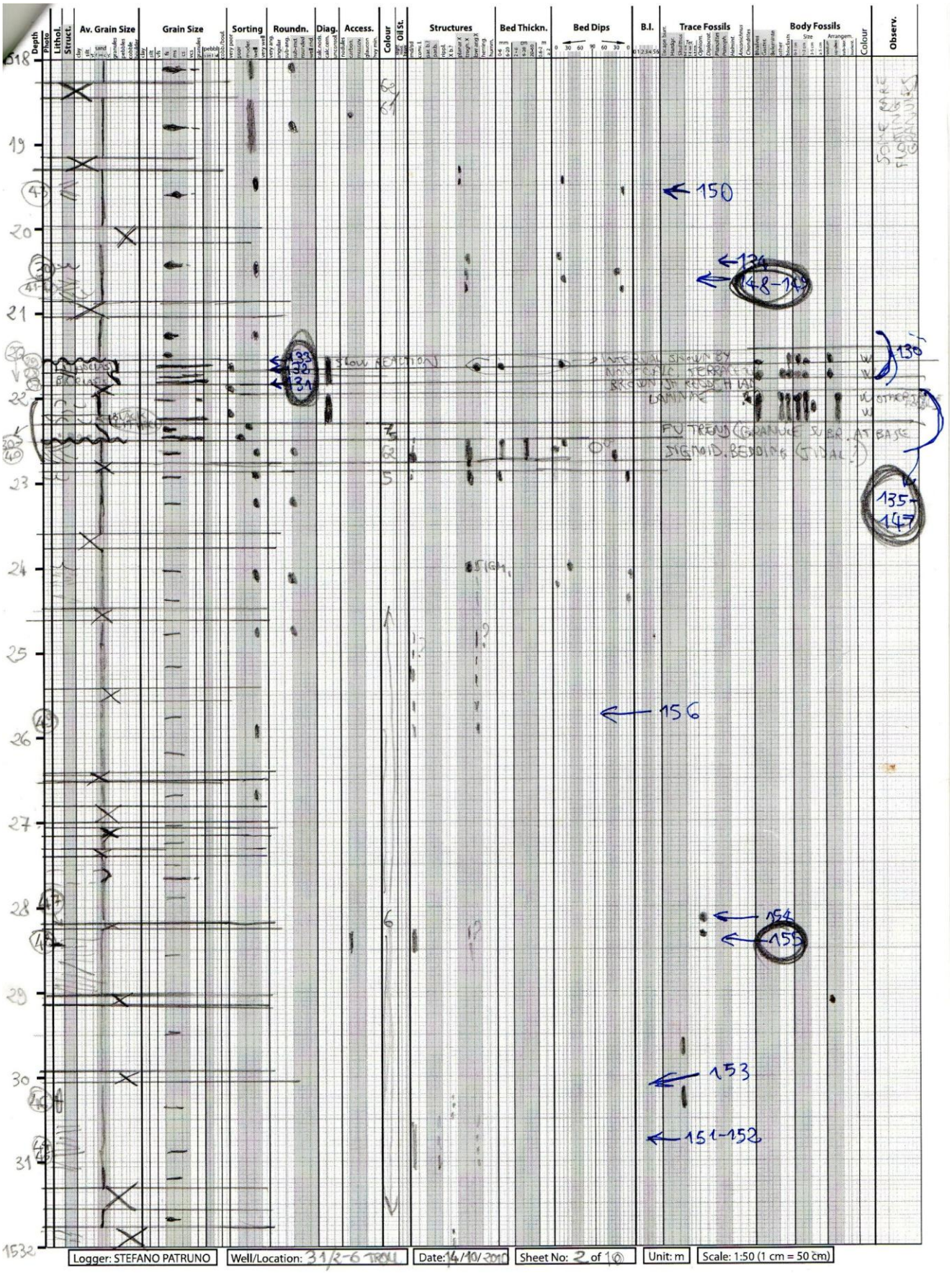
Depth
Photo
Lithol.
Struct.
Av. Grain Size
Grain Size
Sorting
Roundn.
Diag.
Access.
Colour
Oil St.
Structures
Bed Thickn.
Bed Dips
B.I.
Trace Fossils
Body Fossils
Observ.
Logger: STEFANO PATRUNO
Well/Location: 31/2-6 TROLL
Date: 14/10/2010
Sheet No: 2 of 10
Unit: m
Scale: 1:50 (1 cm = 50 cm)

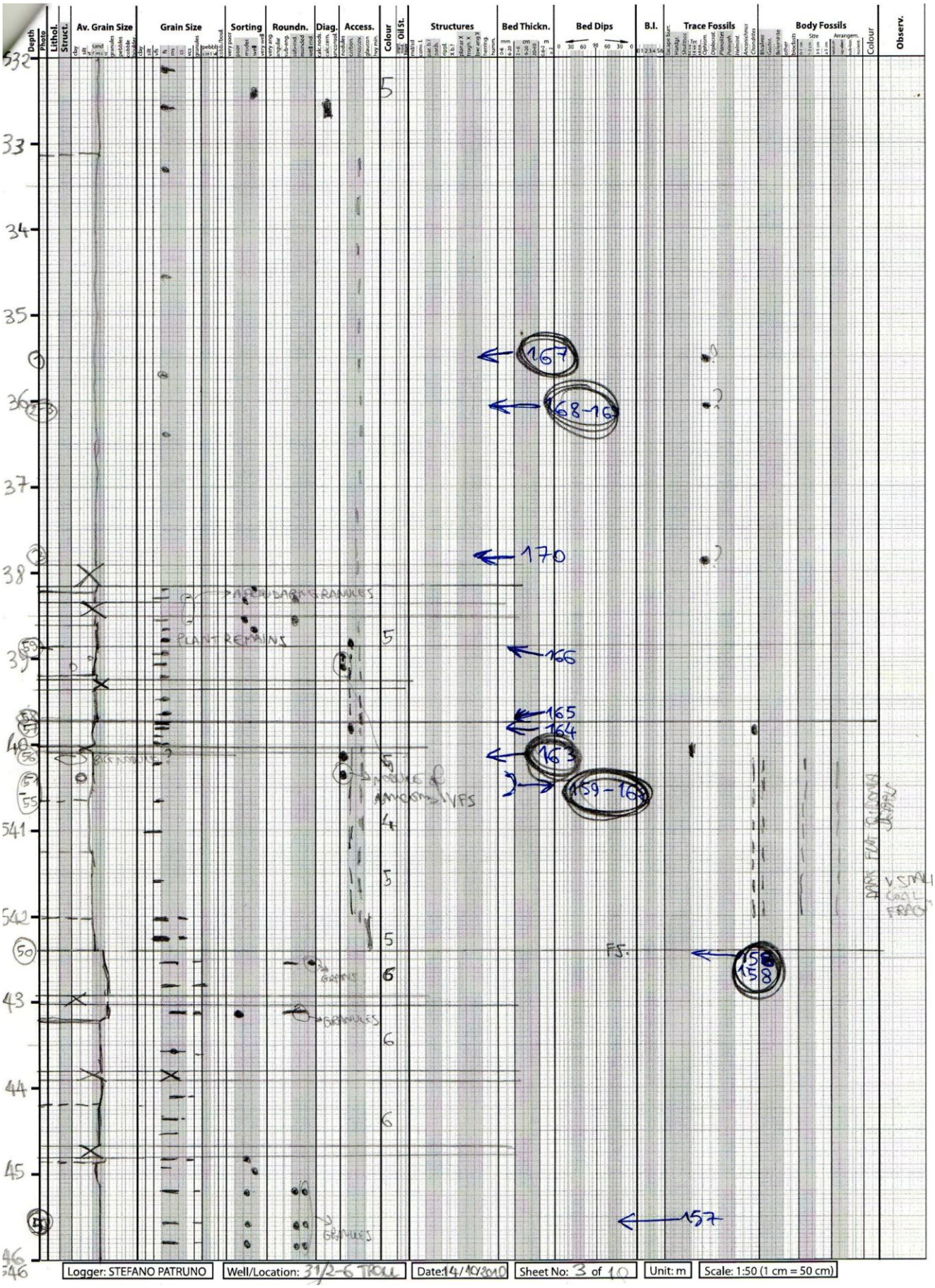
Depth
Photo
Lithol.
Struct.
Av. Grain Size
Grain Size
Sorting
Roundn.
Diag.
Access.
Colour
Oil St.
Structures
Bed Thickn.
Bed Dips
B.I.
Trace Fossils
Body Fossils
Observ.
167
168-16
170
166
165
164
163
159-162
157
PLANT REMAINS
BIOTURBATION
Logger: STEFANO PATRUNO
Well/Location: 31/2-6 TROLL
Date: 14/10/2010
Sheet No: 3 of 10
Unit: m
Scale: 1:50 (1 cm = 50 cm)

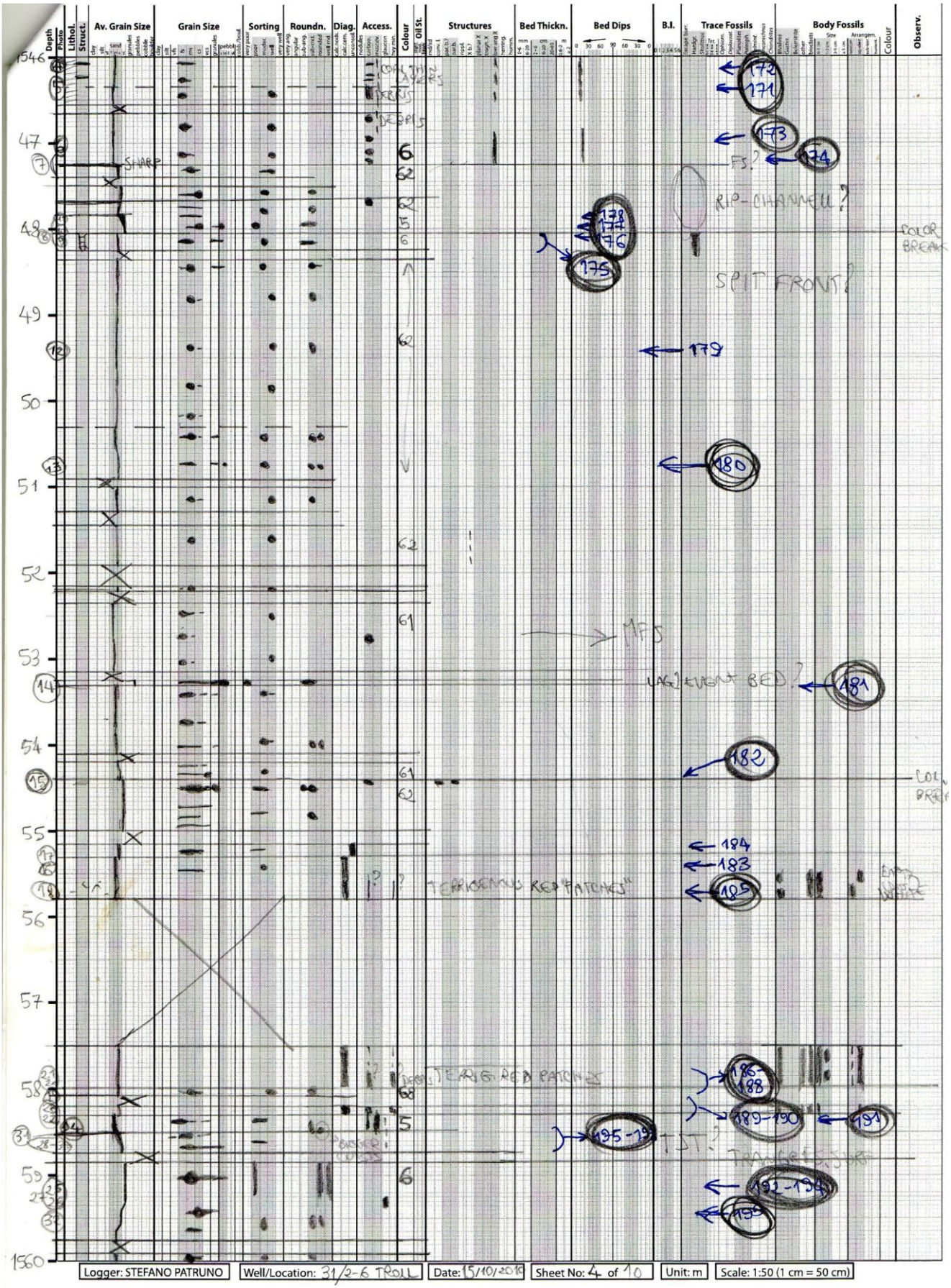
Depth
Photo
Lithol.
Struct.
Av. Grain Size
Grain Size
Sorting
Roundn.
Diag.
Access.
Colour
Oil St.
Structures
Bed Thickn.
Bed Dips
B.I.
Trace Fossils
Body Fossils
Observ.
SHARP
RIP-CHANNEL?
SPIT FRONT?
COLOR BREAK
MFS
LAG? EVENT BED?
TERRIGENOUS RED PATCHES"
TST?
Logger: STEFANO PATRUNO
Well/Location: 31/2-6 TROLL
Date: 15/10/2010
Sheet No: 4 of 10
Unit: m
Scale: 1:50 (1 cm = 50 cm)

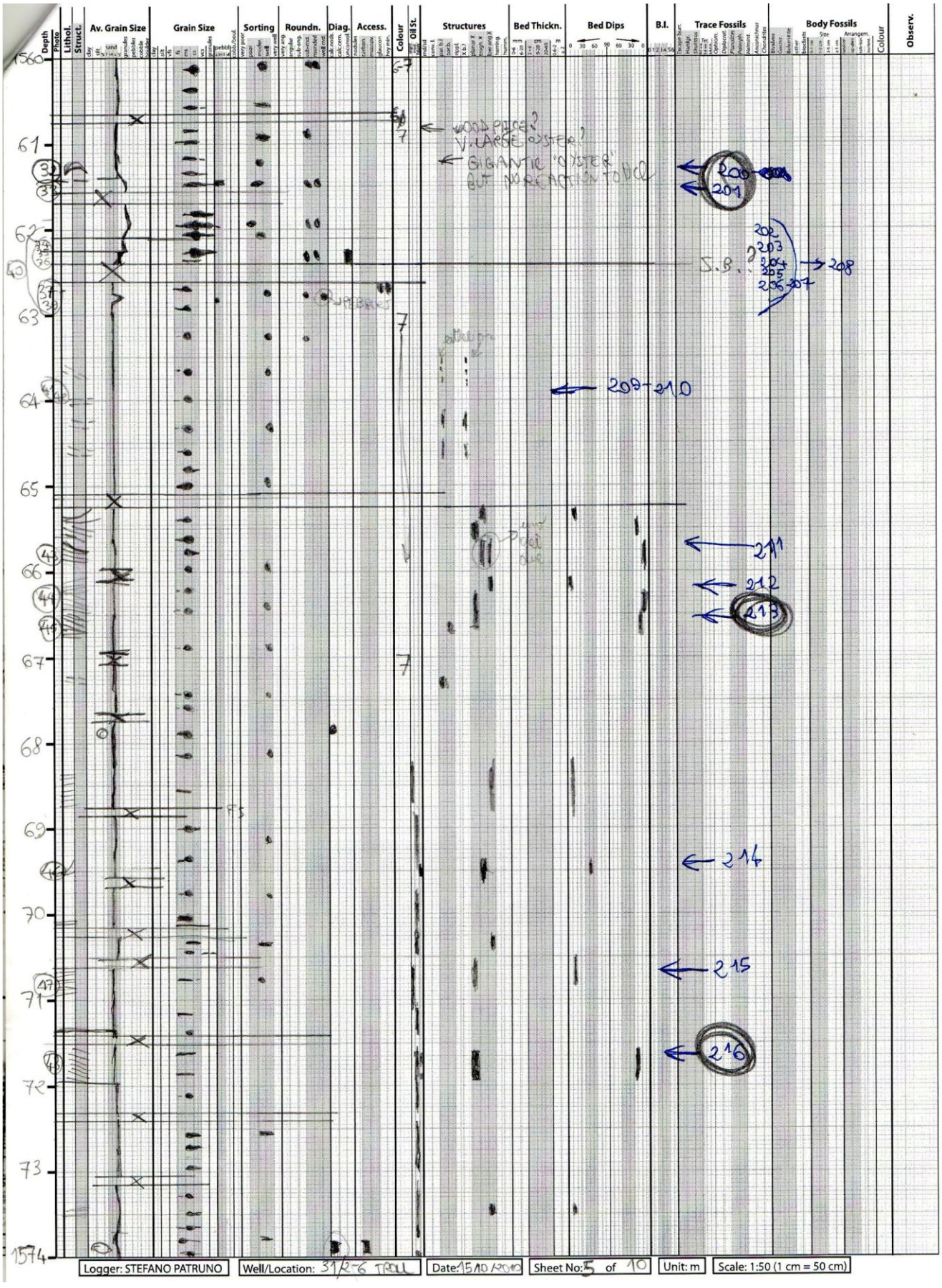
Depth
Photo
Lithol.
Struct.
Av. Grain Size
Grain Size
Sorting
Roundn.
Diag.
Access.
Colour
Oil St.
Structures
Bed Thickn.
Bed Dips
B.I.
Trace Fossils
Body Fossils
Observ.
WOOD PIECE?
V. LARGE OYSTER?
GIGANTIC "OYSTER"
BUT UNREACTION TOUCH
S.B.?
208
209-210
211
212
213
214
215
216
Logger: STEFANO PATRUNO
Well/Location: 31/2-6 TROLL
Date: 15/10/2010
Sheet No: 5 of 10
Unit: m
Scale: 1:50 (1 cm = 50 cm)

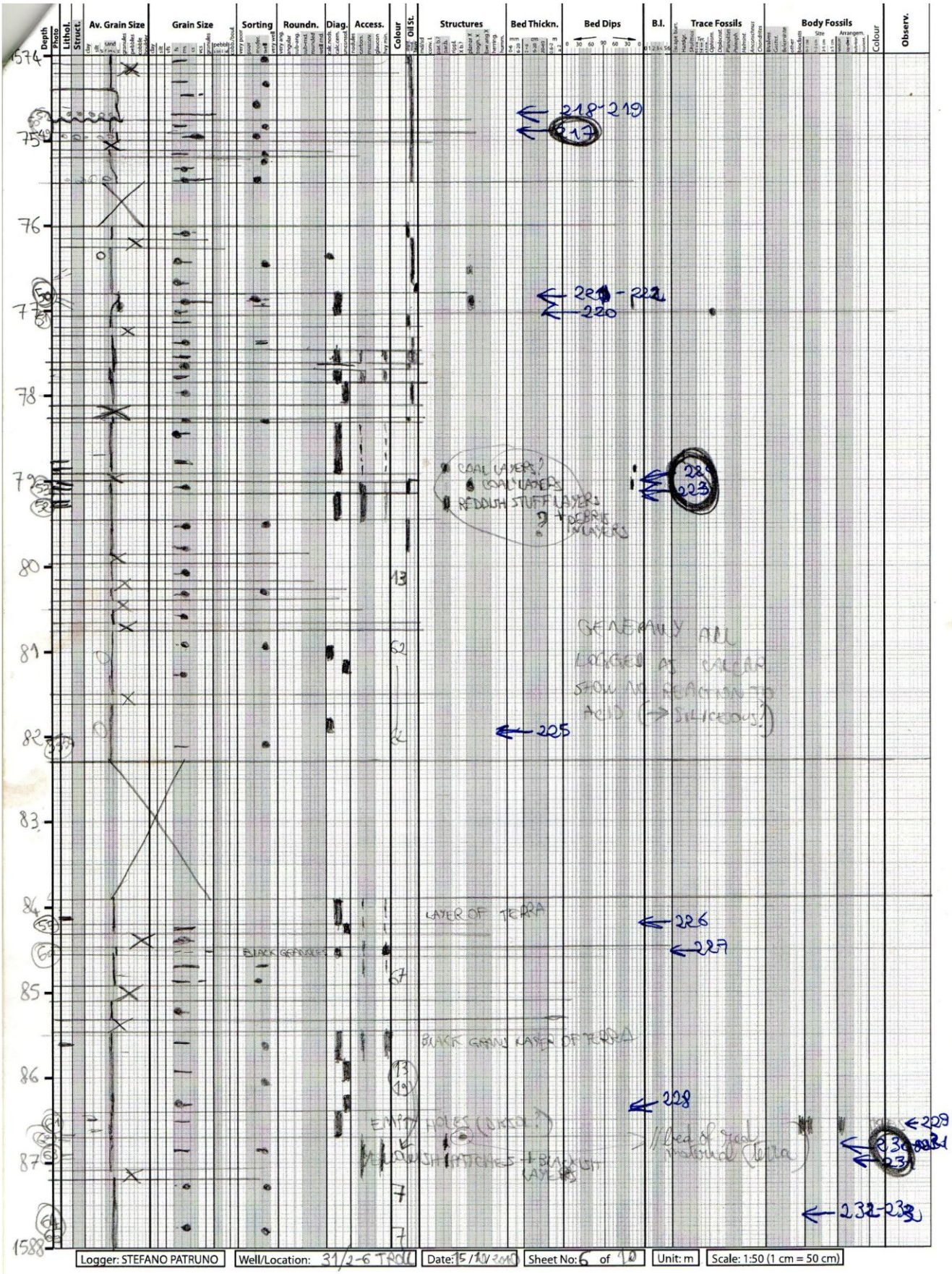
Depth
Photo
Lithol.
Struct.
Av. Grain Size
Grain Size
Sorting
Roundn.
Diag.
Access.
Colour
Oil St.
Structures
Bed Thickn.
Bed Dips
B.I.
Trace Fossils
Body Fossils
Observ.
1574
75
76
77
78
79
80
81
82
83
84
85
86
87
1588
218-219
217
220-222
COAL LAYERS?
COAL LAYERS
REDDISH STUFF LAYER:
? DEBRIS
INLAYERS
GENERALLY ALL
LAYERS AS EARLIER
SHOW NO REACTION TO
ACID (→ SILICEOUS?)
225
LAYER OF TERRA
BLACK GRAINS
226
227
BLACK GRAINY LAYER OF TERRA
228
EMPTY HOLES (LIKELY?)
REDDISH PATCHES + BLACK CLAY LAYERS
Head of root
mineralized (Terra)
229
230-231
232-233
Logger: STEFANO PATRUNO
Well/Location: 31/2-6 TAGL
Date: 15/10/2006
Sheet No: 6 of 10
Unit: m
Scale: 1:50 (1 cm = 50 cm)

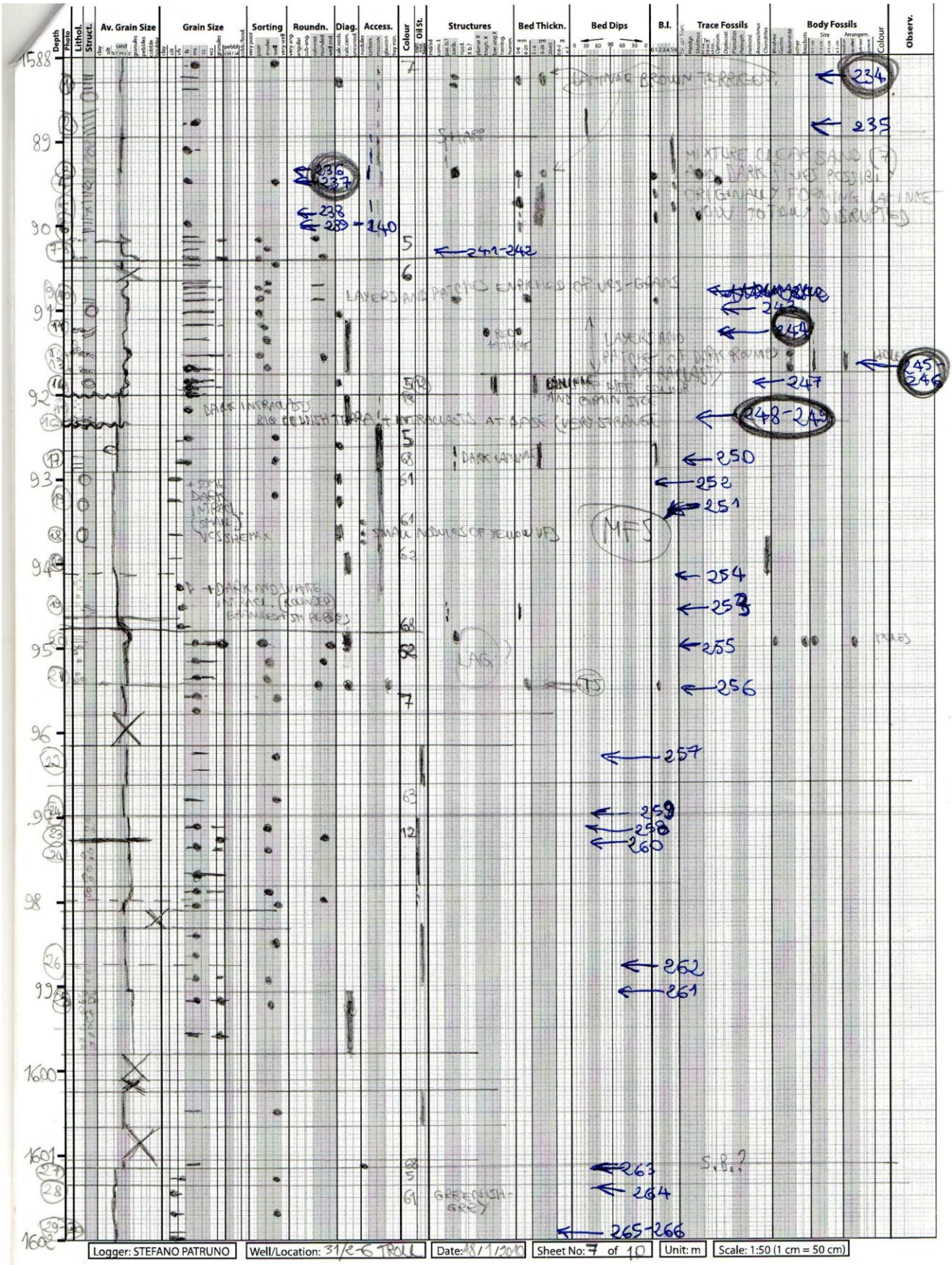
Depth
Photo
Lithol.
Struct.
Av. Grain Size
Grain Size
Sorting
Roundn.
Diag.
Access.
Colour
Oil St.
Structures
Bed Thickn.
Bed Dips
B.I.
Trace Fossils
Body Fossils
Observ.
Logger: STEFANO PATRUNO
Well/Location: 31/2-6 TROLL
Date: 18/1/2010
Sheet No: 7 of 10
Unit: m
Scale: 1:50 (1 cm = 50 cm)

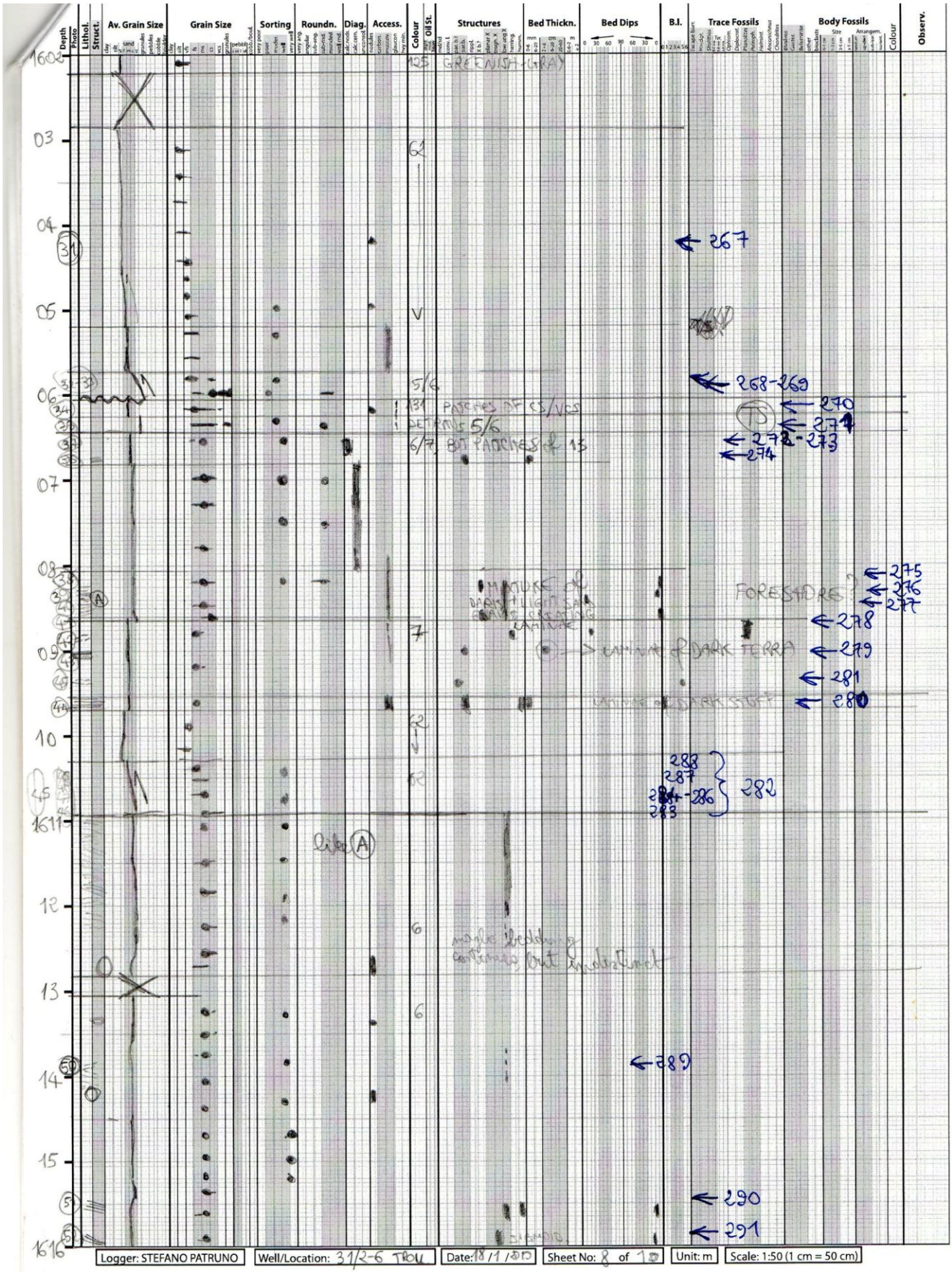
Depth
Photo
Lithol.
Struct.
Av. Grain Size
Grain Size
Sorting
Roundn.
Diag.
Access.
Colour
Oil St.
Structures
Bed Thickn.
Bed Dips
B.I.
Trace Fossils
Body Fossils
Observ.
GREENISH (GRAY)
PATCHES OF CS/VCS
DETRITUS 5/6
BIT PATCHES of 13
FORESHORE?
LAMINAE of DARK TERRA
LAMINAE of DARK STUFF
Logger: STEFANO PATRUNO
Well/Location: 31/2-6 TROLL
Date: 18/11/2010
Sheet No: 8 of 10
Unit: m
Scale: 1:50 (1 cm = 50 cm)

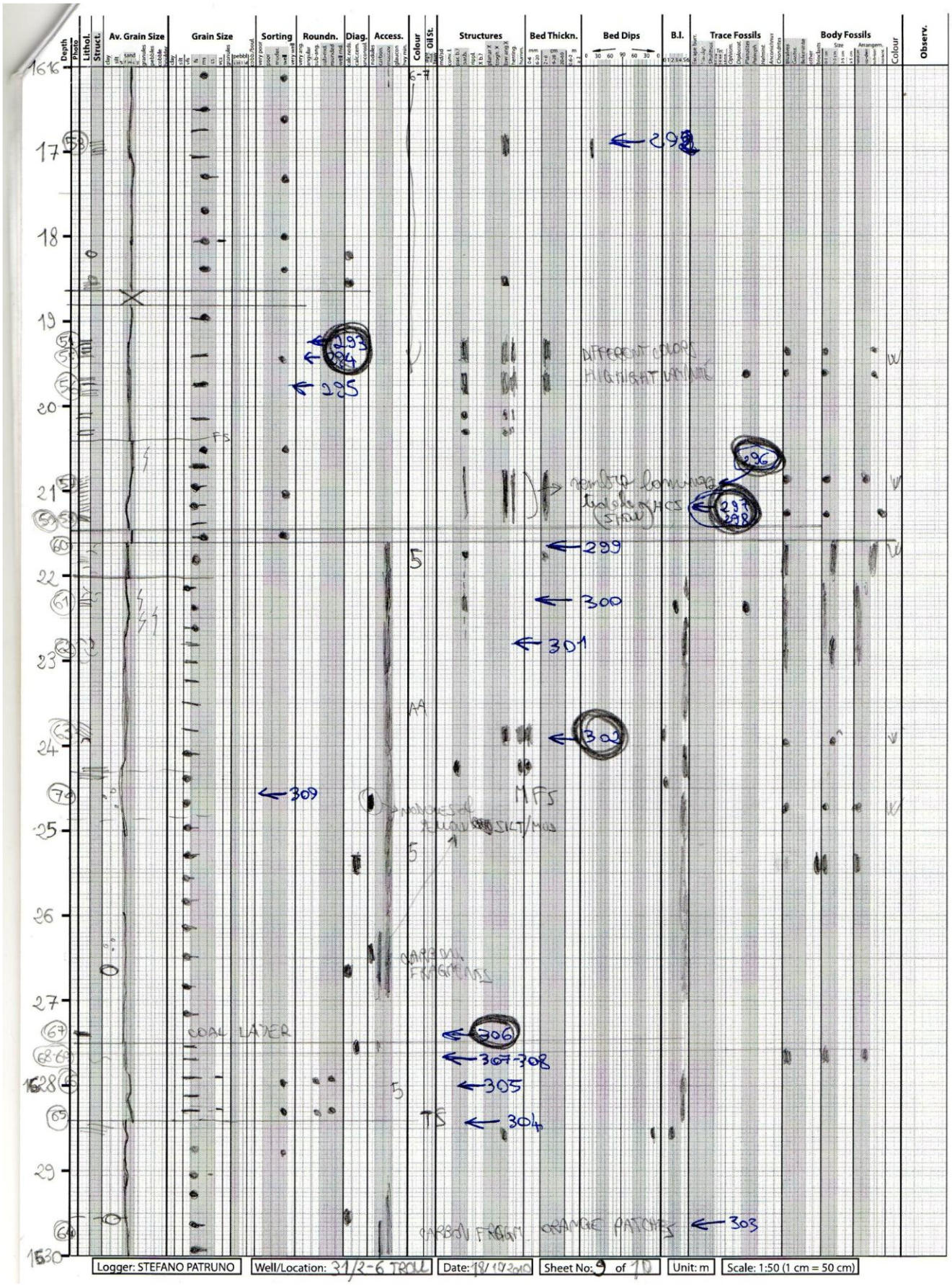
Depth
Photo
Lithol.
Struct.
Av. Grain Size
Grain Size
Sorting
Roundn.
Diag.
Access.
Colour
Oil St.
Structures
Bed Thickn.
Bed Dips
B.I.
Trace Fossils
Body Fossils
Observ.
Logger: STEFANO PATRUNO
Well/Location: 31/2-6 TROLL
Date: 19/10/2010
Sheet No: 9 of 10
Unit: m
Scale: 1:50 (1 cm = 50 cm)

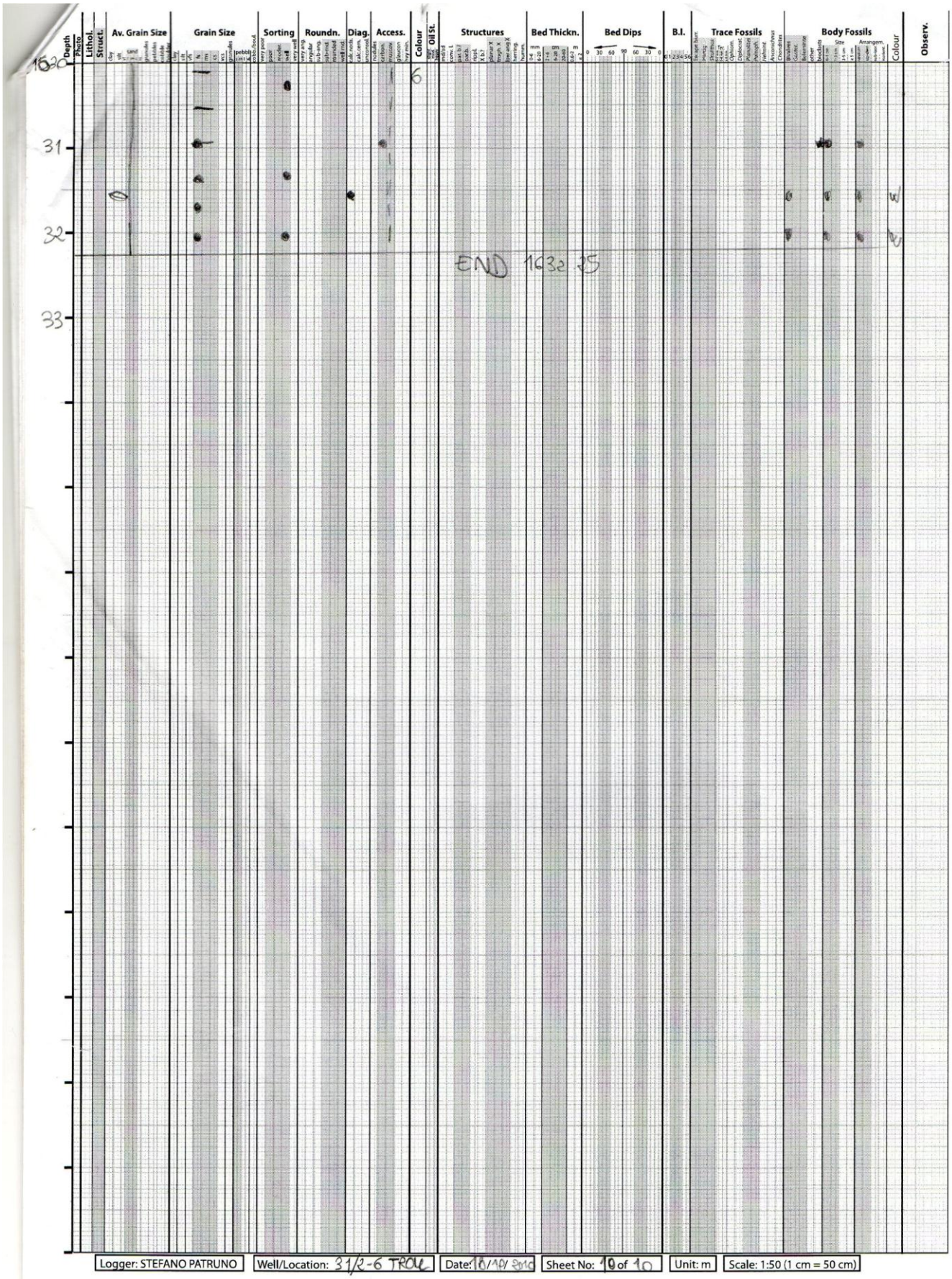
Depth
Photo
Lithol.
Struct.
Av. Grain Size
Grain Size
Sorting
Roundn.
Diag.
Access.
Colour
Oil St.
Structures
Bed Thickn.
Bed Dips
B.I.
Trace Fossils
Body Fossils
Arrangem.
Observ.
1620
31
32
33
END 1632.35
Logger: STEFANO PATRUNO
Well/Location: 31/2-6 TROLL
Date: 10/AD/2010
Sheet No: 10 of 10
Unit: m
Scale: 1:50 (1 cm = 50 cm)

31/2-8

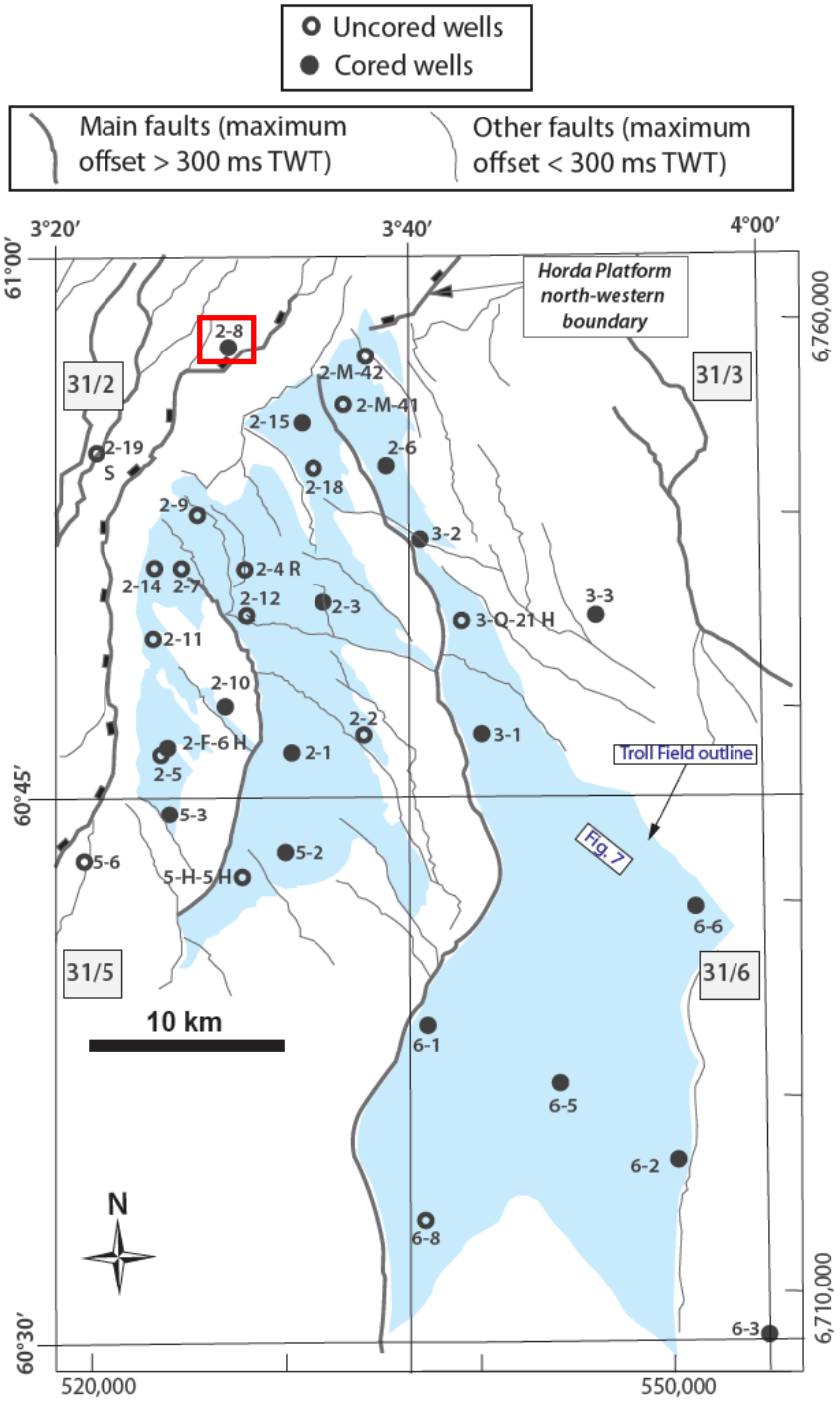
Uncored wells
Cored wells
Main faults (maximum offset > 300 ms TWT)
Other faults (maximum offset < 300 ms TWT)
3°20′
3°40′
4°00′
61°00′
60°45′
60°30′
6,760,000
6,710,000
520,000
550,000
Horda Platform north-western boundary
Troll Field outline
Fig. 7
31/2
31/3
31/5
31/6
10 km
N
2-8
2-M-42
2-M-41
2-15
2-19 S
2-18
2-6
2-9
3-2
2-14
2-7
2-4 R
2-12
2-3
3-Q-21 H
3-3
2-11
2-10
2-2
3-1
2-F-6 H
2-5
2-1
5-3
5-6
5-H-5 H
5-2
6-6
6-1
6-5
6-2
6-8
6-3

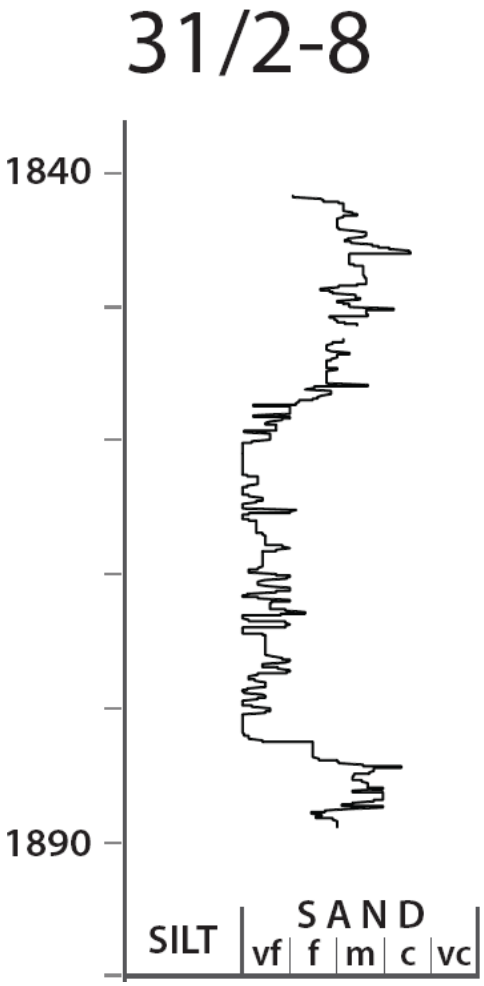
31/2-8
1840
1890
SILT
SAND
vf
f
m
c
vc

A/S NORSKE SHELL | Well: 31/2-8 | Core No. 1

CORE DESCRIPTION

Cored from 1841,8 to 1851,5 Recovered: 9,68 m 100 % Core size: 4"

Formation: JU Date: 11.07.82 Described by: P. Immerz Corehead: CB 303 Sheet: 1 of 3

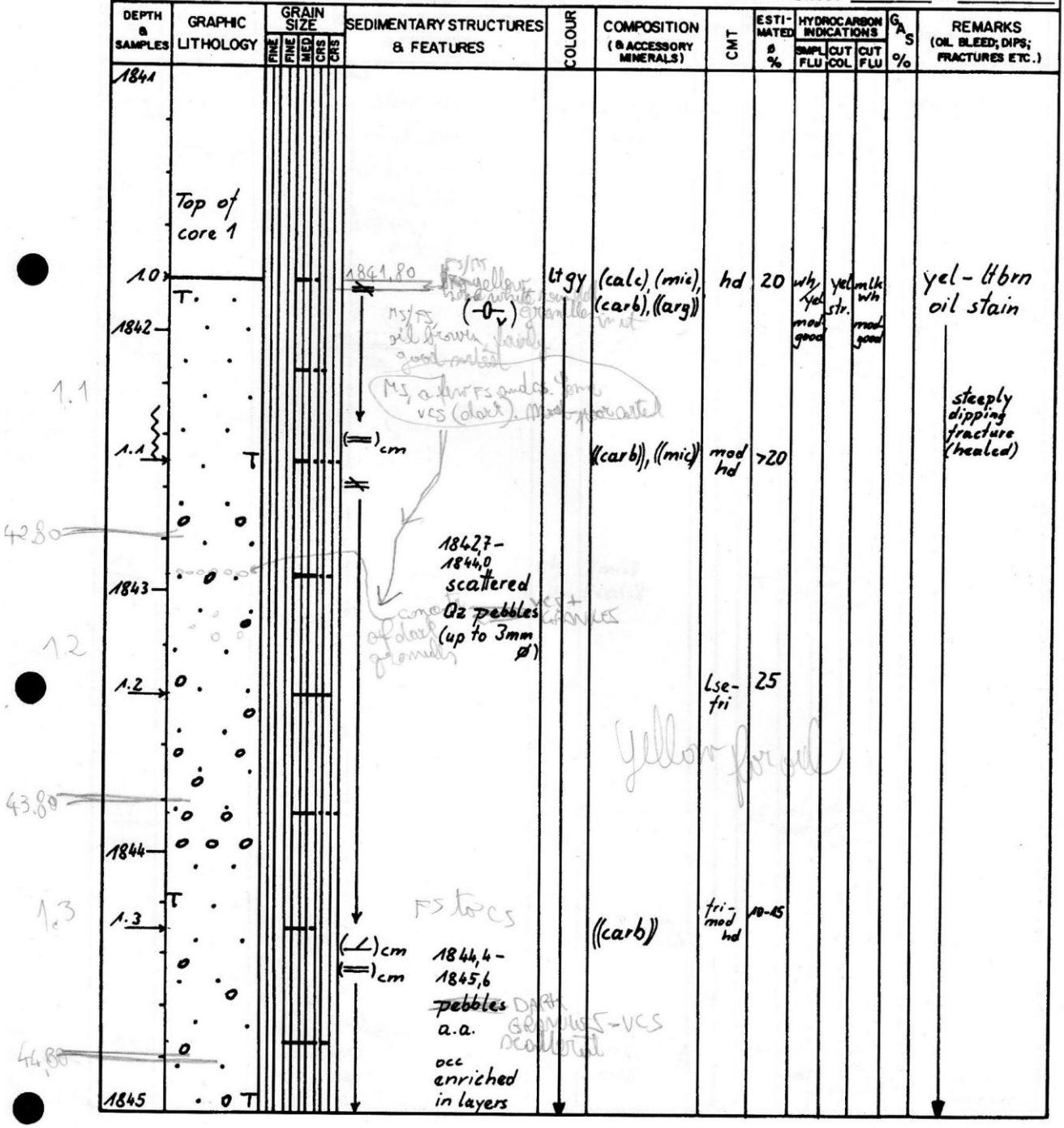

A/S NORSKE SHELL	Well: 31/2-8	Core No. 1

CORE DESCRIPTION

Cored from ________ to ________ Recovered: ________ m ________ % ____ Core size: ________

Formation: ________ Date: ________ Described by: ________ Corehead: ________ Sheet: 2 of 3

DEPTH & SAMPLES	GRAPHIC LITHOLOGY	GRAIN SIZE	SEDIMENTARY STRUCTURES & FEATURES	COLOUR	COMPOSITION (& ACCESSORY MINERALS)	CMT	ESTIMATED Ø %	HYDROCARBON INDICATIONS SMPL FLU	CUT COL	CUT FLU	GAS %	REMARKS (OIL BLEED; DIPS; FRACTURES ETC.)
1845 1.4			(═) FS/MS, some CS mod. poor sorting, a few VCS dark altered yellow for oil → VCS/GRANS (dark) in between. Lower both. No coarser than above (MS/G) → MS/CS yellow oil, some VCS to pebble, small dark pebbles	Ltgy	((mic)), (pyr), ((calc))	fri-mod hd	25	yel mod	yel-brn strm	mlk wh good		Ltbrn oil stain
1846 1.5			FS/CS (less coarse than above. Rest grains are VCS at max) coating (SURFACE/CORE)	wh/Ltgy			30	yel good	yel-brn strm	bl-wh mod-good		
1.6 1847			(═) ≠ FS/MS, some CS in between, dark for oil, (⊥) (═) few quartzy (glossy) and dark VCS granules, floor(?) ≠	wh/Ltgy	((mic)) ((calc))		15	yel good	yel-brn strm	mlk wh good		
1.7 1848			FS/CS, some quartzy VCS/granules; mainly MS, some FS and CS	wh/Ltgy	(calc), (pyr), → belly dark brown		15	yel good	yel-brn strm	mlk wh good		
1.8 1849			(⊥)cm (═) FS and some MS ≠ FS to CS	Ltgy	((mic)), ((carb))		15-20	yel good	yel-brn strm	mlk wh good		no oil stain in hard bands

1.4 — 1.5 — 4680 — 1.6 — 47.30 — 1,7 — 48.80

A/S NORSKE SHELL | Well: 31/2-8 | Core No. 1

CORE DESCRIPTION

Cored from _____ to _____ Recovered: _____ m _____ % Core size: _____

Formation: _____ Date: _____ Described by: _____ Corehead: Sheet: 3 of 3

DEPTH & SAMPLES	GRAPHIC LITHOLOGY	GRAIN SIZE (FINE / FINE / MED / CRS / CRS)	SEDIMENTARY STRUCTURES & FEATURES	COLOUR	COMPOSITION (& ACCESSORY MINERALS)	CMT	ESTIMATED ø %	HYDROCARBON INDICATIONS: SMPL FLU	CUT COL	CUT FLU	GAS %	REMARKS (OIL BLEED; DIPS; FRACTURES ETC.)
1849	T		cm-dm			tri-mod hd						lt-mdbrn oil stain
1.9				ltgy	(carb) (calc)		20	yel good	yel-brn strm	wh mod good		
1850												
1.10				ltgy			20	yel good	yel strm	wh good		
1851			dm									
1.11	T			ltgy pink	(mic), (calc), (carb)		20	yel good	yel strm	wh good		
	End of core 1											
1852												

A/S NORSKE SHELL | Well: 31/2-8 | Core No. 2

CORE DESCRIPTION

Cored from 1851,5 to 1869,7 Recovered: 17,2 m 95 % Core size: 4"

Formation: JU Date: 12.07.67 Described by: P. Immerz Corehead: CB 303

Sheet: 1 of 5

DEPTH & SAMPLES	GRAPHIC LITHOLOGY	GRAIN SIZE (FINE / FINE / MED / CRS / CRS)	SEDIMENTARY STRUCTURES & FEATURES	COLOUR	COMPOSITION (& ACCESSORY MINERALS)	CMT	ESTIMATED %	HYDROCARBON INDICATIONS: SMPL FLU	CUT COL	CUT FLU	GAS %	REMARKS (OIL BLEED; DIPS; FRACTURES ETC.)
1851	core 1											
	Top of core 2											
	not recovered											
1852												
2.3 52.50			(=) FS to CS quartzy vcs floating (⊥)	dkgy-blk	arg	hd	⅟	—	—	—		
2.1 1853 2.4			FS to MS, a few cs floating	ltgy	(calc)	fri-lse	20	yel good	yel-brn strm	milk wh good		yel oil stain
53.50			FS/MS, more abund cs/vcs/granules floating (dark ch, quartzy, subr-subang) (⊥) mostly MS, some cs and vcs FS/MS, a few rare cs									
2.5 2.2 1854			CEM=3.6 (⊕)? some lith of above, less and less dark brown oil stained as we go down	wh-ltgy	(calc) ((arg))	hd	5-10	yel good	yel-brn strm	milk wh good		yel oil stain
54.50			FS/MS, none (⊕)? SS/granules (dark) more common at lower part									
2.6 2.3 1855			(=) dm CEM=3 FS/MS none cs mst above abruptly from only brown to dk	ltgy	(carb), (mic), calc-calc	hd-hd	3	yel good	yel-brn strm	milk wh good		yel/ltbrn oil stain

A/S NORSKE SHELL | Well: 31/2-8 | Core No. 2

CORE DESCRIPTION

Cored from _____ to _____ Recovered: _____ m _____ % Core size: _____

Formation: _____ Date: _____ Described by: _____ Corehead: Sheet: 2 of 5

DEPTH & SAMPLES	GRAPHIC LITHOLOGY	GRAIN SIZE	SEDIMENTARY STRUCTURES & FEATURES	COLOUR	COMPOSITION (& ACCESSORY MINERALS)	CMT	ESTIMATED Ø %	HYDROCARBON INDICATIONS: SMPL FLU	HYDROCARBON INDICATIONS: CUT COL	HYDROCARBON INDICATIONS: CUT FLU	GAS %	REMARKS (OIL BLEED; DIPS; FRACTURES ETC.)
1855			dm									
33.50												
2.7				ltgy	calc, (arg) (mic) - mic	hd	1	yel good ptch	yel-brn slow	milk wh mod		
1856												
56.50												
2.8				ltgy	calc, (arg), (mic) - mic (carb) - carb	hd	1	yel good ptch	yel-brn slow	milk wh wk		patchy, ltbrn oil stain
1857			dm; 1-3 mm ø									colour change from lt to mdgy
2.9				lt-md gy	mic, (arg) ((calc)), carb	mod hd	20	yel md-good ptch	yel-brn strm	milk wh good		smell; bioturbation can be observed in carb stks only
1858												
2.10				lt-mdgy	mic - mic carb, ((calc)), (arg) - arg	mod hd	<10	yel good ptch	yel-brn blm	milk wh mod-good		smell
58.50												
1859			(mould only)									

A/S NORSKE SHELL | Well: 31/2-8 | Core No. 2

CORE DESCRIPTION

Cored from _____ to _____ Recovered: _____ m _____ % Core size: _____

Formation: _____ Date: _____ Described by: _____ Corehead: Sheet: 3 of 5

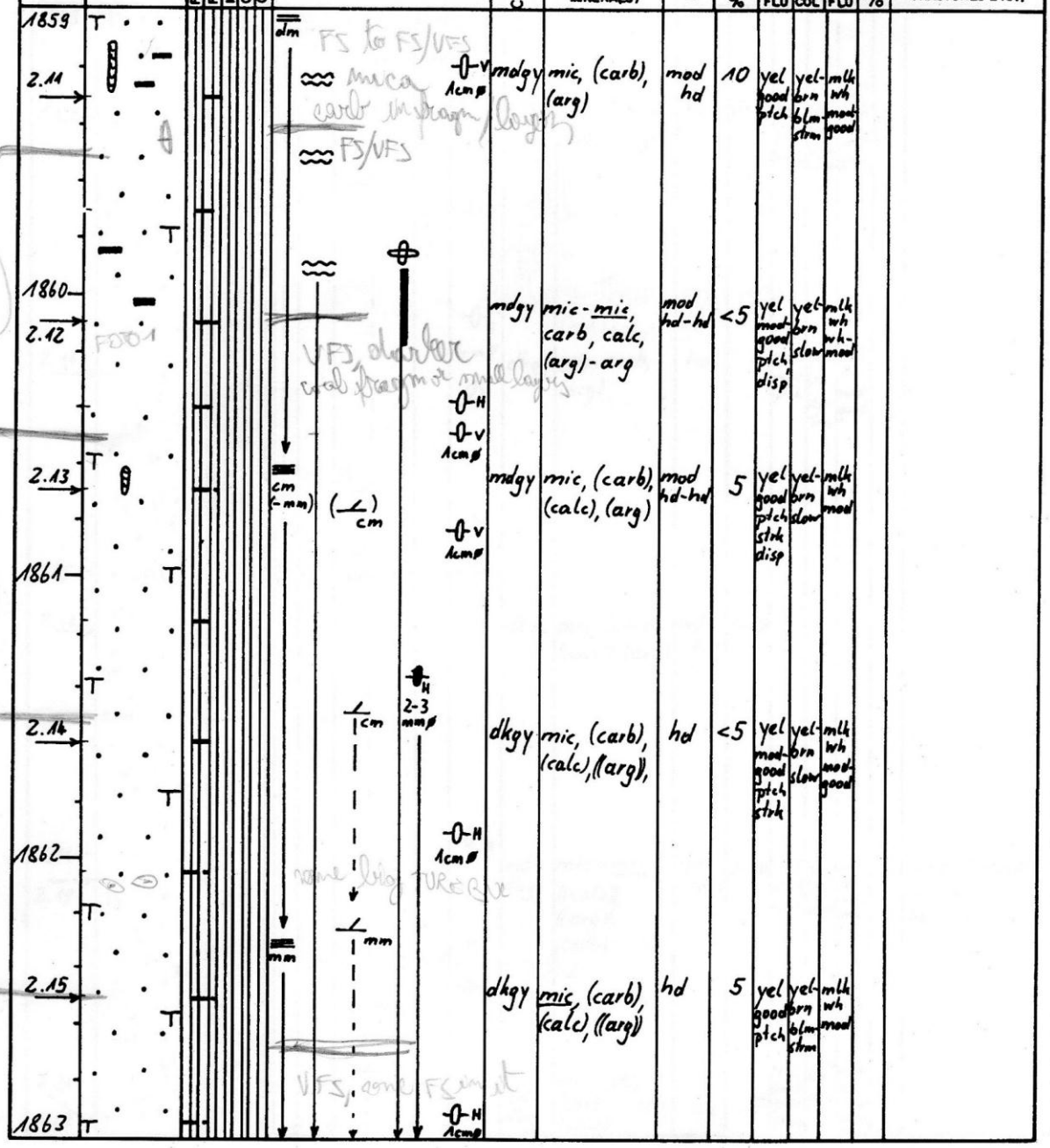

A/S NORSKE SHELL | Well: 31/2-8 | Core No. 2

CORE DESCRIPTION

Cored from _____ to _____ Recovered: _____ m _____ % Core size: _____

Formation: _____ Date: _____ Described by: _____ Corehead: Sheet: 4 of 5

DEPTH & SAMPLES	GRAPHIC LITHOLOGY	GRAIN SIZE (FINE / FINE / MED / CRS / CRS)	SEDIMENTARY STRUCTURES & FEATURES	COLOUR	COMPOSITION (& ACCESSORY MINERALS)	CMT	ESTIMATED Ø %	HYDROCARBON INDICATIONS: SMPL FLU	CUT COL.	CUT FLU	GAS %	REMARKS (OIL BLEED; DIPS; FRACTURES ETC.)
1863			mm (-cm); mm; 2-3 mm Ø H									
2.16				dkgy	mic, (carb), (calc), (arg)	hd	5-10	yel good ptch	yel-brn bl-strm	mlk wh mod-good		
1864			H									
2.17			1cm Ø	dkgy	mic, carb, (arg)	hd	5	yel mod ptch	yel-brn bl-strm	mlk wh mod-good		
1865			(mould only)									
2.18				dkgy	mic, (carb) ((calc)), (arg)	hd-hd	5-10					
1866			H									
2.19				md-dkgy	mic-mic ((calc)), ((arg)), (carb)	hd-mdhd	5-10	yel good ptch	yel-brn strm	mlk wh mod-good		good fluorescence in burrows
			H									
2.20				md-dkgy	mic-mic (carb)-carb, (calc)	hd	5	yel mod-good ptch	cl, slow	mlk wh mod-good		
1867												

A/S NORSKE SHELL | Well: 31/2-8 | Core No. 2

CORE DESCRIPTION

Cored from _____ to _____ Recovered: _____ m _____ % Core size: _____

Formation: _____ Date: _____ Described by: _____ Corehead: Sheet: 5 of 5

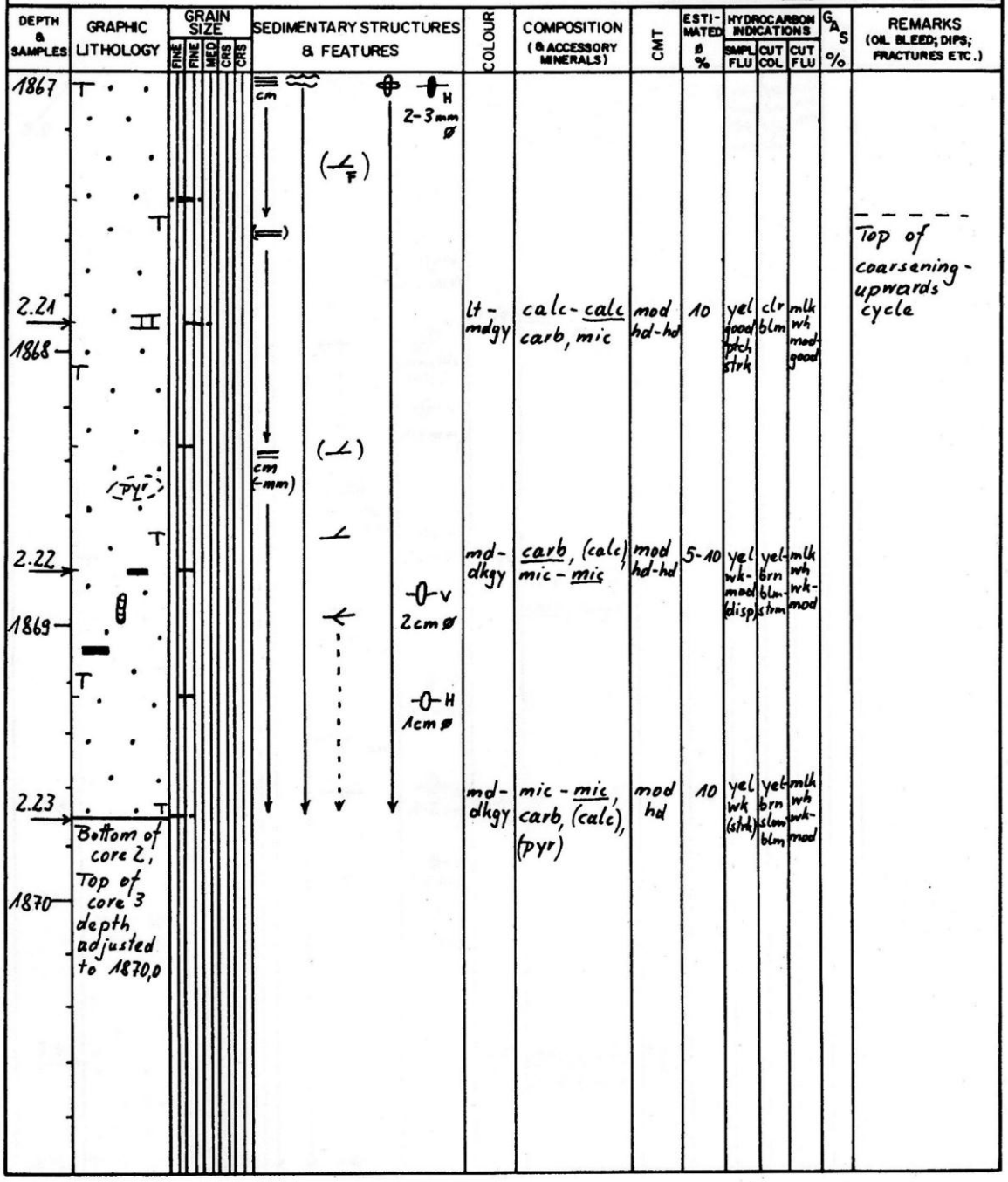

A/S NORSKE SHELL | Well: 31/2-8 | Core No. 3

depth adjusted

CORE DESCRIPTION

Cored from 1870,0 to 1888,5 Recovered: 18,9 m 102 % Core size: 4"

Formation: JU Date: 12.07.82 Described by: P. Immerz Corehead: CB 303

Sheet: 1 of 5

DEPTH & SAMPLES	GRAPHIC LITHOLOGY	GRAIN SIZE	SEDIMENTARY STRUCTURES & FEATURES	COLOUR	COMPOSITION (& ACCESSORY MINERALS)	CMT	ESTIMATED %	HYDROCARBON INDICATIONS: SMPL FLU	HYDROCARBON INDICATIONS: CUT COL.	HYDROCARBON INDICATIONS: CUT FLU	GAS %	REMARKS (OIL BLEED; DIPS; FRACTURES ETC.)
1870			cm f-mm	md-dkgy	mic (carb) - carb (calc) - calc	mod hd-hd	5-10	yel mod strk disp	yel-brn bl-wh slow	milk wh mod		
3.0												
			V 1-2 cm ø									
3.1			cm	mdgy	calc, mic, carb, (arg),	hd	<5	yel wk-mod disp	clr slow	milk wh wk		
1871			(moulds only)									
			V 1-2 mm ø									
			cm									
			H 1cm ø									
3.2				mdgy	mic - mic carb - carb calc, (arg)	hd	<5	yel wk disp		very weak		
1872			cm									
			H 1-2 mm ø									
			cm									
			V 1-2 cm ø	md-dkgy	mic, (calc), (carb) - carb	hd	<5					
3.3			H 1-2 mm ø									
1873			H 1cm ø									+ = syndepositional mini-faults
3.4				md-dkgy	mic, (calc), (arg), (carb)	hd-hd	<5					
1874												

ALL TURBIDITES are MED TO SMALL! (even before)

A/S NORSKE SHELL | Well: 31/2-8 | Core No. 3

CORE DESCRIPTION

Cored from _____ to _____ Recovered: _____ m _____ % Core size: _____

Formation: _____ Date: _____ Described by: _____ Corehead: Sheet: 2 of 5

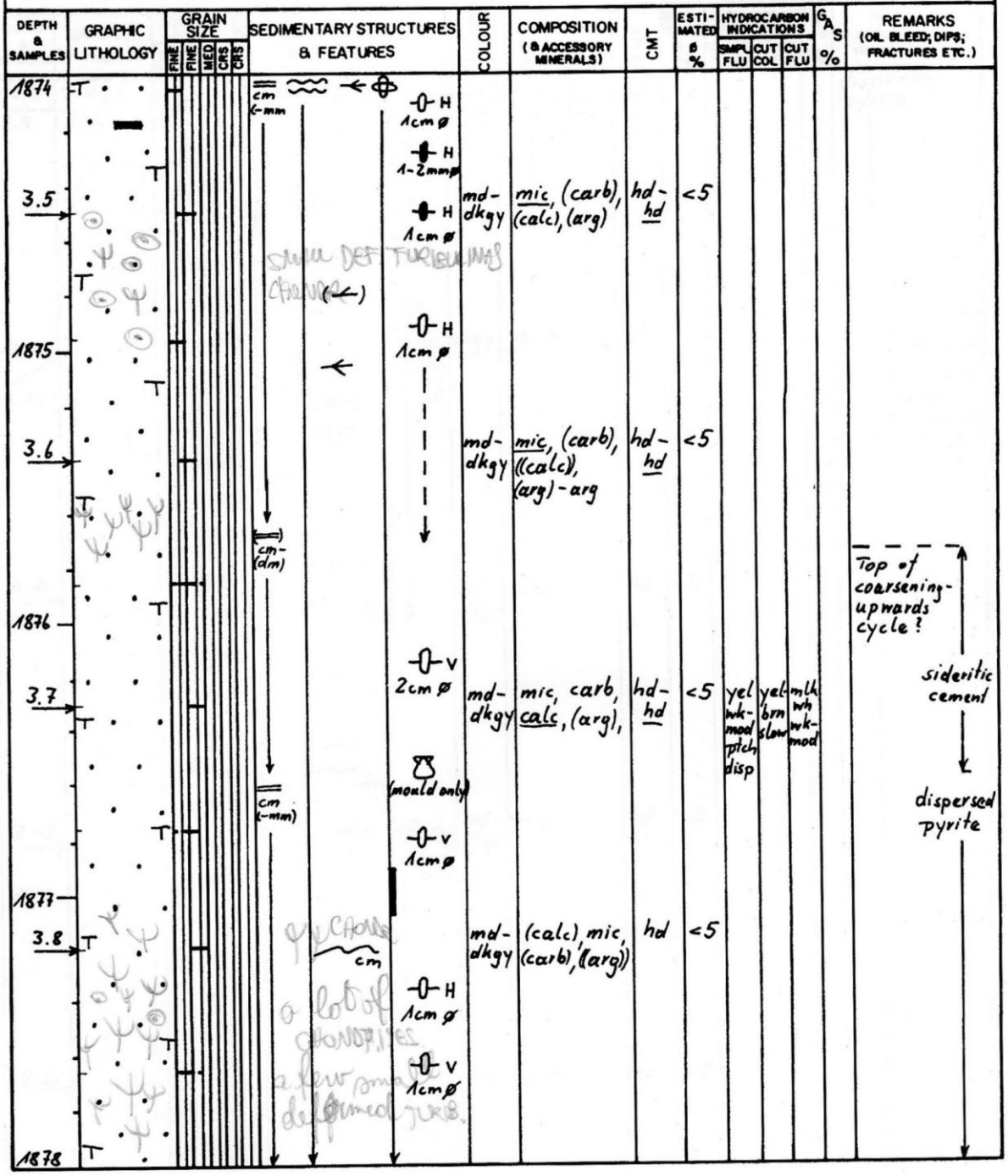

A/S NORSKE SHELL | Well: 31/2-8 | Core No. 3

CORE DESCRIPTION

Cored from _____ to _____ Recovered: _____ m _____ % Core size: _____

Formation: _____ Date: _____ Described by: _____ Corehead: Sheet: 3 of 5

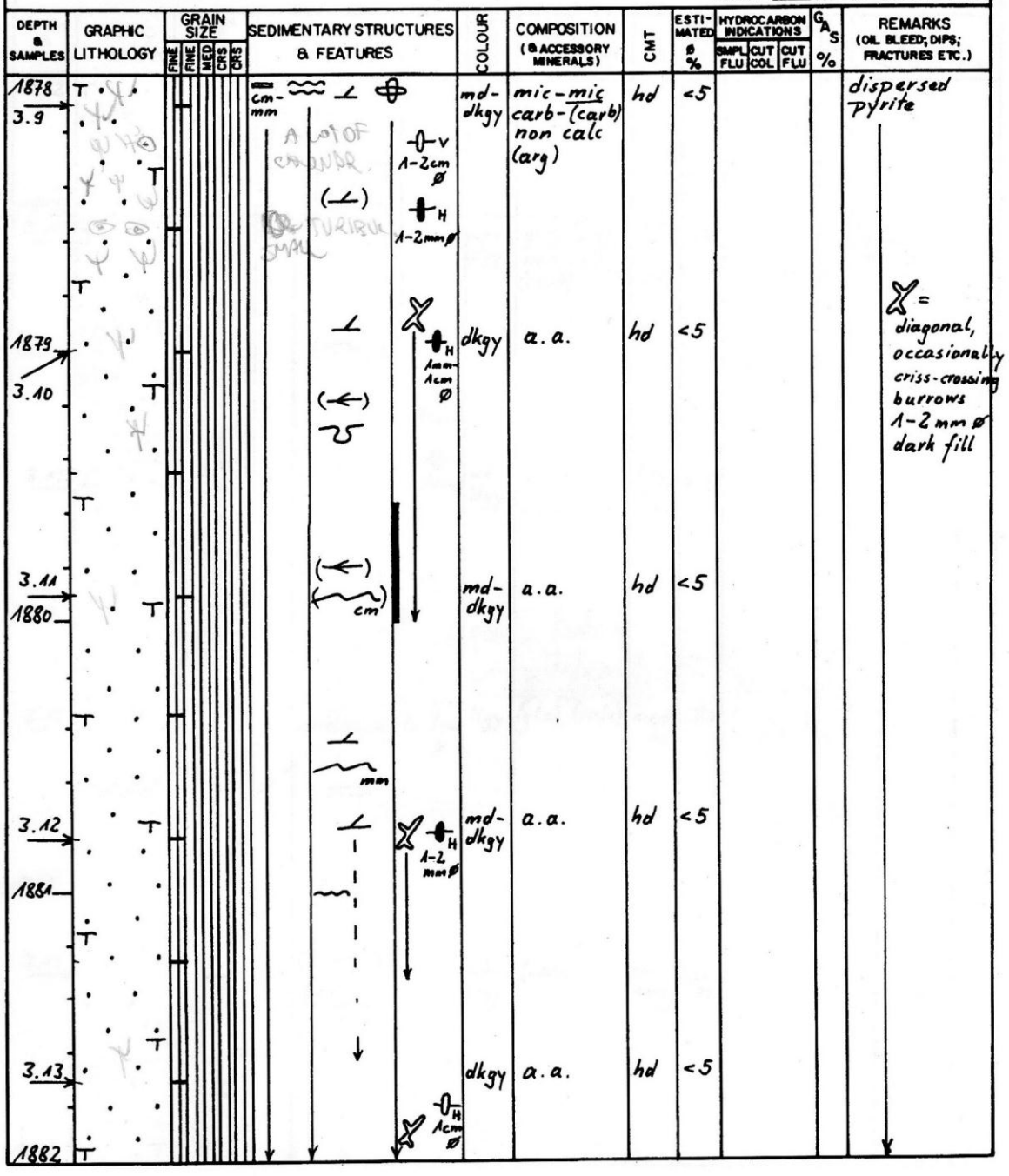

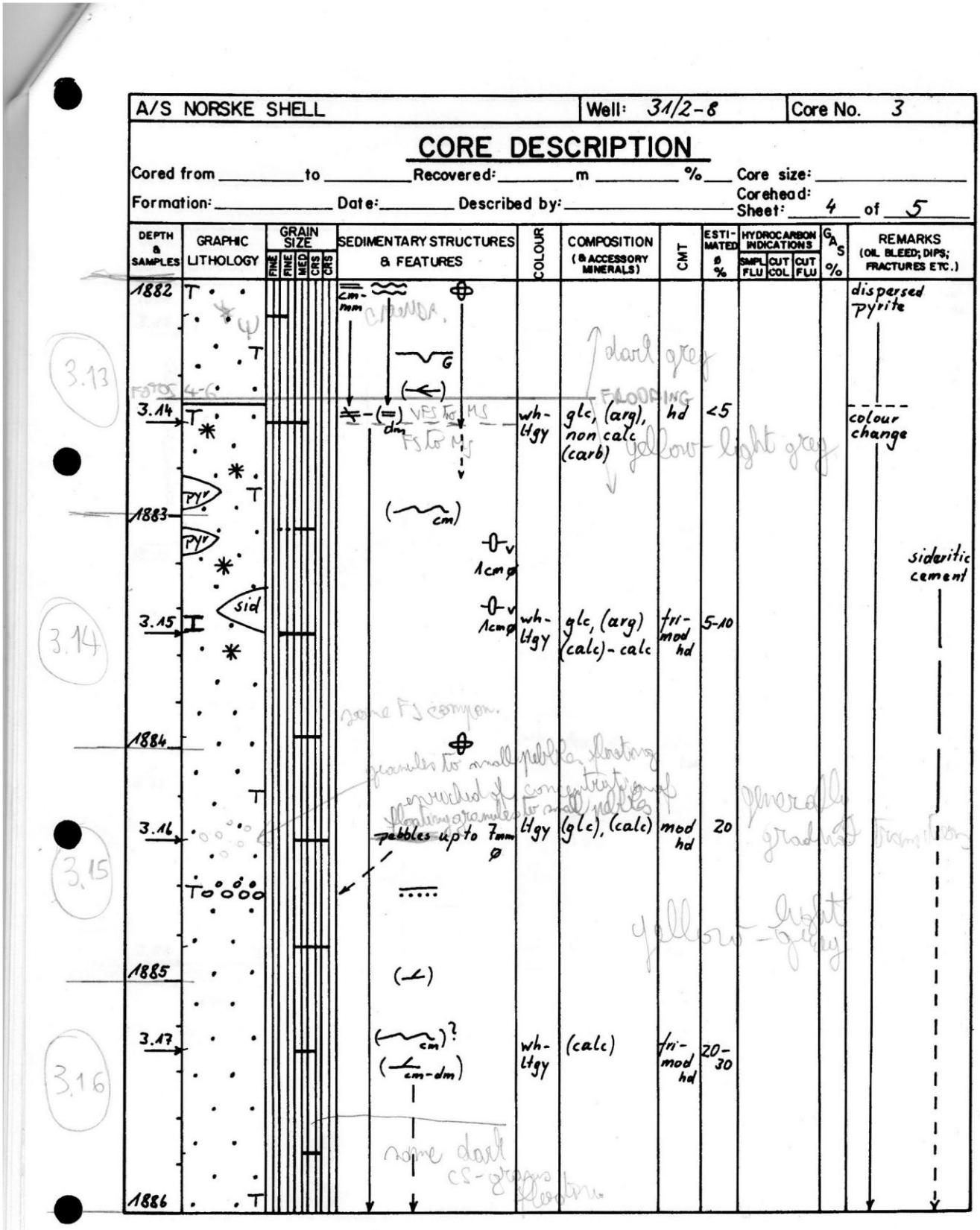
A/S NORSKE SHELL
Well: 31/2-8
Core No. 3
CORE DESCRIPTION
Cored from ____ to ____ Recovered: ____ m ____ % Core size: ____
Formation: ____ Date: ____ Described by: ____ Corehead:
Sheet: 4 of 5
DEPTH & SAMPLES
GRAPHIC LITHOLOGY
GRAIN SIZE
SEDIMENTARY STRUCTURES & FEATURES
COLOUR
COMPOSITION (& ACCESSORY MINERALS)
CMT
ESTIMATED Ø %
HYDROCARBON INDICATIONS
GAS %
REMARKS (OIL BLEED; DIPS; FRACTURES ETC.)
1882
1883
1884
1885
1886
3.13
3.14
3.15
3.16
3.17
wh-ltgy
glc, (arg), non calc (carb)
hd
<5
dispersed pyrite
colour change
sideritic cement
glc, (arg) (calc) - calc
tri-mod hd
5-10
(glc), (calc)
mod hd
20
(calc)
tri-mod hd
20-30
dark grey
yellow-light grey
FLOODING
pebbles up to 7mm Ø
1cm Ø
sid
PYr

A/S NORSKE SHELL | Well: 31/2-8 | Core No. 3

CORE DESCRIPTION

Cored from _____ to _____ Recovered: _____ m _____ % Core size: _____

Formation: _____ Date: _____ Described by: _____ Corehead: Sheet: 5 of 5

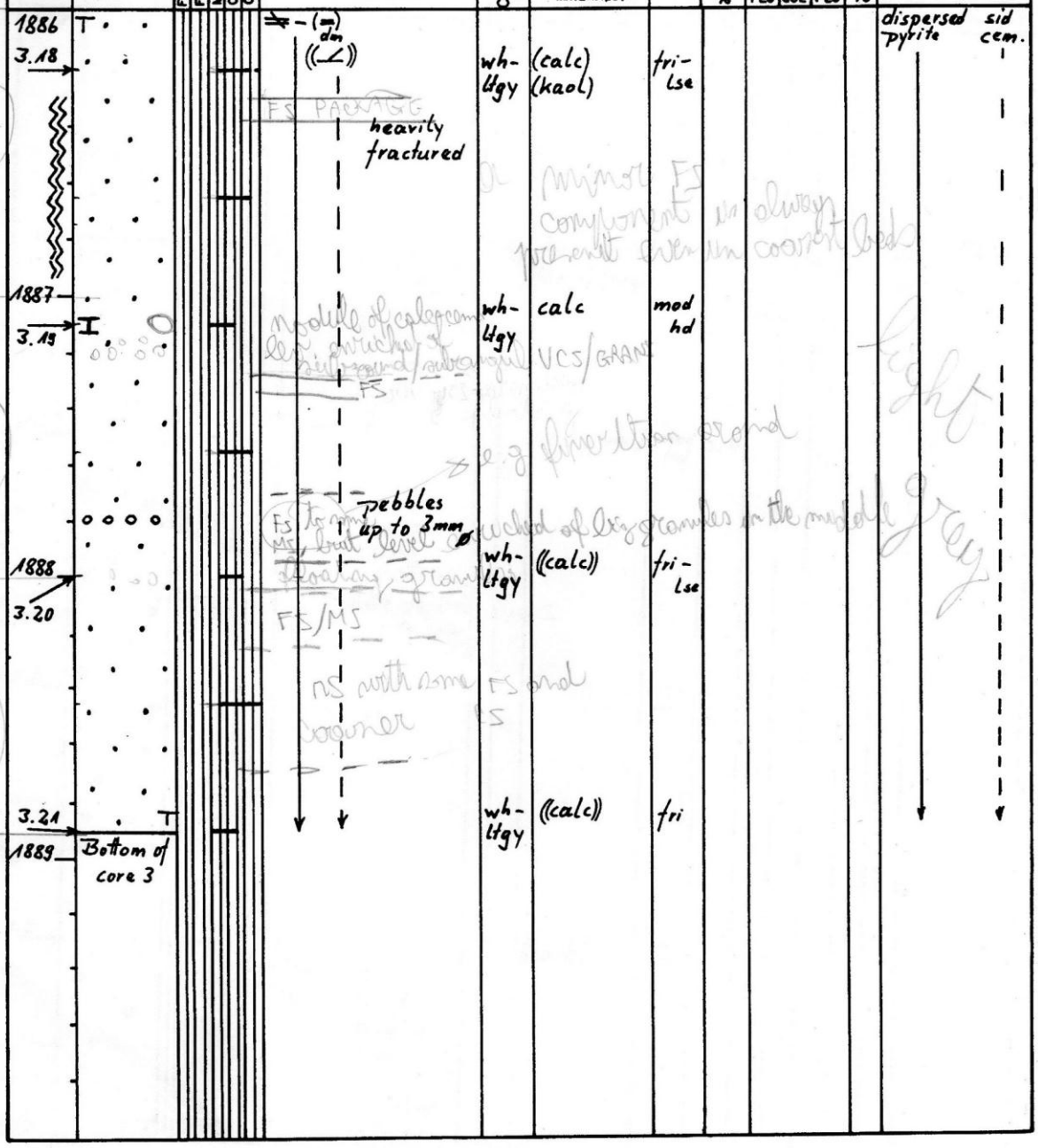

1mm = 2cm
1m = 5cm ⇒ 1 m = 0.05 m ⇒ 1:20

31/2-15

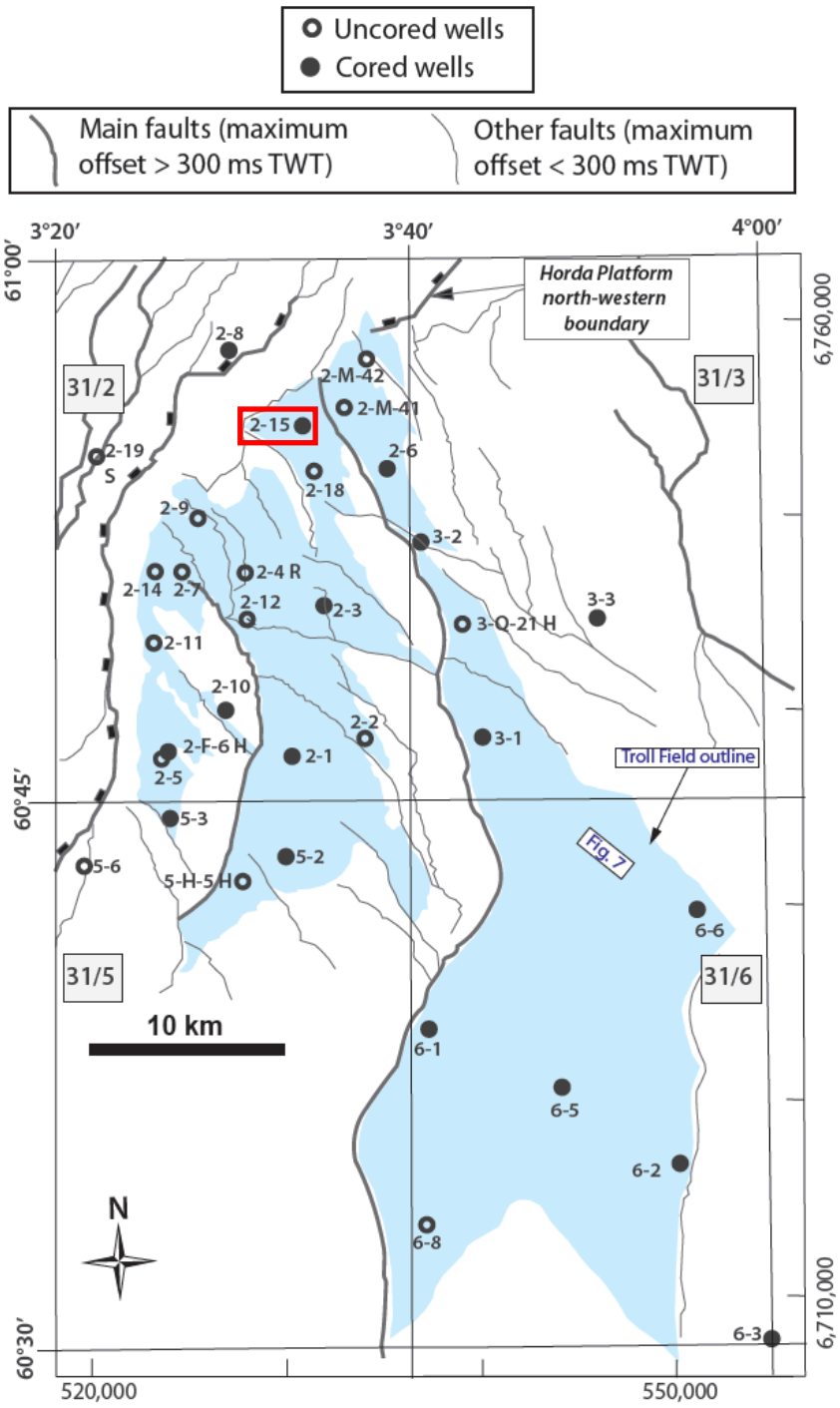
Uncored wells
Cored wells
Main faults (maximum offset > 300 ms TWT)
Other faults (maximum offset < 300 ms TWT)
3°20′
3°40′
4°00′
61°00′
60°45′
60°30′
6,760,000
6,710,000
520,000
550,000
Horda Platform north-western boundary
31/2
31/3
31/5
31/6
2-8
2-M-42
2-M-41
2-15
2-19 S
2-18
2-6
2-9
3-2
2-14
2-7
2-4 R
2-12
2-3
3-Q-21 H
3-3
2-11
2-10
2-2
3-1
2-F-6 H
2-1
2-5
Troll Field outline
Fig. 7
5-3
5-6
5-H-5 H
5-2
6-6
6-1
6-5
6-2
6-8
6-3
10 km
N

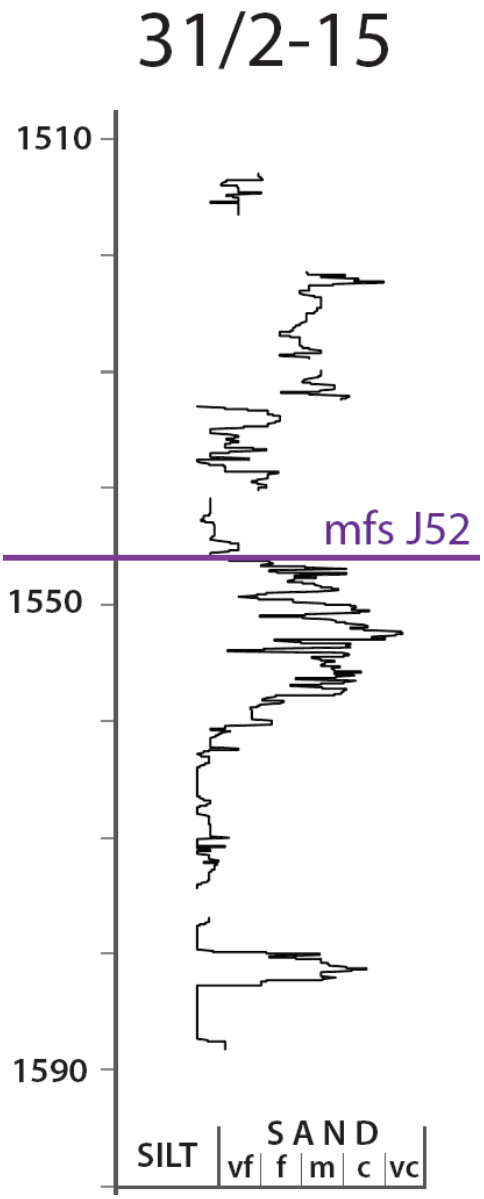
31/2-15
1510
1550
1590
mfs J52
SILT
SAND
vf
f
m
c
vc

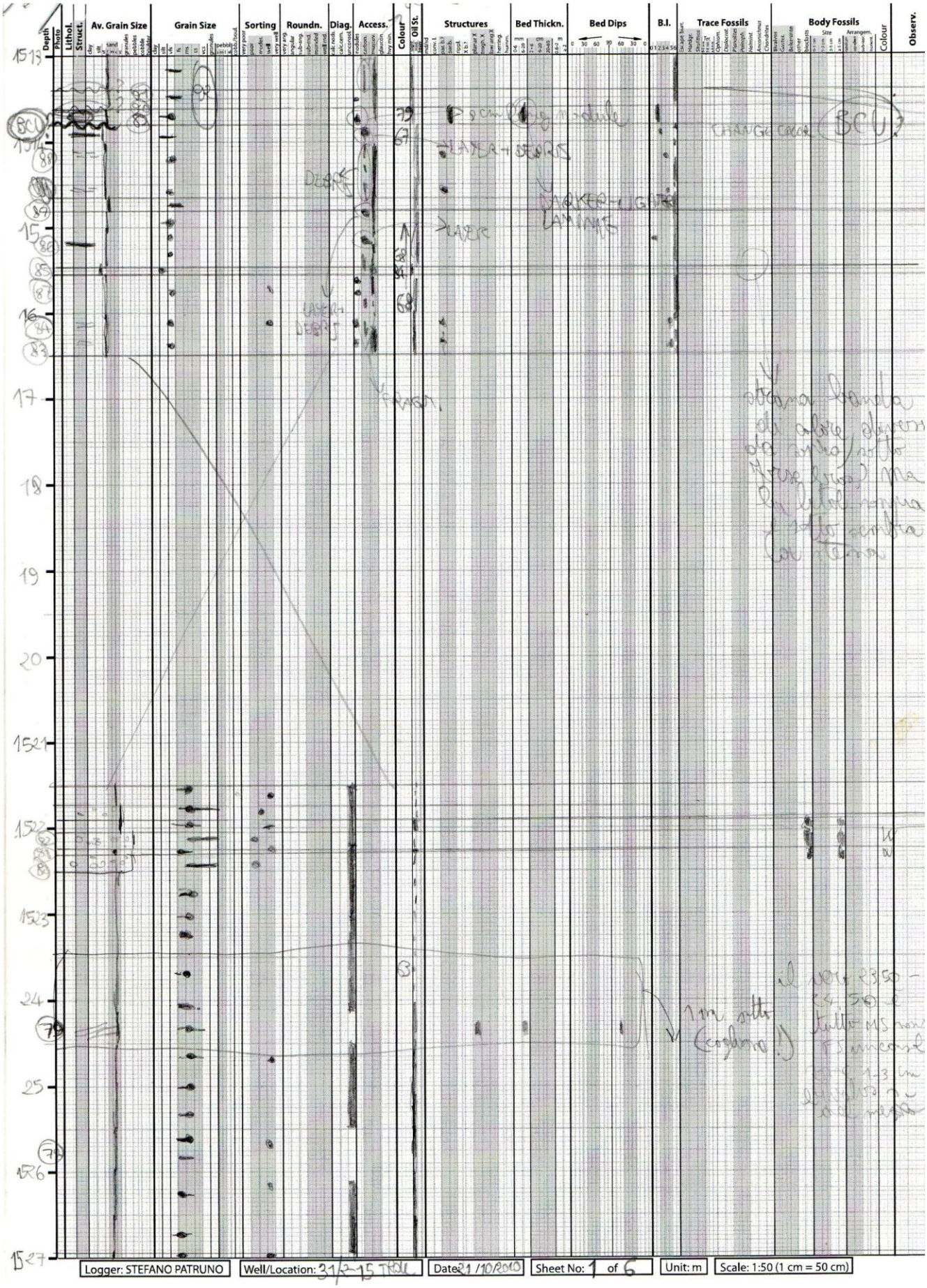
Depth
Photo
Lithol.
Struct.
Av. Grain Size
Grain Size
Sorting
Roundn.
Diag.
Access.
Colour
Oil St.
Structures
Bed Thickn.
Bed Dips
B.I.
Trace Fossils
Body Fossils
Observ.
Logger: STEFANO PATRUNO
Well/Location: 31/2-15 THOR
Date: 21/10/2010
Sheet No: 1 of 6
Unit: m
Scale: 1:50 (1 cm = 50 cm)

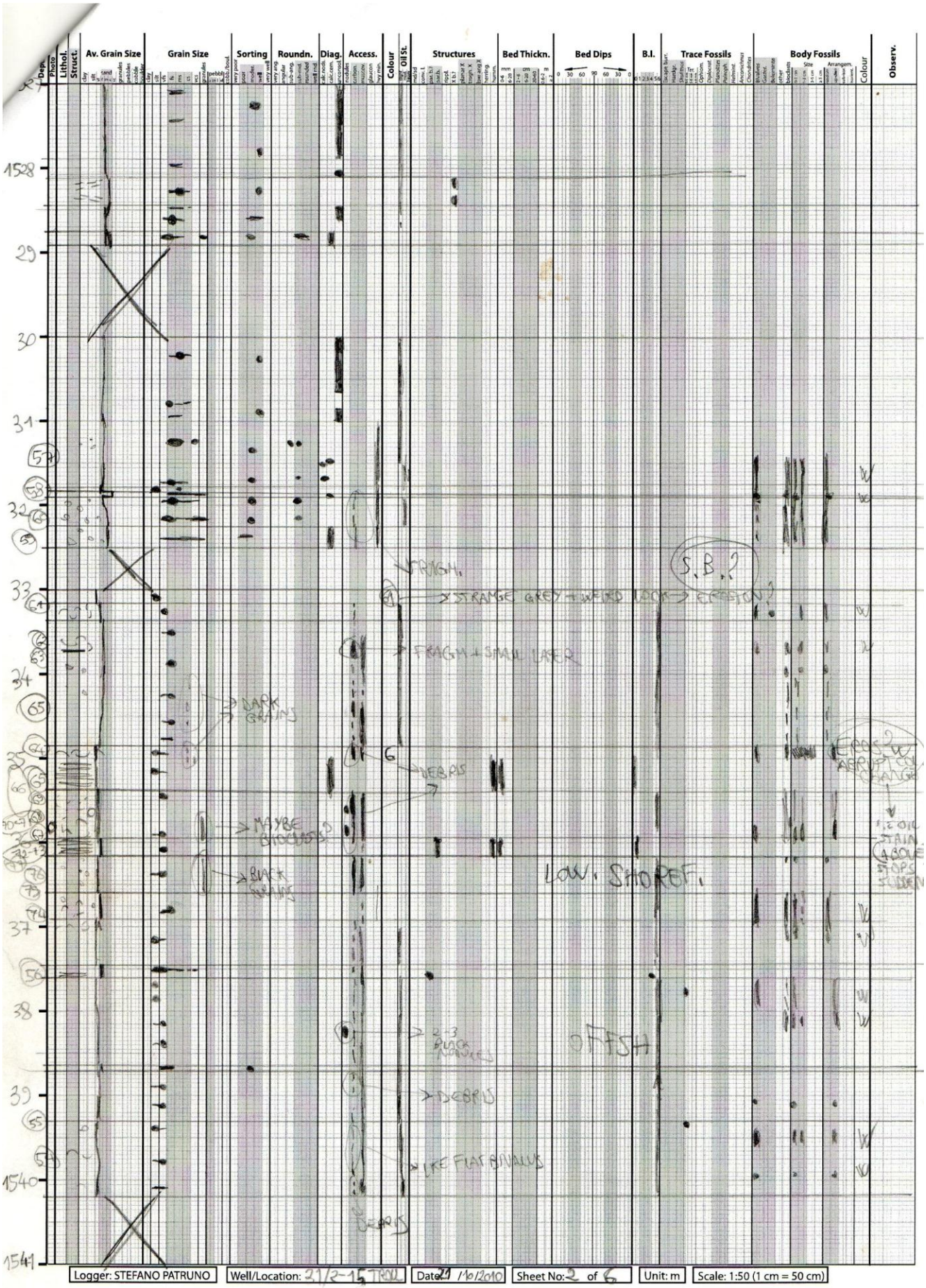
Depth
Photo
Lithol.
Struct.
Av. Grain Size
Grain Size
Sorting
Roundn.
Diag.
Access.
Colour
Oil St.
Structures
Bed Thickn.
Bed Dips
B.I.
Trace Fossils
Body Fossils
Observ.
Colour
1528
29
30
31
32
33
34
1540
1541
S.B.?
STRANGE GREY + WEIRD LOOK → EROSION?
FRAGM + SMALL LAER
DARK GRAINS
DEBRIS
MAYBE BIOCLASTS
BLACK MINERALS
LOW. SHOREF.
OFFSH
2-3 BLACK MINERALS
DEBRIS
LIKE FLAT BIVALVE
DEBRIS
Logger: STEFANO PATRUNO
Well/Location: 21/2-15 TROLL
Date: 29/10/2010
Sheet No: 2 of 6
Unit: m
Scale: 1:50 (1 cm = 50 cm)

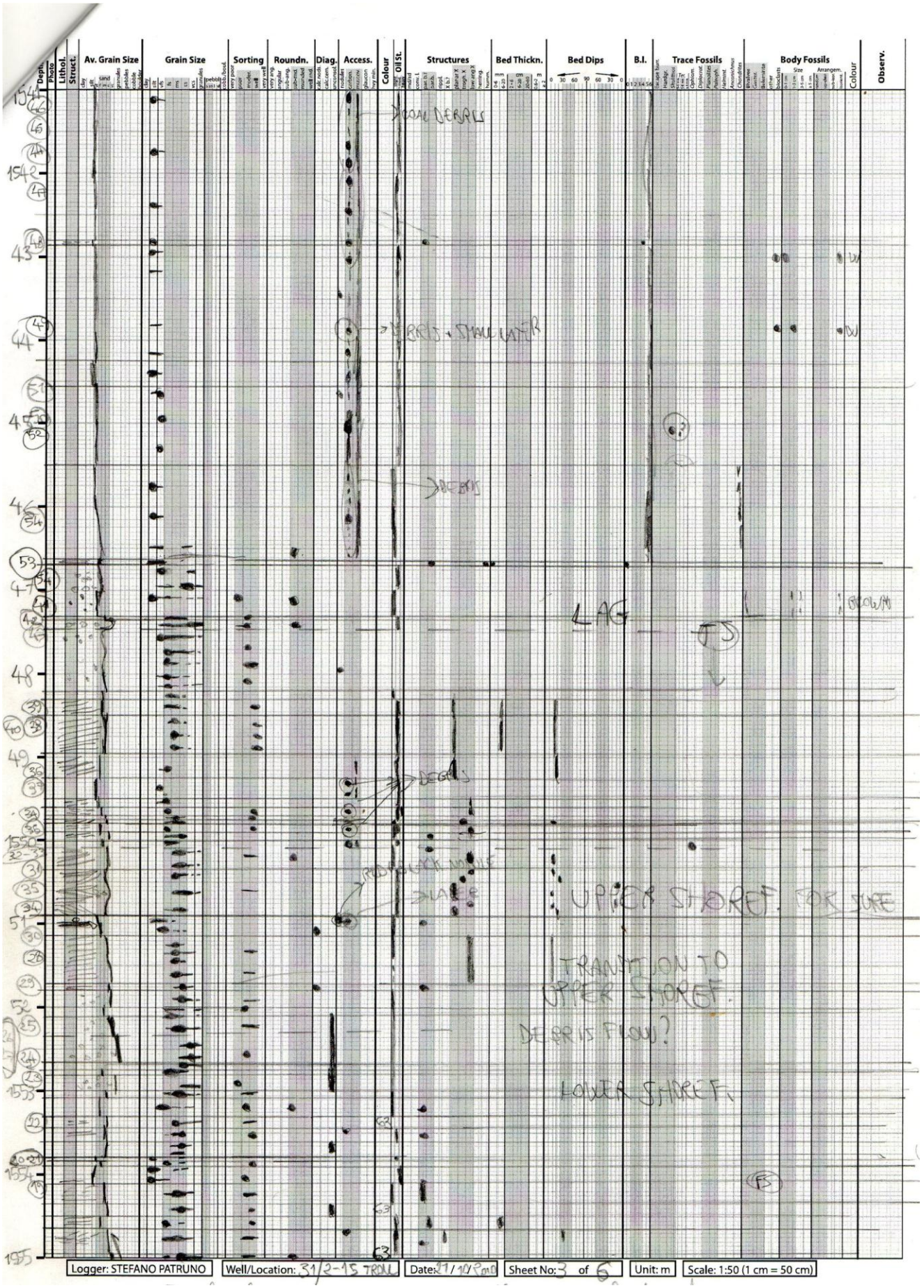
Depth
Photo
Lithol.
Struct.
Av. Grain Size
Grain Size
Sorting
Roundn.
Diag.
Access.
Colour
Oil St.
Structures
Bed Thickn.
Bed Dips
B.I.
Trace Fossils
Body Fossils
Observ.
DEBRIS
LAG
FS
UPPER SHOREF. FOR SURE
TRANSITION TO UPPER SHOREF.
DEBRIS FLOW?
LOWER SHOREF.
Logger: STEFANO PATRUNO
Well/Location: 31/2-15 TROLL
Date: 21/10/2010
Sheet No: 3 of 6
Unit: m
Scale: 1:50 (1 cm = 50 cm)

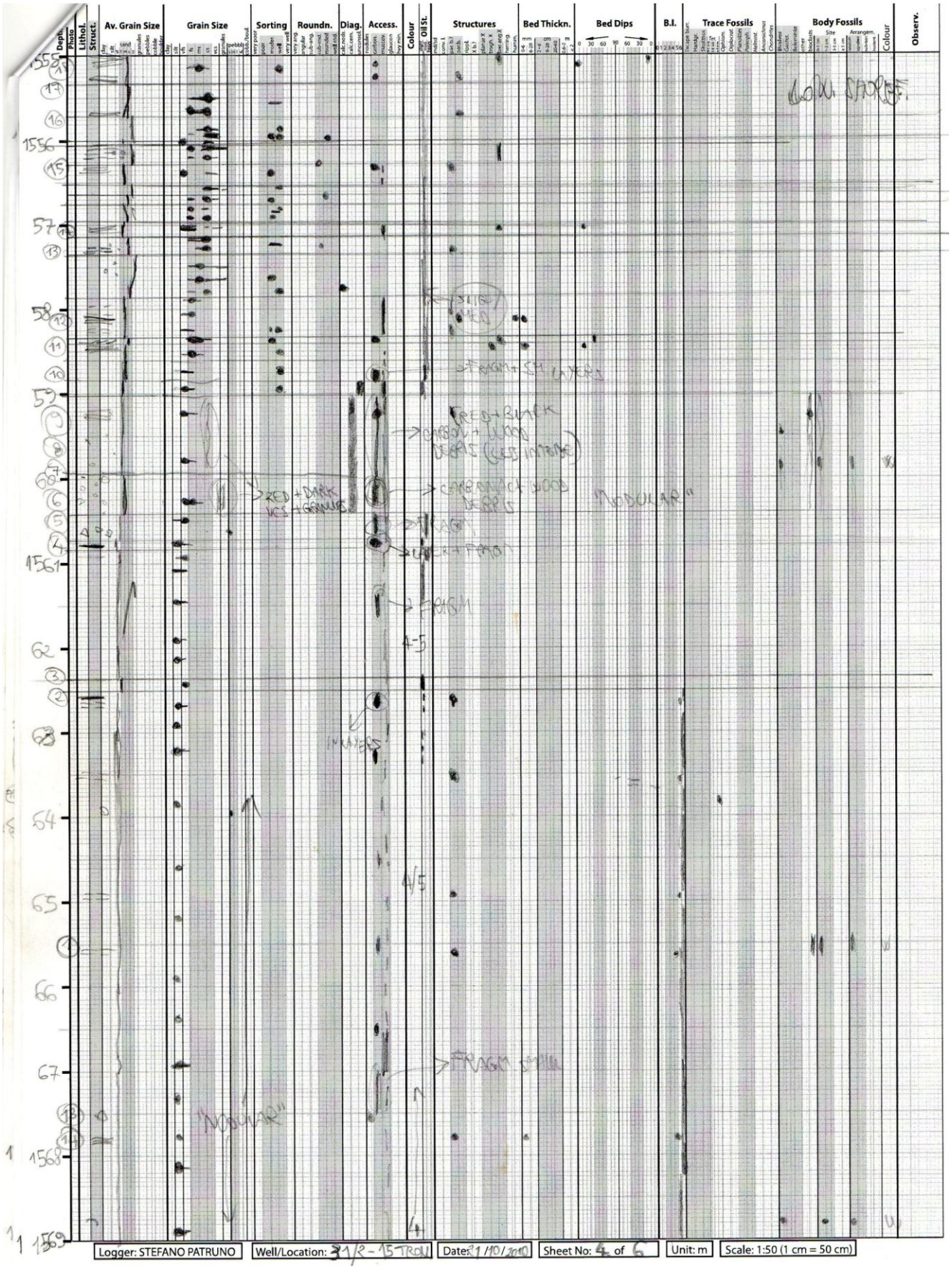
Depth
Photo
Lithol.
Struct.
Av. Grain Size
Grain Size
Sorting
Roundn.
Diag.
Access.
Colour
Oil St.
Structures
Bed Thickn.
Bed Dips
B.I.
Trace Fossils
Body Fossils
Observ.
Logger: STEFANO PATRUNO
Well/Location: 31/2 - 15 TROLL
Date: 21/10/2010
Sheet No: 4 of 6
Unit: m
Scale: 1:50 (1 cm = 50 cm)

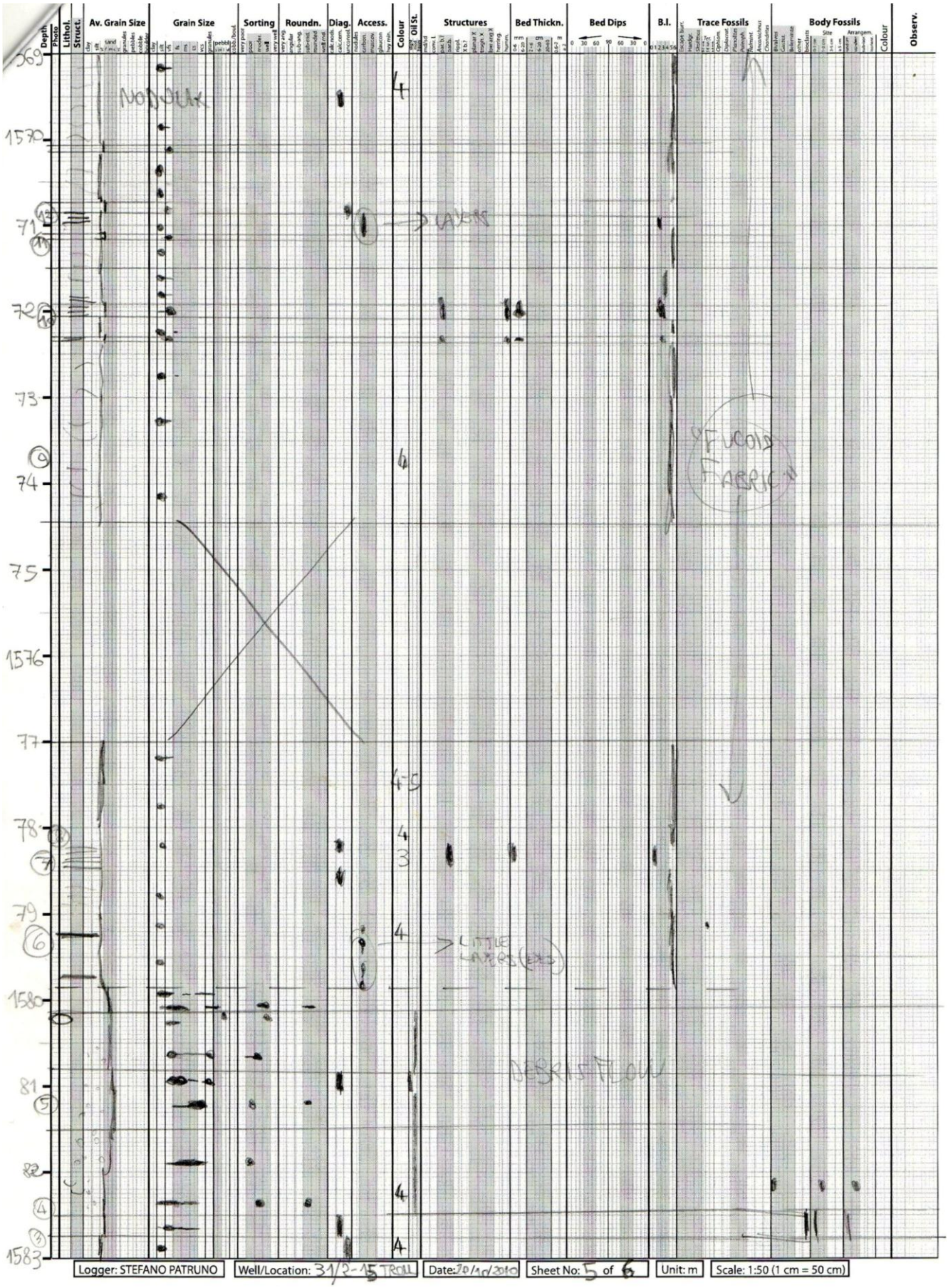
Depth
Photo
Lithol.
Struct.
Av. Grain Size
Grain Size
Sorting
Roundn.
Diag.
Access.
Colour
Oil St.
Structures
Bed Thickn.
Bed Dips
B.I.
Trace Fossils
Body Fossils
Observ.
NODULAR
LAYERS
FUCOID FABRIC
LITTLE LAYERS (CM)
DEBRIS FLOW
Logger: STEFANO PATRUNO
Well/Location: 31/2-15 TROLL
Date: 20/10/2010
Sheet No: 5 of 6
Unit: m
Scale: 1:50 (1 cm = 50 cm)

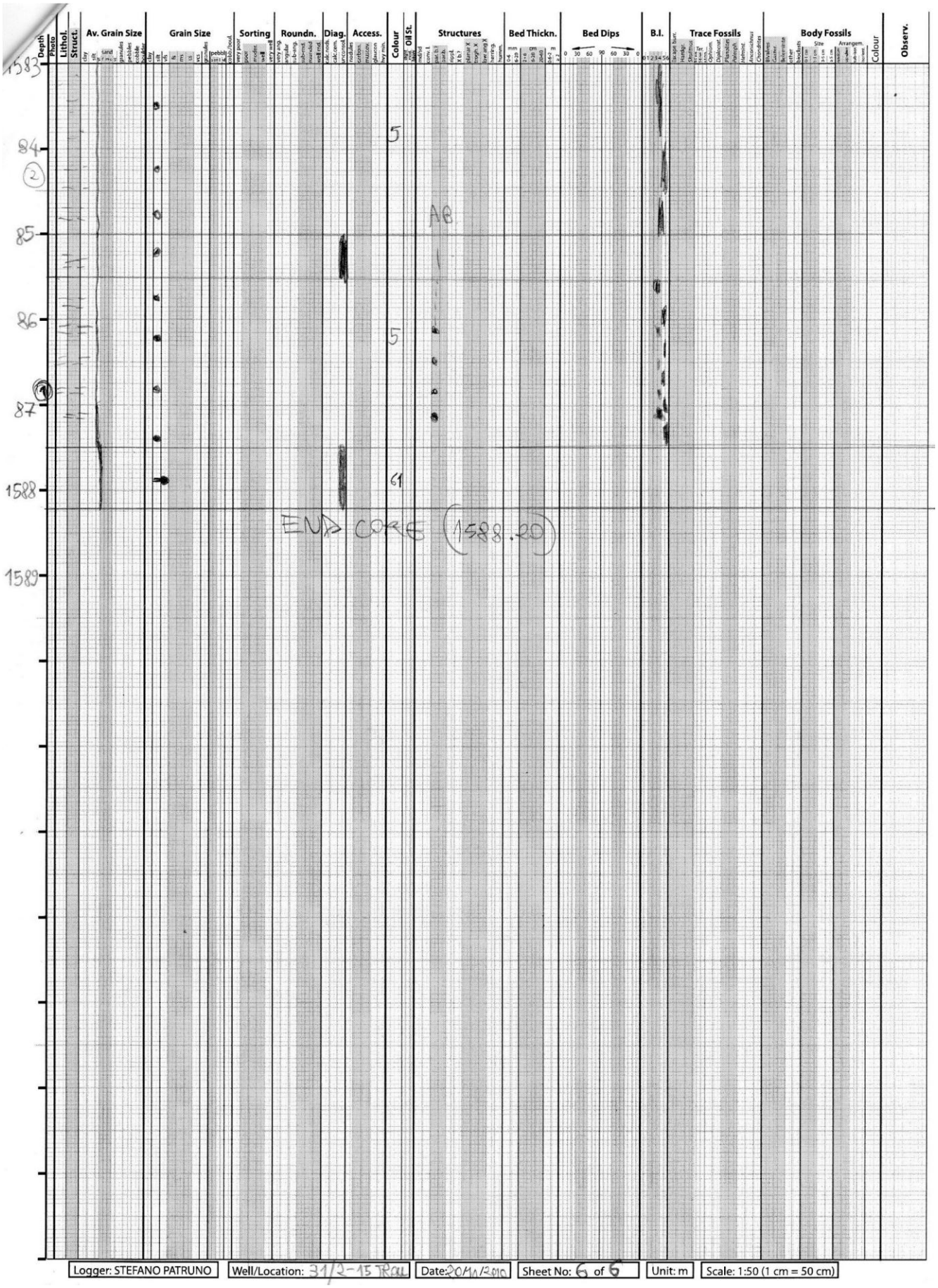
Depth
Photo
Lithol.
Struct.
Av. Grain Size
Grain Size
Sorting
Roundn.
Diag.
Access.
Colour
Oil St.
Structures
Bed Thickn.
Bed Dips
B.I.
Trace Fossils
Body Fossils
Observ.
1583
84
85
86
87
1588
1589
AB
END CORE (1588.20)
Logger: STEFANO PATRUNO
Well/Location: 31/2-15 TROLL
Date: 20/11/2010
Sheet No: 6 of 6
Unit: m
Scale: 1:50 (1 cm = 50 cm)

31/2-F 6H

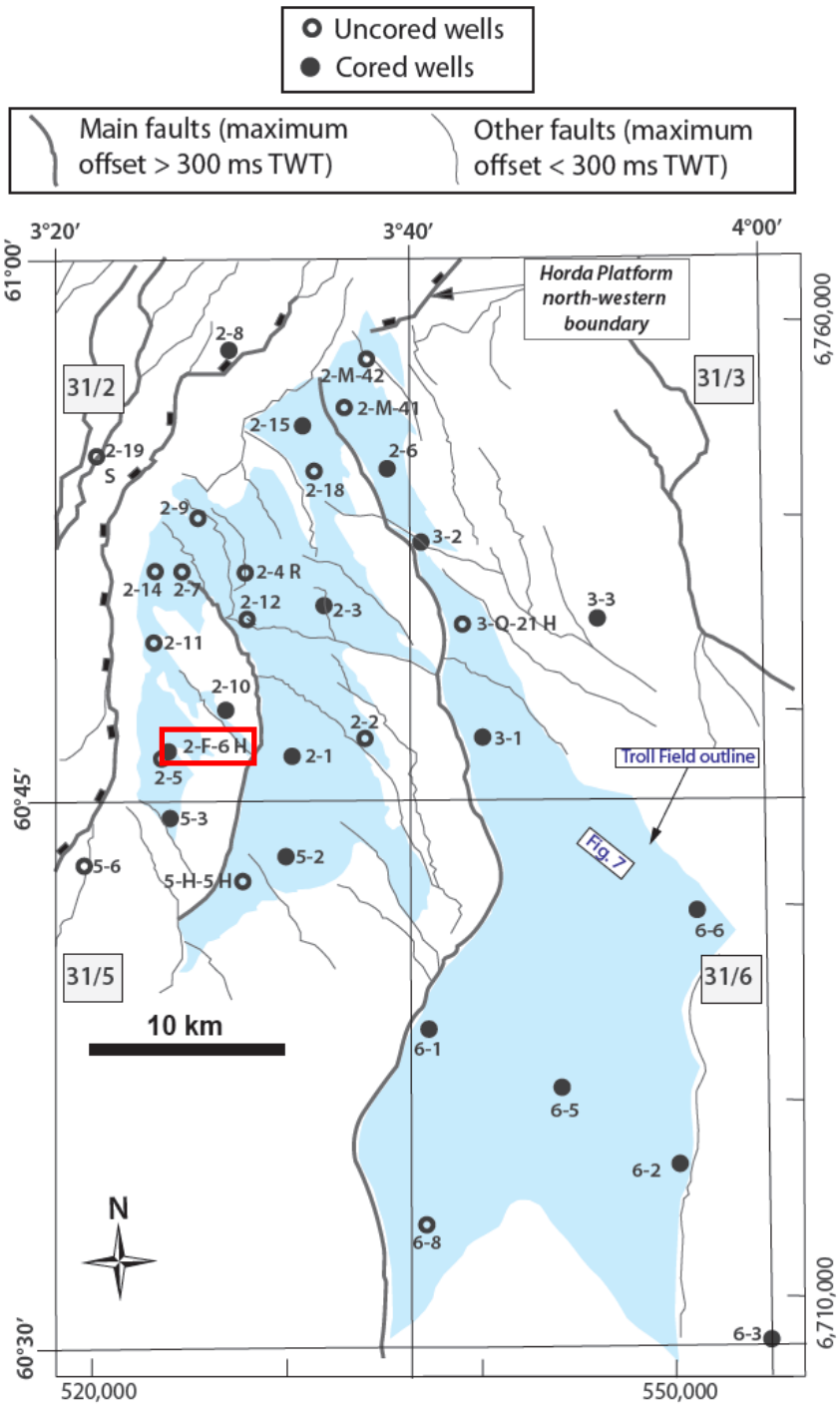
Uncored wells
Cored wells
Main faults (maximum offset > 300 ms TWT)
Other faults (maximum offset < 300 ms TWT)
3°20′
3°40′
4°00′
61°00′
60°45′
60°30′
6,760,000
6,710,000
520,000
550,000
Horda Platform north-western boundary
31/2
31/3
31/5
31/6
2-8
2-M-42
2-M-41
2-15
2-19 S
2-6
2-18
2-9
3-2
2-14
2-7
2-4 R
2-12
2-3
3-3
3-Q-21 H
2-11
2-10
2-2
3-1
2-F-6 H
2-5
2-1
Troll Field outline
Fig. 7
5-3
5-6
5-H-5 H
5-2
6-6
10 km
6-1
6-5
6-2
6-8
6-3
N

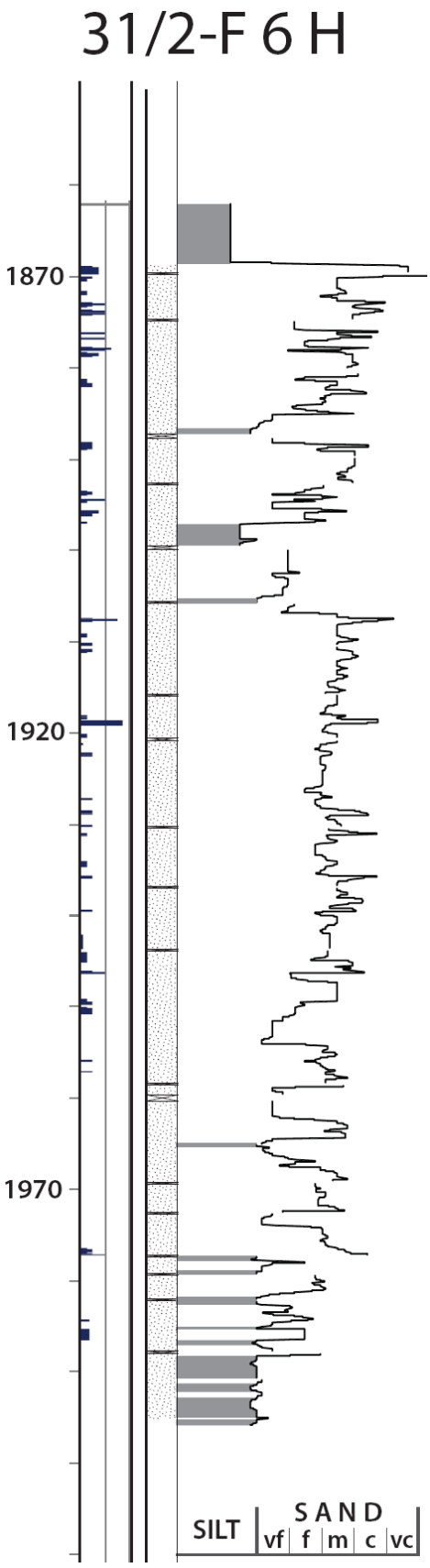
31/2-F 6 H
1870
1920
1970
SILT
SAND
vf
f
m
c
vc

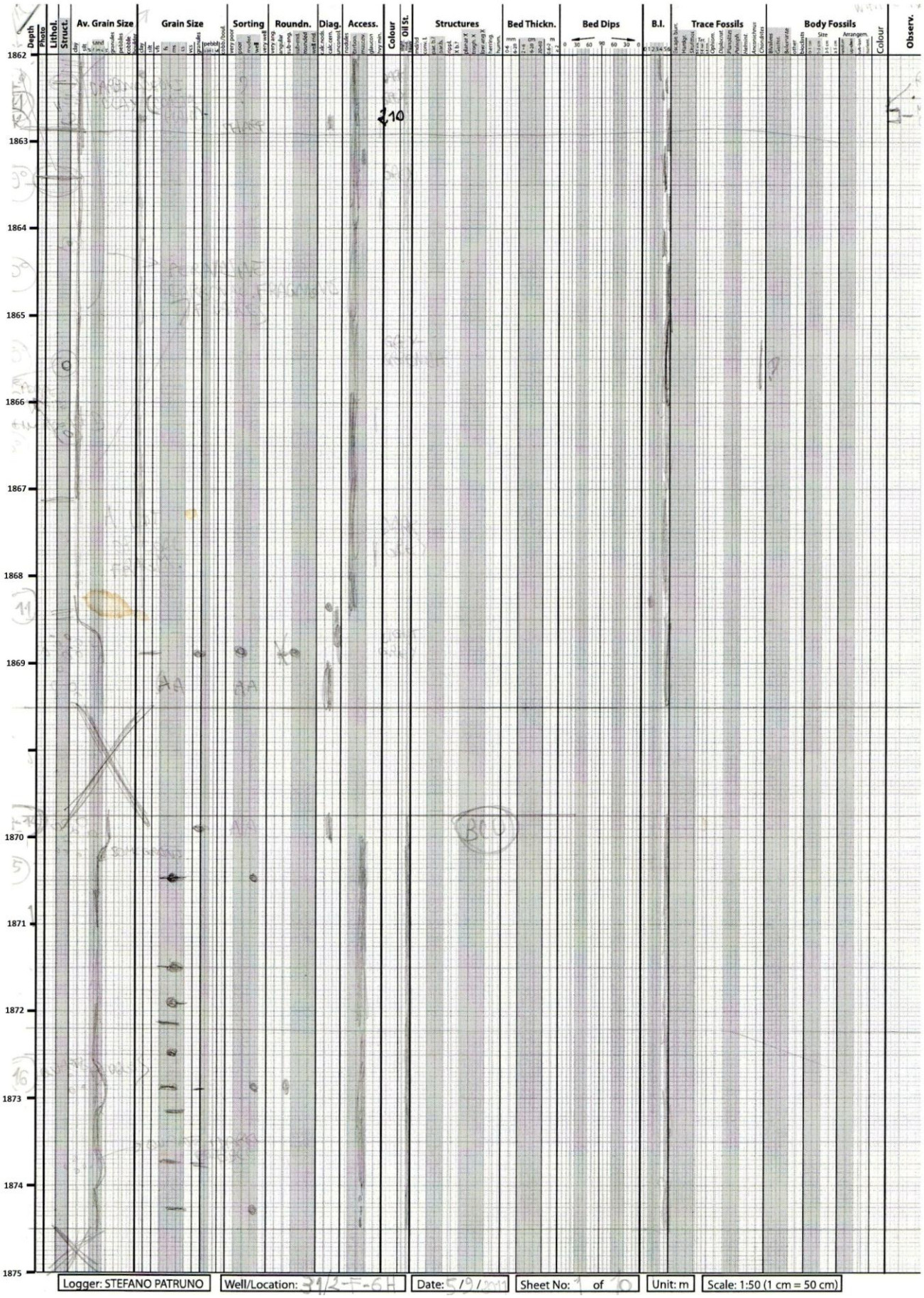
Depth
Photo
Lithol.
Struct.
Av. Grain Size
Grain Size
Sorting
Roundn.
Diag.
Access.
Colour
Oil St.
Structures
Bed Thickn.
Bed Dips
B.I.
Trace Fossils
Body Fossils
Observ.
1862
1863
1864
1865
1866
1867
1868
1869
1870
1871
1872
1873
1874
1875
Logger: STEFANO PATRUNO
Well/Location: 31/3-F-6H
Date: 5/9/2011
Sheet No: 1 of 10
Unit: m
Scale: 1:50 (1 cm = 50 cm)

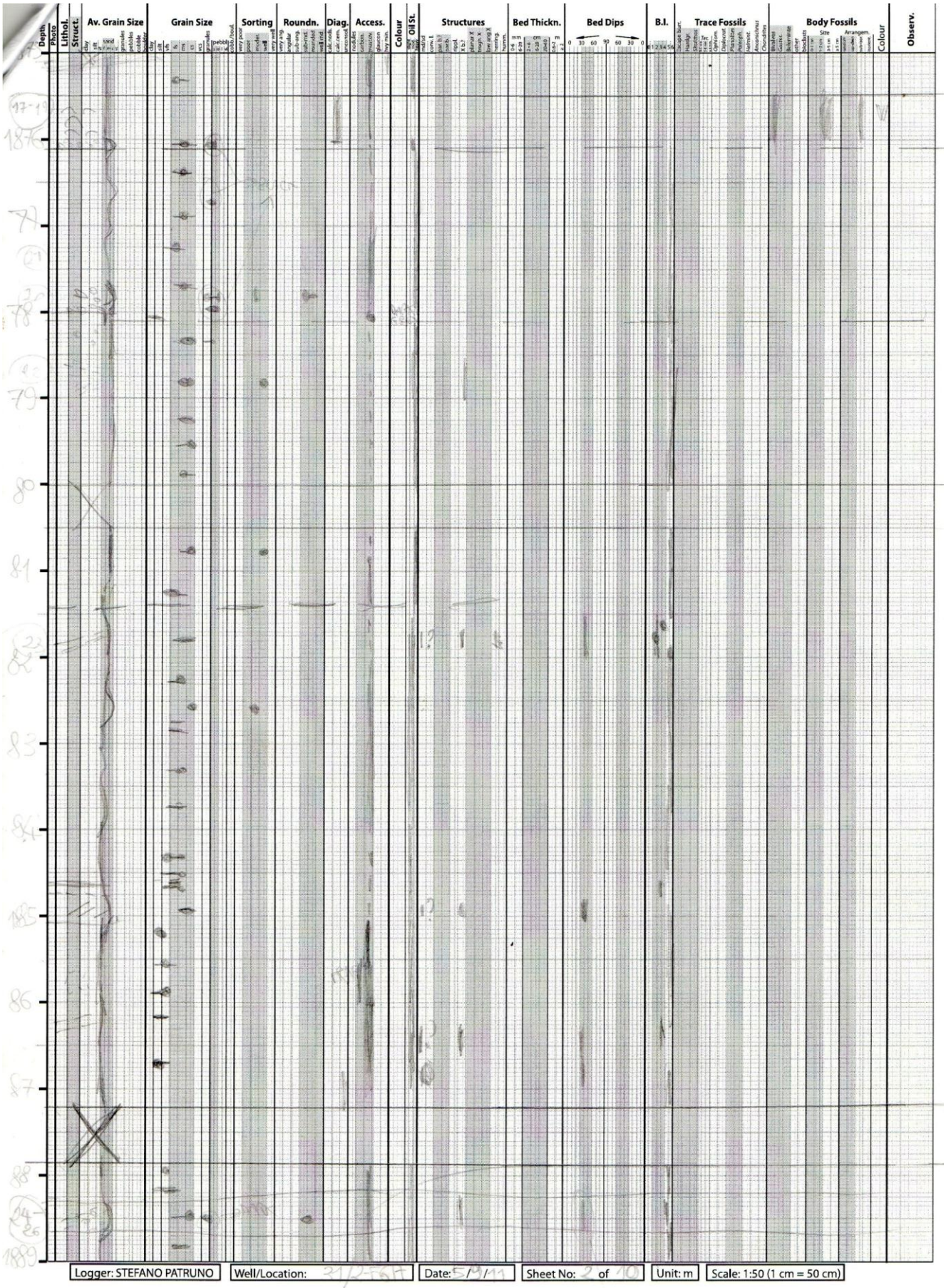
Depth
Photo
Lithol.
Struct.
Av. Grain Size
Grain Size
Sorting
Roundn.
Diag.
Access.
Colour
Oil St.
Structures
Bed Thickn.
Bed Dips
B.I.
Trace Fossils
Body Fossils
Observ.
Logger: STEFANO PATRUNO
Well/Location:
Date: 5/9/11
Sheet No: 2 of 10
Unit: m
Scale: 1:50 (1 cm = 50 cm)

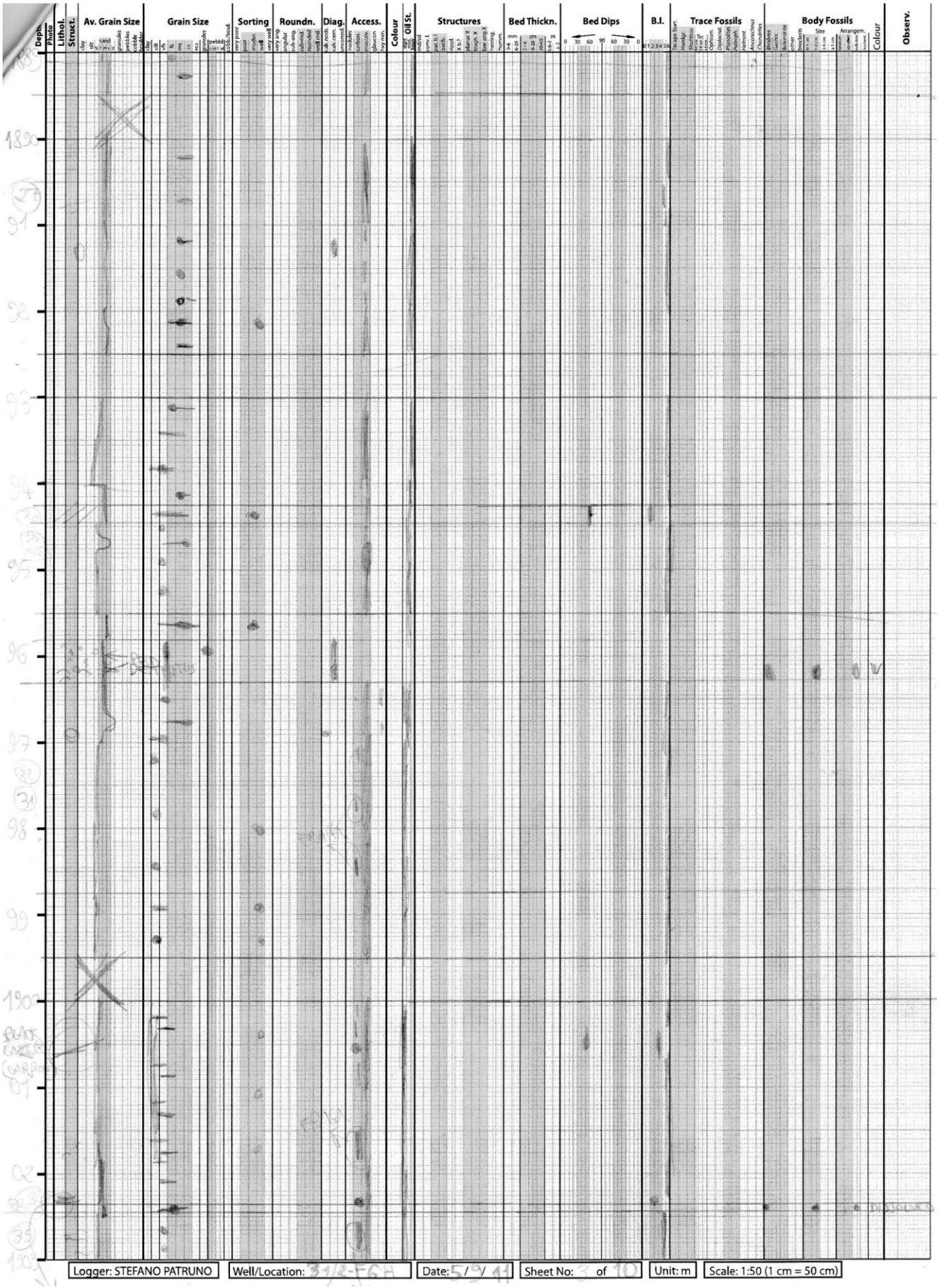
Depth
Photo
Lithol.
Struct.
Av. Grain Size
Grain Size
Sorting
Roundn.
Diag.
Access.
Colour
Oil St.
Structures
Bed Thickn.
Bed Dips
B.I.
Trace Fossils
Body Fossils
Observ.
Logger: STEFANO PATRUNO
Well/Location:
Date: 5 / 9 / 11
Sheet No: of 10
Unit: m
Scale: 1:50 (1 cm = 50 cm)

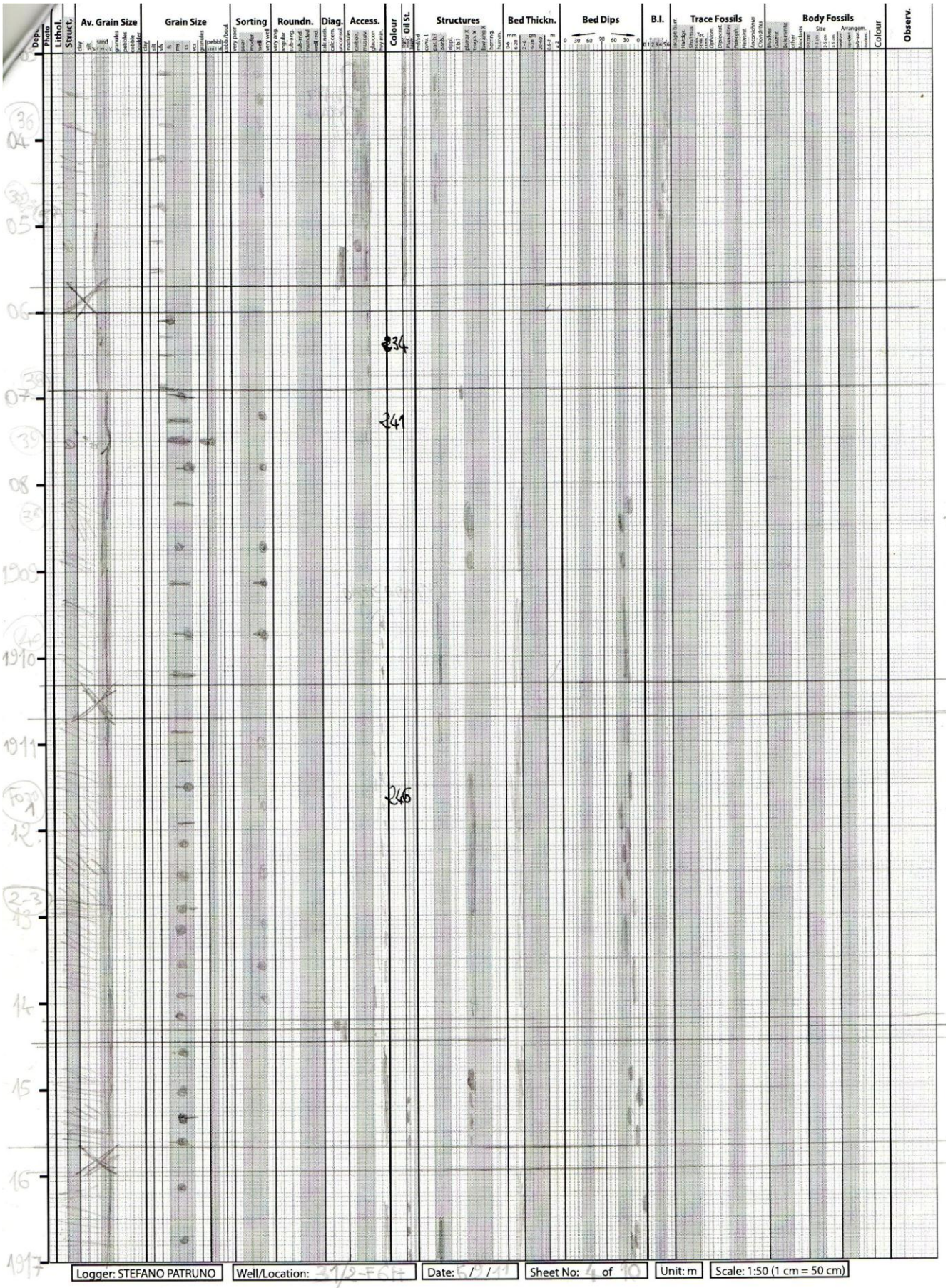
Dep.
Photo
Lithol.
Struct.
Av. Grain Size
Grain Size
Sorting
Roundn.
Diag.
Access.
Colour
Oil St.
Structures
Bed Thickn.
Bed Dips
B.I.
Trace Fossils
Body Fossils
Observ.
Colour
234
241
246
Logger: STEFANO PATRUNO
Well/Location: 31/2-F6T
Date: / /
Sheet No: 4 of 10
Unit: m
Scale: 1:50 (1 cm = 50 cm)

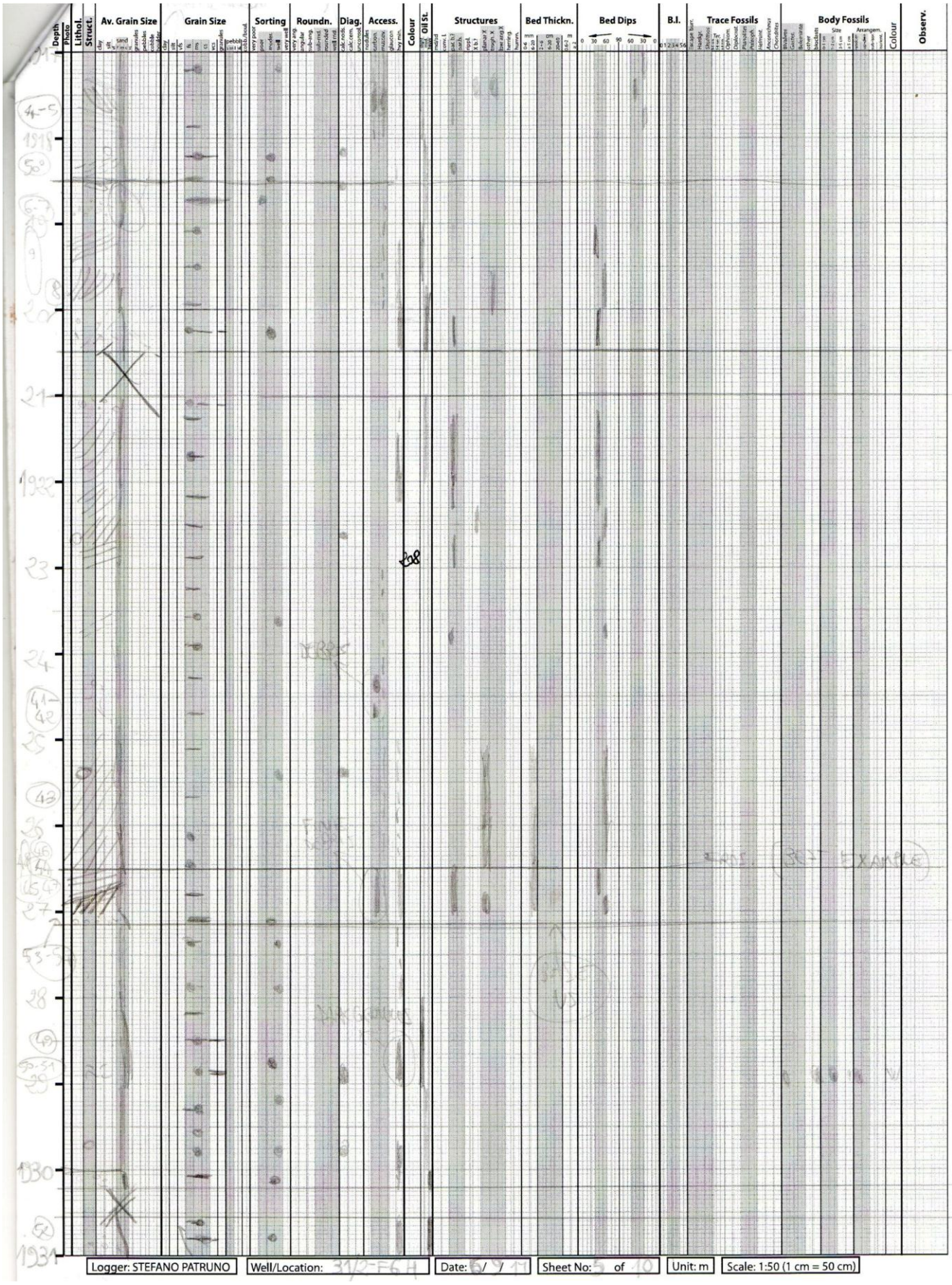
Depth
Photo
Lithol.
Struct.
Av. Grain Size
Grain Size
Sorting
Roundn.
Diag.
Access.
Colour
Oil St.
Structures
Bed Thickn.
Bed Dips
B.I.
Trace Fossils
Body Fossils
Observ.
Logger: STEFANO PATRUNO
Well/Location: 31/2-F6H
Date: 6/ 9/ 11
Sheet No: 5 of 10
Unit: m
Scale: 1:50 (1 cm = 50 cm)

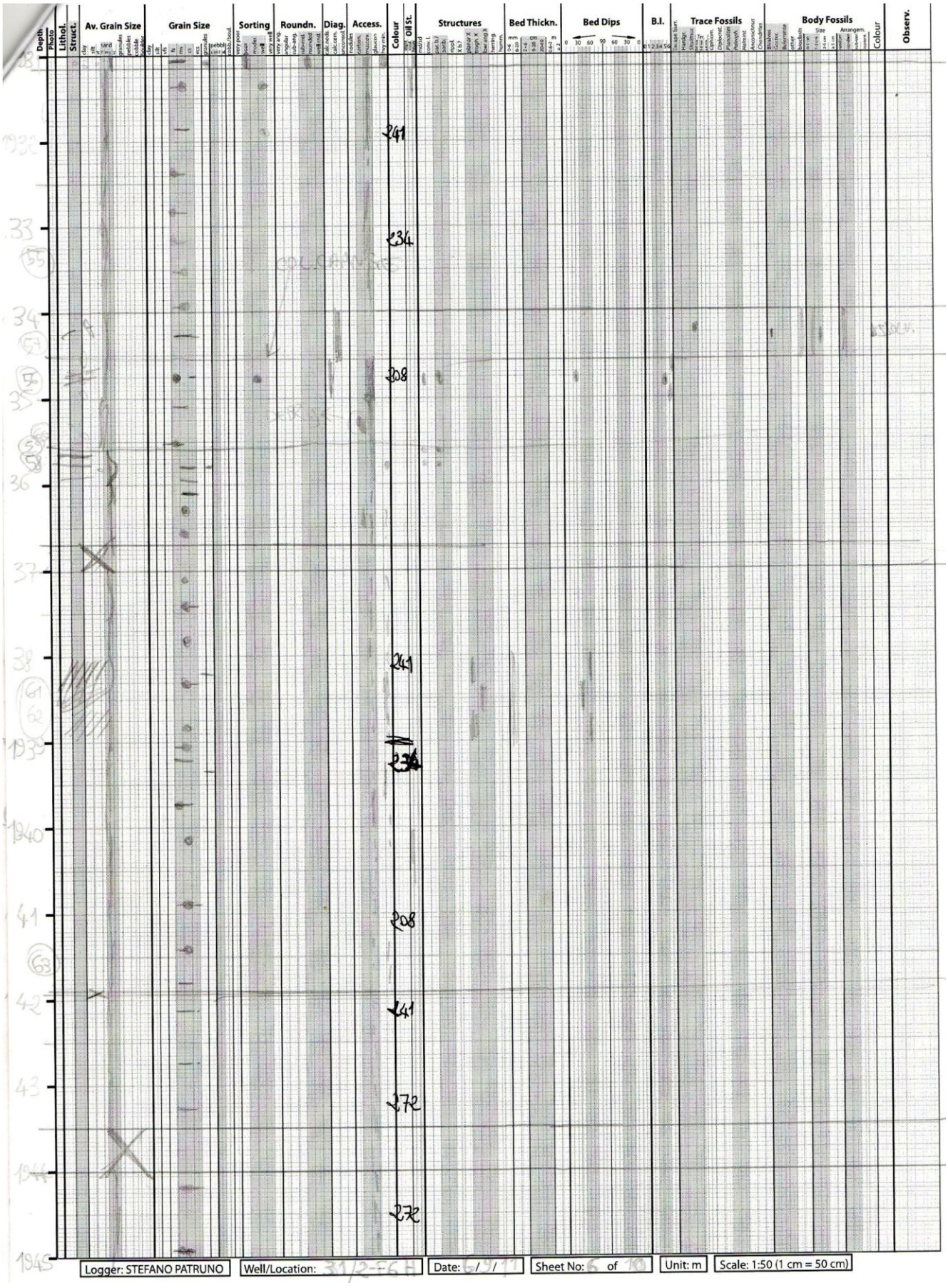
Depth
Photo
Lithol.
Struct.
Av. Grain Size
Grain Size
Sorting
Roundn.
Diag.
Access.
Colour
Oil St.
Structures
Bed Thickn.
Bed Dips
B.I.
Trace Fossils
Body Fossils
Colour
Observ.
Logger: STEFANO PATRUNO
Well/Location: 31/2-F6 H
Date: / /
Sheet No: 6 of 10
Unit: m
Scale: 1:50 (1 cm = 50 cm)

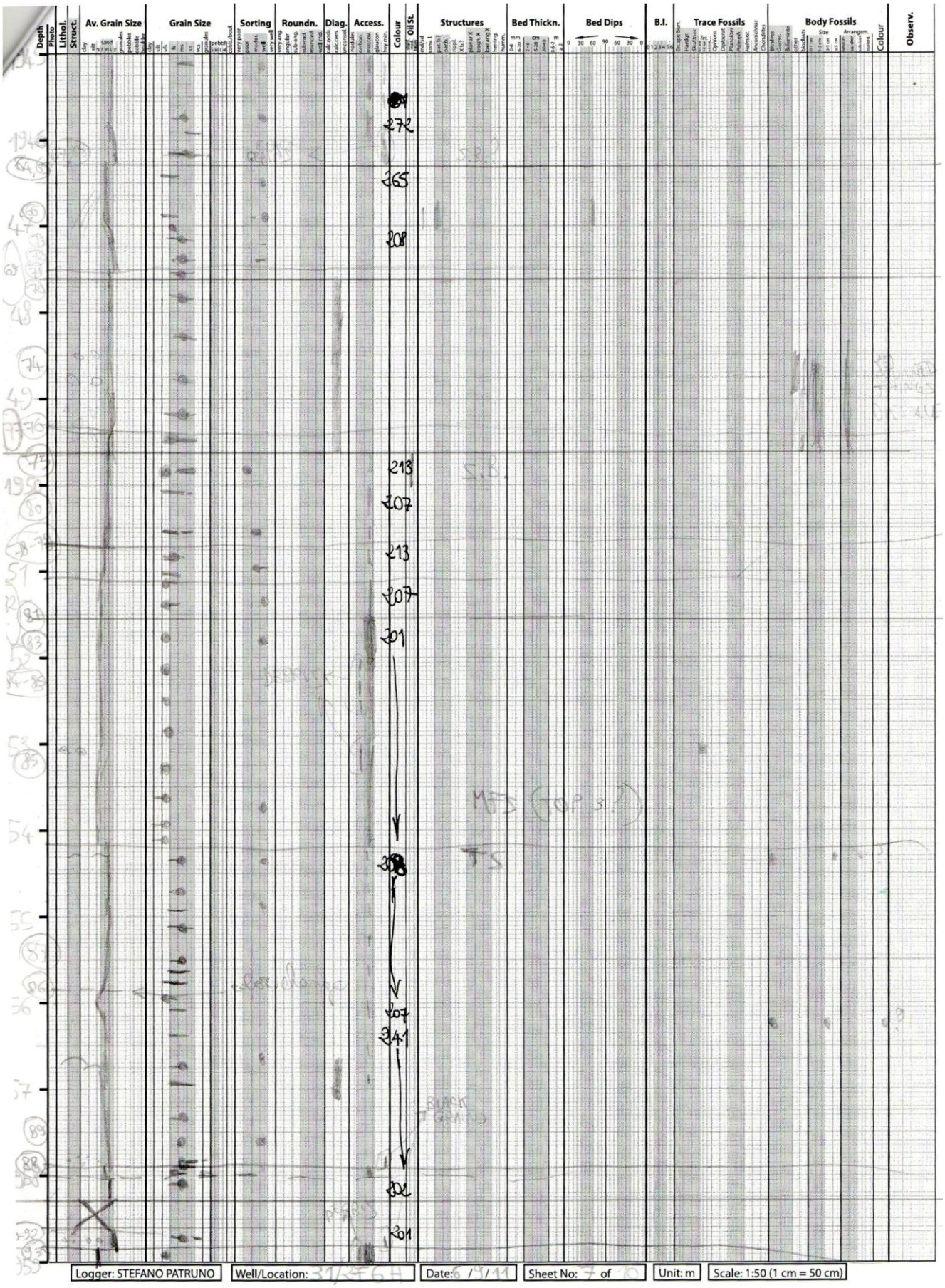
Depth
Photo
Lithol.
Struct.
Av. Grain Size
Grain Size
Sorting
Roundn.
Diag.
Access.
Colour
Oil St.
Structures
Bed Thickn.
Bed Dips
B.I.
Trace Fossils
Body Fossils
Observ.
272
265
208
213
207
213
207
201
207
241
201
Logger: STEFANO PATRUNO
Well/Location:
Date: / /
Sheet No: of
Unit: m
Scale: 1:50 (1 cm = 50 cm)

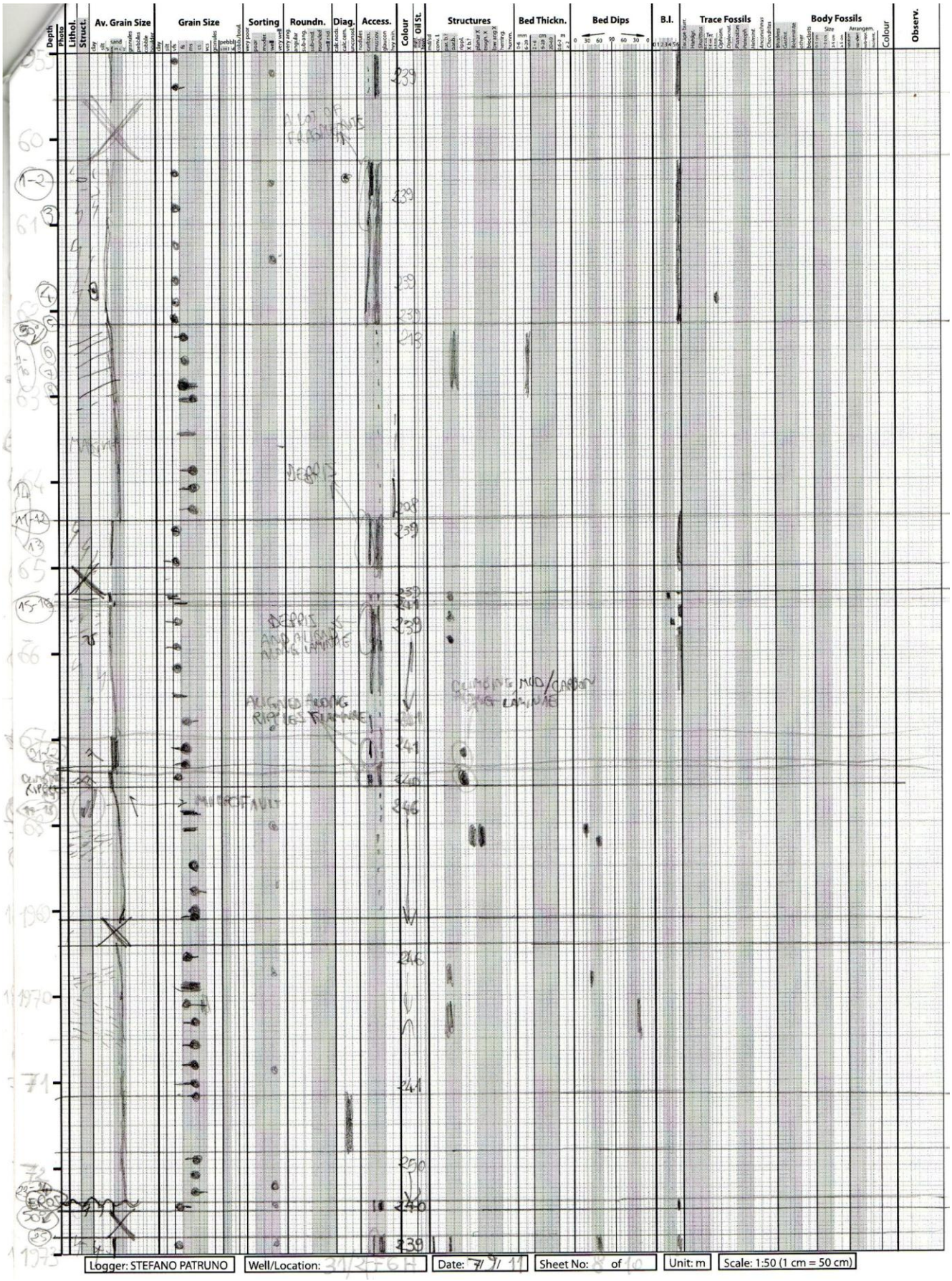
Depth
Photo
Lithol.
Struct.
Av. Grain Size
Grain Size
Sorting
Roundn.
Diag.
Access.
Colour
Oil St.
Structures
Bed Thickn.
Bed Dips
B.I.
Trace Fossils
Body Fossils
Observ.
DEBRIS
DEBRIS AND ALGAL MUDSTONE LAMINAE
ALGAL MUD/GRAINSTONE LAMINAE
Logger: STEFANO PATRUNO
Well/Location:
Date:
Sheet No:
of
Unit: m
Scale: 1:50 (1 cm = 50 cm)

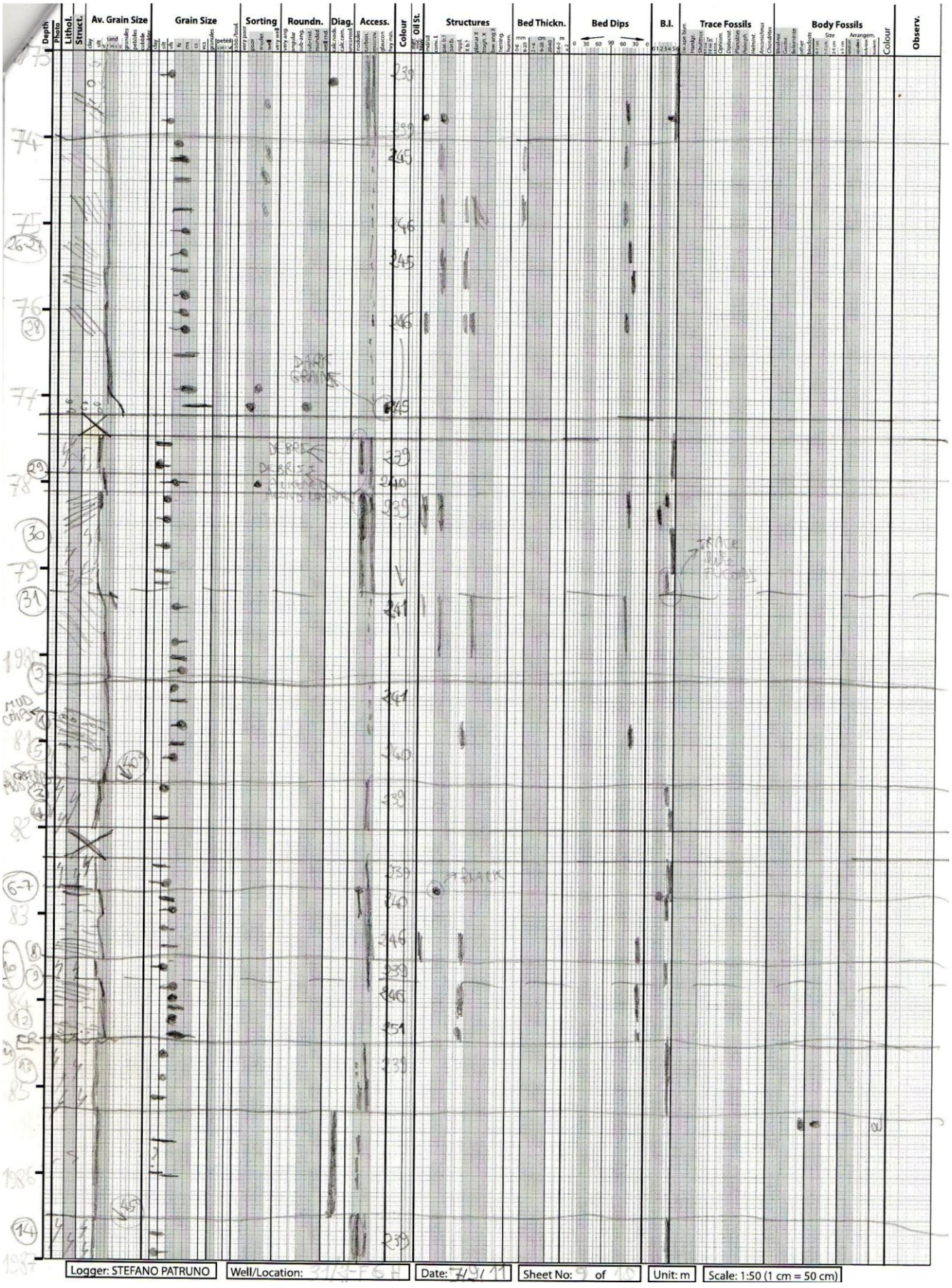
Depth
Photo
Lithol.
Struct.
Av. Grain Size
Grain Size
Sorting
Roundn.
Diag.
Access.
Colour
Oil St.
Structures
Bed Thickn.
Bed Dips
B.I.
Trace Fossils
Body Fossils
Observ.
Logger: STEFANO PATRUNO
Well/Location:
Date:
Sheet No:
of
Unit: m
Scale: 1:50 (1 cm = 50 cm)

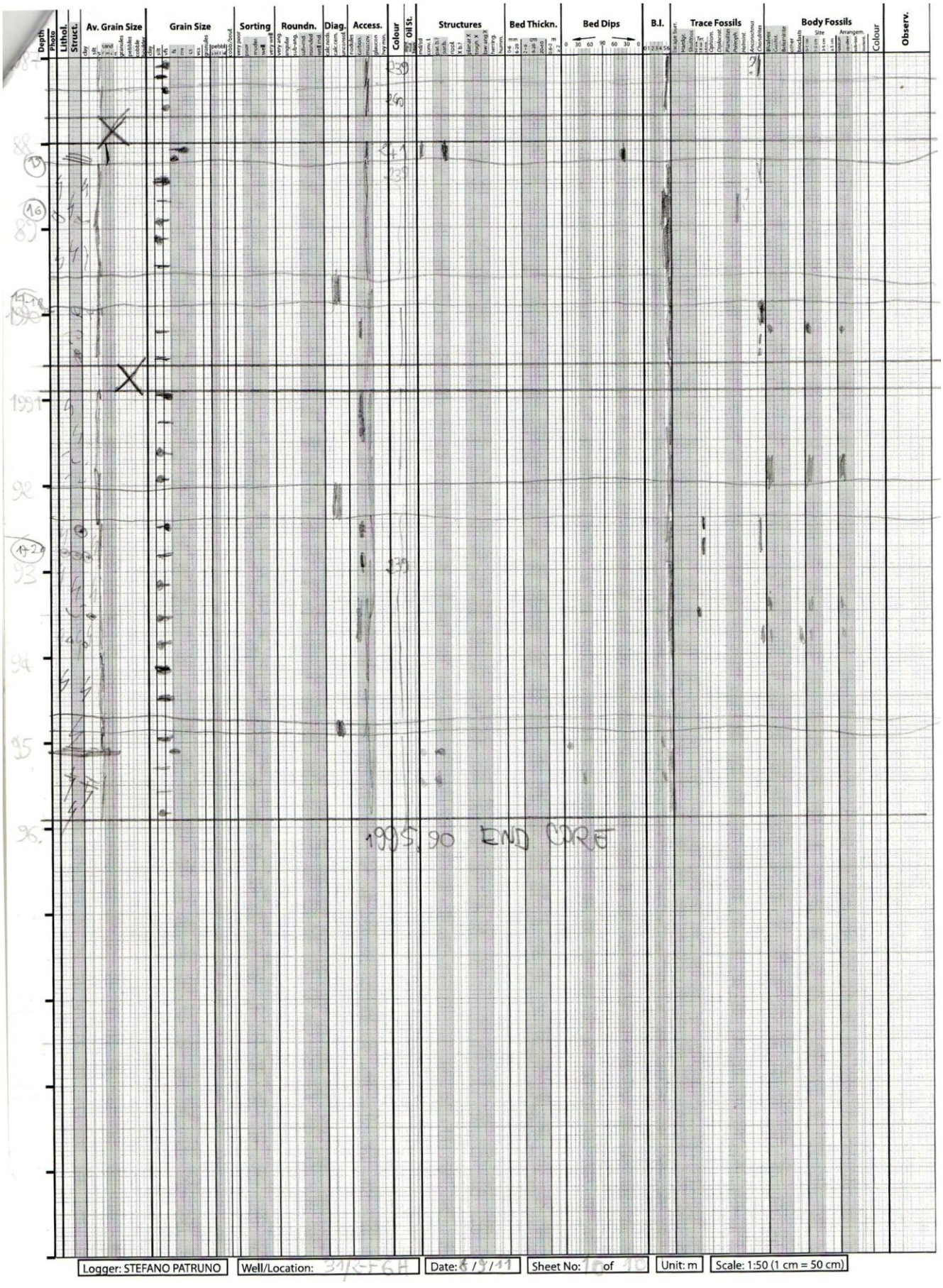
Depth
Photo
Lithol.
Struct.
Av. Grain Size
Grain Size
Sorting
Roundn.
Diag.
Access.
Colour
Oil St.
Structures
Bed Thickn.
Bed Dips
B.I.
Trace Fossils
Body Fossils
Observ.
1995.90 END CORE
Logger: STEFANO PATRUNO
Well/Location: 31/5-F6H
Date: 8/9/11
Sheet No: 16 of 16
Unit: m
Scale: 1:50 (1 cm = 50 cm)

31/3-1

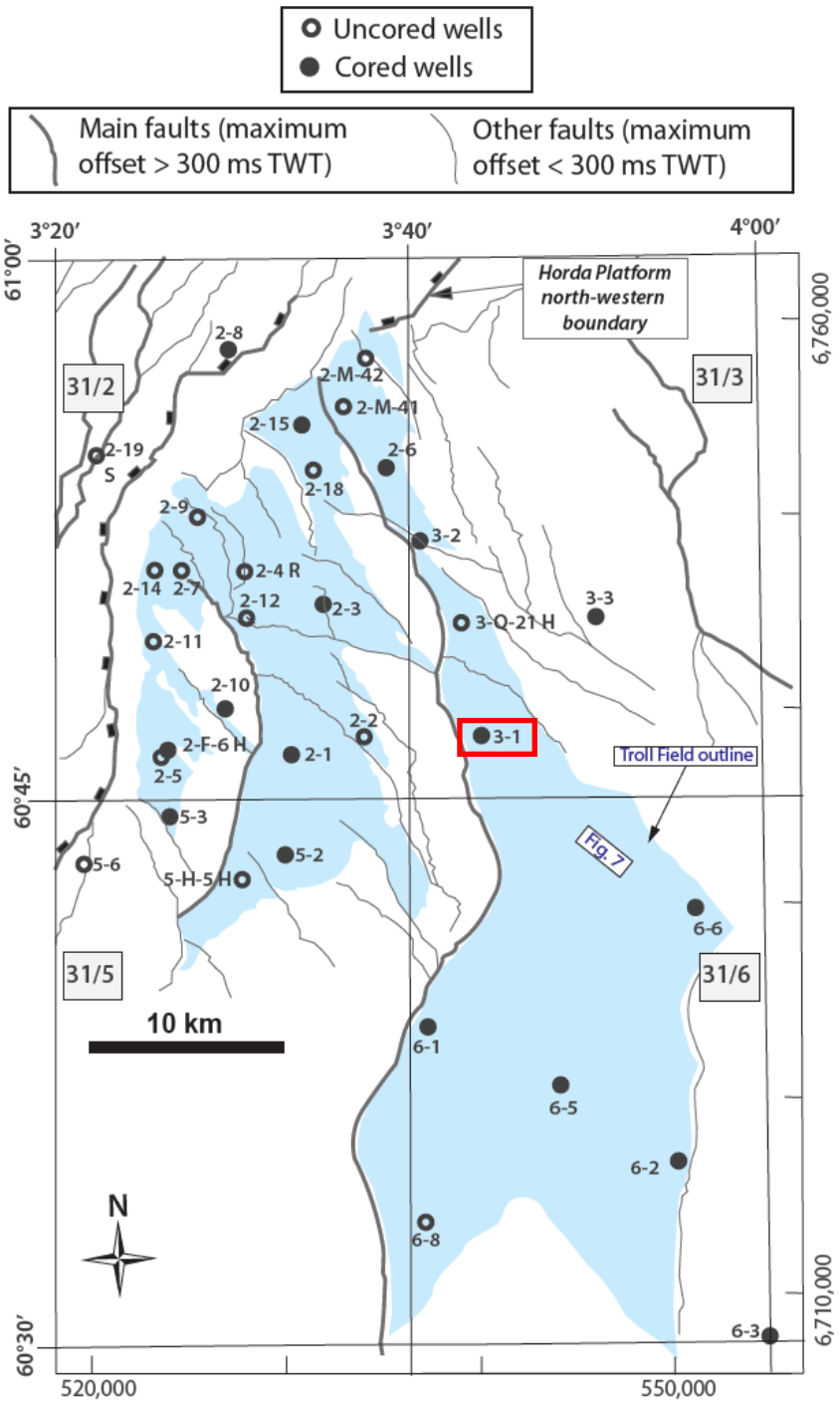
Uncored wells
Cored wells
Main faults (maximum offset > 300 ms TWT)
Other faults (maximum offset < 300 ms TWT)
3°20′
3°40′
4°00′
61°00′
60°45′
60°30′
6,760,000
6,710,000
520,000
550,000
Horda Platform north-western boundary
31/2
31/3
31/5
31/6
2-8
2-M-42
2-M-41
2-15
2-19 S
2-6
2-18
2-9
3-2
2-14
2-7
2-4 R
2-12
2-3
3-3
3-Q-21 H
2-11
2-10
2-2
3-1
2-F-6 H
2-1
2-5
Troll Field outline
5-3
5-2
5-6
5-H-5 H
Fig. 7
6-6
10 km
6-1
6-5
6-2
N
6-8
6-3

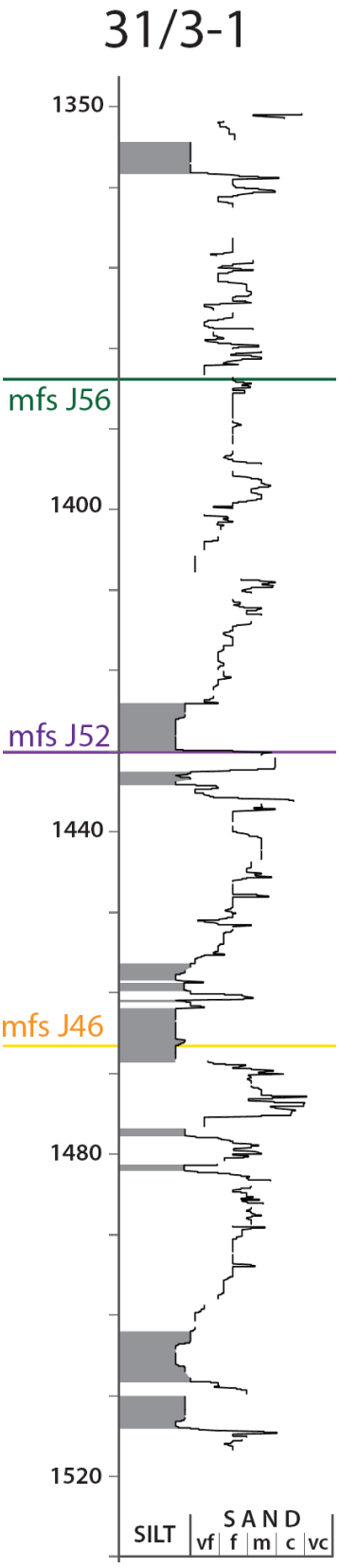
31/3-1
1350
mfs J56
1400
mfs J52
1440
mfs J46
1480
1520
SILT
SAND
vf
f
m
c
vc

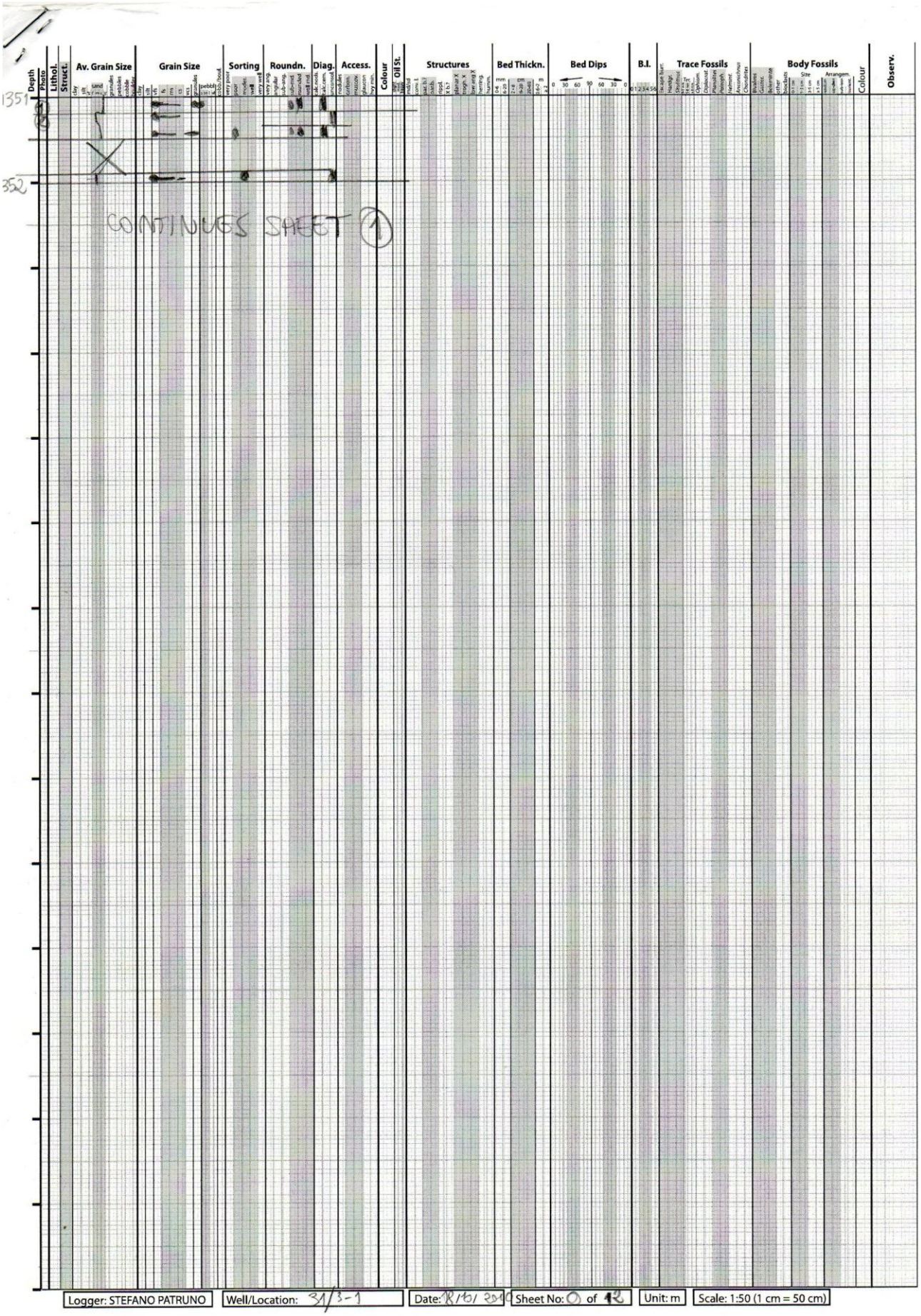
Depth
Photo
Lithol.
Struct.
Av. Grain Size
Grain Size
Sorting
Roundn.
Diag.
Access.
Colour
Oil St.
Structures
Bed Thickn.
Bed Dips
B.I.
Trace Fossils
Body Fossils
Observ.
1351
352
CONTINUES SHEET 1
Logger: STEFANO PATRUNO
Well/Location: 31/3-1
Date: 18/10/ 2010
Sheet No: 01 of 12
Unit: m
Scale: 1:50 (1 cm = 50 cm)

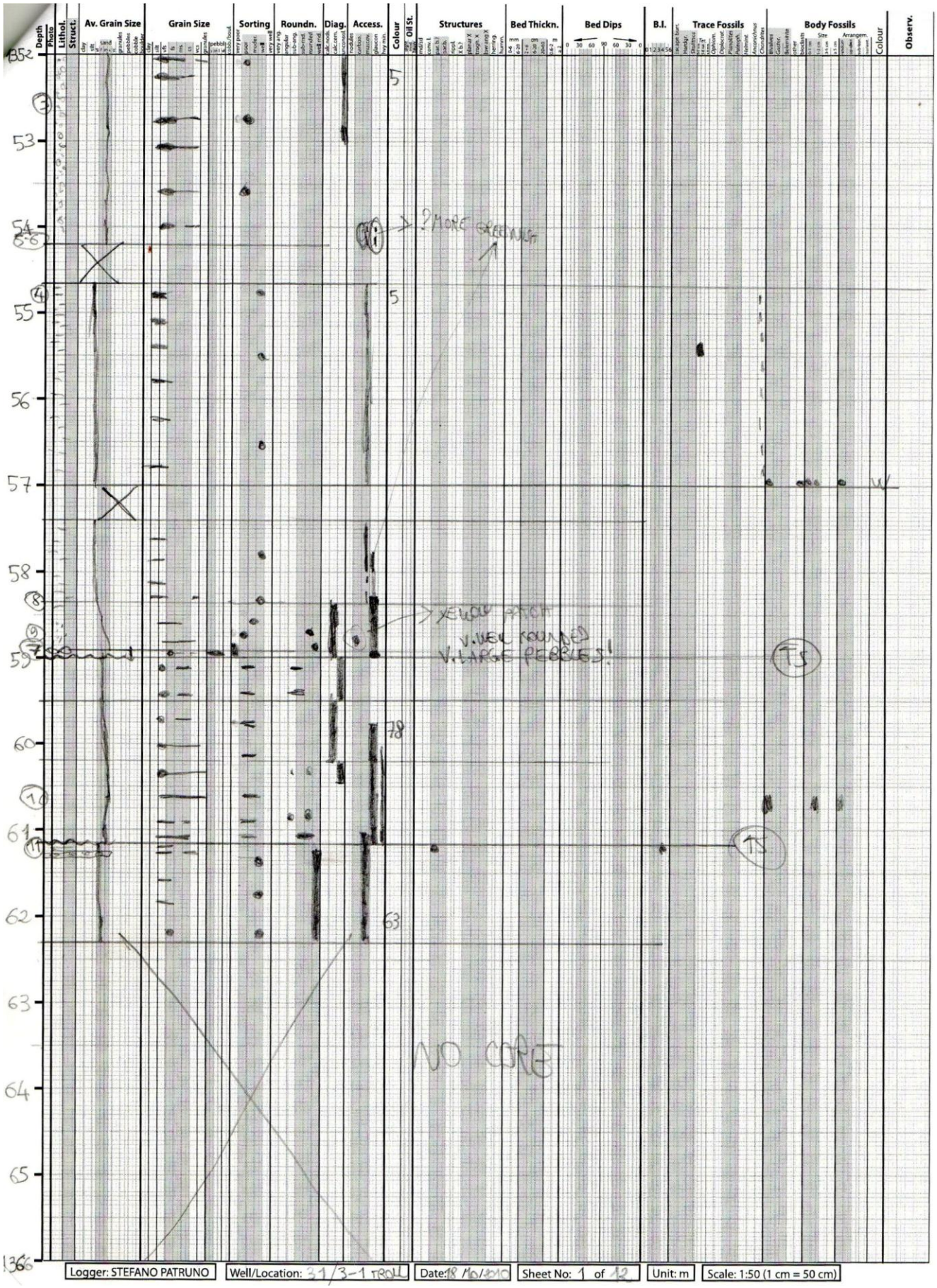
Depth
Photo
Lithol.
Struct.
Av. Grain Size
Grain Size
Sorting
Roundn.
Diag.
Access.
Colour
Oil St.
Structures
Bed Thickn.
Bed Dips
B.I.
Trace Fossils
Body Fossils
Observ.
2 MORE GREENER
V.WELL ROUNDED
V.LARGE PEBBLES!
NO CORE
TS
TS
Logger: STEFANO PATRUNO
Well/Location: 31/3-1 TROLL
Date: 18/10/2010
Sheet No: 1 of 12
Unit: m
Scale: 1:50 (1 cm = 50 cm)

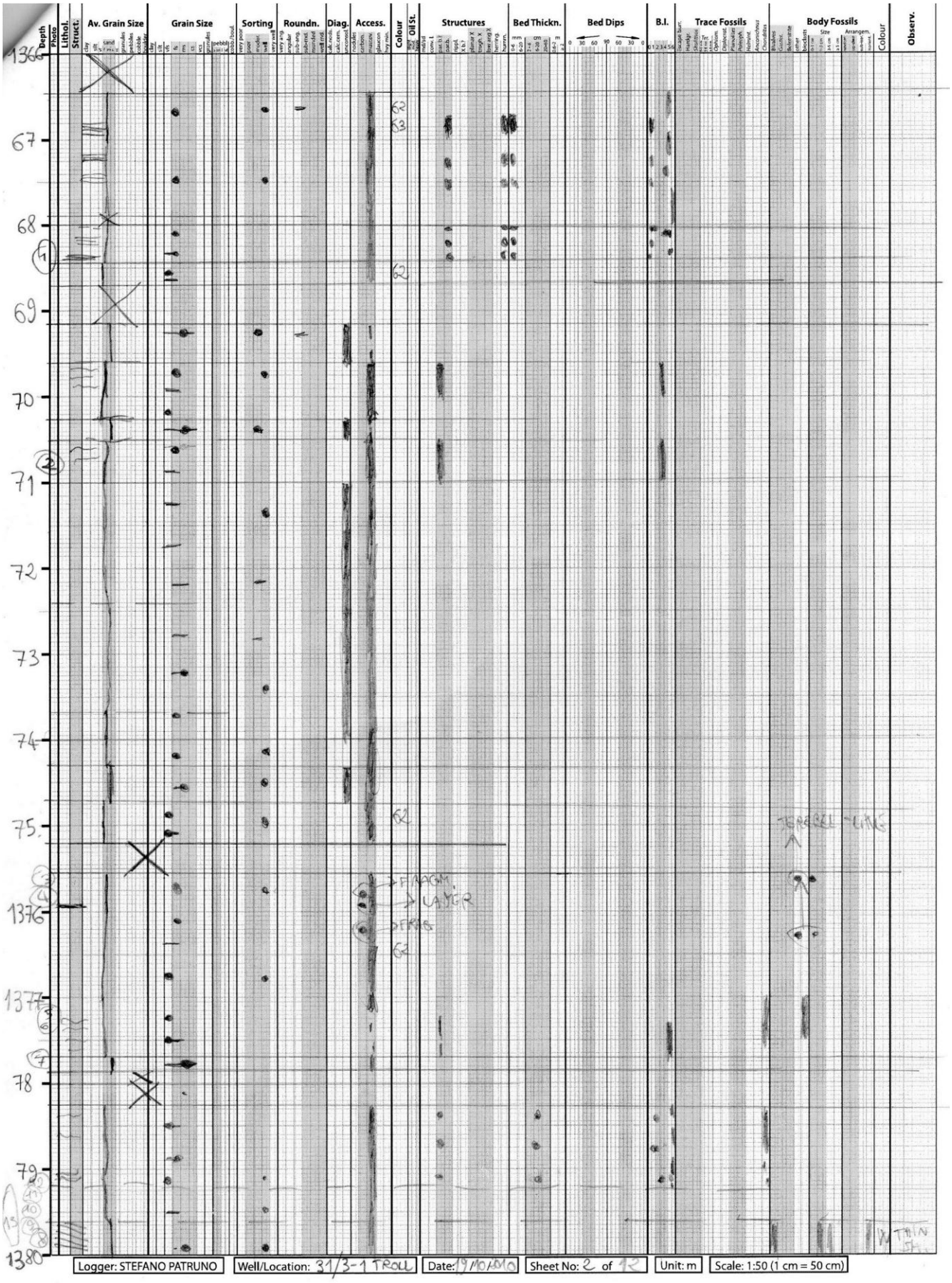
Depth
Photo
Lithol.
Struct.
Av. Grain Size
Grain Size
Sorting
Roundn.
Diag.
Access.
Colour
Oil St.
Structures
Bed Thickn.
Bed Dips
B.I.
Trace Fossils
Body Fossils
Observ.
1366
67
68
69
70
71
72
73
74
75
1376
1377
78
79
1380
FRAGM.
LAYER
DEBRIS
TERRACE LINE
Logger: STEFANO PATRUNO
Well/Location: 31/3-1 TROLL
Date: 19/10/1990
Sheet No: 2 of 12
Unit: m
Scale: 1:50 (1 cm = 50 cm)

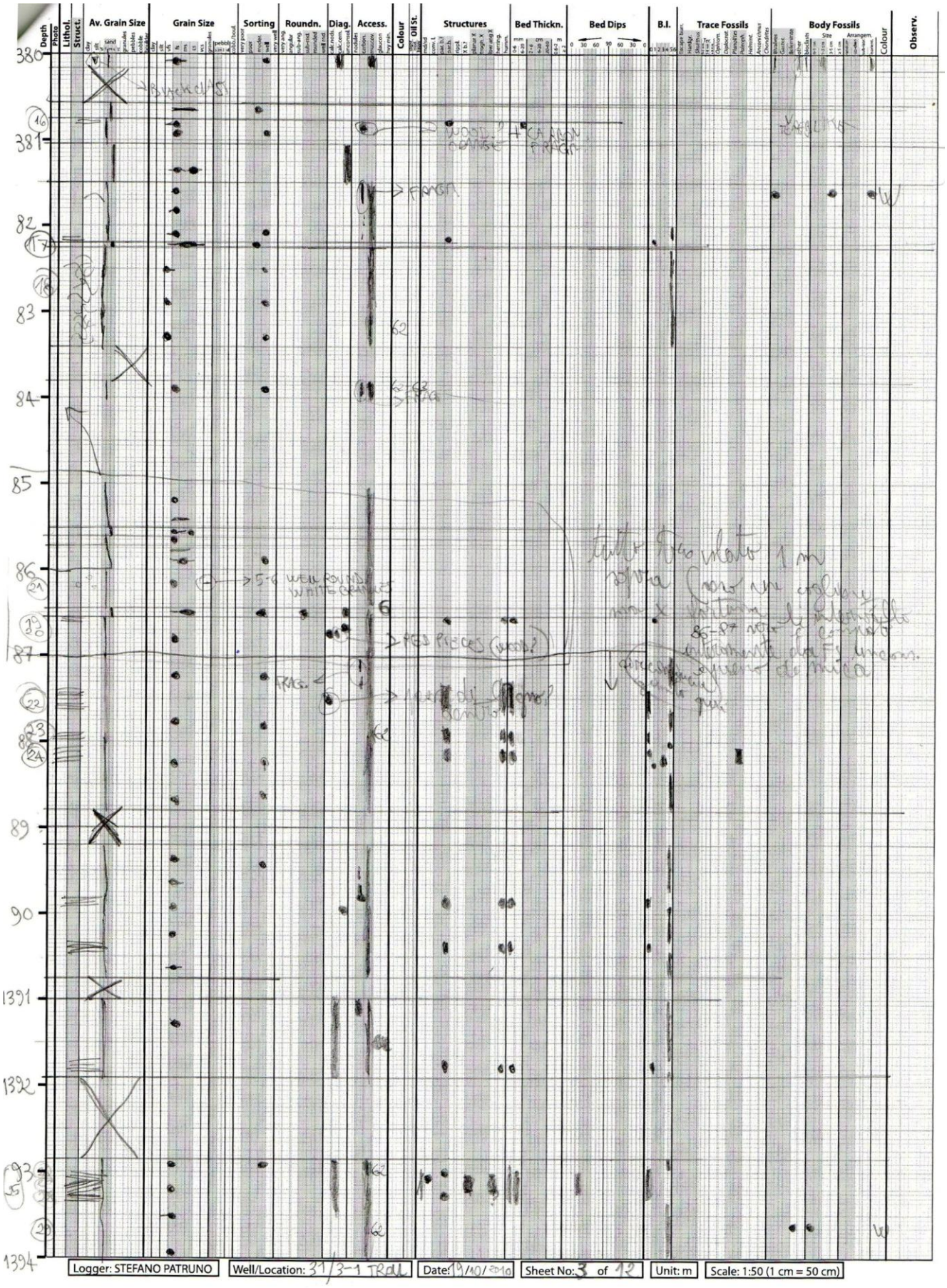
Depth
Photo
Lithol.
Struct.
Av. Grain Size
Grain Size
Sorting
Roundn.
Diag.
Access.
Colour
Oil St.
Structures
Bed Thickn.
Bed Dips
B.I.
Trace Fossils
Body Fossils
Observ.
380
381
82
83
84
85
86
87
89
90
1391
1392
1394
Logger: STEFANO PATRUNO
Well/Location: 31/3-1 TROLL
Date: 19/10/2010
Sheet No: 3 of 12
Unit: m
Scale: 1:50 (1 cm = 50 cm)

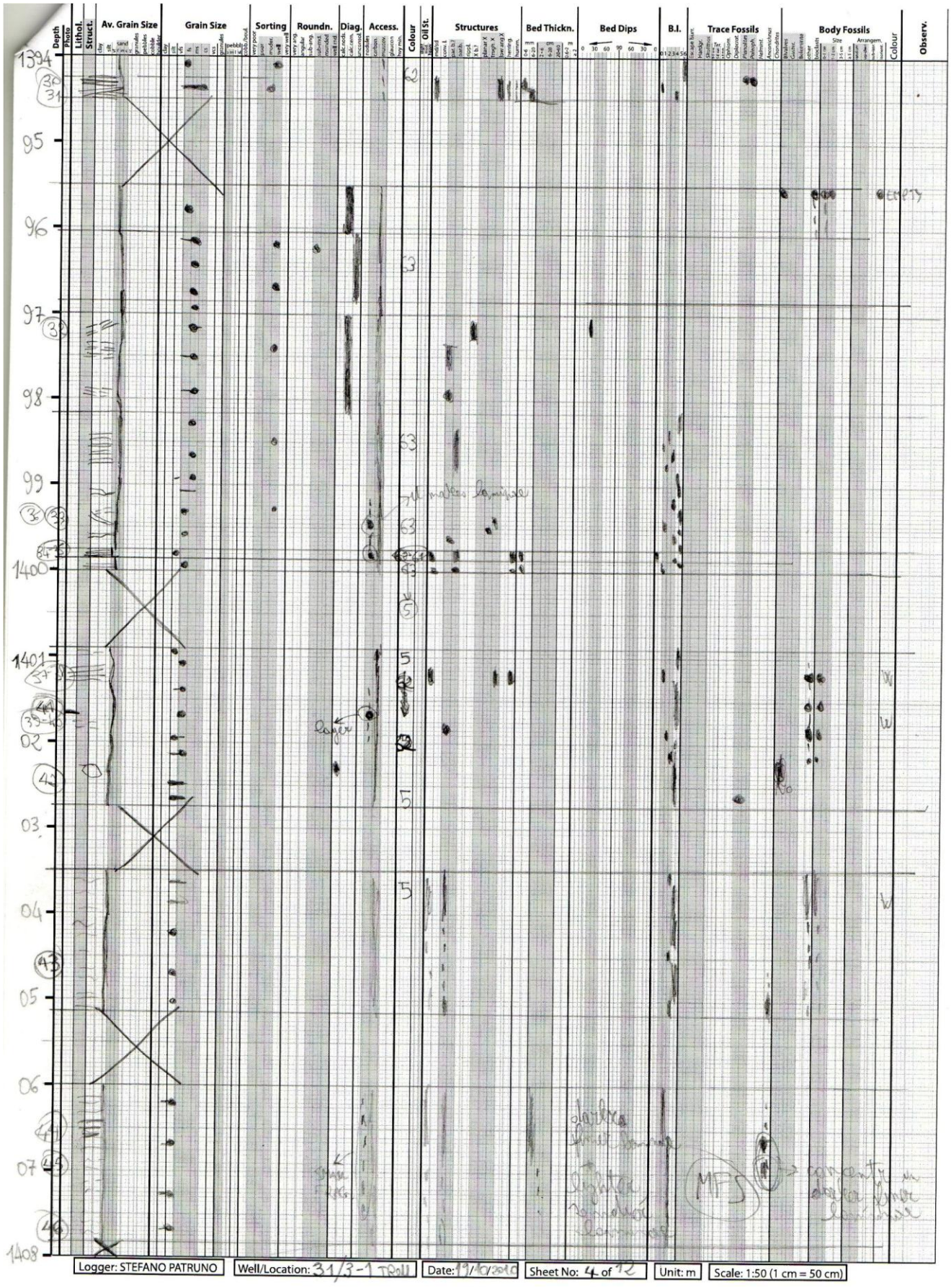
Depth
Photo
Lithol.
Struct.
Av. Grain Size
Grain Size
Sorting
Roundn.
Diag.
Access.
Colour
Oil St.
Structures
Bed Thickn.
Bed Dips
B.I.
Trace Fossils
Body Fossils
Observ.
1394
95
96
97
98
99
1400
1401
02
03
04
05
06
07
1408
Logger: STEFANO PATRUNO
Well/Location: 31/3-1 TROLL
Date: 19/10/2010
Sheet No: 4 of 12
Unit: m
Scale: 1:50 (1 cm = 50 cm)

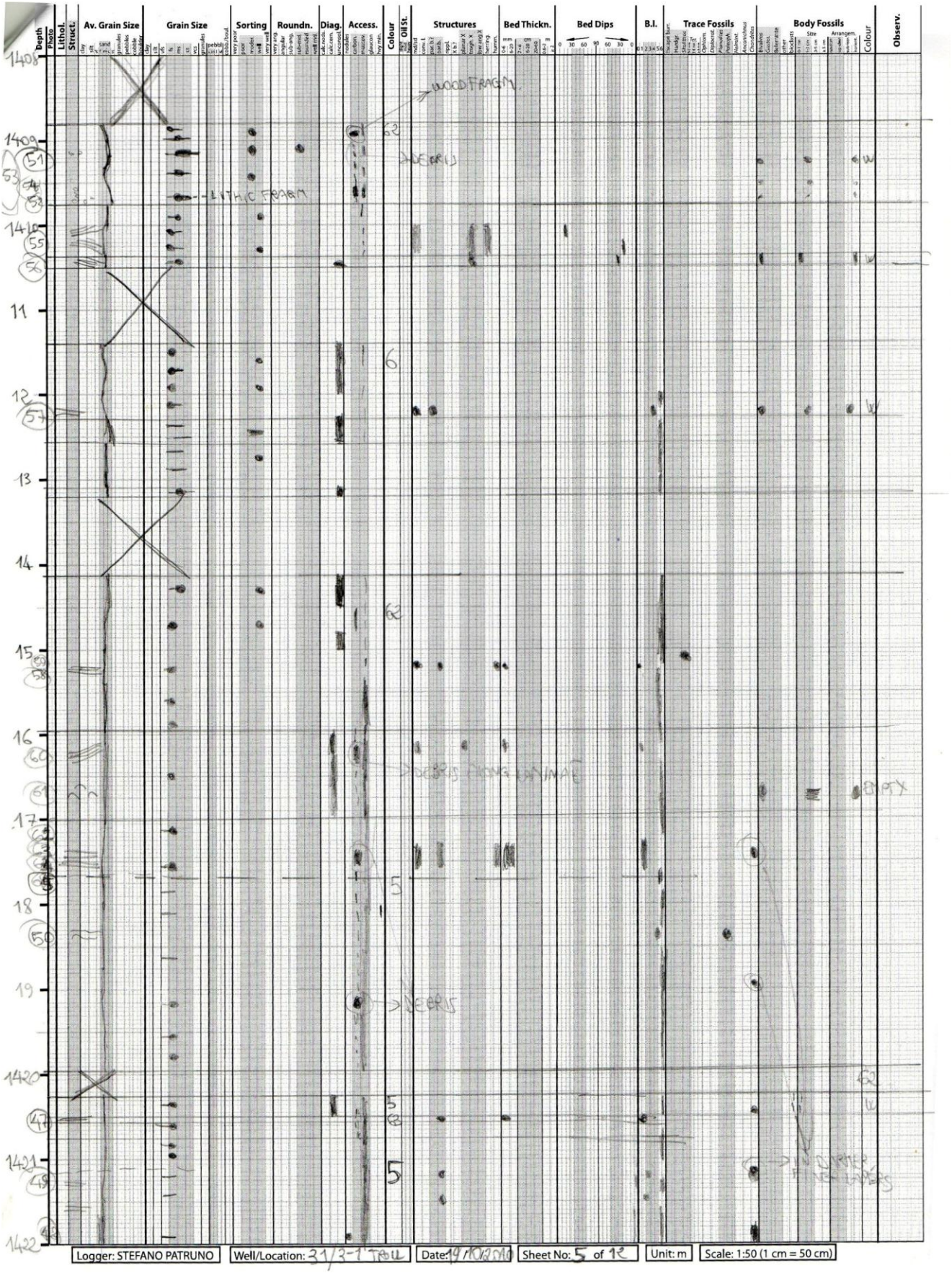
Depth
Photo
Lithol.
Struct.
Av. Grain Size
Grain Size
Sorting
Roundn.
Diag.
Access.
Colour
Oil St.
Structures
Bed Thickn.
Bed Dips
B.I.
Trace Fossils
Body Fossils
Observ.
WOOD FRAGM.
LITHIC FRAGM.
Logger: STEFANO PATRUNO
Well/Location: 31/3-1
Date: 19/10/2010
Sheet No: 5 of 12
Unit: m
Scale: 1:50 (1 cm = 50 cm)

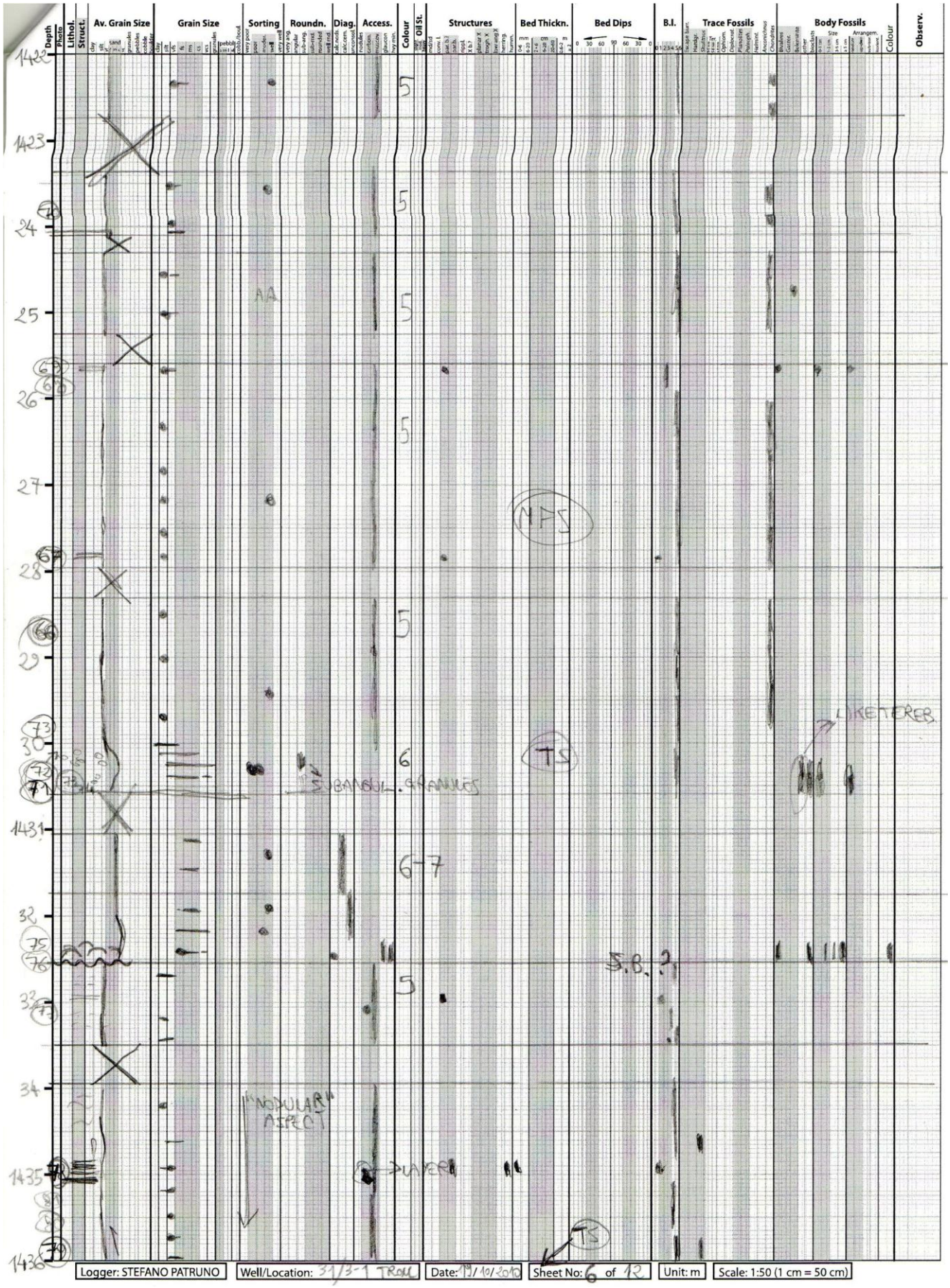
Depth
Photo
Lithol.
Struct.
Av. Grain Size
Grain Size
Sorting
Roundn.
Diag.
Access.
Colour
Oil St.
Structures
Bed Thickn.
Bed Dips
B.I.
Trace Fossils
Body Fossils
Observ.
1422
1423
24
25
26
27
28
29
30
1431
32
34
1435
1436
AA
MFS
TS
BANDUL. GRANULES
LIKETERER
"NODULAR" ASPECT
PLANEER
S.B. ?
TS
Logger: STEFANO PATRUNO
Well/Location: 31/3-1 TROLL
Date: 19/10/2010
Sheet No: 6 of 12
Unit: m
Scale: 1:50 (1 cm = 50 cm)

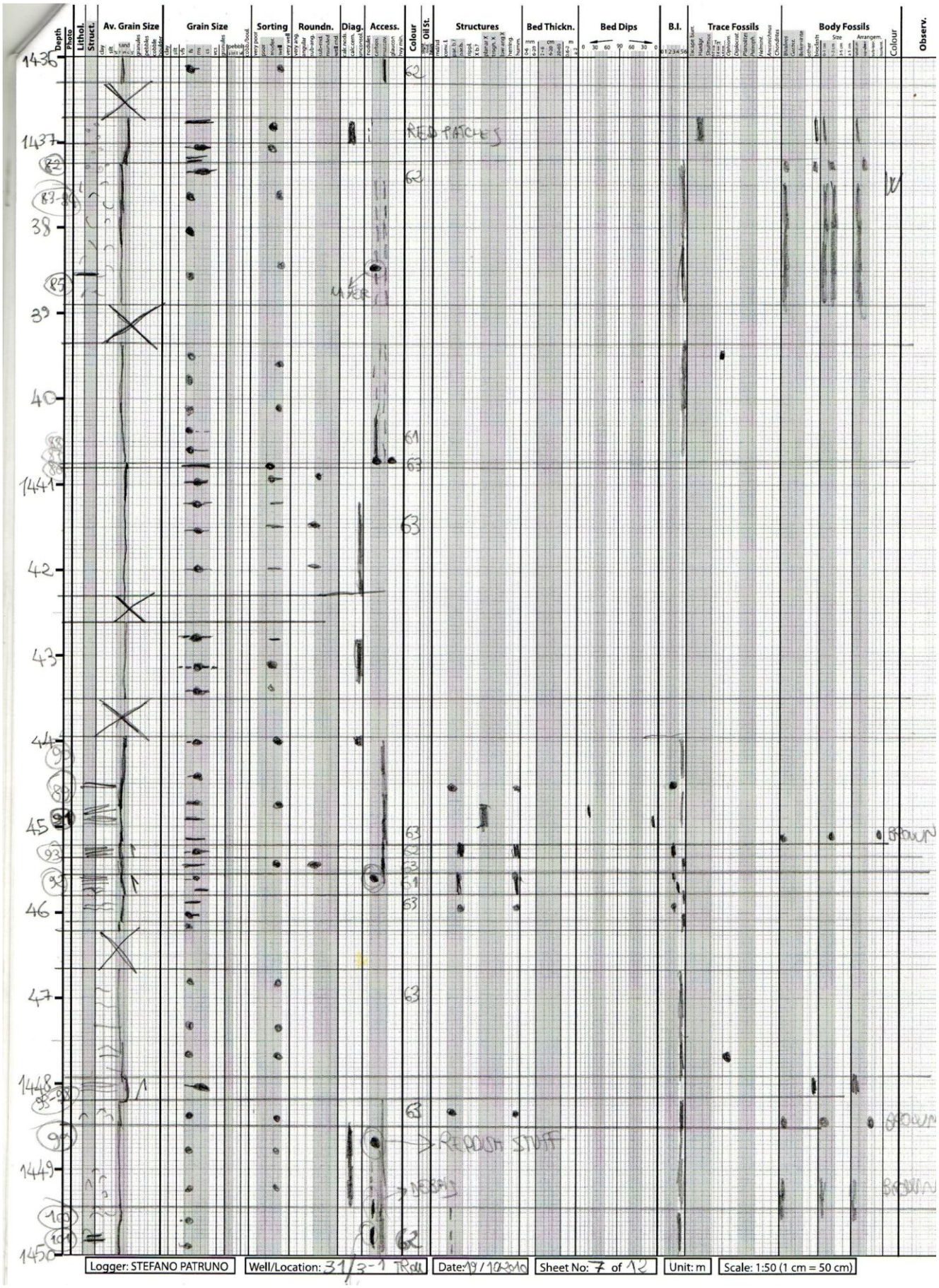
Depth
Photo
Lithol.
Struct.
Av. Grain Size
Grain Size
Sorting
Roundn.
Diag.
Access.
Colour
Oil St.
Structures
Bed Thickn.
Bed Dips
B.I.
Trace Fossils
Body Fossils
Observ.
RED PATCHES
BROWN
BROWN
BROWN
Logger: STEFANO PATRUNO
Well/Location: 31/3-1 TRdl
Date: 19/10-2010
Sheet No: 7 of 12
Unit: m
Scale: 1:50 (1 cm = 50 cm)

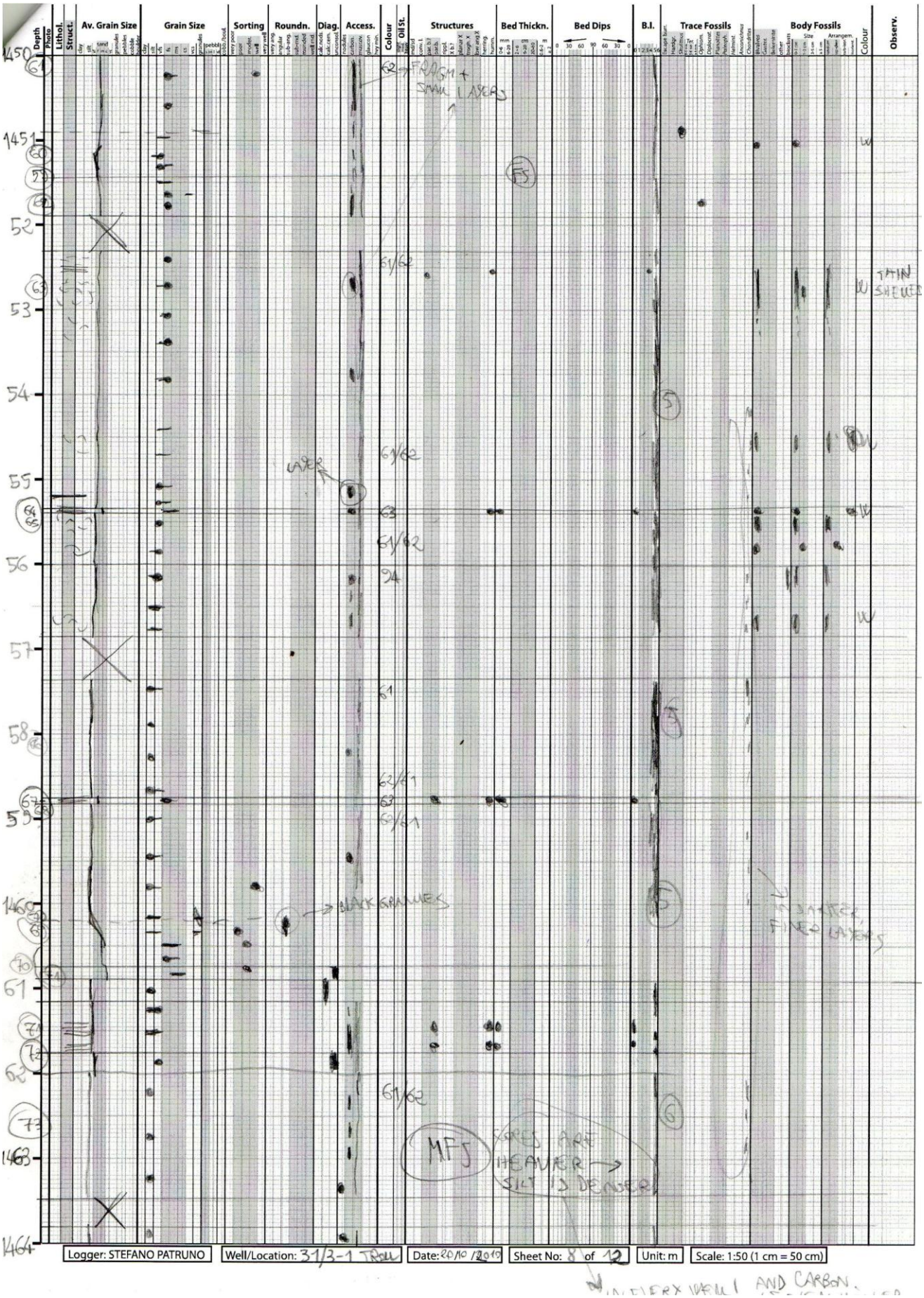
Depth
Photo
Lithol.
Struct.
Av. Grain Size
Grain Size
Sorting
Roundn.
Diag.
Access.
Colour
Oil St.
Structures
Bed Thickn.
Bed Dips
B.I.
Trace Fossils
Body Fossils
Observ.
1450
1451
52
53
54
55
56
57
58
59
1460
61
62
1463
1464
LAYER
BLACK GRAINES
MFS
DARKER PART
HEAVIER →
SLIGHTLY DENSER
DARK LAMINATED LAYERS
Logger: STEFANO PATRUNO
Well/Location: 31/3-1
Date: 20/10/2019
Sheet No: 8 of 12
Unit: m
Scale: 1:50 (1 cm = 50 cm)

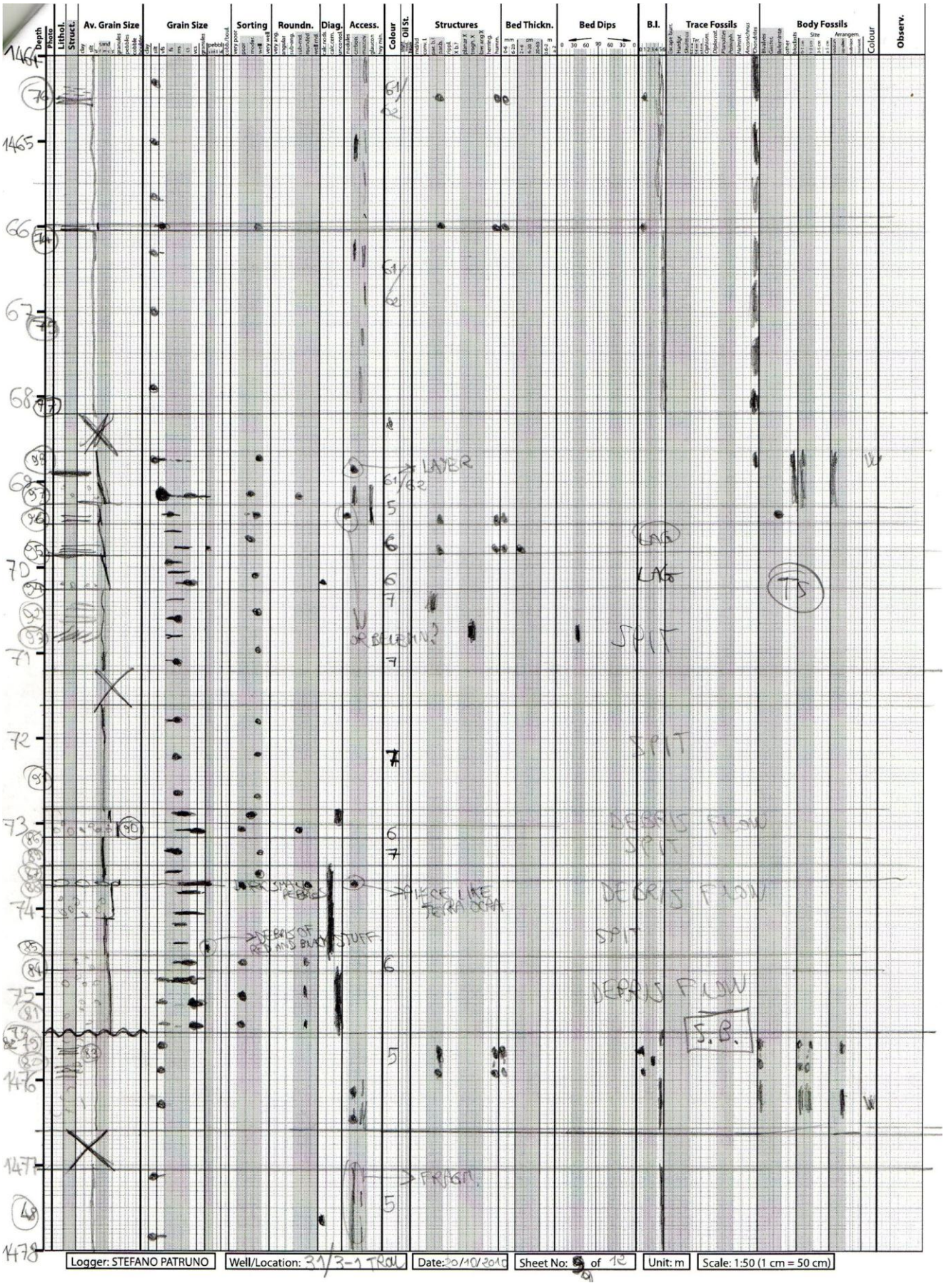
Depth
Photo
Litholl.
Struct.
Av. Grain Size
Grain Size
Sorting
Roundn.
Diag.
Access.
Colour
Oil St.
Structures
Bed Thickn.
Bed Dips
B.I.
Trace Fossils
Body Fossils
Observ.
LAYER
SPIT
DEBRIS FLOW
S.B.
Logger: STEFANO PATRUNO
Well/Location: 31/3-1 TROLL
Date: 30/10/2010
Sheet No: 9 of 12
Unit: m
Scale: 1:50 (1 cm = 50 cm)

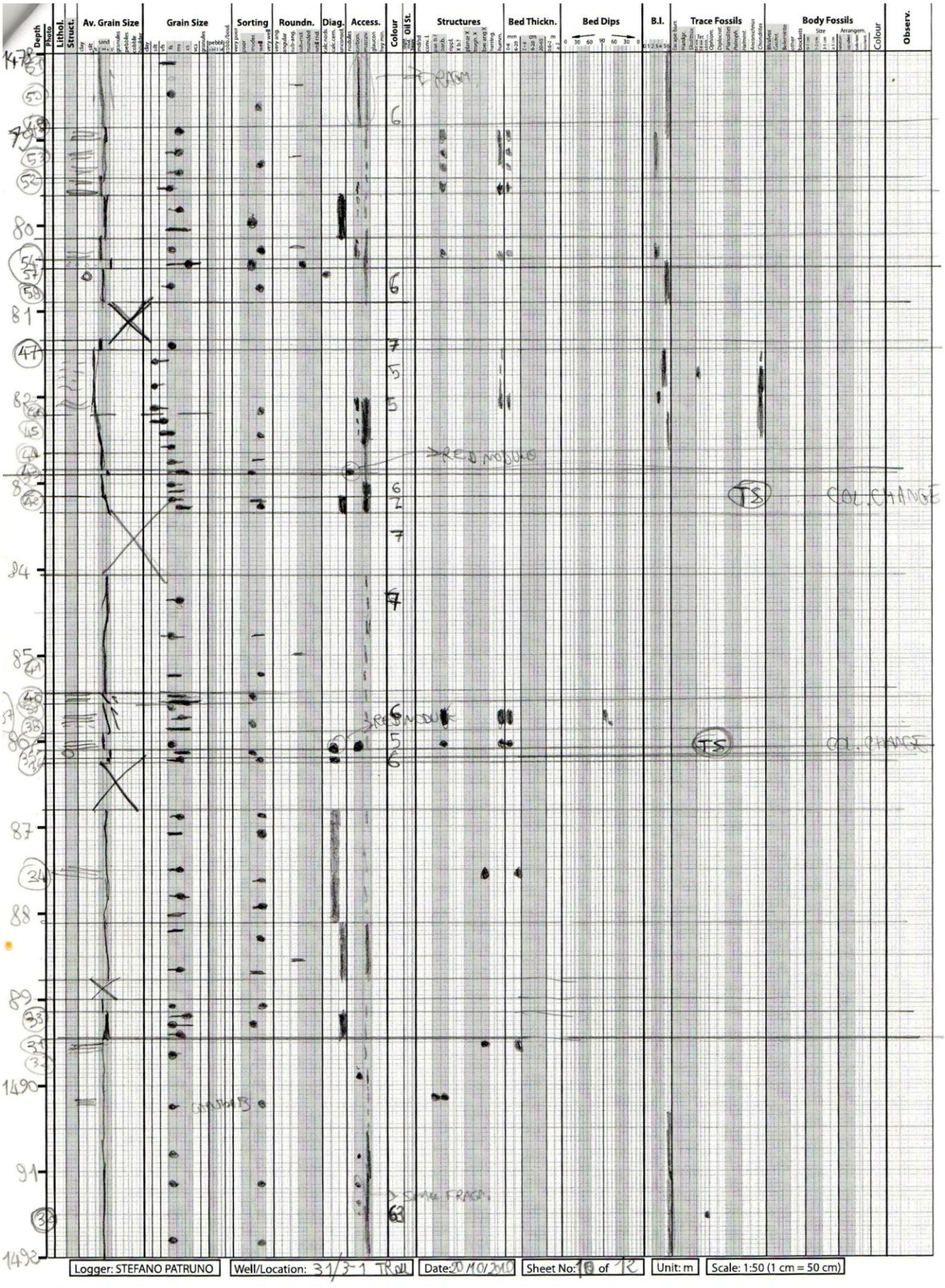
Depth
Photo
Lithol.
Struct.
Av. Grain Size
Grain Size
Sorting
Roundn.
Diag.
Access.
Colour
Oil St.
Structures
Bed Thickn.
Bed Dips
B.I.
Trace Fossils
Body Fossils
Observ.
Logger: STEFANO PATRUNO
Well/Location: 31/3-1 TROLL
Date: 30/10/2010
Sheet No: 10 of 12
Unit: m
Scale: 1:50 (1 cm = 50 cm)

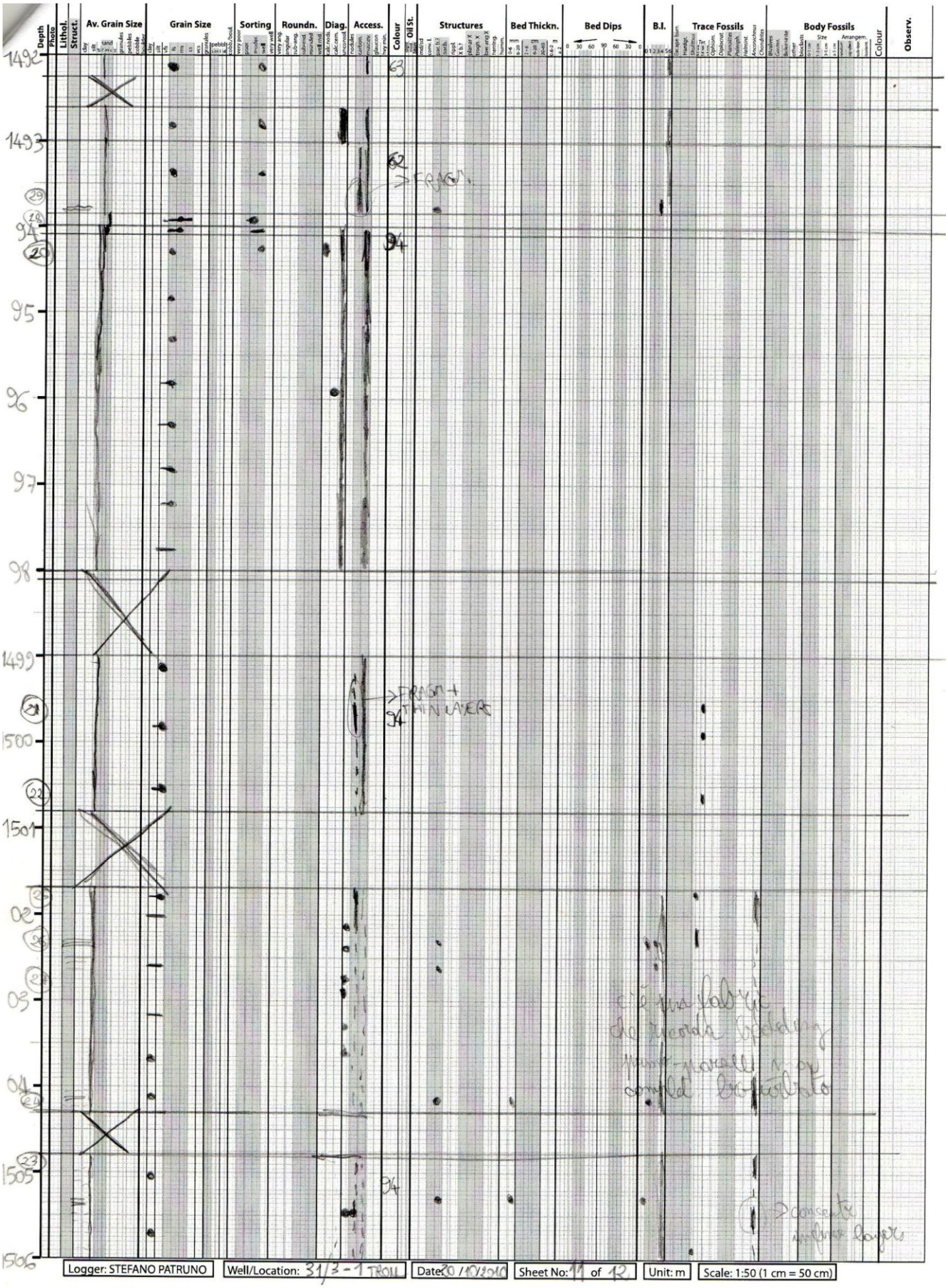
Depth
Photo
Lithol.
Struct.
Av. Grain Size
Grain Size
Sorting
Roundn.
Diag.
Access.
Colour
Oil St.
Structures
Bed Thickn.
Bed Dips
B.I.
Trace Fossils
Body Fossils
Observ.
1492
1493
94
95
96
97
98
1499
1500
1501
02
03
04
1505
1506
FRAGM.
FRAGM + THIN LAYERS
Logger: STEFANO PATRUNO
Well/Location: 31/3-1 TROLL
Date: 20 / 10 / 2010
Sheet No: 11 of 12
Unit: m
Scale: 1:50 (1 cm = 50 cm)

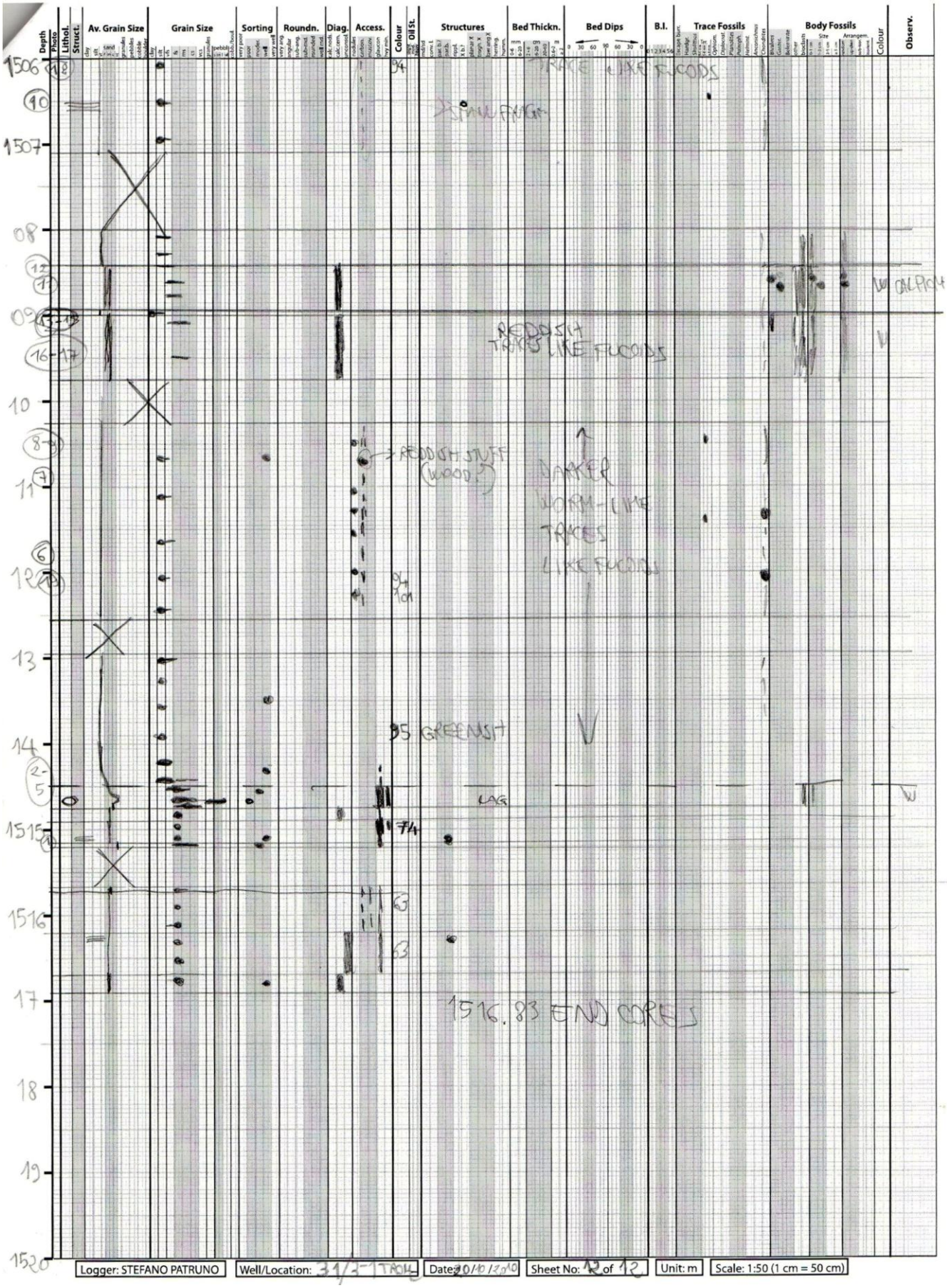
Depth
Photo
Lithol.
Struct.
Av. Grain Size
Grain Size
Sorting
Roundn.
Diag.
Access.
Colour
Oil St.
Structures
Bed Thickn.
Bed Dips
B.I.
Trace Fossils
Body Fossils
Observ.
1506
1507
1510
1515
1516
1517
1518
1519
1520
RARE LIKE FUCODS
REDDISH TAKES LIKE FUCODS
REDDISH STUFF (WOOD?)
DARKER WORM-LIKE TAKES LIKE FUCODS
95 GREENISH
LAG
1516.83 END CORE
Logger: STEFANO PATRUNO
Well/Location: 31/2-1 TROLL
Date: 20/10/2010
Sheet No: 12 of 12
Unit: m
Scale: 1:50 (1 cm = 50 cm)

31/3-2

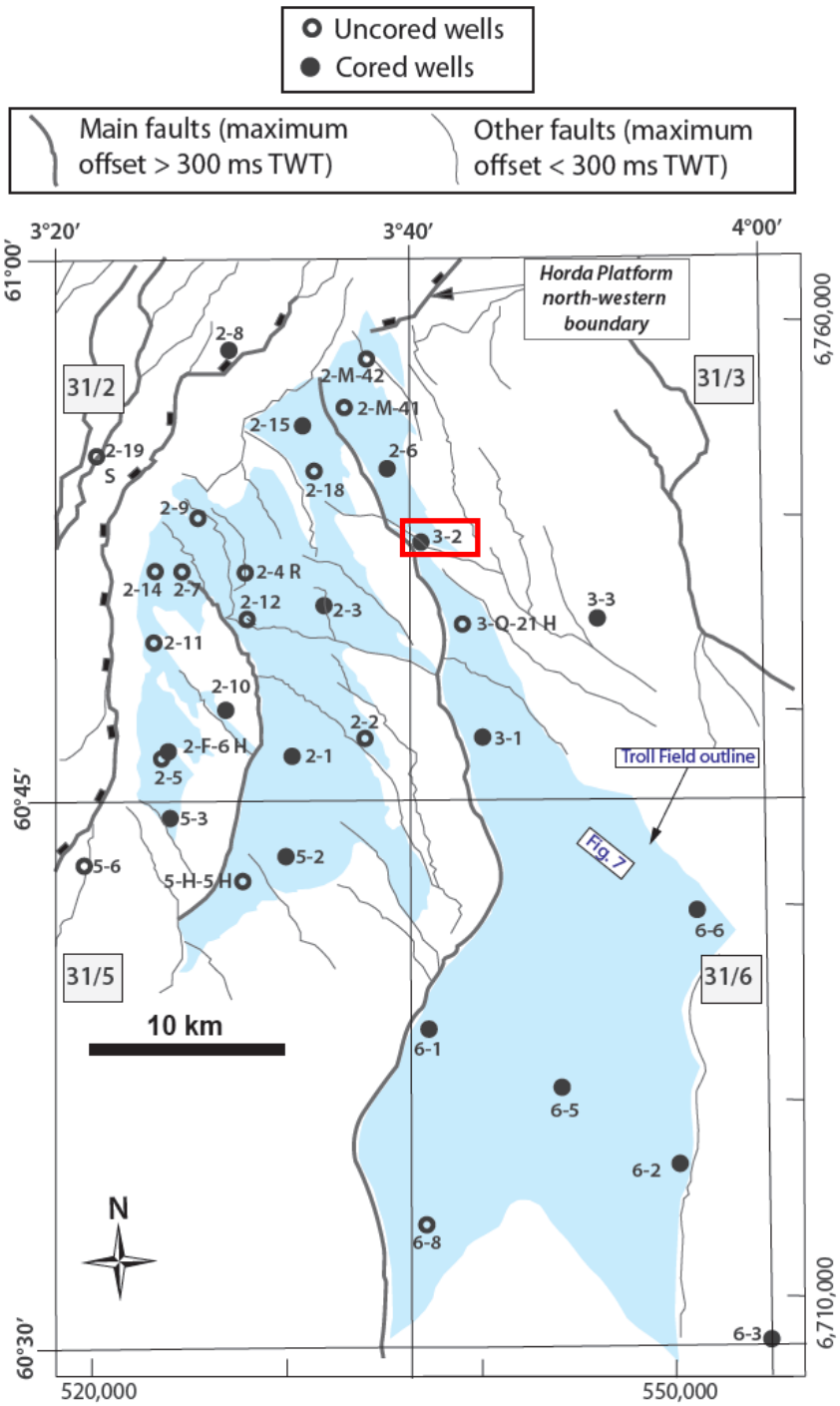
Uncored wells
Cored wells
Main faults (maximum offset > 300 ms TWT)
Other faults (maximum offset < 300 ms TWT)
3°20′
3°40′
4°00′
61°00′
60°45′
60°30′
6,760,000
6,710,000
520,000
550,000
Horda Platform north-western boundary
31/2
31/3
31/5
31/6
2-8
2-M-42
2-M-41
2-15
2-19 S
2-6
2-18
2-9
3-2
2-14
2-7
2-4 R
2-12
2-3
3-3
3-Q-21 H
2-11
2-10
2-2
3-1
2-F-6 H
2-5
2-1
Troll Field outline
Fig. 7
5-3
5-6
5-H-5 H
5-2
6-6
10 km
6-1
6-5
6-2
6-8
6-3
N

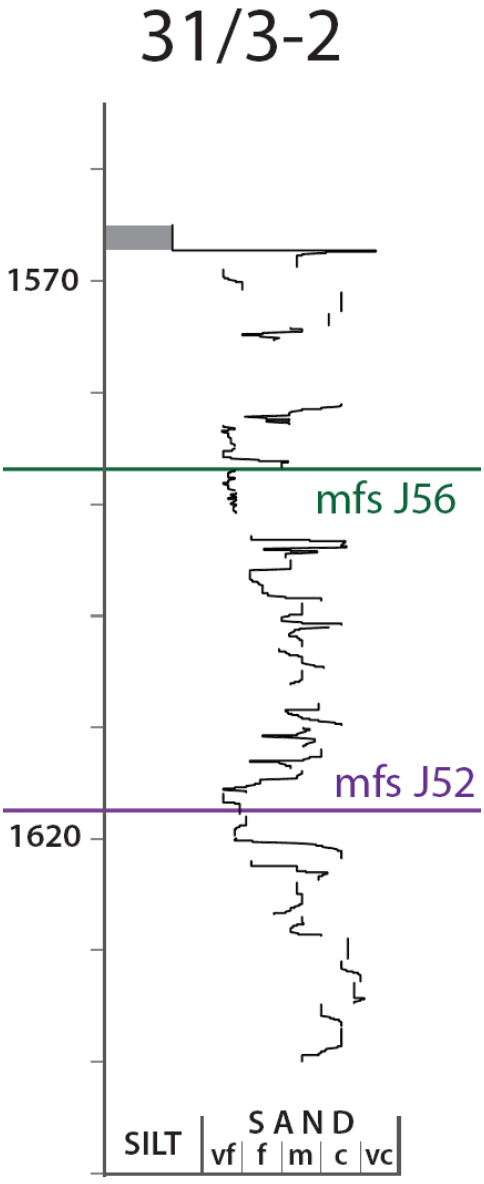
31/3-2
1570
mfs J56
mfs J52
1620
SILT
SAND
vf
f
m
c
vc

Norsk Hydro

Well no.	Core report	Core no's
31/3-2		1

Interval	Area	Cut	Date
1565 - 1570 m	Troll	1565 - 1581 m	24.3.84
Scale	**Well R.K.B.**	**Recovery**	**Geologist**
1:25	25 m	1565 - 1575.5 (65.6%)	Häger/Edvardsen

Depth scale	Recovery	Lithological column	Depths	Lithological descriptions	Shows
1565		" M		**Sh:** gy blk - brn blk, mod hd - firm, subfis, in pt fis, sl slty - slty, carb, sl micro-mic, non - v sl calc.	No show.
1566		" " C " C		**Clyst:** brn blk, mod hd, blky - subfis, sl slty, carb, sl micro-mic, non calc.	No show.
1567		" " M		**Clyst:** slty, micro-mic, else a/a.	No show.
		C "			
1568		" M C M		**Sd/Sst:** lt brn gy, m - f, tr crs, v fri - lse, subang - subrnd, sl slty mtx, sl mic, mod srtd, fair vis por.	Gd HC odour, lt brn oil stn, 100% bright yel flu, strong inst strmg bl wh cut, v pale straw vis cut, strong yel wh flu resd, pale straw vis resd.
		" "	1568.75 m Sealed sample 1569		
1569		C M " " M C M		**Sst:** brn blk, vf - slty, pt grdg **Slst,** mod hd, subang, v mic, carb, mod srtd, no vis por.	40% flu a/a, mod slow strmg blu wh flu cut, no vis cut.
1570		M " "		**Sst:** brn gy - m dk gy, vf - slty, mod hd, subang, v mic, carb, mod srtd, no vis por.	100% bright yel flu, mod strong fast strmg blu wh flu cut, v pale straw vis cut.

Norsk Hydro

Well no.	Core report	Core no's
31/3-2		1

Interval	Area	Cut	Date
1570 - 1575 m	Troll	1565 - 1581 m	24.3.84.
Scale	**Well R.K.B.**	**Recovery**	**Geologist**
1:25	25 m	1565 - 1575.5 m (65.5%)	J. Edvardsen/K.O. Häger

Depth	Recovery	Lithological column	Depths	Lithological descriptions	Shows
1570		M, C		Transitional GRDY VFS/FS	
		M	1570.75 m Sealed sample		
1571		C	1571	**Sst:** brn gy, pred vf - slty, minor crs - f pbly, firm, fri, subang - subrnd, weak silic cmt, sl mic, sl carb, poor srtg (bimodal), poor vis por.	Gd HC odour, lt brn - brn gy oil stn (90%), 100% bright yel flu, mod strong fast - inst strmg blu wh flu cut, straw vis cut, strong yel wh flu resd, lt amber vis resd.
1572		C	1572.75 m Sealed sample	**Sst/Sd:** lt brn gy - brn gy, crs - f pbly, minor m, v fri - lse, subang - subrnd, rr rnd, poor srtg, excellent vis por.	Flu a/a, mod strong, inst strmg blu wh flu cut, pale straw vis cut, strong yel wh flu resd, v pale straw vis resd.
1573		C	1573	**Sst/Sd:** pred m - crs, minor f pbly, else as for 1572 m.	Show as for 1572 m.
1574		C, M	1574 m Sealed sample 1574.25	**Sst/Sd:** brn gy, m - crs, minor v crs, v fri - lse, subang, tr subrnd, mod srtd, excellent vis por.	Fast strmg flu cut, else as for 1572 m.
1575					

Well	Core report	Core no's

Norsk Hydro

Well no.	Core report	Core no's
31/3 - 2		1

Interval	Area	Cut	Date
1575 - 1575.5 m	Troll	1565 - 1581 m	24.3.84.
Scale	**Well R.K.B.**	**Recovery**	**Geologist**
1:25	25 m	1565 - 1575.5 m (65.6%)	J. Edvardsen/K.O. Häger

Depth scale	Re-covery	Lithological column	Depths	Lithological descriptions	Shows
1575			1575.2 m	**Sst/Sd/** brn gy - m dk gy, pred crs - f pbly, minor m - f, firm - v fri, subang - subrand, v sl mic, poor srtg, gd vis por.	Gd HC odour, brn gy oil stn, 80% spotty bright - mod strong yel flu, fast - inst strmg milky wh flu cut, v pale straw vis cut, mod strong yel wh flu resd, no vis resd.
1575.3		M·M·C	1575.5 m		
1576				**Sst:** lt brn gy - lt olv gy, clr Qtz, f - m, pred m, fri, pred subrnd, tr arg mtx, mica - v mica, sl carb, well srtd, poor - fair vis por.	30 - 40% vis oil stn, 90 - 100% bright yel flu, strong inst strmg blu wh flu cut, pale straw vis cut, strong yel wh flu resd, lt amber vis resd.
1577		Not recovered			
1578					
1579					
1580					

Well	Core report	Core no's
31/3 - 2	3 of 3	1

Norsk Hydro

Well no.	Core report	Core no's
31/3-2		2

Interval	Area	Cut	Date
1581 - 1586 m	Troll	1581 - 1593 m	26.3.84
Scale	**Well R.K.B.**	**Recovery**	**Geologist**
1:25	25 m	1581 - 1590.7 (80.8%)	J. Edvardsen /K.O. Häger

Depth scale	Re-covery	Lithological column	Depths	Lithological descriptions	Shows
1581				**Sst/Sd:** m lt gy - lt brn gy, pred m - crs, minor v crs - pbly, v fri - lse, subang, tr subrnd, tr slt mtx, poor srtg, v good vis por.	Fair HC odour, 40% spotty mod strong yel wh flu. mod strong fast - slow strmg milky wh flu cut, mod yel wh flu resd, no vis cut.
1582		C		**Sst:** olv gy - lt gy, clr Qtz, crs - f pbly, hd, subang, tr subrnd, v well calc cmtd, poor srtg, no vis por.	Tr spotty flu a/a, no cut.
			1582.75 m Sealed sample 1583		
1583		M		**Sst:** olv yg - m dk gy, vf - f, tr slt, mod hd, subang, tr calc cmt, thin carb lam, thin mica lam, well srtd, poor vis por.	90% spotty flu a/a, inst - fast strmg mod strong milky wh flu cut, amber vis cut, strong yel flu resd, pale straw vis resd.
1584		M		**Sst:** olv gy - m dk gy, vf - f, tr slty, mod hd, subang, thin (1 - 2 mm) v mica lam, well srtd, poor vis por.	30% spotty flu a/a, mod strong fast - slow strmg milky wh flu cut, lt amber vis cut, strong yel wh flu resd, pale straw vis resd.
			1584.75 m Sealed sample 1585		
1585		M		**Sst:** glau, sl mica, else as for 1584 m.	100% mod strong yel wh flu, fast - inst strmg milky wh flu cut, lt amber vis cut, strong yel wh flu resd, pale straw vis resd.
1586		C			

Well	Core report	Core no's
31/3 - 2	1 of 2	2

Norsk Hydro

Well no.	Core report	Core no's
31/3-2		2

Interval	Area	Cut	Date
1586 - 1590.7 m	Troll	1581 - 1593 m	26.3.84.
Scale	**Well R.K.B.**	**Recovery**	**Geologist**
1:25	25 m	1581 - 1590.7 (80.8%)	J. Edvardsen/K.O. Häger

Depth scale	Recovery	Lithological column	Depths	Lithological descriptions	Shows
1586		C		**Sst:** olv gy - m dk gy, clr Qtz, m - f, tr crs, mod hd - fri, subang - subrnd, tr weak calc cmt, sl tr arg mtx, carb, fair srtg, poor vis por.	30 - 40% spotty mod strong dull yel flu, inst strmg mod milky wh flu cut, no vis cut, strong yel wh flu resd, straw vis resd.
		C	1586.75 m Sealed sample		
1587		C M	1587	**Sst:** lt brn gy - olv gy, m - f, firm - fri, pred subang, tr subrnd, tr weak calc cmt, carb strks, well srtd, mod vis por.	40 - 50% spotty mod strong yel wh flu, slow strmg mod milky wh flu cut, no vis cut, strong yel wh flu resd, tr amber vis resd.
		C			
1588		M		**Sst:** olv gy - m dk gy, clr Qtz, f - vf, firm, fri, subang, tr subrnd, tr slt mtx, carb, mica, mod srtd, poor vis por.	60% spotty mod strong yel flu slow - non strmg milky wh flu cut, no vis cut, mod strong yel wh flu resd, tr amber vis resd.
		M	1588.75 m Sealed sample		
1589		C	1589	**Sst:** pred vf - slty, minor f, else as for 1588 m.	20% spotty dull yel flu, slow strmg mod milky wh flu cut, no vis cut, mod strong yel wh flu resd.
1590		M C		**Sst:** olv gy - m dk gy, clr Qtz, vf - slty, minor f, firm, fri, subang, tr weak calc ctm, carb, mica, mod srtd, poor vis por.	40% spotty mod strong yel flu, slow - non strmg mod milky wh flu cut, no vis cut, flu resd a/a.
		Not recovered	1590.7 m	**Sst:** as for 1590 m.	as for 1590 m.
1591					

Well	Core report	Core no's
31/3 - 2	2 of 2	2

Norsk Hydro

Well no.	Core report	Core no's
31/3-2		3

Interval	Area	Cut	Date
1593 - 1598 m	Troll	1593 - 1608 m	26.3.84
Scale	**Well R.K.B.**	**Recovery**	**Geologist**
1:25	25 m	1593 - 1606.25 (88%)	H ä ger/ Edvardsen

Depth scale	Re-covery	Lithological column	Depths	Lithological descriptions	Shows
1593		C		**Sh:** brn blk, firm, fis, sl slty, sl micro-mid, sl carb, non calc.	No show.
1594		M C C C C C		**Sst/Sd:** lt brn gy, m - v crs, tr pbly, v fri - lse, subang, rr subrnd, mod srtd, v good vis por.	30% spotty dull yel flu, fast strmg mod weak mlky wh flu cut, no vis cut, weak yel wh flu resd.
1595		C M	1594.75 m Sealed sample 1595	**Sst:** Lt brn gy, f - v crs, tr f pbly mod hd - fri, pt mod - well calc cmtd, poor srtg, mod vis por.	Show a/a.
1596		M C M C	1596m Sealed sample 1596.25	**Sst:** olv gy - m lt gy, pred f, minor vf, tr m, firm, subang, tr weak calc cmt, mica, sl carb, fairly well srtd, poor vis por.	No show.
1597		M C		**Sst:** olv gy - brn gy, f - vf, tr m, v hd, subang, v well calc cmt, mica, carb, tr pyr, mod srtd, no vis por.	No show.
1598		M			

Well	Core report	Core no's
31/3 - 2	1 of 3	3

Norsk Hydro

Well no.	Core report	Core no's
31/3-2		3

Interval	Area	Cut	Date
1598 - 1603 m	Troll	1593 - 1608 m	26.3.84.
Scale	**Well R.K.B.**	**Recovery**	**Geologist**
1:25	25 m	1593 - 1606.25 (88%)	J. Edvardsen/K.O. Häger

Depth scale	Recovery	Lithological column	Depths	Lithological descriptions	Shows
1598		M		**Sst:** olv gy - brn gy, f - vf, tr m, tr slt, v hd, subang, v well calc cmtd, carb lam, v mica lam, tr pyr, mod srtd, no vis por.	No show.
		M	1598.75 m Sealed sample		
1599		C	1599	**Sst:** brn gy, m - crs, tr f, mod hd, fri, subang - subrnd, tr weak calc cmt, sl mica, sl carb, mod srtd, good vis por.	No show.
		M			
		C			
1600		M		**Sst:** dk gy, f - vf, v hd, subang, v well calc cmtd, v mica, carb, fairly well srtd, no vis por.	No show.
		M			
		C	1600.75 m Sealed sample		
		C	1601	**St/Sd:** brn gy, m - crs, tr v crs, firm, v fri - lse, subang, tr subrnd, v sl carb, v sl mica, well srtd, excellent vis por.	No show.
		M			
1602		C		**Sst/Sd:** brn gy - lt brn gy, m - crs, tr f & v crs, firm, v fri, subang, tr subrnd, carb, mica, well srtd, excellent vis por.	No show.
		M			
1603			1602.75 m Sealed sample 1603		

Well	Core report	Core no's
31/3 - 2	2 of 3	3

Norsk Hydro

Well no.	Core report	Core no's
31/3-2		3

Interval	Area	Cut	Date
1603 - 1606.25 m	Troll	1593 - 1608 m	26.3.84.
Scale	**Well R.K.B.**	**Recovery**	**Geologist**
1:25	25 m	1593 - 1606.25 (88%)	J. Edvardsen/K.O. Hæger

Depth scale	Recovery	Lithological column	Depths	Lithological descriptions	Shows
1603		M C		**Sst:** brn gy, f - m, tr vf, firm, fri, subang, tr weak calc cmt, sl carb, sl mica, well srtd, fair vis por.	No show.
1604		M C		**Sst/Sd:** brn gy, f - crs, firm, v fri - lse, subang, v sl carb, poor srtg, fair vis por.	No show.
1605		M C	1604.75 m Sealed sample 1605 m	**Sst/Sd:** pred m - crs, else as for 1604 m.	No show.
1606		C	1606	**Sst:** m dk gy, m - f, v hd, subang - subrnd, well calc cmtd, carb, mica, mod srtd, no vis por.	No show.
			1606.25 m	**Sh:** brn blk, mod hd, fis, slty, mica, carb, pyr, calc - sl calc.	
1607		Not recovered			
1608					

Well	Core report	Core no's
31/3 - 2	3 of 3	3

Norsk Hydro

Well no.	Core report	Core no's
31/3-2		4

Interval	Area	Cut	Date
1608 - 1613 m	Troll	1608 - 1626 m	27.3.84.
Scale	**Well R.K.B.**	**Recovery**	**Geologist**
1:25	25 m	1608 - 1626 (100%)	J. Edvardsen/K.O. Häger

Depth scale	Recovery	Lithological column	Depths	Lithological descriptions	Shows
1608				**Sst/Sd/** lt brn gy - m dk gy, m - crs, tr v crs, firm, fri, subang, tr subrnd, fairly well srtd, gd vis por.	No show.
1609		M		**Sst/Sd:** olv gy - m lt gy, m - f, firm, fri, v sl mica, well srtd, gd vis por.	No show.
1610		M C	1609.75 m Sealed sample 1610	**Sst:** lt olv gy, m - crs, firm, fri, subang, v sl calc cmtd, rr carb, tr mica, mod srtd, gd vis por.	No show.
1611		M C	1611.75 m Sealed sample	**Sst:** m lt gy, pred m, firm, fri, subang - subrnd, tr carb, tr mica, fairly well srtd, gd vis por.	No show.
1612		M	1612	**Sst:** lt olv gy - olv gy, m, lse - fri, subang - subrnd, v sl slty mtx, fairly well srtd, gd vis por.	No show.
1613					

Well	Core report	Core no's
31/3 - 2	1 of 4	4

Norsk Hydro

Well no.	Core report	Core no's
31/3-2		4

Interval	Area	Cut	Date
1613 - 1618 m	Troll	1608 - 1626 m	27.3.84.
Scale	**Well R.K.B.**	**Recovery**	**Geologist**
1:25	25 m	1608 - 1626 (100%)	J. Edvardsen/K.O. Hæger

Depth scale	Recovery	Lithological column	Depths	Lithological descriptions	Shows
1613		M		**Sst:** lt olv gy, pred m, lse, fri, subang, tr mica, fairly well srtd.	No shows.
		C	1613.75 m Sealed sample		
1614		M	1614	**Sst:** m lt gy, f - m, v hd, subang - subrnd, v well calc cmtd, tr mica, tr carb, tr pyr, mod srtd, no vis por.	
		C			
1615		M		**Sst:** m dk gy, f - vf, firm, subrnd - subang, slty mtx, arg lam, carb, mica, poorly srtd, poor vis por.	
			1615.75 m Sealed sample		
1616		M	1616	**Sst:** m lt gy, pred m, firm, subang, tr subrnd, tr mica, well srtd, gd vis por.	
		C			
1617		M		**Sst:** m dk gy - dk gy, f - vf, tr slt, firm, subrnd, mica, carb, arg lam, poorly srtd, no vis por.	
		C	1617.75 m Sealed sample		
1618			1618		

Well	Core report	Core no's
31/3 - 2	2 of 4	4

Norsk Hydro

Well no.	Core report	Core no's
31/3-2		4

Interval	Area	Cut	Date
1618 - 1623 m	Troll	1608 - 1626 m	27.3.84.
Scale	**Well R.K.B.**	**Recovery**	**Geologist**
1:25	25 m	1608 - 1626 (100%)	J. Edvardsen/K.O. Hæger

Depth scale	Re-covery	Lithological column	Depths	Lithological descriptions	Shows
1618		M, C		**Sst:** m dk gy - dk gy, f - vf, tr slt, firm, subrnd, mica, carb, arg lam, poorly srtd, no vis por.	No shows.
1619		M, C		**Slst:** brn blk - olv blk, firm, flaggy vf sdy, mica - micro-mic, carb, sl calc.	
1620		M, C	1619.75 m Sealed sample 1620	**Sst:** brn blk, vf - slt, firm, v sl calc cmt, arg mtx, mica, carb, mod srtd, no vis por.	
1621		M, C	1621.75 m Sealed sample 1622	**Sst:** m lt gy, f - m, fri, firm, sl calc cmt, sl mica, tr carb, mod srtd, mod vis por.	
1622		C		**Sst:** m dk gy, vf - f, v hd, subrnd, sucrosic, v well calc cmt, mica and carb, fairly well srtd, no vis por.	
1623		M			

Well	Core report	Core no's
31/3 - 2	3 of 4	4

Norsk Hydro

Well no.	Core report	Core no's
31/3-2		4

Interval	Area	Cut	Date
1623 - 1626 m	Troll	1608 - 1626 m	27.3.84.
Scale	**Well R.K.B.**	**Recovery**	**Geologist**
1:25	25 m	1608 - 1626 m (100%)	J. Edvardsen/K.O. Hæger

Depth scale	Recovery	Lithological column	Depths	Lithological descriptions	Shows
1623				**Sst:** lt brn gy, m - crs, minor v crs - pbly, lse - fri, subang - ang, v sl mica, poorly srtd, gd vis por.	No shows.
1624		M	1623.75 m Sealed sample 1624	**Sst:** m lt gy - lt brn gy, pred m, tr pbls, lse - fri, subang, v sl mica, mod srtd, gd vis por.	
1625		M		**Sst:** f - m, else a/a.	
1626		M C M C		**Sst:** brn blk, vf - slt, firm, v sl calc cmt, arg mtx, mica, carb, mod srtd, no vis por.	

Well	Core report	Core no's
31/3 - 2	4 of 4	4

Norsk Hydro

Well no.	Core report	Core no's
31/3 - 2		5

Interval	Area	Cut	Date
1626 - 1631 m	Troll	1626.0 - 1640.0 m	27.3.84.
Scale	**Well R.K.B.**	**Recovery**	**Geologist**
1:25	25 m	1626.0 - 1640.0 m (100%)	Nilsen/Finnerud

Depth scale	Recovery	Lithological column	Depths	Lithological descriptions	Shows
1626		M		**Sst:** lt gy, f - m, fri, sl mic, v sl calc, sl carb, mod - well srtd, gd vis por.	No show.
1627		M		**Sst:** a/a, pred f, tr kao, non calc, gd vis por.	
		M	1627.75 m Sealed sample		
1628		C	1628	**Sst:** lt gy, f - m, rr crs, fri, sl mic, tr kao, pos kao shell frags, v sl carb, mod srtd, gd vis por.	
1629			1629	**Sst:** lt gy, m - v crs, fri tr kao, poor srtg, gd vis por.	
		C	1629.75 m Sealed sample		
1630		M	1630	**Sst:** lt gy, m - v crs, rr pbly fri, sl mic, tr kao, v sl carb, poor srtd, gd vis por.	
1631					

Well	Core report	Core no's
31/3 - 2	1 of 3	5

Norsk Hydro

Well no.	Core report	Core no's
31/3-2		5

Interval	Area	Cut	Date
1631 - 1636 m	Troll	1626.0 - 1640.0 m	27.3.84.
Scale	**Well R.K.B.**	**Recovery**	**Geologist**
1:25	25 m	1626.0 - 1640.0 m (100%)	Nilsen/Finnerud

Depth scale	Re-covery	Lithological column	Depths	Lithological descriptions	Shows
1631		M	MS-VCS	**Sst:** a/a pred m, mod srtd, gd vis por.	No show.
		M.	1631.75 m Sealed sample 1632	**Sst:** lt gy, f - v crs - pbly, fri, sl mic, tr rock frags, poor srtg, gd vis por.	
1632				MS-VCS, some FS, poor sorting	
		M			
1633			1633	**Sst:** lt gy, m - v crs, v hd, calc cmt, sl mic, poor srtg, no vis por.	
				CEM=3 FS-VCS, some granules floating poor sorting	
			1633.75 m Sealed sample 1634		
1634				**Sst:** lt gy, f - pbly, fri, tr garnets, tr pyr, tr rock frags, poor srtg, gd vis por.	
				FS-VCS some granules and small-med. very well rounded pebbles floating (pebbles qtz, sh, lgt, qtz)	
		M	1635	**Sst:** a/a, pred crs - pbly, tr garnets, tr pyr, sl mic, tr weathered rock frags, poor srtg, gd vis por.	
1635				MS-CS (50%-3/8)	
			1635.75 m Sealed sample 1636 m	module of calc. cem.	
1636					

Well	Core report	Core no's
31/3 - 2	2 of 3	5

Norsk Hydro

Well no.	Core report	Core no's
31/3-2		5

Interval	Area	Cut	Date
1636 - 1640 m	Troll	1626.0 - 1640.0 m	27.3.84.
Scale	**Well R.K.B.**	**Recovery**	**Geologist**
1:25	25 m	1626 - 1640.0 m (100%)	Nilsen/Finnerud

Depth scale	Re-covery	Lithological column	Depths	Lithological descriptions	Shows
1636				**Sst:** a/a, tr kao, v few garnets, gd vis por.	No show.
1637		M		**Sst:** a/a, f - m - loc crs, sl mic - mic, tr pt dissolved shell frags, tr kao, poor - mod srtg, gd vis por.	
			1637.75 m Sealed sample 1638		
1638		M		**Sst:** a/a.	
1639				**Sst:** lt gy, m - v crs - pbly, v hd, calc cmtd, sl mic, thick walled bivalves, mod - poor srtg, no vis por.	
		M			
1640			1639.85	**Sst:** lt gy, fri, f - m pred m, mod well srtd, sl mic, tr kao, tr garnets, gd vis por.	

Well	Core report	Core no's
31/3 - 2	3 of 3	5

31/3-3

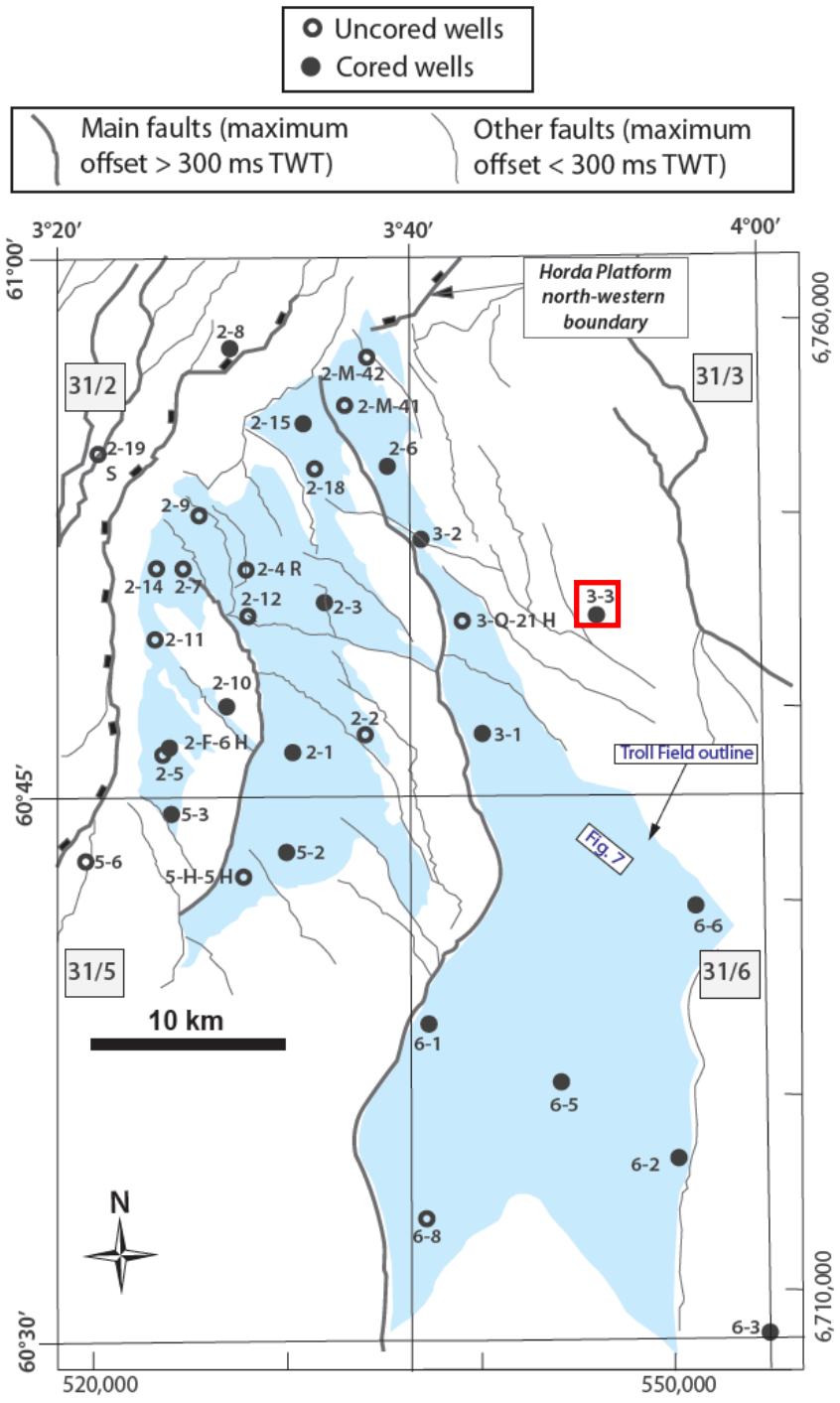
Uncored wells
Cored wells
Main faults (maximum offset > 300 ms TWT)
Other faults (maximum offset < 300 ms TWT)
3°20′
3°40′
4°00′
61°00′
60°45′
60°30′
6,760,000
6,710,000
520,000
550,000
Horda Platform north-western boundary
31/2
31/3
31/5
31/6
2-8
2-M-42
2-M-41
2-15
2-19 S
2-6
2-18
2-9
3-2
2-4 R
2-14
2-7
2-12
2-3
3-3
3-Q-21 H
2-11
2-10
2-2
3-1
2-F-6 H
2-5
2-1
Troll Field outline
5-3
5-2
5-6
5-H-5 H
Fig. 7
6-6
10 km
6-1
6-5
6-2
N
6-8
6-3

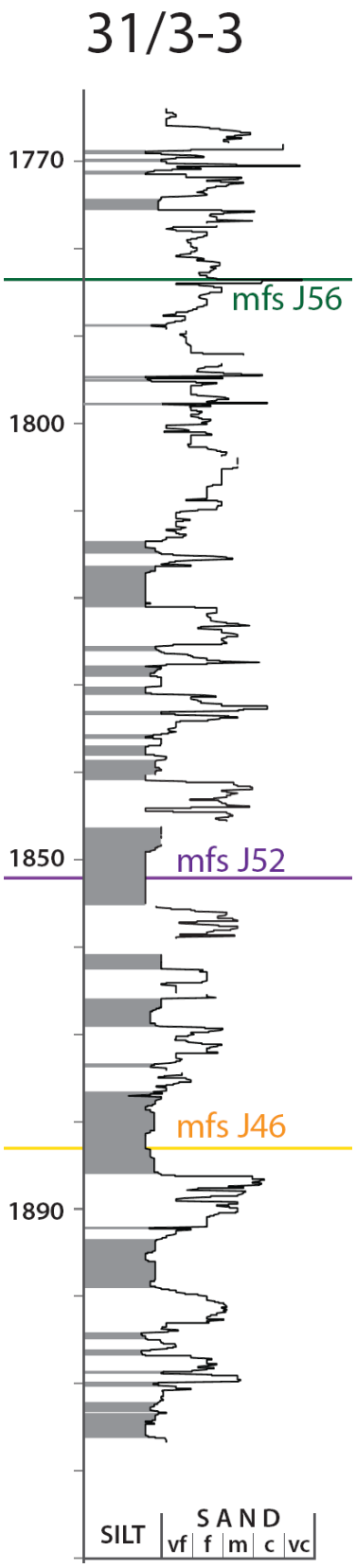
31/3-3
1770
mfs J56
1800
1850
mfs J52
mfs J46
1890
SILT
SAND
vf
f
m
c
vc

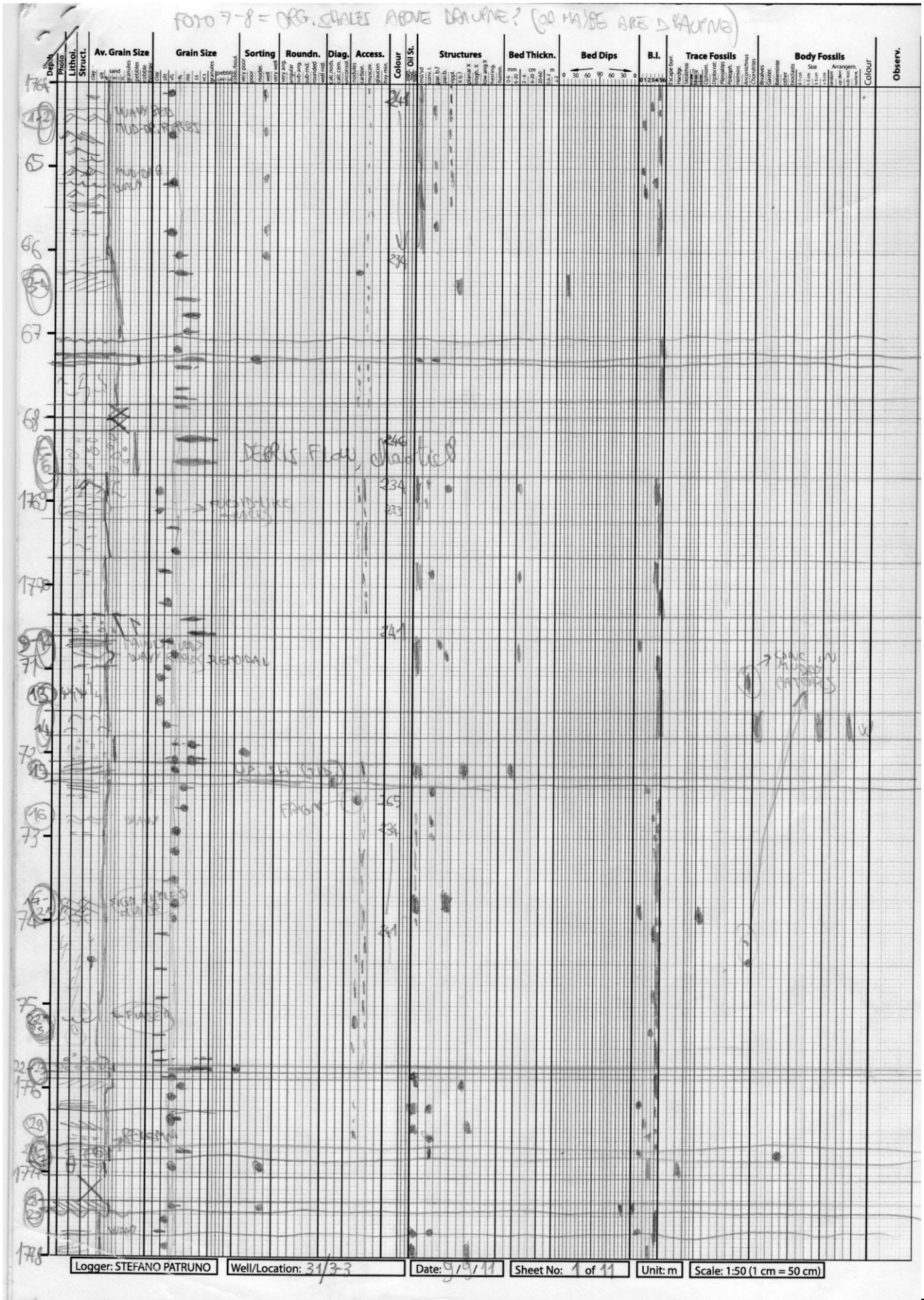
FOTO 7-8 = ORG. SHALES ABOVE DAUNIE? (OR MAYBE ARE DAUNIE)
Depth
Photo
Lithol.
Struct.
Av. Grain Size
Grain Size
Sorting
Roundn.
Diag.
Access.
Colour
Oil St.
Structures
Bed Thickn.
Bed Dips
B.I.
Trace Fossils
Body Fossils
Observ.
DEBRIS FLOW, chaotic
Logger: STEFANO PATRUNO
Well/Location: 31/3-3
Date: 9/9/11
Sheet No: 1 of 11
Unit: m
Scale: 1:50 (1 cm = 50 cm)

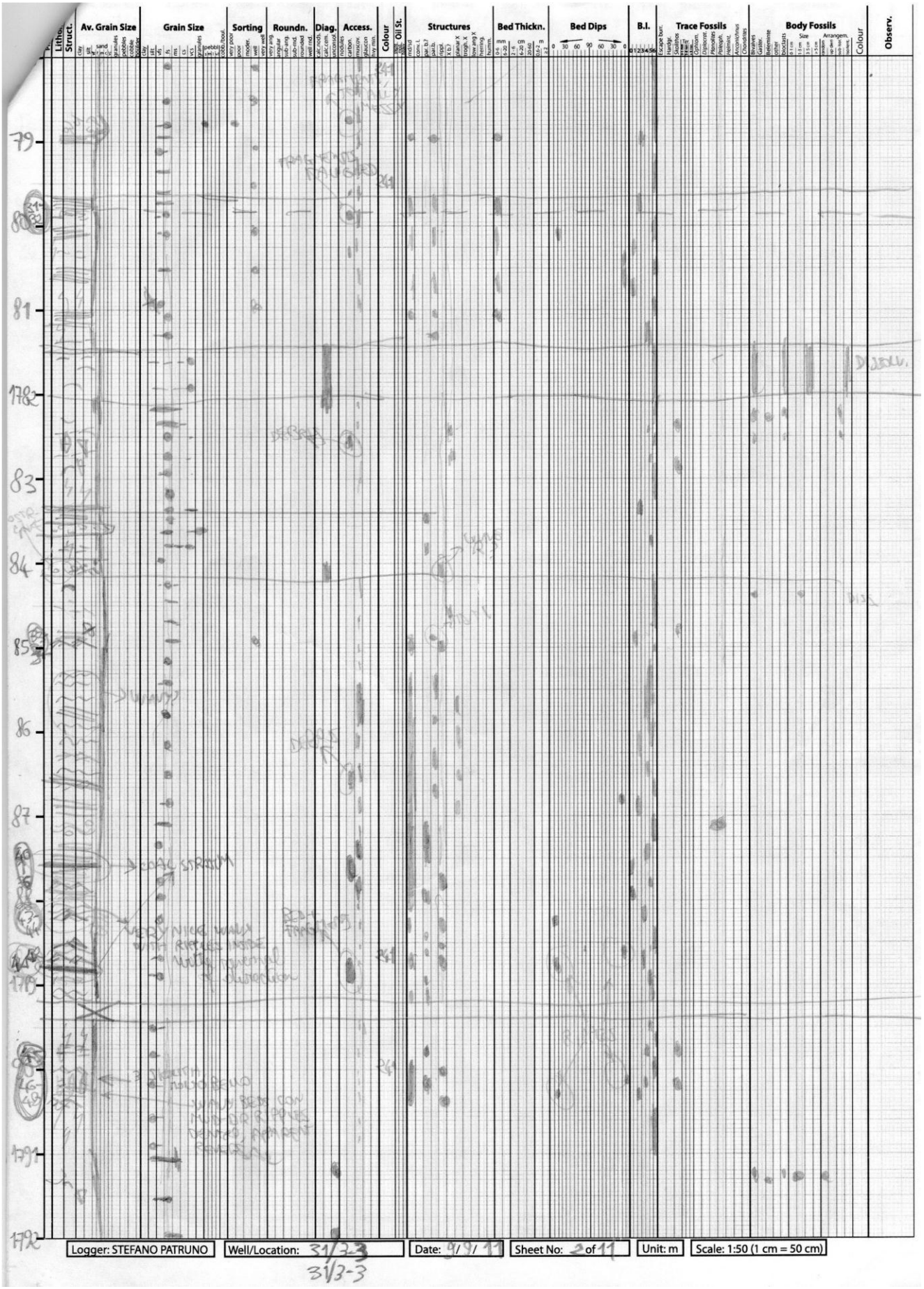
Lithol. Struct.
Av. Grain Size
Grain Size
Sorting
Roundn.
Diag.
Access.
Colour
Oil St.
Structures
Bed Thickn.
Bed Dips
B.I.
Trace Fossils
Body Fossils
Observ.
79
80
81
1782
83
84
85
86
87
1791
1792
Logger: STEFANO PATRUNO
Well/Location: 31/3-3
31/3-3
Date: 9/9/11
Sheet No: 2 of 11
Unit: m
Scale: 1:50 (1 cm = 50 cm)

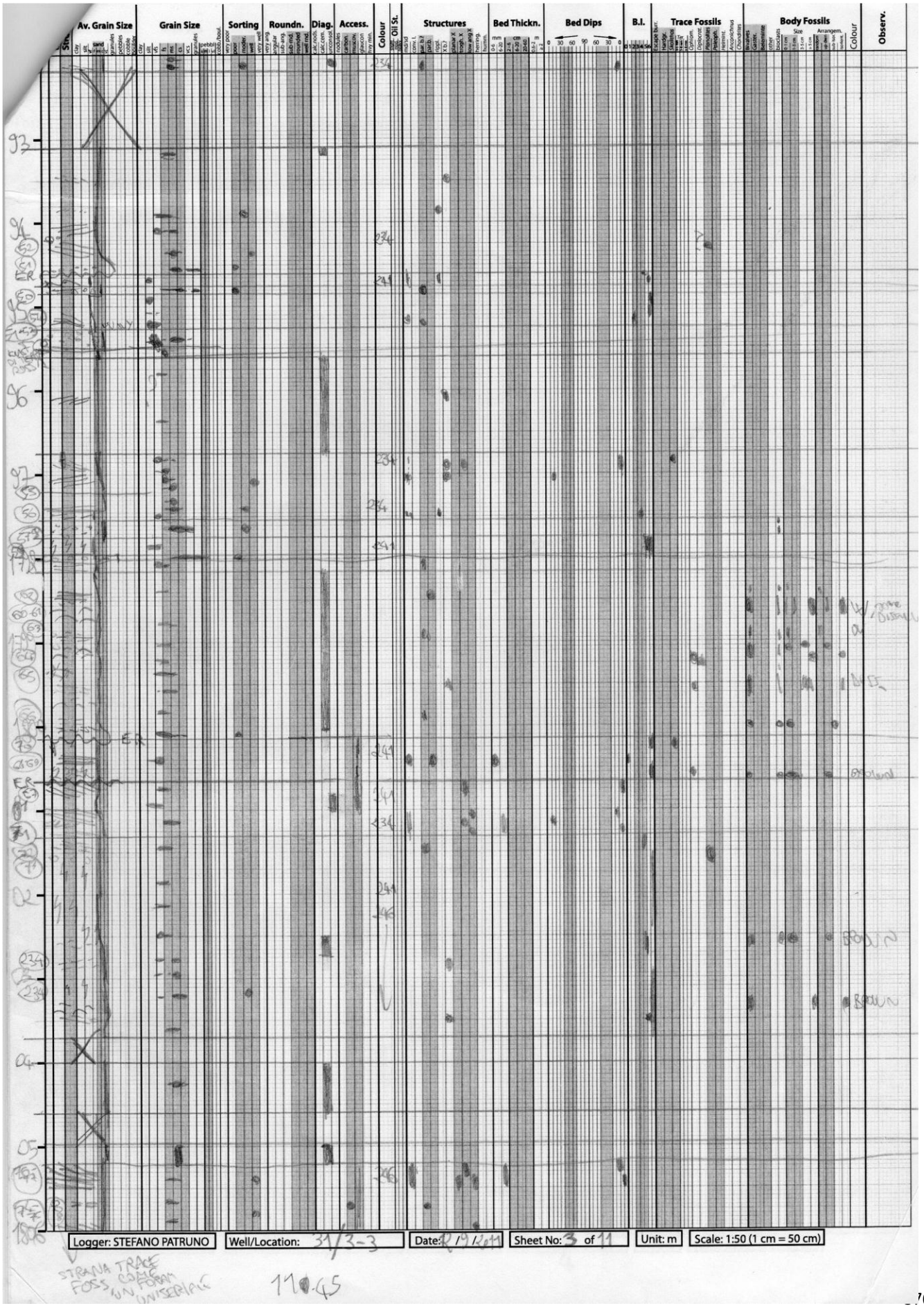
Av. Grain Size
Grain Size
Sorting
Roundn.
Diag.
Access.
Colour
Oil St.
Structures
Bed Thickn.
Bed Dips
B.I.
Trace Fossils
Body Fossils
Observ.
Logger: STEFANO PATRUNO
Well/Location: 31/3-3
Date: 2 / 9 / 2011
Sheet No: 3 of 11
Unit: m
Scale: 1:50 (1 cm = 50 cm)

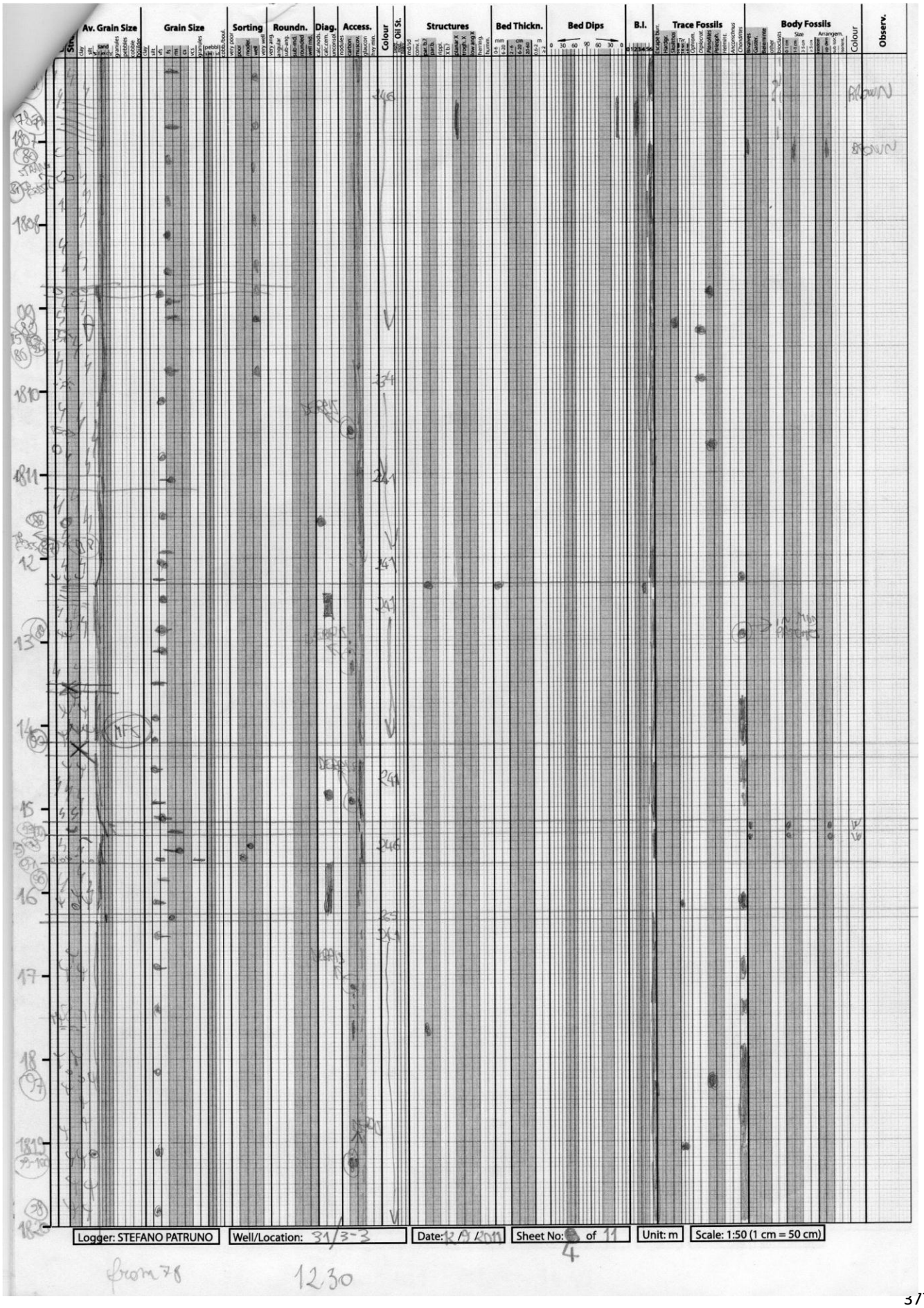
Av. Grain Size
Grain Size
Sorting
Roundn.
Diag.
Access.
Colour
Oil St.
Structures
Bed Thickn.
Bed Dips
B.I.
Trace Fossils
Body Fossils
Observ.
Logger: STEFANO PATRUNO
Well/Location: 31/3-3
Date: 12/8/2011
Sheet No: 5 of 11
Unit: m
Scale: 1:50 (1 cm = 50 cm)
from 78
1230

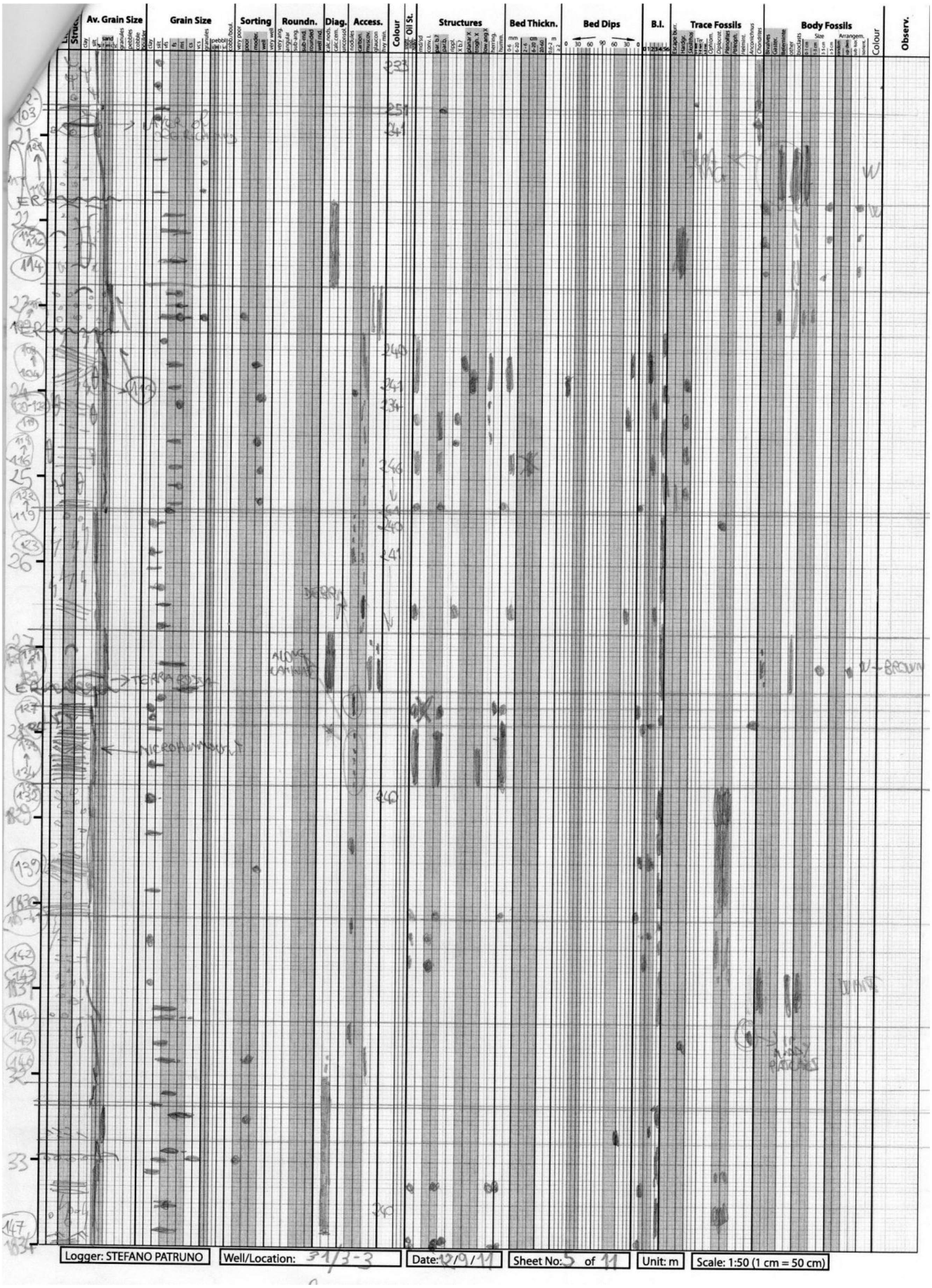
Av. Grain Size
Grain Size
Sorting
Roundn.
Diag.
Access.
Colour
Oil St.
Structures
Bed Thickn.
Bed Dips
B.I.
Trace Fossils
Body Fossils
Colour
Observ.
Logger: STEFANO PATRUNO
Well/Location: 31/3-3
Date: 12/9/11
Sheet No: 5 of 11
Unit: m
Scale: 1:50 (1 cm = 50 cm)

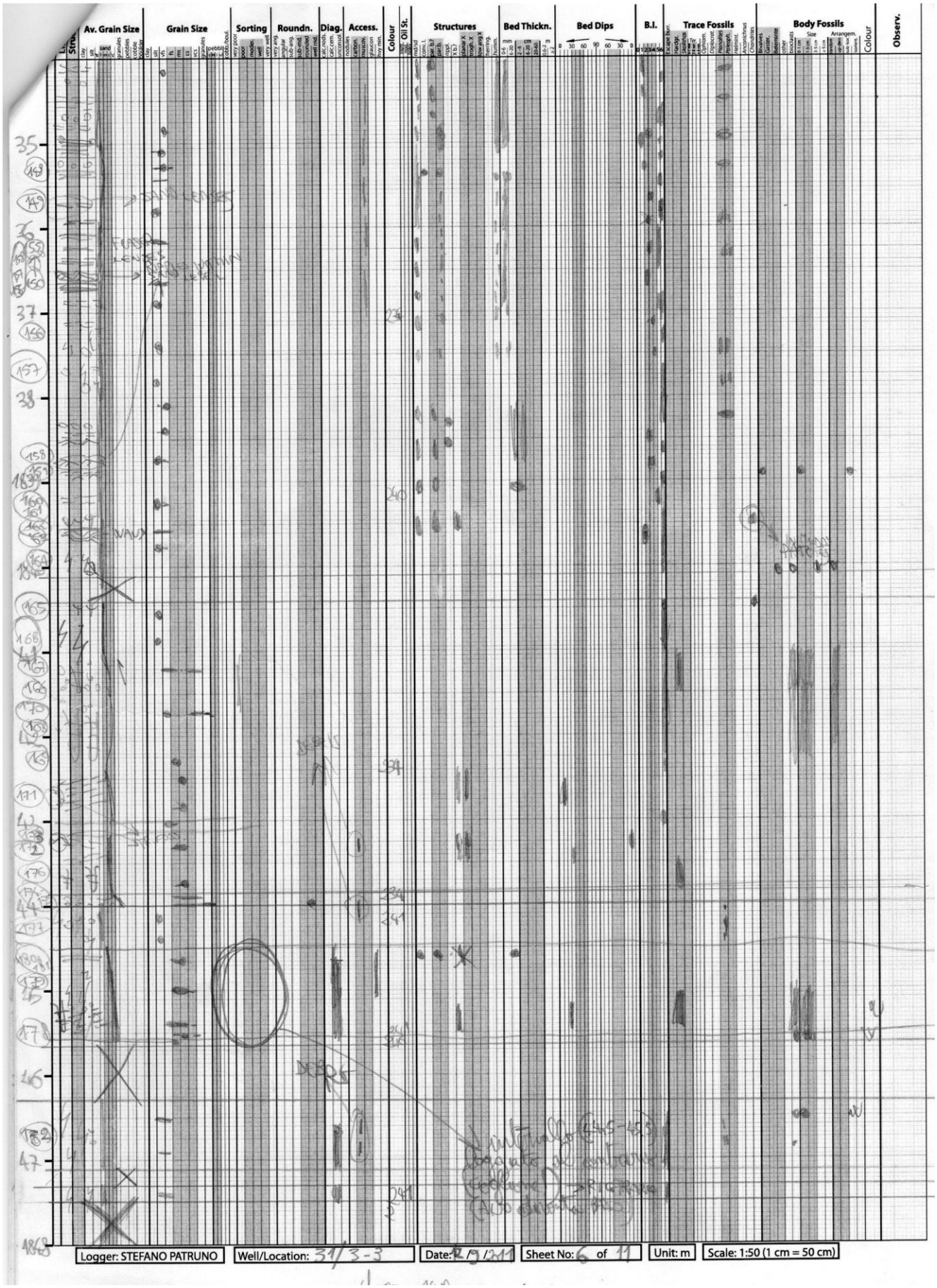
Av. Grain Size
Grain Size
Sorting
Roundn.
Diag.
Access.
Colour
Oil St.
Structures
Bed Thickn.
Bed Dips
B.I.
Trace Fossils
Body Fossils
Observ.
Logger: STEFANO PATRUNO
Well/Location: 31/3-3
Date: 2/9/2011
Sheet No: 6 of 11
Unit: m
Scale: 1:50 (1 cm = 50 cm)

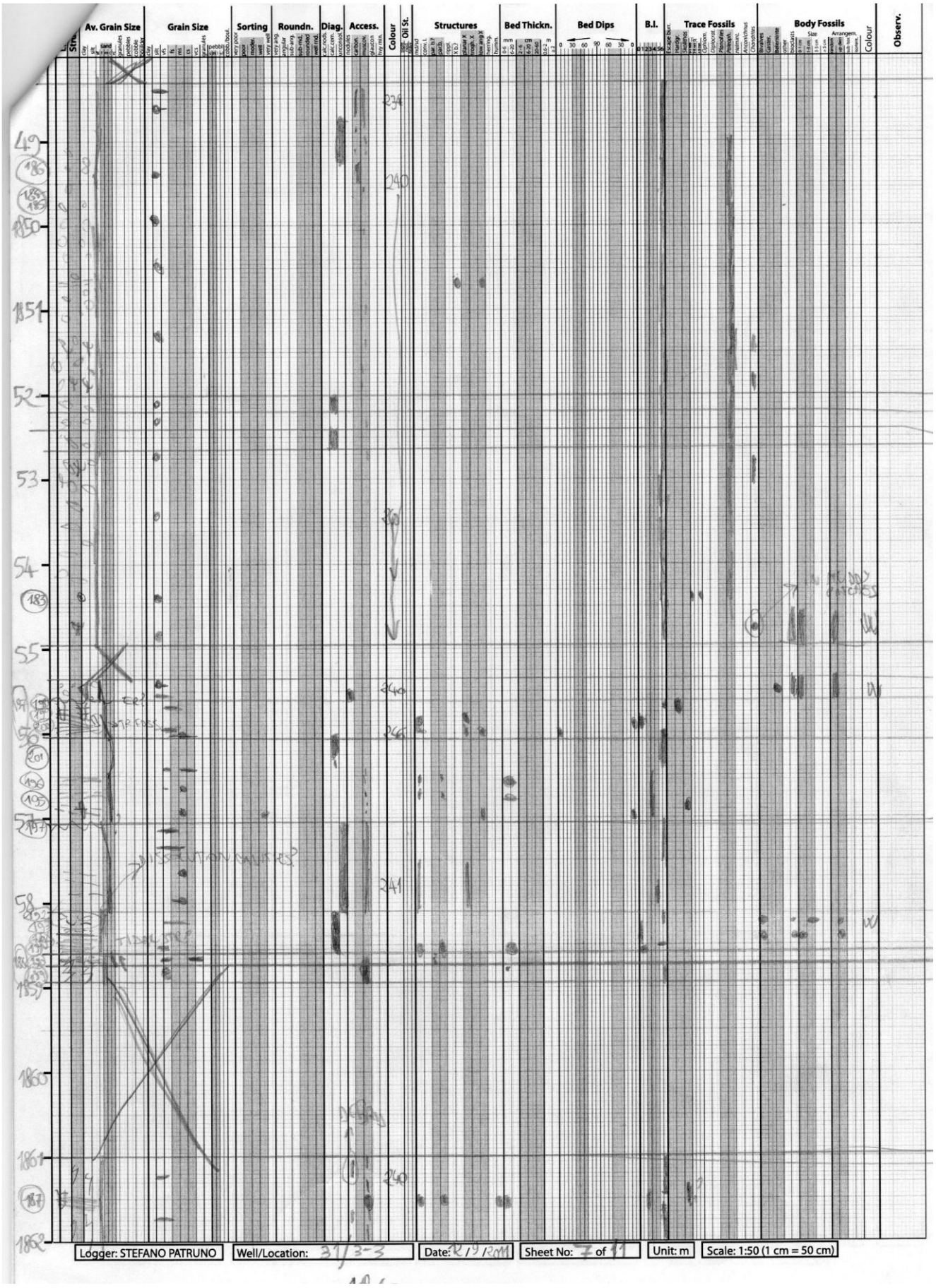
Av. Grain Size
Grain Size
Sorting
Roundn.
Diag.
Access.
Colour
Oil St.
Structures
Bed Thickn.
Bed Dips
B.I.
Trace Fossils
Body Fossils
Observ.
Logger: STEFANO PATRUNO
Well/Location: 37/3-3
Date: 8/9/2011
Sheet No: 7 of 11
Unit: m
Scale: 1:50 (1 cm = 50 cm)

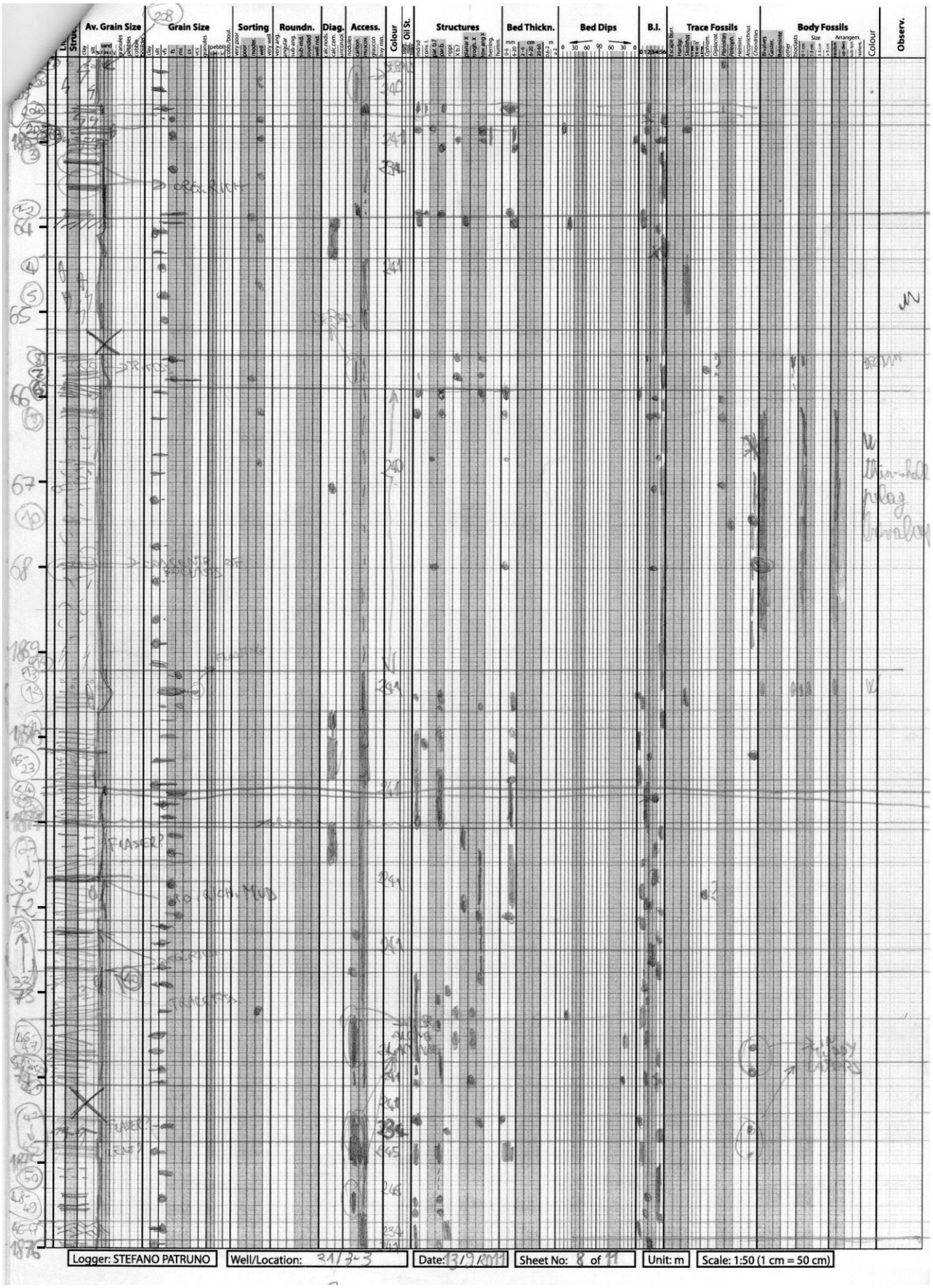
Av. Grain Size
Grain Size
Sorting
Roundn.
Diag.
Access.
Colour
Oil St.
Structures
Bed Thickn.
Bed Dips
B.I.
Trace Fossils
Body Fossils
Observ.
Logger: STEFANO PATRUNO
Well/Location:
Date:
Sheet No: 8 of 11
Unit: m
Scale: 1:50 (1 cm = 50 cm)

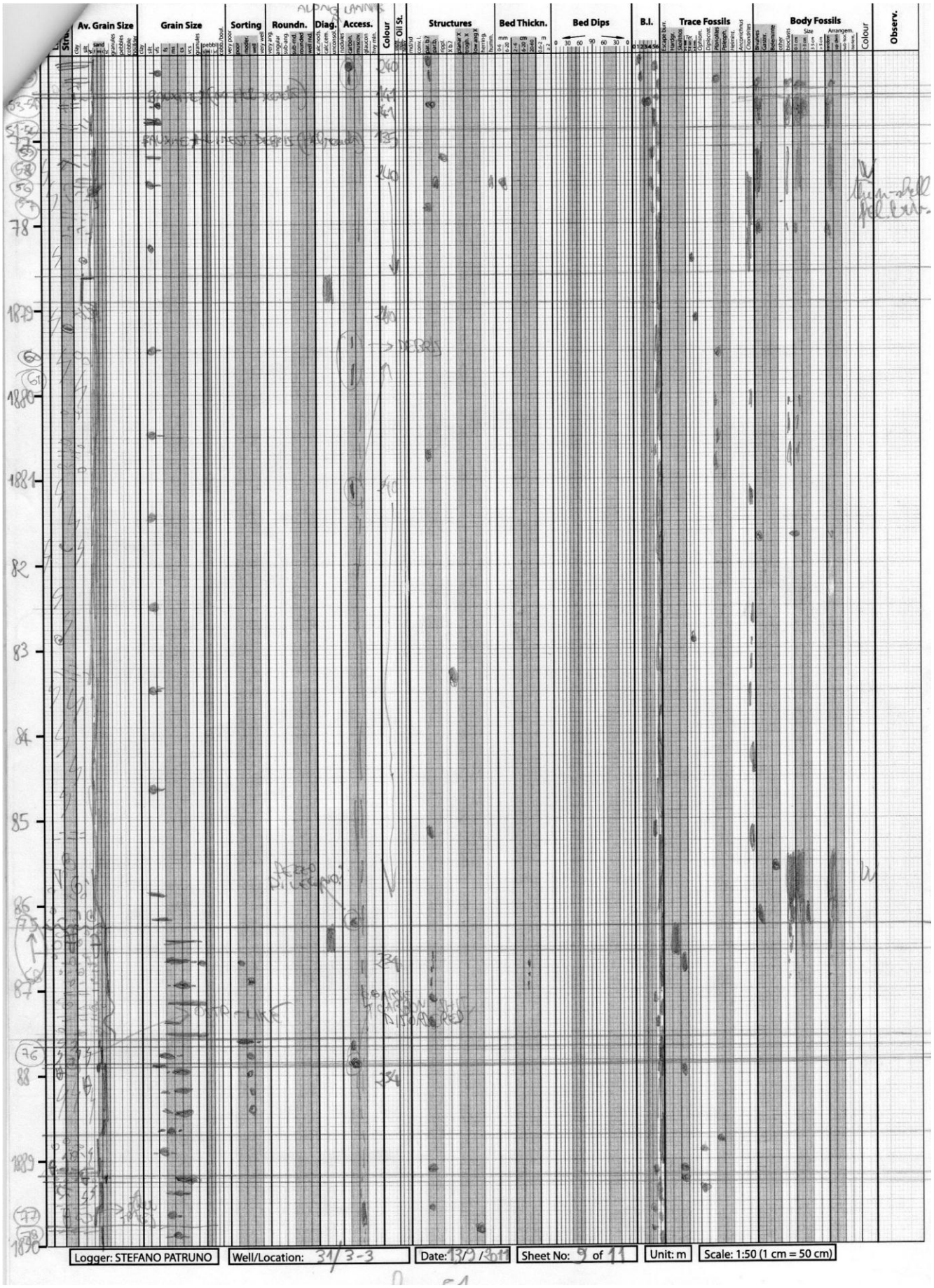
Str.
Av. Grain Size
Grain Size
Sorting
Roundn.
Diag.
Access.
Colour
Oil St.
Structures
Bed Thickn.
Bed Dips
B.I.
Trace Fossils
Body Fossils
Observ.
Logger: STEFANO PATRUNO
Well/Location: 31/3-3
Date: 13/3/2011
Sheet No: 9 of 11
Unit: m
Scale: 1:50 (1 cm = 50 cm)

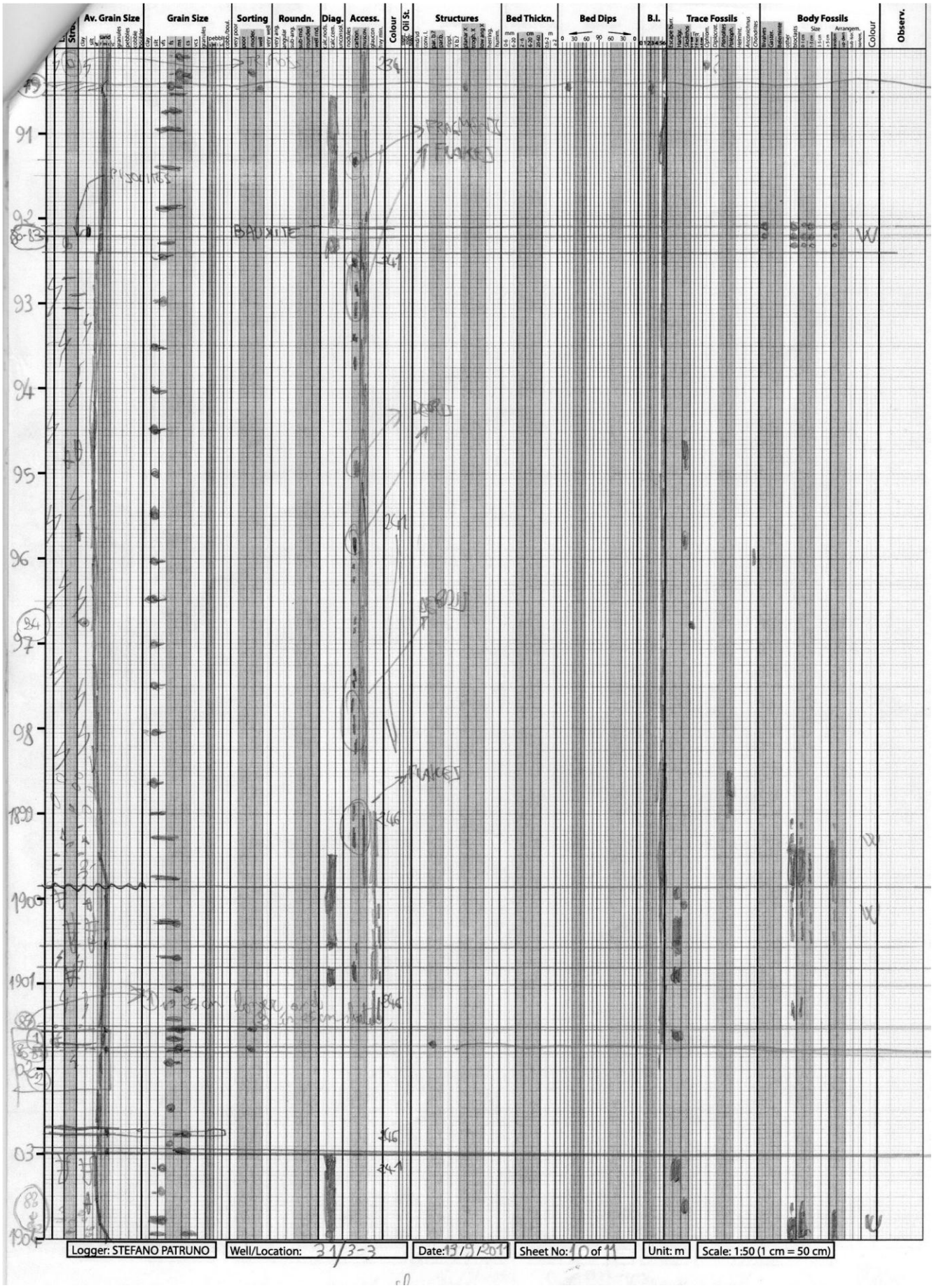
Av. Grain Size
Grain Size
Sorting
Roundn.
Diag.
Access.
Colour
Oil St.
Structures
Bed Thickn.
Bed Dips
B.I.
Trace Fossils
Body Fossils
Observ.
BAUXITE
Logger: STEFANO PATRUNO
Well/Location: 31/3-3
Date: 13/5/2011
Sheet No: 10 of 11
Unit: m
Scale: 1:50 (1 cm = 50 cm)

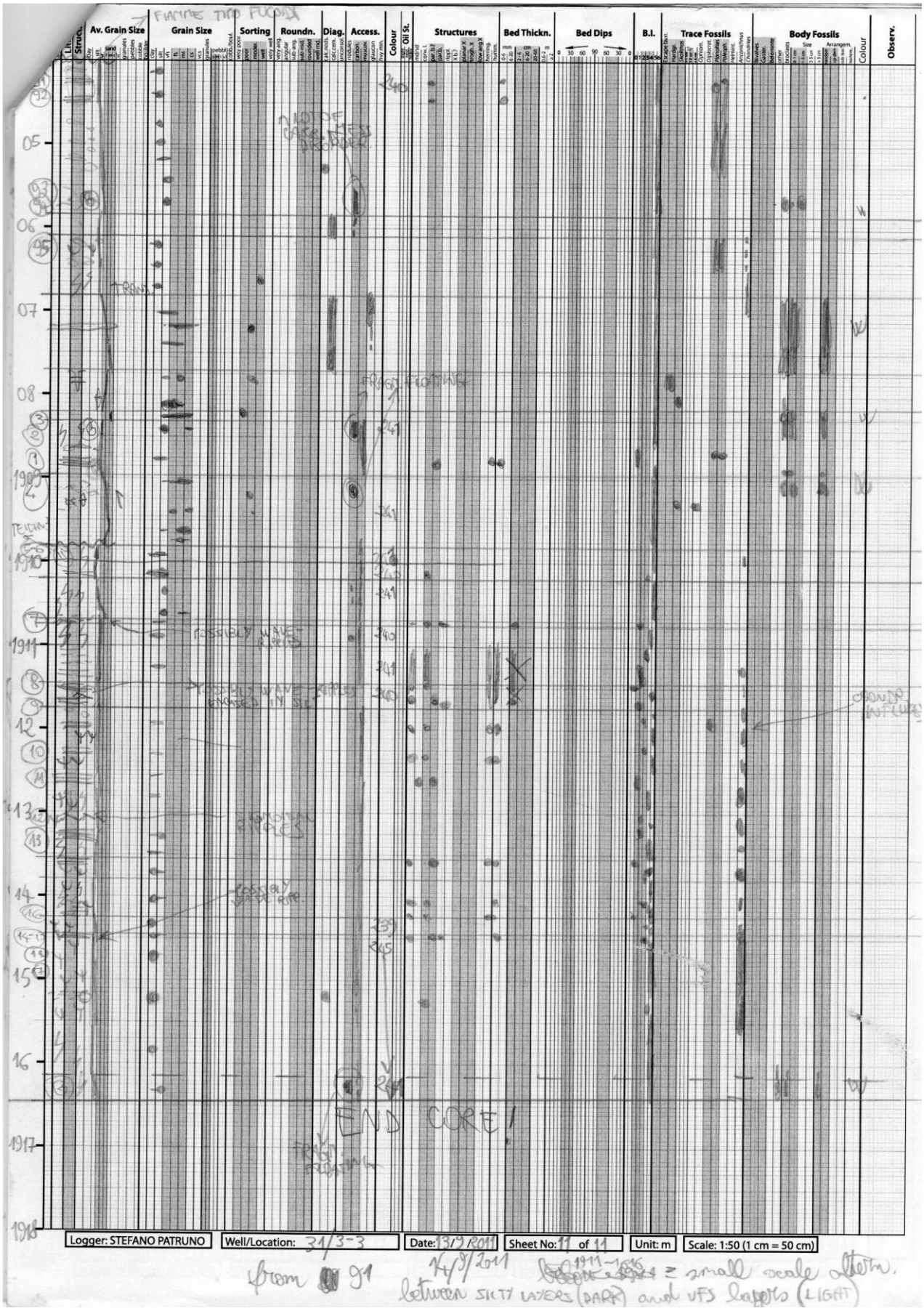
Lith.
Struc.
Av. Grain Size
Grain Size
Sorting
Roundn.
Diag.
Access.
Colour
Oil St.
Structures
Bed Thickn.
Bed Dips
B.I.
Trace Fossils
Body Fossils
Observ.
FRATTURE TIPO FUCOIDI
END CORE!
Logger: STEFANO PATRUNO
Well/Location: 21/3-3
Date: 13/9/2011
Sheet No: 11 of 11
Unit: m
Scale: 1:50 (1 cm = 50 cm)
14/9/2011
between SILTY LAYERS (DARK) and VFS laygers (LIGHT)

31/5-3

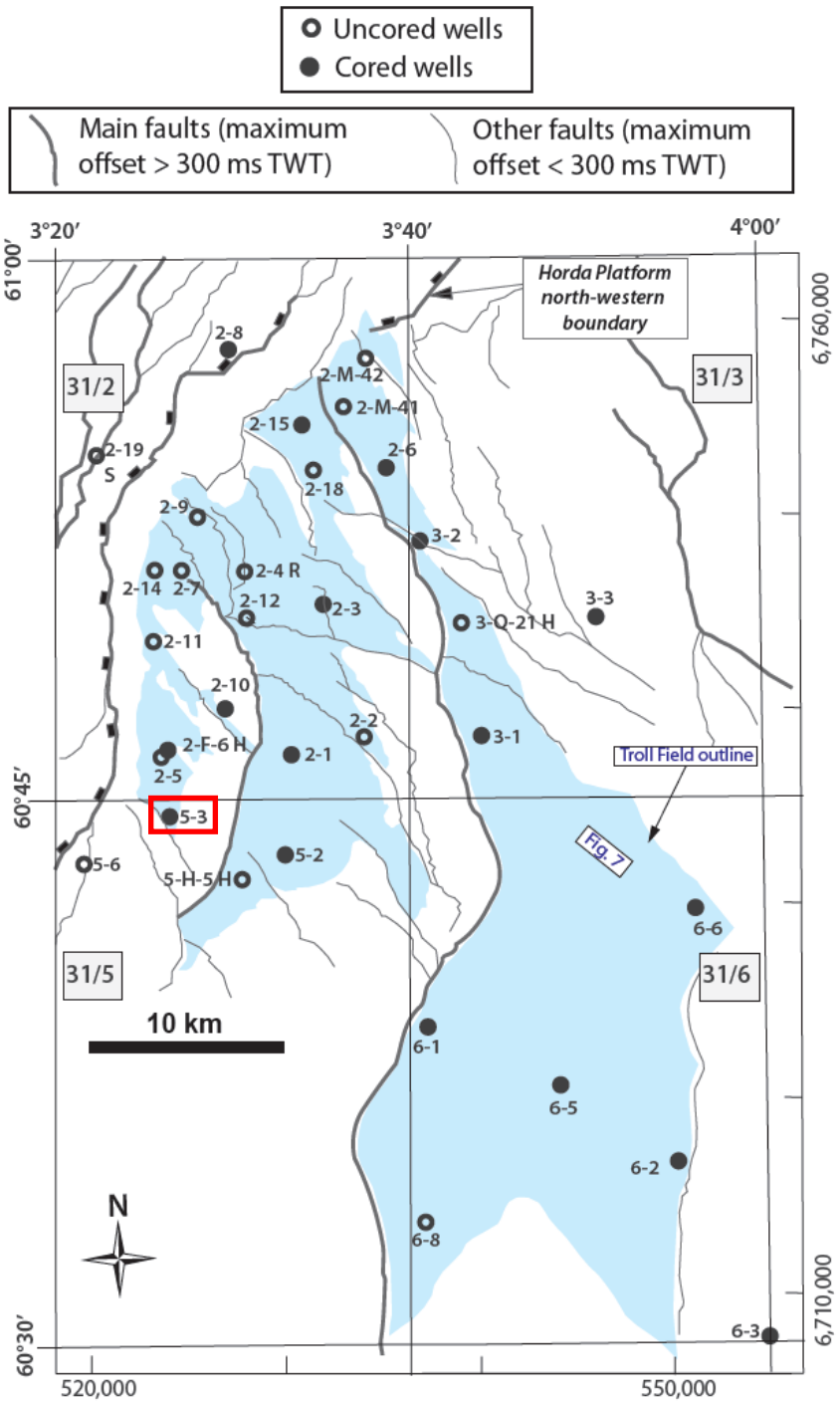
Uncored wells
Cored wells
Main faults (maximum offset > 300 ms TWT)
Other faults (maximum offset < 300 ms TWT)
3°20′
3°40′
4°00′
61°00′
60°45′
60°30′
6,760,000
6,710,000
520,000
550,000
Horda Platform north-western boundary
31/2
31/3
31/5
31/6
2-8
2-M-42
2-M-41
2-15
2-19 S
2-6
2-18
2-9
3-2
2-14
2-7
2-4 R
2-12
2-3
3-3
3-Q-21 H
2-11
2-10
2-2
3-1
2-F-6 H
2-1
2-5
5-3
5-6
5-H-5 H
5-2
Troll Field outline
Fig. 7
6-6
10 km
6-1
6-5
6-2
6-8
6-3
N

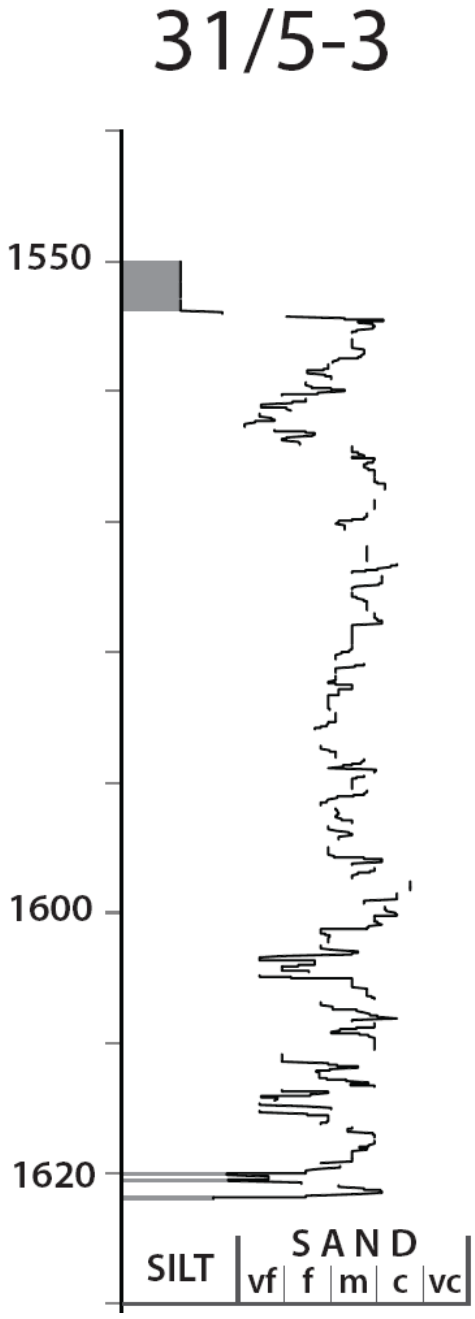
31/5-3
1550
1600
1620
SILT
SAND
vf
f
m
c
vc

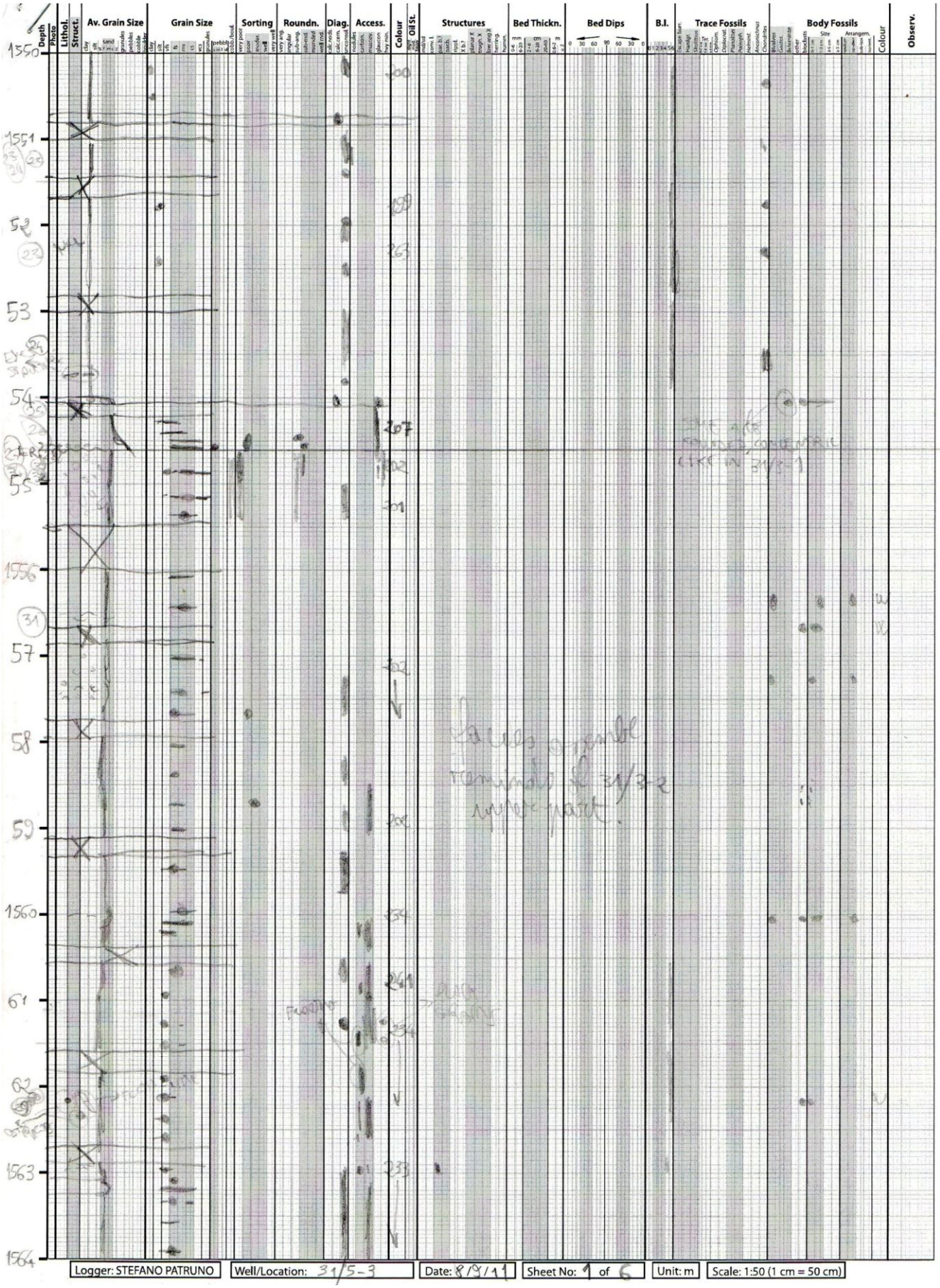
Depth
Lithol.
Struct.
Av. Grain Size
Grain Size
Sorting
Roundn.
Diag.
Access.
Colour
Oil St.
Structures
Bed Thickn.
Bed Dips
B.I.
Trace Fossils
Body Fossils
Observ.
1550
1551
52
53
54
55
1556
57
58
59
1560
61
62
1563
1564
Logger: STEFANO PATRUNO
Well/Location: 31/5-3
Date: 8/9/11
Sheet No: 1 of 6
Unit: m
Scale: 1:50 (1 cm = 50 cm)

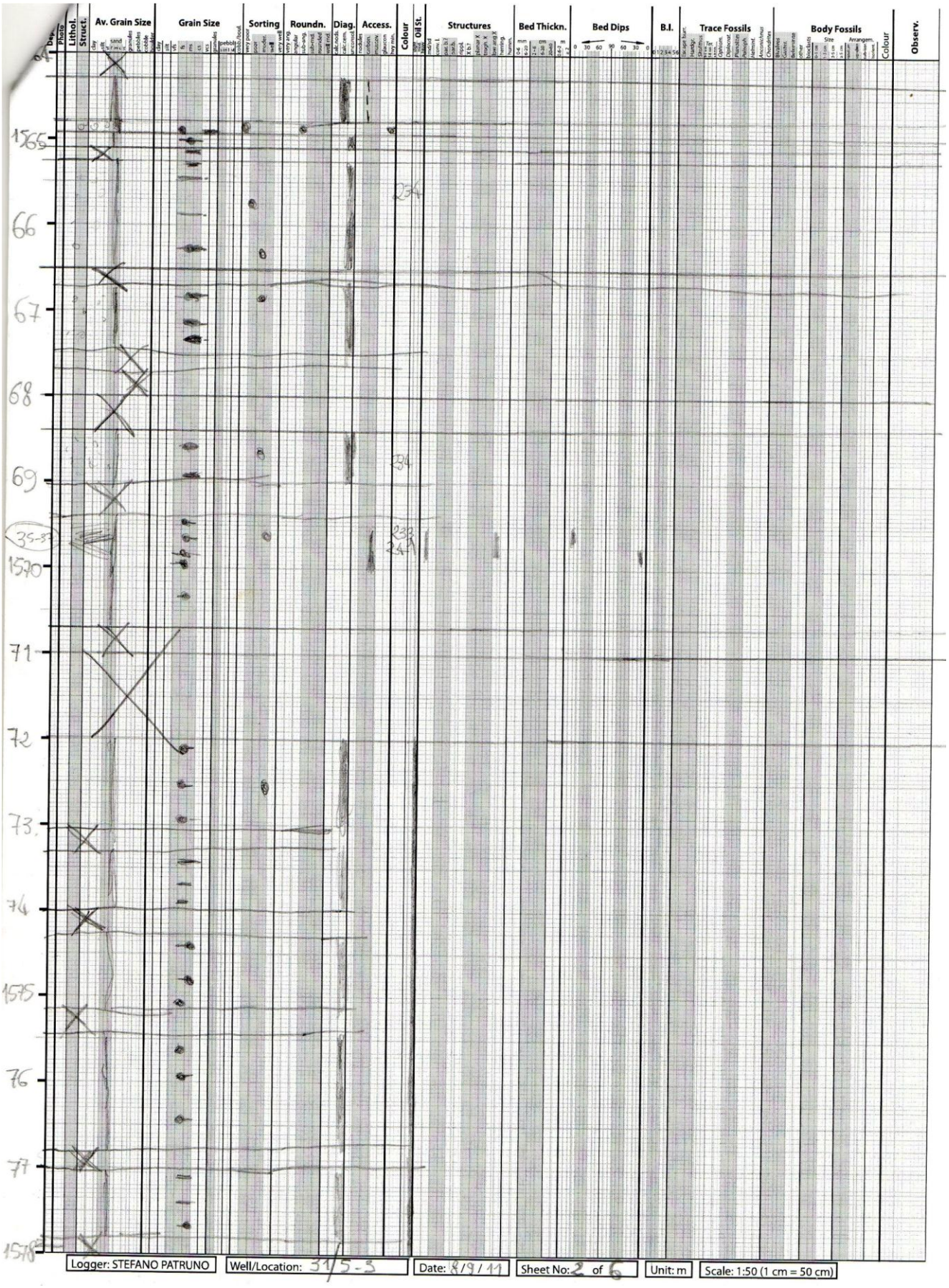
Depth
Photo
Lithol.
Struct.
Av. Grain Size
Grain Size
Sorting
Roundn.
Diag.
Access.
Colour
Oil St.
Structures
Bed Thickn.
Bed Dips
B.I.
Trace Fossils
Body Fossils
Observ.
1565
66
67
68
69
35-37
1570
71
72
73
74
1575
76
77
1578
234
34
232
24
Logger: STEFANO PATRUNO
Well/Location: 31/5-3
Date: 8/9/11
Sheet No: 2 of 6
Unit: m
Scale: 1:50 (1 cm = 50 cm)

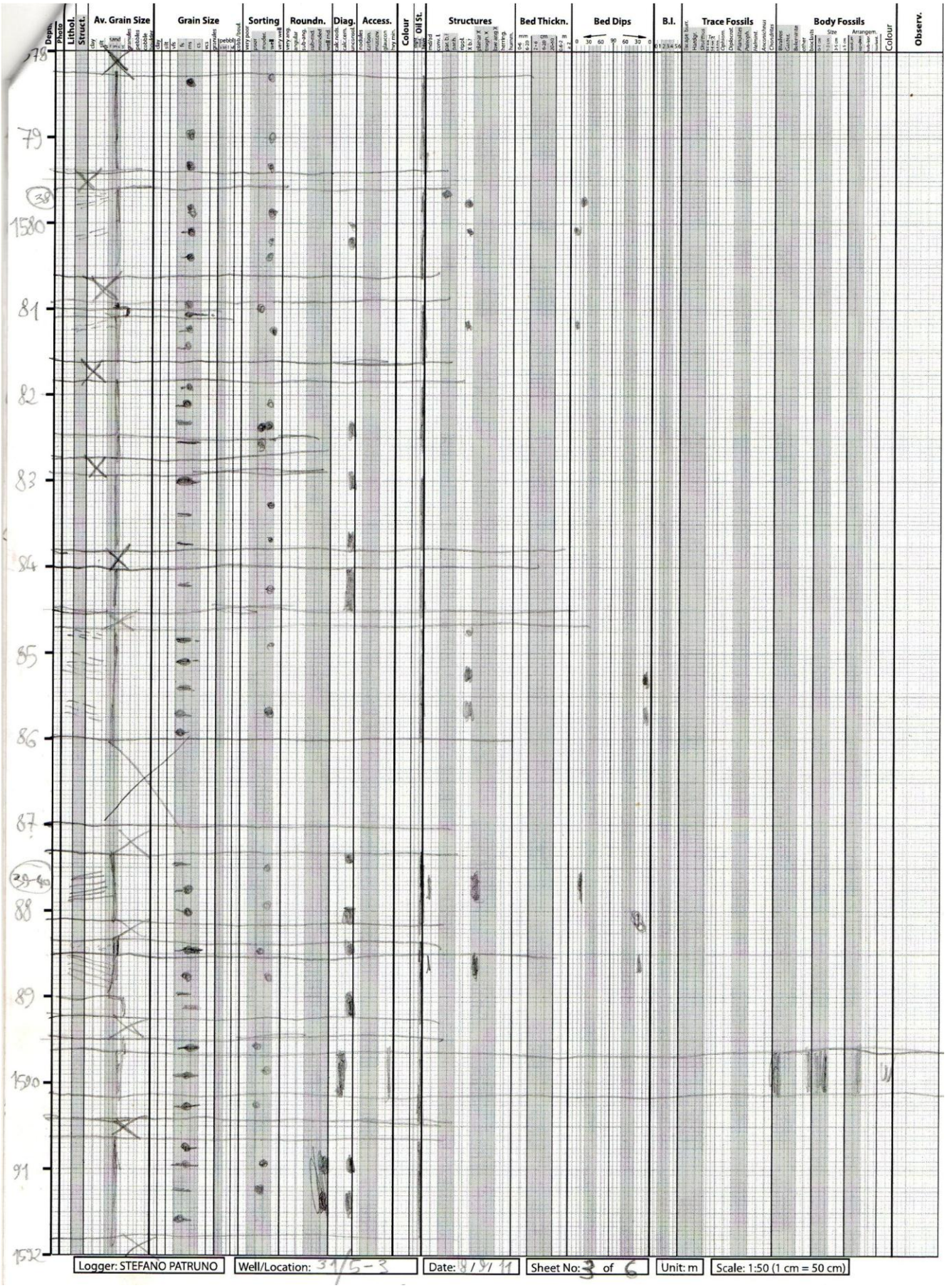
Depth
Photo
Lithol.
Struct.
Av. Grain Size
Grain Size
Sorting
Roundn.
Diag.
Access.
Colour
Oil St.
Structures
Bed Thickn.
Bed Dips
B.I.
Trace Fossils
Body Fossils
Observ.
78
79
38
1580
81
82
83
84
85
86
87
39-40
88
89
1590
91
1592
Logger: STEFANO PATRUNO
Well/Location: 31/5-3
Date: 8 / 9 / 11
Sheet No: 3 of 6
Unit: m
Scale: 1:50 (1 cm = 50 cm)

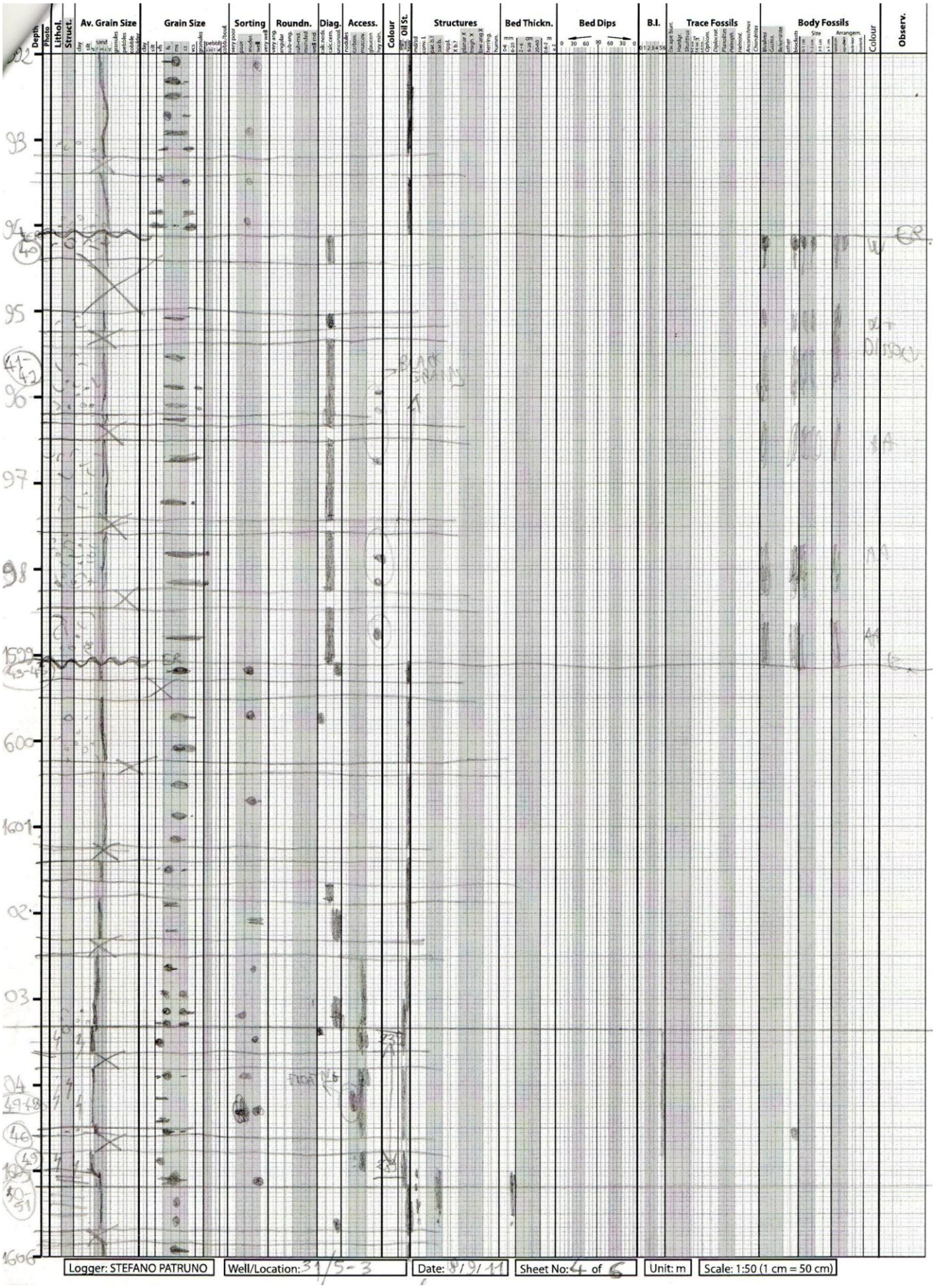
Depth
Photo
Lithol.
Struct.
Av. Grain Size
Grain Size
Sorting
Roundn.
Diag.
Access.
Colour
Oil St.
Structures
Bed Thickn.
Bed Dips
B.I.
Trace Fossils
Body Fossils
Observ.
Logger: STEFANO PATRUNO
Well/Location: 31/5-3
Date: 8/9/11
Sheet No: 4 of 6
Unit: m
Scale: 1:50 (1 cm = 50 cm)

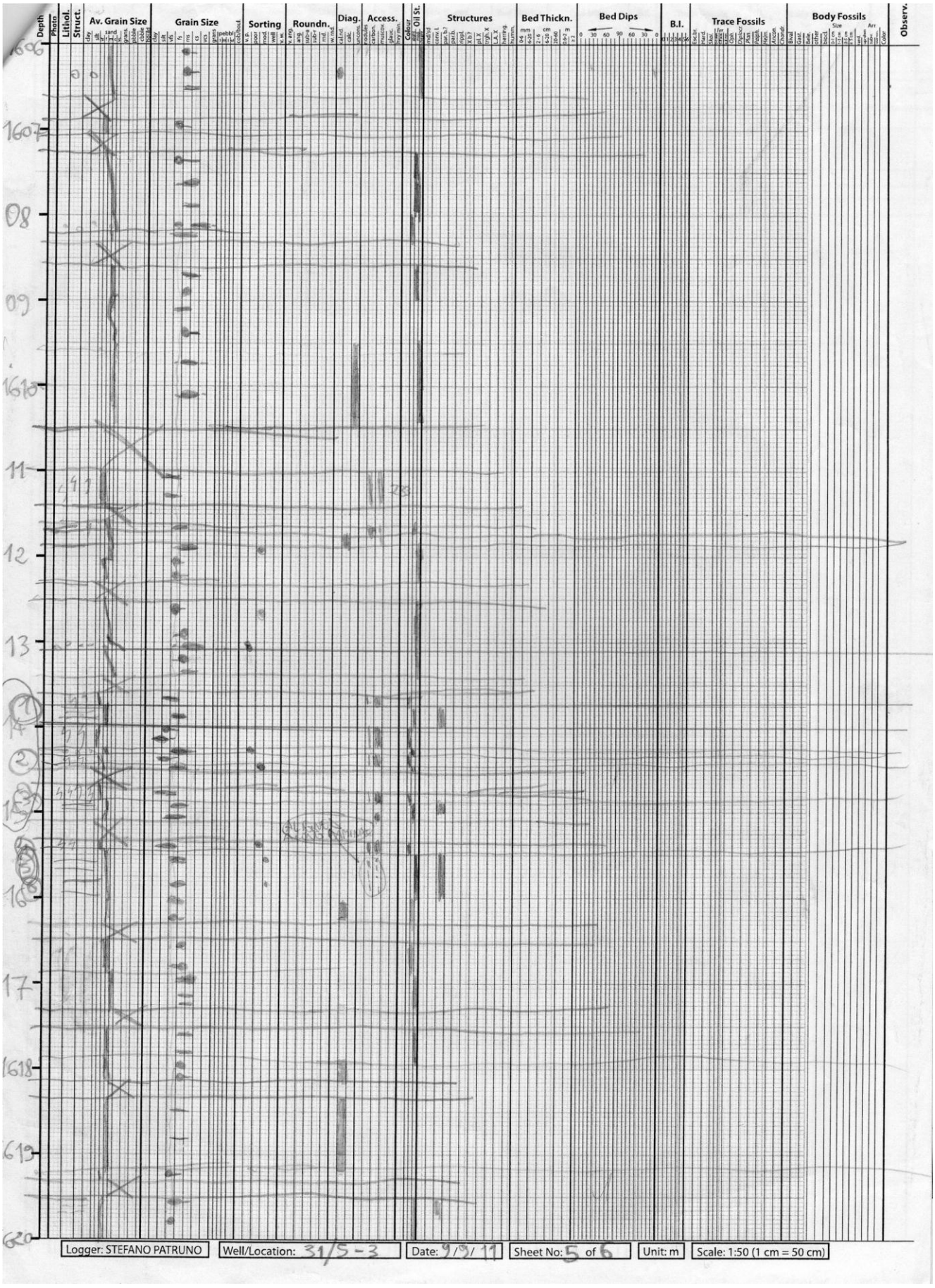
Depth
Photo
Lithol.
Struct.
Av. Grain Size
Grain Size
Sorting
Roundn.
Diag.
Access.
Colour
Oil St.
Structures
Bed Thickn.
Bed Dips
B.I.
Trace Fossils
Body Fossils
Observ.
Logger: STEFANO PATRUNO
Well/Location: 31/5-3
Date: 9/9/11
Sheet No: 5 of 6
Unit: m
Scale: 1:50 (1 cm = 50 cm)

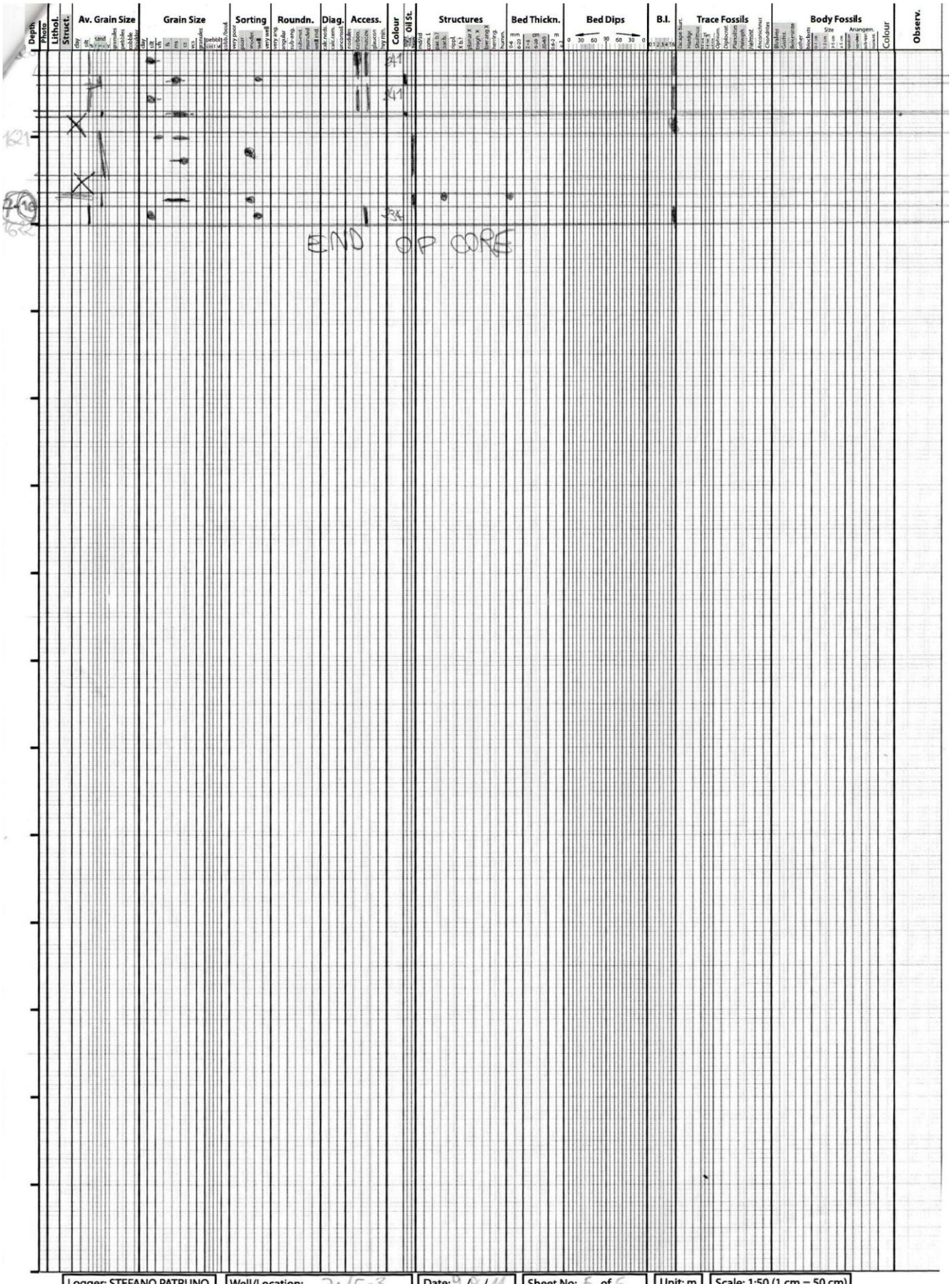
Depth
Photo
Lithol.
Struct.
Av. Grain Size
Grain Size
Sorting
Roundn.
Diag.
Access.
Colour
Oil St.
Structures
Bed Thickn.
Bed Dips
B.I.
Trace Fossils
Body Fossils
Observ.
END OF CORE
Logger: STEFANO PATRUNO
Well/Location: 24/5-3
Date: 4 / 9 / 11
Sheet No: 6 of 6
Unit: m
Scale: 1:50 (1 cm = 50 cm)

31/6-1

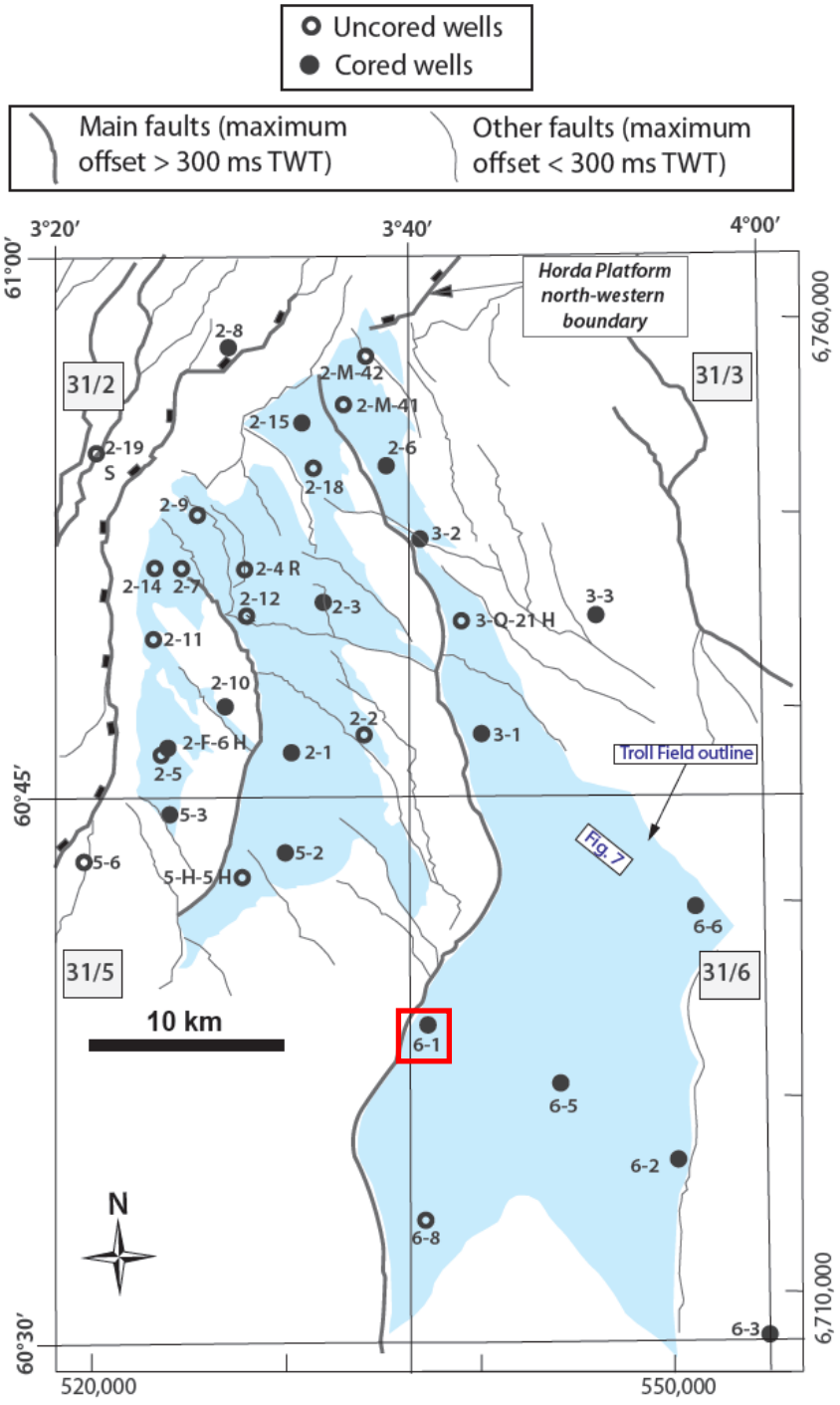
Uncored wells
Cored wells
Main faults (maximum offset > 300 ms TWT)
Other faults (maximum offset < 300 ms TWT)
3°20′
3°40′
4°00′
61°00′
60°45′
60°30′
6,760,000
6,710,000
520,000
550,000
Horda Platform north-western boundary
31/2
31/3
31/5
31/6
Troll Field outline
Fig. 7
10 km
N
2-8
2-M-42
2-M-41
2-15
2-19 S
2-6
2-18
2-9
3-2
2-14
2-7
2-4 R
2-12
2-3
3-Q-21 H
3-3
2-11
2-10
2-2
3-1
2-F-6 H
2-5
2-1
5-3
5-6
5-H-5 H
5-2
6-6
6-1
6-5
6-2
6-8
6-3

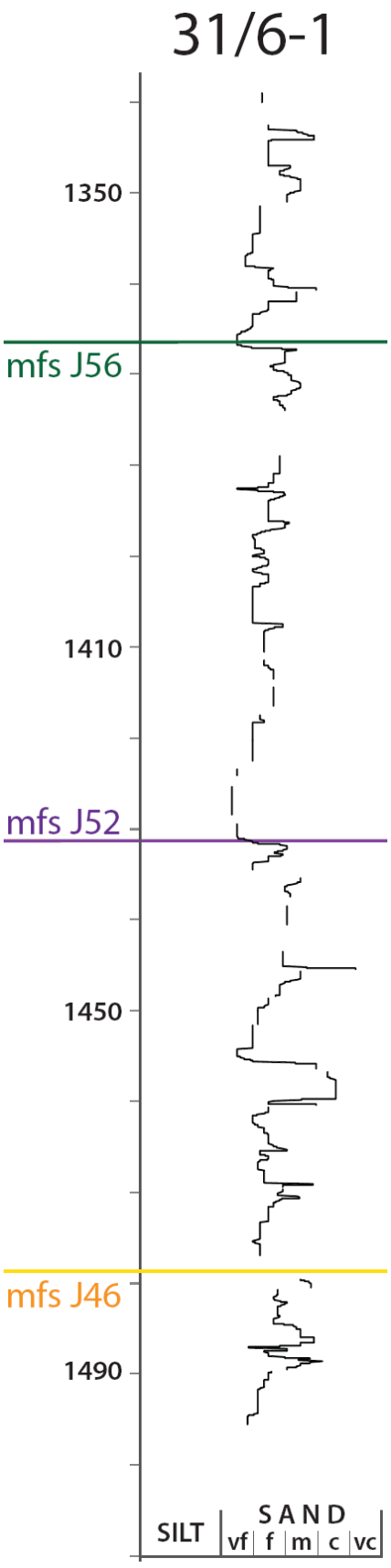
31/6-1
1350
mfs J56
1410
mfs J52
1450
mfs J46
1490
SILT
SAND
vf
f
m
c
vc

Norsk Hydro

Note: Lithological interpretation based on spot sample descriptions every meter due to coring with fibre glass inner barrel.

Well no.	Core report	Core no's
31/6-1		1

Interval	Area	Cut	Date
1341 - 1349 m	Norwegian North Sea	1341 - 1349 m	29.7.83.
Scale	**Well R.K.B.**	**Recovery**	**Geologist**
1:50	25 m	0	Midtkandal/Lømo

Depth scale	Re-covery	Lithological column	Depths	Lithological descriptions	Shows
1342				Cuttings sample:	
1343				**Clyst,** gy blk, sft - firm, slky, micro-mic, tr carb, calc.	
1344		No recovery		Tr **Lst,** v lt gy, pink gy, mod-red brn, mod hd - hd, blky, arg, micro-xln. tr **Calcite.**	
1345				tr **Dol,** pale - dk yel brn, dusky yel brn, blky, arg, micro-xln.	
1346				rr **Sd,** clr - fros Qtz, crs - v crs, subrnd - subang.	
1347				rr **Sst,** clr Qtz, vf - f, mod hd, fri, subrnd, calc cmt, abn glau, well srtd, poor vis por.	
1348				**Slst,** clr gy, mod hd, blky, micro-mic, rr carb, calc.	
1349			1349 m	tr **Pyr** mod.	
				rr **Carb mat,** blk, brn blk, firm, blky, occ slty.	

Well	Core report	Core no's
31/6 - 1	1 of 1	1

Norsk Hydro

Note: Lithological interpretation based on spot sample descriptions evert meter (-) due to coring with fibre glass inner barrel.

Well no.	Core report	Core no's
31/6-1		2

Interval	Area	Cut	Date
1350 - 1352.5 m	Norwegian North Sea	1350 - 1352.5 m	29.7.83.
Scale	**Well R.K.B.**	**Recovery**	**Geologist**
1:25	25 m	1350 - 1351 m (40%)	Rønning/Godvik

Depth scale	Re-covery	Lithological column	Depths	Lithological descriptions	Shows
1351			1351 m	**Sst:** m dk gy - dk grn, with wh specs, f - m, tr crs, v hd, subrnd - rnd, v glau as f crs nods, (rnd), v calc cmt, tr pyr, rr wood frags, mod srtd, no vis por.	No shows.
1352		No recovery	1352.5 m		

Well	Core report	Core no's
31/6 - 1	1 of 1	2

Norsk Hydro

Note: Lithological interretation based on spot sample deseriptions every meter (-) due to coring with fibre glass inner barrel.

Well no.	Core report	Core no's
31/6-1		3

Interval	Area	Cut	Date
1352.5 - 1361.5 m	Norwegian North Sea	1352.5 - 1361.5 m	30.7.83.
Scale 1:50	**Well R.K.B.** 25 m	**Recovery** 1352.5 - 1361.0 m (89%)	**Geologist** Rønning/Godvik

Depth scale	Re-covery	Lithological column	Depths	Lithological descriptions	Shows
1352.5		M	1352.5 m	**Sst:** m dk gy - dk grn, vf - m hd, subrnd, v calc cmt, v glau, in pt v pyr, tr mic, mod srtd, no vis por.	No shows.
1353				**Sst:** vf, a/a.	
1354		M		**Sst:** clr Qtz, vf - f, v fri - lse, subang, v sl calc cmt, glau, tr mic, sl pyr, well srtd, gd por.	
1355		M			
1356		M		**Sst:** vf, a/a.	
1357		M			
1358		M		**Sst:** pred m, a/a.	
1359		M			
1360		M		**Sst:** f - m, a/a.	
1361		Not recovered	1361.0 m	**Sst:** f, a/a.	
1362					

Well	Core report	Core no's
36/6 - 1	1 of 1	3

Norsk Hydro

Note: Lithological interpretation based on spot sample descriptions evert meter (-) due to coring with fibre glass inner barrel.

Well no.	Core report	Core no's
31/6-1		4

Interval	Area	Cut	Date
1361.5 - 1371 m	Norwegian North Sea	1361.5 - 1371 m	31.7.83.
Scale	**Well R.K.B.**	**Recovery**	**Geologist**
1:50	25 m	1361 - 1370.75 m (97%)	Godvik/Rønning

Depth scale	Re-covery	Lithological column	Depths	Lithological descriptions	Shows
1361.5			1361.5 m	**Clyst:** gy blk - blk, v hd, blky in pt sl subfis, tr micro-mic, v calc, brecciated, calc vns.	No shows.
1362				**Sst:** m dk gy - olv gy, clr - milky Qtz, vf - f, pred f, lse - fri, subang - subrnd, tr calc cmt, mica - mica, tr pyr, well srtd, gd vis por.	
1363					
1364				**Sst:** a/a, v mica, sl calc.	
1365				**Sst:** a/a, mica, calc.	
1366				**Sst:** a/a, v mica.	
1367				**Sst:** a/a, w/shell frags, calc tubes.	
1368					
1369				**Sst:** a/a, pred vf, inpt v hd, v calc cmt, no vis por.	
1370			1370.10 m	**Sst:** a/a, lse.	
1371		Not recovered	1370.75 m	**Sst:** a/a, m, fri - occ firm, sl silic cmt, v micro pyr, well srtd, fair - gd por.	

Well	Core report	Core no's
31/6 - 1	1 of 1	4

Norsk Hydro

Note: Lithological interpretation based on spot sample descriptions every meter (-) due to coring with fibre glass inner barrel.

Well no.	Core report	Core no's
31/6-1		5

Interval	Area	Cut	Date
1371 - 13819 m	Norwegian North Sea	1371 - 1389 m	31.7.83.
Scale	**Well R.K.B.**	**Recovery**	**Geologist**
1:50	25 m	1371 - 1384.10 m (72,7%)	Godvik/Rønning

Depth scale	Recovery	Lithological column	Depths	Lithological descriptions	Shows
			1371 m	**Sst:** m dk gy - elv gy, clr - milky Qtz g, m, subang - subrnd, fri, sl silic cmt, mica, micro-pyr, well srtd, pair - gd vis por.	No shows.
1372			Caps waxed	**Sst:** m dk gy - dk gy, clr - milky Qtz g, vf - f, pud vf, subang - subrnd, hd - v hd, v calc cmt, mica, well srtd, no vis por.	
1373				**Sst:** m gy - m dk gy, clr - milky Qtz g, vf - f, pud f, subang - subrnd, brn - fri, tr calc cmt, mica - v mica, well srtd, gd vis por.	
1374				**Sst:** m dk gy, vf, no calc cmt, v mica, tr glau, poor vis por, else a/a.	
1375			Caps waxed		
1376					
1377				**Sst:** vf - f, occ m, pud f, fair vis por, else a/a.	
1378			Caps waxed	**Sst:** m gy - m dk gy, clr - milky Qtz g, f - m, occ crs, subang - subrnd, pud subrnd, lse - fri tr, mica, tr Glau, mod srtd, gd vis por.	
1379				**Sst:** vf - f, pud f, tr foss frags, well srtd, else a/a.	
1380			Caps waxed	**St:** f - m, subang - subrnd, rr Glau, else a/a.	
1381			1381 m	**Sst:** m, tr f, tr crs, tr Glau, else a/a.	

Norsk Hydro

Note: Lithological interpretation based on spot sample descriptions every meter (-) due to coring with fibre glass inner barrel.

Well no.	Core report	Core no's
31/6-1		5

Interval	Area	Cut	Date
1381 - 1389 m	Norwegian North Sea	1371 - 1389 m	31.7.83.
Scale	**Well R.K.B.**	**Recovery**	**Geologist**
1:50	25 m	1371 -1384.10 m (72,7%)	Godvik/Rønning

Depth scale	Re-covery	Lithological column	Depths	Lithological descriptions	Shows
1382		C M M C	1381 m	**Sst:** m gy - m dk gy, clr - milky Qtz g, m, tr f, tr cs, subang - subrnd, lse - fri, tr mica, tr Glau, well srtd, gd vis por.	No shows.
1383		M C M		**Sst:** m gy - m dk gy, clr - milky Wtz g, ~~vf - f,~~ subang - subrnd, v hd, v calc cmt, mica, well srtd, no vis por.	
1384		M	Caps waxed 1384.10 m	**Sst:** m gy - m dk gy, clr - milky Qtz g, f - m, subang - subrnd, lse - fri, mica, tr Glau, well srtd, gd vis por.	
1385				**Sst:** f - m pudf, v mica, else a/a.	
1386					
1387					
1388					
1389			1389 m		

Well	Core report	Core no's
31/6 - 1	2 of 2	5

Norsk Hydro

Note: Lithological interpretation based on spot sample descriptions evert meter (-) due to coring with fibre glass inner barrel.

Well no.	Core report	Core no's
31/6-1		6

Interval	Area	Cut	Date
1389 - 1399 m	Norwegian North Sea	1389 - 1407.5 m	1.8.83.
Scale	**Well R.K.B.**	**Recovery**	**Geologist**
1:50	25 m	1389 - 1407.3 m (99%)	Rønning/Godvik

Depth scale	Re-covery	Lithological column	Depths	Lithological descriptions	Shows
1389		M, C			
1390		C, M		**Sst:** m - dk gy, f, lse - fri, subang, sl silic cmt and sl calc cmt, mica, tr pyr, rr glau, tr carb tr shell frags, well srtd, gd vis por.	No show.
1391		M, C			
1392		M		**Sst:** a/a, vf - m pred f, fri.	Tr weak pl yel wh flu, weak fast strmg wh flu cut, wh flu resd.
1393		M		**Sst:** a/a, pred m, fri - lse.	no show.
1394		M		**Sst:** a/a, vf - m, fri, sl calc cmt.	tr weak pl yel wh flu, weak fast strmg wh flu cut, wh flu resd.
1395		M		**Sst:** a/a, hd, v calc cmt, no vis por.	No show.
1396		M, C		**Sst:** a/a, f, fri.	
1397		M		**Sst:** a/a, f - m.	
1398		M		**Sst:** a/a, f - m, lse.	
1399				**Sst:** a/a, fri.	

Well	Core report	Core no's
30/6 - 1	1 of 2	6

Norsk Hydro

Note: Lithological interpretation based on spot sample descriptions every meter (-) due to coring with fibre glass inner barrel.

Well no.	Core report	Core no's
31/6-1		6

Interval	Area	Cut	Date
1399 - 1407.5 m	Norwegian North Sea	1389 - 1407.5 m	1.8.83.
Scale	**Well R.K.B.**	**Recovery**	**Geologist**
1:50	25 m	1389 - 1407.3 m (99%)	Rønning/Godvik

Depth scale	Re-covery	Lithological column	Depths	Lithological descriptions	Shows
1399		M			
1400		C M		**Sst:** m - dk gy, vf - f, lse - fri, subang, tr slic cmt, tr calc cmt, mica, rr glau, tr pyr, sl carb, tr shell frags, well srtd, gd vis por.	No show.
1401		M		**Sst:** a/a, fri - mod hd, calc cmt v mica.	
1402		M		**Sst:** a/a, fri.	
1403		M C		**Sst:** a/a, f - m.	No flu, v slow weak blu wh flu cut, wh flu resd.
1404		M		**Sst:** a/a, f.	No show.
1405		M C			
1406		M		**Sst:** a/a, vf - f, fri, calc cmt, lam.	
1407		M		**Sst:** a/a, fri - mod hd, calc cmt.	
		Not recovered	1407.3 m		

Well	Core report	Core no's
31/6 - 1	2 of 2	6

Norsk Hydro

Note: Lithological interpretation based on spot sample descriptions evert meter (-) due to coring with fibre glass inner barrel.

Well no.	Core report	Core no's
31/6-1		7

Interval	Area	Cut	Date
1407.5 - 1417 m	Norwegian North Se	1407.5 - 1425.5 m	2.8.83.
Scale 1:50	**Well R.K.B.** 25 m	**Recovery** 1407.5 - 1424.2 m (93%)	**Geologist** Rønning/Godvik

Depth scale	Re-covery	Lithological column	Depths	Lithological descriptions	Shows
1408		M C	1407.5 m	**Sst:** m - dk gy, clr Qtz, f - m, fri - firm, subang - subrnd, sl silic and calc cmt, mica, tr pyr, sl carb, well srtd, gd por.	No show.
1409		M			Tr weak pl yel flu weak fast strng, wh flu cut, pl yel wh flu resd.
1410		M		**Sst:** a/a, m, hd, v calc cmt, no vis por.	No show.
1411		M C		**Sst:** a/a, f - m, fri, silic cmt.	Tr weak pl yel flu, weak fast strmg wh flu cut, pl yel wh flu resd.
1412		M C		**Sst:** dk gy - gy blk, vf - f, tr m, mod hd - hd, calc cmt, v carb, tr plnt rem, mica, sl pyr no vis por.	No show.
1413		M		**Sst:** m - dk gy, clr Qtz, f - m, prod m, fri, sl calc cmt, v mica, com shell frags, well srtd, fair - gd vis por.	Tr, v weak pl yel flu, v weak fast strmg bl wh flu cut, yel wh flu resd.
1414		M C		**Sst:** a/a, f, lse.	No show.
1415		M			
1416		M C			
1417		M		**Sst:** a/a, fri - occ mod hd, sl silic - calc cmt.	

Well	Core report	Core no's
31/6 - 1	1 of 2	7

Norsk Hydro

Note: Lithological interpretation based on spot sample descriptions every meter (-) due to coring with fibre glass inner barrel.

Well no.	Core report	Core no's
31/6-1		7

Interval	Area	Cut	Date
1417 - 1425.5 m	Norwegian North Sea	1407.5 - 1425.5 m	2.8.83.
Scale	**Well R.K.B.**	**Recovery**	**Geologist**
1:50	25 m	1407.5 - 1424.2 m (93%)	Rønning/Godvik

Depth scale	Recovery	Lithological column	Depths	Lithological descriptions	Shows
1417		M C	NO CORE AVAL.	**Sst:** m - dk gy, clr Qtz, vf - f, fri - firm, subang - subrnd, sl silic + calc cmt, mica, tr pyr, sl carb, well srtd, gd vis por.	No shows.
1418		C M		**Sst:** dk gy - gy blk, vf, fri - firm, subang, sl calc cmt, slty, arg, mica, carb, tr pyr, poor - mod srtd, poor vis por.	
1419		C M			
1420		C M			
1421		M		**Sst:** a/a, hd, v calc cmt.	
1422		C M M		**Sst:** a/a, fri - firm.	
1423		C M	NO CORE AV.		
1424		M	1424.2 m		
1425		Not recovered			
1426					

Well	Core report	Core no's
31/6 - 1	2 of 2	7

Norsk Hydro

Note: Lithological interpretation based on spot sample descriptions every meter (-) due to coring with fibre glass inner barrel.

Well no.	Core report	Core no's
31/6-1		8

Interval	Area	Cut	Date
1425.5 - 1435 m	Norwegian North Sea	1425.5 - 1443.5 m	3.8.83.
Scale	**Well R.K.B.**	**Recovery**	**Geologist**
1:50	25 m	1425.5 - 1440.5 m (83.3%)	Godvik/Rønning

Depth scale	Re-covery	Lithological column	Depths	Lithological descriptions	Shows
1425.5			1425.5 m	**Sst:** dk gy - gy blk, clr - milky Qtz g, vf, subang, fri - firm, sl calc cmt, slty, sl arg, v mica, tr carb, poor - mod srtd, poor vis por.	Non - rr v weak pale yel flu, weak slow - fast strmg wh flu cmt, bright yel wh flu resd, no vis resd.
1426					
1427				**Sst:** tr shell frags, else a/a.	
1428					
1429				**Slst:** dk gy - gy blk, firm, v mica, tr carb, grdg vf **Sst,** sl arg, non calc.	
1430					
1431				**Sst:** m gy - m dk gy, clr - milky Qtz g, vf, subang, hd, v calc cmt, tr mica, rr Pyr, well srtd, no vis por.	No show.
1432				**Sst:** m gy - olv gy, clr - milky Qtz g, vf - m pred f, subang - subrnd, fri, sl calc cmt, tr mica, rr pyr, mod srtd, gd vis por.	Non - rr weak pale yel flu, weak slow - fast strmg wh flu cut, pale yel wh flu resd, no vis resd.
1433				**Sst:** m dk gy - olv gy, clr - milky Qtz g, vf - f, subang - subrnd, fri, tr mica, tr blk specs, tr shell frags, well srtd, gd vis por.	
1434				**Sst:** vf, fri - firm, sl calc and sl silic cmt, else a/a.	Bright yel wh flu resd, else a/a.
1435					

Well	Core report	Core no's
31/6 - 1	1 of 2	8

Norsk Hydro

Note: Lithological interpretation based on spot sample descriptions every meter (-) due to coring with fibre glass inner barrel.

Well no.	Core report	Core no's
31/6-1		8

Interval	Area	Cut	Date
1435 - 1443.5 m	Norwegian North Sea	1425.5 - 1443.5 m	3.8.83.
Scale 1:50	**Well R.K.B.** 25 m	**Recovery** 1425.5 - 1440.5 m (83.3%)	**Geologist** Godvik/Rønning

Depth scale	Re-covery	Lithological column	Depths	Lithological descriptions	Shows
1436		M, M	NO CORE AVAIL.	**Sst:** m dk gy - olv gy, clr milky, occ smoky Qtz g, f - m, subang - subrnd, fri - firm, sl calc end silic cmt, tr mica, tr blk specs, tr shell frags, well srtd, gd vis por.	Non - rr weak pale yel flu, weak slow - fast strmg wh flu cut, bright yel wh flu resd, no vis resd.
1437		M			
1438		M	NO CORE AVAIL.	**Sst:** m gy - olv gy, vf - m, pred m, tr crs, mod srtd, else a/a.	No show.
1439		M			
1440		M	1440.5 m		
1441		Not recovered			
1442					
1443			1443.5 m		

Well	Core report	Core no's
31/6 - 1	2 of 2	8

Norsk Hydro

Note: Lithological interpretation based on spot sample descriptions every meter (-) due to coring with fibre glass inner barrel.

Well no.	Core report	Core no's
31/6-1		9

Interval	Area	Cut	Date
1443.5 - 1453 m	Norwegian North Sea	1443.5 - 1461.5 m	4.8.83.
Scale 1:50	**Well R.K.B:** 25 m	**Recovery** 1443.5 - 1461.5 m (100%)	**Geologist** Rønning/Godvik

Depth scale	Recovery	Lithological column	Depths	Lithological descriptions	Shows
1443.5			1443.5 m		
1444		M C		**Sst:** dk gy, clr Qtz, f - m hd, subang - subrnd, v calc cmt, tr mica, Ammonite shell, well srtd, no vis por.	No show.
1445		M C		**Sst:** m - m dk gy, clr Qtz, pred m, f - crs, fri, subang - subrnd, sl silic + calc cmt, mica, carb, tr pyr, well srtd, fair - gd por.	Distinct HC odour, no flu, no cut.
1446		M M			
1447		M			
1448		M M C		**Sst:** dk gy, clr Qtz, f - m, hd, subang - subrnd, v calc cmt, tr mica well srtd, no vis por.	No show.
1449		M C M		**Sst:** m - m dk gy, clr Qtz, f, fri, subang, sl silic cmt, mica, rr pyr, sl carb, shell frags, well srtd, gd vis por.	Weak HC odour, no flu, no cut.
1450		M C			
1451		M M		**Sst:** a/a, bcm fri - firm, sl calc cmt, v mica.	Distinct HC odour, no flu, weak fast strmg bl wh flu cut, bl wh flu resd.
1452		M C M C C M		**Sst:** dk gy, vf, firm, subang, silic + calc cmt, mica, carb, tr pyr, arg lam, mod srtd, pr, fair vis por.	Weak HC odour no flu, no cut.
1453		M		**Slst:** dk gy - brn blk, mod hd, vf sdy grdg **Sst,** arg, mica, carb, no vis por.	

Well	Core report	Core no's
31/6 - 1	1 of 2	9

Norsk Hydro

Note: Lithological interpretation based on spot sample descriptions every meter (-) due to coring with fibre glass inner barrel.

Well no.	Core report	Core no's
31/6-1		9

Interval	Area	Cut	Date
1453 - 1461.5 m	Norwegian North Sea	1443.5 - 1461.5 m	4.8.83.
Scale	**Well R.K.B.**	**Recovery**	**Geologist**
1:50	25 m	1443.5 - 1461.5 m (100%)	Godvik/Rønning

Depth scale	Re-covery	Lithological column	Depths	Lithological descriptions	Shows
1453		C M		**Slst:** dk gy - brn blk, mod hd, vf sdy grdg **Sst,** arg, mica, carb, no vis por.	Weak HC odour, no flu, no cut.
1454		C M		**Slst:** a/a, bcm v sdy, plnt rems.	
1455		M C		**Slst/Sst:** a/a.	
1456		M		**Sst:** m - dk gy, clr Qtz, crs - v crs, fri, subrnd - rnd, sl silic cmt, slt mtx, tr mica, tr pyr, well srtd poor vis por.	Distinct HC odour, no flu, no cut.
1457		M		**Sst:** a/a, bcm hd, v calc cmt, no vis por.	No show.
1458		M		**Sst:** m gy, crs - v crs, lse - fri, rnd, sl silic cmt, sl carb, tr pyr, mica, well srtd, fair vis por.	Strong HC odour, no flu, no cut.
1459		M			
1460		M		**Sst:** a/a, pred crs, m - v crs.	
1461		M C	1461.5 m	**Sst:** a/a, v crs - grnls and f - m, fri - mod hd, silic cmt, bimodal srtd, fair vis por.	
1462				**Sst/Slst:** dk gy - brn blk, firm, vf sdy, arg, mica, carb, tr pyr, no vis por.	

Well	Core report	Core no's
31/6 - 1	2 of 2	9

Norsk Hydro

Note: Lithological interpretation based on spot sample descriptions every meter due to coring with fibre glass inner barrel.

Well no.	Core report	Core no's
31/6-1		10

Interval	Area	Cut	Date
1461.5 - 1471 m	Norwegian North Sea	1461.5 - 1479.5 m	5.8.83.
Scale 1:50	**Well R.K.B.** 25 m	**Recovery** 1461.5 - 1477.05 m (86%)	**Geologist** Rønning/Godvik

Depth scale	Recovery	Lithological column	Depths	Lithological descriptions	Shows
1461			1461.5 m		
1462				**Sst/Slst:** dk gy - brn blk, vf, mod hd, v slty, arg, lam, carb, mica, tr pyr, sl calc, burrows, no vis por.	Weak HC odour, no flu, no flu cut.
1463				**Sst:** olv gy - m gy, vf - f, fri - mod hd, subang, sl silic cmt, arg + slt lam, mica, carb, plnt rem, tr pyr, com shell frags, fair - pr vis por.	
1464				**St:** a/a, f - fri, well srtd, gd vis por.	Strong HC odour, no flu, no cut.
1465				**Sst:** a/a, vf - f, calc cmt, fair vis por.	Weak HC odour, no flu, no cut.
1466					
1467					
1468				**Sst:** a/a, pred f, fri - firm, sl calc cmt, poor - fair vis por.	
1469					
1470				**Sst:** m gy, clr Qtz, f - m, fri, subang - subrnd, tr calc cmt, tr mica, tr pyr, tr carb, shell frags, well srtd, gd no por.	Strong HC odour, no flu, v weak fast strmg bl wh flu cut, bl wh flu resd.
1471				**Sst:** m gy, clr Qtz, f - v crs, pred crs, lse - fri, subang - md, sl silic cmt. bimodal well srtd, fair por.	Strong HC odour, no flu, no flu cut.

Well	Core report	Core no's
31/6 - 1	1 of 2	10

Norsk Hydro

Note: Lithological interpretation based on spot sample descriptions every meter (-) due to coring with fibre glass inner barrel.

Well no.	Core report	Core no's
31/6-1		10

Interval	Area	Cut	Date
1461.5 - 1491 m	Norwegian North Sea	1461.5 - 1479.5 m	5.8.83.
Scale 1:50	**Well R.K.B.** 25 m	**Recovery** 1461.5 - 1477.05 m (86%)	**Geologist** Godvik/Rønning

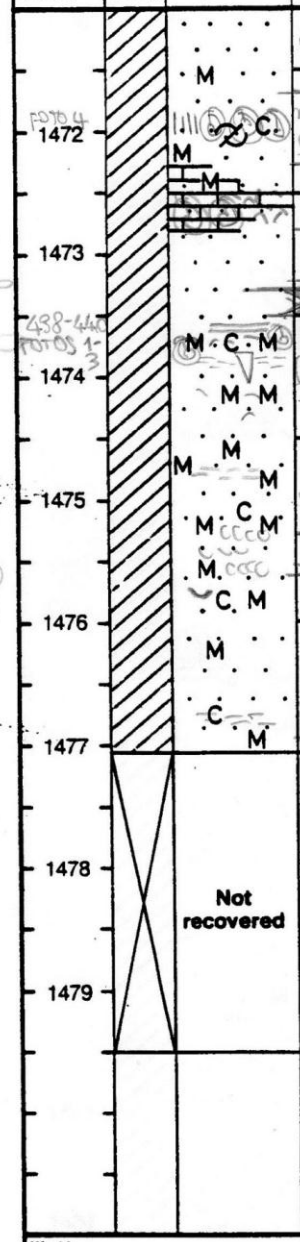

Depth scale	Recovery	Lithological column	Depths	Lithological descriptions	Shows
1472–1477			1461.5 – 1477.05 m	**Sst:** m gy - olv gy, clr - milky Qtz g, vf - f, subang - subrnd, fri - firm, sl calc cmt, tr carb, tr mica, tr shell frags, tr blk specs, well srtd, gd vis por.	No dir flu, v weak slow strmg wh flu cut, yel wh. flu resd, no vis resd.
				Sst: m dk gy - dk gy, clr Qtz g, vf - f, subang - subrnd, v hd, v calc / dol, cmt, tr mica, tr blk, specs, well srtd, no vis por.	No show.
				Sst: m gy - olv gy, clr - milky Qtz g, vf - f, subang - subrnd, fri - firm, sl calc cmt, v mica, tr carb, tr blk specs, tr shell frags, well srtd, gd vis por.	No dir flu, v weak slow strmg wh flu cut, yel wh flu resd, no vis resd.
				Sst: vf, else a/a.	
				Sst: vf, mica, else a/a.	
				Sst: m dk gy - olv gy, clr - milky, occ smoky Qtz g, m - crs, fri, sl calc cmt, subang - subrnd, tr mica, well srtd, gd vis por.	No show.
1477–1479		Not recovered	1477.05 m – 1479.5 m		

Well	Core report	Core no's
31/1 - 6	2 of 2	10

Norsk Hydro

Note: Lithological interpretation based on spot sample descriptions every meter (-) due to coring with fibre glass inner barrel.

Well no.	Core report	Core no's
31/6-1		11

Interval	Area	Cut	Date
1479.5 - 1489 m	Norwegian North Sea	1479.5 - 1498 m	6.8.83.
Scale	**Well R.K.B.**	**Recovery**	**Geologist**
1:50	25 m	1479.5 - 1497.75 m (99%)	Kalgraff/Godvik

Depth scale	Re-covery	Lithological column	Depths	Lithological descriptions	Shows
1479			1479.5 m		
1480		M		**Sst:** m dk gy, clr - milky Qtz, f - m, fri - lse, subang - subrnd, tr mica, silic cmt, tr carb, well srtd, gd vis por.	Gd petroliferous odour, no str, no flu, v weak int - fast strmg wh flu cut, weak duell yel flu resd, no vis cut.
1481		C			
1482		M		**Sst:** m dk gy - dk gy, clr - milky Qtz, m - crs, loc pbly, subang - subrnd, tr mica, tr silic, rr tr calc cmt, shell frags, mod srtd, gd vis por.	Gd petroliferaus odour, no stn, no flu, weak fast strmg wh yel flu cmt, weak yel wh flu resd, no vis cut.
1483		M			
1484		C		**Sst:** m dk gy, clr - milky, rr tr smokey Qtz, f - m, fri - lse, subang - subrnd, tr mica, mica cmt, rr tr carb cmt, tr carb, well srtd, gd vis por.	
1485		M M M		**St/Lst:** m dk gy - dk gy, clr Qtz, vf - f, v hd, subang - subrnd, v calc cmt, v mica, mod srtd, no vis por.	
1486		C		**Sst:** dk gy - olv gy, clr - milky Qtz, vf - crs, pred m, lse - fri, subang - subrnd, tr mica, tr carb, tr pyr, silic cmt, mod srtd, gd vis por.	No shows.
1487		M			
1488					
1489		M C			

Well	Core report	Core no's
31/6 - 1	1 of 2	11

Norsk Hydro

Note: Lithological interpretation based on spot sample descriptions every meter (-) due to coring with fibre glass inner barrel.

Well no.	Core report	Core no's
31/6-1		11

Interval	Area	Cut	Date
1489 - 1497.75 m	Norwegian North Sea	1479.5 - 1498 m	6.8.83.
Scale 1:50	**Well R.K.B.** 25 m	**Recovery** 1479.5 - 1497.75 m (99%)	**Geologist** Kalgraff/Godvik

Depth scale	Recovery	Lithological column	Depths	Lithological descriptions	Shows
1489		M		**Sst:** m dk gy - olv gy, clr - milky Qtz, vf - m, pred vf, fri, subang - subrnd v mica - carb, tr pyr, sl calc, lam, v slty grdg **Slst,** mod srtd, poor vis por.	Gd petroliferous odour, no stn, tr weak spotted, lam wh yel flu, weak cmt strmg yel wh flu cut, weak yel wh flu resd, no vis cut, no resd vis cut.
1490		M			
1491		M		**Sst/Slst:** olv gy, loc clr Qtz, vf, subang - subrnd, micro-mic, mica, carb, tr pyr, sl calc, sl lam, burrows v slty grdg **Slst,** mod srtd, poor - no vis por.	
1492		C M			
1493		M		**Sst:** dk gy - olv gy, clr - milky Qtz, vf, fri - mod hd, subang - subrnd, micro-mic, mica, carb, v arg, loc v slty grdg **Slst,** mod srtd.	Gd petroliferous odour, no stn, no flu, weak cmt strmg yel wh flu cut, weak yel wh flu resd.
1494		M			
1495		M		**Sst/Slst:** a/a.	Gd petroliferous odour, no stn, no dir flu, weak inst strmg wh flu cut, weak wh flu resd.
1496		M			
1497		M C			
1498			1497.75 m 1498 m		

Well	Core report	Core no's
31/6 - 1	2 of 2	11

31/6-2

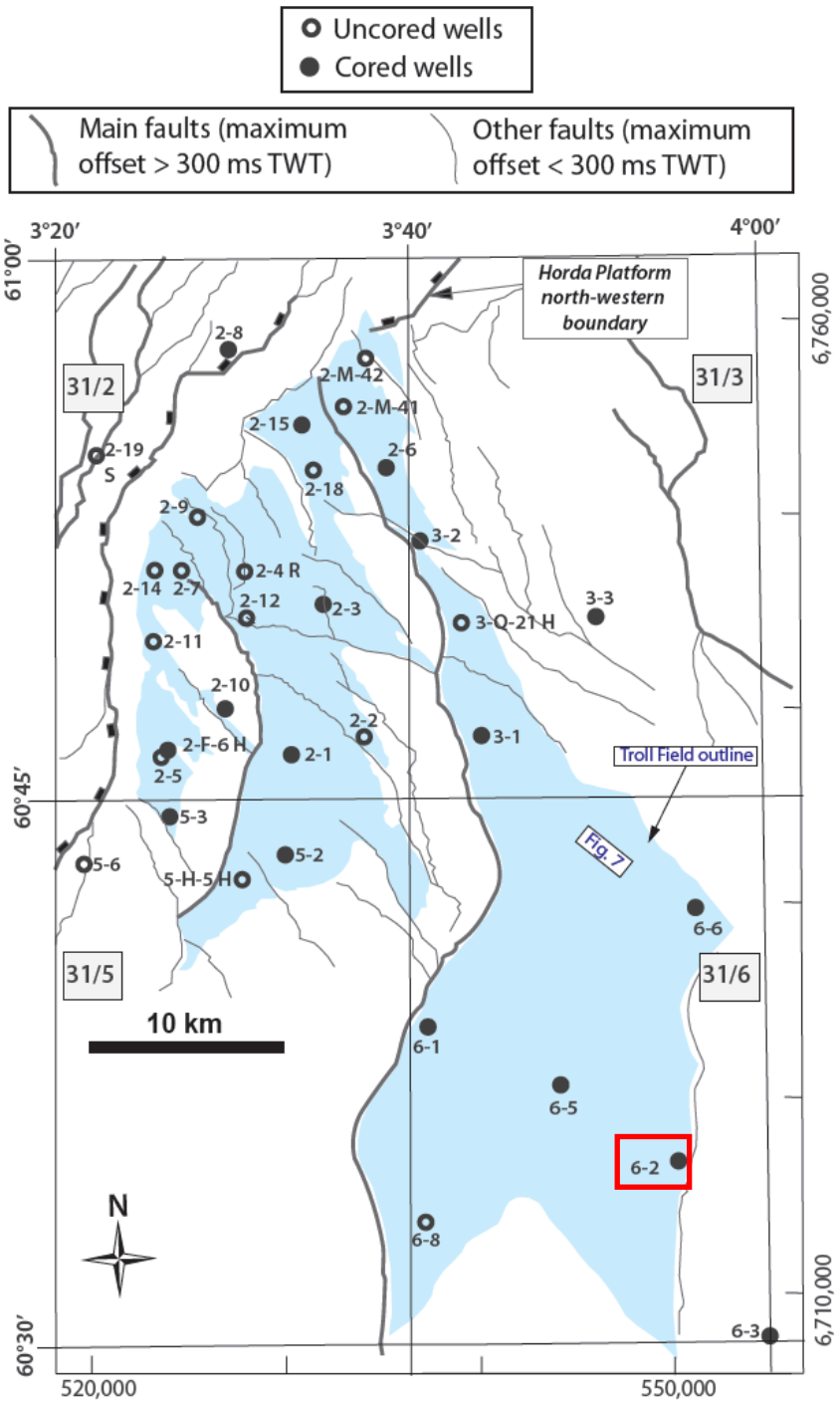
Uncored wells
Cored wells
Main faults (maximum offset > 300 ms TWT)
Other faults (maximum offset < 300 ms TWT)
3°20′
3°40′
4°00′
61°00′
60°45′
60°30′
6,760,000
6,710,000
520,000
550,000
Horda Platform north-western boundary
Troll Field outline
Fig. 7
31/2
31/3
31/5
31/6
10 km
N
2-8
2-M-42
2-M-41
2-15
2-19 S
2-6
2-18
2-9
3-2
2-14
2-7
2-4 R
2-12
2-3
3-Q-21 H
3-3
2-11
2-10
2-2
3-1
2-F-6 H
2-5
2-1
5-3
5-2
5-6
5-H-5 H
6-6
6-1
6-5
6-2
6-8
6-3

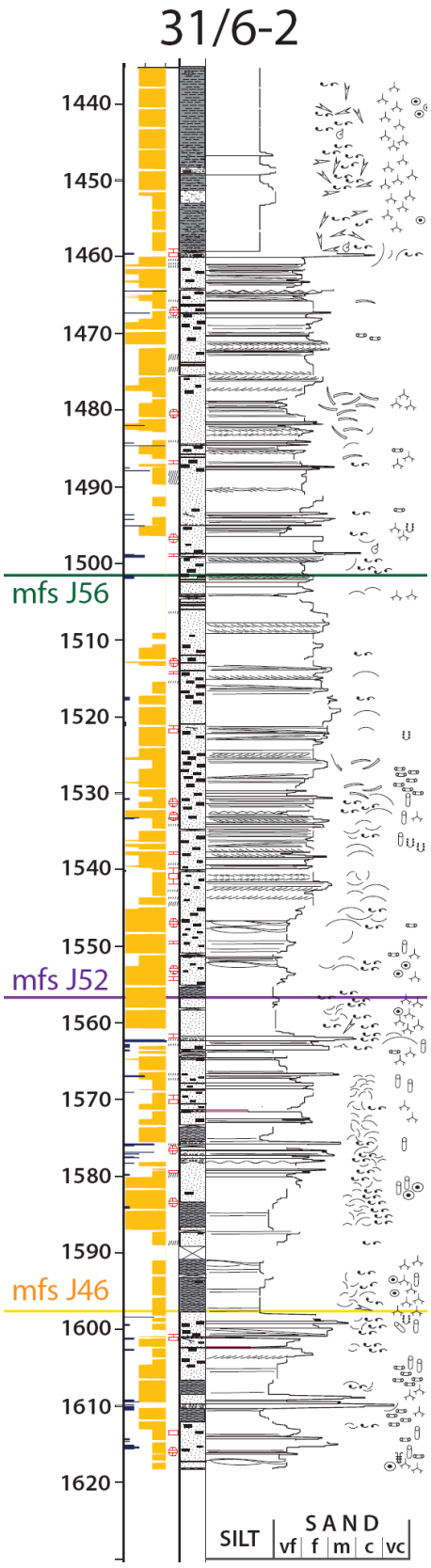
31/6-2
1440
1450
1460
1470
1480
1490
1500
mfs J56
1510
1520
1530
1540
1550
mfs J52
1560
1570
1580
1590
mfs J46
1600
1610
1620
SILT
SAND
vf
f
m
c
vc

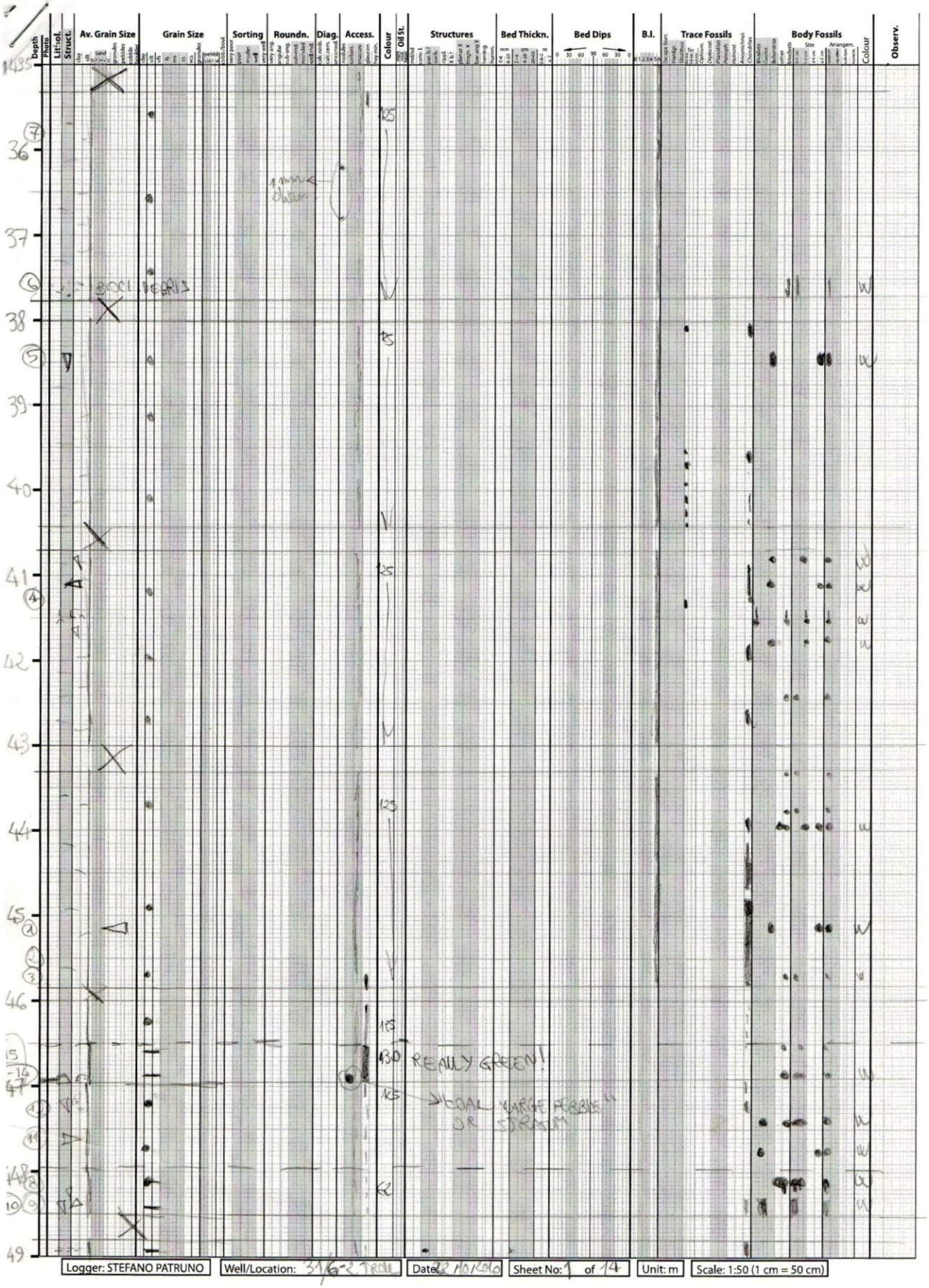
Depth
Photo
Lith.
Struct.
Av. Grain Size
Grain Size
Sorting
Roundn.
Diag.
Access.
Colour
Oil St.
Structures
Bed Thickn.
Bed Dips
B.I.
Trace Fossils
Body Fossils
Observ.
REALLY GREEN!
COAL
Logger: STEFANO PATRUNO
Well/Location:
Date:
Sheet No: 1 of 14
Unit: m
Scale: 1:50 (1 cm = 50 cm)

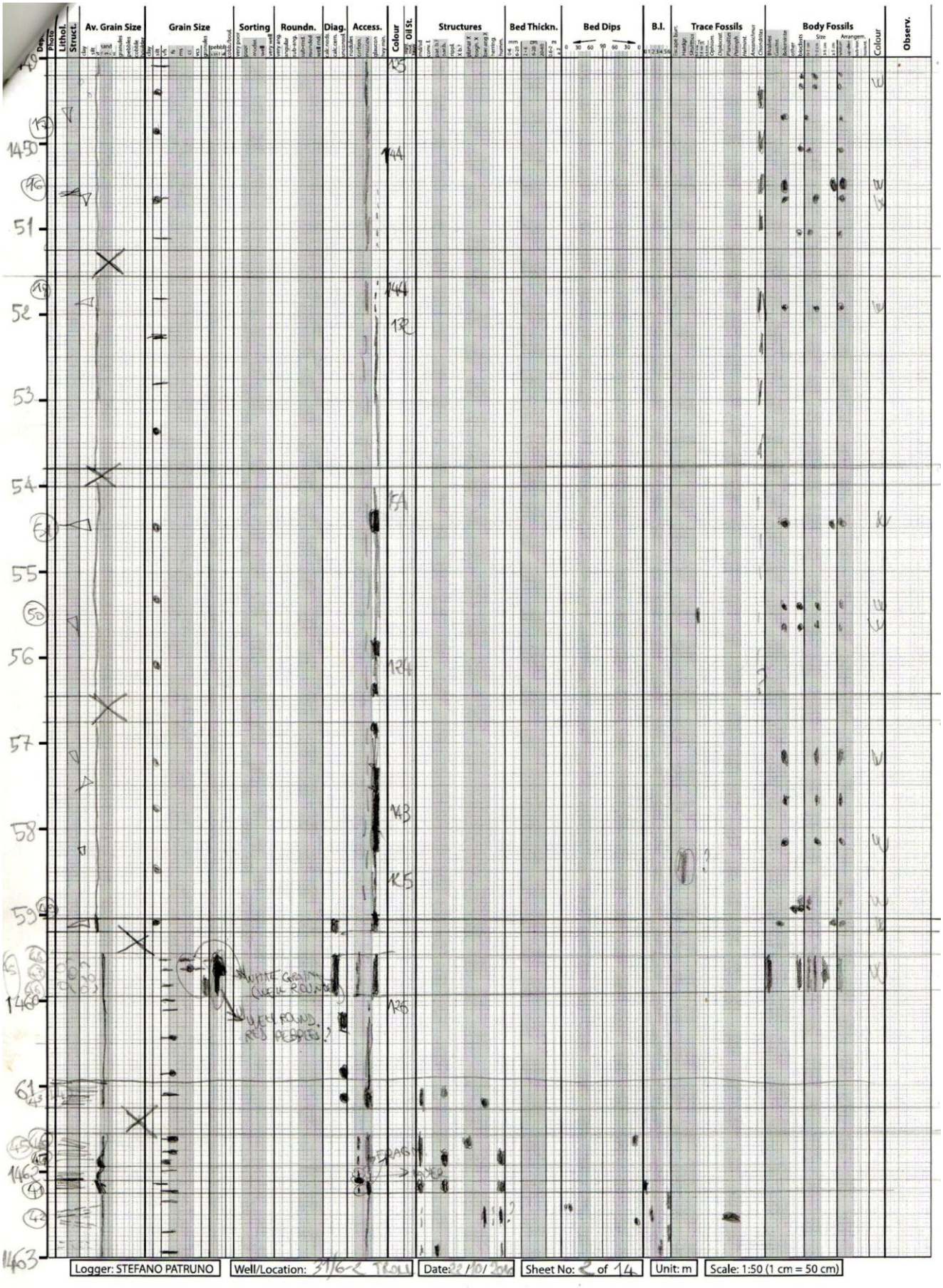
Dep.
Photo
Lithol.
Struct.
Av. Grain Size
Grain Size
Sorting
Roundn.
Diag.
Access.
Colour
Oil St.
Structures
Bed Thickn.
Bed Dips
B.I.
Trace Fossils
Body Fossils
Observ.
WHITE GRAIN QUITE ROUND
DARK ROUND RED PEBBLES?
BRASH
Logger: STEFANO PATRUNO
Well/Location: 31/6-2 TROLL
Date: 22/10/2006
Sheet No: 2 of 14
Unit: m
Scale: 1:50 (1 cm = 50 cm)

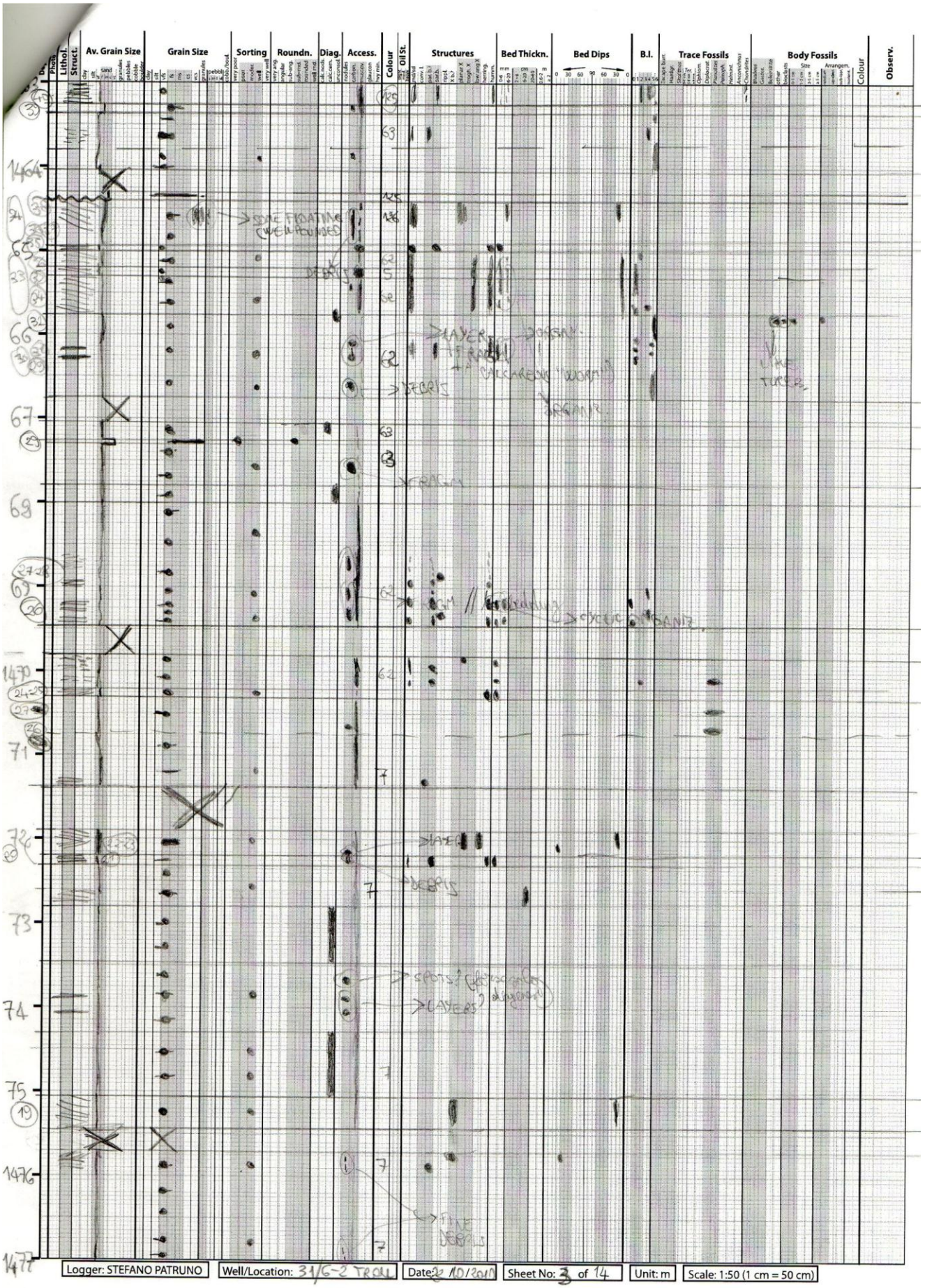
Lithol.
Struct.
Av. Grain Size
Grain Size
Sorting
Roundn.
Diag.
Access.
Colour
Oil St.
Structures
Bed Thickn.
Bed Dips
B.I.
Trace Fossils
Body Fossils
Observ.
Logger: STEFANO PATRUNO
Well/Location: 31/6-2 TROLL
Date: 22/10/2019
Sheet No: 3 of 14
Unit: m
Scale: 1:50 (1 cm = 50 cm)

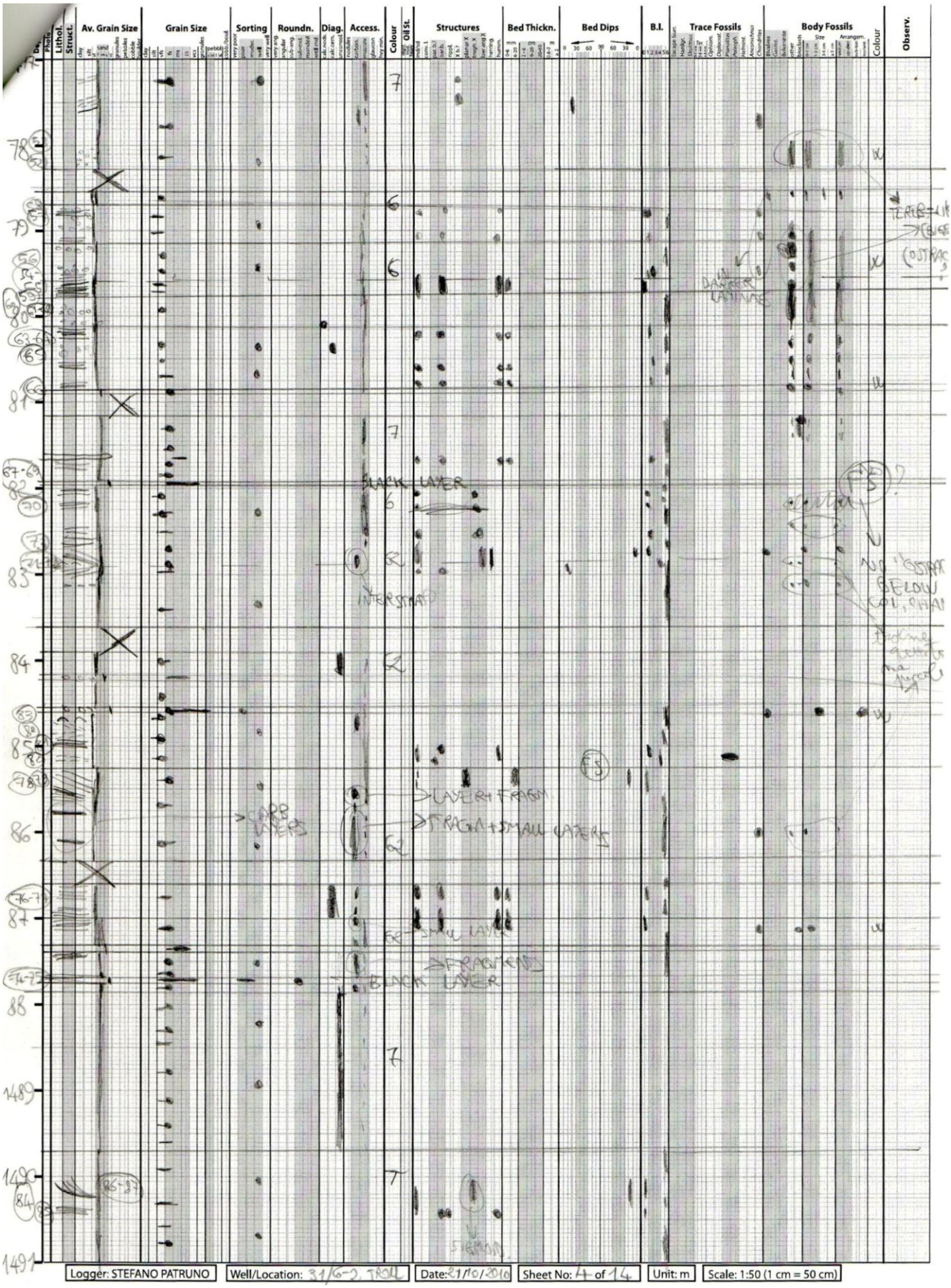
Depth
Facies
Lithol.
Struct.
Av. Grain Size
Grain Size
Sorting
Roundn.
Diag.
Access.
Colour
Oil St.
Structures
Bed Thickn.
Bed Dips
B.I.
Trace Fossils
Body Fossils
Size
Arrangem.
Colour
Observ.
BLACK LAYER
INTERSTRAT
LAYER FRAGM
FRAGM+SMALL LAYERS
BLACK LAYER
Logger: STEFANO PATRUNO
Well/Location: 31/6-2, TROLL
Date: 21/10/2010
Sheet No: 4 of 14
Unit: m
Scale: 1:50 (1 cm = 50 cm)

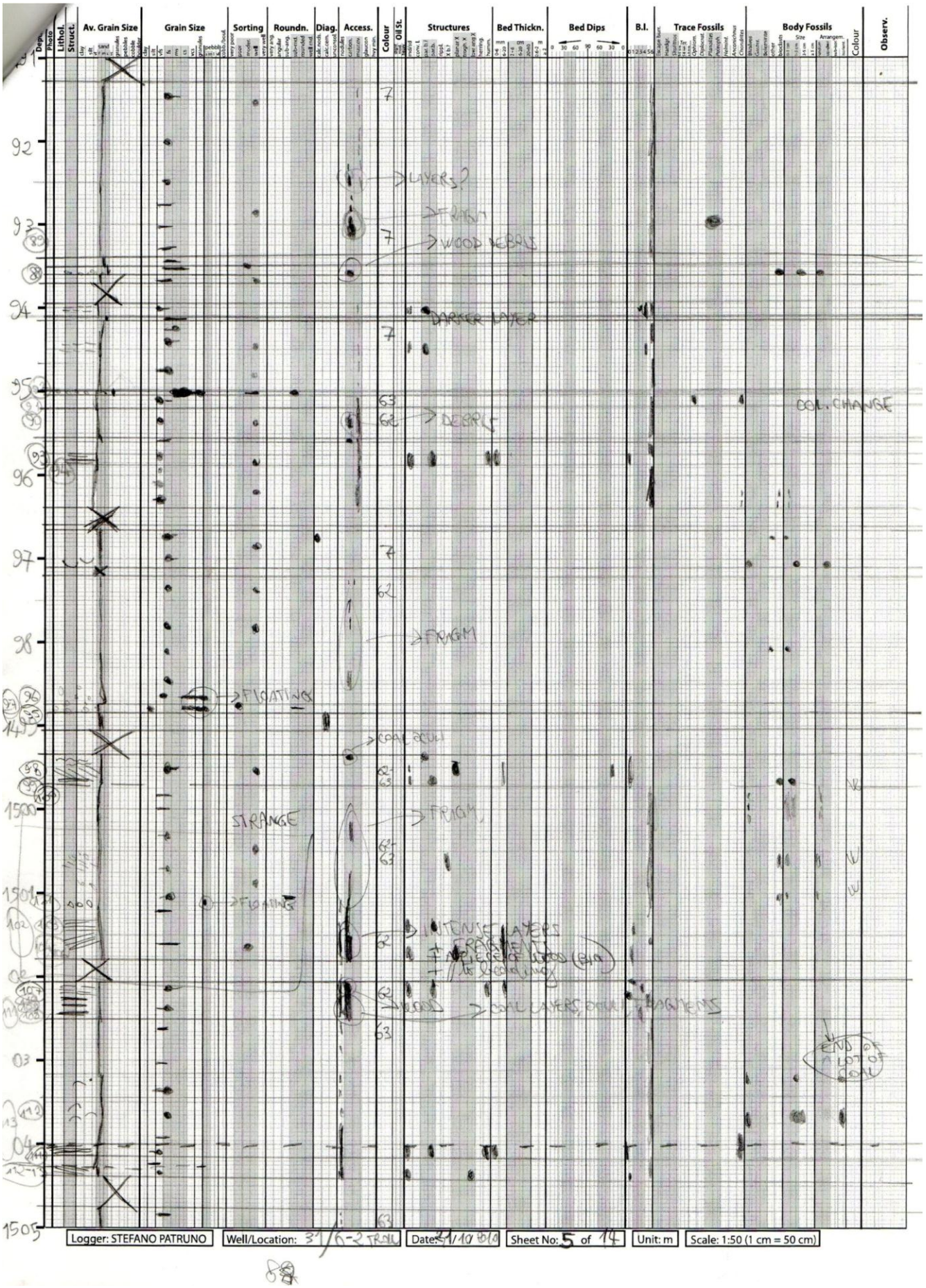
Depth
Photo
Lithol.
Struct.
Av. Grain Size
Grain Size
Sorting
Roundn.
Diag.
Access.
Colour
Oil St.
Structures
Bed Thickn.
Bed Dips
B.I.
Trace Fossils
Body Fossils
Observ.
LAYERS?
WOOD DEBRIS
DARKER LAYER
COL. CHANGE
DEBRIS
FRAGM
FLOATING
CORAL DEBRIS
STRANGE
FRAGM.
INTENSE LAYERS
END OF CORE
Logger: STEFANO PATRUNO
Well/Location: 3
Date:
Sheet No: 5 of 14
Unit: m
Scale: 1:50 (1 cm = 50 cm)

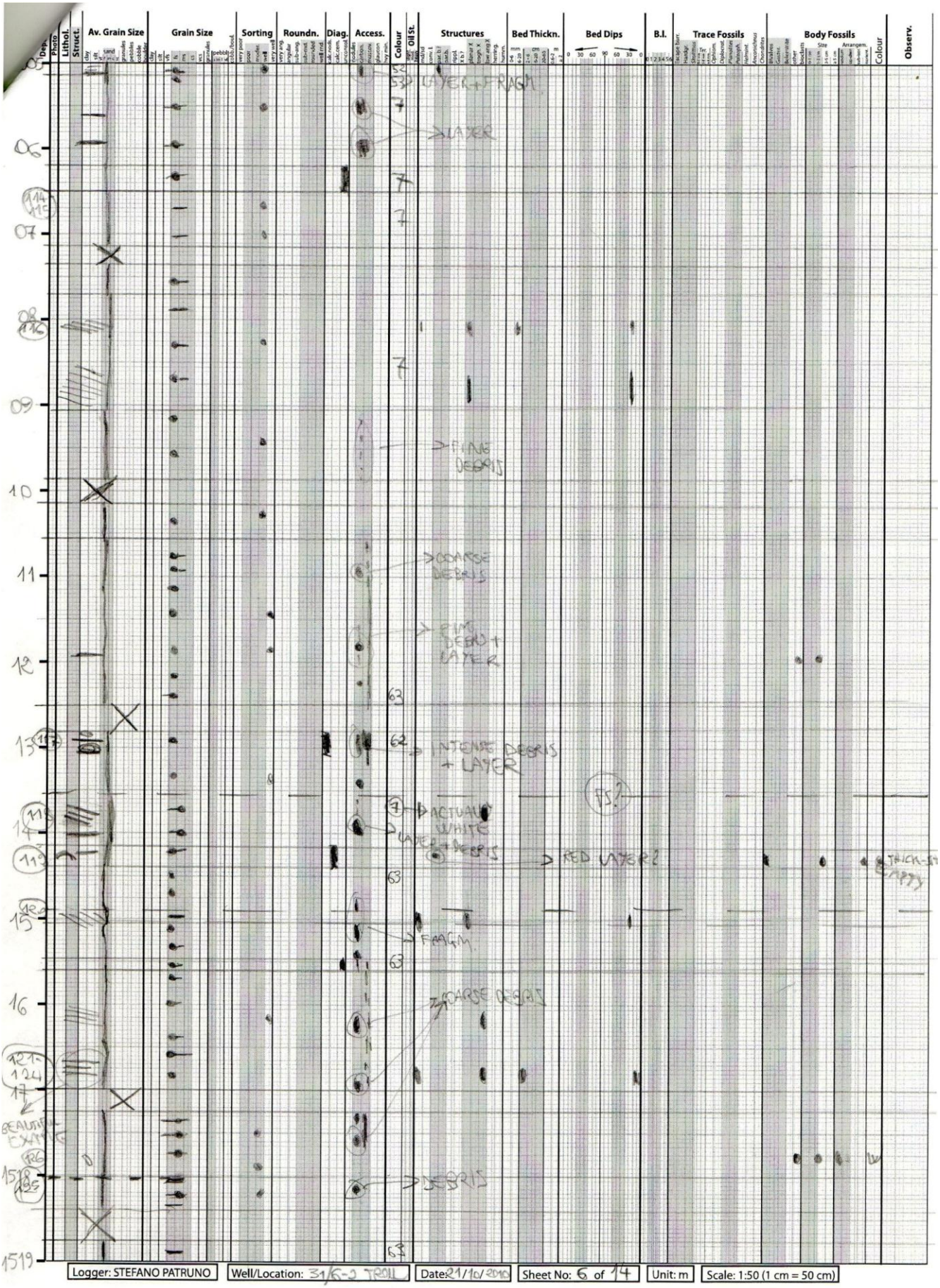
Depth
Photo
Lithol.
Struct.
Av. Grain Size
Grain Size
Sorting
Roundn.
Diag.
Access.
Colour
Oil St.
Structures
Bed Thickn.
Bed Dips
B.I.
Trace Fossils
Body Fossils
Observ.
LAYER + FRAGM
LAYER
FINE DEBRIS
COARSE DEBRIS
FINE DEBRIS LAYER
INTENSE DEBRIS + LAYER
ACTUAL WHITE LAYER + DEBRIS
RED LAYER?
FRAGM.
COARSE DEBRIS
DEBRIS
THICK-SI
CAPPY
BEAUTIFUL EXAMPLE
Logger: STEFANO PATRUNO
Well/Location: 31/6-3 TROLL
Date: 21/10/2010
Sheet No: 6 of 14
Unit: m
Scale: 1:50 (1 cm = 50 cm)

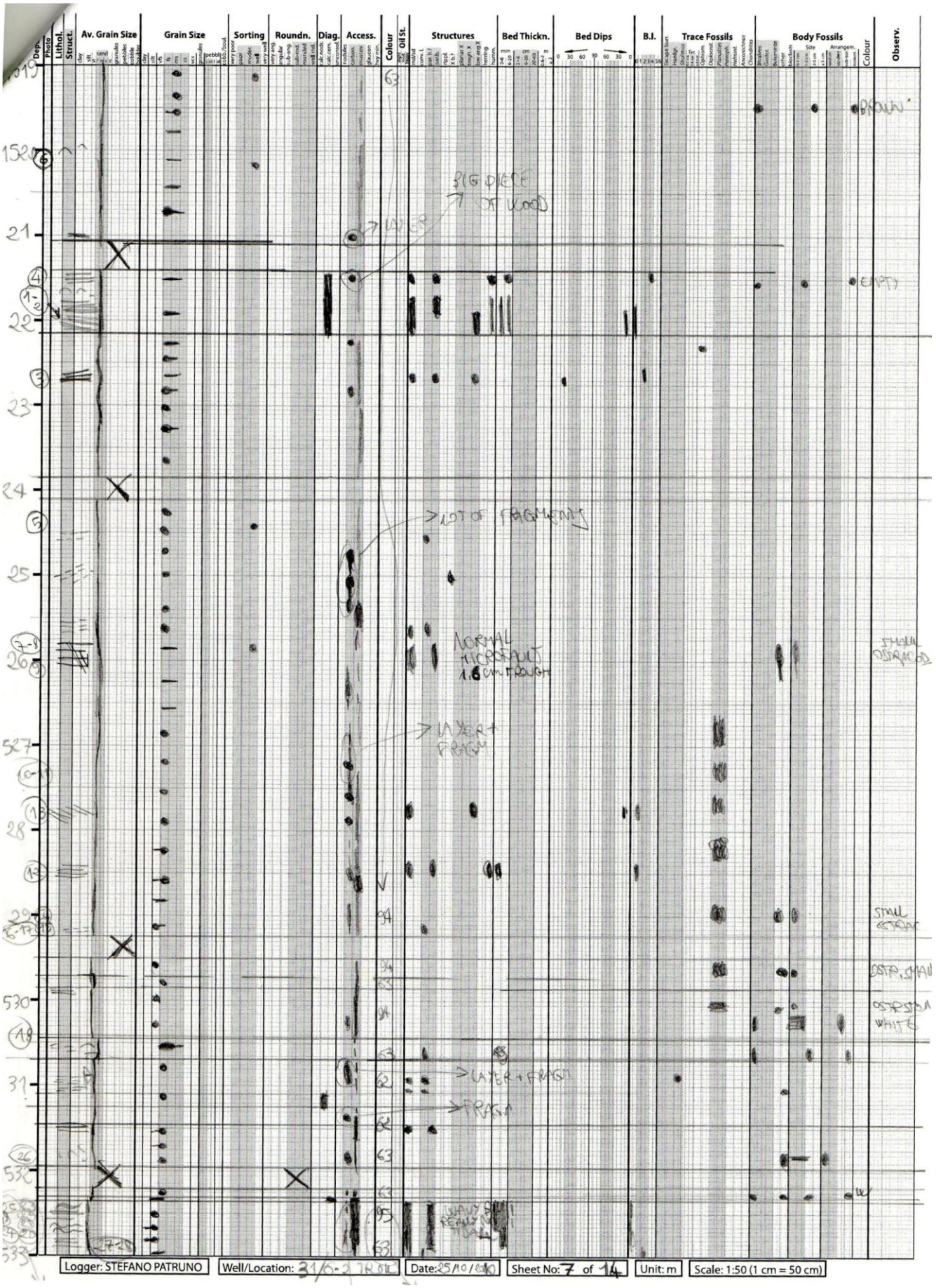
Depth
Facies
Lithol.
Struct.
Av. Grain Size
Grain Size
Sorting
Roundn.
Diag.
Access.
Colour
Oil St.
Structures
Bed Thickn.
Bed Dips
B.I.
Trace Fossils
Body Fossils
Observ.
BIG PIECE OF WOOD
LOT OF FRAGMENTS
NORMAL MICROFAULT 1.6 cm THROW
LAYER + FRAG
Logger: STEFANO PATRUNO
Well/Location:
Date:
Sheet No: 7 of 14
Unit: m
Scale: 1:50 (1 cm = 50 cm)

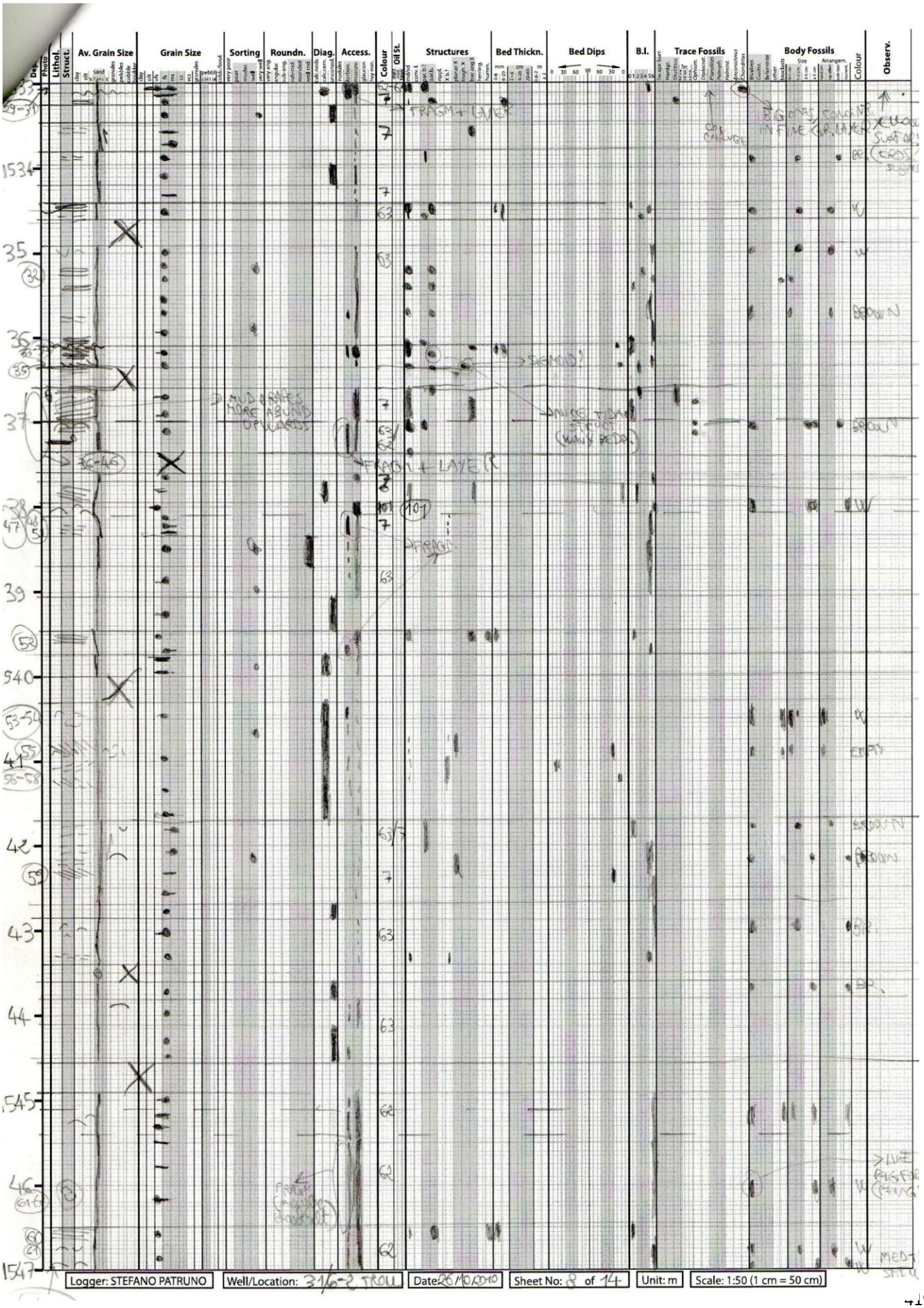
Dep. Photo
Lithol. Struct.
Av. Grain Size
Grain Size
Sorting
Roundn.
Diag.
Access.
Colour
Oil St.
Structures
Bed Thickn.
Bed Dips
B.I.
Trace Fossils
Body Fossils
Observ.
Colour
Logger: STEFANO PATRUNO
Well/Location: 31/6-2 TROLL
Date: 26/10/2010
Sheet No: 8 of 14
Unit: m
Scale: 1:50 (1 cm = 50 cm)

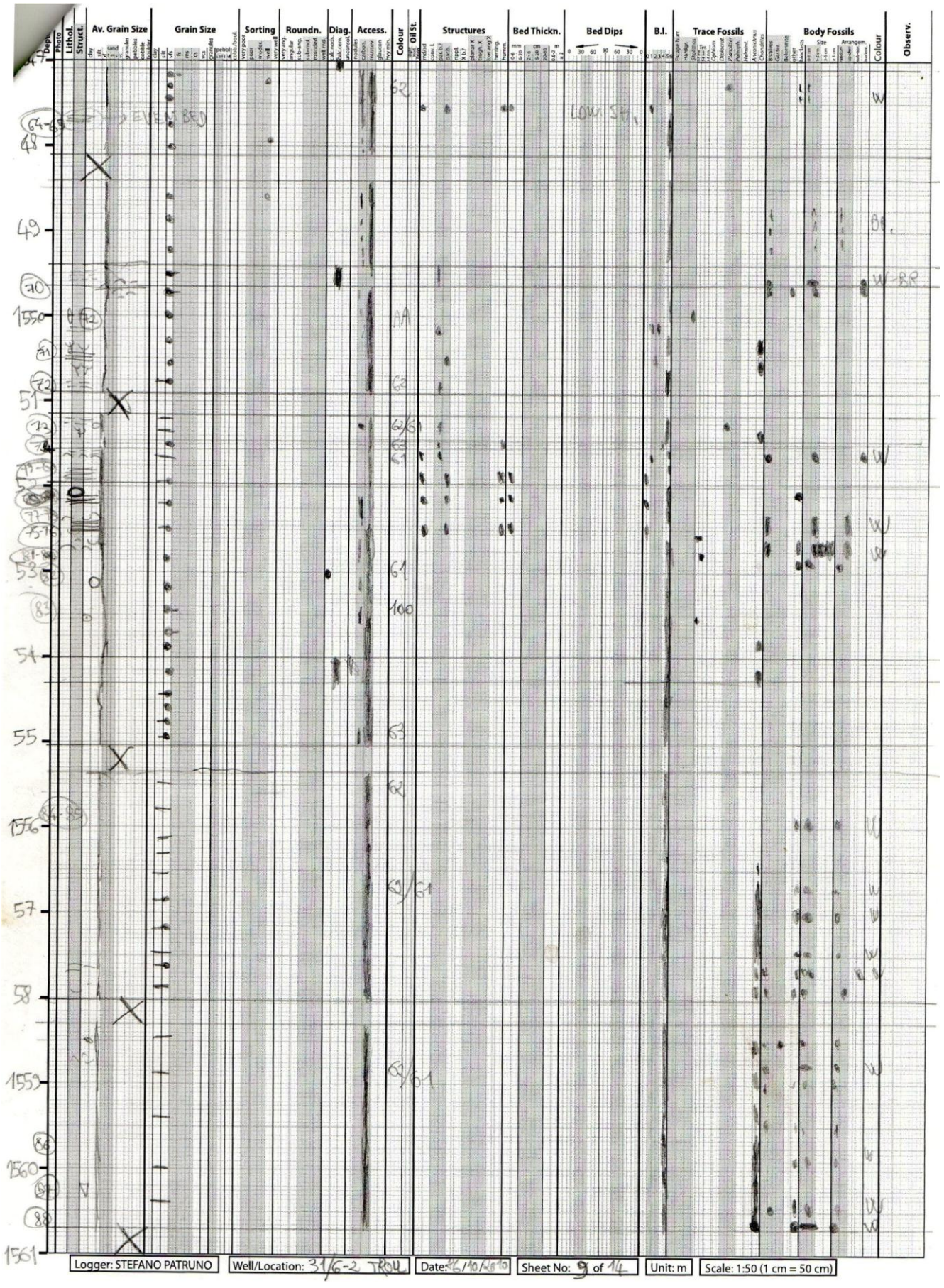
Depth
Photo
Lithol.
Struct.
Av. Grain Size
Grain Size
Sorting
Roundn.
Diag.
Access.
Colour
Oil St.
Structures
Bed Thickn.
Bed Dips
B.I.
Trace Fossils
Body Fossils
Observ.
Logger: STEFANO PATRUNO
Well/Location: 31/6-2
Date: 6/10/2010
Sheet No: 9 of 14
Unit: m
Scale: 1:50 (1 cm = 50 cm)

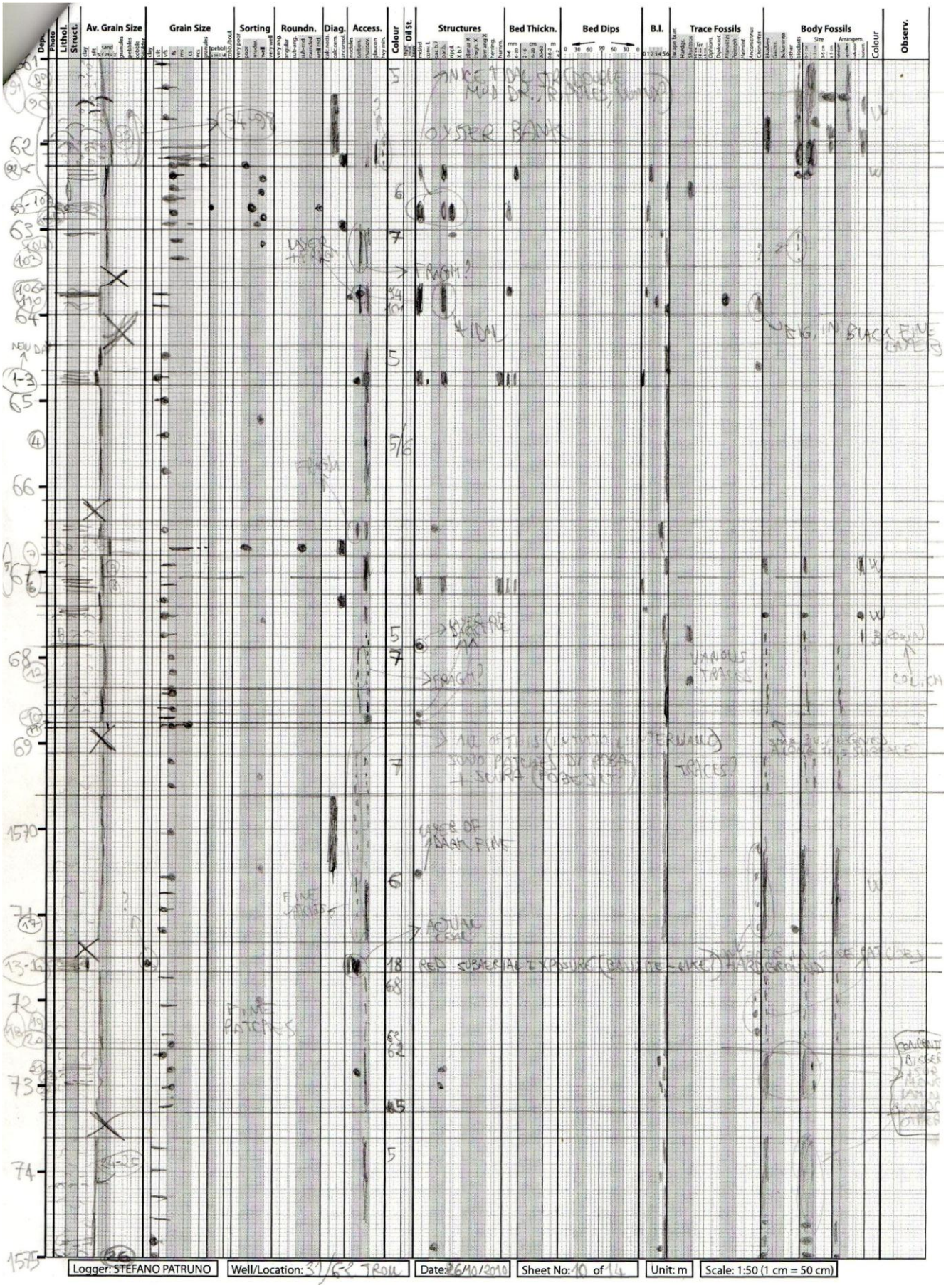
Dep.
Photo
Lithol.
Struct.
Av. Grain Size
Grain Size
Sorting
Roundn.
Diag.
Access.
Colour
Oil St.
Structures
Bed Thickn.
Bed Dips
B.I.
Trace Fossils
Body Fossils
Observ.
OYSTER BANK
RED SUBAERIAL EXPOSURE
Logger: STEFANO PATRUNO
Well/Location: 37/5-2 TROLL
Date: 26/10/2010
Sheet No: 10 of 14
Unit: m
Scale: 1:50 (1 cm = 50 cm)

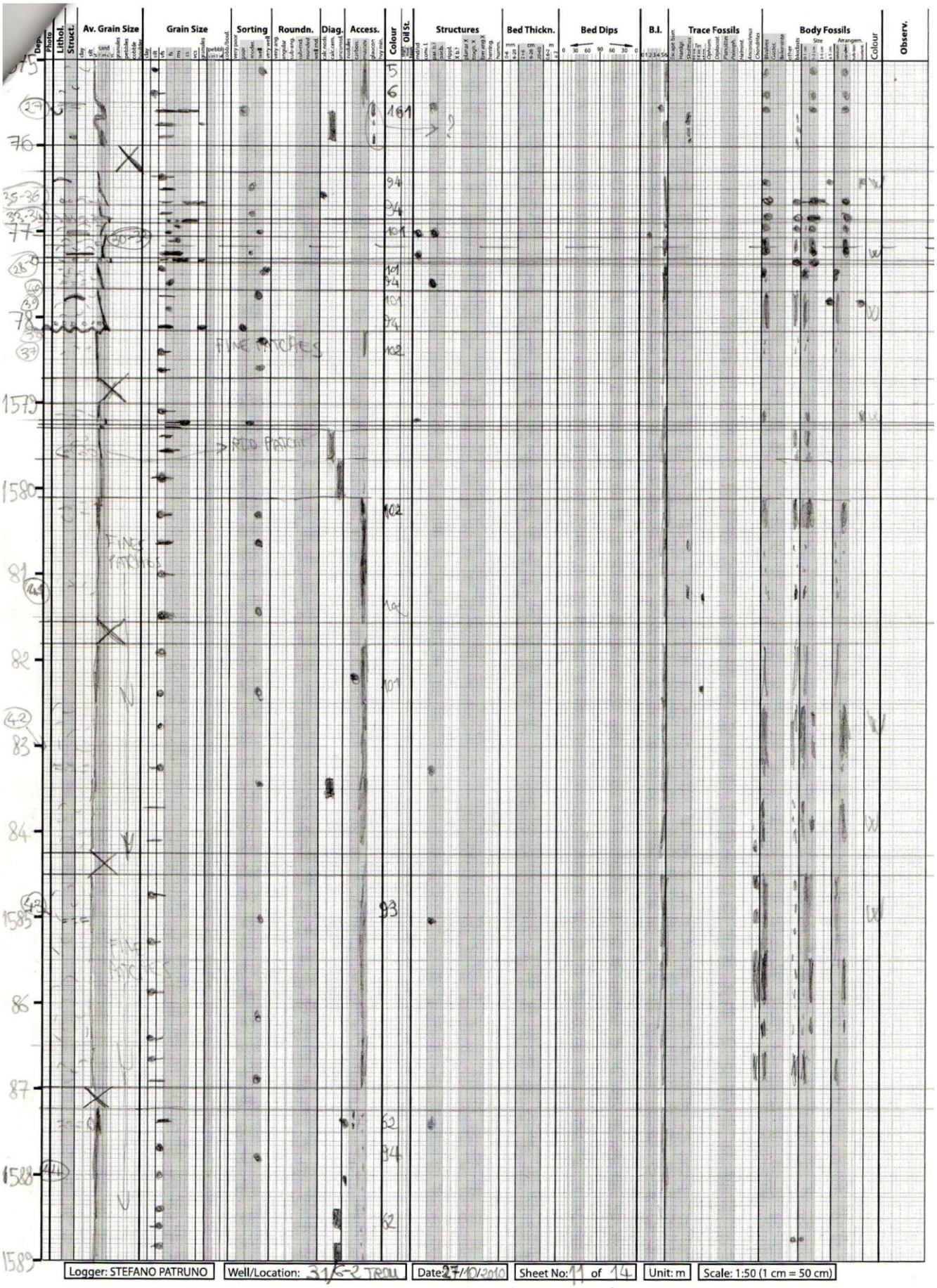
Depth
Photo
Lithol.
Struct.
Av. Grain Size
Grain Size
Sorting
Roundn.
Diag.
Access.
Colour
Oil St.
Structures
Bed Thickn.
Bed Dips
B.I.
Trace Fossils
Body Fossils
Observ.
FINE PATCHES
RED PATCH
Logger: STEFANO PATRUNO
Well/Location: 31/6-2 TROLL
Date: 27/10/2010
Sheet No: 11 of 14
Unit: m
Scale: 1:50 (1 cm = 50 cm)

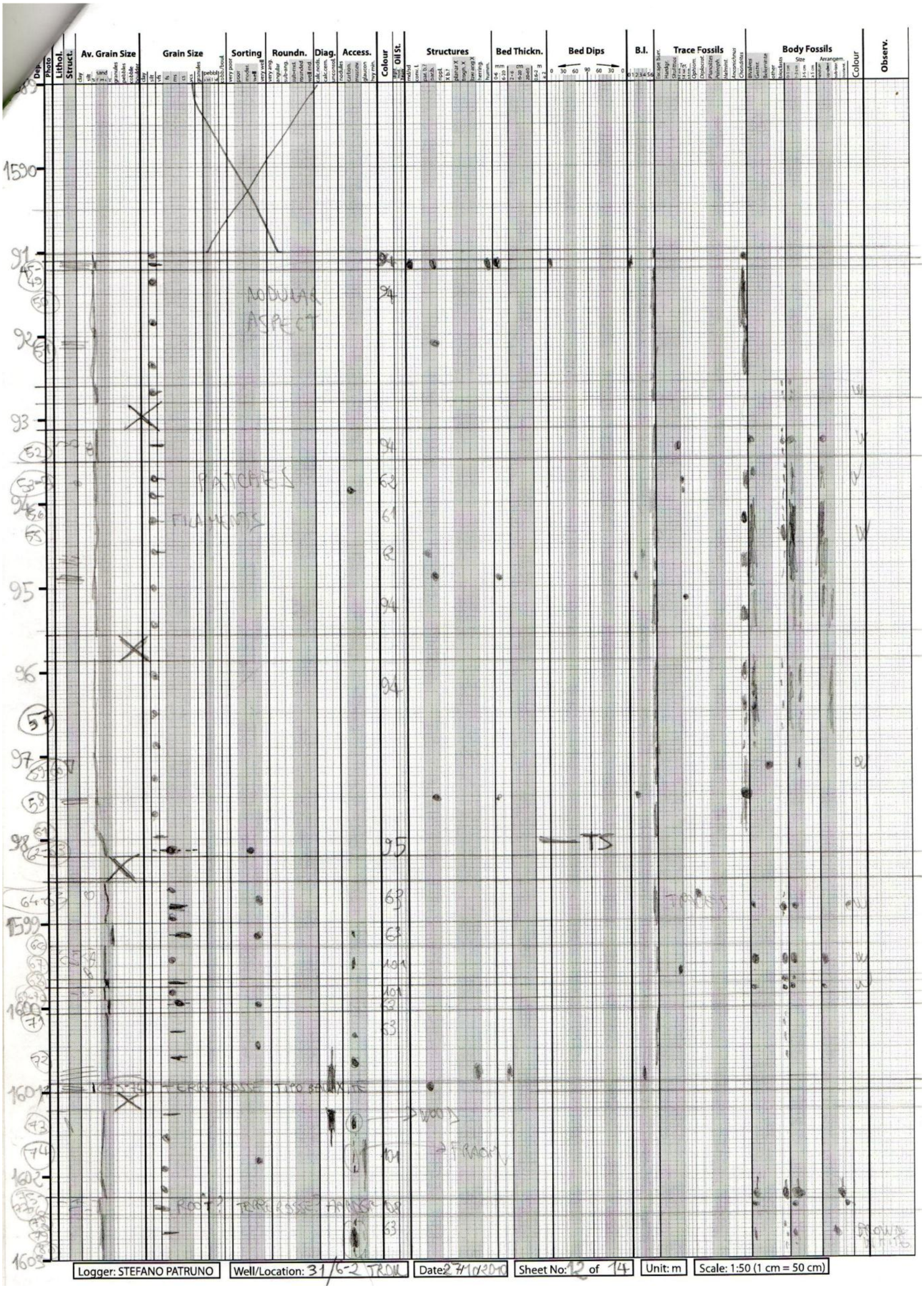
Depth
Photo
Lithol.
Struct.
Av. Grain Size
Grain Size
Sorting
Roundn.
Diag.
Access.
Colour
Oil St.
Structures
Bed Thickn.
Bed Dips
B.I.
Trace Fossils
Body Fossils
Colour
Observ.
1590
1599
1600
1601
1602
1603
NODULAR ASPECT
PATCHES
TS
TERRE ROSSE TIPO BAUXITE
WOOD
ROOT?
Logger: STEFANO PATRUNO
Well/Location: 31/6-2 TROLL
Date: 27/10/2010
Sheet No: 12 of 14
Unit: m
Scale: 1:50 (1 cm = 50 cm)

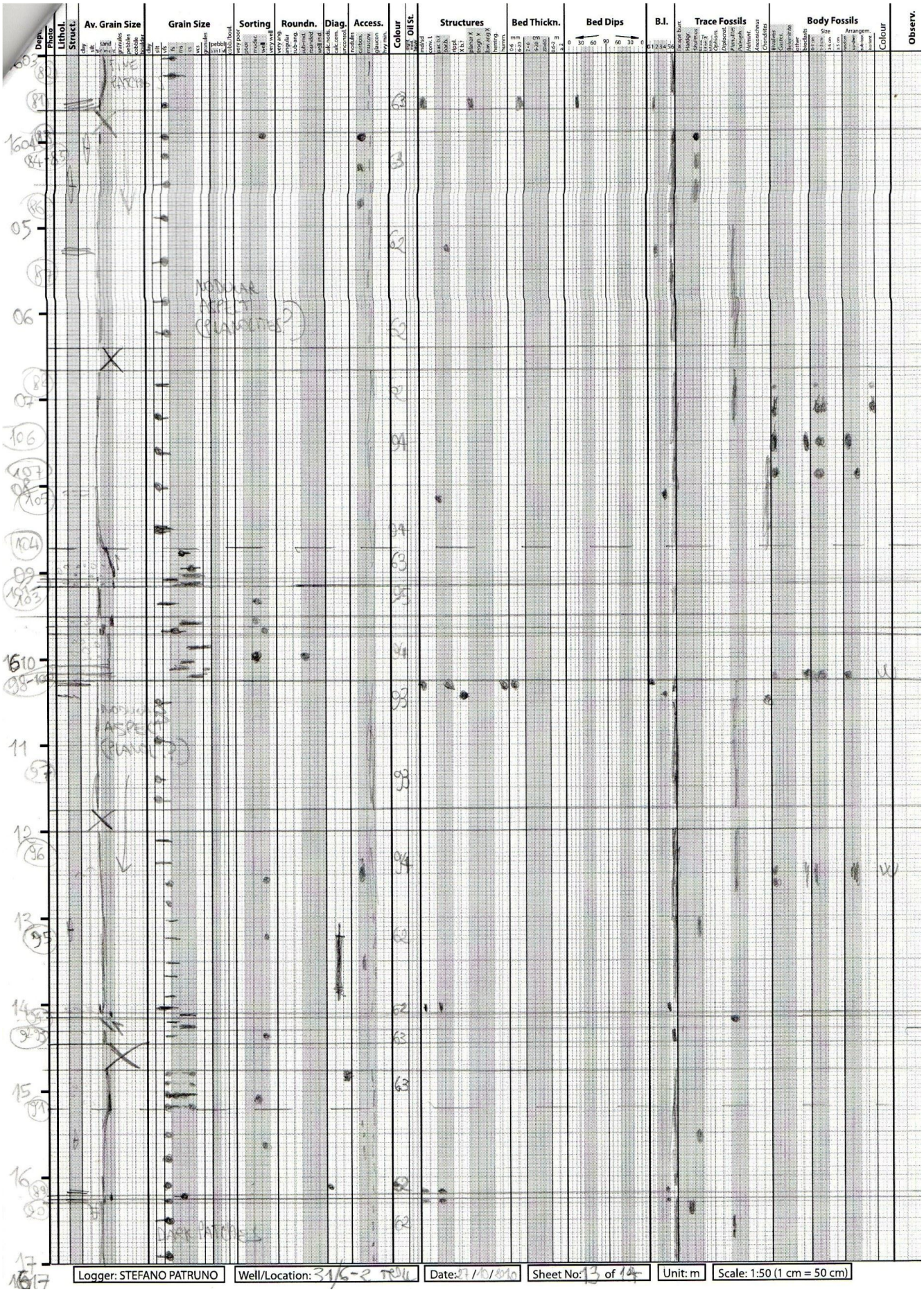
Depth
Photo
Lithol.
Struct.
Av. Grain Size
Grain Size
Sorting
Roundn.
Diag.
Access.
Colour
Oil St.
Structures
Bed Thickn.
Bed Dips
B.I.
Trace Fossils
Body Fossils
Observ.
NODULAR ASPECT (PLANOLITES?)
DARK PATCHES
Logger: STEFANO PATRUNO
Well/Location: 31/6-3
Date: 27/10/2010
Sheet No: 13 of 14
Unit: m
Scale: 1:50 (1 cm = 50 cm)

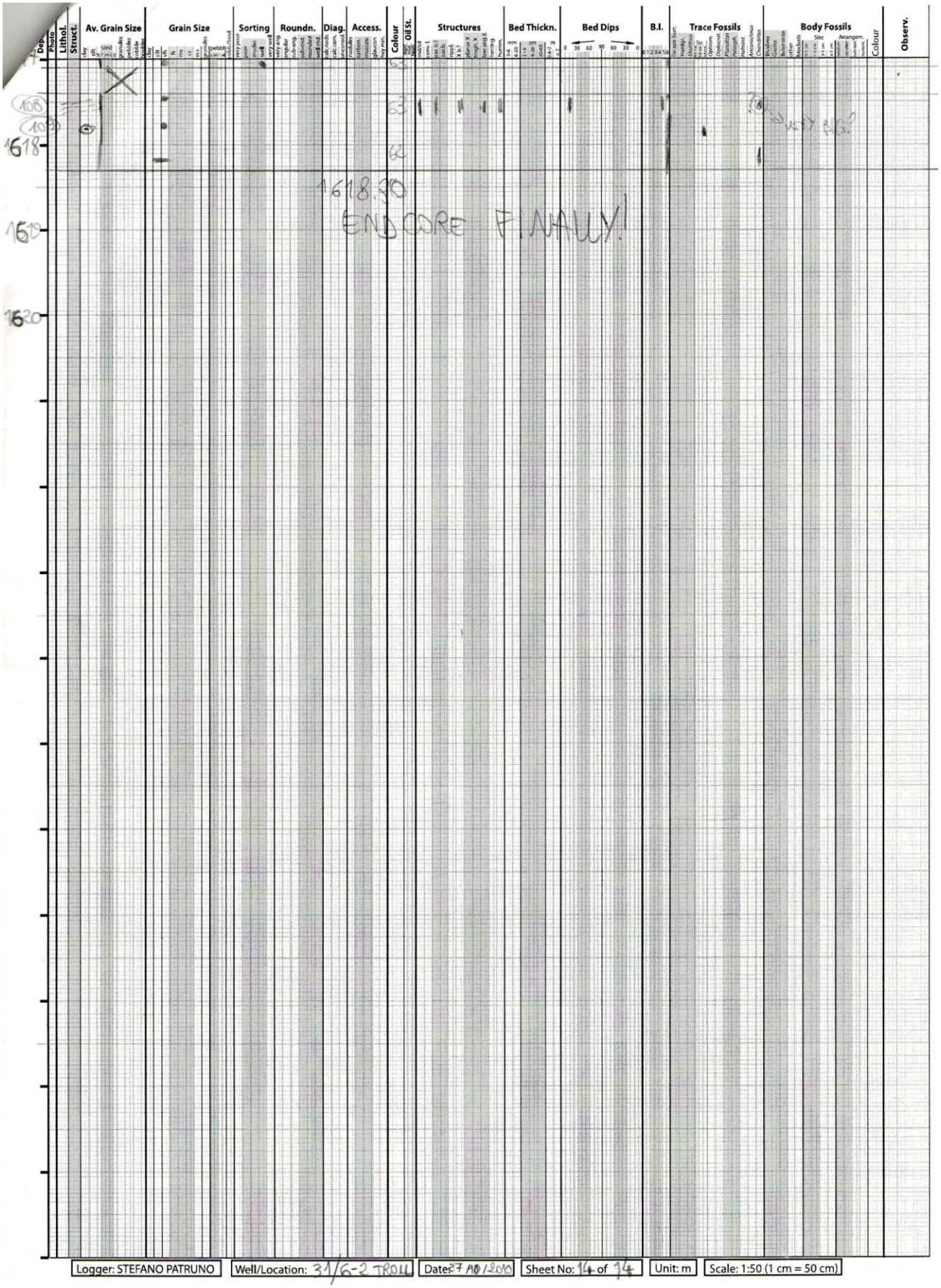
Dep.
Photo
Lithol.
Struct.
Av. Grain Size
Grain Size
Sorting
Roundn.
Diag.
Access.
Colour
Oil St.
Structures
Bed Thickn.
Bed Dips
B.I.
Trace Fossils
Body Fossils
Observ.
1618.30
END CORE F. MAUX!
Logger: STEFANO PATRUNO
Well/Location: 31/6-2 TROLL
Date: 27 AUG/2010
Sheet No: 14 of 14
Unit: m
Scale: 1:50 (1 cm = 50 cm)

31/6-3

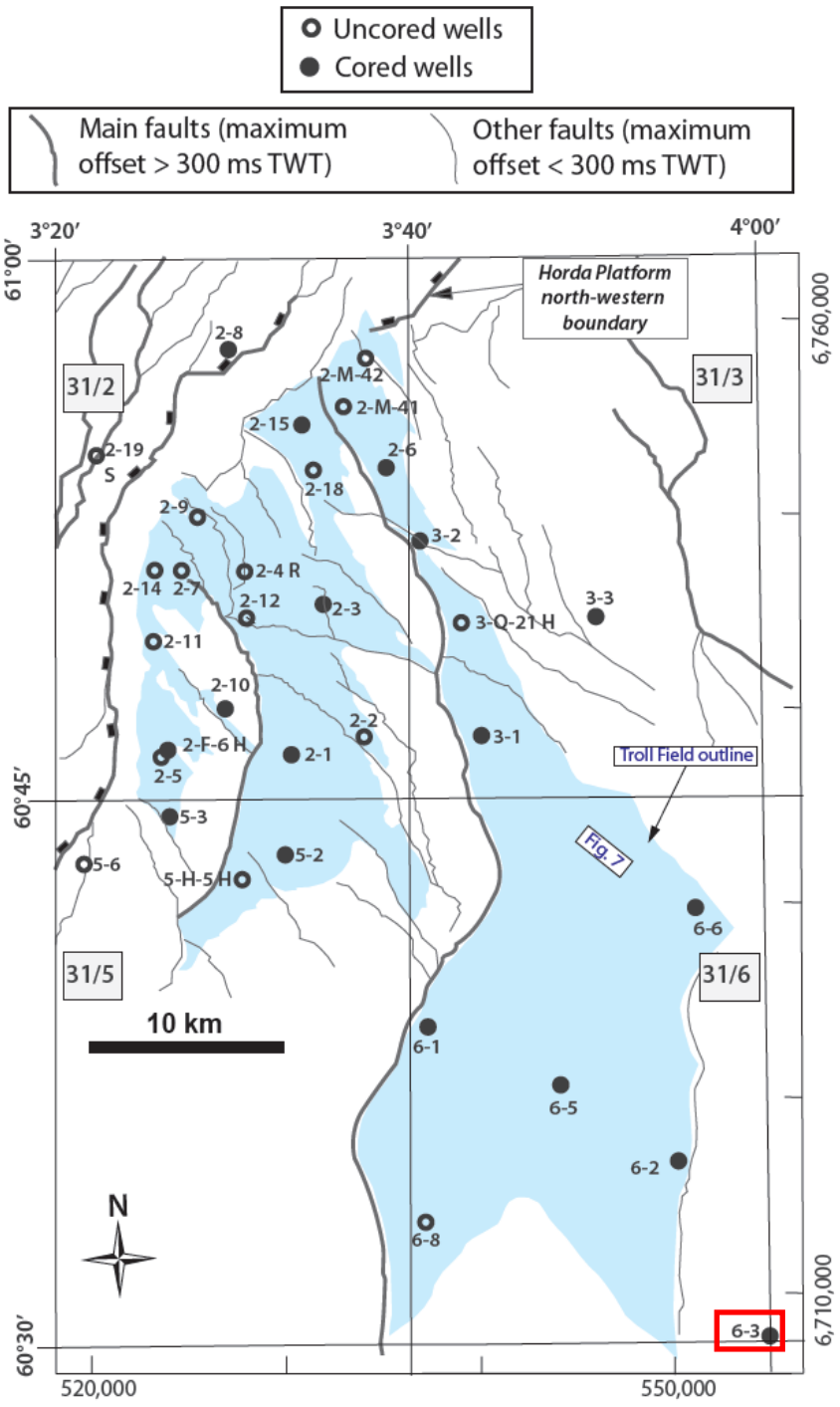
Uncored wells
Cored wells
Main faults (maximum offset > 300 ms TWT)
Other faults (maximum offset < 300 ms TWT)
3°20′
3°40′
4°00′
61°00′
60°45′
60°30′
6,760,000
6,710,000
520,000
550,000
Horda Platform north-western boundary
31/2
31/3
31/5
31/6
Troll Field outline
Fig. 7
10 km
N
2-8
2-M-42
2-M-41
2-15
2-19 S
2-6
2-18
2-9
3-2
2-14
2-7
2-4 R
2-12
2-3
3-3
3-Q-21 H
2-11
2-10
2-2
3-1
2-F-6 H
2-5
2-1
5-3
5-2
5-6
5-H-5 H
6-6
6-1
6-5
6-2
6-8
6-3

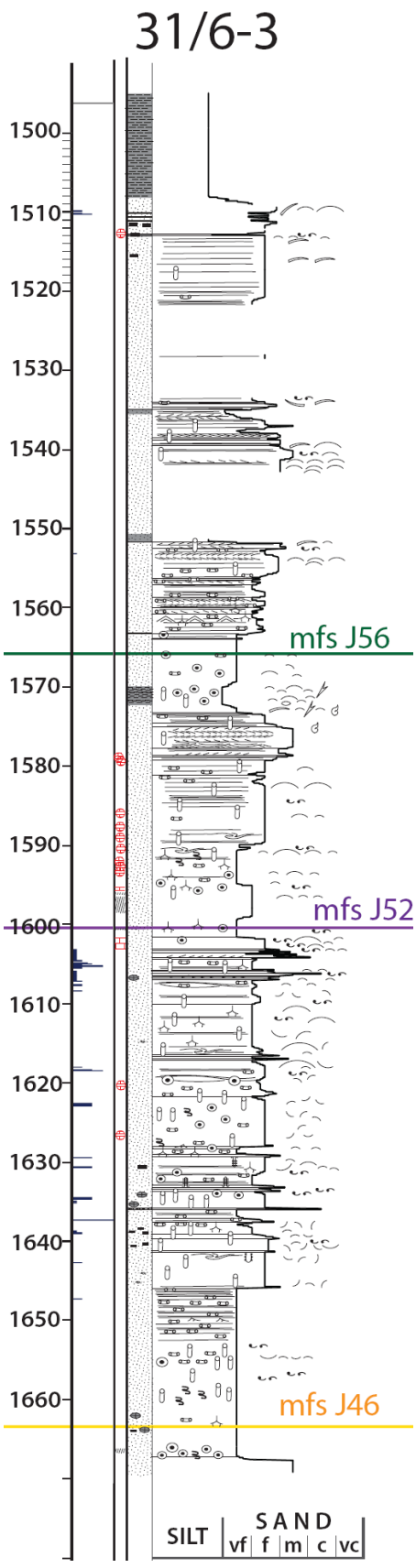
31/6-3
1500
1510
1520
1530
1540
1550
1560
1570
1580
1590
1600
1610
1620
1630
1640
1650
1660
mfs J56
mfs J52
mfs J46
SILT
SAND
vf
f
m
c
vc

NAME: 31/6-3 LOCATION: TROLL EAST
DATE: 19-01-2016 UNIT: m
SHEET No.: 1 SCALE: 1: 50

DEPTH (m)	LITHOLOGY	HANDSPECIMENS & PHOTOGRAPHS	GRAIN SIZE & SEDIMENTARY STRUCTURES (CLAY, SILT, V.F. F. M. C. V.C. SAND, GRANULE, PEBBLE, COBBLE, BOULDER)	DESCRIPTION	INTERP'N (1): DEPOSITIONAL PROCESS	INTERP'N (2): DEPOSITIONAL ENVIRONMENT
1495						
1496		1-1/5		(B)		
1497		1-2/5	Foto 1 142	grey to grey-yellowish to grey marly siltstone with white shells scattered within → BELEMNITES see Foto		
1498		1-3/5				
1499		1-4/5	Foto 4 145			
1500		1-5/5	ABS			
1501		2-1/10	CEM=1	presence of scattered nodules either (B) darker or lighter		
1502		2-2/10		(B)		
1503		2-3/10				
1504		2-4/10	(B)(B)(B) Foto 2 143	(B)(B) discreet levels with shell concentration belemnites rarer below 2/10		
1505		2-5/10	CEM=1			
1506		2-6/10	CEM=1			
1507		2-7/10		interval with a little less light (=5): some minute bioturbation		
		2-8/10	Foto 3 144	a few very large to large pebbles (reddish)		

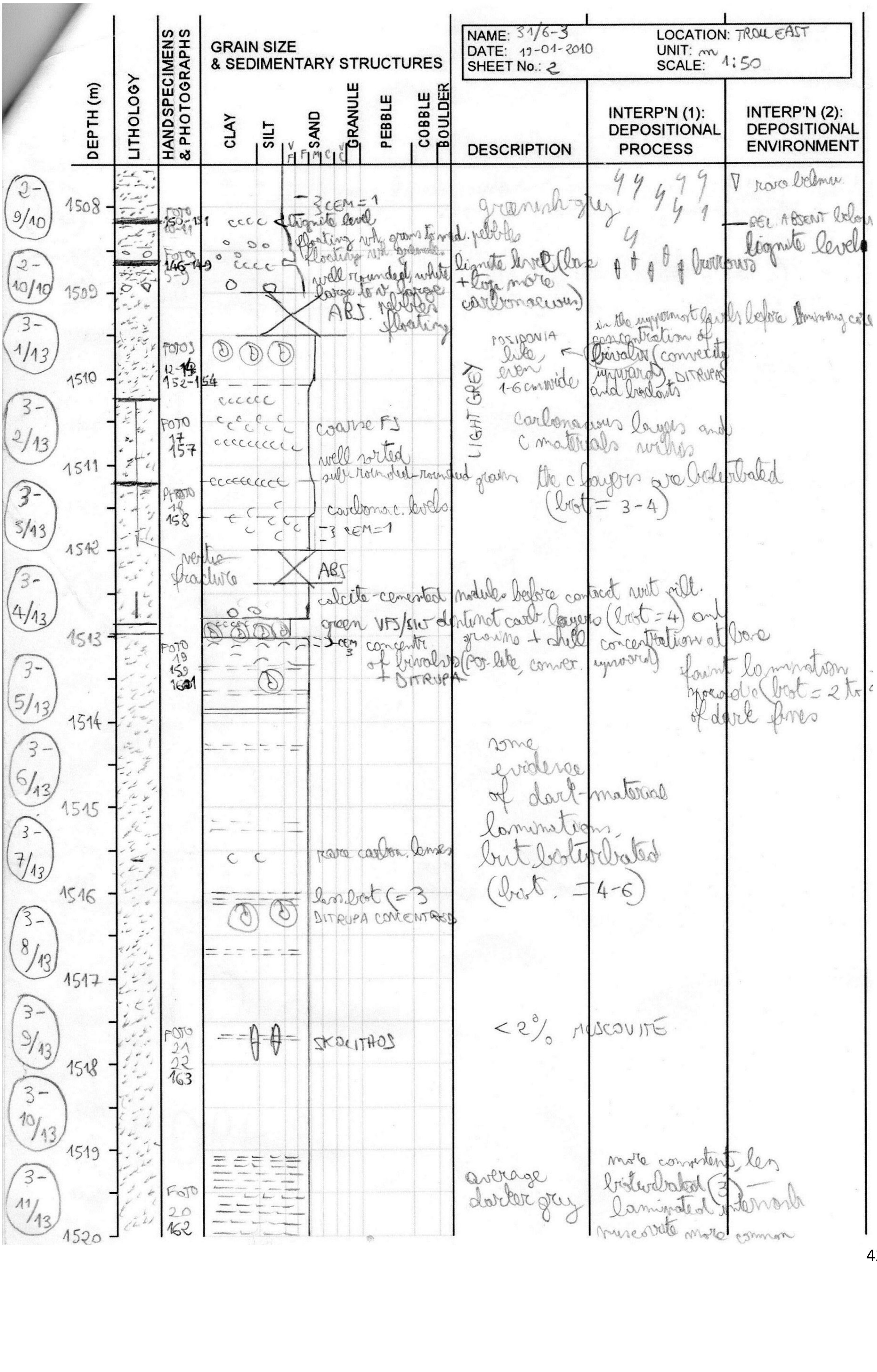
NAME: 31/6-3
DATE: 19-01-2010
SHEET No.: 2
LOCATION: TROLL EAST
UNIT: m
SCALE: 1:50
DEPTH (m)
LITHOLOGY
HANDSPECIMENS & PHOTOGRAPHS
GRAIN SIZE & SEDIMENTARY STRUCTURES
CLAY
SILT
SAND
GRANULE
PEBBLE
COBBLE
BOULDER
DESCRIPTION
INTERP'N (1): DEPOSITIONAL PROCESS
INTERP'N (2): DEPOSITIONAL ENVIRONMENT
1508
1509
1510
1511
1512
1513
1514
1515
1516
1517
1518
1519
1520
greenish-grey
lignite level
ABS.
LIGHT GREY
coarse FS
well sorted
carbonac. levels
CEM=1
ABS
calcite-cemented nodules before contact with silt.
rare carbon. lenses
DITRUPA CONCENTRATED
SKOLITHOS
< 2% MUSCOVITE
average darker grey
rare belemn.
BEL. ABSENT below lignite level
some evidence of dark-material laminations but bioturbated (biot. = 4-6)
muscovite more common

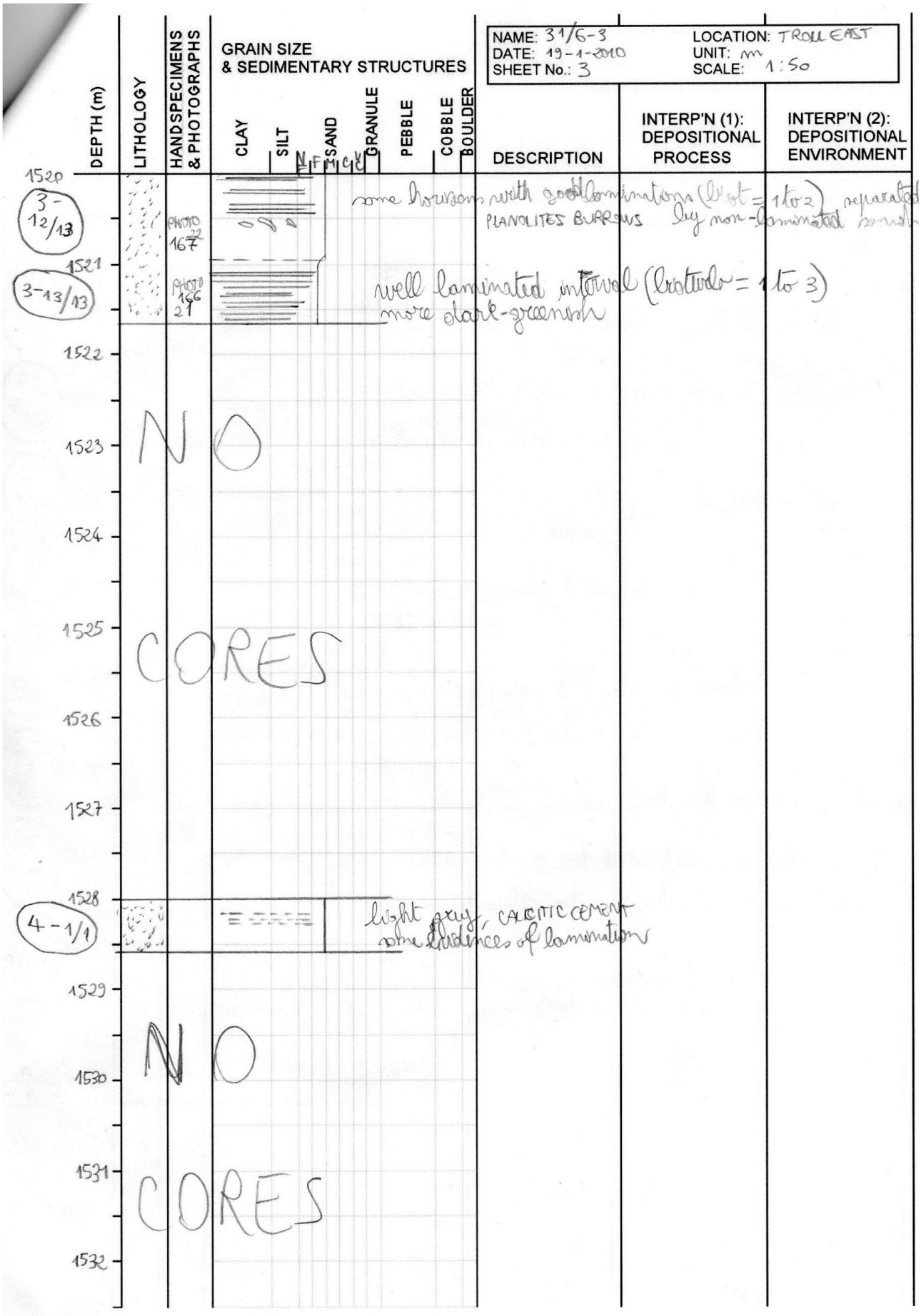
NAME: 31/6-3
DATE: 19-1-2010
SHEET No.: 3
LOCATION: TROLL EAST
UNIT: m
SCALE: 1:50
DEPTH (m)
LITHOLOGY
HANDSPECIMENS & PHOTOGRAPHS
GRAIN SIZE & SEDIMENTARY STRUCTURES
CLAY
SILT
SAND
GRANULE
PEBBLE
COBBLE
BOULDER
DESCRIPTION
INTERP'N (1): DEPOSITIONAL PROCESS
INTERP'N (2): DEPOSITIONAL ENVIRONMENT
1520
1521
1522
1523
1524
1525
1526
1527
1528
1529
1530
1531
1532
3-12/13
PHOTO 167
3-13/13
PHOTO 166 27
some horizons with good laminations (bioturb = 1 to 2) separated
PLANOLITES BURROWS by non-laminated sands
well laminated interval (bioturb = 1 to 3)
more dark-greenish
NO
CORES
4-1/1
light grey, CALCITIC CEMENT
some evidences of lamination
NO
CORES

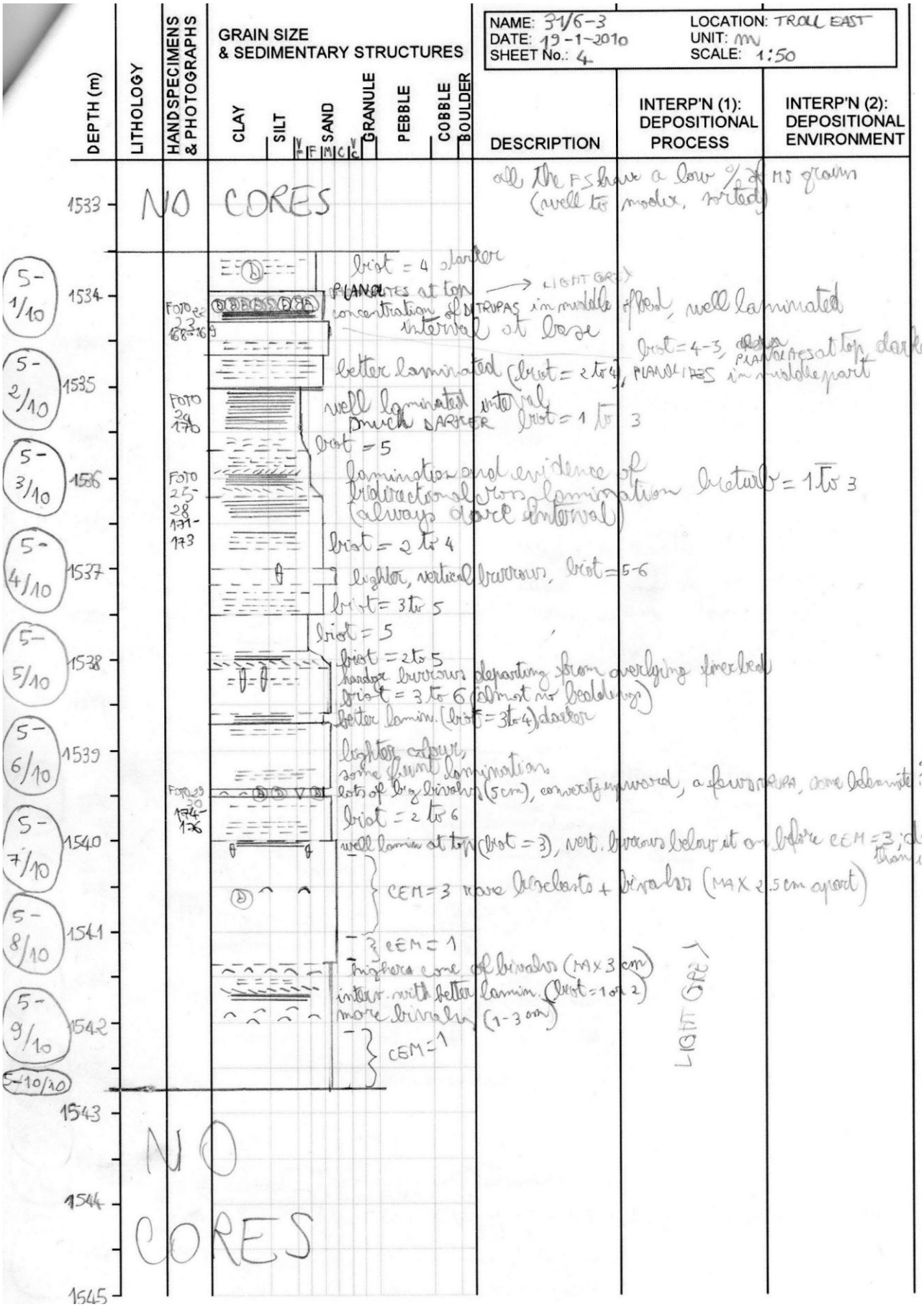
NAME: 31/6-3
DATE: 19-1-2010
SHEET No.: 4
LOCATION: TROLL EAST
UNIT: MV
SCALE: 1:50
GRAIN SIZE & SEDIMENTARY STRUCTURES
DEPTH (m)
LITHOLOGY
HANDSPECIMENS & PHOTOGRAPHS
CLAY
SILT
SAND
GRANULE
PEBBLE
COBBLE
BOULDER
DESCRIPTION
INTERP'N (1): DEPOSITIONAL PROCESS
INTERP'N (2): DEPOSITIONAL ENVIRONMENT
NO CORES
NO CORES
LIGHT GREY

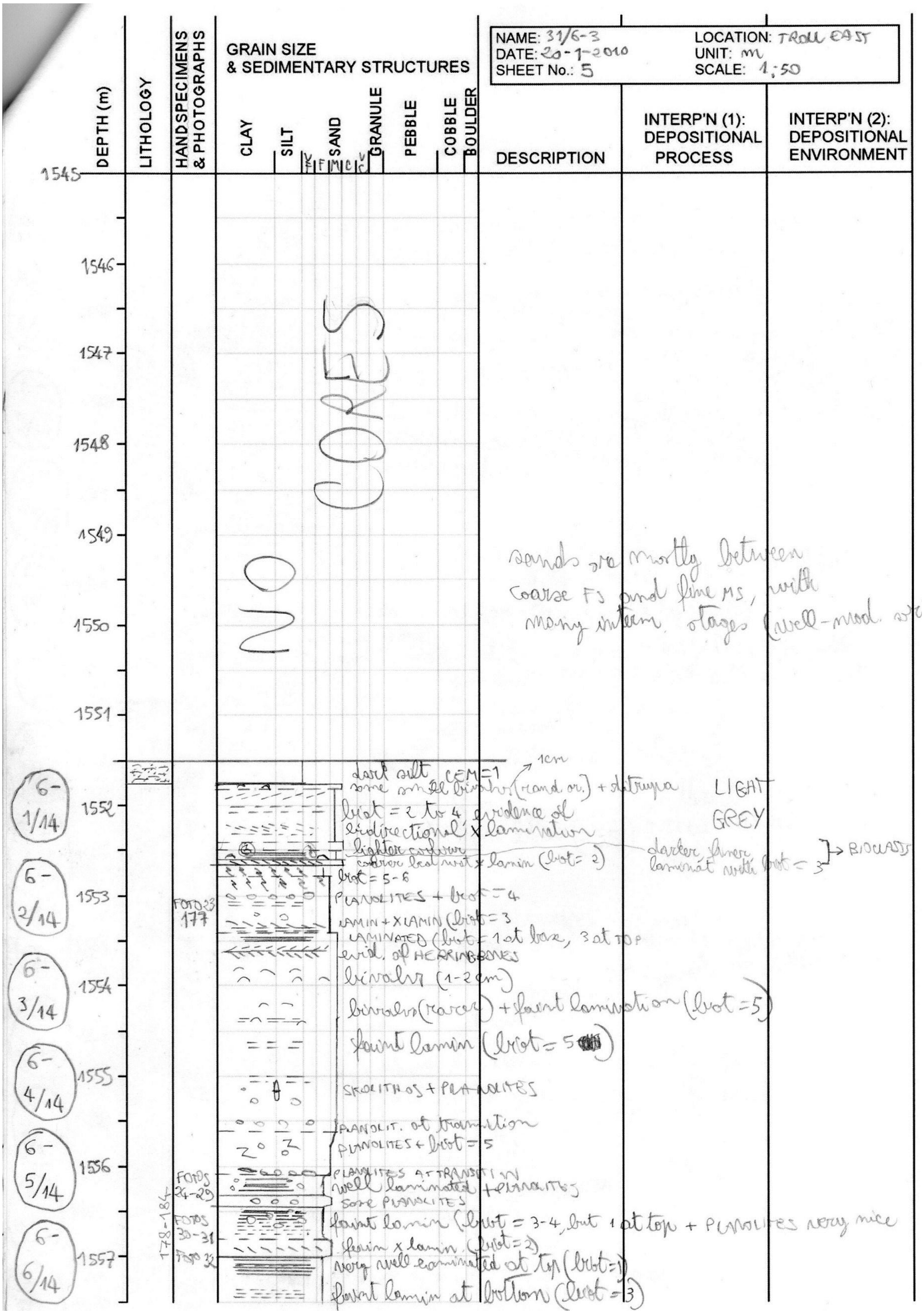
NAME: 31/6-3
DATE: 20-1-2010
SHEET No.: 5
LOCATION: TROLL EAST
UNIT: m
SCALE: 1:50
DEPTH (m)
LITHOLOGY
HANDSPECIMENS & PHOTOGRAPHS
GRAIN SIZE & SEDIMENTARY STRUCTURES
CLAY
SILT
SAND
GRANULE
PEBBLE
COBBLE
BOULDER
DESCRIPTION
INTERP'N (1): DEPOSITIONAL PROCESS
INTERP'N (2): DEPOSITIONAL ENVIRONMENT
1545
1546
1547
1548
1549
1550
1551
1552
1553
1554
1555
1556
1557
NO CORES
sands are mostly between coarse FS and fine MS, with many interm. stages (well-mod. sr
6-1/14
6-2/14
6-3/14
6-4/14
6-5/14
6-6/14
dark silt CEM=1
1cm
some small bivalv. (rand. or.) + skitrupa
LIGHT GREY
biot = 2 to 4 evidence of bidirectional x lamination
lighter colour
coarser bed with x lamin (biot = 2)
darker, finer laminat with biot = 3
BIOCLASTS
biot = 5-6
FOTO 23 177
PLANOLITES + biot = 4
LAMIN + XLAMIN (biot = 3
LAMINATED (biot = 1 at base, 3 at TOP
evid. of HERRINGBONES
bivalv (1-2 cm)
bivalv (rarer) + faint lamination (biot = 5)
faint lamin (biot = 5
SKOLITHOS + PLANOLITES
PLANOLIT. at transition
PLANOLITES + biot = 5
FOTOS 24-29
PLANOLITES AT TRANSITION
well laminated + PLANOLITES
some PLANOLITES
178-184
FOTOS 30-31
faint lamin (biot = 3-4, but 1 at top + PLANOLITES very nice
lamin x lamin (biot = 2)
FOTO 32
very well laminated at top (biot = 1)
faint lamin at bottom (biot = 3)

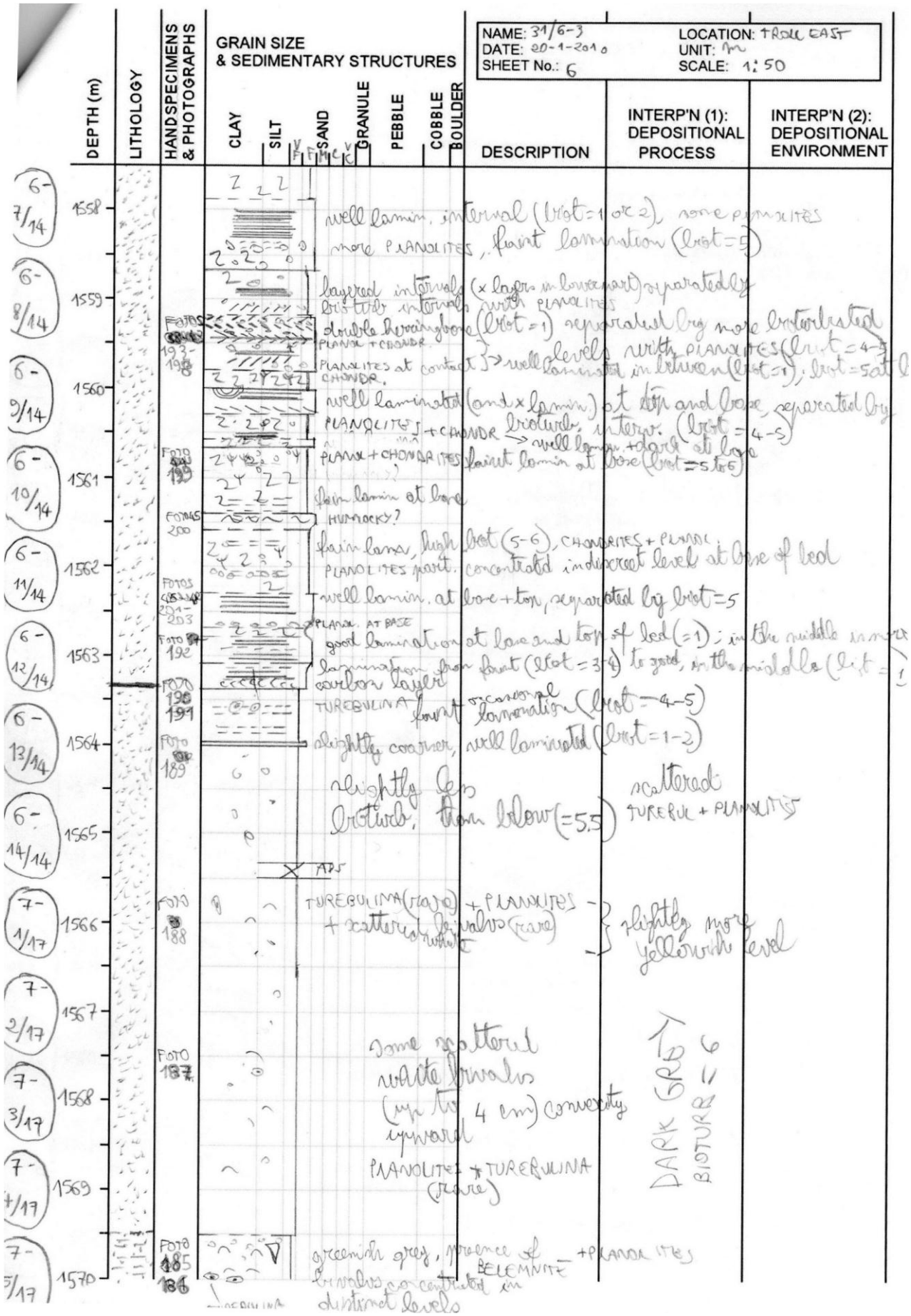
NAME: 31/6-3
DATE: 20-1-2010
SHEET No.: 6
LOCATION: TROLL EAST
UNIT: Nm
SCALE: 1:50
DEPTH (m)
LITHOLOGY
HANDSPECIMENS & PHOTOGRAPHS
GRAIN SIZE & SEDIMENTARY STRUCTURES
CLAY
SILT
SAND
GRANULE
PEBBLE
COBBLE
BOULDER
DESCRIPTION
INTERP'N (1): DEPOSITIONAL PROCESS
INTERP'N (2): DEPOSITIONAL ENVIRONMENT
1558
1559
1560
1561
1562
1563
1564
1565
1566
1567
1568
1569
1570
well lamin. interval (biot=1 or 2), some PLANOLITES
more PLANOLITES, faint lamination (biot=5)
layered interval (x layers in lower part) separated by
bioturb intervals with PLANOLITES
double bioturbabore (biot=1) separated by more interlaminated
PLANOLITES + CHONDR.
PLANOLITES at contact } => well levels with PLANOLITES (biot=4-5)
CHONDR. well laminated in between (biot=1), biot=5 at t
well laminated (cm to x lamin) at top and base, separated by
PLANOLITES + CHONDR bioturb. interv. (biot=4-5)
=> well lamin + bore at base
PLANOLITES + CHONDRITES faint lamin at base (biot=5 to 6)
faint lamin at base
HUMMOCKY?
faint lamin, high biot (5-6), CHONDRITES + PLANOLITES part. concentrated in discreet levels at base of bed
well lamin. at base + top, separated by biot=5
PLANOLITES AT BASE
good lamination at base and top of bed (=1); in the middle in
laminations from faint (biot=3-4) to good, in the middle (biot=
carbon layer
TUREBULINA
occasional laminations (biot=4-5)
slightly coarser, well laminated (biot=1-2)
slightly less bioturb. than below (=5.5)
scattered TUREBUL + PLANOLITES
ATS
TUREBULINA (rare) + PLANOLITES + scattered bivalves (rare)
slightly more yellowish level
some scattered white bivalves (up to 4 cm) convexity upward
PLANOLITES + TUREBULINA (rare)
DARK GREY BIOTURB
greenish grey, presence of BELEMNITE + PLANOLITES
bivalves concentrated in discreet levels
TUREBULINA
FOTOS 193-198
FOTOS 200
FOTOS 201-203
FOTO 192
FOTO 190 191
FOTO 189
FOTO 188
FOTO 187
FOTO 185 186
6-7/14
6-8/14
6-9/14
6-10/14
6-11/14
6-12/14
6-13/14
6-14/14
7-1/17
7-2/17
7-3/17
7-4/17
7-5/17

NAME: 31/6-3 LOCATION: TROLL EAST
DATE: 20-1-2010 UNIT: m
SHEET No.: 7 SCALE: 1:50

DEPTH (m)	LITHOLOGY	HANDSPECIMENS & PHOTOGRAPHS	GRAIN SIZE & SEDIMENTARY STRUCTURES (CLAY, SILT, SAND VF F M C VC, GRANULE, PEBBLE, COBBLE, BOULDER)	DESCRIPTION	INTERP'N (1): DEPOSITIONAL PROCESS	INTERP'N (2): DEPOSITIONAL ENVIRONMENT
1570				highly bioturb. (= 6) scattered Teichichnus + white bivalves? concentrated in discreet levels	CHONDRITES + PLANOLITES throughout	the white bivalves in this levels are very flattened (ag
1571		205 FOTO 41; FOTO 40 204		ABS; concentr. of bivalves; long vertical burrows		
1572		FOTO 42 206		CEM = 3; rare bivalves, with valves still closes		
1573		209 210 FOTO 45/46; 207 208 FOTO 43 44		very bioturb., concentr. of upward convex bivalves + DITRUPA in the centre of biot; concentrat. of shells + DITRUPA at transition → even BELEMNITES and other bioclasts very bioturb.		
1574		212 214 FOTOS 46-49		discreet laminated intervals (top + centre, biot = 2-4); concentr. of PLANOLITES in the centre; SKOLITHOS biot = 6		
1575		211 FOTO 45		discreet laminated levels (biot = 4) separ. by biot = 6; x lamin (biot = 2-3) at base + top, separated by biot = 6; presence of white bioclasts		
1576		215-219 FOTOS 1-5		very nice HERRINGBONES biot = 1		
1577		220 221 FOTOS 6-7				
1578						
1579				nodules of calcite-cem sands; very faint lamin (biot = 5-6)		
1580				NODULE of calcite-cem. sand; occasional very faint lam. (biot = 5-6); scattered PLANOLITES, a few bivalves (convex upward) RARE; very well bioturbated		
1581				darker, PLANOLITES, faint lamin (biot = 4-5); concentr. of PLANOLITES		↓ more dark (greener)
1582		222 FOTO 8		PLANOLITES + faint lamin (biot = 5); CEM = 1; concentr. of big (ca 4-5 cm) bivalves		

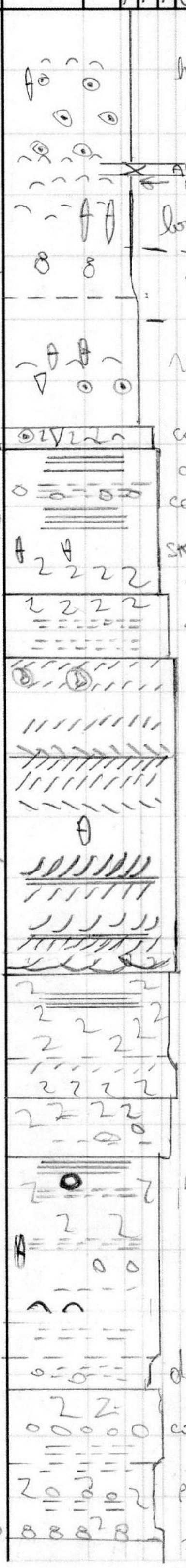

Core box labels (left margin): 7-5/17, 7-6/17, 7-7/17, 7-8/17, 7-9/17, 7-10/17, 7-11/17, 7-12/17, 7-13/17, 7-14/17, 7-15/17, 7-16/17, 7-17/17

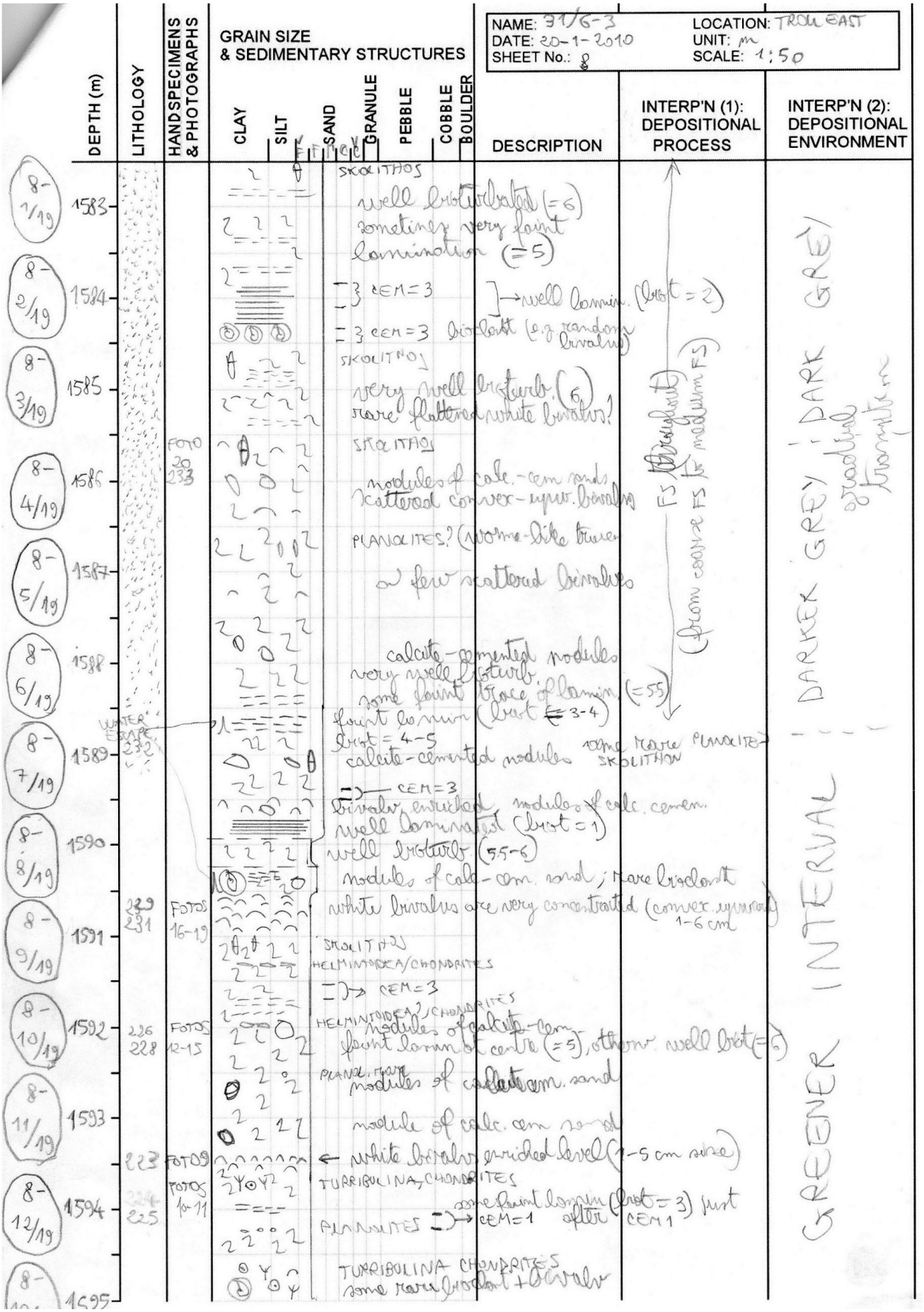
NAME: 31/6-3
DATE: 20-1-2010
SHEET No.: 8
LOCATION: TROLL EAST
UNIT: m
SCALE: 1:50
DEPTH (m)
LITHOLOGY
HANDSPECIMENS & PHOTOGRAPHS
GRAIN SIZE & SEDIMENTARY STRUCTURES
CLAY
SILT
SAND
GRANULE
PEBBLE
COBBLE
BOULDER
DESCRIPTION
INTERP'N (1): DEPOSITIONAL PROCESS
INTERP'N (2): DEPOSITIONAL ENVIRONMENT
GREENER INTERVAL
DARKER GREY / DARK GREY

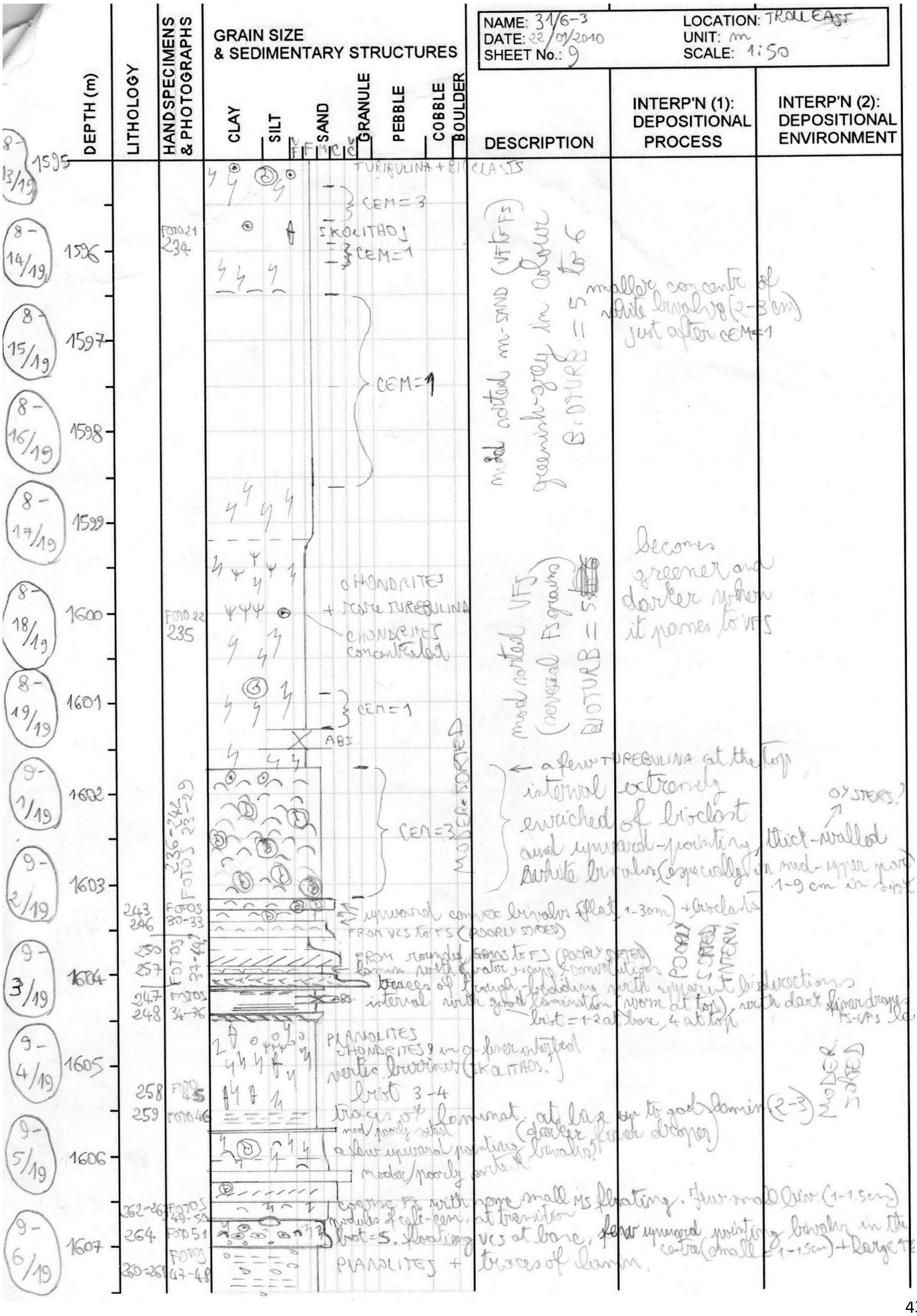
NAME: 31/6-3
DATE: 22/07/2010
SHEET No.: 9
LOCATION: TROLL EAST
UNIT: m
SCALE: 1:50
DEPTH (m)
LITHOLOGY
HANDSPECIMENS & PHOTOGRAPHS
GRAIN SIZE & SEDIMENTARY STRUCTURES
CLAY
SILT
SAND
VF F M C VC
GRANULE
PEBBLE
COBBLE
BOULDER
DESCRIPTION
INTERP'N (1): DEPOSITIONAL PROCESS
INTERP'N (2): DEPOSITIONAL ENVIRONMENT
1595
1596
1597
1598
1599
1600
1601
1602
1603
1604
1605
1606
1607
TUREBULINA + BIOCLASTS
CEM=3
SKOLITHOS
CEM=1
CEM=1
CHONDRITES
+ rare TUREBULINA
CHONDRITES concentrated
CEM=1
ABS
CEM=3
MODER. SORTED
mod sorted m-SAND (VF to FS)
greenish-grey in colour
BIOTURB = 5 to 6
smaller concentr. of white bivalves (2-3 cm)
just after CEM=1
mod sorted VFS
(several FS grains)
BIOTURB = 5
becomes greener and darker when it passes to VFS
a few TUREBULINA at the top
interval extremely enriched of bioclast and upward-pointing thick-walled white bivalves (especially in mid-upper part) 1-9 cm in size
OYSTERS?
upward convex bivalves flat (1-3 cm) + bioclasts
FROM VCS to FS (POORLY SORTED)
FROM rounded grains to FS (POORLY SORTED)
lamin. with water escape & convolution
traces of trough-bedding with apparent bidirections
interval with good lamination (worn at top) with dark finer drapes FS-VFS
biot = 1-2 at base, 4 at top
ABS.
POORLY SORTED INTERV.
PLANOLITES
CHONDRITES in finer interbed
vertic. burrows (SKOLITHOS)
biot 3-4
traces of laminat. at base up to good lamin. (2-3)
mod/poorly sorted
a few upward pointing bivalves (darker, finer drapes)
moder/poorly sorted
MODER. SORTED
coarse FS with some small MS floating. Few small biv. (1-1.5 cm)
nodules of calc-cem at transition
biot = 5. floating VCS at base, few upward pointing bivalves in the centre (small = 1-1.5 cm) + large
PLANOLITES + traces of lamin.
FOTO 21 234
FOTO 22 235
FOTOS 236-242 23-29
243 246 FOTOS 30-33
255 257 FOTOS 37-44
247 248 FOTOS 34-36
258 FOTO 45
259 FOTO 46
262-263 FOTOS 49-50
264 FOTO 51
260-261 FOTOS 47-48
8-13/19
8-14/19
8-15/19
8-16/19
8-17/19
8-18/19
8-19/19
9-1/19
9-2/19
9-3/19
9-4/19
9-5/19
9-6/19

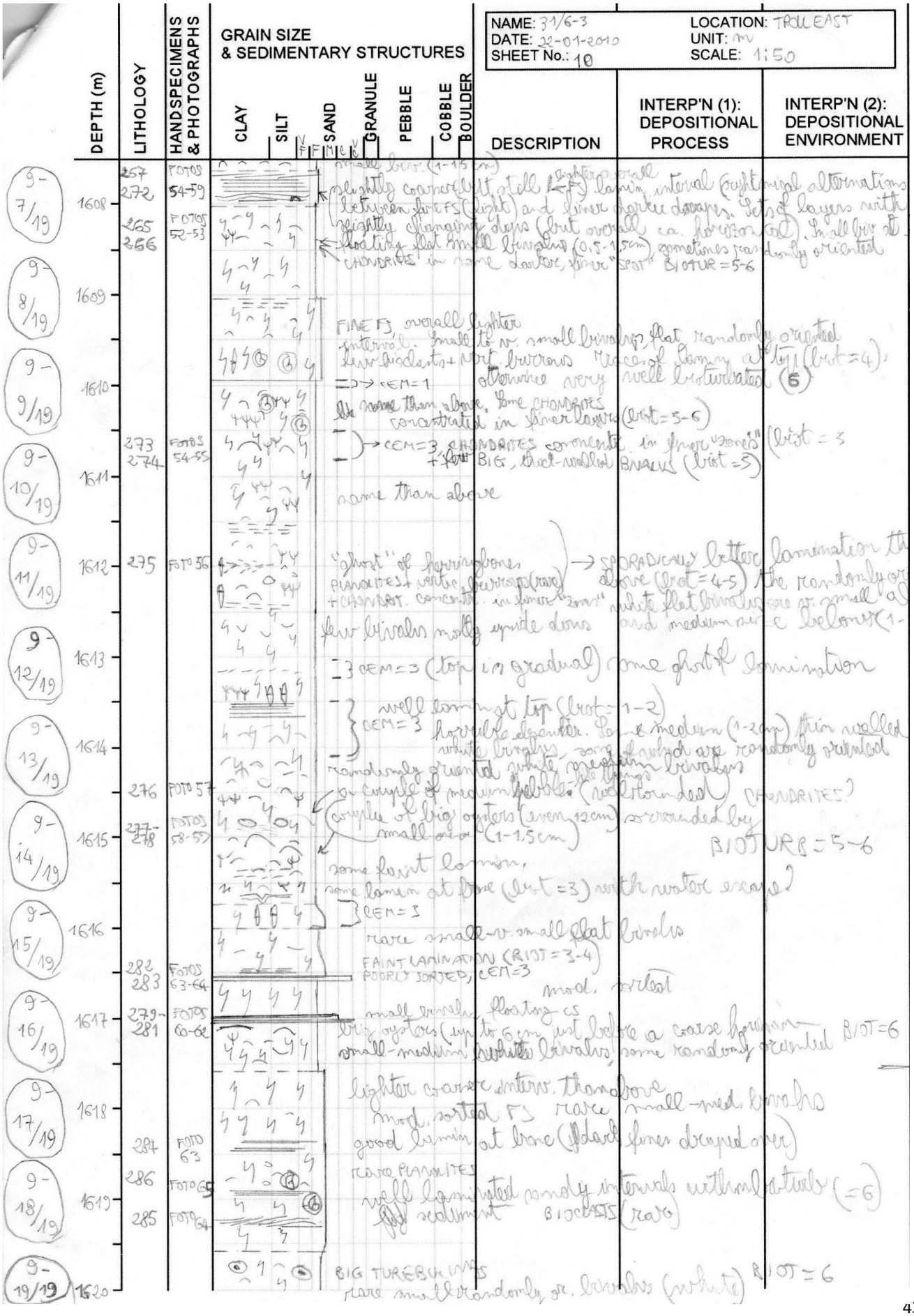
NAME: 31/6-3
DATE: 22-01-2010
SHEET No.: 10
LOCATION: TROLL EAST
UNIT: Nv
SCALE: 1:50
DEPTH (m)
LITHOLOGY
HANDSPECIMENS & PHOTOGRAPHS
GRAIN SIZE & SEDIMENTARY STRUCTURES
CLAY
SILT
SAND
GRANULE
PEBBLE
COBBLE
BOULDER
DESCRIPTION
INTERP'N (1): DEPOSITIONAL PROCESS
INTERP'N (2): DEPOSITIONAL ENVIRONMENT
9-7/19
9-8/19
9-9/19
9-10/19
9-11/19
9-12/19
9-13/19
9-14/19
9-15/19
9-16/19
9-17/19
9-18/19
9-19/19
1608
1609
1610
1611
1612
1613
1614
1615
1616
1617
1618
1619
1620
FOTOS 54-59
FOTOS 52-53
FOTOS 54-55
FOTO 56
FOTO 57
FOTOS 58-59
FOTOS 63-64
FOTOS 60-62
FOTO 63
FOTO 65
FOTO 64
BIOTURB=5-6
BIOT=6

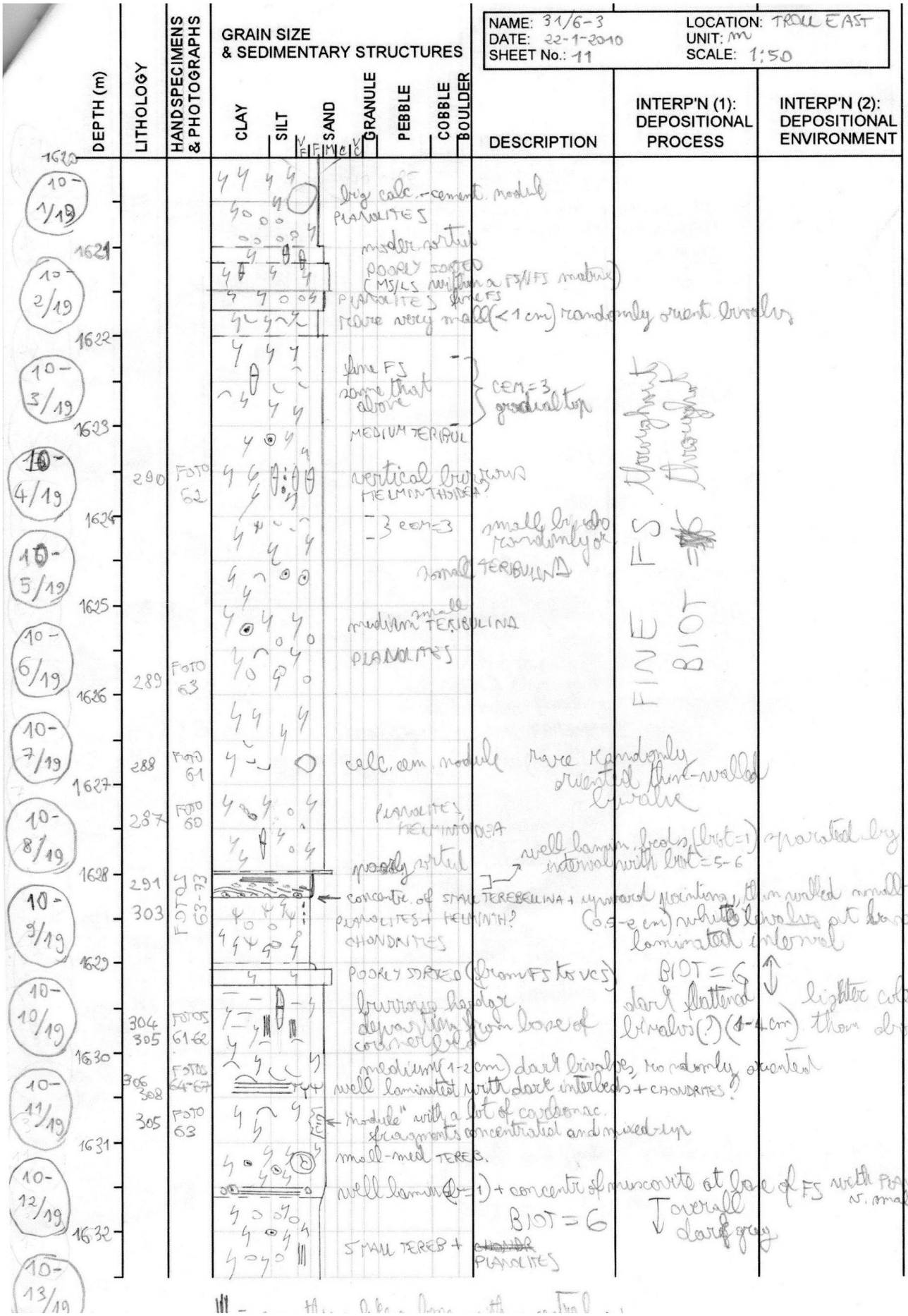
NAME: 31/6-3
DATE: 22-1-2010
SHEET No.: 11
LOCATION: TROLL EAST
UNIT: m
SCALE: 1:50
GRAIN SIZE & SEDIMENTARY STRUCTURES
DEPTH (m)
LITHOLOGY
HANDSPECIMENS & PHOTOGRAPHS
CLAY
SILT
SAND
GRANULE
PEBBLE
COBBLE
BOULDER
DESCRIPTION
INTERP'N (1): DEPOSITIONAL PROCESS
INTERP'N (2): DEPOSITIONAL ENVIRONMENT
1620
1621
1622
1623
1624
1625
1626
1627
1628
1629
1630
1631
1632
10-1/19
10-2/19
10-3/19
10-4/19
10-5/19
10-6/19
10-7/19
10-8/19
10-9/19
10-10/19
10-11/19
10-12/19
10-13/19
290
289
288
287
291
303
304
305
306
308
FOTO 62
FOTO 63
FOTO 61
FOTO 60
FOTOS 63-73
FOTOS 61-62
FOTOS 64-67
FOTO 63
big calc.-cement. nodule
PLANOLITES
moder. sorted
POORLY SORTED (MS/LS within a FS/MFS matrix)
PLANOLITES in FS
rare very small (<1 cm) randomly oriented burrows
fine FS
zone that above
CEM=3 gradual top
MEDIUM TERIBUL
vertical burrows HELMINTHOIDEA
small burrows randomly or
small TEREBULINA
medium small TEREBULINA
PLANOLITES
calc. cem. nodule
rare randomly oriented thin-walled burrow
PLANOLITES, HELMINTHOIDEA
poorly sorted
well lamin. fecals (bio=1) separated by interval with bio=5-6
concentr. of SMALL TEREBELLINA + upward pointing, thin walled small (0.5-2 cm) white burrows at base of laminated interval
PLANOLITES + HELMINTH?
CHONDRITES
POORLY SORTED (from FS to VCS)
BIOT=6
burrowed hardgr. dark flattened burrows (?) (1-4 cm) lighter colour than ab
separating from base of conformable
medium (1-2 cm) dark burrows, randomly oriented
well laminated with dark interbeds + CHONDRITES?
"nodule" with a lot of carbonac. fragments concentrated and mixed up
small-med TEREB.
well lamin (bio=1) + concentr of muscovite at base of FS with PLANOL N. small
BIOT=6
overall dark grey
SMALL TEREB + PLANOLITES
FINE BIOT
LS

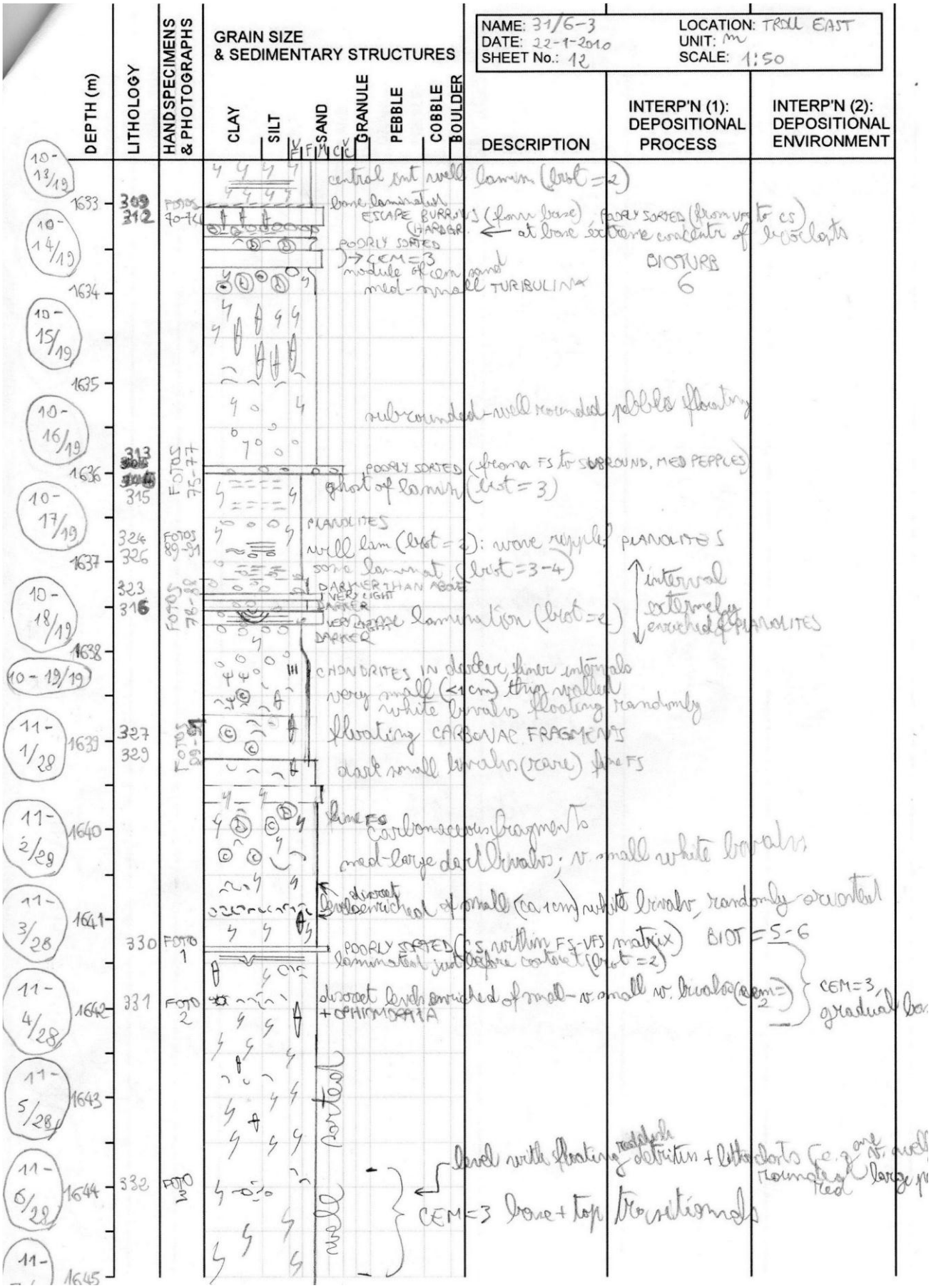
NAME: 31/6-3
DATE: 22-1-2010
SHEET No.: 12
LOCATION: TROLL EAST
UNIT: m
SCALE: 1:50
DEPTH (m)
LITHOLOGY
HANDSPECIMENS & PHOTOGRAPHS
GRAIN SIZE & SEDIMENTARY STRUCTURES
CLAY
SILT
SAND
GRANULE
PEBBLE
COBBLE
BOULDER
DESCRIPTION
INTERP'N (1): DEPOSITIONAL PROCESS
INTERP'N (2): DEPOSITIONAL ENVIRONMENT
BIOTURB 6
PLANOLITES
CHONDRITES
CARBONACEOUS FRAGMENTS
FOTOS 70-76
FOTOS 75-77
FOTOS 89-91
FOTOS 78-88
FOTO 1
FOTO 2
FOTO 3
1633
1634
1635
1636
1637
1638
1639
1640
1641
1642
1643
1644
1645


NAME: 31/6-3
DATE: 25-1-2010
SHEET No.: 13
LOCATION: TROLL EAST
UNIT: Nn
SCALE: 1:50
DEPTH (m)
LITHOLOGY
HANDSPECIMENS & PHOTOGRAPHS
GRAIN SIZE & SEDIMENTARY STRUCTURES
CLAY
SILT
SAND
VF F M C VC
GRANULE
PEBBLE
COBBLE
BOULDER
DESCRIPTION
INTERP'N (1): DEPOSITIONAL PROCESS
INTERP'N (2): DEPOSITIONAL ENVIRONMENT
11-7/28
1645
11-8/28
1646
333
FOTO 4
11-9/28
1647
334
336
FOTOS 5-7
11-10/28
1648
11-11/28
1649
11-12/28
1650
337
340
FOTOS 8-11
11-13/28
1651
11-14/28
1652
11-15/28
1653
341
FOTO 12
11-16/28
1654
11-17/28
1655
342
FOTO 13
11-18/28
1656
11-19/28
1657
laminations of yellowish FS well dark greenish finer material
overall dark greenish colour
very well bioturbated (6)

NAME: 31/6-3
DATE: 25-1-2010
SHEET No.: 14

LOCATION: TROLL EAST
UNIT: m
SCALE: 1:50

DEPTH (m)	LITHOLOGY	HANDSPECIMENS & PHOTOGRAPHS	GRAIN SIZE & SEDIMENTARY STRUCTURES (CLAY, SILT, VF, F, M SAND, C, VC, GRANULE, PEBBLE, COBBLE, BOULDER)	DESCRIPTION	INTERP'N (1): DEPOSITIONAL PROCESS	INTERP'N (2): DEPOSITIONAL ENVIRONMENT
(11-20/28) 1658					well- moder. sorted throughout	very well bioturb. (=6) greyish internal transition greenish coloured
(11-21/28) 1659						
(11-22/28) 1660	343	FOTO 14		= particular worm-like fossil traces		
(11-23/28) 1661						
(11-24/28) 1662	344	FOTO 15		"nodules" of apparent coarser gr. size (VFS/FS) CHONDR.? few PLANOL?		
(11-25/28) 1663						
(11-26/28) 1664				few carbonaceous remains + some "nodules" of apparently coarser grain size (VFS/FS)		
(11-27/28) 1665				very very bioturb. (there's nothing in it)		
(11-28/28)						
1666			NO DATA	VFS, but not micaceous at all (throughout)		
(12-1/29)				⟹ CEM=1		
	347	FOTO 18		scattered med-big TURIBUL.		
1667	346	FOTO 17		small-medium TURIBULUS more conc.		
(12-2/29)	343	FOTO 16		worm trace ← 5 cm of CEM=3 just above contact		
1668				MS grains within FS matrix (mod. sorted		
(12-3/29) 1669						

31/6-5

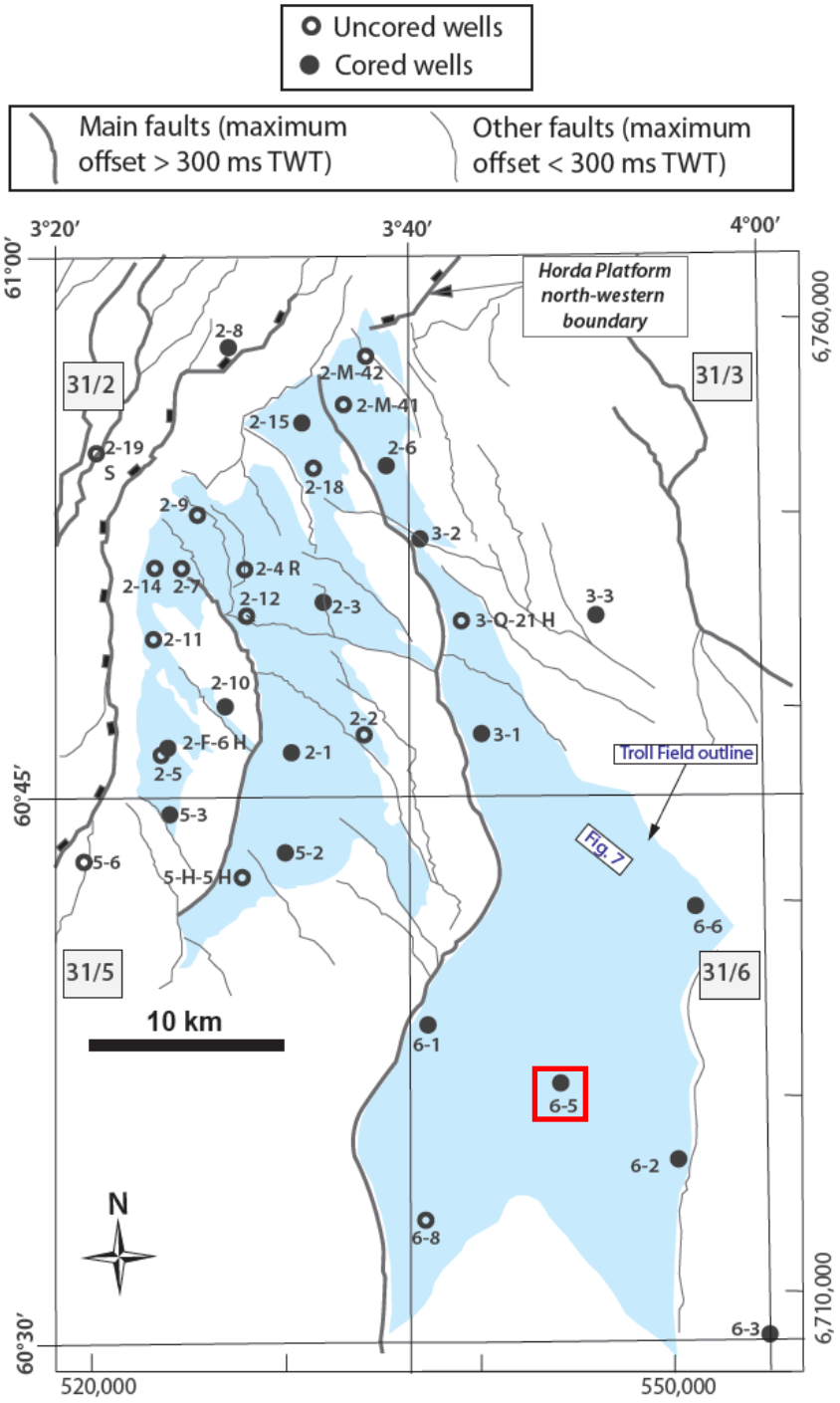
Uncored wells
Cored wells
Main faults (maximum offset > 300 ms TWT)
Other faults (maximum offset < 300 ms TWT)
3°20′
3°40′
4°00′
61°00′
60°45′
60°30′
6,760,000
6,710,000
520,000
550,000
Horda Platform north-western boundary
Troll Field outline
Fig. 7
31/2
31/3
31/5
31/6
10 km
N
2-8
2-M-42
2-M-41
2-15
2-19 S
2-6
2-18
2-9
3-2
2-14
2-7
2-4 R
2-12
2-3
3-Q-21 H
3-3
2-11
2-10
2-2
3-1
2-F-6 H
2-5
2-1
5-3
5-6
5-H-5 H
5-2
6-6
6-1
6-5
6-2
6-8
6-3

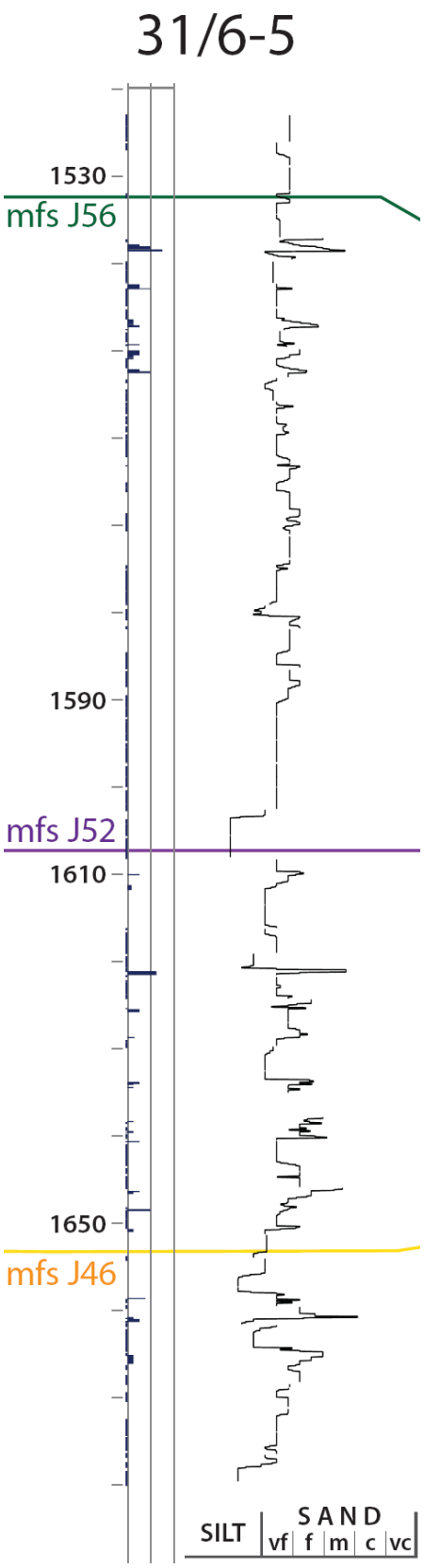
31/6-5
1530
mfs J56
1590
mfs J52
1610
1650
mfs J46
SILT
SAND
vf
f
m
c
vc

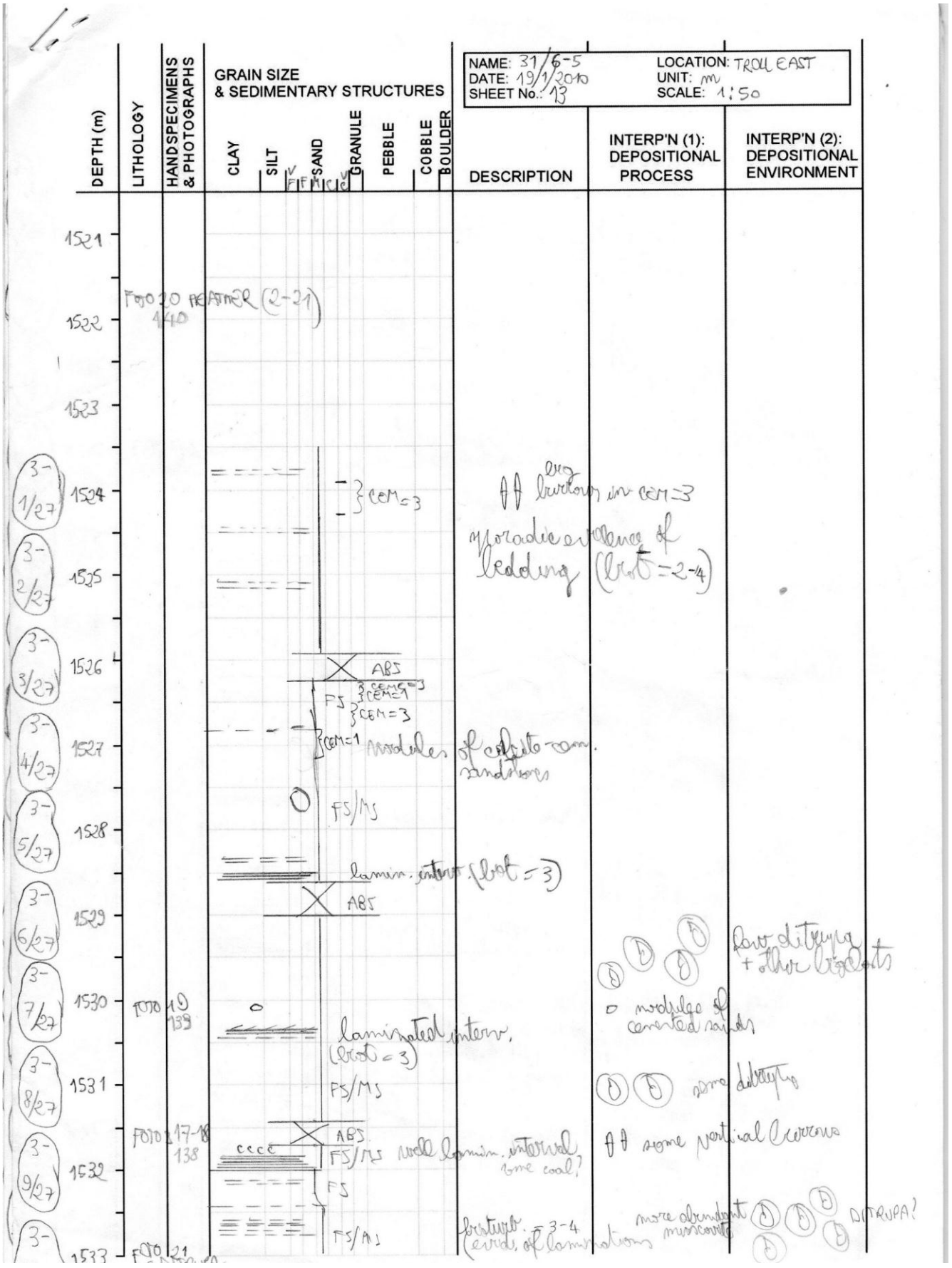
NAME: 31/6-5
DATE: 19/1/2010
SHEET No.: 13
LOCATION: TROLL EAST
UNIT: m
SCALE: 1:50
DEPTH (m)
LITHOLOGY
HANDSPECIMENS & PHOTOGRAPHS
GRAIN SIZE & SEDIMENTARY STRUCTURES
CLAY
SILT
SAND
GRANULE
PEBBLE
COBBLE
BOULDER
DESCRIPTION
INTERP'N (1): DEPOSITIONAL PROCESS
INTERP'N (2): DEPOSITIONAL ENVIRONMENT
1521
1522
1523
1524
1525
1526
1527
1528
1529
1530
1531
1532
1533
FOTO 20 FEATHER (2-21)
1410
3-1/27
3-2/27
3-3/27
3-4/27
3-5/27
3-6/27
3-7/27
3-8/27
3-9/27
3-
FOTO 19
1359
FOTO 17-18
1338
FOTO 21
CEM=3
CEM=1
ABS
FS
FS/MS
laminated interv. (bioT=3)
ccccc
FS/MS well lamin. interval, some coal?
bioturb. 3-4 (evids. of lamination)
more abundant mussels
DITRUPA?

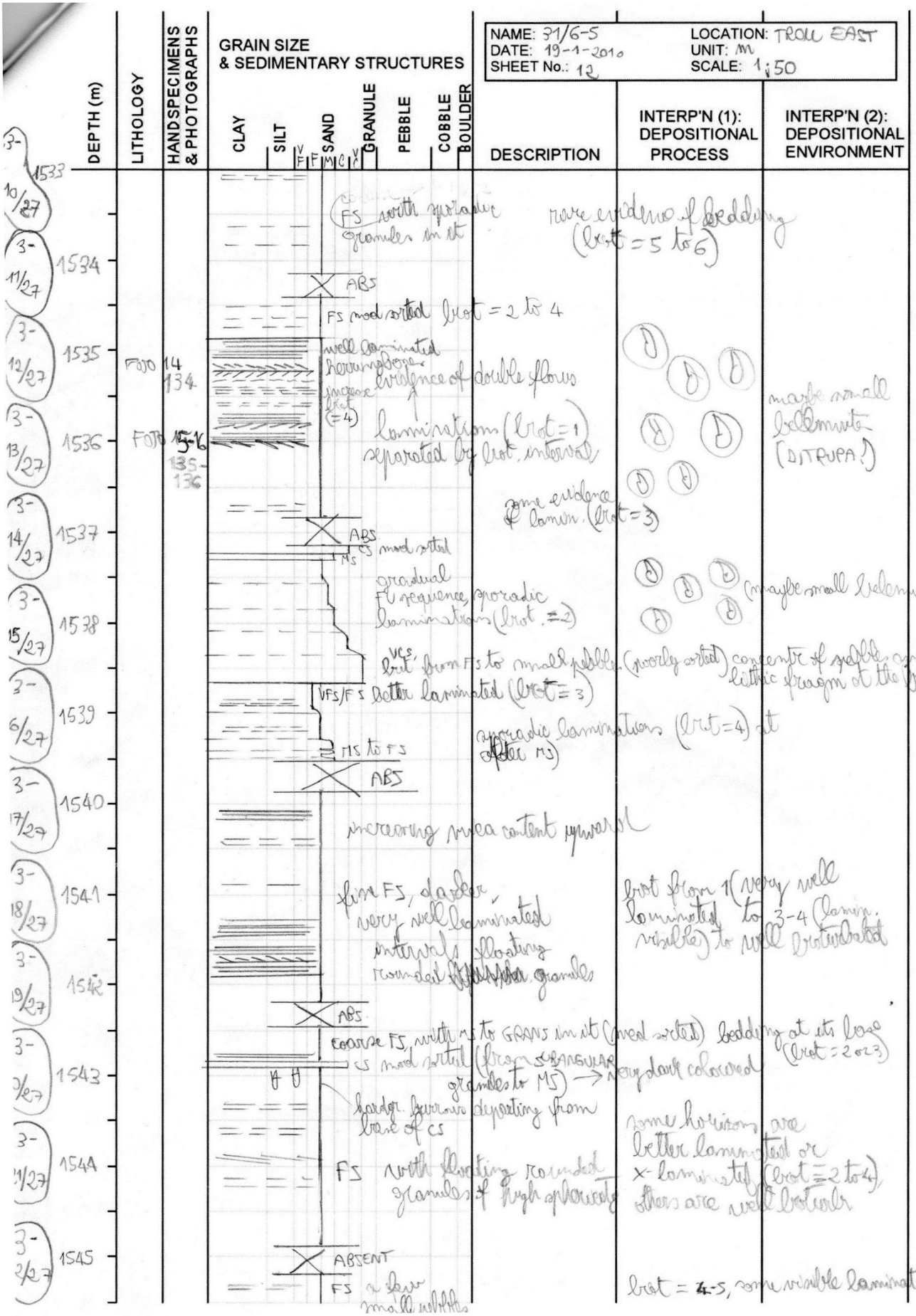
NAME: 31/6-5
DATE: 19-1-2010
SHEET No.: 12
LOCATION: TROLL EAST
UNIT: m
SCALE: 1:50
DEPTH (m)
LITHOLOGY
HANDSPECIMENS & PHOTOGRAPHS
GRAIN SIZE & SEDIMENTARY STRUCTURES
CLAY
SILT
SAND
GRANULE
PEBBLE
COBBLE
BOULDER
DESCRIPTION
INTERP'N (1): DEPOSITIONAL PROCESS
INTERP'N (2): DEPOSITIONAL ENVIRONMENT
1533
1534
1535
1536
1537
1538
1539
1540
1541
1542
1543
1544
1545
FOTO 14 134
FOTO 15-16 135-136
ABS
FS
CS
MS
VFS/FS
ABSENT

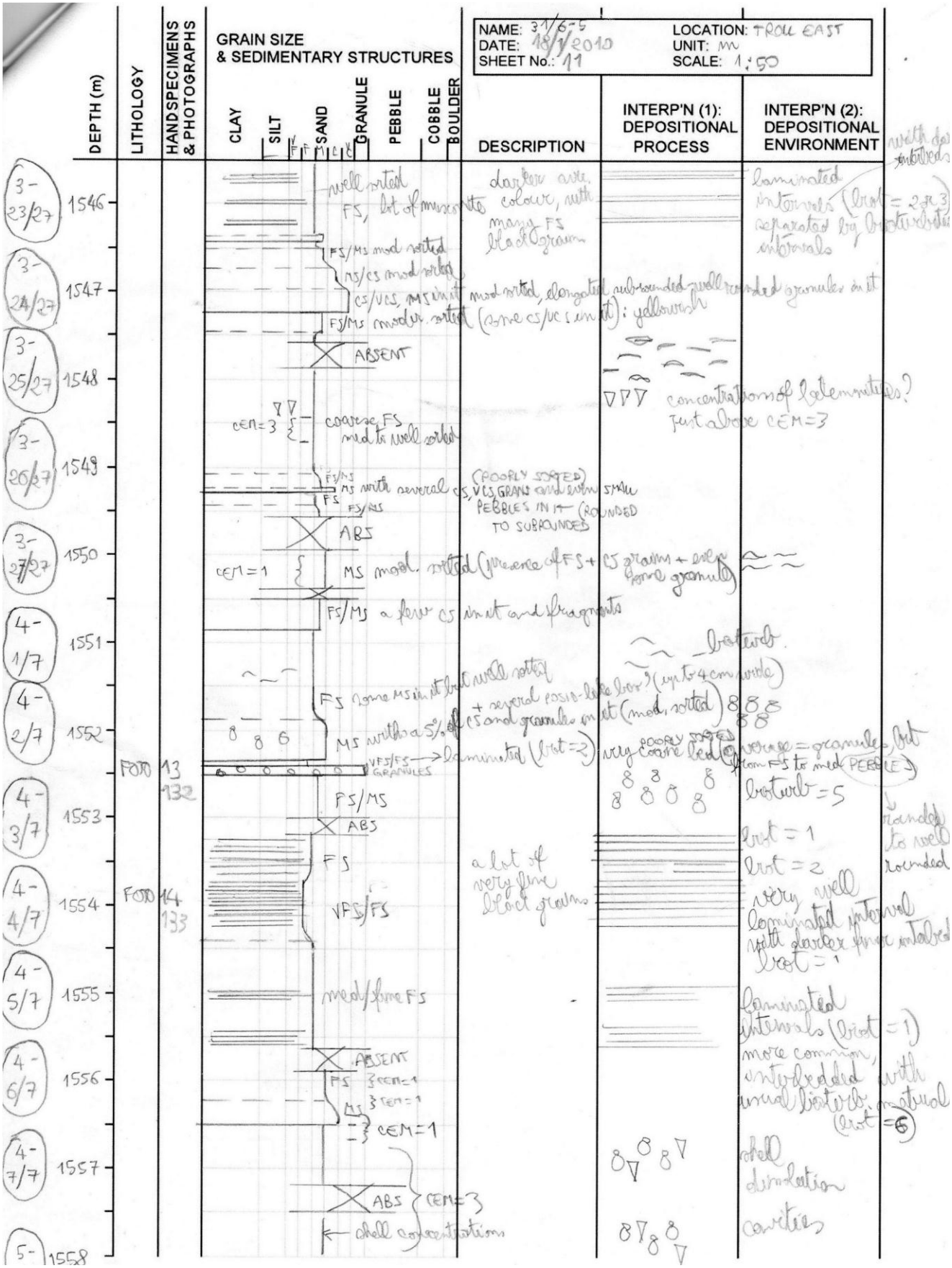
NAME: 31/6-5
DATE: 18/1 2010
SHEET No.: 11
LOCATION: TROLL EAST
UNIT: M
SCALE: 1:50
DEPTH (m)
LITHOLOGY
HANDSPECIMENS & PHOTOGRAPHS
GRAIN SIZE & SEDIMENTARY STRUCTURES
CLAY
SILT
SAND
GRANULE
PEBBLE
COBBLE
BOULDER
DESCRIPTION
INTERP'N (1): DEPOSITIONAL PROCESS
INTERP'N (2): DEPOSITIONAL ENVIRONMENT
3-23/27
1546
3-24/27
1547
3-25/27
1548
3-26/27
1549
3-27/27
1550
4-1/7
1551
4-2/7
1552
4-3/7
1553
4-4/7
1554
4-5/7
1555
4-6/7
1556
4-7/7
1557
5-
1558
FOTO 13
132
FOTO 14
133
well sorted FS, lot of muscovite
darker arg. colour, with many FS black grains
FS/MS mod sorted
MS/CS mod sorted
CS/VCS, MS inset
mod sorted, elongated, subrounded well rounded granules in it
FS/MS moder. sorted (some CS/VCS inset): yellowish
ABSENT
CEM=3
coarse FS mod to well sorted
concentrations of belemnites? just above CEM=3
FS/MS
MS with several CS, VCS GRAINS and even SMALL PEBBLES IN IT (ROUNDED TO SUBROUNDED)
FS
FS/MS
ABS
CEM=1
MS mod. sorted (presence of FS + CS grains + even some granules)
FS/MS a few CS inset and fragments
FS some MS inset
well sorted
+ several fossil-like bor? (up to 4cm wide)
+ CS and granules inset (mod. sorted)
MS with a 5% of
VFS/FS GRANULES
laminated (lint=2)
very poorly sorted
coarse lead
average = granule (but from FS to med PEBBLE)
bioturb=5
FS/MS
ABS
lint = 1
FS
a lot of very fine black grains
lint = 2
very well laminated interval with planar fine interbed
VFS/FS
lint = 1
med/fine FS
laminated intervals (lint = 1) more common, interbedded with several bioturb. interval (int = 5)
ABSENT
FS CEM=1
MS CEM=1
shell dissolution cavities
ABS
CEM=3
← shell concentrations

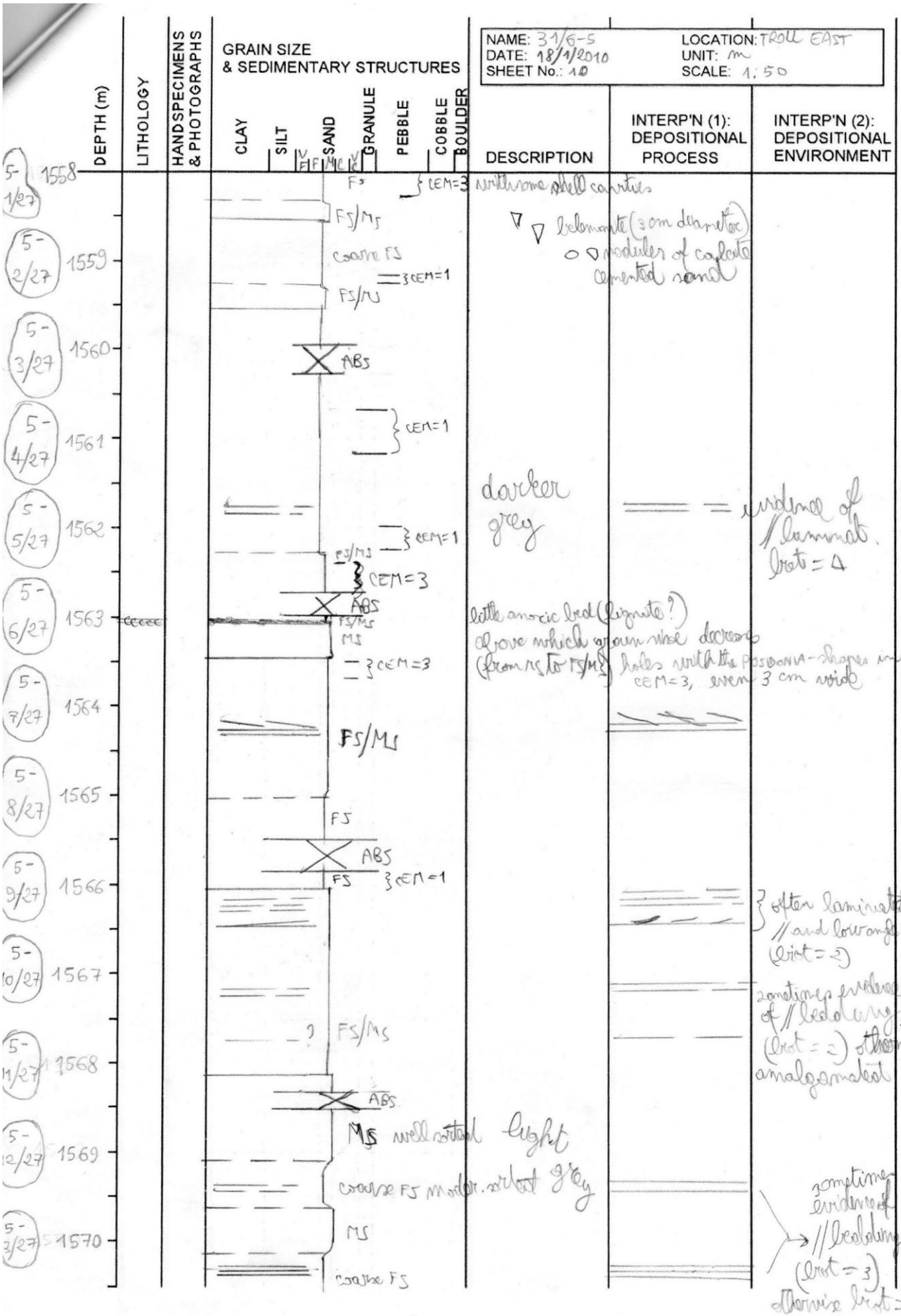
NAME: 31/6-5
DATE: 18/1/2010
SHEET No.: 10
LOCATION: TROLL EAST
UNIT: m
SCALE: 1:50
DEPTH (m)
LITHOLOGY
HANDSPECIMENS & PHOTOGRAPHS
GRAIN SIZE & SEDIMENTARY STRUCTURES
CLAY
SILT
SAND
GRANULE
PEBBLE
COBBLE
BOULDER
DESCRIPTION
INTERP'N (1): DEPOSITIONAL PROCESS
INTERP'N (2): DEPOSITIONAL ENVIRONMENT
5-1/27
1558
5-2/27
1559
5-3/27
1560
5-4/27
1561
5-5/27
1562
5-6/27
1563
5-7/27
1564
5-8/27
1565
5-9/27
1566
5-10/27
1567
5-11/27
1568
5-12/27
1569
5-13/27
1570
FS
CEM=3
with some shell convites
FS/MS
clomonte (3 cm diameter)
nodules of calcite cemented sand
coarse FS
CEM=1
ABS
darker grey
evidence of // laminat. (cat = 4)
little anoxic bed (lignite?) above which grain size decreases (from MS to FS/MS)
holes with the POSIDONIA-shapes in CEM=3, even 3 cm wide
MS
FS/MS
often laminated // and low angle X (cat = 2)
sometimes evidence of // bedding (cat = 2) otherwise amalgamated
MS well sorted light
coarse FS moder. sorted grey
sometime evidence of // bedding (cat = 3) otherwise cat = 6

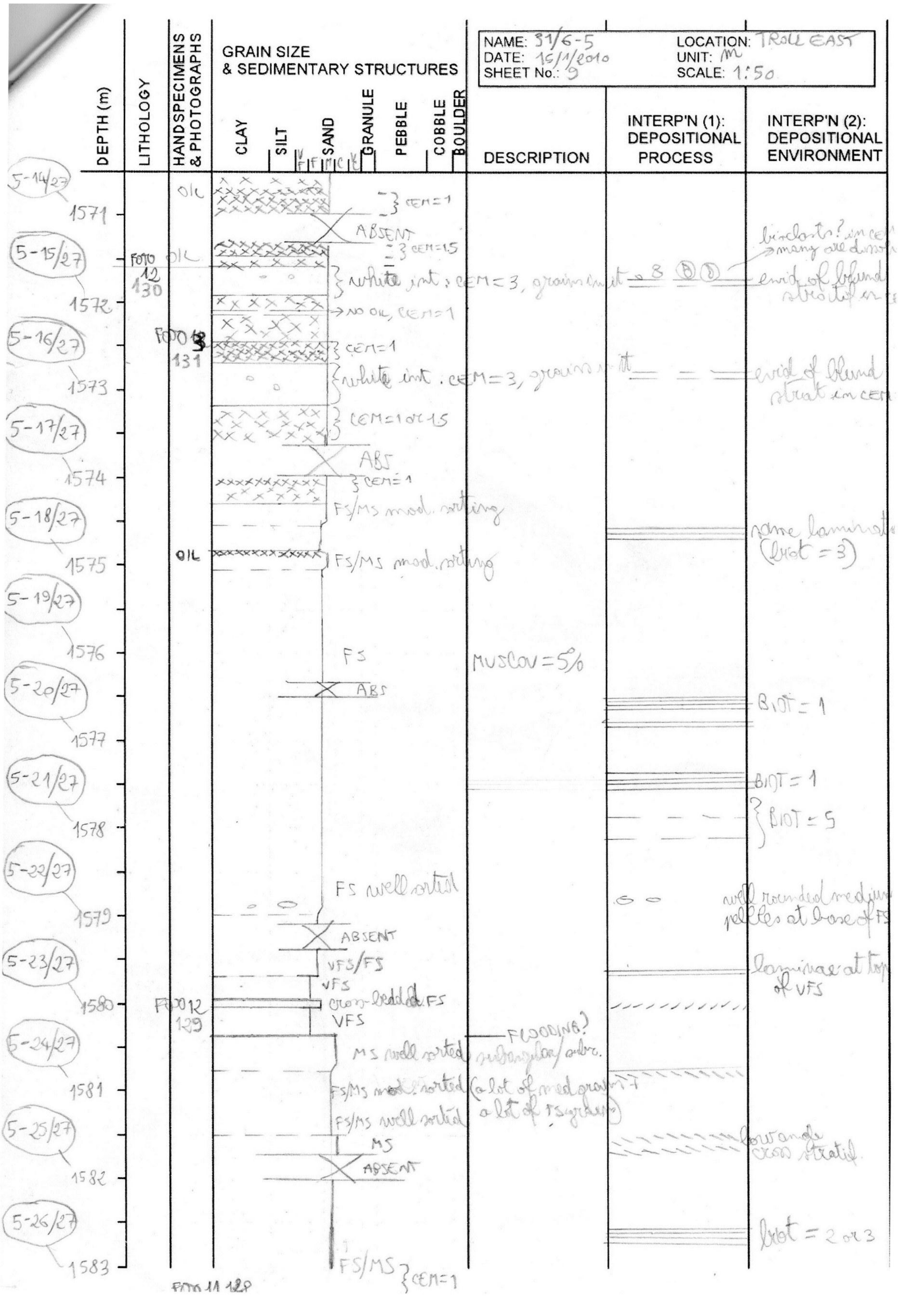
NAME: 31/6-5
DATE: 15/1/2010
SHEET No.: 9
LOCATION: TROLL EAST
UNIT: m
SCALE: 1:50
DEPTH (m)
LITHOLOGY
HANDSPECIMENS & PHOTOGRAPHS
GRAIN SIZE & SEDIMENTARY STRUCTURES
CLAY
SILT
SAND
GRANULE
PEBBLE
COBBLE
BOULDER
DESCRIPTION
INTERP'N (1): DEPOSITIONAL PROCESS
INTERP'N (2): DEPOSITIONAL ENVIRONMENT
1571
1572
1573
1574
1575
1576
1577
1578
1579
1580
1581
1582
1583
5-14/27
5-15/27
5-16/27
5-17/27
5-18/27
5-19/27
5-20/27
5-21/27
5-22/27
5-23/27
5-24/27
5-25/27
5-26/27
OIL
CEM=1
ABSENT
CEM=1.5
NO OIL, CEM=1
CEM=1 or 1.5
ABS
FS/MS mod. sorting
FS
MUSCOV=5%
BIOT=1
BIOT=5
FS well sorted
VFS/FS
VFS
VFS
FLOODING?
MS well sorted
FS/MS well sorted
MS
FS/MS
CEM=1

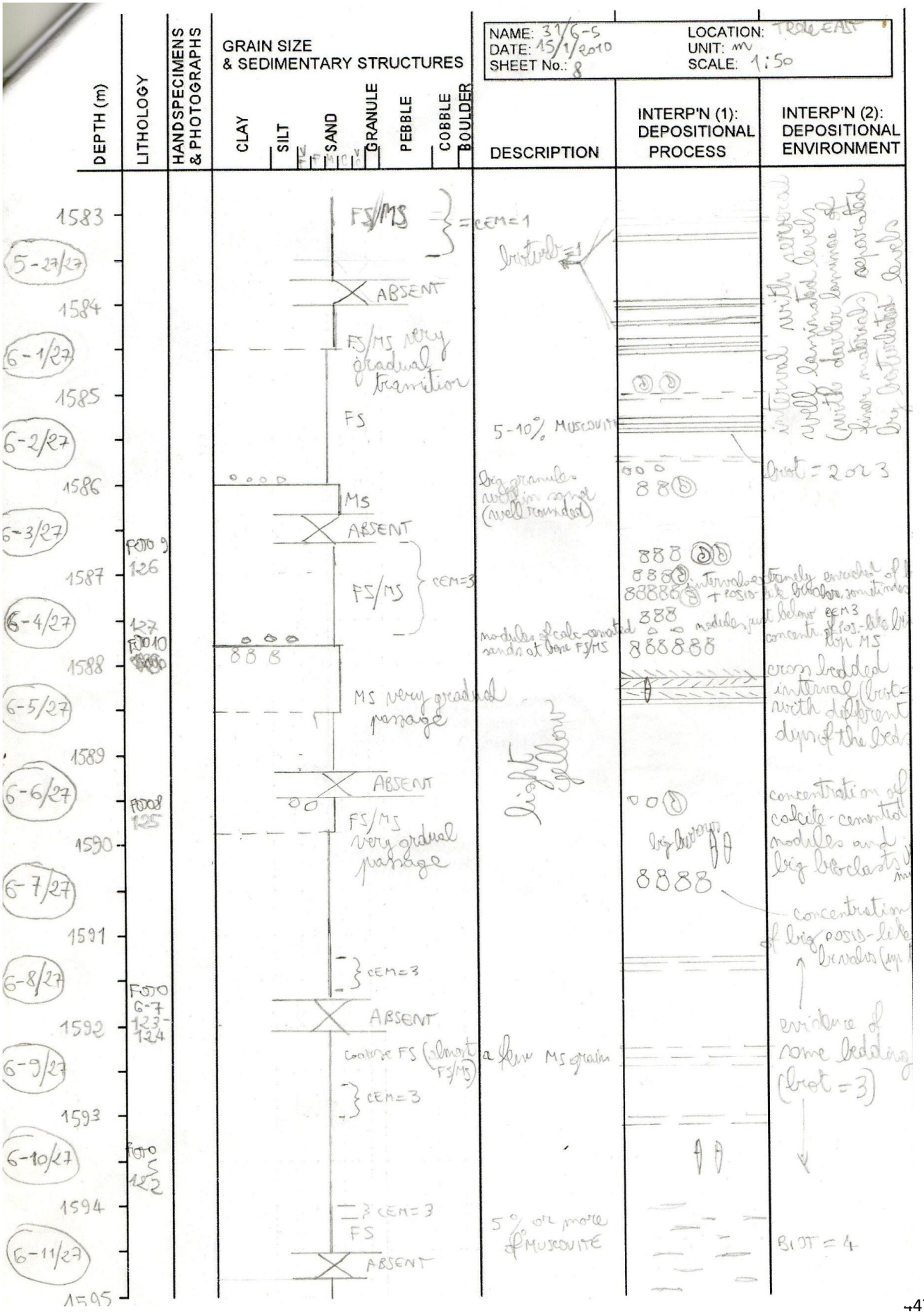
NAME: 31/6-5
DATE: 15/1/2010
SHEET No.: 8
LOCATION: TROLL EAST
UNIT: MV
SCALE: 1:50
DEPTH (m)
LITHOLOGY
HANDSPECIMENS & PHOTOGRAPHS
GRAIN SIZE & SEDIMENTARY STRUCTURES
CLAY
SILT
SAND
GRANULE
PEBBLE
COBBLE
BOULDER
DESCRIPTION
INTERP'N (1): DEPOSITIONAL PROCESS
INTERP'N (2): DEPOSITIONAL ENVIRONMENT
1583
1584
1585
1586
1587
1588
1589
1590
1591
1592
1593
1594
1595
FS/MS
=CEM=1
ABSENT
FS/MS very gradual transition
FS
5-10% MUSCOVITE
MS
ABSENT
FS/MS
CEM=3
MS very gradual passage
ABSENT
FS/MS very gradual passage
CEM=3
ABSENT
coarse FS (almost FS/MS)
a few MS grain
CEM=3
FS
CEM=3
ABSENT
5% or more of MUSCOVITE
BIOT = 4
6-1/27
6-2/27
6-3/27
6-4/27
6-5/27
6-6/27
6-7/27
6-8/27
6-9/27
6-10/27
6-11/27
FOTO 9 126
FOTO 10 127
FOTO 8 125
FOTO 7 123-124
FOTO 5 122

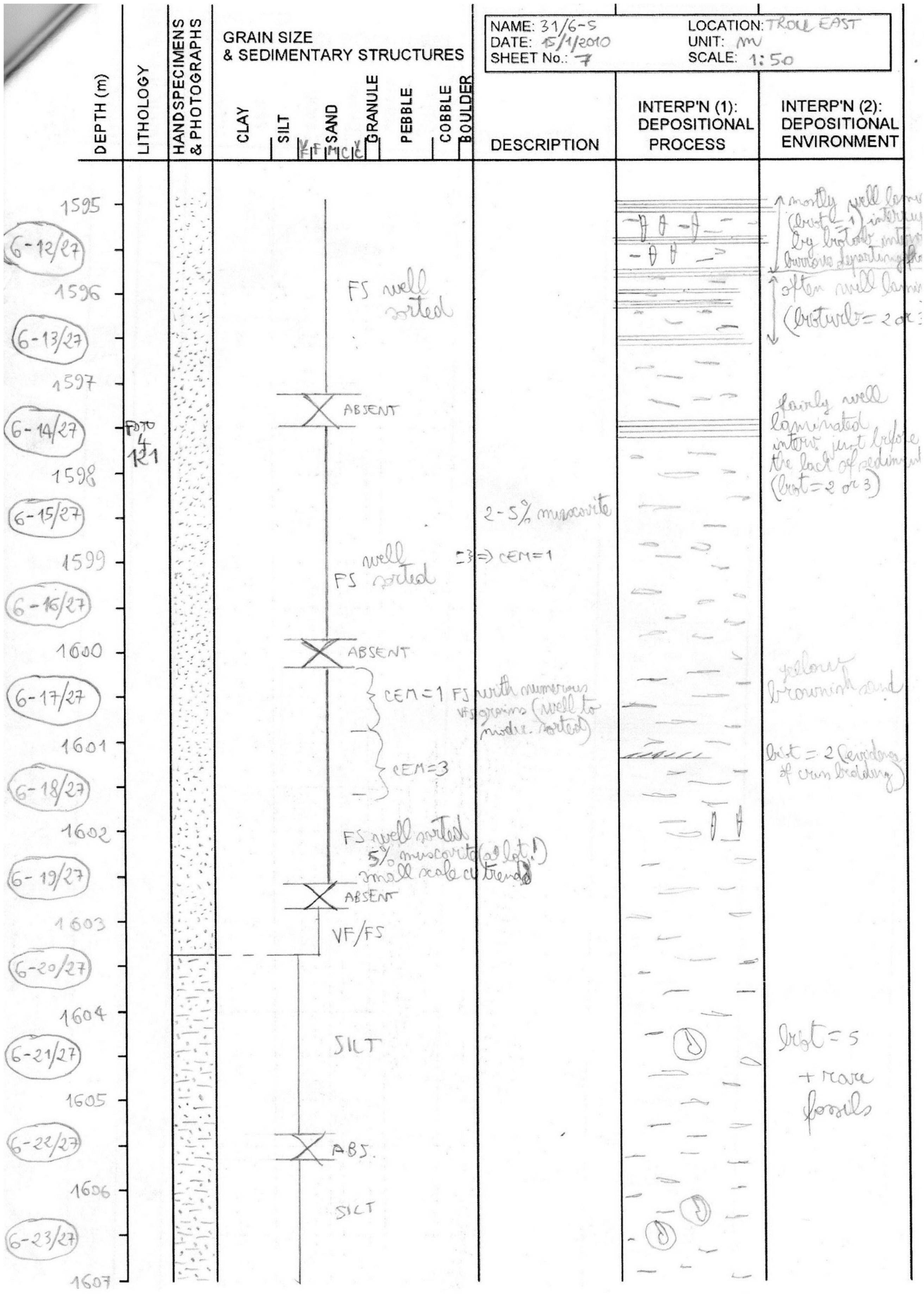
NAME: 31/6-5
DATE: 15/1/2010
SHEET No.: 7
LOCATION: TROLL EAST
UNIT: MV
SCALE: 1:50
DEPTH (m)
LITHOLOGY
HANDSPECIMENS & PHOTOGRAPHS
GRAIN SIZE & SEDIMENTARY STRUCTURES
CLAY
SILT
SAND
VF F M C VC
GRANULE
PEBBLE
COBBLE
BOULDER
DESCRIPTION
INTERP'N (1): DEPOSITIONAL PROCESS
INTERP'N (2): DEPOSITIONAL ENVIRONMENT
1595
6-12/27
1596
6-13/27
1597
6-14/27
1598
6-15/27
1599
6-16/27
1600
6-17/27
1601
6-18/27
1602
6-19/27
1603
6-20/27
1604
6-21/27
1605
6-22/27
1606
6-23/27
1607
FOTO 4 121
FS well sorted
ABSENT
2-5% muscovite
FS well sorted
CEM=1
ABSENT
CEM=1 FS with numerous VF grains (well to moder. sorted)
CEM=3
FS well sorted
5% muscovite (a lot!)
small scale cu trends
ABSENT
VF/FS
SILT
ABS.
SILT
often well laminated
fairly well laminated
yellow brownish sand
biot = 5
+ rare fossils

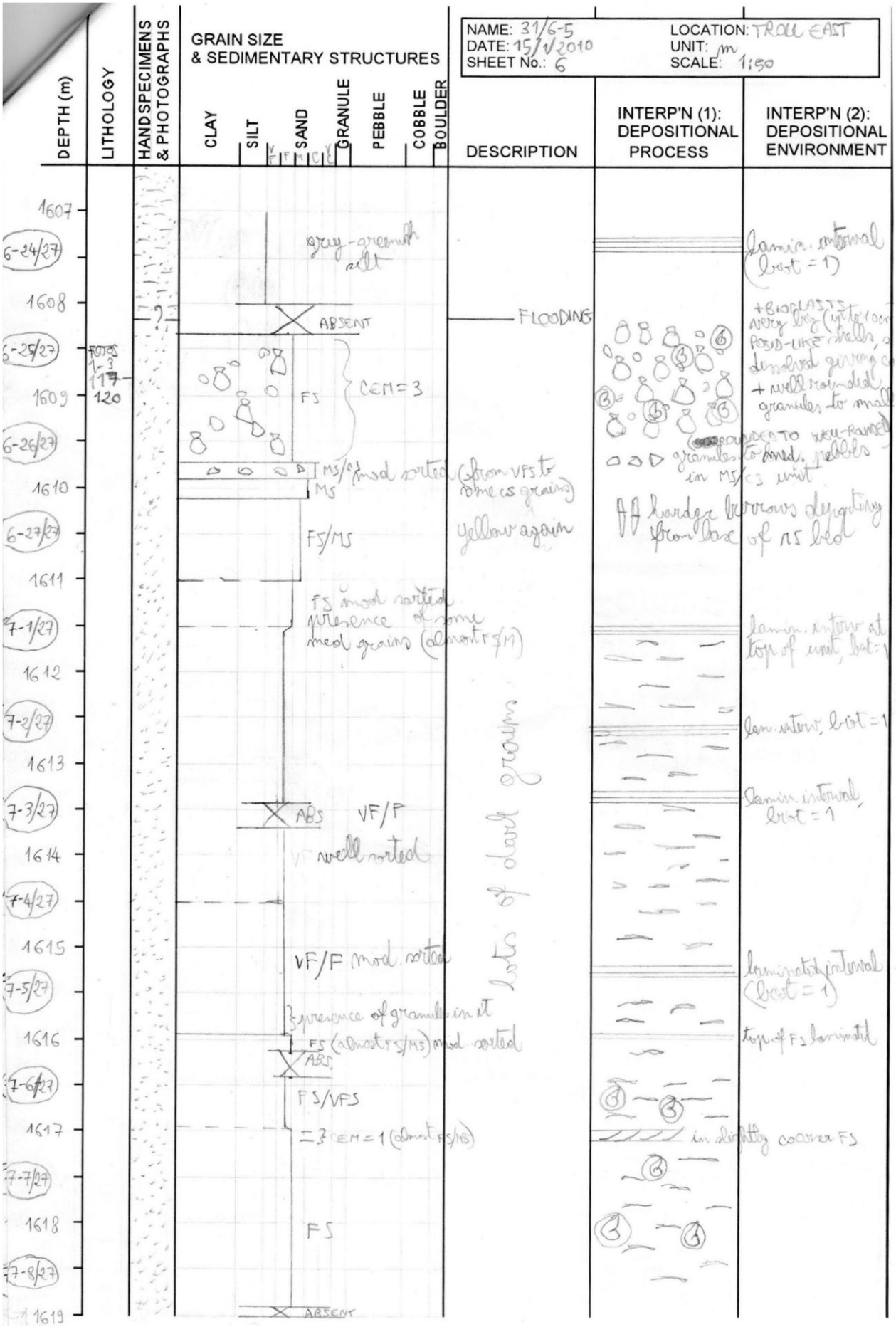
NAME: 31/6-5
DATE: 15/1/2010
SHEET No.: 6
LOCATION: TROLL EAST
UNIT: m
SCALE: 1:50
DEPTH (m)
LITHOLOGY
HANDSPECIMENS & PHOTOGRAPHS
GRAIN SIZE & SEDIMENTARY STRUCTURES
CLAY
SILT
SAND
GRANULE
PEBBLE
COBBLE
BOULDER
DESCRIPTION
INTERP'N (1): DEPOSITIONAL PROCESS
INTERP'N (2): DEPOSITIONAL ENVIRONMENT
1607
1608
1609
1610
1611
1612
1613
1614
1615
1616
1617
1618
1619
6-24/27
6-25/27
6-26/27
6-27/27
7-1/27
7-2/27
7-3/27
7-4/27
7-5/27
7-6/27
7-7/27
7-8/27
FOTOS 1-3 117-120
grey-greenish silt
ABSENT
FLOODING
FS
CEM=3
MS/cs mod sorted (from VFS to some cs grains)
MS
FS/MS
yellow again
FS mod sorted presence of some med grains (almost FS/M)
ABS
VF/F
well sorted
VF/F mod. sorted
lots of dark grains
presence of granules in it
FS (almost FS/MS) mod sorted
ABS
FS/VFS
=3 CEM=1 (almost FS/MS)
FS
ABSENT
granules to med. pebbles in MS/cs unit
harder brown layer of MS bed
lamin. interval (biot = 1)
+BIOCLASTS very big (up to 1 cm) POND-LIKE shells, + well rounded granules to mall
lamin. interval, biot = 1
lamin. interval, biot = 1
laminated interval (biot = 1)
top of FS laminite
in slightly coarser FS

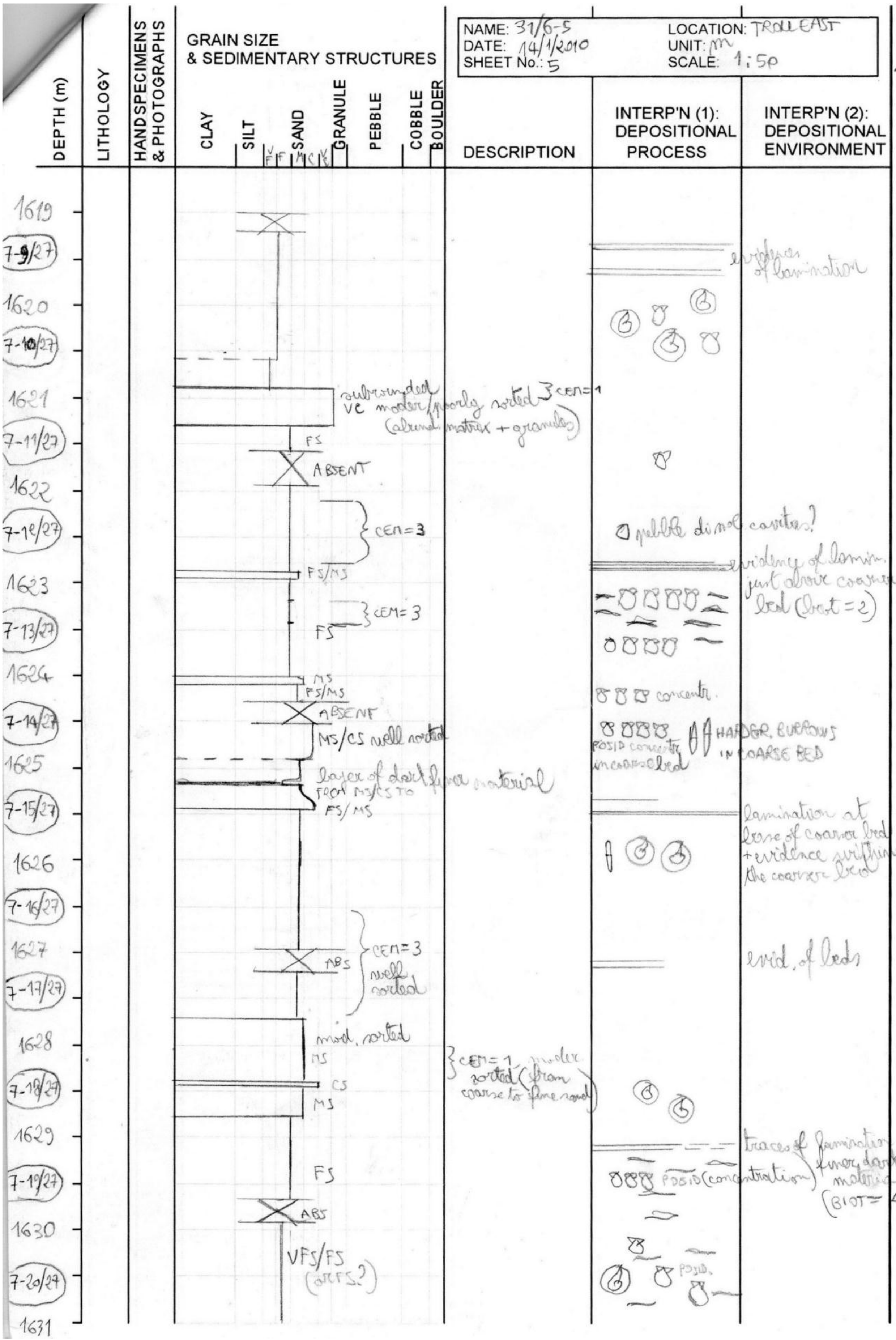
NAME: 31/6-5
DATE: 14/1/2010
SHEET No.: 5
LOCATION: TROLL EAST
UNIT: m
SCALE: 1:50
DEPTH (m)
LITHOLOGY
HANDSPECIMENS & PHOTOGRAPHS
GRAIN SIZE & SEDIMENTARY STRUCTURES
CLAY
SILT
SAND
GRANULE
PEBBLE
COBBLE
BOULDER
DESCRIPTION
INTERP'N (1): DEPOSITIONAL PROCESS
INTERP'N (2): DEPOSITIONAL ENVIRONMENT
1619
1620
1621
1622
1623
1624
1625
1626
1627
1628
1629
1630
1631
subrounded VC moder./poorly sorted } CEM=1
(abund. matrix + granules)
FS
ABSENT
CEM=3
FS/MS
CEM=3
FS
MS
FS/MS
ABSENT
MS/CS well sorted
layer of dark finer material
FROM MS/CS TO FS/MS
ABS
CEM=3
well sorted
mod. sorted
MS
CS
MS
CEM=1 moder. sorted (from coarse to fine sand)
FS
ABS
VFS/FS (or FS?)
evidence of lamination
pebble di mol cavities?
evidence of lamin. just above coarse bed (biot=2)
concentr.
POSID concentr. in coarse bed
HARDER BURROWS IN COARSE BED
lamination at base of coarse bed + evidence within the coarse bed
evid. of beds
traces of lamination of finer darker material
POSID (concentration)
(BIOT=4)
POSID.

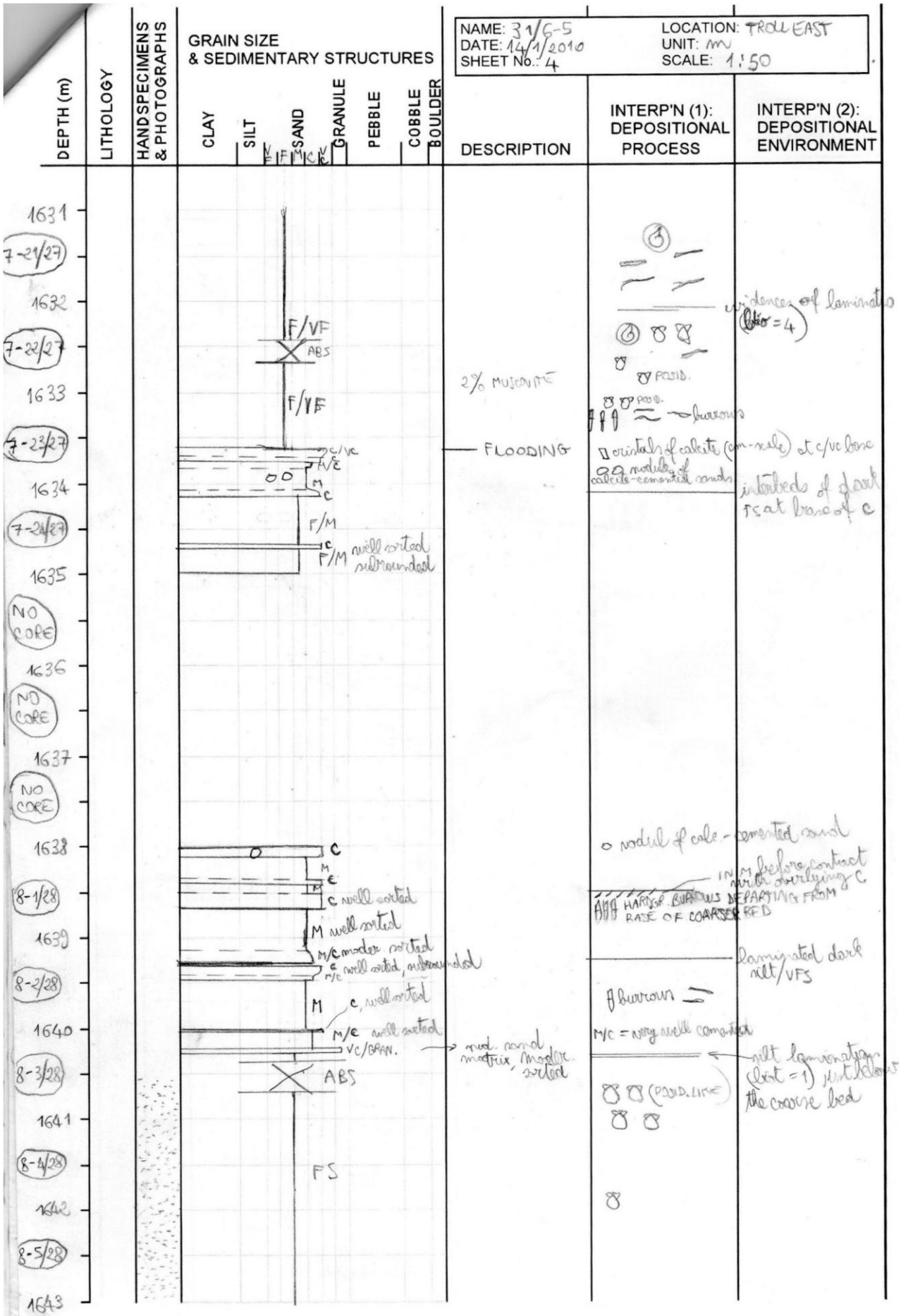
NAME: 31/6-5
DATE: 14/1/2010
SHEET No.: 4
LOCATION: TROLL EAST
UNIT: m
SCALE: 1:50
DEPTH (m)
LITHOLOGY
HANDSPECIMENS & PHOTOGRAPHS
GRAIN SIZE & SEDIMENTARY STRUCTURES
CLAY
SILT
SAND
GRANULE
PEBBLE
COBBLE
BOULDER
DESCRIPTION
INTERP'N (1): DEPOSITIONAL PROCESS
INTERP'N (2): DEPOSITIONAL ENVIRONMENT
1631
7-21/27
1632
7-22/27
1633
7-23/27
1634
7-24/27
1635
NO CORE
1636
NO CORE
1637
NO CORE
1638
8-1/28
1639
8-2/28
1640
8-3/28
1641
8-4/28
1642
8-5/28
1643
F/VF
ABS
F/VF
c/vc
F/c
M
c
F/M
c
F/M well sorted subrounded
2% MUSCOVITE
FLOODING
evidences of laminatio
(Lam = 4)
FOSS.
burrows
orientals of calcite (cm-scale) at c/vc base
99 nodules of calcite-cemented sands
interbeds of dark silt at base of c
c
M
c
c well sorted
M well sorted
M/c moder. sorted
c
M/c well sorted, subrounded
M
c, well sorted
M/c well sorted
VC/GRAN.
red. round matrix, moderately sorted
ABS
FS
o nodul of calc-cemented sand
IN
HARPER BURROWS DEPARTING FROM
RAISE OF COARSER
RED
laminated dark silt/VFS
burrows
M/c = very well cemented
silt laminations (Lam = 1) just below the coarse bed
(POSS. LIKE)

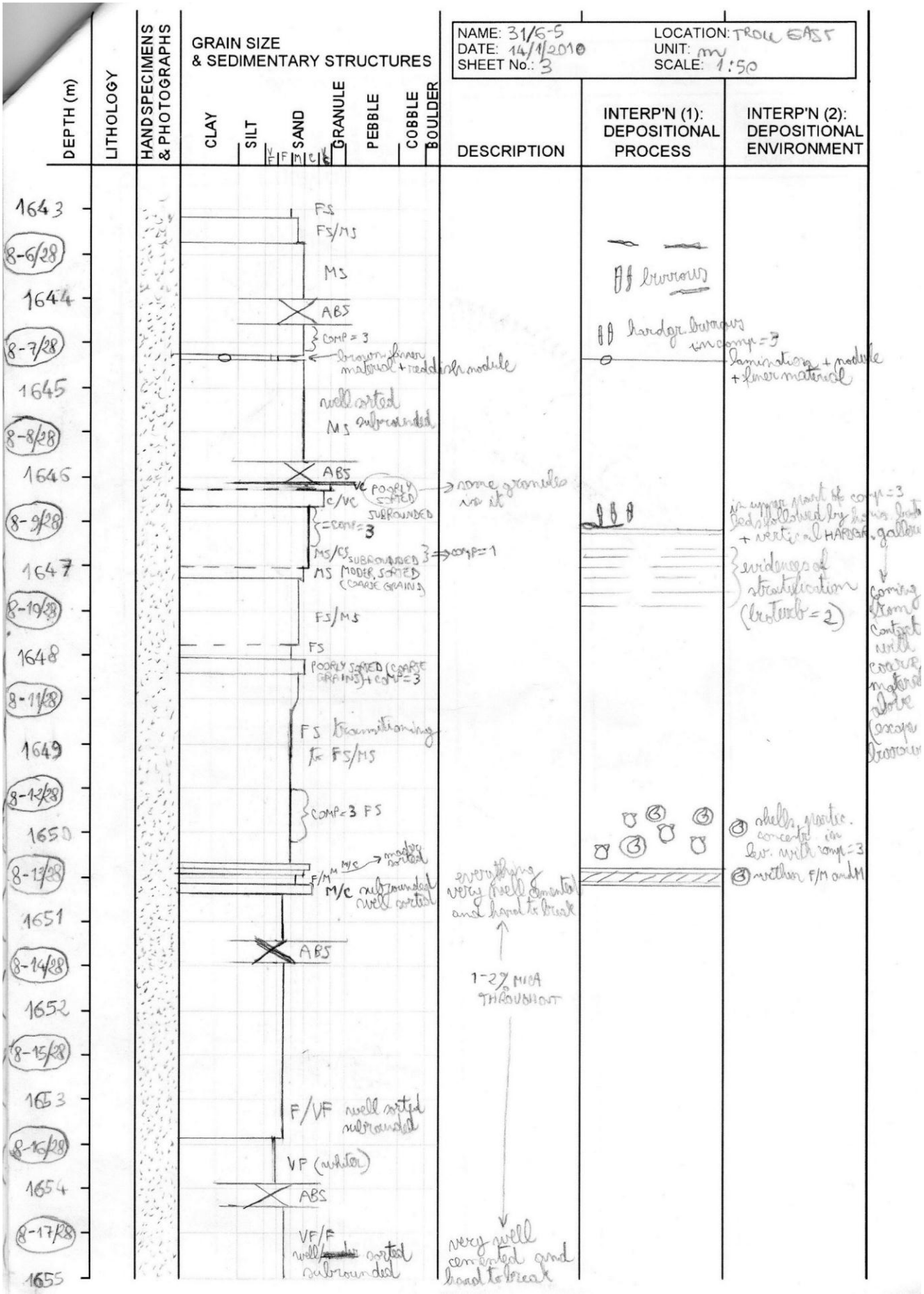
NAME: 31/6-5
DATE: 14/1/2010
SHEET No.: 3
LOCATION: TROLL EAST
UNIT: mv
SCALE: 1:50
DEPTH (m)
LITHOLOGY
HAND SPECIMENS & PHOTOGRAPHS
GRAIN SIZE & SEDIMENTARY STRUCTURES
CLAY
SILT
SAND
GRANULE
PEBBLE
COBBLE
BOULDER
DESCRIPTION
INTERP'N (1): DEPOSITIONAL PROCESS
INTERP'N (2): DEPOSITIONAL ENVIRONMENT
1643
8-6/28
1644
8-7/28
1645
8-8/28
1646
8-9/28
1647
8-10/28
1648
8-11/28
1649
8-12/28
1650
8-13/28
1651
8-14/28
1652
8-15/28
1653
8-16/28
1654
8-17/28
1655
FS
FS/MS
MS
ABS
COMP = 3
brown-grey material + reddish
well sorted
MS subrounded
ABS
VC POORLY SORTED
C/VC
SUBROUNDED
COMP = 3
MS/CS SUBROUNDED
COMP = 1
MS MODER. SORTED (COARSE GRAINS)
FS/MS
FS
POORLY SORTED (COARSE GRAINS) + COMP = 3
FS lamin/ripp
to FS/MS
COMP < 3 FS
F/M M/C
matrix supported
M/C subrounded well sorted
ABS
F/VF well sorted subrounded
VF (white)
ABS
VF/F well sorted subrounded
burrows
hardgr. burrows in comp = 3
lamination + nodule + finer material
in upper part of comp = 3 beds followed by
+ vertical
evidences of stratification (bioturb = 2)
coming from contact with coarse material above (escape burrows)
shells, greatest concentr. in bur. with comp = 3
neither F/M and M
everything very well cemented and hard to break
1-2% MICA THROUGHOUT
very well cemented and hard to break

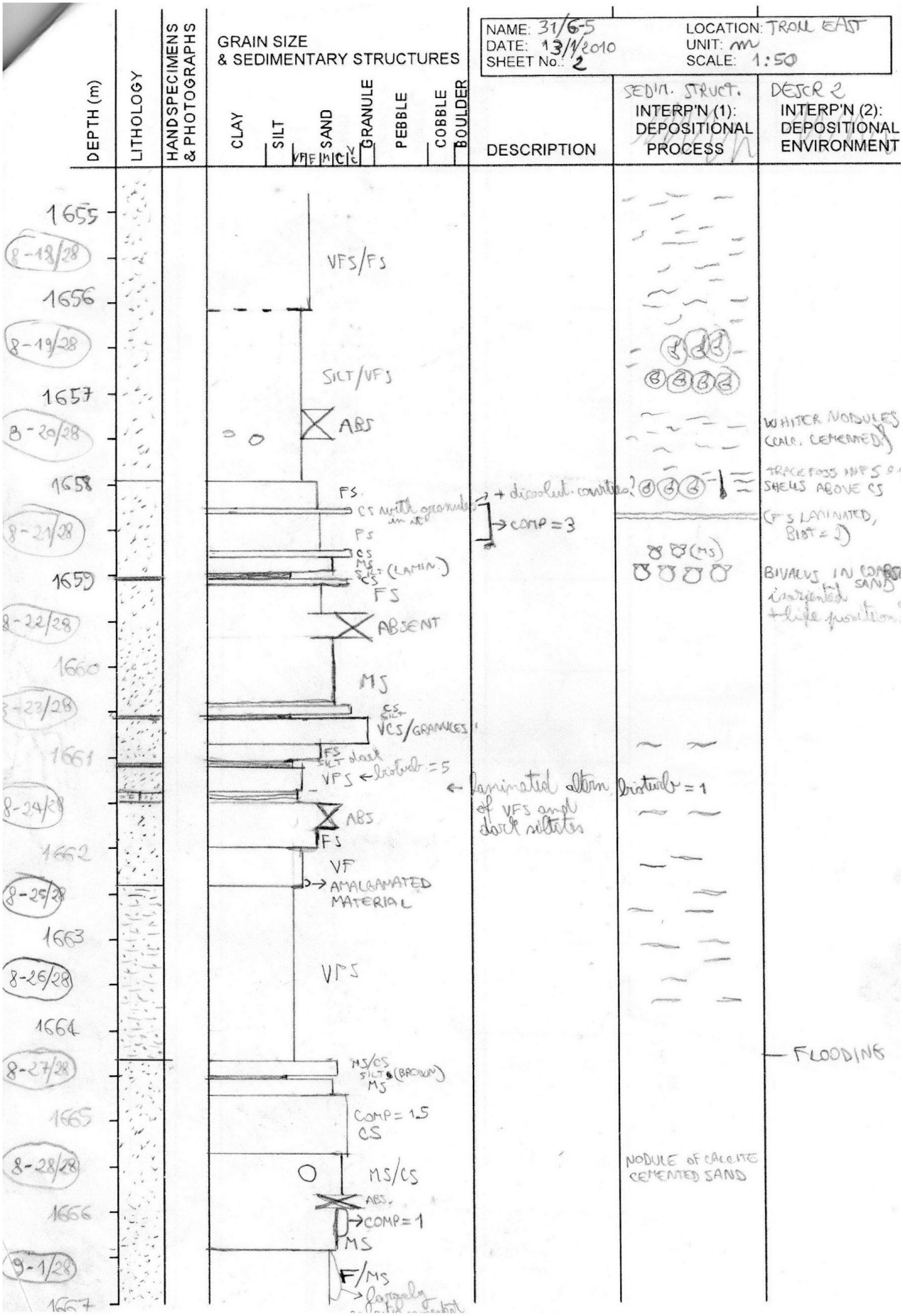
NAME: 31/6-5
DATE: 13/1/2010
SHEET No.: 2
LOCATION: TROLL EAST
UNIT: m
SCALE: 1:50
DEPTH (m)
LITHOLOGY
HANDSPECIMENS & PHOTOGRAPHS
GRAIN SIZE & SEDIMENTARY STRUCTURES
CLAY
SILT
SAND
VF F M C VC
GRANULE
PEBBLE
COBBLE
BOULDER
DESCRIPTION
SEDIM. STRUCT. INTERP'N (1): DEPOSITIONAL PROCESS
DESCR 2 INTERP'N (2): DEPOSITIONAL ENVIRONMENT
1655
1656
1657
1658
1659
1660
1661
1662
1663
1664
1665
1666
1667
VFS/FS
SILT/VFS
ABS
FS
CS with granules
+ dissolut. cavities?
COMP = 3
FS
CS
MS
CS
(LAMIN.)
FS
ABSENT
MS
CS
VCS/GRANULES
FS
SILT dark
VFS
bioturb = 5
laminated alternations of VFS and dark siltstone
bioturb = 1
ABS
FS
VF
AMALGAMATED MATERIAL
VFS
MS/CS
SILT
MS
(BROWN)
COMP = 1.5
CS
MS/CS
ABS.
COMP = 1
MS
F/MS
WHITISH NODULES (CALC. CEMENTED)
TRACE FOSS. IN FS & SHELLS ABOVE CS
(FS LAMINATED, BIOT = 1)
BIVALVES IN COARSE SAND
FLOODING
NODULE OF CALCITE CEMENTED SAND

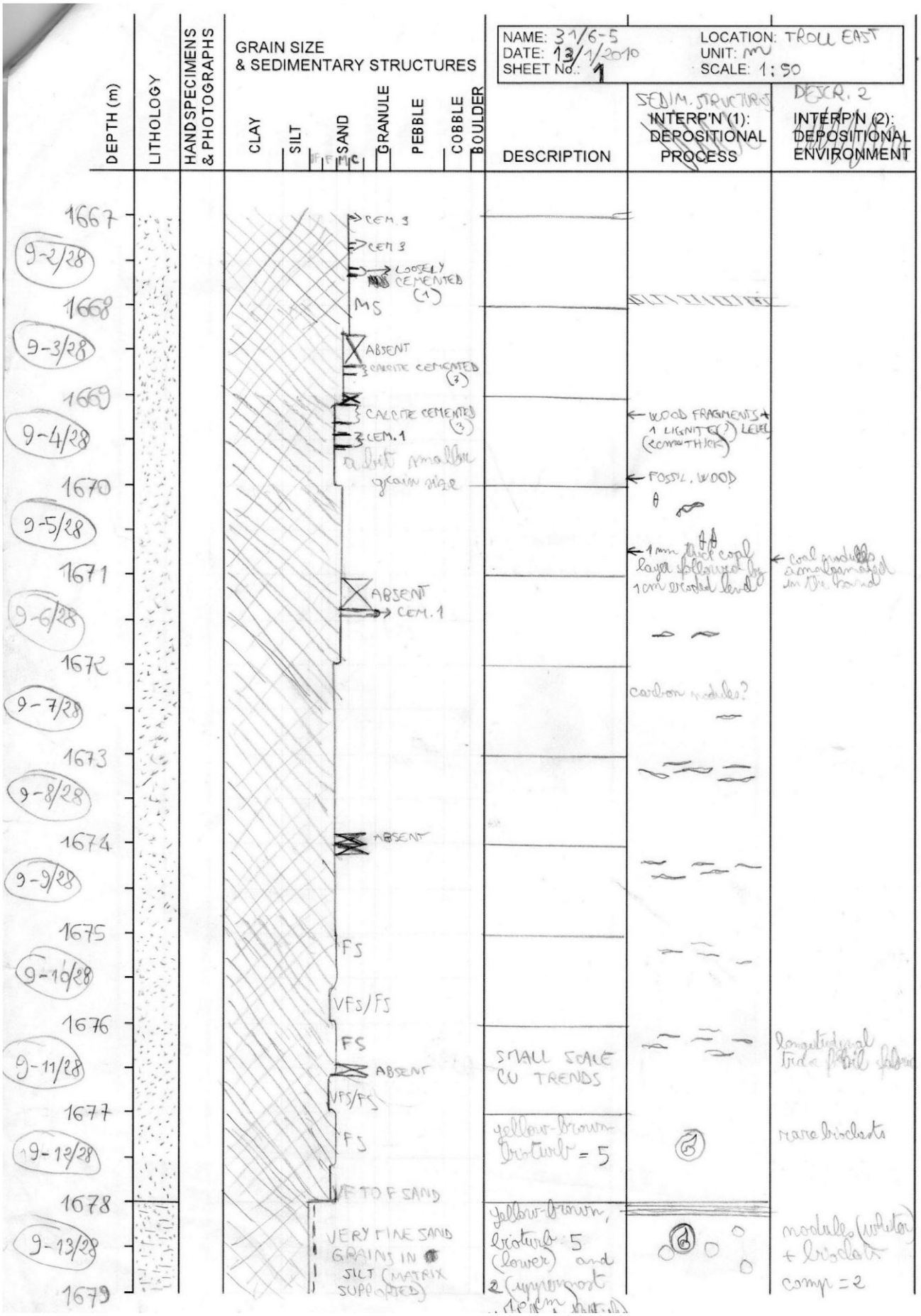
NAME: 31/6-5
DATE: 13/1/2010
SHEET NO.: 1
LOCATION: TROLL EAST
UNIT: MU
SCALE: 1:50
DEPTH (m)
LITHOLOGY
HANDSPECIMENS & PHOTOGRAPHS
GRAIN SIZE & SEDIMENTARY STRUCTURES
CLAY
SILT
SAND
GRANULE
PEBBLE
COBBLE
BOULDER
DESCRIPTION
SEDIM. STRUCTURES
INTERP'N (1): DEPOSITIONAL PROCESS
DESCR. 2
INTERP'N (2): DEPOSITIONAL ENVIRONMENT
1667
1668
1669
1670
1671
1672
1673
1674
1675
1676
1677
1678
1679
9-2/28
9-3/28
9-4/28
9-5/28
9-6/28
9-7/28
9-8/28
9-9/28
9-10/28
9-11/28
9-12/28
9-13/28
CEM.3
CEM.3
LOOSELY CEMENTED (1)
MS
ABSENT
CALCITE CEMENTED (3)
CALCITE CEMENTED (3)
CEM.1
a bit smaller grain size
ABSENT
CEM.1
ABSENT
FS
VFS/FS
FS
ABSENT
VFS/FS
FS
VF TO F SAND
VERY FINE SAND GRAINS IN SILT (MATRIX SUPPORTED)
WOOD FRAGMENTS + 1 LIGNITIC LEVEL (2CM THICK)
FOSSIL WOOD
1mm thick coal layer followed by 1cm eroded bed
coal fragments amalgamated in the sand
carbon nodules?
SMALL SCALE CU TRENDS
yellow-brown bioturb = 5
yellow-brown bioturb = 5 (lower) and 2 (uppermost 10cm thick)
longitudinal
rare bioclasts
nodules (siderite) + bioclasts
comp = 2

31/6-6

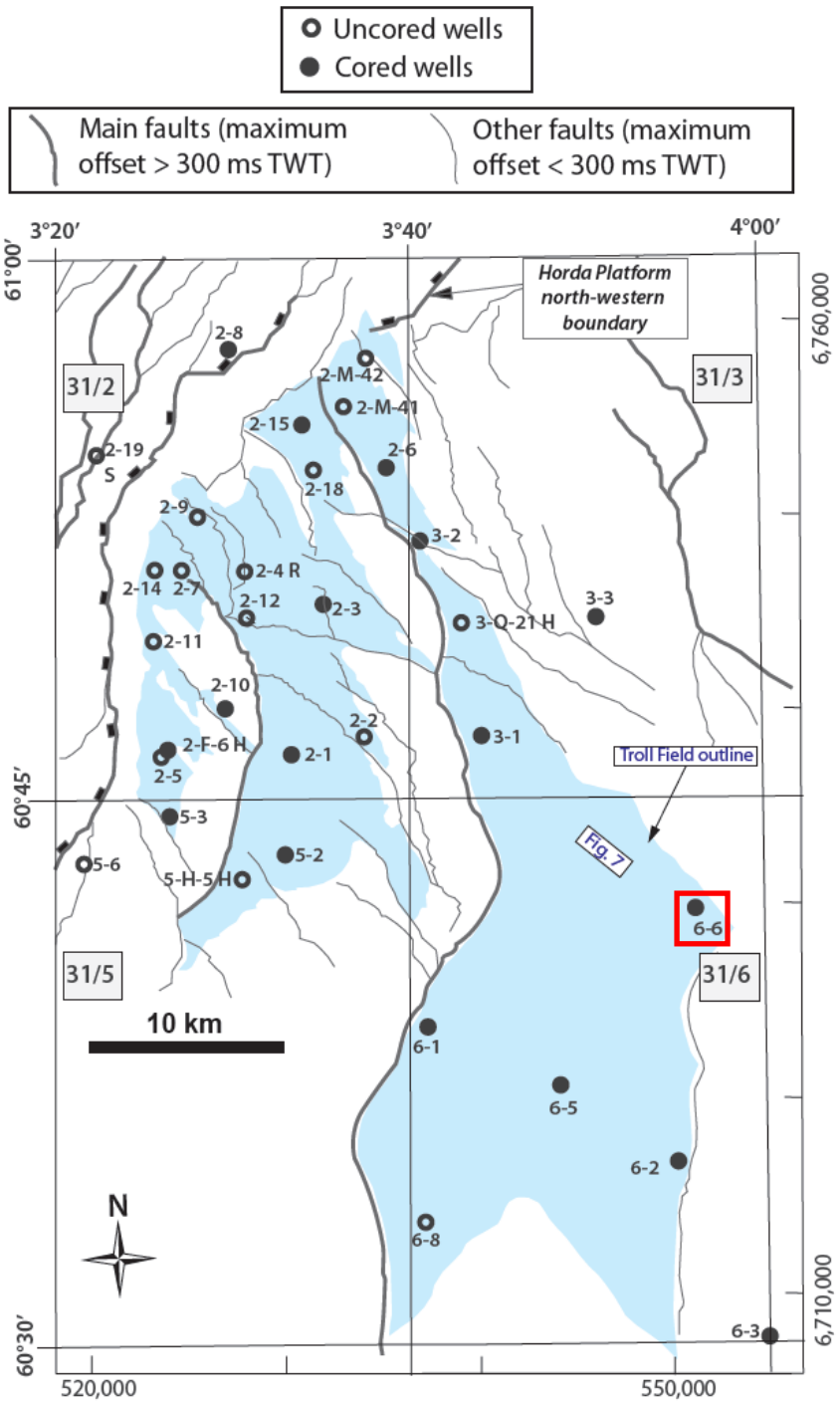
Uncored wells
Cored wells
Main faults (maximum offset > 300 ms TWT)
Other faults (maximum offset < 300 ms TWT)
3°20′
3°40′
4°00′
61°00′
60°45′
60°30′
6,760,000
6,710,000
520,000
550,000
Horda Platform north-western boundary
31/2
31/3
31/5
31/6
Troll Field outline
Fig. 7
10 km
N
2-8
2-M-42
2-M-41
2-15
2-19 S
2-6
2-18
2-9
3-2
2-14
2-7
2-4 R
2-12
2-3
3-Q-21 H
3-3
2-11
2-10
2-2
3-1
2-F-6 H
2-5
2-1
5-3
5-6
5-H-5 H
5-2
6-6
6-1
6-5
6-2
6-8
6-3

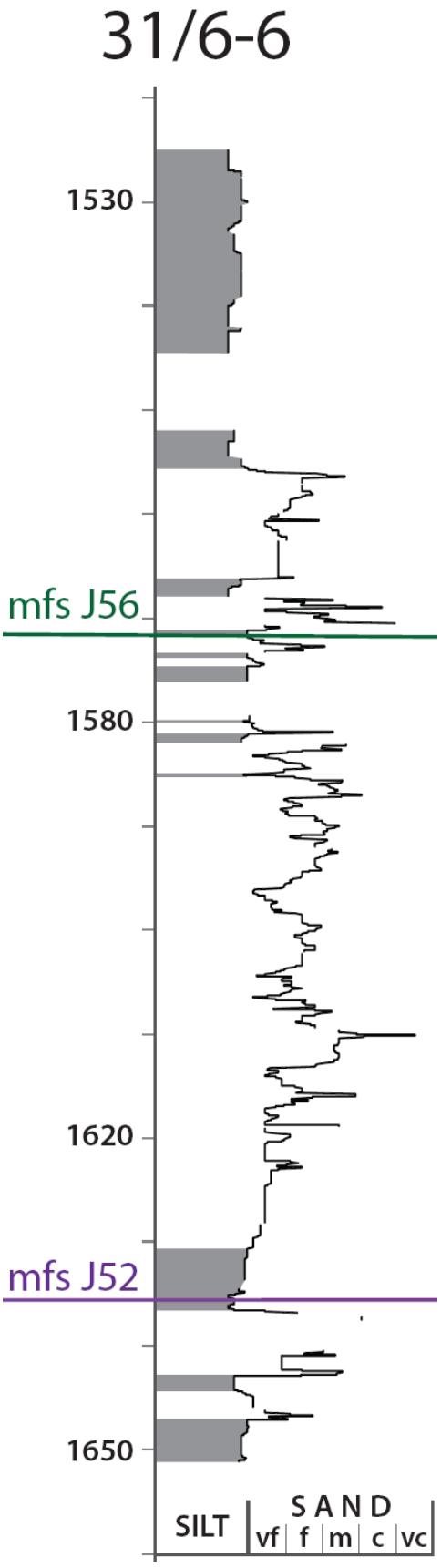
31/6-6
1530
mfs J56
1580
1620
mfs J52
1650
SILT
SAND
vf
f
m
c
vc

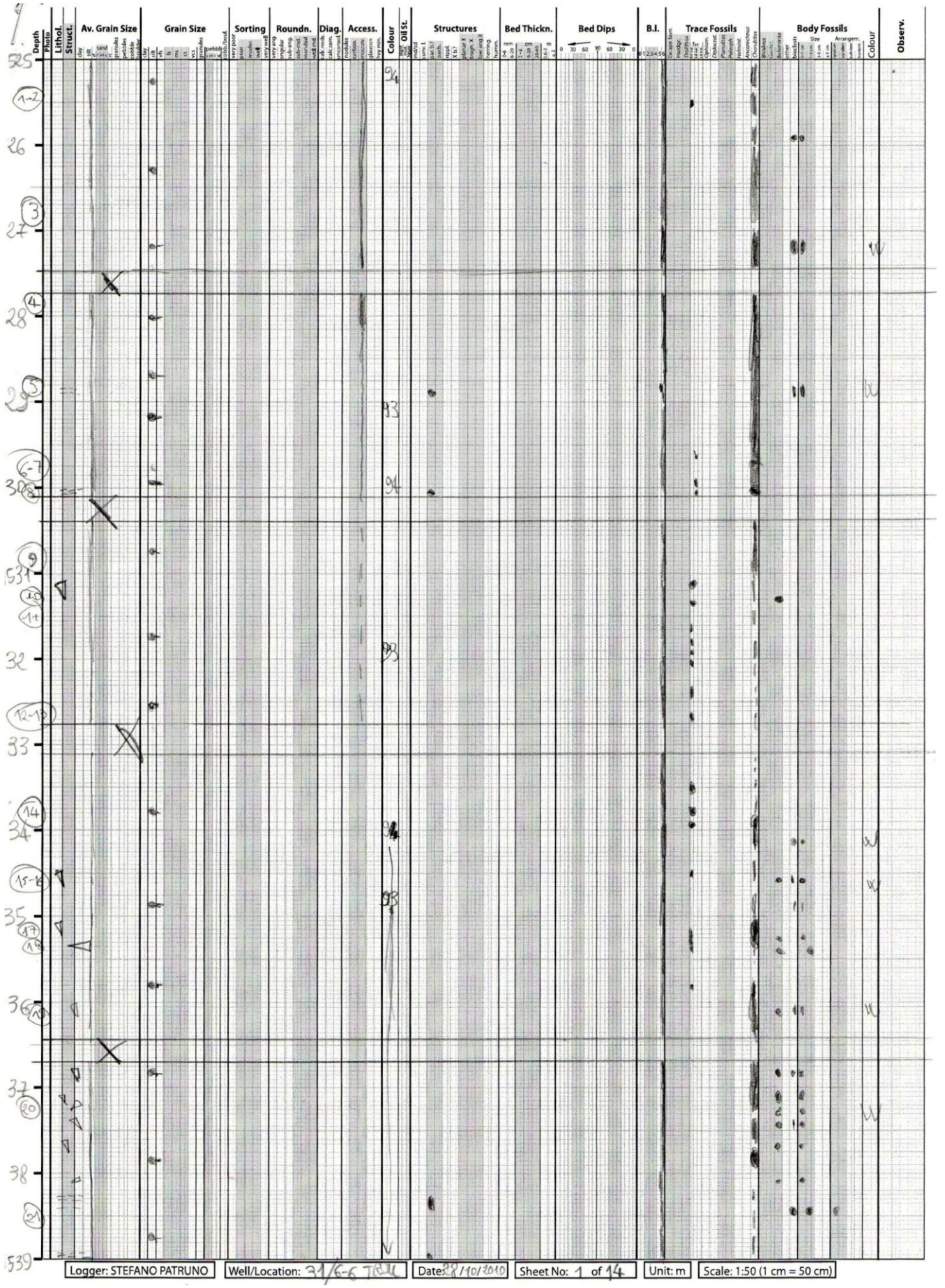
Depth
Photo
Lithol.
Struct.
Av. Grain Size
Grain Size
Sorting
Roundn.
Diag.
Access.
Colour
Oil St.
Structures
Bed Thickn.
Bed Dips
B.I.
Trace Fossils
Body Fossils
Observ.
Logger: STEFANO PATRUNO
Well/Location: 31/6-6
Date: 28/10/2010
Sheet No: 1 of 14
Unit: m
Scale: 1:50 (1 cm = 50 cm)

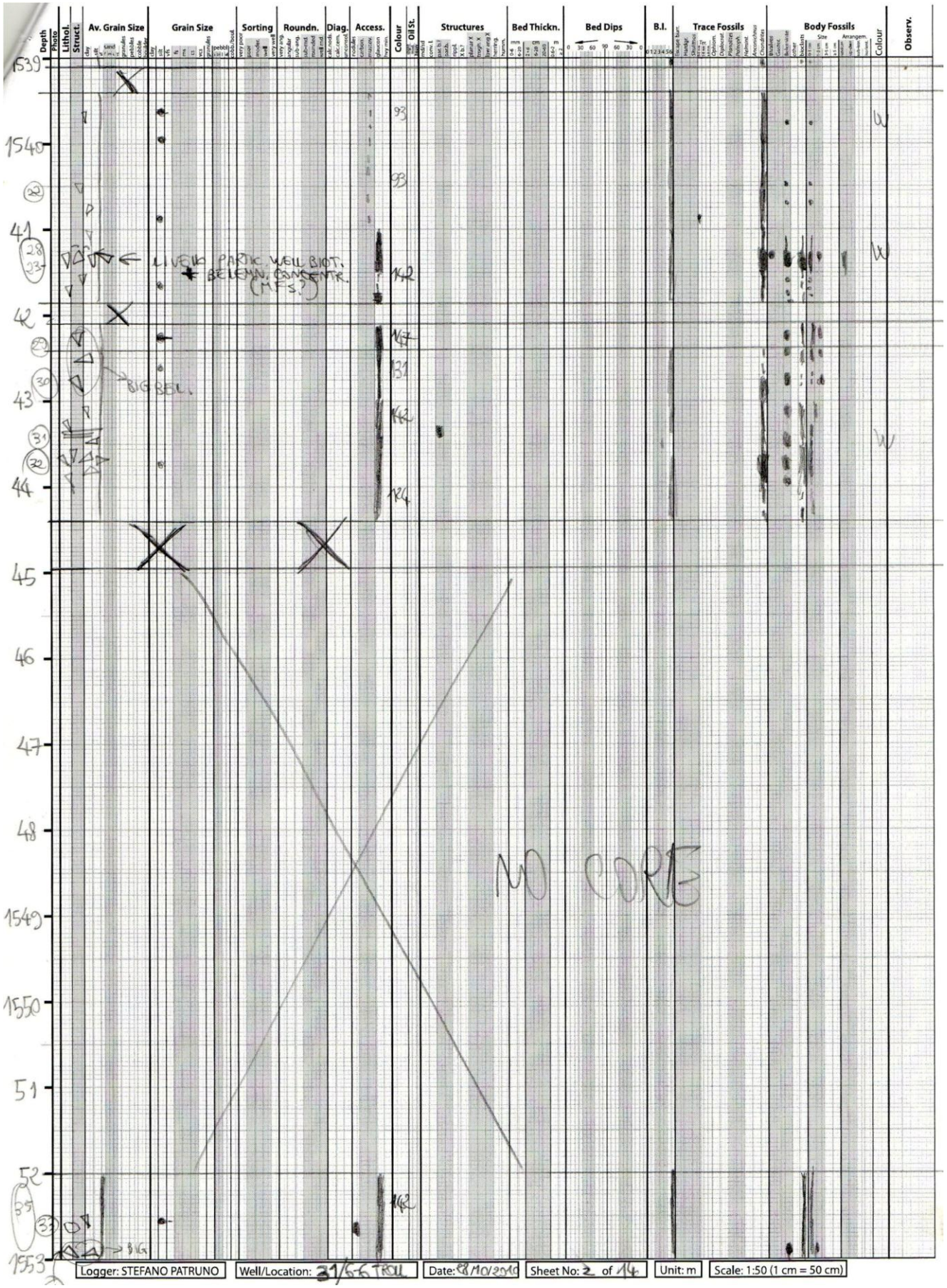
Depth
Photo
Lithol.
Struct.
Av. Grain Size
Grain Size
Sorting
Roundn.
Diag.
Access.
Colour
Oil St.
Structures
Bed Thickn.
Bed Dips
B.I.
Trace Fossils
Body Fossils
Observ.
1539
1540
41
42
43
44
45
46
47
48
1549
1550
51
52
1553
LIVE W. PARTIC. WELL BIOT. BELEMN. CONCENTR. (MFS?)
BIG BELL.
NO CORE
Logger: STEFANO PATRUNO
Well/Location: 31/6-5 TROLL
Date: 28/10/2010
Sheet No: 2 of 14
Unit: m
Scale: 1:50 (1 cm = 50 cm)

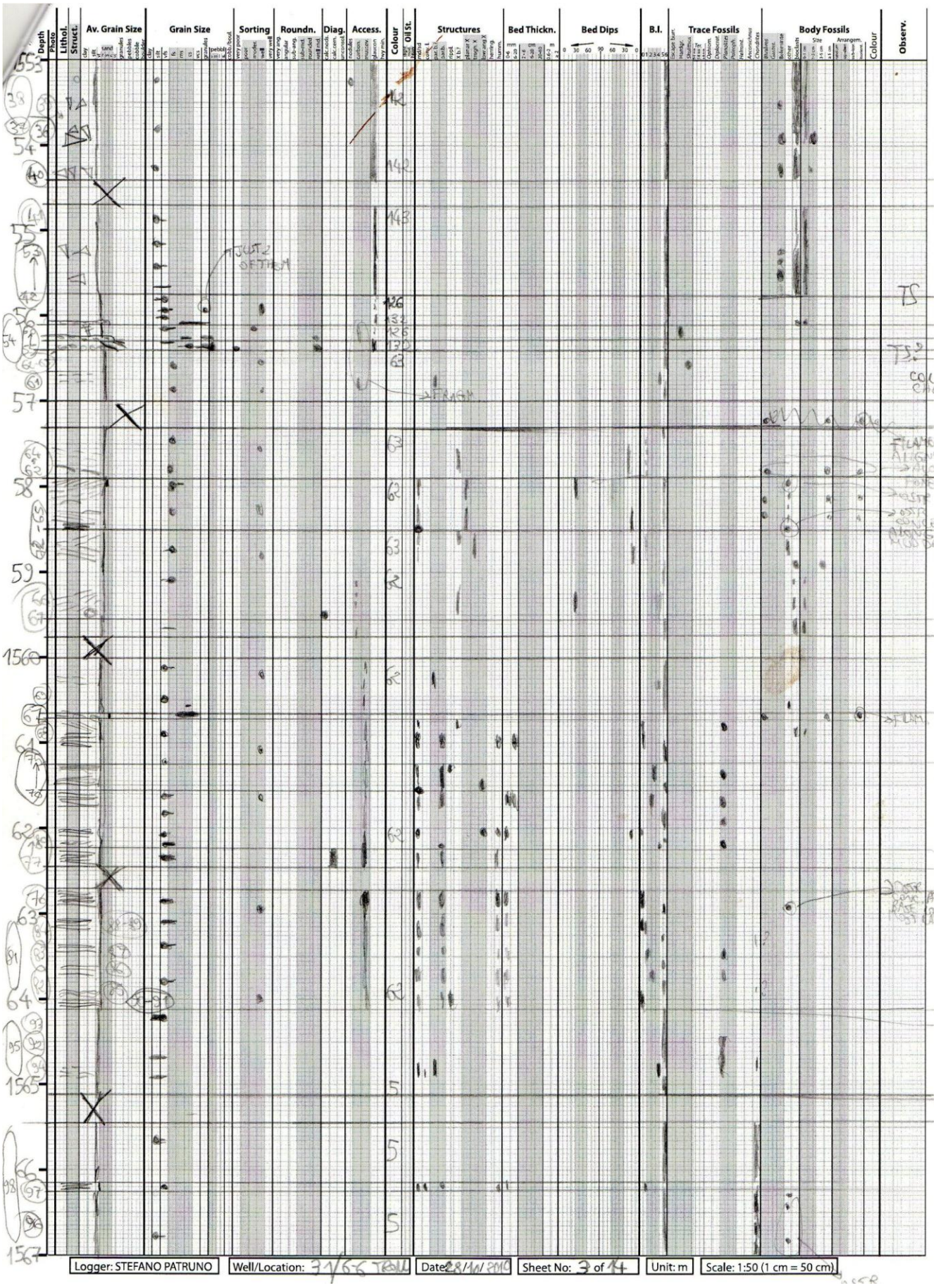
Depth
Photo
Lithol.
Struct.
Av. Grain Size
Grain Size
Sorting
Roundn.
Diag.
Access.
Colour
Oil St.
Structures
Bed Thickn.
Bed Dips
B.I.
Trace Fossils
Body Fossils
Observ.
Logger: STEFANO PATRUNO
Well/Location:
Date:
Sheet No: 3 of 14
Unit: m
Scale: 1:50 (1 cm = 50 cm)

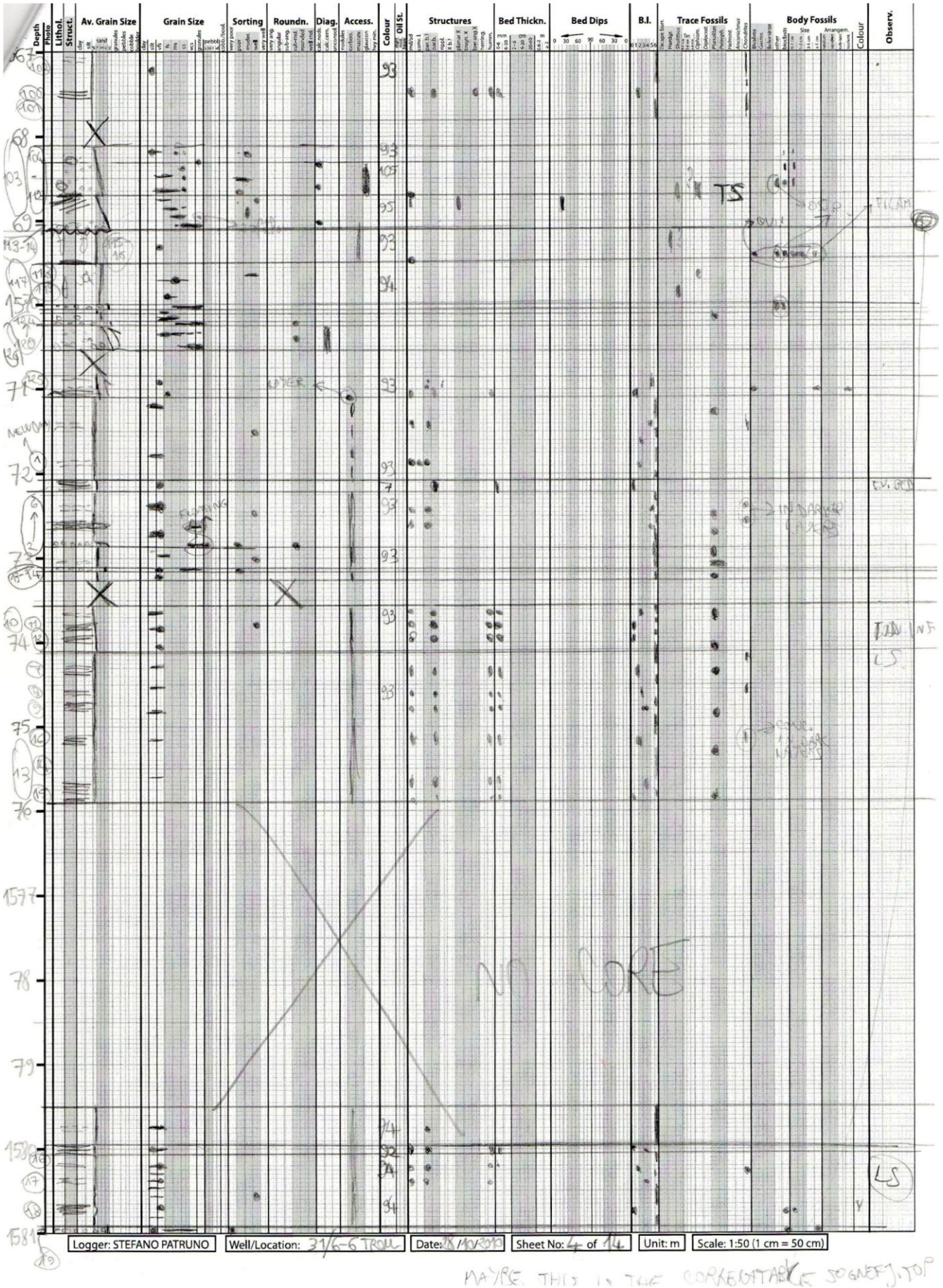
Depth
Photo
Lithol.
Struct.
Av. Grain Size
Grain Size
Sorting
Roundn.
Diag.
Access.
Colour
Oil St.
Structures
Bed Thickn.
Bed Dips
B.I.
Trace Fossils
Body Fossils
Observ.
Logger: STEFANO PATRUNO
Well/Location: 31/6-6 TROLL
Date: 28/10/2010
Sheet No: 4 of 14
Unit: m
Scale: 1:50 (1 cm = 50 cm)
NO MORE

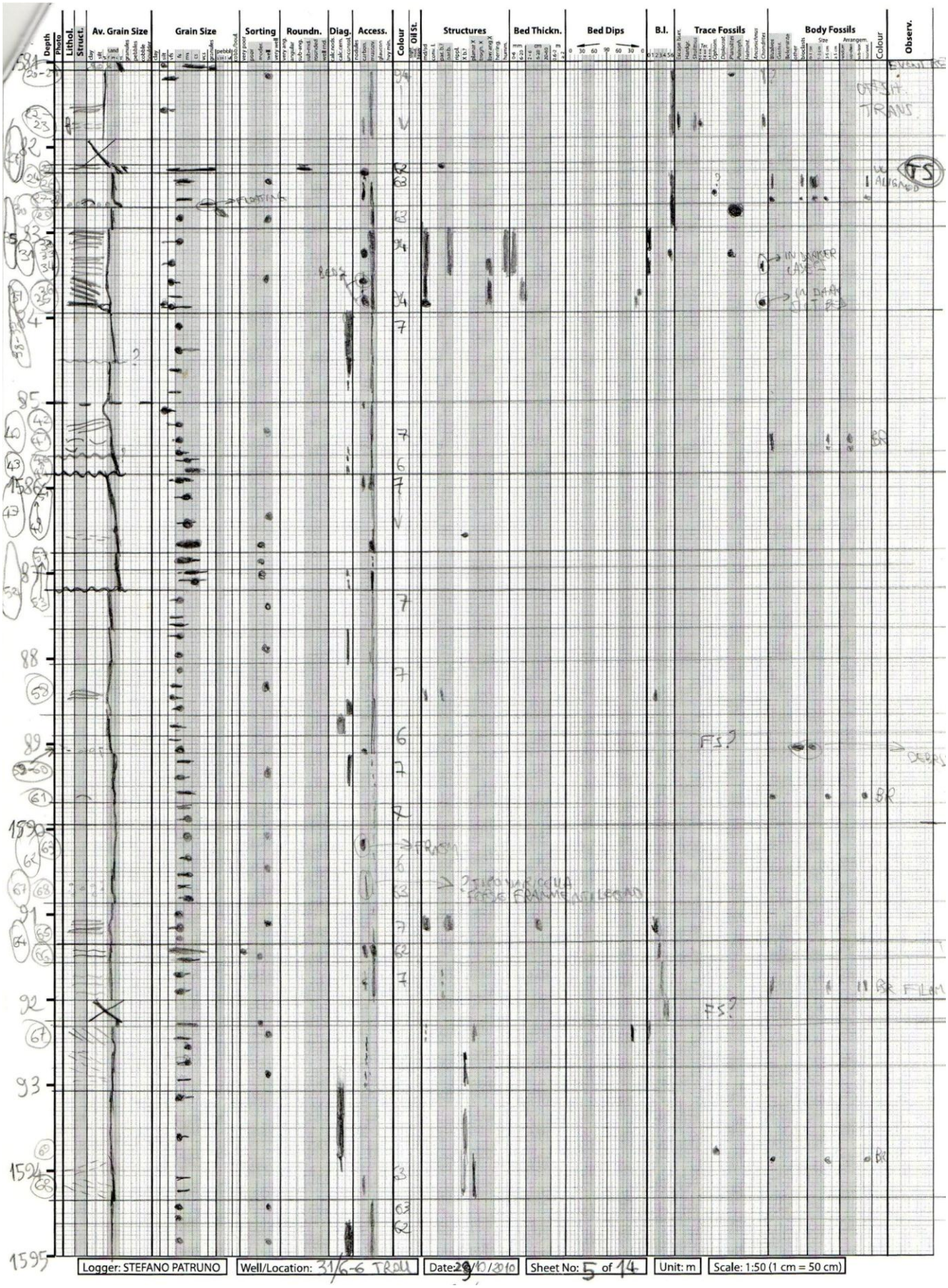
Depth
Photo
Lithol.
Struct.
Av. Grain Size
Grain Size
Sorting
Roundn.
Diag.
Access.
Colour
Oil St.
Structures
Bed Thickn.
Bed Dips
B.I.
Trace Fossils
Body Fossils
Observ.
Logger: STEFANO PATRUNO
Well/Location: 31/6-6 TROLL
Date: 29/10/2010
Sheet No: 5 of 14
Unit: m
Scale: 1:50 (1 cm = 50 cm)

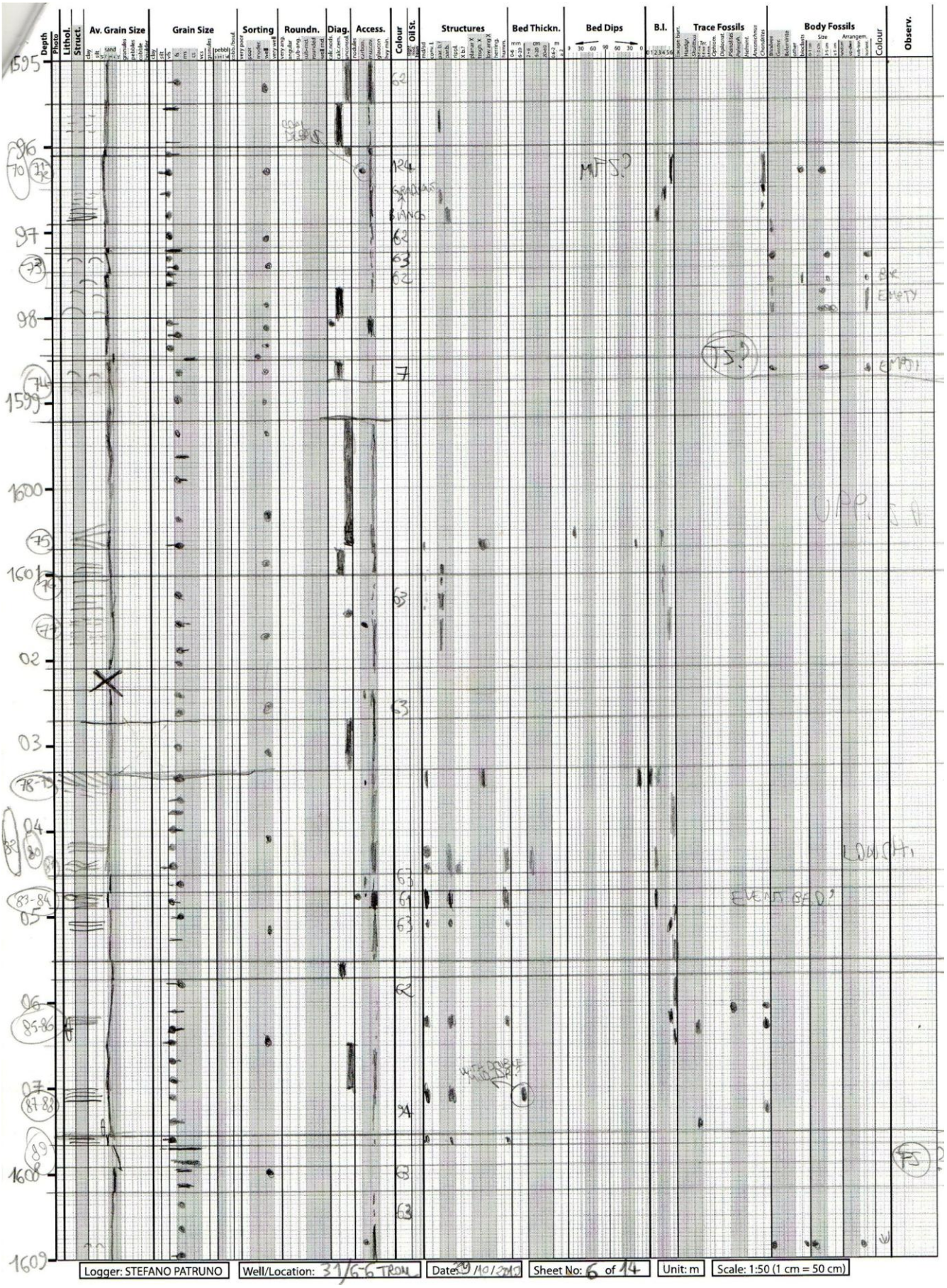
Depth
Photo
Lithol.
Struct.
Av. Grain Size
Grain Size
Sorting
Roundn.
Diag.
Access.
Colour
Oil St.
Structures
Bed Thickn.
Bed Dips
B.I.
Trace Fossils
Body Fossils
Observ.
1595
1596
1597
1598
1599
1600
1601
1602
1603
1604
1605
1606
1607
1608
1609
MFS?
TS?
UPP. SH
LOWER
EVENT BED?
Logger: STEFANO PATRUNO
Well/Location: 31/6-6 TROLL
Date: 29/10/2013
Sheet No: 6 of 14
Unit: m
Scale: 1:50 (1 cm = 50 cm)

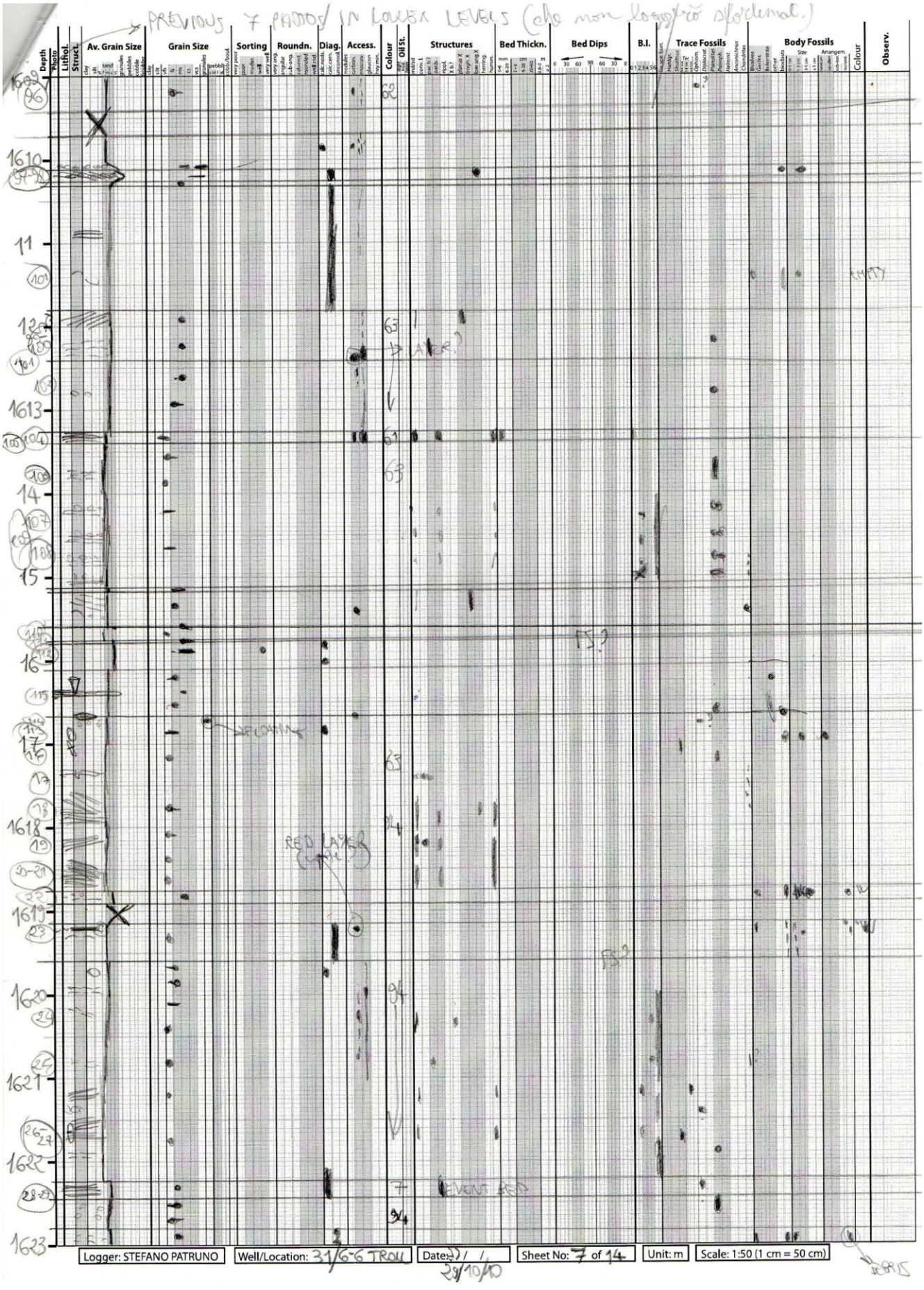
PREVIOUS 7 PAGES IN LOWER LEVELS (che non loggerò sfortunat.)
Depth
Photo
Lithol.
Struct.
Av. Grain Size
Grain Size
Sorting
Roundn.
Diag.
Access.
Colour
Oil St.
Structures
Bed Thickn.
Bed Dips
B.I.
Trace Fossils
Body Fossils
Observ.
Logger: STEFANO PATRUNO
Well/Location: 31/6-6 TROLL
Date: / /
Sheet No: 7 of 14
Unit: m
Scale: 1:50 (1 cm = 50 cm)

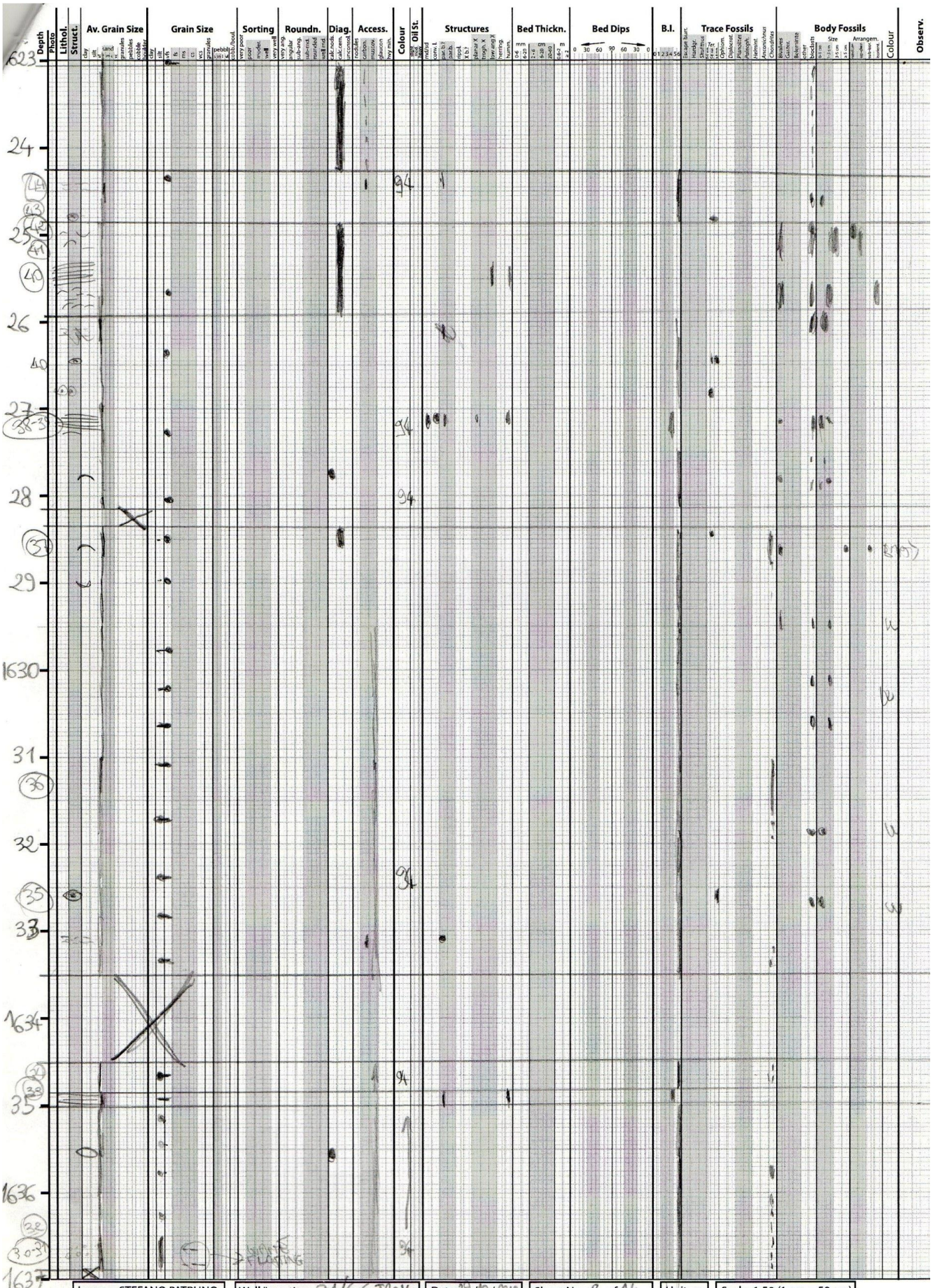
Depth
Photo
Lithol.
Struct.
Av. Grain Size
Grain Size
Sorting
Roundn.
Diag.
Access.
Colour
Oil St.
Structures
Bed Thickn.
Bed Dips
B.I.
Trace Fossils
Body Fossils
Observ.
Logger: STEFANO PATRUNO
Well/Location: 31/6-6 TROLL
Date: 29 / 10 / 2010
Sheet No: 8 of 14
Unit: m
Scale: 1:50 (1 cm = 50 cm)

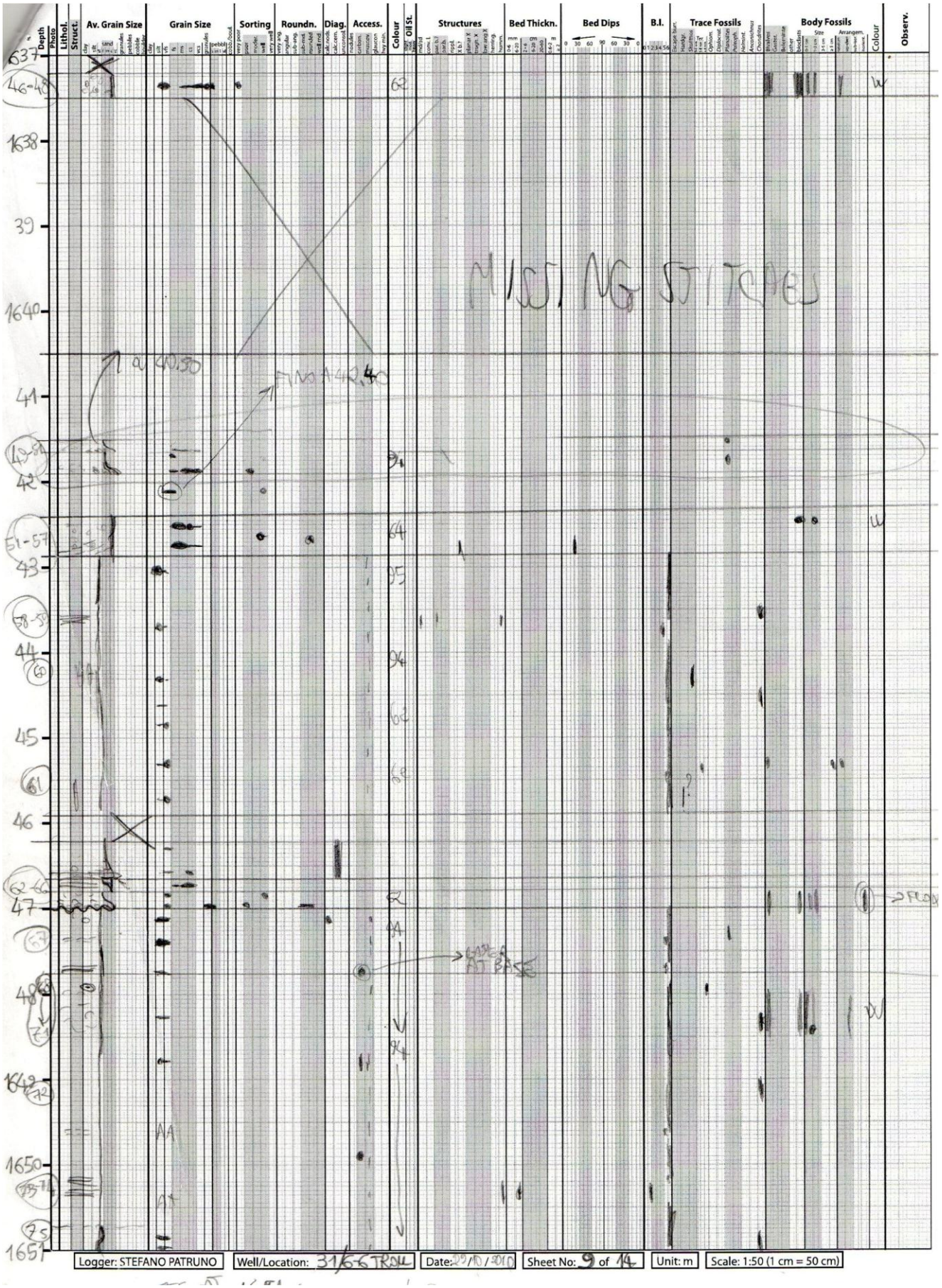
Depth
Lithol.
Struct.
Photo
Av. Grain Size
Grain Size
Sorting
Roundn.
Diag.
Access.
Colour
Oil St.
Structures
Bed Thickn.
Bed Dips
B.I.
Trace Fossils
Body Fossils
Observ.
MISSING STITCHES
Logger: STEFANO PATRUNO
Well/Location: 31/6-6 TROLL
Date: 29/10/2010
Sheet No: 9 of 14
Unit: m
Scale: 1:50 (1 cm = 50 cm)

32/4-1

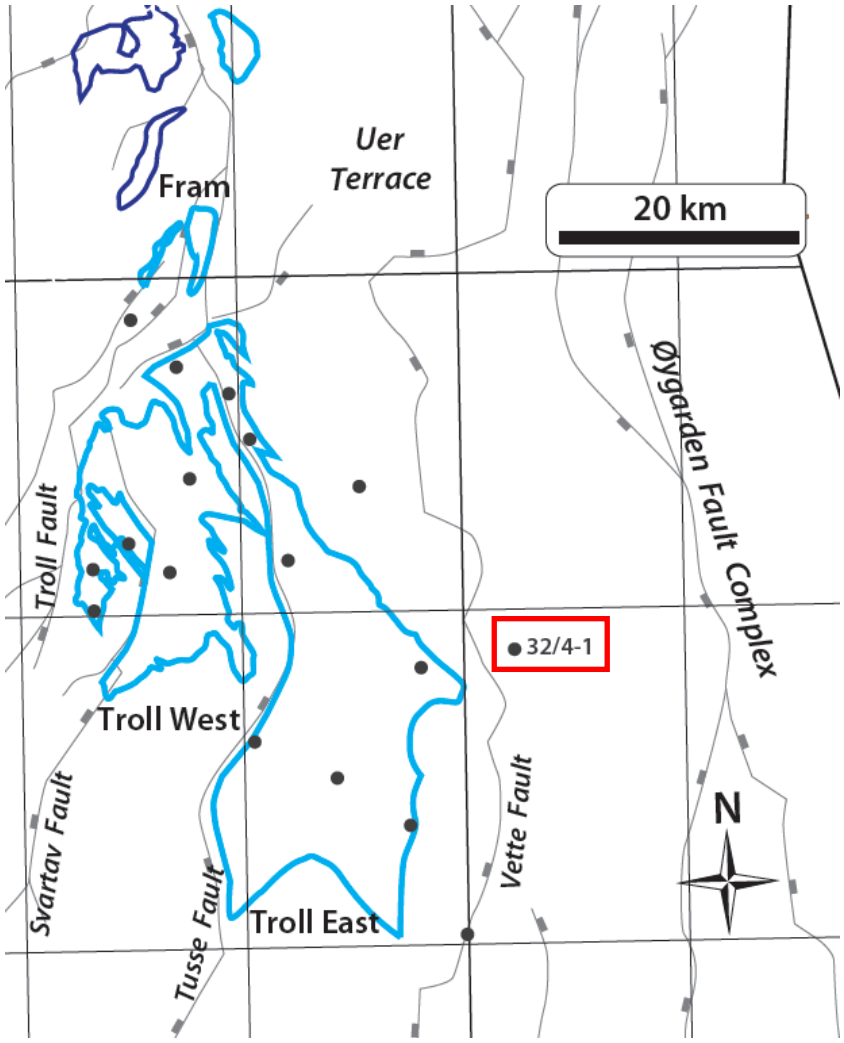
Fram
Uer
Terrace
20 km
Troll Fault
Øygarden Fault Complex
32/4-1
Troll West
Svartav Fault
Tusse Fault
Troll East
Vette Fault
N

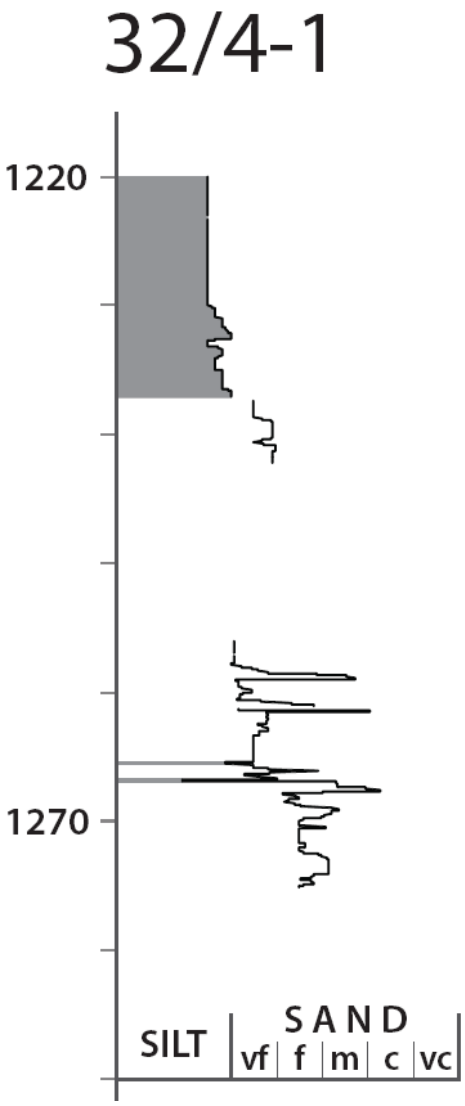
32/4-1
1220
1270
SILT
SAND
vf
f
m
c
vc

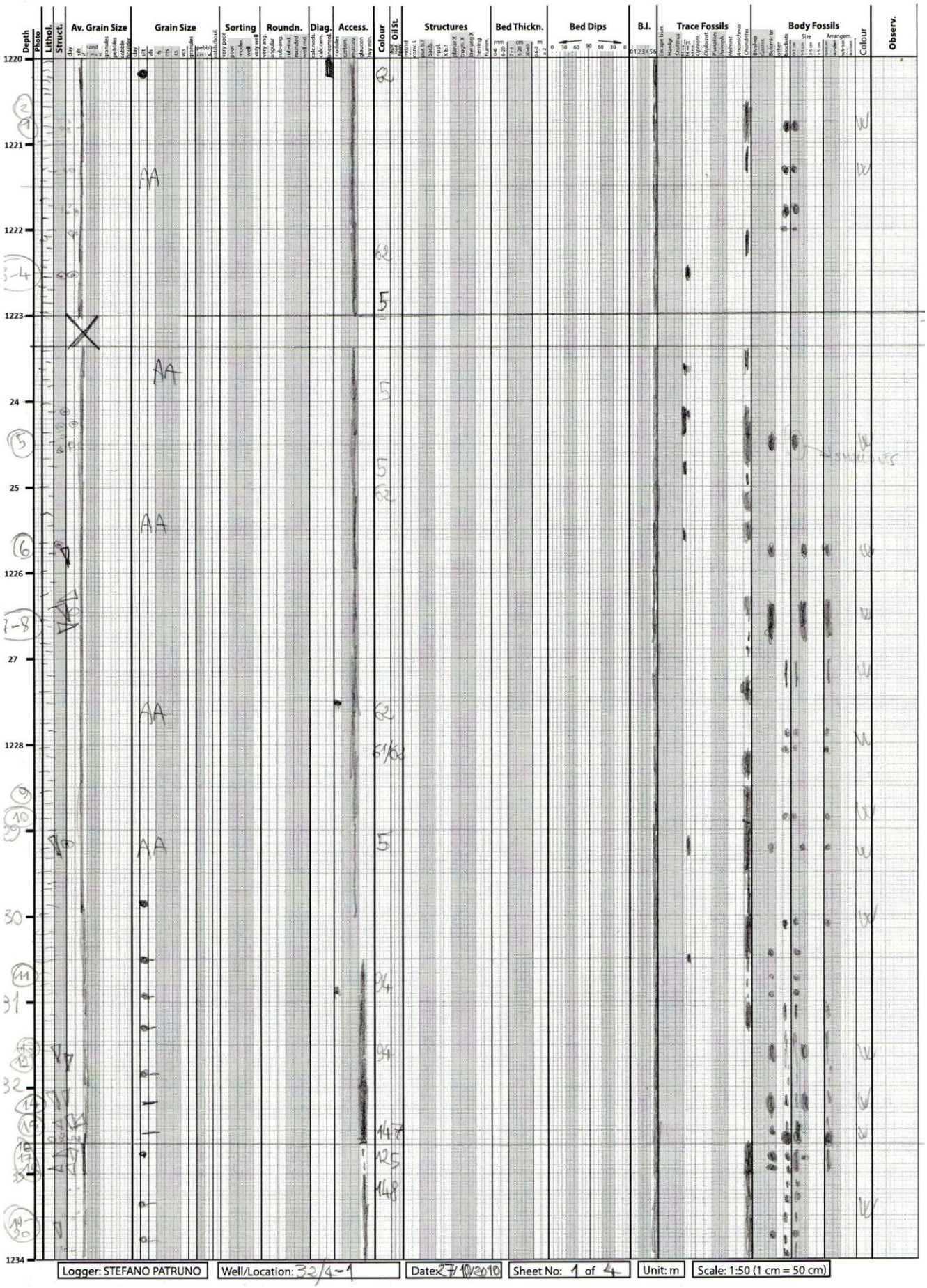
Depth
Photo
Lithol.
Struct.
Av. Grain Size
Grain Size
Sorting
Roundn.
Diag.
Access.
Colour
Oil St.
Structures
Bed Thickn.
Bed Dips
B.I.
Trace Fossils
Body Fossils
Observ.
Logger: STEFANO PATRUNO
Well/Location: 32/4-1
Date: 27/10/2010
Sheet No: 1 of 4
Unit: m
Scale: 1:50 (1 cm = 50 cm)

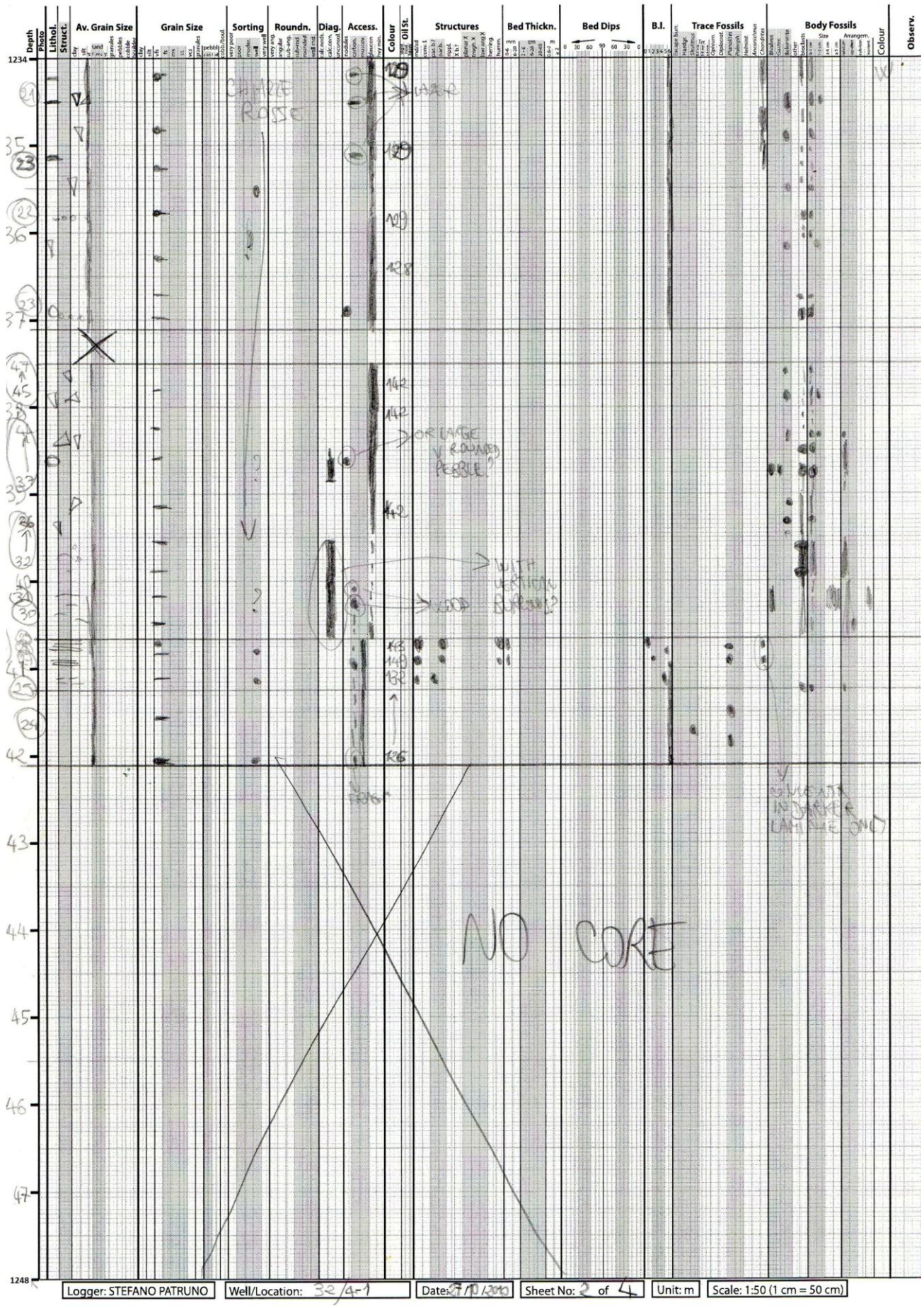
Depth
Photo
Lithol.
Struct.
Av. Grain Size
Grain Size
Sorting
Roundn.
Diag.
Access.
Colour
Oil St.
Structures
Bed Thickn.
Bed Dips
B.I.
Trace Fossils
Body Fossils
Observ.
1234
1248
CHANNEL ROSSE
FOR LARGE V. ROUNDED PEBBLE?
WITH VERTICAL BURROWS?
NO CORE
Logger: STEFANO PATRUNO
Well/Location: 32/4-1
Date: 7/10/2010
Sheet No: 2 of 4
Unit: m
Scale: 1:50 (1 cm = 50 cm)

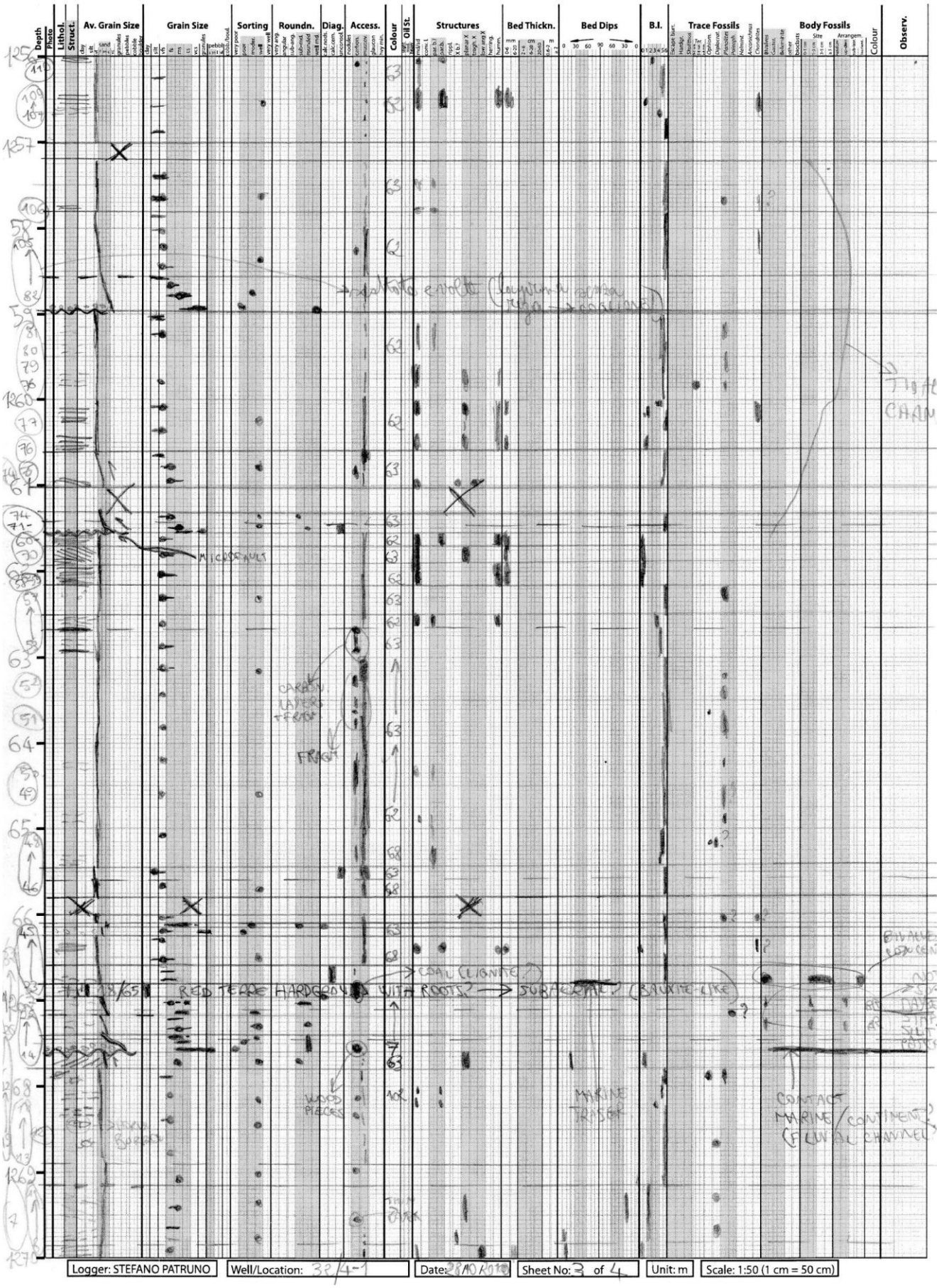
Depth
Photo
Lithol.
Struct.
Av. Grain Size
Grain Size
Sorting
Roundn.
Diag.
Access.
Colour
Oil St.
Structures
Bed Thickn.
Bed Dips
B.I.
Trace Fossils
Body Fossils
Observ.
MICRODAULS
CARBON LAYERS + ROOTS
FRACT
WOOD PIECES
MARINE TRACES
CONTACT MARINE / CONTINENTAL (FLUVIAL CHANNEL)
Logger: STEFANO PATRUNO
Well/Location: 32/4-1
Date: 28/10/2018
Sheet No: 3 of 4
Unit: m
Scale: 1:50 (1 cm = 50 cm)

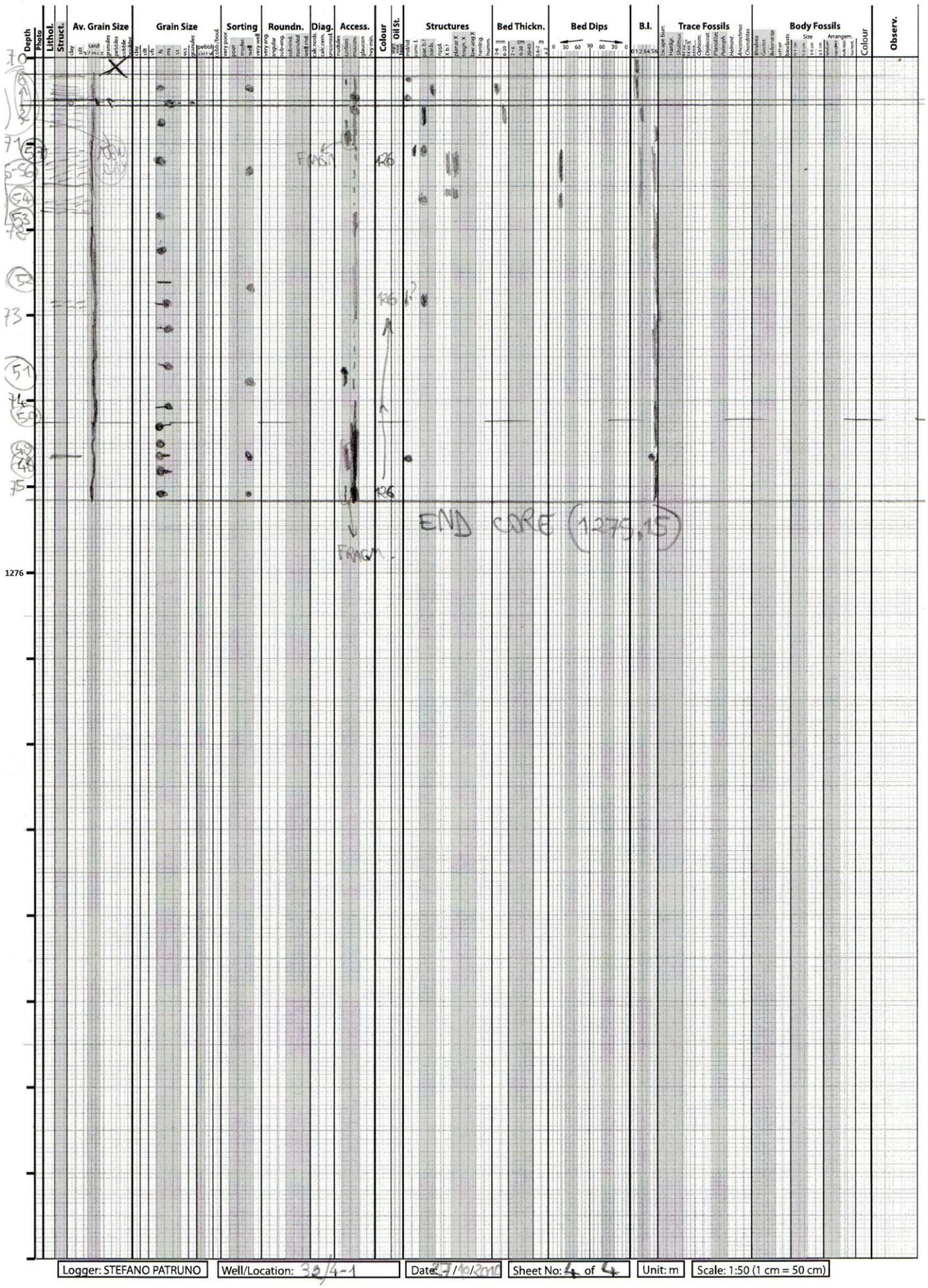
Depth
Photo
Lithol.
Struct.
Av. Grain Size
Grain Size
Sorting
Roundn.
Diag.
Access.
Colour
Oil St.
Structures
Bed Thickn.
Bed Dips
B.I.
Trace Fossils
Body Fossils
Observ.
FRAG?
END CORE (1275,15)
FRAGM.
Logger: STEFANO PATRUNO
Well/Location: 35/4-1
Date: 27/10/2010
Sheet No: 4 of 4
Unit: m
Scale: 1:50 (1 cm = 50 cm)